frontiers | Research Topics

# Influenza viruses: Infection, pathogenesis, and host responses

**Edited by**
Quanjiao Chen, Yizhi Tao and Dayan Wang

**Published in**
Frontiers in Microbiology

ISSN 1664-8714
ISBN 978-2-83252-189-2
DOI 10.3389/978-2-83252-189-2

## About Frontiers

Frontiers is more than just an open access publisher of scholarly articles: it is a pioneering approach to the world of academia, radically improving the way scholarly research is managed. The grand vision of Frontiers is a world where all people have an equal opportunity to seek, share and generate knowledge. Frontiers provides immediate and permanent online open access to all its publications, but this alone is not enough to realize our grand goals.

## Frontiers journal series

The Frontiers journal series is a multi-tier and interdisciplinary set of open-access, online journals, promising a paradigm shift from the current review, selection and dissemination processes in academic publishing. All Frontiers journals are driven by researchers for researchers; therefore, they constitute a service to the scholarly community. At the same time, the *Frontiers journal series* operates on a revolutionary invention, the tiered publishing system, initially addressing specific communities of scholars, and gradually climbing up to broader public understanding, thus serving the interests of the lay society, too.

## Dedication to quality

Each Frontiers article is a landmark of the highest quality, thanks to genuinely collaborative interactions between authors and review editors, who include some of the world's best academicians. Research must be certified by peers before entering a stream of knowledge that may eventually reach the public - and shape society; therefore, Frontiers only applies the most rigorous and unbiased reviews. Frontiers revolutionizes research publishing by freely delivering the most outstanding research, evaluated with no bias from both the academic and social point of view. By applying the most advanced information technologies, Frontiers is catapulting scholarly publishing into a new generation.

## What are Frontiers Research Topics?

Frontiers Research Topics are very popular trademarks of the *Frontiers journals series*: they are collections of at least ten articles, all centered on a particular subject. With their unique mix of varied contributions from Original Research to Review Articles, Frontiers Research Topics unify the most influential researchers, the latest key findings and historical advances in a hot research area.

Find out more on how to host your own Frontiers Research Topic or contribute to one as an author by contacting the Frontiers editorial office: frontiersin.org/about/contact

# Influenza viruses: Infection, pathogenesis, and host responses

**Topic editors**

Quanjiao Chen — Wuhan Institute of Virology, Chinese Academy of Sciences (CAS), China

Yizhi Tao — Rice University, United States

Dayan Wang — Chinese National Influenza Center, China

**Citation**

Chen, Q., Tao, Y., Wang, D., eds. (2023). *Influenza viruses: Infection, pathogenesis, and host responses*. Lausanne: Frontiers Media SA.

doi: 10.3389/978-2-83252-189-2

# Table of contents

frontiers in Microbiology

ORIGINAL RESEARCH
published: 27 September 2021
doi: 10.3389/fmicb.2021.730449

# A Cross-Reactive Monoclonal Antibody Against Neuraminidases of Both H9N2 and H3N2 Influenza Viruses Shows Protection in Mice Challenging Models

*Fei Wang[1,2†], Zhimin Wan[1,2,3†], Jinsen Wu[1,2], Yajuan Wang[1,2], Hui Fu[1,2], Hongxia Shao[1,2,3], Kun Qian[1,2,3], Wei Gao[1,2,3*], Jianqiang Ye[1,2,3*] and Aijian Qin[1,2,3*]*

[1] Ministry of Education Key Lab for Avian Preventive Medicine, Yangzhou University, Yangzhou, China, [2] Jiangsu Co-innovation Center for Prevention and Control of Important Animal Infectious Diseases and Zoonoses, Yangzhou, China, [3] Joint International Research Laboratory of Agriculture and Agri-Product Safety of Ministry of Education of China, Yangzhou University, Yangzhou, China

Neuraminidases (NAs) of H9N2 avian influenza virus (AIV) and H3N2 human seasonal influenza virus (HSIV) share similar antigenic structures. However, there are few reports on epitopes shared by these two NAs. We previously reported a monoclonal antibody (mAb) 1G8 against the NA of H9N2 AIV with neuraminidase inhibition (NI) ability. In this study, 1G8 was shown to cross-react with and inhibit the NA of H3N2 HSIV. In a passive transfer experiment, 1G8 provided protection to mice challenged with rescued H1N2 viruses carrying H9N2 NA or H3N2 NA. Mutation at amino acid position 199 was also selected and proved to be crucial for H3N2 HSIV to escape from mAb 1G8. Moreover, we found that residue 199 contributed to inducing broad protective antibodies without the influence of the *N*-linked glycosylation at amino acid position 200 in NAs. Residues as residue 199, which are not shielded by glycosylation modification, would form ideal epitopes for developing universal vaccine and protective antibodies.

**Keywords: monoclonal antibody, neuraminidase, H9N2, H3N2, influenza virus, cross-react, protection**

OPEN ACCESS

***Edited by:***
*Dayan Wang,*
*Chinese National Influenza Center, China*

***Reviewed by:***
*Qingbing Zheng,*
*Xiamen University, China*
*Ahmed Mohamed Kandeil,*
*St. Jude Children's Research Hospital, United States*

****Correspondence:***
*Wei Gao*
*wgao@yzu.edu.cn*
*Jianqiang Ye*
*jqye@yzu.edu.cn*
*Aijian Qin*
*aijian@yzu.edu.cn*

*† These authors have contributed equally to this work*

***Specialty section:***
*This article was submitted to Virology, a section of the journal Frontiers in Microbiology*

***Received:*** *25 June 2021*
***Accepted:*** *30 August 2021*
***Published:*** *27 September 2021*

***Citation:***
*Wang F, Wan Z, Wu J, Wang Y, Fu H, Shao H, Qian K, Gao W, Ye J and Qin A (2021) A Cross-Reactive Monoclonal Antibody Against Neuraminidases of Both H9N2 and H3N2 Influenza Viruses Shows Protection in Mice Challenging Models. Front. Microbiol. 12:730449. doi: 10.3389/fmicb.2021.730449*

## INTRODUCTION

H9N2 subtype avian influenza virus (AIV) is one of the most prevalent influenza viruses in poultry and has caused substantial economic loss in poultry production (Bi et al., 2020; Carnaccini and Perez, 2020). Although H9N2 AIV infections in humans were rarely reported, the neuraminidase (NA) and other internal genes have been involved in generation of many highly pathogenic influenza viruses (Lin et al., 2000; Gao et al., 2013; Gu et al., 2014; Jianzhong et al., 2014; Liu et al., 2018). H3N2 subtype influenza virus is a human seasonal influenza virus (HSIV) and predominates in recent influenza seasons. H3N2 HSIV infection can cause severe respiratory system injury in humans, especially in the elderly (Kissling et al., 2017). Although H9N2 AIV and H3N2 HSIV share the same N2 subtype, there were few reports on same antigenic epitopes between them but universal epitopes among all subtypes of NAs (Doyle et al., 2013; Stadlbauer et al., 2019).

Neuraminidase is an important surface protein and antigen of influenza virus, which is a tetramer structure and plays an important role in helping newborn virus release from infected cells (Varghese et al., 1983). In the case of preexisted vaccination, antibodies targeting the NA active center can block the releasing of newborn virus (Eichelberger and Wan, 2015). However, as flexible as hemagglutinin (HA), NA can also escape from antibodies and inhibitors by amino acid mutations (Sandbulte et al., 2011; Wang et al., 2021). Many amino acid positions of H9N2 NA have been reported to be involved in escape from monoclonal antibodies (mAbs) and antibody pressure induced by vaccines (Wang et al., 2021). To control H3N2 HSIV, the best-matched strains for vaccination are updated every year, but antigenic drifts in NA have also been reported to help virus evade from the humoral immunity (Wan et al., 2019; Powell and Pekosz, 2020).

Conserved epitopes in HA and NA are crucial for developing universal influenza vaccines (Krammer and Palese, 2013; Wohlbold and Krammer, 2014). However, even if HA or NA belongs to the same subtype, the evolutionary directions might be different because of being prevalent in diverse hosts and exposed to various vaccinations (Lee et al., 2019). H9N2 AIV and H3N2 HSIV share the same N2 subtype and homologous sequences, while there were few reports on similar antigenic structure between them. In the present study, mAb 1G8 against the NA of H9N2 AIV was proved to cross-react with the NA of H3N2 HSIV and protect mice from viral challenge. Our research may facilitate the development of protective antibodies against N2 subtype AIV and HSIV in future.

## MATERIALS AND METHODS

### Viruses, Cells, and Monoclonal Antibodies

A/Chicken/Jiangsu/H1/2019 (JSH1) H9N2 virus (accession numbers: MN515351 and MT459203) was isolated from poultry in China (Wang et al., 2021). A/Canine/Jiangsu/06/2010 (JS06) H3N2 virus (accession number: JN247616 to JN247623) was isolated from canine in China (Lin et al., 2012). All viruses were grown in 9-day-old embryonated SPF chicken eggs. Allantoic fluid of each virus was harvested at 120 h postinoculation and stored at −70°C. Madin-Darby canine kidney (MDCK) cells, African green monkey kidney-originated COS-1 cells, and human lung carcinomatous A549 cells were maintained in DMEM supplemented with 10% FBS at 37°C in 5% $CO_2$. mAbs 1G8 and A7E6 were prepared as previously described (Wang et al., 2021). Ascitic fluid of each mAb was prepared in 8-week-old mice and purified with protein G column (GE, Boston, MA, United States).

### Reassortant Viruses Rescued by Reverse Genetics

Reassortant viruses were rescued by reverse genetics as previously reported (Shao et al., 2015). NA gene of A/Chicken/Jiangsu/H1/2019 (JSH1) H9N2 virus was amplified by reverse transcription-polymerase chain reaction (RT-PCR). NA gene of A/Beijing/PUMCH06/2017 (PUMCH06) H3N2 virus (accession number: MG759370.1) was synthetized by GenScript Co., Ltd., Nanjing, China. The NA genes and the other seven genes (HA, PA, PB1, PB2, NP, NS, and M) of A/Puerto Rico/8/34 (PR8) H1N1 virus were cloned into the pDP2002 vector by the Exnase II (Vazyme, Nanjing, China). The reassortant viruses rgH1N2(JSH1) and rgH1N2(PUMCH06) were rescued by transfection in COS-1 cells. Briefly, 1 μg of each plasmid was transfected into COS-1 cells with 16 μl of TransIT®-LT1 Transfection Reagent (Mirus, Madison, WI, United States). The culture medium was changed into Opti-MEM with 2 μg/ml TPCK-Trypsin at 6 h posttransfection. The recued viruses in supernatants of transfected cells were collected at 72 h posttransfection. Nine-day-old SPF eggs were used for expended culture of rescued viruses. Allantoic fluid of each virus was collected on the fifth day postinoculation and preserved at −70°C for further research.

### Immunofluorescence Assay

Briefly, COS-1 cells infected with viruses were fixed with cold acetone-alcohol at 48 h post-infection. After incubation of mAb 1G8 for 30 min, the fixed cells were washed three times with PBS and incubated with FITC conjugated goat anti-mouse-IgG(H + L) antibody (Jackson Immunoresearch, PA, United States) as secondary antibody. After 30 min, the cells were washed three times again and observed under inverted fluorescence microscopy (Olympus, Tokyo, Japan).

### Viral Growth Kinetics

A549 cells in 6-well plates were infected with rgH1N2(JSH1) and rgH1N2(PUMCH06) at a multiplicity of infection (MOI) of 0.01, respectively. The supernatants from the infected cells were collected at 12, 24, 36, 48, 60, and 72 h post-infection, and the viruses were titrated by median tissue infective dose ($TCID_{50}$) assay in MDCK cells as previously described (Jin et al., 2019). Briefly, the collected supernatants were serially diluted from $10^{-1}$ to $10^{-11}$ with Opti-MEM medium that contained 2 μg/mL TPCK-treated trypsin. MDCK cells in 96-well plates were infected with diluted virus. Three days later, HA titer of each well was tested with 0.5% chicken red blood cells and $TCID_{50}$ was calculated according to Reed-Muench assay.

### Neuraminidase Inhibition Assay

The inhibition of NA activity by 1G8 was measured with enzyme-linked lectin assay (ELLA) and 4-(methylumbelliferyl)-*N*-acetylneuraminic acid (Mu-NANA) assay as previously described (Wan et al., 2016).

In ELLA, mixtures of serial-diluted mAb and predetermined viruses were incubated in fetuin (Sigma-Aldrich, Shanghai, China) coated wells at 37°C for 16 h. After washing with PBST for six times, peanut agglutinin conjugated with peroxidase (PNA-HRP) (Sigma-Aldrich, Shanghai, China) were added and incubated at room temperature for 2 h. The plates were washed with PBST for six times, followed by addition of tetramethylbenzidine (TMB) substrate. The reaction was finally stopped with 1% SDS and absorbance at $OD_{650}$ was read.

In Mu-NANA assay, mixtures of serial-diluted mAb and predetermined viruses were incubated in black 96-well plate at 37°C for 30 min. Mu-NANA substrate (Sigma-Aldrich, Shanghai, China) was added and incubated for 1 h at 37°C. The reaction was finally stopped with 0.2 M $Na_2CO_3$ and read with excitation range 350–365 nm and emission range 440–460 nm.

## Mice Experiments

For mice experiments, the BALB/c mice were purchased from Experimental Animal Center of Yangzhou University (Yangzhou, China). All animal experiments were done in accordance with the institutional animal care guidelines, and the protocol (number 06R015) was approved by the Animal Care Committee at Yangzhou University.

In the prophylactic experiment, eleven 6-week-old BALB/c mice per group were first intraperitoneally injected with 5 mg/kg mAb, and 2 h later, mice were anesthetized with 0.2 mL 1.25% avertin by intraperitoneal injection and infected with rgH1N2(JSH1) and rgH1N2(PUMCH06), respectively, at a dose of $10^7$ $TCID_{50}$ by intranasal inoculation. On day 3 and 6 post-infection, three mice from each group were euthanized, and lungs were collected and the viral load in the lungs was titrated in MDCK cells by $TCID_{50}$ assay. The lung tissues with representative pathological changes collected at the sixth day post-infection in prophylactic experiment were fixed with 4% paraformaldehyde for histopathological analysis. The other five infected mice in per group were monitored daily for body weight loss and any clinical signs. The mice with the body weight loss more than 25% were euthanized.

In the therapeutic experiment, five 6-week-old BALB/c mice per group were anesthetized and infected with rgH1N2(JSH1) and rgH1N2(PUMCH06) with a dose of $10^8$ $TCID_{50}$ by intranasal inoculation. Mice of each group received 5, 2.5, 1, 0.5 mg/kg mAb 1G8 or 5 mg/kg mAb A7E6 by intraperitoneal injection at 48 h post-infection. The body weight of each group was monitored daily. The mice with the body weight loss more than 25% were euthanized.

## Selection of Monoclonal Antibody Escape Mutants

Escape mutants of rgH1N2(PUMCH06) and JS06 H3N2 canine influenza virus (CIV) were selected with mAb 1G8 as previously reported (Wang et al., 2021). Briefly, 50 μL allantoic fluid of each virus was incubated with 0.5 mL mAb at 37°C for 30 min and then inoculated into 9-day-old SPF embryonated chicken eggs. Allantoic fluid of the virus was collected on 5th day post-inoculation and NA gene of each virus was amplified with RT-PCR assays for sequencings. Mutant viruses were cloned by limiting dilution in 9-day-old embryonated chicken eggs and plaque assay, followed by further NA sequencing.

## Sequence Alignments and Phylogenetic Analysis

Twenty-two NA amino acid sequences (accession number: ABP49330.1, AJM70556.1, ALM05426.1, ANG55885.1, ALT67802.1, AQS25225.1, AEM75969.1, ACD88721.1, ADP07897.1, AHZ43615.1, AGG81752.1, AGG83215.1, ASV60611.1, AGG82970.1, AGG83292.1, CAC69608.1, AKF35396.1, AQS26225.1, AFC35440.1, AFC35430.1, AKC43905.1, and AGX84936.1) belong to 11 different NA subtypes were analyzed using multiple sequence alignment by MEGA X.[1] The phylogenetic tree was constructed with MEGA X in neighbor-joining method and 1000 boot-strap replicates.

## Statistical Analysis

The data analysis was performed by GraphPad Prism v.5 (GraphPad Software Inc.). All results of viral growth, NI assays and mouse experiments were indicated as the mean ± SEM.

# RESULTS

## Monoclonal Antibody 1G8 Inhibits Enzymatic Activity of H9N2 and H3N2 Neuraminidase

Rescued reassortant viruses rgH1N2(PUMCH06) and rgH1N2(JSH1) were generated with NA gene of JSH1 H9N2 virus or PUMCH06 H3N2 virus and 7 other genes of PR8 H1N1 virus. Rescued viruses were tested with mAb 1G8 in immunofluorescence assay (IFA) (**Figure 1A**). The IFA results showed that mAb 1G8 reacted with both rgH1N2(PUMCH06) virus and rgH1N2(JSH1) virus but not PR8 virus, indicating that mAb 1G8 could recognize NAs of not only H9N2 AIV but also H3N2 HSIV.

rgH1N2(PUMCH06) and rgH1N2(JSH1) exhibited similar replication kinetics in A549 cells (**Figure 1B**), which indicated that recombinant viruses with either avian-origin or human-origin N2-subtype NA can grow well in A549 cells. rgH1N2(JSH1) viruses had slightly lower reproduction level than rgH1N2(PUMCH06) in A549 cells at first 24 h postinfection, but rgH1N2(JSH1) viruses posed comparatively higher titers of viruses after 36 h postinfection.

In NI assays, mAb 1G8 showed significant inhibition effect on rgH1N2(JSH1) virus both in ELLA and Mu-NANA assay (**Figure 1C**). Although mAb 1G8 posed weaker inhibition activity to NA of rgH1N2(PUMCH06) virus compared with that to rgH1N2(JSH1) virus, significant inhibition to NA of rgH1N2(PUMCH06) virus can take place at high concentration of mAb 1G8, especially in ELLA. In the negative control group, mAb A7E6 cannot inhibit NA activity of the rgH1N2 viruses even at very high concentration. Results of NI assays implied that mAb 1G8 can inhibit NA activity of not only current H9N2 AIVs but also prevalent H3N2 HSIVs.

## Monoclonal Antibody 1G8 Protects Mice Against Viruses Bearing H9N2 and H3N2 Neuraminidase

To test if mAb 1G8 has protective activity *in vivo*, we assessed the efficacy in prophylaxis and therapy of mAb 1G8 against recombinant H1N2 viruses in mice. In the prophylactic

[1] www.megasoftware.net

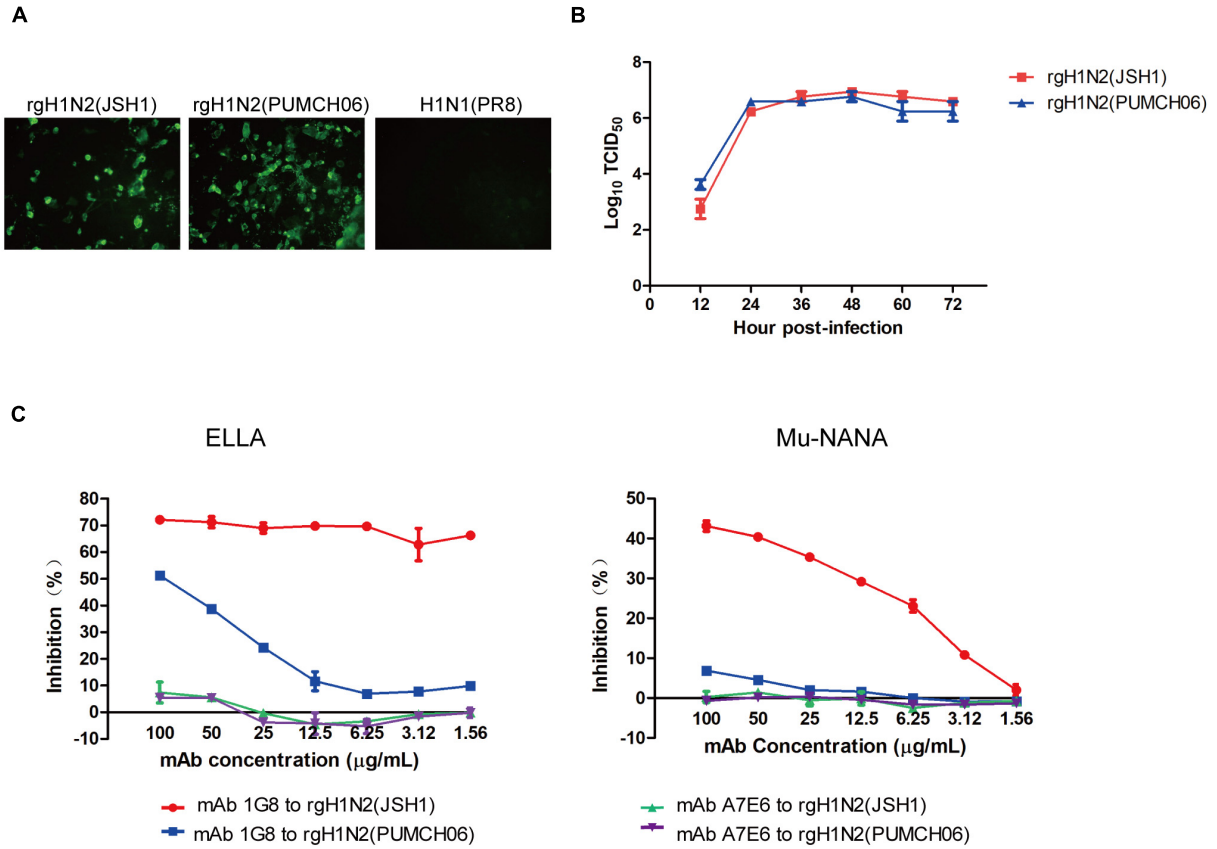


**FIGURE 1 |** Generation of rgH1N2 viruses and reactivity to mAb 1G8. **(A)** Reactivity of mAb 1G8 to rgH1N2(JSH1), rgH1N2(PUMCH06), and H1N1(PR8) viruses in IFA. **(B)** Viral growth kinetics of rgH1N2 viruses in A549 cells. **(C)** NI activity of mAb 1G8 to rgH1N2 viruses measured by ELLA and Mu-NANA assay. The mAb A7E6 was used as negative control. All data of viral growth kinetics and NI assay were performed with Graphpad Prism v.5 and represented as mean ± SEM.

experiment, 1G8 provided 100% protection at a dose of 5 mg/kg for mice challenged with $10^7$ $TCID_{50}$ of rgH1N2(JSH1) or rgH1N2(PUMCH06) (**Figures 2B,D**). The continuous weight losses of mice in 1G8 group infected with two viruses were only observed at the first 4 days, and the body weight recovered quickly right about less than 90% (**Figures 2A,C**). Whereas, the body weight of the negative control group, which was treated with mAb A7E6, continuously decreased on the first week and only one mouse in each group recovered on the second week.

The administration of mAb 1G8 also resulted in a reduction of viral load in lungs of the challenged mice (**Figures 2E,F**). Especially for the 1G8 group infected with rgH1N2(JSH1) virus, two of three mice were viral positive in lungs at third day postinfection, and only one viral positive in lungs collected at sixth day postinfection was detected. Consistent to viral load in lungs, the histopathological analysis results of infected mice showed that 1G8 resulted in less lesions and inflammations in lungs at sixth day postinfection compared with the control mAb (**Figure 2G**). The 1G8-treated mice had only mild alveolitis, while the negative control mAb A7E6-treated mice had severe pulmonary interstitial pneumonia and alveolitis. The alveolar structure of control mAb-treated mice is destroyed compared with the 1G8-treated mice, especially in those challenged with rgH1N2(JSH1).

In the therapeutic experiment, 1G8 still provided 100% protection at a dose of 5 mg/kg for mice challenged with $10^8$ $TCID_{50}$ rgH1N2(JSH1) virus or rgH1N2(PUMCH06) virus (**Figures 3B,D**). Lower doses of mAb 1G8 did not provide 100% protection. At a dose of 2.5 mg/kg 1G8, only 40% of the animals survived. However, mice treated with lower doses of 1G8 showed slower weight loss and death in contrast with mice treated with the negative control mAb A7E6 (**Figures 3A,C**).

## Mutations at Amino Acid Position 199 of Neuraminidase Help Virus Escape From Monoclonal Antibody 1G8

To identify if 1G8 targets the same epitope in NA of H3N2 HSIV as previously reported for H9N2 AIV (Wan et al., 2016), escape mutant of rgH1N2(PUMCH06) selected by 1G8 was characterized. The K199R (N2 numbering) mutation in NA was found in selected escape mutant of rgH1N2(PUMCH06) virus.

The NI activity of 1G8 to the mutant virus was also measured with ELLA and MuNANA assays (**Figures 4A,B**). Compared with the rgH1N2(PUMCH06) virus containing K199 in NA,

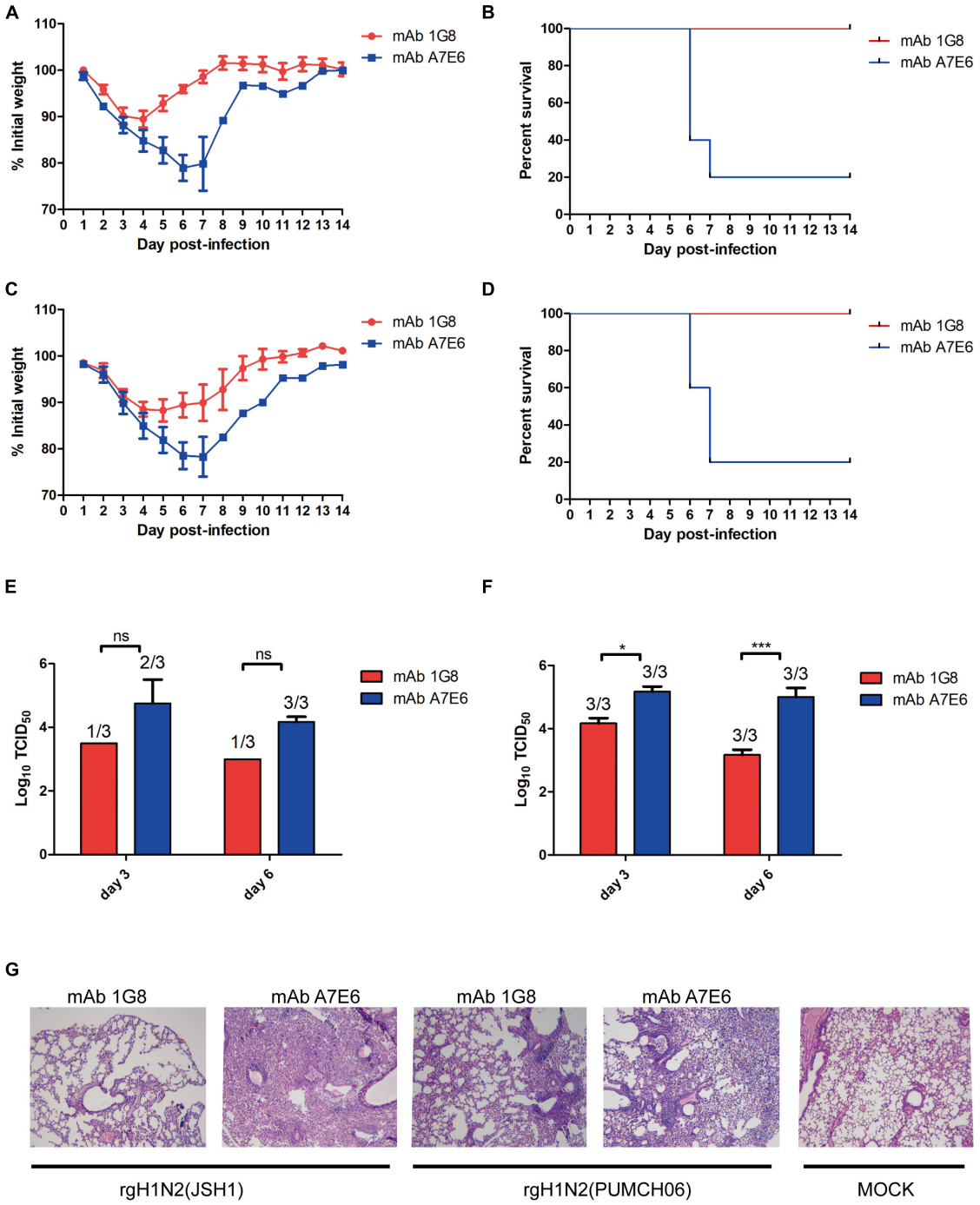


**FIGURE 2 |** *In vivo* protective effect of mAb 1G8 in prophylactic experiment. The mean percentage of the mice body weight **(A)** and the survival curves **(B)** of BALB/c mice ($n$ = 5 per group) treated with mAb 1G8 or mAb A7E6 after challenge with $10^7$ $TCID_{50}$ rgH1N2(JSH1) viruses. The mean percentage of the mice body weight **(C)** and the survival curves **(D)** of BALB/c mice treated with mAb 1G8 or mAb A7E6 after challenge with $10^7$ $TCID_{50}$ rgH1N2(PUMCH06) viruses. Viral titers in lungs of mice treated with mAb 1G8 or mAb A7E6 were determined on days 3 and 6 postinfection of $10^7$ $TCID_{50}$ rgH1N2(JSH1) viruses **(E)** or rgH1N2(PUMCH06) viruses **(F)**. The $p$-values were calculated using two-way ANOVA using Dunnett's multiple comparisons test with a 95% CI (ns, not significant; $^*p < 0.05$; $^{***}p < 0.0001$). **(G)** Histological analysis of lungs from uninfected mice and infected mice treated with mAb 1G8 or mAb A7E6. The photos were taken in 100-fold magnification.

substituting R199 reduced the inhibitory effect of 1G8. Residue K199 is conserved in the current H3N2 HSIV, while R199 is a dominant residue in NA of H3N2 CIV. However, mAb 1G8 can still well react with JS06 H3N2 CIV, which has a R199 in NA. Therefore, another escape mutant with R199E mutation in NA of H3N2 CIV was selected with mAb 1G8. Whereas, mAb

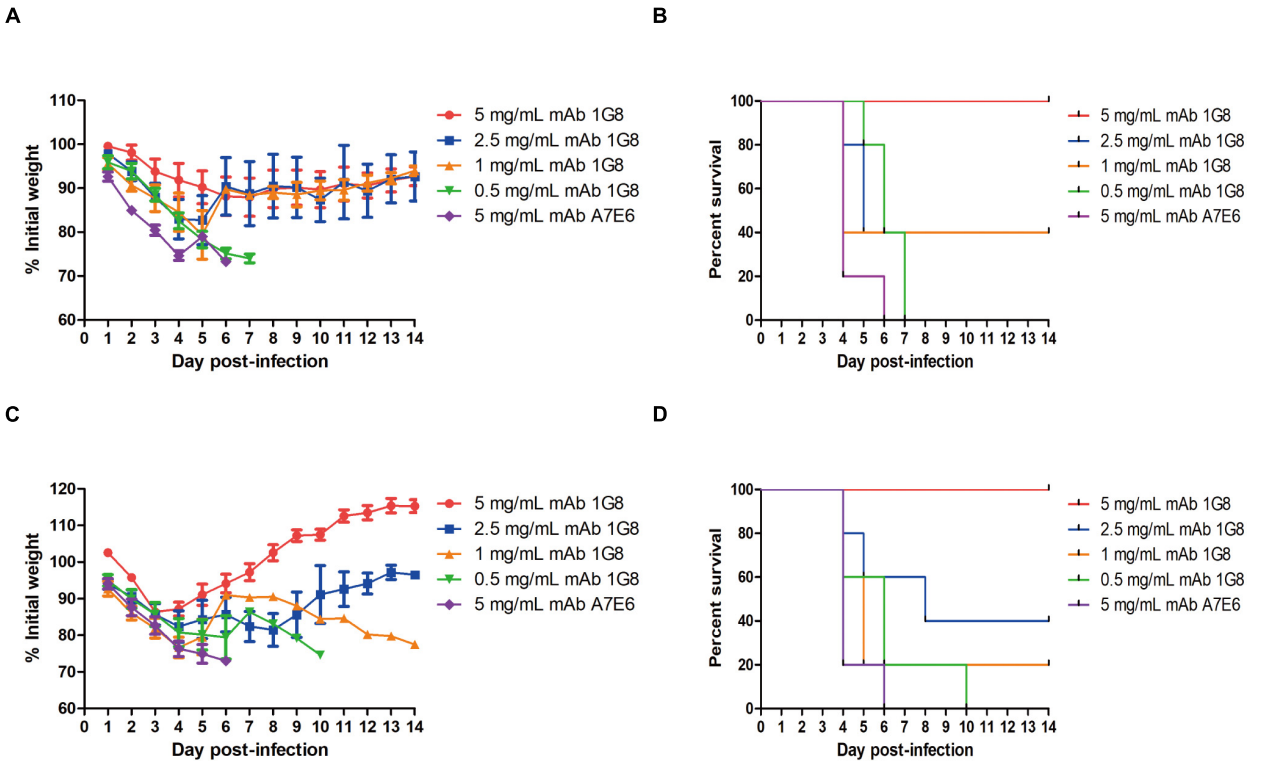


**FIGURE 3 |** *In vivo* protective effect of mAb 1G8 in therapeutic experiment. **(A)** The mean percentage of mice body weight of BALB/c mice ($n$ = 5 per group) challenged with $10^8$ $TCID_{50}$ rgH1N2(JSH1) viruses and treated with mAb 1G8 (5, 2.5, 1, and 0.5 mg/kg) or mAb A7E6 (5 mg/kg). **(B)** The survival curves of BALB/c mice ($n$ = 5 per group) challenged with $10^8$ $TCID_{50}$ rgH1N2(JSH1) viruses and treated with mAb 1G8 (5, 2.5, 1, and 0.5 mg/kg) or mAb A7E6 (5 mg/kg). **(C)** The mean percentage of body weight of BALB/c mice challenged with $10^8$ $TCID_{50}$ rgH1N2(PUMCH06) viruses and treated with mAb 1G8 (5, 2.5, 1, and 0.5 mg/kg) or mAb A7E6 (5 mg/kg). All data were performed with Graphpad Prism 5 and represented as mean ± SEM. **(D)** The survival curves of BALB/c mice challenged with $10^8$ $TCID_{50}$ rgH1N2(PUMCH06) viruses and treated with mAb 1G8 (5, 2.5, 1, and 0.5 mg/kg) or mAb A7E6 (5 mg/kg).

1G8 showed very strong NI effect on WT H3N2 CIV but very weak NI effect on the selected mutant of the H3N2 CIV with an R199E mutation in NA in both ELLA and Mu-NANA assay (**Figures 4C,D**). All results indicated that, K199R mutation is crucial for H3N2 HSIV to escape from mAb 1G8. While E199 is the key residue for H3N2 CIV to escape from mAb 1G8, which is consistent with our previous report in H9N2 AIV (Wan et al., 2016).

## *N*-Linked Glycosylation at Residue 200 Does Not Shield Epitope(s) Containing Residue 199

Position 199 locates close to the NA active center and plays an important role in inducing protective antibodies against H3N2 HSIVs (Gulati et al., 2002; Kirkpatrick Roubidoux et al., 2021). Human-derived antibodies targeting position 199 in NA showed broadly protective effect against multiple NA subtypes of viruses *in vivo* (Stadlbauer et al., 2019). However, the *N*-linked glycosylation sites at positions 200 to 202 were conserved in all group II NA subtypes except N3 (**Figures 5A,B**), which may form sugar chain modification and block the antibody binding with residue 199 by steric hindrance. Interestingly, structure analysis result shows that the sugar chain of each *N*-linked glycosylation at residue 200 in N2, N6, N7, and N9 is fixed on the adjacent NA monomer but not an active glycan shield. Although group II NA type virus except the N3 subtype virus have different glycosylation modifications at N200, the *N*-acetylglucosamine (NAG) of each sugar chain bind with the G454 or G394 in adjacent NA monomer by the hydrogen bond (**Figure 5C**). The alignment result also shows that G454 is highly conserved in viruses of all group II NA subtypes (**Figure 5B**).

Although, the gap among monomers and epitopes around residue 454 are buried by the sugar chain, which may result in less cross-reactive bodies against group I and group II NA subtype viruses. While the fixed sugar chain of the *N*-linked glycosylation at position 200 leaves enough space for the residue 199 being fully exposed to the antibodies (**Figure 5D**). All in all, residue 199 is able to take part in inducing protective antibodies without the influence by the *N*-linked glycosylation at residue 200.

## DISCUSSION

N2-subtype influenza viruses have caused two pandemic disasters in humans. The first one was caused by H2N2 influenza virus

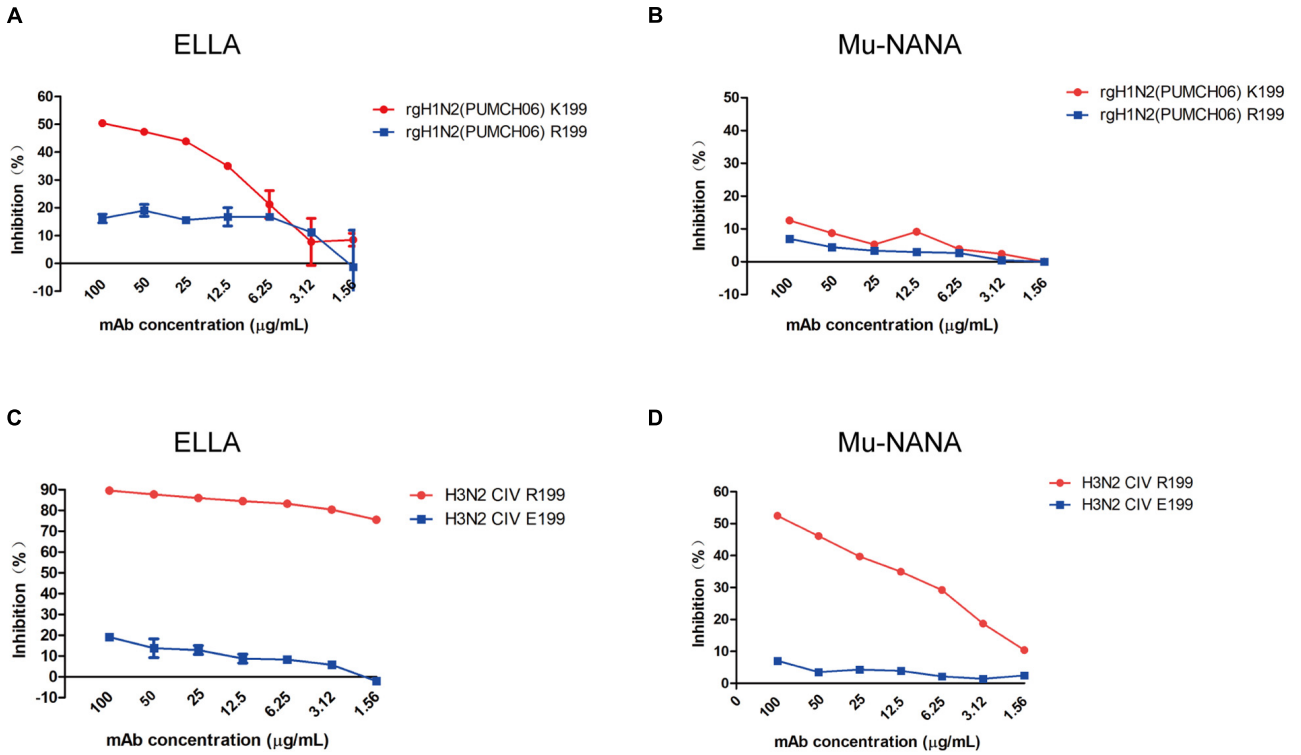


**FIGURE 4 |** Neuraminidase inhibition ability of mAb 1G8 to mutant viruses. The NI activity of mAb 1G8 to rgH1N2(PUMCH06) viruses with K199 or R199 in NA were measured in both ELLA **(A)** and Mu-NANA assay **(B)**. The NI activity of mAb 1G8 to JS06 CIVs with R199 or E199 in NA were measured in both ELLA **(C)** and Mu-NANA assay **(D)**. All data of NI assay were performed with Graphpad Prism v.5 and represented as mean ± SEM.

in 1957, which had an avian-born NA (Kilbourne, 2006). H3N2 influenza virus resulted in the second one and evolved into seasonal flu since its first outbreak in 1968 (Kilbourne, 2006). H9N2 AIV cannot transmit from human to human, but H9N2 infections have been reported in humans (Peacock et al., 2019). Although both H9N2 AIV and H3N2 HSIV belong to the N2 subtype, there used to be few reports on the same antigenic epitopes or antigenic structures between two NAs.

We previously reported a mAb 1G8 against NA of H9N2 AIV, which possesses NI activity (Wan et al., 2016; Wang et al., 2020). We now further identified that mAb 1G8 cannot only cross-react with NAs of H9N2 AIV and H3N2 HSIV but also have NI activity to them in NI assays.

In our mice challenge model, mAb 1G8 also shows protective effect in both prophylactic and therapeutic experiments. Lower viral load and less lesions in mouse lungs were detected with treatment of 5 mg/kg 1G8. Less and slower progress of deaths occurred in mice treated with 1G8 compared with control groups in the therapeutic experiment. Mutations and *N*-linked glycosylation have been reported for NA of H9N2 AIVs after 2011 and H3N2 HSIVs circulating since 2016 and contributed to escape from humoral immunity (Wan et al., 2019; Powell and Pekosz, 2020; Wang et al., 2021), while mAb 1G8 cannot only show well reactivity and inhibition activity to the NAs of these viruses, it also poses great protection against rgH1N2 viruses challenge.

Our previous research identified mutations D198N and K199E in NA which can help H9N2 AIV escape from mAb 1G8 (Wan et al., 2016). In this study, mutation K199R was selected in NA of H3N2 HSIV with mAb 1G8, which indicates that position 199 is also a crucial binding site for mAb 1G8 reacting with human-origin N2-subtype NA. Both mAbs B10 and Mem 5 interact with residue 199 in NA of H3N2 HSIV by the CDR2 within the heavy chain (Venkatramani et al., 2006; Wan et al., 2019). Moreover, broadly protective human antibodies 1G04, 1E01, and 1G01 also bind residue 199 in NA by CDR2 in the light chain (Stadlbauer et al., 2019), which indicates epitopes with residue 199 are crucial for NA-specific protective antibodies.

Antibodies against NA of seasonal H1N1 viruses can provide sufficient protection *in vivo* against the lethal H5N1 AIV challenge (Sandbulte et al., 2007; Frobert et al., 2010; Rockman et al., 2013). Furthermore, influenza infection can induce broadly cross-reactive and protective NA antibodies (Chen et al., 2018). In conclusion, this mAb 1G8 can also inhibit NA activity and show protection in mice challenged with rgH1N2 viruses, which would be a good candidate for developing antibody drugs to both AIVs and HSIVs. Moreover, we find that residue 199 in NA is not buried by the *N*-linked glycans at position 200 and is fully exposed for the binding of antibodies. The epitope targeted by mAb 1G8, which includes position 199 can be further studied in the future for development of ideal universal influenza vaccine.

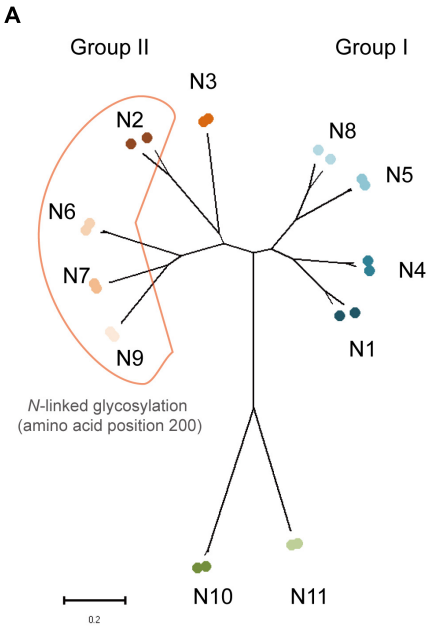


B

| Subtype | NA amino acid position (N2 numbering) 196-207 | | | | | | | | | | | | | 450-459 | | | | | | | | |
|---|---|---|---|---|---|---|---|---|---|---|---|---|---|---|---|---|---|---|---|---|---|---|
| H18N11 | G | - | - | - | D | G | F | V | S | I | L | Y | G | G | S | M | P | D | V | N | W | G |
| H18N11 | G | - | - | - | D | G | F | V | S | I | L | Y | G | G | S | M | P | D | V | N | W | G |
| H17N10 | G | R | D | R | N | S | F | I | M | I | K | Y | N | S | P | V | Q | N | I | N | W | D |
| H17N10 | G | R | D | R | N | S | F | I | M | I | K | Y | N | S | P | V | Q | N | I | N | W | D |
| H7N9 | G | P | N | N | N | A | S | A | V | I | W | Y | T | E | F | L | G | Q | W | N | W | P |
| H11N9 | G | P | N | N | N | A | S | A | V | I | W | Y | T | E | F | L | G | Q | W | N | W | P |
| H3N8 | G | P | D | N | Q | A | V | A | V | V | N | Y | D | H | K | I | A | S | W | S | W | H |
| H4N8 | G | P | D | A | K | A | V | A | V | V | H | Y | D | H | E | I | A | D | W | S | W | H |
| H7N7 | G | N | N | D | N | A | T | A | T | V | Y | Y | P | I | S | V | G | S | G | S | F | P |
| H10N7 | G | N | N | D | N | A | T | A | T | V | Y | Y | P | I | S | V | G | S | G | S | F | P |
| H10N6 | G | P | N | N | N | A | S | A | V | V | W | Y | K | E | R | L | G | S | W | S | W | H |
| H4N6 | G | P | N | N | N | A | S | A | V | V | W | Y | K | E | R | L | G | S | W | S | W | H |
| H6N5 | G | A | D | D | D | A | Y | A | V | I | H | Y | S | S | E | V | P | G | W | S | W | D |
| H11N5 | G | A | D | D | D | A | Y | A | V | I | H | Y | S | S | E | V | P | G | W | S | W | D |
| H10N4 | G | P | D | A | T | A | V | A | V | L | K | Y | N | S | D | T | T | G | W | S | W | P |
| H8N4 | G | P | D | T | T | A | V | A | V | L | K | Y | N | S | D | T | T | G | W | S | W | P |
| H11N3 | G | N | D | N | D | A | S | A | Q | I | I | Y | D | N | E | P | G | S | G | N | W | P |
| H7N3 | G | N | D | N | D | A | S | A | Q | I | I | Y | D | N | E | P | G | S | G | N | W | P |
| H9N2 | G | D | D | R | N | A | T | A | S | F | I | Y | S | G | T | Y | G | T | G | S | W | P |
| H3N2 | G | D | D | K | N | A | T | A | S | F | I | Y | S | G | T | Y | G | T | G | S | W | P |
| H1N1 | G | P | D | D | E | A | V | A | V | L | K | Y | N | S | D | T | V | D | W | S | W | P |
| H5N1 | G | P | D | N | G | A | V | A | V | L | K | Y | N | S | D | T | V | G | W | S | W | P |

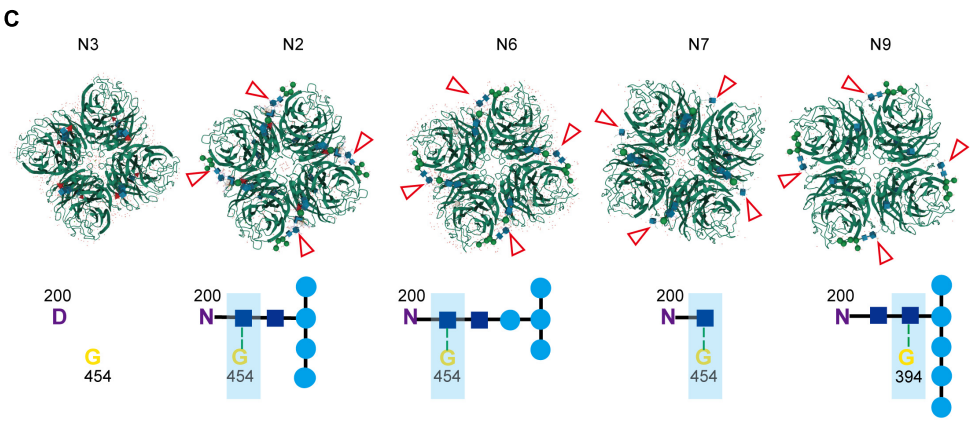


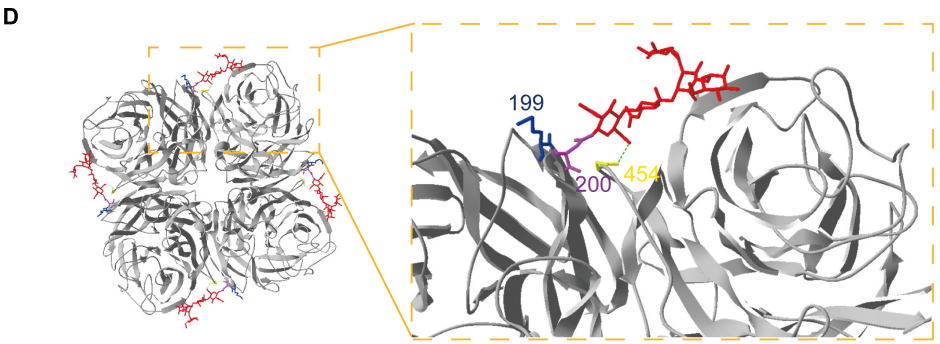


**FIGURE 5 |** Structural and alignment analysis of residue 199 in NAs. **(A)** The distribution of *N*-linked glycosylation at amino acid position 200 in NA subtypes was shown in phylogenetic tree. **(B)** NA amino acid sequences of 22 strains belong to 11 subtypes was analyzed by alignment with MEGA X. The amino acids from position 196 to 207 and 450 to 459 were shown. Amino acids involved in forming the position 200 *N*-linked glycosylation site and residue 454 were marked in red. **(C)** Locations of different *N*-linked glycosylation modification at position 200 in group II NAs (PDB: 4HZV, 1NN2, 4QN6, 4QN3, and 3NN9) were analyzed online with Mol viewer in RCSB PDB. The glycosylation modification in NA tetramer was shown above and marked with red triangles. The hydrogen bond between *N*-acetylglucosamine (NAG) and glycine at position 454 or 394 was shown with green dot line below. **(D)** Status of residue 199 in case of *N*-linked glycosylation modification at residue 200 was analyzed by Swiss PDB Deep-viewer. The structure of N2 (PDB:4GZX) was used for analysis. The sugar chain was marked in red. Residues 199, 200, and 454 were individually labeled with blue, purple, and yellow. Hydrogen bond between NAG and G454 (or G394) is shown with green dotted line.

## DATA AVAILABILITY STATEMENT

The datasets presented in this study can be found in online repositories. The names of the repository/repositories and accession number(s) can be found in the article/supplementary material.

## ETHICS STATEMENT

The animal study was reviewed and approved by the Animal Care Committee at Yangzhou University.

## AUTHOR CONTRIBUTIONS

FW and ZW wrote the manuscript. FW, YW, JW, ZW, and HF performed the experiment and data analysis. FW, AQ, WG, ZW, JY, KQ, and HS designed the study. All authors have reviewed and approved the final vision of this manuscript.

## FUNDING

This work was supported by the National Key Research and Development Program of China (2017YFD0501100) and a project funded by the priority academic program development of Jiangsu higher education institutions.

## ACKNOWLEDGMENTS

We show thanks to Yongjie Liu from the Nanjing Agriculture University for providing A/Canine/Jiangsu/06/2010 (JS06) H3N2 virus used in the study.

## REFERENCES

Bi, Y., Li, J., Li, S., Fu, G., and Shi, W. (2020). Dominant subtype switch in avian influenza viruses during 2016-2019 in China. *Nat. Commun.* 11:5909. doi: 10.1038/s41467-020-19671-3

Carnaccini, S., and Perez, D. R. (2020). H9 influenza viruses: an emerging challenge. *Cold Spring Harbor Perspect. Med.* 10:a038588. doi: 10.1101/cshperspect.a038588

Chen, Y.-Q., Wohlbold, T. J., Zheng, N.-Y., Huang, M., Huang, Y., Neu, K. E., et al. (2018). Influenza infection in humans induces broadly cross-reactive and protective neuraminidase-reactive antibodies. *Cell* 173, 417.e10–429.e10. doi: 10.1016/j.cell.2018.03.030

Doyle, T. M., Hashem, A. M., Li, C., Van Domselaar, G., Larocque, L., Wang, J., et al. (2013). Universal anti-neuraminidase antibody inhibiting all influenza A subtypes. *Antivir. Res.* 100, 567–574. doi: 10.1016/j.antiviral.2013.09.018

Eichelberger, M. C., and Wan, H. (2015). Influenza neuraminidase as a vaccine antigen. *Curr. Top. Microbiol. Immunol.* 386, 275–299. doi: 10.1007/82_2014_398

Frobert, E., Bouscambert-Duchamp, M., Escuret, V., Mundweiler, S., Barthélémy, M., Morfin, F., et al. (2010). Anti N1 cross-protecting antibodies against H5N1 detected in H1N1 infected people. *Curr. Microbiol.* 61, 25–28. doi: 10.1007/s00284-009-9571-z

Gao, R., Cao, B., Hu, Y., Feng, Z., Wang, D., Hu, W., et al. (2013). Human infection with a novel avian-origin influenza A (H7N9) virus. *N. Engl. J. Med.* 368, 1888–1897. doi: 10.1056/NEJMoa1304459

Gu, M., Chen, H., Li, Q., Huang, J., Zhao, M., Gu, X., et al. (2014). Enzootic genotype S of H9N2 avian influenza viruses donates internal genes to emerging zoonotic influenza viruses in China. *Vet. Microbiol.* 174, 309–315. doi: 10.1016/j.vetmic.2014.09.029

Gulati, U., Hwang, C. C., Venkatramani, L., Gulati, S., Stray, S. J., Lee, J. T., et al. (2002). Antibody epitopes on the neuraminidase of a recent H3N2 influenza virus (A/Memphis/31/98). *J. Virol.* 76, 12274–12280. doi: 10.1128/jvi.76.23.12274-12280.2002

Jianzhong, S., Guohua, D., Xianying, Z., Huihui, K., Xiaoyu, W., Kunpeng, L., et al. (2014). Novel influenza A(H7N2) virus in chickens. Jilin province, China, 2014. *Emerg. Infect. Dis.* 20, 1719–1722. doi: 10.3201/eid2010.140869

Jin, F., Dong, X., Wan, Z., Ren, D., Liu, M., Geng, T., et al. (2019). A single mutation N166D in hemagglutinin affects antigenicity and pathogenesis of H9N2 avian influenza virus. *Viruses* 11:709. doi: 10.3390/v11080709

Kilbourne, E. (2006). Influenza pandemics of the 20th Century. *Emerg. Infect. Dis.* 12, 9–14. doi: 10.3201/eid1201.051254

Kirkpatrick Roubidoux, E., McMahon, M., Carreño, J. M., Capuano, C., Jiang, K., Simon, V., et al. (2021). Identification and characterization of novel antibody epitopes on the N2 neuraminidase. *mSphere* 6:e00958-20 . doi: 10.1128/mSphere.00958-20

Kissling, E., Rondy, M., and I-Move/I-Move+ study team. (2017). Early 2016/17 vaccine effectiveness estimates against influenza A(H3N2): I-MOVE multicentre case control studies at primary care and hospital levels in Europe. *Eurosurveillance* 22:30464. doi: 10.2807/1560-7917.es.2017.22.7.30464

Krammer, F., and Palese, P. (2013). Influenza virus hemagglutinin stalk-based antibodies and vaccines. *Curr. Opin. Virol.* 3, 521–530. doi: 10.1016/j.coviro.2013.07.007

Lee, R. T. C., Chang, H. H., Russell, C. A., Lipsitch, M., and Maurer-Stroh, S. (2019). Influenza A hemagglutinin passage bias sites and host specificity mutations. *Cells* 8:958. doi: 10.3390/cells8090958

Lin, Y., Zhao, Y. B., Zeng, X. J., Lu, C. P., and Liu, Y. J. (2012). Complete genome sequence of an H3N2 canine influenza virus from dogs in jiangsu. *China. J. Virol.* 86:11402. doi: 10.1128/JVI.01946-12

Lin, Y. P., Shaw, M., Gregory, V., Cameron, K., Lim, W., Klimov, A., et al. (2000). Avian-to-human transmission of H9N2 subtype influenza A viruses: relationship between H9N2 and H5N1 human isolates. *Proc. NatI. Acad. Sci. U.S.A.* 97, 9654–9658. doi: 10.1073/pnas.160270697

Liu, K., Gu, M., Hu, S., Gao, R., Li, J., Shi, L., et al. (2018). Genetic and biological characterization of three poultry-origin H5N6 avian influenza viruses with all internal genes from genotype S H9N2 viruses. *Arch. Virol.* 163, 947–960. doi: 10.1007/s00705-017-3695-4

Peacock, T. H. P., James, J., Sealy, J. E., and Iqbal, M. (2019). A global perspective on H9N2 avian influenza virus. *Viruses* 11:620. doi: 10.3390/v11070620

Powell, H., and Pekosz, A. (2020). Neuraminidase antigenic drift of H3N2 clade 3c.2a viruses alters virus replication, enzymatic activity and inhibitory antibody binding. *PLoS Pathog.* 16:e1008411. doi: 10.1371/journal.ppat.1008411

Rockman, S., Brown, L. E., Barr, I. G., Gilbertson, B., Lowther, S., Kachurin, A., et al. (2013). Neuraminidase-inhibiting antibody is a correlate of cross-protection against lethal H5N1 influenza virus in ferrets immunized with seasonal influenza vaccine. *J. Virol.* 87, 3053–3061. doi: 10.1128/JVI.02434-12

Sandbulte, M., Jimenez, G., Boon, A., Smith, L., Treanor, J., and Webby, R. (2007). Cross-reactive neuraminidase antibodies afford partial protection against H5N1 in mice and are present in unexposed humans. *PLoS Med.* 4:e59. doi: 10.1371/journal.pmed.0040059

Sandbulte, M. R., Westgeest, K. B., Jin, G., Xiyan, X., Klimov, A. I., Russell, C. A., et al. (2011). Discordant antigenic drift of neuraminidase and hemagglutinin in H1N1 and H3N2 influenza viruses. *Proc. NatI. Acad. Sci. U.S.A.* 108, 20748–20753. doi: 10.1073/pnas.1113801108

Shao, H., Fan, Z., Wan, Z., Tian, X., and Ye, J. (2015). An efficient and rapid influenza gene cloning strategy for reverse genetics system. *J. Virol. Methods* 222, 91–94. doi: 10.1016/j.jviromet.2015.06.001

Stadlbauer, D., Zhu, X., McMahon, M., Turner, J. S., Wohlbold, T. J., Schmitz, A. J., et al. (2019). Broadly protective human antibodies that target the active site of influenza virus neuraminidase. *Science* 366, 499–504. doi: 10.1126/science.aay0678

Varghese, J. N., Laver, W. G., and Colman, P. M. (1983). Structure of the influenza virus glycoprotein antigen neuraminidase at 2.9 Å resolution. *Nature* 303, 35–40. doi: 10.1038/303035a0

Venkatramani, L., Bochkareva, E., Lee, J. T., Gulati, U., Graeme Laver, W., Bochkarev, A., et al. (2006). An epidemiologically significant epitope of a 1998 human influenza virus neuraminidase forms a highly hydrated interface in the NA–Antibody complex. *J. Mol. Biol.* 356, 651–663. doi: 10.1016/j.jmb.2005.11.061

Wan, H., Gao, J., Yang, H., Yang, S., Harvey, R., Chen, Y. Q., et al. (2019). The neuraminidase of A(H3N2) influenza viruses circulating since 2016 is antigenically distinct from the A/Hong Kong/4801/2014 vaccine strain. *Nat. Microbiol.* 4, 2216–2225. doi: 10.1038/s41564-019-0522-6

Wan, Z., Ye, J., Sang, J., Shao, H., Qian, K., Jin, W., et al. (2016). Identification of amino acids in H9N2 influenza virus neuraminidase that are critical for the binding of two mouse monoclonal antibodies. *Vet. Microbiol.* 187, 58–63. doi: 10.1016/j.vetmic.2016.03.011

Wang, F., Wang, Y., Wan, Z., Shao, H., Qian, K., Ye, J., et al. (2020). Generation of a recombinant chickenized monoclonal antibody against the neuraminidase of H9N2 avian influenza virus. *AMB Express* 10:151. doi: 10.1186/s13568-020-01086-4

Wang, F., Wu, J., Wang, Y., Wan, Z., Shao, H., Qian, K., et al. (2021). Identification of key residues involved in the neuraminidase antigenic variation of H9N2 influenza virus. *Emerg. Microbes Infect.* 10, 210–219. doi: 10.1080/22221751.2021.1879602

Wohlbold, T. J., and Krammer, F. (2014). In the shadow of hemagglutinin: a growing interest in influenza viral neuraminidase and its role as a vaccine antigen. *Viruses* 6, 2465–2494. doi: 10.3390/v6062465

**Conflict of Interest:** The authors declare that the research was conducted in the absence of any commercial or financial relationships that could be construed as a potential conflict of interest.

**Publisher's Note:** All claims expressed in this article are solely those of the authors and do not necessarily represent those of their affiliated organizations, or those of the publisher, the editors and the reviewers. Any product that may be evaluated in this article, or claim that may be made by its manufacturer, is not guaranteed or endorsed by the publisher.

frontiers in Microbiology

ORIGINAL RESEARCH
published: 04 October 2021
doi: 10.3389/fmicb.2021.729914

# Tetrameric Neuraminidase of Influenza A Virus Is Required to Induce Protective Antibody Responses in Mice

*Xiren Deng, Qimin Wang, Mei Liu, Qinwen Zheng, Fan Wu* and Jinghe Huang**

*Shanghai Public Health Clinical Center and Key Laboratory of Medical Molecular Virology (MOE/NHC/CAMS), School of Basic Medical Sciences, Shanghai Medical College, Fudan University, Shanghai, China*

Influenza neuraminidase (NA) is able to induce cross-subtype immunity and is considered as a promising target for the development of universal influenza vaccines. However, commercial influenza vaccines only induced low NA-specific immune responses due to the low amounts and the denatured conformation of NA proteins in current inactivated or split influenza vaccines. Here we investigated the protective efficacy of recombinant tetrameric and monomeric NA proteins to determine whether the conformation contributed to induce protective immunity. We found that H1N1$_{PR8}$NA tetramer (NA$_{tet}$) could provide complete homologous protection against A/PR8 (H1N1) virus infection in mice, while the protection of H1N1$_{PR8}$NA monomer (NA$_{mono}$) was moderate. Higher levels of NA-reactive binding and inhibition antibodies and less weight loss were observed in the H1N1$_{PR8}$NA$_{tet}$-vaccinated group. Similarly, H5N1$_{VN}$NA$_{tet}$ immunization exhibited a preferable heterologous protection than H5N1$_{VN}$NA$_{mono}$, but neither H7N9$_{SH}$NA$_{tet}$ nor H7N9$_{SH}$NA$_{mono}$ vaccination showed heterosubtypic protection. We also compared the effect of three adjuvants, aluminum, 3′3′-cGAMP (cGAMP), and Poly(I:C), on the humoral response and protective efficacy induced by H1N1$_{PR8}$NA$_{tet}$. H1N1$_{PR8}$NA$_{tet}$ protein adjuvanted with aluminum was observed to exhibited better capacity in inducing NA-specific humoral immunity and preventing weight loss than with cGAMP or Poly(I:C). In conclusion, our data demonstrate that tetrameric NA with natural conformation is required to induce protective anti-NA immunity. The NA tetramer could provide homologous protection and subtype-specific cross-protection. In addition, the aluminum adjuvant is preferable in recombinant NA protein vaccination.

**Keywords: influenza virus, neuraminidase, protein, vaccine, cross-protection**

OPEN ACCESS

***Edited by:***
*Dayan Wang,*
*Chinese National Influenza Center, China*

***Reviewed by:***
*Juan Pu,*
*China Agricultural University, China*
*Sujuan Chen,*
*Yangzhou University, China*

****Correspondence:***
*Fan Wu*
*wufan@fudan.edu.cn*
*Jinghe Huang*
*jinghehuang@fudan.edu.cn*

***Specialty section:***
*This article was submitted to Virology, a section of the journal Frontiers in Microbiology*

***Received:*** *24 June 2021*
***Accepted:*** *30 August 2021*
***Published:*** *04 October 2021*

***Citation:***
*Deng X, Wang Q, Liu M, Zheng Q, Wu F and Huang J (2021) Tetrameric Neuraminidase of Influenza A Virus Is Required to Induce Protective Antibody Responses in Mice. Front. Microbiol. 12:729914. doi: 10.3389/fmicb.2021.729914*

## INTRODUCTION

The seasonal epidemics and less frequently global pandemics of influenza viruses result in high morbidity and mortality every year. Vaccination is the most effective way to prevent influenza circulation. The currently licensed vaccines, including inactivated and attenuated influenza vaccines, induce protection mainly by eliciting neutralizing antibodies (NAbs) against the major

glycoprotein, hemagglutinin (HA), of influenza virus (Vogel and Manicassamy, 2020). Vaccine efficacy depends on the antigenic similarities of HA proteins between the vaccine and circulating strains. However, the continuous and extensive antigenic variation of HA protein allows influenza viruses to easily escape from the protection of vaccines. The vaccine components need to be updated yearly based on the prediction of circulating influenza strains. The mismatch of vaccine and circulating strains, as in the 2009–2010 and 2017–2018 influenza seasons, resulted in a significant increase of influenza-related morbidity and mortality. A universal vaccine may overcome the shortage of the current influenza vaccines and provide cross-protection against multiple influenza subtypes.

Neuraminidase (NA) protein is the second most abundant glycoprotein on the membrane of influenza virion. The native influenza NA protein is a tetramer with enzymatic activity (Saito et al., 1995; Wu et al., 2009; Da Silva et al., 2013) that can cleave off the terminal sialic acid from N-linked glycans to facilitate viral release and transmission (Krammer et al., 2018; Eichelberger and Monto, 2019). Serologic studies showed that individuals with higher NA-specific antibody titers were less likely to be infected by influenza virus with the same NA subtypes (Murphy et al., 1972; Monto and Kendal, 1973). NA inhibition (NAI) antibody titers were independently correlated with lower morbidity and decreased viral shedding in influenza-infected individuals (Couch et al., 2013; Stadlbauer et al., 2019). Although there are 11 different subtypes of NA proteins, N10 and N11 NA are unique to bats (Tong et al., 2012, 2013). The antigenic variation of NA protein is relatively low compared to that of HA protein (Couch et al., 2013; Stadlbauer et al., 2019). Furthermore, NA-specific monoclonal antibodies isolated from influenza-infected individuals provide cross-protection against multiple influenza virus strains (Chen et al., 2018; Stadlbauer et al., 2019; Yasuhara et al., 2019). Therefore, NA protein is considered a candidate for the development of universal influenza vaccines. Recent studies have shown that expressed or purified NA proteins could induce robust NA-based immunity and protect against influenza virus infection (Liu et al., 2015; Wohlbold et al., 2015; McMahon et al., 2020), indicating that the NA protein is immunogenic in both animal models and humans. In contrast, commercial inactivated and split influenza vaccines only induced low levels of NA-specific immune response (Wohlbold et al., 2015; Krammer et al., 2018). Several factors were suggested to contribute to the low immunogenicity of NA in inactivated and split influenza vaccines. First, the amount of NA proteins is relatively lower than HA in the vaccine formula (Sridhar et al., 2015; Wohlbold et al., 2015); second, NA seems to have immune subdominance to HA when both antigens were administered (Johansson et al., 1987; Krammer et al., 2018); and third, the NA conformation in the vaccine formula may be changed during vaccine manufacturing (McMahon et al., 2020).

In this paper, we investigated the factors that potentially affect the immune response and protective efficacy induced by NA protein in BALB/c mouse models. We compared the difference of the protective efficacy between tetrameric and monomeric NA proteins and investigated the humoral responses induced by tetrameric and monomeric NA proteins. We also assessed the influence of adjuvants on the humoral response and protective efficacy induced by H1N1$_{PR8}$NA$_{tet}$ tetramer.

# MATERIALS AND METHODS

## Cells and Viruses

Madin Darby canine kidney (MDCK) and human embryonic kidney 293 (HEK293T) cells were obtained from the American Type Culture Collection and grown in complete high-glucose Dulbecco's modified Eagle's medium (DMEM, HyClone) supplemented with antibiotics (100 units/ml penicillin and 100 μg/ml streptomycin, HyClone) and 10% fetal bovine serum (FBS, Gibco). Expi293F (Thermo Fisher Scientific) cells were grown in SMM 293-TII expression medium (Sino Biological Inc.).

The influenza A virus (IAV) used in this study was the mouse-adapted strain A/Puerto Rico/8/1934 (H1N1). The IAV was propagated in MDCK cells in serum-free DMEM media in the presence of 1 μg/ml TPCK-trypsin (Sigma-Aldrich). The median tissue culture infective dose and median lethal dose ($LD_{50}$) of viruses were calculated by the Reed and Munch method.

## Expression and Purification of Recombinant Proteins

Recombinant NA proteins derived from A/Puerto Rico/8/1934 (H1N1), A/Shanghai/37T/2009 (H1N1), A/Hong Kong/16/68 (H3N2), A/Vietnam/1204 (H5N1), and A/Shanghai/4664T/2013 (H7N9)—referred to as H1N1$_{PR8}$NA, H1N1$_{p09}$NA, H3N2$_{HK}$NA, H5N1$_{VN}$NA, and H7N9$_{SH}$NA, respectively—were expressed in Expi293F cells and purified by Ni-nitrilotriacetic acid (NTA) beads (GE Healthcare). Briefly, the NA ectodomains with additional N-terminal Igκ-light chain secretion sequence, followed by a hex-histidine tag (HHHHHH), a human vasodilator stimulating phosphoprotein (VASP) tetramerization domain (SSSDYSDLQRVKQELLEEVKKELQKVKEEIIEAFVQELRKRG), and a thrombin cleavage site (SLVPRGSPSRS) were constructed into eukaryotic expressing plasmid pcDNA3.1 to express NA tetramer (NA$_{tet}$). The monomeric NA (NA$_{mono}$) proteins were constructed in the same way as NA$_{tet}$ but without the VASP domain. Recombinant NA proteins were purified from the supernatant of transiently transfected Expi293F cells by Ni-NTA beads. The concentration of proteins was adjusted to 1 mg/ml with phosphate-buffered saline (PBS) and frozen at −80°C.

## Western Blotting and Cross-Linking SDS-PAGE

Recombinant NA proteins were then analyzed by Western blotting. Briefly, 2 μg of NA were mixed with 4× SDS-loading buffer containing 10% β-mercaptoethanol. The samples were heated for 10 min at 98°C and were afterward loaded on an SDS gradient gel (4–20% Precast Protein Improve Gels, Yeasen Biotechnology Inc.). The gel was run for 100 min at 120 V, and Western blotting transfer was performed. Following the transfer onto the nitrocellulose membrane, the membrane was

blocked with TBS with 0.1% Tween 20 (TBS-T) containing 5% milk powder for 2 h at room temperature (RT). Then, mouse anti-HIS primary antibody (Younuoke Biotechnology Inc.) was added for 12 h at 4°C (1:1,000 dilution in TBS-T containing 1% milk). The membrane was washed three times with TBS-T after 12 h, and a secondary goat anti-mouse horse radish peroxidase (HRP) antibody (Jackson Immuno Research) was added for 1 h at RT (diluted 1:1,000 in PBS-T containing 1% milk). The membrane was then washed three times with TBS-T before it was visualized using Pierce Chemiluminescence (ECL) Western Blotting Substrate (as per the instructions of the manufacturer) on Tanon-5200 Chemiluminescent Imaging System (Tanon Science and Technology).

The extent of tetramerization and/or multimerization was investigated by cross-linking of NA with glutaraldehyde (Sigma-Aldrich). Briefly, 5 μg of NA was diluted in 25 μl of PBS in the presence of 0.3 mM of glutaraldehyde cross-linker. The mixture was incubated at RT for 5 min, and then glutaraldehyde was quenched by adding 1 M Tris–HCl buffer (pH 8.0) to a final concentration of 50 mM. Afterward, the protein samples were loaded on 4–20% SDS gradient gel. The gel was run for 60 min at 180 V and confirmed by Coomassie staining.

## Neuraminidase Enzymatic Activity Assay

The enzymatic activity of recombinant NA proteins was determined by the cleavage of two specific substrates of NA, 2′-(4-methylumbelliferyl)-α-D-N-acetylneuraminic acid (MUNANA) (Job et al., 2018; Ju et al., 2018) and fetuin (Prevato et al., 2015; Biuso et al., 2019) as previously described, with minor modifications.

For the MUNANA-based enzymatic activity assay, twofold gradient diluted recombinant NA proteins that range from 0.0015625 to 1.6 μg/ml in morpholine ethanesulfonic acid (MES) buffer (32.5 mM MES and 2 mM $CaCl_2$, pH 6.5) were incubated with 20 mM MUNANA (Sigma-Aldrich) at 37°C for 40 min. The reaction was stopped by adding a stopping buffer (0.2 M glycine and 0.2 M NaOH, pH 10.7), and the degree of fluorescence was detected by EnSight Multimode plate reader (PerkinElmer).

For the fetuin-based enzyme-linked lectin assay (ELLA), MaxiSorp Nunc-immuno 96-well plates were coated with 100 μl of fetuin (Sigma-Aldrich) at a concentration of 50 μg/ml and refrigerated at 4°C overnight. The plates were blocked with 200 μl blocking buffer (PBS containing 1% FBS and 5% dry milk) for 1 h at RT and washed six times with PBS-T solution. Following the blocking, 50 μl of the sample diluent [Dulbecco's phosphate buffered saline (DPBS) with 1% bovine serum albumin and 0.5% Tween 20] and 50 μl of serially diluted recombinant NA protein or purified virus were then added to the fetuin-coated plates and mixed well. The plates were then incubated for 14–16 h at 37°C before being washed six times with PBS-T. After the extensive wash, the NA enzymatic activity was detected by horse-radish peroxidase-labeled peanut agglutinin (Sigma Aldrich) and developed with the 3,3′,5,5′-tetramethylbenzidine substrate (Sigma-Aldrich). The reaction was stopped by the addition of 2 N $H_2SO_4$ after 20 min of incubation. The optical density (OD) values were read at 450 nm on a Multiskan FC plate reader (Thermo Fisher Scientific).

## Mice Experiments

Female BALB/c mice (6–8 weeks old) from the Laboratory Animal Center of Shanghai Public Health Clinical Center (SHPHCC) were used for all animal experiments. The protocols were reviewed and approved by the Ethics Committee of SHPHCC (approval no. 2019-A019-01/02).

To compare the immunogenicity and protective efficacy of tetrameric and monomeric NA proteins, the mice were intraperitoneally (i.p.) immunized with 20 μg $H1N1_{PR8}NA_{tet}$, $H5N1_{VN}NA_{tet}$, $H7N9_{SH}NA_{tet}$, $H1N1_{PR8}NA_{mono}$, $H5N1_{VN}NA_{mono}$, and $H7N9_{SH}NA_{mono}$, respectively. The antigens were diluted in 100 μl PBS and mixed with aluminum adjuvant (1:1). The mice were immunized with PBS as control. To investigate the influence of adjuvants on the immunogenicity of NA tetramers, the mice were intraperitoneally immunized with 20 μg $H1N1_{PR8}NA_{tet}$ protein mixed with aluminum (i.p.), 3′3′-cGAMP (cGAMP; intradermally, i.d.) and Poly(I:C) (i.p.), respectively. Aluminum is a strong inducer of Th2 responses (Rudicell et al., 2019). cGAMP is a Th1 immune response inducer as an "ideal" adjuvant for cutaneous vaccination (Wang et al., 2016). The TLR3 agonist Poly(I:C) also promotes Th1-dominant immunity, and it is commonly used as intraperitoneal immune adjuvant (Moriyama et al., 2017). These three adjuvants were all purchased from InvivoGen. The mice were boosted with the same immunogen 2 weeks later.

Sera were collected 1 week after the final immunization to detect NA-specific antibodies. The mice were intranasally challenged with 5 $LD_{50}$ of A/Puerto Rico/8/34 (H1N1) virus 2 weeks after the final immunization to evaluate the protective efficacy. The weight loss and survival rates of mice were monitored for 14 days after the challenge.

## Enzyme-Linked Immunosorbent Assay

The NA-specific antibodies were measured by enzyme-linked immunosorbent assay (ELISA). To explore the immunogenicity of tetrameric and monomeric NA proteins, the sera samples which were collected 1 week after the final immunization were tested for NA-reactive antibodies by ELISA, including NA-specific binding antibodies to the respective immunogen, cross-subtype binding antibodies against NA of A/PR8 (H1N1), and NAI antibodies. The subtypes of NA-specific antibodies were also analyzed. Briefly, MaxiSorp Nunc-immuno 96-well plates (Thermo Fisher Scientific) were coated with 2 μg/ml NA proteins (100 μl/well) in carb/bicarb coating buffer (10 mM $Na_2CO_3$, 40 mM $NaHCO_3$, and pH 9.6) at 4°C overnight. To detect the NA-specific antibodies, the respective immunogen to sera of immunized mice was coated. To detect the cross-binding activity of mice sera, the tetrameric NA protein of $H1N1_{PR8}NA_{tet}$ was coated. The plates were washed three times with PBS-T (PBS containing 0.05% Tween 20) and blocked with blocking buffer (PBS containing 1% FBS and 5% dry milk) for 1 h at RT. The sera were fourfold serially diluted starting at 1:100 in disruption buffer (PBS containing 5% FBS, 2% BSA, and 1% Triton X-100). Then, 50 μl of diluted serum was added to each well and incubated for 1 h at RT. After three times of washing with PBS-T, bound antibodies

were detected by horseradish peroxidase-labeled goat-anti mouse IgG antibody (Jackson Immuno Research) and substrate ABTS (Thermo Fisher Scientific). The OD was measured at 405 nm on a Multiskan FC plate reader (Thermo Fisher Scientific). The isotypes of NA-specific antibodies were determined by ELISA with Mouse Monoclonal Antibody Isotyping Reagents (Sigma-Aldrich) following the instructions of the manufacturer. The antibody titers were defined as the highest sera dilution at which the OD values were twice of those by the control sera.

### Neuraminidase Inhibition Assay

The plates were coated and blocked as fetuin-based ELLA as described above. While the plates were blocked, pre-challenge mouse sera were fourfold serially diluted starting at 1:40 in PBS in a new U-bottom, 96-well plate. Then, the split A/PR8 (H1N1) virus was added to each well of the serially diluted serum plate, and the plates were incubated at 37°C for 1 h. The amount of split A/PR8 (H1N1) virus used in the NAI assay corresponded to 90% of the maximum signal. After incubation, 100 μl of the serum/virus mixture was added on the blocked fetuin-coated plates and incubated for 16–18 h at 37°C. The remainder of the NAI assay was performed as ELLA as described above. The values of test wells obtained from the plate reader were divided by the average value for virus-only control wells and then multiplied by a factor of 100 to obtain the NA activity. Percent inhibition was calculated by subtracting the NA activity from 100.

### Statistical Analysis

The survival rate was compared by log-rank test. Antibody titers, viral titers, and body weights among groups were compared by one- or two-way ANOVA. A $P$-value $< 0.05$ was considered significant. All the statistical analyses were performed by GraphPad Prism, version 8.00 (GraphPad Software, San Diego, CA, United States).

## RESULTS

### Neuraminidase Tetramers, but Not Monomers, Exhibited Enzymatic Activity

The NA tetramers and monomers were expressed using Expi293F cells and purified by Ni-NTA. The proteins were analyzed by Western blotting (**Figures 1A**,**B**) and cross-linking SDS-PAGE (**Figures 1C,D**). The bands of NA tetramers stabilized by the VASP domain were observed as monomers on Western blotting (**Figure 1A**), while they showed bands consistent with tetramers when cross-linked (**Figure 1C**). The monomeric NA proteins exhibited as monomers on Western blotting (**Figure 1B**) and showed some level on dimer or tetramer formation when cross-linked but was mostly monomeric (**Figure 1D**). The enzymatic activity of NA tetramers and monomers was characterized using two NA-specific substrates, MU-NANA and fetuin, respectively. These assays measured the amount of 4-methylumbelliferone cleaved by the influenza virus NA from the MUNANA or the amount of NA cleaved-fetuin from the intact fetuin. For the results of MUNANA-based enzymatic activity assays, as shown in **Figures 1E**,**F**, the NA tetramers exhibited enzymatic activity, while the NA monomers did not. The same results were also observed in fetuin-based enzymatic activity assays; the tetrameric NA showed high enzymatic activity, but the monomeric NA did not (**Figures 1G**,**H**). Taken together, these results suggest that the enzymatic activity depends on the tetrameric conformation of the NA proteins.

### Tetrameric Neuraminidase Protein Induced Better Protection Against Influenza Challenge in Mice Than Monomeric Neuraminidase

To investigate the protective efficacy of tetrameric NA vs. monomeric NA, the mice were immunized with NA tetramers or monomers as per the schedule shown in **Figure 2A**. As shown in **Figures 2B–G**, all the mice in the PBS control group showed signs of influenza, such as huddling or ruffled fur, from 2 to 3 days and died after the challenge with A/PR8 (H1N1) virus. The median survival days in the control group was 7 days. Vaccination with either $H1N1_{PR8}NA_{tet}$ or $H1N1_{PR8}NA_{mono}$ significantly protected the mice against the lethal dose of the A/PR8 (H1N1) influenza challenge (**Figures 2B**,**C**). All the $H1N1_{PR8}NA_{tet}$-immunized mice and 6/8 of $H1N1_{PR8}NA_{mono}$-immunized mice survived the influenza virus challenge (**Figure 2B**). Although the survival rates were not significantly different between the tetramer- and monomer-immunized mice, the mice immunized with $H1N1_{PR8}NA_{tet}$ showed significantly less weight loss compared with those immunized with $H1N1_{PR8}NA_{mono}$ (**Figure 2C**).

The cross-subtype protection was evaluated in mice that were immunized with H5N1 and H7N9 NA by heterosubtypic challenge with A/PR8 (H1N1) virus. As shown in **Figures 2D**,**E**, immunization with H5N1 NA tetramer significantly improved the survival of mice post-challenge with the A/PR8 (H1N1) virus. Then, 75% (6/8) of the mice that were immunized with $H5N1_{VN}NA_{tet}$ tetramer survived, while all the mice in the control group died. However, the protection induced by H5N1 NA monomer is significantly weaker than that induced by tetramer ($p < 0.05$, log-rank test), with only 37.5% (3/8) of $H5N1_{VN}NA_{mono}$-immunized mice surviving. No protection was observed in mice that were immunized with either $H7N9_{SH}NA_{tet}$ or $H7N9_{SH}NA_{mono}$ proteins (**Figures 2E**,**F**), indicating that protection induced by the NA protein is subtype-specific. Similar results were observed in tetrameric H1N1 and H3N2 NA proteins immunization. Tetrameric $H1N1_{pdm09}NA$ induced moderate cross-protection against A/PR8 (H1N1) virus infection while $H3N2_{HK}NA$ not (**Supplementary Figure S2**).

### Neuraminidase Tetramers Exhibited Better Abilities in Inducing Neuraminidase-Specific, Cross-Binding, and Neuraminidase Inhibition Antibodies That Were Related to Protection

To explore the immunogenicity of tetrameric and monomeric NA proteins, the sera samples which were collected 1 week after the final immunization (**Figure 2A**) were tested for NA-reactive antibodies, including NA-specific binding antibodies to the respective immunogen, cross-subtype binding antibodies

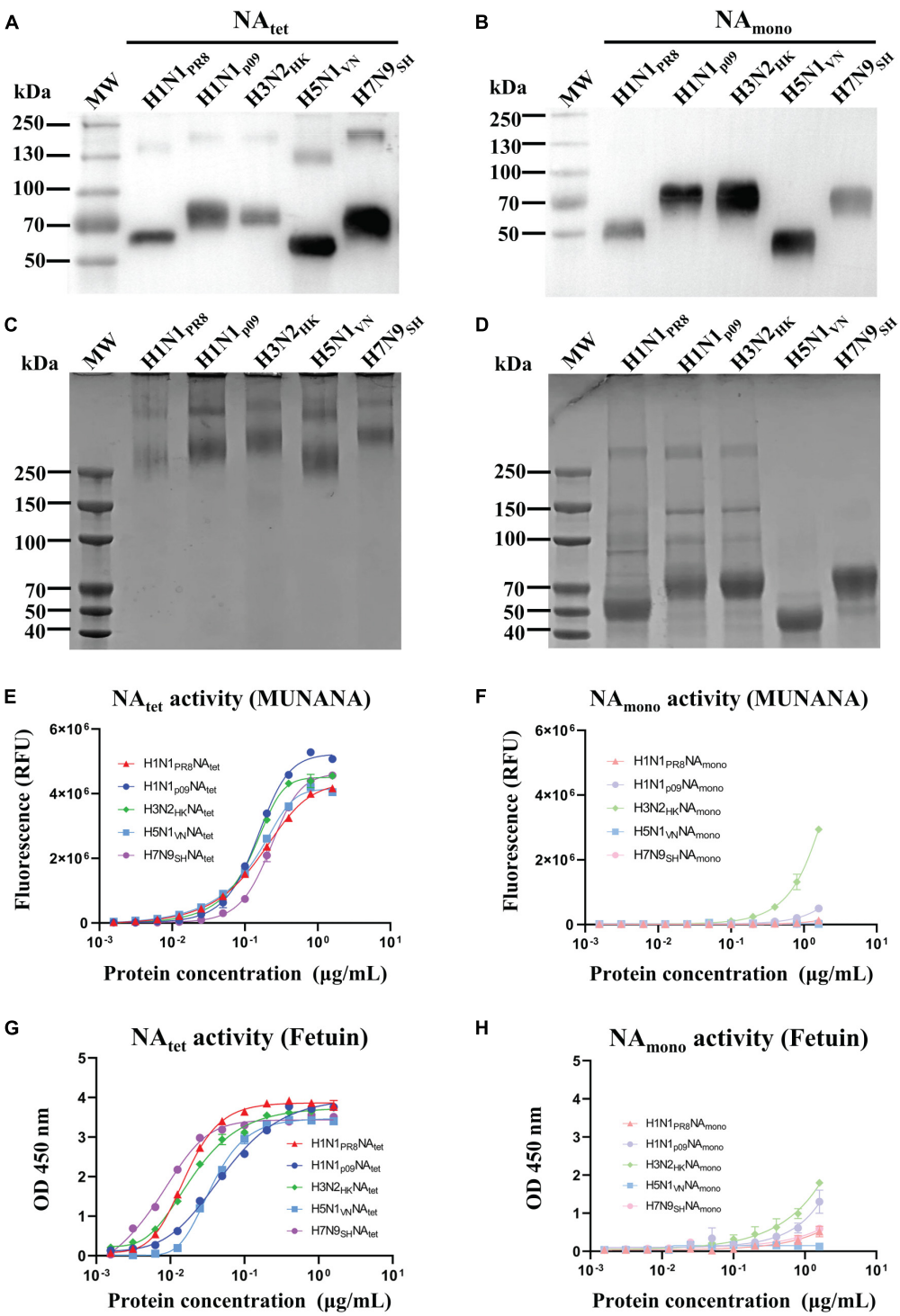


**FIGURE 1 |** Expression, purification, and characterization of recombinant neuraminidase (NA) proteins. Tetrameric and monomeric NA proteins derived from A/Puerto Rico/8/1934 (H1N1), A/Shanghai/37T/2009 (H1N1), A/Hong Kong/16/68 (H3N2), A/Vietnam/1204 (H5N1), and A/Shanghai/4664T/2013 (H7N9) were expressed by the Expi293F cell expression system and purified by Ni-nitrilotriacetic acid (NTA). **(A,B)** Purified NA proteins were confirmed by Western blotting. **(C,D)** Cross-linking SDS-PAGE of tetrameric and monomeric recombinant NA proteins. **(E,F)** MUNANA-based enzymatic activity assays were used to determine the enzymatic activity of recombinant NA proteins. **(G,H)** Fetuin-based enzymatic activity assays were used to determine the enzymatic activity of recombinant NA proteins.

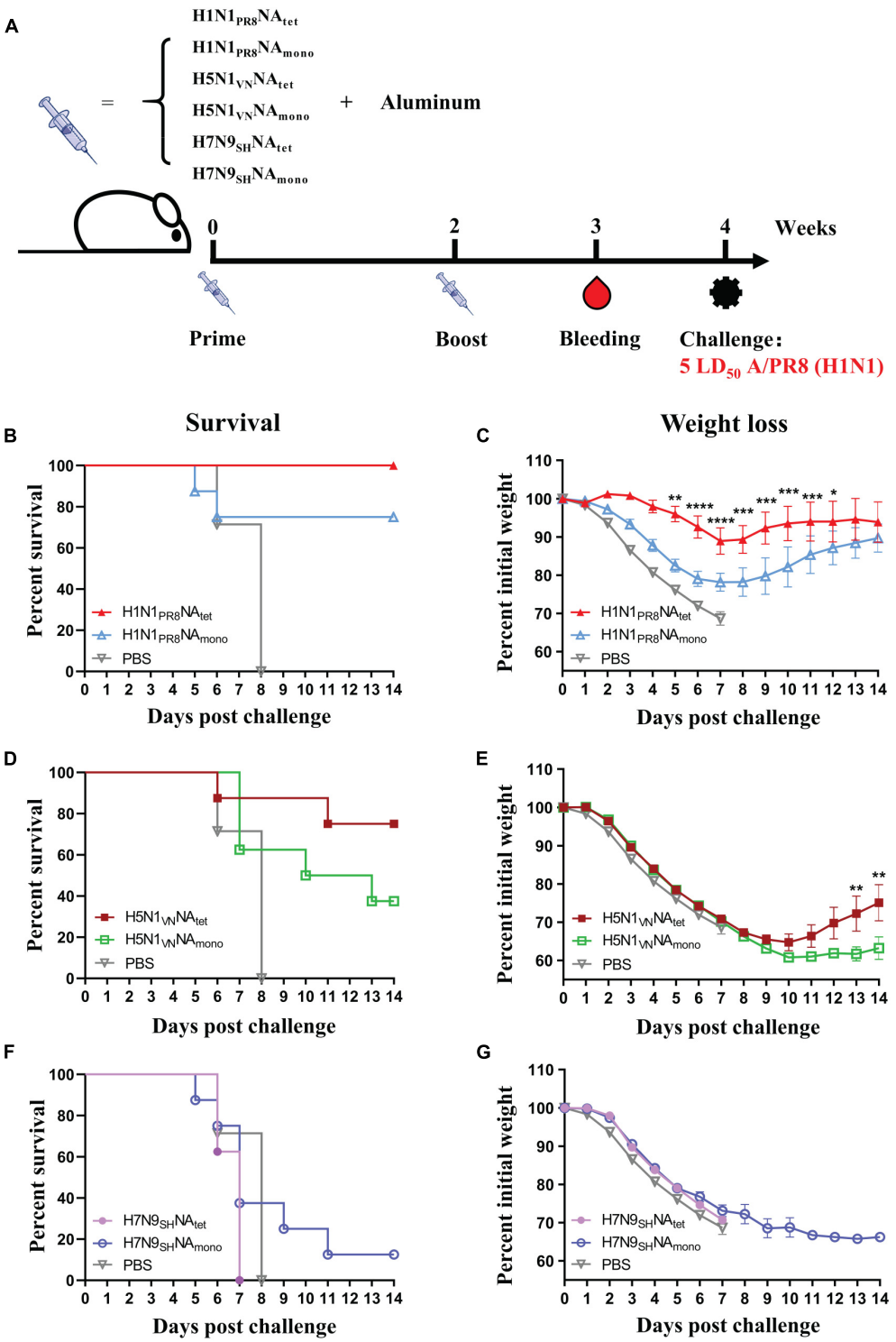


**FIGURE 2 |** Protective efficacy of tetrameric neuraminidase (NA) vs. monomeric NA. **(A)** The experimental design for immunization and challenge studies. Six- to eight-week-old BALB/c mice ($n$ = 8 in each group) were immunized twice at 2-week interval with 20 μg of $H1N1_{PR8}NA_{tet}$, $H5N1_{VN}NA_{tet}$, $H7N9_{SH}NA_{tet}$, $H1N1_{PR8}NA_{mono}$, $H5N1_{VN}NA_{mono}$, and $H7N9_{SH}NA_{mono}$ proteins adjuvanted with aluminum (i.p.), respectively. Sera were collected at 1 week after the final immunization; then, the mice were challenged with 5 $LD_{50}$ of A/PR8 (H1N1) virus intranasally (i.n.) at 2 weeks after the final immunization. **(B–G)** Survival rates **(B,D,F)** and weight loss **(C,E,G)** were monitored for 14 days post-infection.

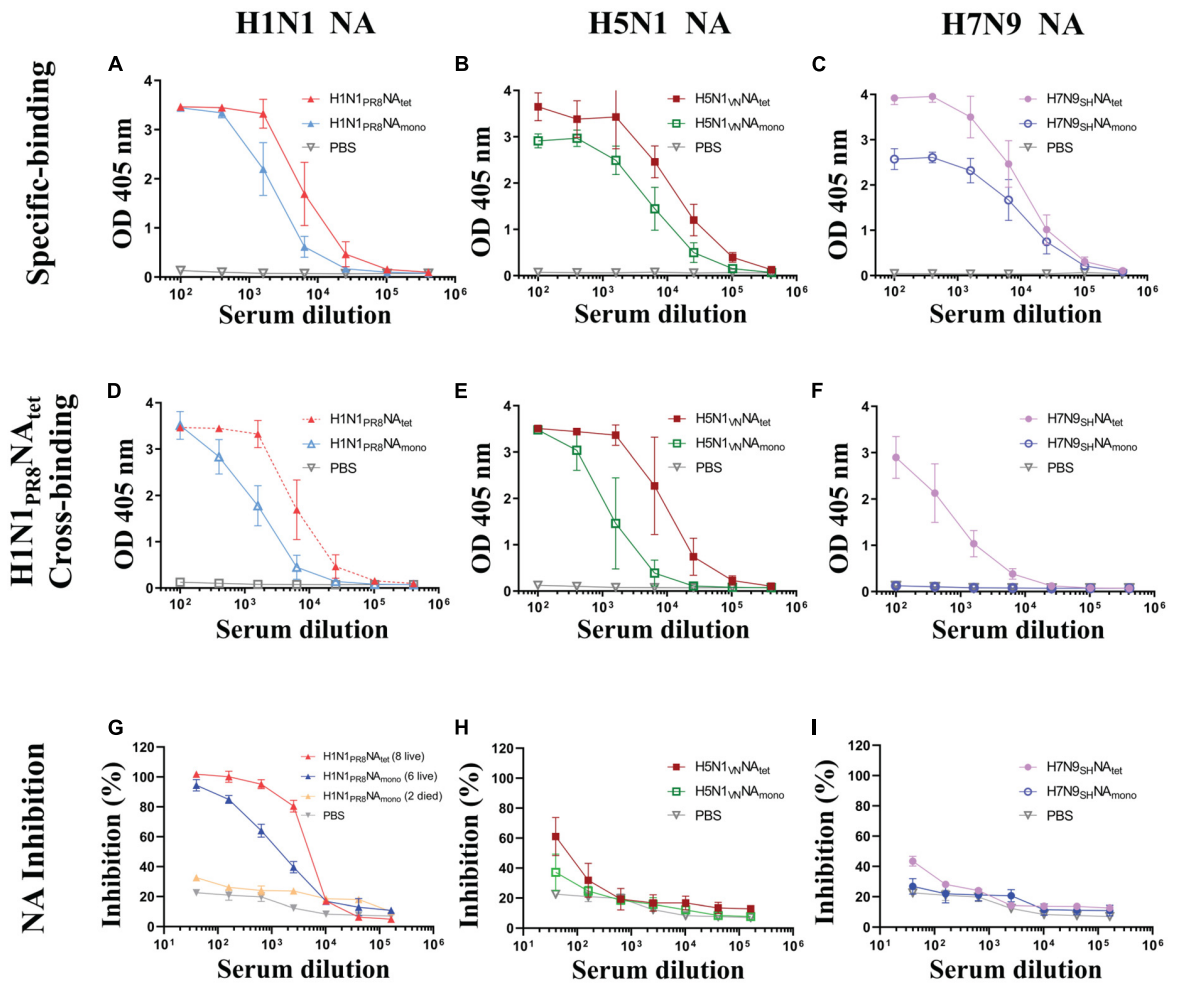


**FIGURE 3 |** Humoral response induced tetrameric and monomeric neuraminidase (NA) proteins. The experimental design for immunization and challenge studies was identical to that detailed in the legend of **Figure 2A**. Serum were collected at 1 week after the final immunization. **(A–C)** The sera of mice vaccinated, respectively, with H1N1$_{PR8}$NA$_{tet}$ and H1N1$_{PR8}$NA$_{mono}$ **(A)**, H5N1$_{VN}$NA$_{tet}$ and H5N1$_{VN}$NA$_{mono}$ **(B)**, and H7N9$_{SH}$NA$_{tet}$ and H7N9$_{SH}$NA$_{mono}$ **(C)** proteins were tested for NA-specific binding antibody levels to the respective immunogen *via* ELISA. **(D–F)** The same sera whose results are shown in panels **(A–C)** were tested for cross-binding activity to H1N1$_{PR8}$NA$_{tet}$ protein *via* ELISA, respectively. **(G–I)** The same sera mentioned above were tested for NA inhibition (NAI) activity against NA of A/PR8 (H1N1) *via* enzyme-linked lectin assay (ELLA), respectively.

against NA of A/PR8 (H1N1), and NAI antibodies. The subtype of NA-specific antibodies was also analyzed. We firstly evaluated NA-specific binding antibodies against their respective immunogens by ELISA. As shown in **Figure 3A**, both of the H1N1 NA tetramer and monomer induced high levels of binding antibodies to the immunogens after two immunizations in mice. The H1N1 NA tetramer induced higher binding antibodies compared to H1N1 NA monomers (1:25,600 vs. 1:6,400). Similar results were observed between the groups of H5N1$_{VN}$NA$_{tet}$ and H5N1$_{VN}$NA$_{mono}$ (**Figure 3B**) as well as groups of H7N9$_{SH}$NA$_{tet}$ and H7N9$_{SH}$NA$_{mono}$ (**Figure 3C**). These results suggested that the NA tetramer with natural conformation has higher immunogenicity than the monomer.

Then, we evaluated the cross-subtype binding antibodies against H1N1 PR8 NA induced by the H5N1 NA and H7N9 NA proteins. The cross-binding of sera from different mice groups against the H1N1$_{PR8}$NA$_{tet}$ protein was tested by ELISA. Both H1N1 PR8 NA and H5N1 NA induced binding antibodies to H1N1$_{PR8}$NA$_{tet}$ (**Figures 3D,E**). The antibody levels induced by NA tetramer were higher than those by the monomer as previously indicated. The sera from mice immunized with H7N9 NA tetramer weakly reacted with H1N1$_{PR8}$NA$_{tet}$, while the sera from mice immunized with H7N9 NA monomer did not react with H1N1$_{PR8}$NA$_{tet}$ (**Figure 3F**). These results indicated that cross-binding antibodies are related to protection, while antibodies induced by NA proteins were mainly subtype-specific.

We also investigated the subtypes of NA-specific antibodies by isotyping ELISA assays. All tetrameric and monomeric NA proteins mainly induced IgG1 isotype of NA-specific antibodies (**Supplementary Figure S1**), indicating that the NA protein elicited a Th2-directed immune response.

Since it has been reported that the NA-induced protection was correlated with NAI antibodies (Couch et al., 2013; Memoli et al., 2016; Gilchuk et al., 2019; Stadlbauer et al., 2019;

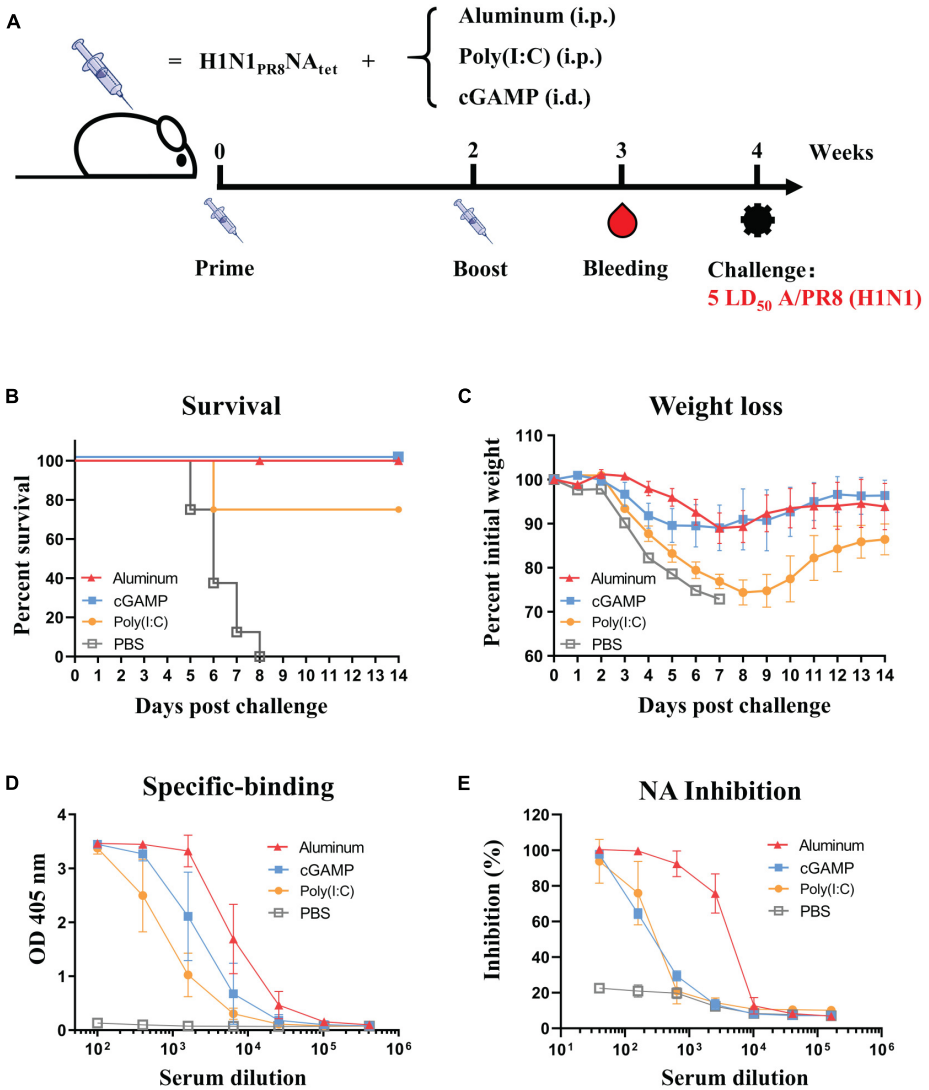


**FIGURE 4 |** Effect of three adjuvants—aluminum, cGAMP, and Poly(I:C)—on the protective efficacy and humoral response induced by H1N1$_{PR8}$NA$_{tet}$ tetramer. **(A)** Six- to eight-week-old BALB/c mice were immunized twice at 2-week interval with 20 μg of H1N1$_{PR8}$NA$_{tet}$ protein adjuvanted with aluminum ($n$ = 8, i.p.), cGAMP ($n$ = 4, i.c.), or Poly(I:C) ($n$ = 4, i.p.), respectively. The mice were immunized with phosphate-buffered saline (PBS) as control ($n$ = 4, i.p.). Sera were collected at 1 week after the final immunization; then, the mice were challenged with 5 LD$_{50}$ of A/PR8 (H1N1) virus intranasally (i.n.) at 2 weeks after the final immunization. **(B,C)** The survival rates **(B)** and weight loss **(C)** were monitored for 14 days post-infection. **(D)** The serum from individual mice in each experimental group was tested for neuraminidase (NA)-specific antibody levels against H1N1$_{PR8}$NA$_{tet}$ protein *via* ELISA. **(E)** The NAI activity of mice serum against NA of A/PR8 (H1N1) was tested *via* enzyme-linked lectin assay (ELLA).

Vogel and Manicassamy, 2020), we evaluated the NAI activity of sera by ELLA. As shown in **Figure 3G**, sera from eight mice immunized with the H1N1$_{PR8}$NA$_{tet}$ tetramer exhibited a higher NAI activity against the NA of A/PR8 (H1N1) than the six survivors that were immunized with H1N1$_{PR8}$NA$_{mono}$. In contrast, the NAI activity was barely detectable in sera from two deceased mice in this group (**Figure 3G**). The NAI activity against the NA of A/PR8 (H1N1) was only weakly detected in mice that were immunized with H5N1 NA tetramer and monomer (**Figure 3H**) and almost not detected in mice that were immunized with H7N9 NA proteins (**Figure 3I**), suggesting that NAI antibodies may be related to protection during influenza virus infection. Taken together, those results mentioned above indicated that NA$_{tet}$ exhibited better ability in inducing NA-specific-, cross- binding-, and NAI antibodies. Furthermore, NA$_{tet}$ proteins provide better homogeneous protection or cross-protection than NA$_{mono}$.

## Adjuvant Effects on the Immunity Induced by Neuraminidase Proteins

We compared the effect of three adjuvants, aluminum, cGAMP, and Poly(I:C), on the protective efficacy and humoral responses induced by the H1N1$_{PR8}$NA$_{tet}$ tetramer. The immunization

and challenge schedule is shown in **Figure 4A**. We found that complete protection against homologous A/PR8 (H1N1) virus challenge was observed in groups of aluminum or cGAMP (**Figures 4B,C**). The protection efficacy in the Poly(I:C) group was lower than those in the aluminum and cGAMP groups, as indicated by both the lower survival rates and weight loss (**Figures 4B,C**). We then evaluated the antibody responses in mice with different adjuvants of groups. Aluminum-adjuvant H1N1PR8NAtet induced the highest NA-specific binding antibodies and NAI antibodies (**Figures 4D,E**). cGAMP-adjuvant H1N1$_{PR8}$NA$_{tet}$ induced higher NA-specific binding antibodies than Poly(I:C)-adjuvant, but both adjuvants induced a similar level of NAI antibodies (**Figures 4D,E**). These results together suggested that tetrameric NA protein with natural conformation adjuvanted with aluminum elicited better protection than with cGAMP or Poly(I:C).

## DISCUSSION

Influenza NA protein has been considered a potential target to develop universal vaccines that can provide cross-protection against different subtypes of influenza virus. The current commercial influenza vaccines are not efficient at inducing NA-specific protective immune response (Wohlbold et al., 2015; Chen et al., 2018; McMahon et al., 2020). Several NA-based vaccines, including recombinant NA proteins (Martinet et al., 1997; Bosch et al., 2010; Subathra et al., 2014; Liu et al., 2015; Wohlbold et al., 2015), DNA vaccines (Sandbulte et al., 2007), and virus-like particles (VLP) vaccines (Quan et al., 2012; Smith et al., 2017; Kim et al., 2019), have been evaluated in experimental animals and successfully provoked protection against influenza viruses. However, the mechanism of NA-induced protection has not been completely understood. Here we evaluated the immune response and protective efficacy of recombinant NA proteins. We found that the NA protein is highly immunogenic and induced protection against influenza viruses. Compared to the NA monomer, the NA tetramer is more immunogenic to induce higher NA-specific and cross-reactive biding antibodies, which are related to protection. The NA-reactive antibodies that bound to the native NA tetramers of the live virus might also play an important a role in inhibiting the viral release and spread of the infection. However, the protection is NA-subtype specific. H7N9$_{SH}$NA$_{tet}$ tetramer could not provide heterosubtypic protection against A/PR8 (H1N1) virus infection. This finding is supported by the report that vaccination with the recombinant NA protein of A/PR8 (H1N1) could provide complete homologous protection against A/PR8 (H1N1) virus infection but not heterosubtypic protection against H3N2 virus (Wohlbold et al., 2015). Since there are 11 known NA subtypes, further studies may be required to explore an immune strategy, such as sequential or mixed immunization, to induce a broad immune response against all the 11 NA subtypes.

It was suggested that the protection induced by the NA protein was mediated by NAI antibodies (Couch et al., 2013; Memoli et al., 2016; Gilchuk et al., 2019; Stadlbauer et al., 2019; Vogel and Manicassamy, 2020). In this paper, we found that the protection induced by the NA protein was correlated with NAI antibodies. High NAI antibodies were detected in sera from the mice that survived the challenge, while NAI antibodies were undetectable in deceased mice. We also observed that NAI antibodies were strain-specific, while H5N1$_{VN}$NA$_{tet}$ induced cross-protection against A/PR8 (H1N1) virus infection without provoking cross-reactive NAI antibodies, which probably depended on the differences among the epitopes around the active enzyme sites (Liu et al., 2015). However, H5N1$_{VN}$NA$_{tet}$ induced high titers of subtype-specific binding antibodies to the NA protein of A/PR8 (H1N1) virus. Those cross-binding antibodies may potentially contribute to partial cross-protection. Further study is required to clarify whether the cross-protection was correlated with the NA-binding antibodies.

In addition, adjuvant is also an important consideration in NA protein-based vaccine design since we found that it worked on the immunity induced by the NA proteins. In contrast, we found that the mice of aluminum and cGAMP groups all survived the lethal influenza virus challenge, although the NAI antibody level of the aluminum group was slightly higher. We speculate that it may refer to the property of adjuvants or immune methods (i.p. vs. i.d.), but this still remains to be further determined. In short, adjuvant aluminum might be preferred for NA protein-based vaccination.

## CONCLUSION

In conclusion, our data suggests that tetrameric NA provides better homologous protection against influenza virus infection, and it could also confer preferable subtype-specific cross-protection. NA-reactive binding and inhibition antibodies are related to protection. Furthermore, aluminum adjuvant is preferential in vaccination of recombinant NA protein than cGAMP and Poly(I:C). We hope that this information could be useful for influenza vaccine formulation and administration.

## DATA AVAILABILITY STATEMENT

The original contributions presented in the study are included in the article/ **Supplementary Material**, further inquiries can be directed to the corresponding authors.

## ETHICS STATEMENT

The animal study was reviewed and approved by the Ethics Committee of Shanghai Public Health Clinical Center.

## AUTHOR CONTRIBUTIONS

JH conceived and designed the experiments and supervised the project. XD, ML, and QZ expressed and purified the recombinant NA proteins. XD performed the MUNANA-based enzymatic activity assay and ELISA and ELLA assays. XD and QW performed the mice experiments. XD, JH, and FW analyzed the data and wrote the

manuscript. All authors have read and agreed to the published version of the manuscript.

## FUNDING

This work was supported by the National Natural Science Foundation of China (31771008 to JH), the National Major Science and Technology Projects of China (2017ZX10202102 to JH and 2018ZX10301403 to FW), the Hundred Talent Program of Shanghai Municipal Health Commission (2018BR08 to JH), and the Chinese Academy of Medical Sciences (2019PT350002 to JH).

## ACKNOWLEDGMENTS

We are thankful for the help from the Laboratory Animal Center of Shanghai Public Clinical Center.

## SUPPLEMENTARY MATERIAL

The Supplementary Material for this article can be found online at: https://www.frontiersin.org/articles/10.3389/fmicb.2021.729914/full#supplementary-material

## REFERENCES

Biuso, F., Palladino, L., Manenti, A., Stanzani, V., Lapini, G., Gao, J., et al. (2019). Use of lentiviral pseudotypes as an alternative to reassortant or Triton X-100-treated wild-type Influenza viruses in the neuraminidase inhibition enzyme-linked lectin assay. *Influenza Other Respir. Viruses* 13, 504–516. doi: 10.1111/irv.12669

Bosch, B. J., Bodewes, R., de Vries, R. P., Kreijtz, J. H. C. M., Bartelink, W., van Amerongen, G., et al. (2010). Recombinant soluble, multimeric HA and NA exhibit distinctive types of protection against pandemic Swine-Origin 2009 A(H1N1) influenza virus infection in ferrets. *J. Virol.* 84, 10366–10374. doi: 10.1128/JVI.01035-10

Chen, Y., Wohlbold, T. J., Zheng, N., Huang, M., Huang, Y., Neu, K. E., et al. (2018). Influenza infection in humans induces broadly cross-reactive and protective neuraminidase-reactive antibodies. *Cell* 173, 417–429. doi: 10.1016/j.cell.2018.03.030

Couch, R. B., Atmar, R. L., Franco, L. M., Quarles, J. M., Wells, J., Arden, N., et al. (2013). Antibody correlates and predictors of immunity to naturally occurring influenza in humans and the importance of antibody to the neuraminidase. *J. Infect. Dis.* 207, 974–981. doi: 10.1093/infdis/jis935

Da Silva, D. V., Nordholm, J., Madjo, U., Pfeiffer, A., and Daniels, R. (2013). Assembly of subtype 1 influenza neuraminidase is driven by both the transmembrane and head domains. *J. Biol. Chem.* 288, 644–653. doi: 10.1074/jbc.M112.424150

Eichelberger, M. C., and Monto, A. S. (2019). Neuraminidase, the forgotten surface antigen, emerges as an influenza vaccine target for broadened protection. *J. Infect. Dis.* 219, S75–S80. doi: 10.1093/infdis/jiz017

Gilchuk, I. M., Bangaru, S., Gilchuk, P., Irving, R. P., Kose, N., Bombardi, R. G., et al. (2019). Influenza H7N9 virus Neuraminidase-specific human monoclonal antibodies inhibit viral egress and protect from lethal influenza infection in mice. *Cell Host Microbe* 26, 715–728. doi:10.1016/j.chom.2019.10.003

Job, E. R., Ysenbaert, T., Smet, A., Christopoulou, I., Strugnell, T., Oloo, E. O., et al. (2018). Broadened immunity against influenza by vaccination with computationally designed influenza virus N1 neuraminidase constructs. *NPJ Vaccines* 3:55. doi: 10.1038/s41541-018-0093-1

Johansson, B. E., Moran, T. M., and Kilbourne, E. D. (1987). Antigen-Presenting B cells and helper T cells cooperatively mediate intravirionic antigenic competition between influenza a virus surface glycoproteins. *Proc. Natl. Acad. Sci. U.S.A.* 84, 6869–6873. doi: 10.1073/pnas.84.19.6869

Ju, H., Zhang, J., Sun, Z., Huang, Z., Qi, W., Huang, B., et al. (2018). Discovery of C-1 modified oseltamivir derivatives as potent influenza neuraminidase inhibitors. *Eur. J. Med. Chem.* 146, 220–231. doi: 10.1016/j.ejmech.2018.01.050

Kim, K., Lee, Y., Park, S., Jung, Y., Lee, Y., Ko, E., et al. (2019). Neuraminidase expressing virus-like particle vaccine provides effective cross protection against influenza virus. *Virology* 535, 179–188. doi: 10.1016/j.virol.2019.07.008

Krammer, F., Fouchier, R. A. M., Eichelberger, M. C., Webby, R. J., Shaw-Saliba, K., Wan, H., et al. (2018). NAction! How can Neuraminidase-Based immunity contribute to better influenza virus vaccines?. *mBio* 9:e02317-32. doi: 10.1128/mBio.02332-17

Liu, W., Lin, C., Tsou, Y., Jan, J., and Wu, S. (2015). Cross-reactive neuraminidase-inhibiting antibodies elicited by immunization with recombinant neuraminidase proteins of H5N1 and pandemic H1N1 influenza a viruses. *J. Virol.* 89, 7224–7234. doi: 10.1128/JVI.00585-15

Martinet, W., Saelens, X., Deroo, T., Neirynck, S., Contreras, R., Min, J. W., et al. (1997). Protection of mice against a lethal influenza challenge by immunization with yeast-derived recombinant influenza neuraminidase. *Eur. J. Biochem.* 247, 332–338. doi: 10.1111/j.1432-1033.1997.00332.x

McMahon, M., Strohmeier, S., Rajendran, M., Capuano, C., Ellebedy, A. H., Wilson, P. C., et al. (2020). Correctly folded - but not necessarily functional - influenza virus neuraminidase is required to induce protective antibody responses in mice. *Vaccine* 38, 7129–7137. doi: 10.1016/j.vaccine.2020.08.067

Memoli, M. J., Shaw, P. A., Han, A., Czajkowski, L., Reed, S., Athota, R., et al. (2016). Evaluation of antihemagglutinin and antineuraminidase antibodies as correlates of protection in an influenza A/H1N1 virus healthy human challenge model. *mBio* 7:e417. doi: 10.1128/mBio.00417-16

Monto, A. S., and Kendal, A. P. (1973). Effect of neuraminidase antibody on Hong Kong influenza. *Lancet* 1, 623–625. doi: 10.1016/S0140-6736(73)92196-X

Moriyama, M., Chino, S., and Ichinohe, T. (2017). Consecutive inoculations of influenza virus vaccine and poly(I:C) protects mice against homologous and heterologous virus challenge. *Vaccine* 35, 1001–1007. doi: 10.1016/j.vaccine.2017.01.025

Murphy, B. R., Kasel, J. A., and Chanock, R. M. (1972). Association of serum anti-neuraminidase antibody with resistance to influenza in man. *N. Engl. J. Med.* 286, 1329–1332. doi: 10.1056/NEJM197206222862502

Prevato, M., Ferlenghi, I., Bonci, A., Uematsu, Y., Anselmi, G., Giusti, F., et al. (2015). Expression and characterization of recombinant, tetrameric and enzymatically active influenza neuraminidase for the setup of an enzyme-linked lectin-based assay. *PLoS One* 10:e135474. doi: 10.1371/journal.pone.0135474

Quan, F., Kim, M., Lee, B., Song, J., Compans, R. W., and Kang, S. (2012). Influenza M1 VLPs containing neuraminidase induce heterosubtypic cross-protection. *Virology* 430, 127–135. doi: 10.1016/j.virol.2012.05.006

Rudicell, R. S., Garinot, M., Kanekiyo, M., Kamp, H. D., Swanson, K., Chou, T. H., et al. (2019). Comparison of adjuvants to optimize influenza neutralizing antibody responses. *Vaccine* 37, 6208–6220. doi: 10.1016/j.vaccine.2019.08.030

Saito, T., Taylor, G., and Webster, R. G. (1995). Steps in maturation of influenza a virus neuraminidase. *J. Virol.* 69, 5011–5017. doi: 10.1128/jvi.69.8.5011-5017.1995

Sandbulte, M. R., Jimenez, G. S., Boon, A. C., Smith, L. R., Treanor, J. J., and Webby, R. J. (2007). Cross-reactive neuraminidase antibodies afford partial protection against H5N1 in mice and are present in unexposed humans. *PLoS Med.* 4:e59. doi: 10.1371/journal.pmed.0040059

Smith, G. E., Sun, X., Bai, Y., Liu, Y. V., Massare, M. J., Pearce, M. B., et al. (2017). Neuraminidase-based recombinant virus-like particles protect against lethal avian influenza A(H5N1) virus infection in ferrets. *Virology* 509, 90–97. doi: 10.1016/j.virol.2017.06.006

Sridhar, S., Brokstad, K. A., and Cox, R. J. (2015). Influenza vaccination strategies: comparing inactivated and live attenuated influenza vaccines. *Vaccines* 3, 373–389. doi: 10.3390/vaccines3020373

Stadlbauer, D., Zhu, X., McMahon, M., Turner, J. S., Wohlbold, T. J., Schmitz, A. J., et al. (2019). Broadly protective human antibodies that target the active site of influenza virus neuraminidase. *Science* 366, 499–504. doi: 10.1126/science.aay0678

Subathra, M., Santhakumar, P., Narasu, M. L., Beevi, S. S., and Lal, S. K. (2014). Evaluation of antibody response in mice against avian influenza a (H5N1) strain neuraminidase expressed in yeast Pichia pastoris. *J. Biosci.* 39, 443–451. doi: 10.1007/s12038-014-9422-3

Tong, S. X., Li, Y., Rivailler, P., Conrardy, C., Alvarez Castillo, D. A., Chen, L. M., et al. (2012). A distinct lineage of influenza A virus from bats. *Proc. Natl. Acad. Sci. U.S.A.* 109, 4269–4274. doi: 10.1073/pnas.1116200109

Tong, S. X., Zhu, X. Y., Li, Y., Shi, M., Zhang, J., Bourgeois, M., et al. (2013). New world bats harbor diverse influenza A viruses. *PLoS Pathog.* 9:e1003657. doi: 10.1371/journal.ppat.1003657

Vogel, O. A., and Manicassamy, B. (2020). Broadly protective strategies against influenza viruses: universal vaccines and therapeutics. *Front. Microbiol.* 11:135. doi: 10.3389/fmicb.2020.00135

Wang, J., Li, P. Y., and Wu, M. X. (2016). Natural STING agonist as an "ideal" adjuvant for cutaneous vaccination. *J. Invest. Dermatol.* 136, 2183–2191. doi: 10.1016/j.jid.2016.05.105

Wohlbold, T. J., Nachbagauer, R., Xu, H., Tan, G. S., Hirsh, A., Brokstad, K. A., et al. (2015). Vaccination with adjuvanted recombinant neuraminidase induces broad heterologous, but not heterosubtypic, cross-protection against influenza virus infection in mice. *mBio* 6:e2556. doi: 10.1128/mBio.02556-14

Wu, Z. L., Ethen, C., Hickey, G. E., and Jiang, W. (2009). Active 1918 pandemic flu viral neuraminidase has distinct N-glycan profile and is resistant to trypsin digestion. *Biochem. Biophys. Res. Commun.* 69, 749–753. doi: 10.1016/j.bbrc.2008.12.139

Yasuhara, A., Yamayoshi, S., Kiso, M., Sakai-Tagawa, Y., Koga, M., Adachi, E., et al. (2019). Antigenic drift originating from changes to the lateral surface of the neuraminidase head of influenza a virus. *Nat. Microbiol.* 4, 1024–1034. doi: 10.1038/s41564-019-0401-1

**Conflict of Interest:** The authors declare that the research was conducted in the absence of any commercial or financial relationships that could be construed as a potential conflict of interest.

**Publisher's Note:** All claims expressed in this article are solely those of the authors and do not necessarily represent those of their affiliated organizations, or those of the publisher, the editors and the reviewers. Any product that may be evaluated in this article, or claim that may be made by its manufacturer, is not guaranteed or endorsed by the publisher.

frontiers in Microbiology

ORIGINAL RESEARCH
published: 16 December 2021
doi: 10.3389/fmicb.2021.751142

# Characterizing the Core Internal Gene Pool of H9N2 Responsible for Continuous Reassortment With Other Influenza A Viruses

*Haoyi Yang[1,2†], Mingda Hu[1†], Boqian Wang[1], Yuan Jin[1], Xingfei Gong[1,2], Long Liang[1], Junjie Yue[1*], Wei Chen[2*] and Hongguang Ren[1*]*

[1] Beijing Institute of Biotechnology, State Key Laboratory of Pathogen and Biosecurity, Academy of Military Medical Sciences, Beijing, China, [2] College of Computer, National University of Defense Technology, Changsha, China

OPEN ACCESS

**Edited by:**
Dayan Wang,
Chinese National Influenza Center, China

**Reviewed by:**
Ye Ge,
Guangdong Ocean University, China
Hongliang Chai,
Northeast Forestry University, China

***Correspondence:**
Junjie Yue
yue_junjie@126.com
Wei Chen
chenwei@nudt.edu.cn
Hongguang Ren
bioren@163.com

[†] These authors have contributed equally to this work

**Specialty section:**
This article was submitted to Virology, a section of the journal Frontiers in Microbiology

**Received:** 31 July 2021
**Accepted:** 30 November 2021
**Published:** 16 December 2021

**Citation:**
Yang H, Hu M, Wang B, Jin Y, Gong X, Liang L, Yue J, Chen W and Ren H (2021) Characterizing the Core Internal Gene Pool of H9N2 Responsible for Continuous Reassortment With Other Influenza A Viruses. Front. Microbiol. 12:751142. doi: 10.3389/fmicb.2021.751142

Reassortment among avian influenza viruses is the main source of novel avian influenza virus subtypes. Studies have shown that the H9N2 virus often donates internal segments to generate novel reassortant avian influenza viruses, acting as a reassortment template. However, the characteristics of the internal pattern of reassortment remain unclear. In this article, we first defined the core gene pool of the internal segments of the H9N2 virus that provide templates for reassortment. We used genetic distance and sequence similarity to define typical clusters in the core gene pool. Then, we analyzed the phylogenetic relationships, feature vector distances, geographic distributions and mutation sites of strains related to the core gene pool. Strains in the same typical clusters have close phylogenetic relationships and feature vector distances. We also found that these typical clusters can be divided into three categories according to their main geographic distribution area. Furthermore, typical clusters in the same geographic area contain some common mutation patterns. Our results suggest that typical clusters in the core gene pool affect the reassortment events of the H9N2 virus in many respects, such as geographic distribution and amino acid mutation sites.

**Keywords: H9N2, reassortment, influenza A virus, evolution, genome**

## INTRODUCTION

H9N2 avian influenza virus (AIV) was first detected in 1966 (Homme and Easterday, 1970). Since then, it has been found to be widespread in avian around the world, especially in the last two decades (Peacock et al., 2019). H9N2 infects hosts and transmits rapidly, as its low pathogenicity gives it high fitness in poultry and other wild birds. In a recent report, H9N2 was found to be the dominant subtype of AIVs among poultry in China (Bi et al., 2020). The first zoonotic event involving H9N2 was reported in 1997 (Peiris et al., 1999). Since then, several cross-species transmissions to humans or swine have been documented (Sun et al., 2020).

A number of AIVs have been reported to infect humans, including H7N9, H5N6, H10N8, H5N1, H6N1, and H7N4 (Guan et al., 1999; Hoffmann et al., 2000; Gao et al., 2013; Chen et al., 2014; Yang et al., 2015; Li et al., 2020; Qu et al., 2020). Some of these human-infecting AIVs [e.g., H7N9, H5N1, H10N8, and H5N6 (Guan et al., 1999; Martin et al., 2011; Chen et al., 2014; Cui et al., 2014;

Yang et al., 2015; Pu et al., 2021)] were found to be reassortant viruses, with H9N2 contributing the internal segments to the reassortants (Liu et al., 2014). Hosts may be coinfected with H9N2 and other AIV subtypes, and in this context, H9N2 may contribute reassortment templates for novel reassortment AIV subtypes. The frequent reassortments among the H9N2 virus and other subtypes of AIVs imply that there may be a core internal gene pool in the H9N2 virus that continuously offers segments for the emergence of novel AIVs.

In this article, we aimed to identify and characterize the core gene pool of H9N2 internal segments and analyze the reassortment events involving the H9N2 virus. Based on a genetic analysis and mathematical relationships calculated for all the H9N2 viruses and other relevant AIVs, we defined typical clusters of each internal segment of the H9N2 virus. Each typical cluster consists of strains that are clustered together according to sequence similarity and evolutionary tree branching information. Strains in the same typical cluster have similar genetic characteristics. Typical clusters with different characteristics constitute the core gene pool of H9N2 internal segments. Then, we extracted feature vectors from the sequences and performed mathematical clustering to cross-validate the results. The clustering results essentially corresponded to the typical clusters. Then, we conducted a more detailed analysis of the biological characteristics of the core gene pool. The results reflect that different typical clusters infect different host species and have different geographic distributions. Mutation site analysis of typical clusters revealed that typical clusters in the same geographic area share some common mutation sites. We further analyzed the relationship between H7N9 and H9N2 using mathematical feature characterization. Most sequences of the H7N9 virus and H9N2 virus clustered together, which is consistent with reported reassortment events and further verifies the rationality of our core H9N2 virus gene pool.

# MATERIALS AND METHODS

## Sequence Data Preparation

All internal segments sequences of H9N2 virus and other relevant AIV subtypes are downloaded from NCBI Influenza Virus Resource (Bao et al., 2008). Only full-length sequences are preserved. Repetitive sequences with the same host, the same country, the same time and the same subtypes are excluded. For the relevant AIVs other than H9N2, sequences with >98% similarity to H9N2 virus are selected judged by blast (Johnson et al., 2008). MAFFT (Katoh and Standley, 2013) are used to align the coding region of the resulting sequences and then Mega (Kumar et al., 2016) is used to manually inspect the sequences. The sequence lengths of different AIV subtypes are slightly different. So, we set a lower threshold for each internal segment sequences, as **Table 1** shows. For MP and NS segments, M1 and NS1 segment are considered in the follow-up study.

We use CD-HIT to initially filter the resulting sequences with a threshold level of 0.98 and retained sequences in clusters which meet all the following rules.

**TABLE 1 |** Lower threshold for internal segments nucleotide sequence length.

| Internal segments | PB2 | PB1 | PA | NP | MP | NS |
|---|---|---|---|---|---|---|
| Sequence length | 2280 | 2274 | 2151 | 1497 | 759 | 693 |

- Cluster contains H9N2 virus sequence(s).
- Besides H9N2 virus sequence(s), cluster contains other AIV subtypes sequences. And there is at least one sequence whose collecting time is no more than 3 years from the collecting time of H9N2 virus sequence(s) in the cluster.
- Besides H9N2 virus sequence(s), cluster contains other AIV subtypes sequences. And there is at least one sequence which has the same host or country with H9N2 virus sequence(s).

After first filtering, our dataset includes 2,583 PB2 sequences, 3,356 PB1 sequences, 3,565 PA sequences, 3,660 NP sequences, 5,757 MP sequences, and 3,325 NS sequences.

## Phylogenetic Tree Construction and Analysis

Maximum-likelihood trees are inferred by IQ-TREE (Nguyen et al., 2015). And ModelFinder is used to find the best partition model automatically (Kalyaanamoorthy et al., 2017). Branch supports are obtained with 1,000 times ultrafast bootstrap (Hoang et al., 2018). Both ModelFinder and the ultrafast bootstrap are implemented in IQ-TREE.

For each evolutionary tree, we use Mean Pairwise Distance (MPD) to cluster AIV strains (Tsirogiannis and Sandel, 2014). The MPD formula is as follows:

$$mpd = \frac{\sum_{\mathrm{i}}^{\mathrm{n}} \sum_{\mathrm{j}}^{\mathrm{n}} \delta_{i,j}}{\binom{\mathrm{n}}{2}}$$

We calculate the median number of leaf nodes and MPD for each internal node. To reduce deviation, we also set a lower threshold for the median number of leaf nodes. We choose the larger one of the median and the threshold as the max number of strains in a cluster, named as *maxNode*. The average MPD of all internal nodes is defined as *meanMPD*.

## Definition of Typical Clusters

When two different strains have a reassortment relationship, we believe that their sequences are similar and they have close phylogenetic distance reflected in the evolutionary tree. For a given subtree *s* of the evolutionary tree, it has two features. $N_s$ reflects the number of strains of subtree *s*, and $mpd_s$ represents the MPD value of subtree *s*. We define a set K(s) which contains all strains in subtree s. To infer the possible genealogy and relationship of strains, we use the following conditions to measure phylogenetic distance between strains: (a) Strains in subtree s with $N_s < maxNode$ have close phylogenetic distance. (b) Strains in subtree s with $mpd_s < meanMPD$ have close phylogenetic distance. Subtree that satisfies one of the above conditions is defined as a cluster.

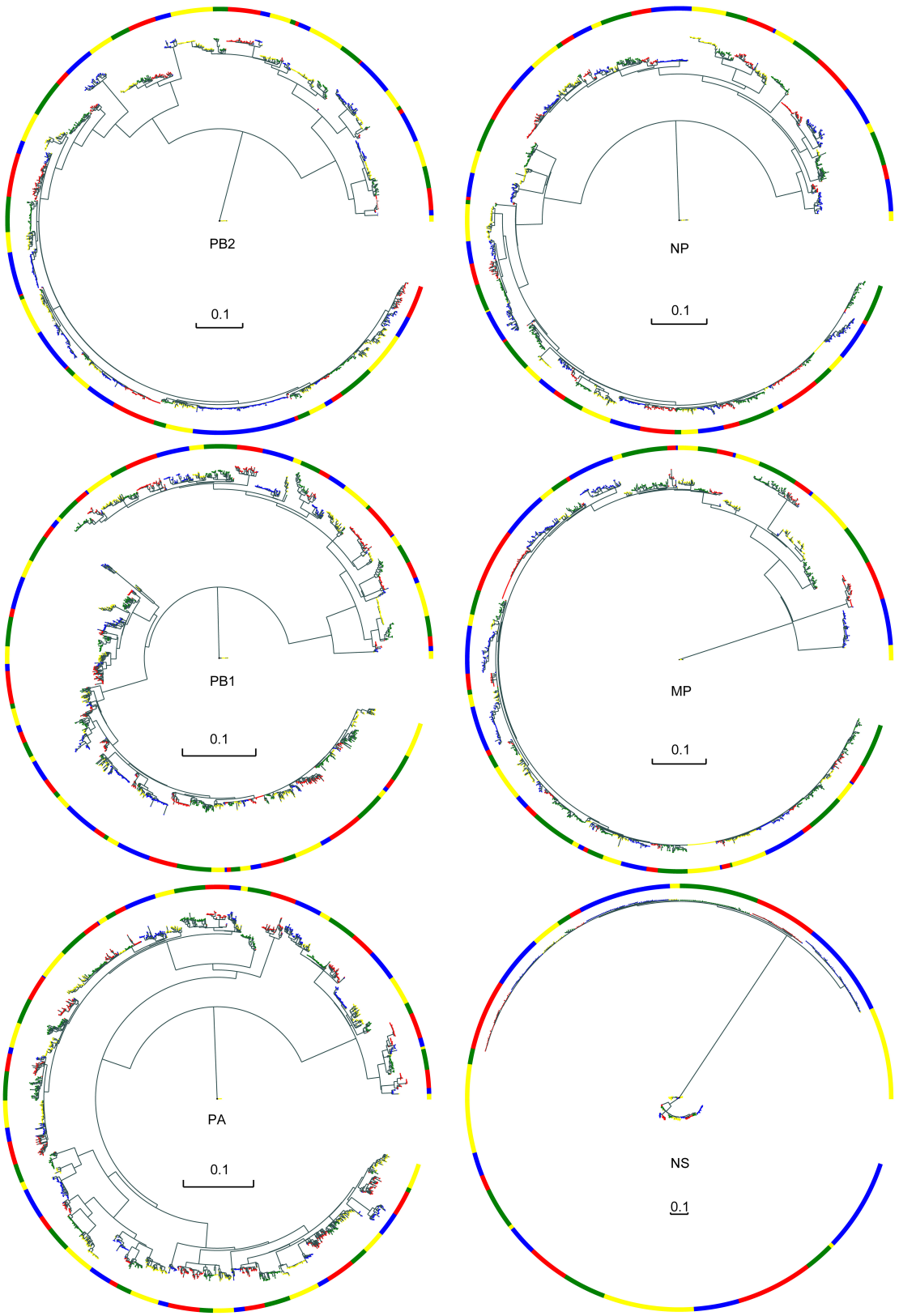


**FIGURE 1 |** Evolutionary trees and typical clusters of the core gene pool. The branches are colored according to their different typical clusters. Color blocks are visual representations of different typical clusters. Each color block represents a typical cluster; the colors themselves have no special meaning.

We analyze the common mutation sites for all strains in a given cluster. A cluster with more than one strains that contains H9N2 virus and has common non-neutral mutations is defined as a typical cluster.

## Feature Extraction

To verify the rationality of typical clusters and characterize each genotype completely, we define a feature vector for each genotype. In DNA/RNA sequences, there are 64 combinations of triplet nucleotide residue sequences (codons). Excluding termination codons, 61 codons remain. Each sequence starts from the initiation codon and every three bases is a codon. Bases included in a sequence compose a set $S$. For each base occurs in the sequence, the frequency of it is defined as $p_i$, $(i \in S)$. For each codon except termination codons, the frequency of it can be defined as $p_{ijk}$, $(i, j, k \in S)$. Trinucleotide relative abundance (TRA) is an extension of dinucleotide relative abundance (DRA; Kariin and Burge, 1995), which reflects the correlation between three adjacent bases. The TRA of a codon is defined as:

$$T_{ijk} = \frac{p_{ijk}}{p_i p_j p_k}$$

Relative synonymous codon usage (RSCU; Sharp et al., 1986) is used to access codon usage bias. For a given codon, the number of times it appears in the sequence is defined as *Obs_codon*. The times that the coded amino acid occurs is defined as *Obs_Amino*, while the number of synonymous codons of the amino acid is denoted as $n$. When those synonymous codons don't have codon usage bias, the expected observation number of them in the sequence is calculated as follows. The RSCU value of a given codon is calculated as follows:

$$Exp\_codon_i = \frac{Obs\_Amino_i}{n}, condon_i \in Amino_i$$

$$RSCU_i = \frac{Obs\_codon_i}{Exp\_codon_i}$$

Considering both TRA value and RSCU value of codons occur in a sequence, our feature vector is the product of RSCU and TRA:

$$V = RSCU \times T$$

As three termination codons are excluded, the feature vector is a 61-dimensional vector.

## Core Gene Pool Characterization

A typical cluster in core gene pool must have long time span or contain large number of AIV subtypes or contain large number of strains. We screen qualifying typical clusters from the typical clusters calculated in the previous section. These qualifying clusters have more than 3-year time span, or the number of AIV subtypes or strains they contain is higher than the median value. We calculate the average center of each screened cluster as the center vector, which can characterize the cluster. Then we calculate a distance matrix among all the screened clusters and show it in the form of a heat map. In addition to mathematical characterization, we also use common amino acid mutation sites and geographic distribution to characterize clusters biologically.

**TABLE 2 |** Numbers of typical clusters for six internal segments.

| Internal segments | PB2 | PB1 | PA | NP | MP | NS |
|---|---|---|---|---|---|---|
| Typical clusters | 55 | 73 | 65 | 56 | 56 | 26 |

## Analysis of Reassortment Events

We find H7N9 virus is the most representative reassortment AIV subtypes which has been reported before. TSNE (Pezzotti et al., 2017) method can reduce the dimensionality of high-dimensional data and map it to two-dimensional or three-dimensional space. To visually show the relationship between H7N9 virus and H9N2 virus, we use TSNE method perform dimensionality reduction visualization on all the feature vectors. Then we mark all H9N2 virus sequences and H7N9 virus sequences in the core gene pool clusters to verify the rationality of our clusters.

# RESULTS

## Phylogenetic Tree Clustering

We downloaded all available internal segment sequences of AIV from NCBI as of October 13, 2020, and finally constructed a genome set including 1,428 PB2 sequences, 1,795 PB1 sequences, 1,988 PA sequences, 1,564 NP sequences, 1,318 MP sequences, and 637 NS sequences. We constructed six phylogenetic trees for the six internal segments. According to the MPD value and similarity of leaf nodes in the phylogenetic trees, sequences of each internal segment were clustered into different clusters, as shown in **Figure 1**. The different colors of the blocks are used only to distinguish between the different typical clusters. Although some typical clusters contain a smaller number of strains, their frequency of occurrence (number of subtypes or number of strains occurring in a year) is high. As a result, we also consider them typical clusters. Additional information about the typical clusters of the six internal segments, including host, location distribution, AIV subtypes and so on, is shown in **Supplementary Figures 1–6**.

Almost all six internal segments had similar numbers of typical clusters and sequences (**Table 2**). The PB1 and PA segments have a larger number of typical clusters and sequences. Thus, they may be more likely to be reassortment templates.

## Mathematical Characterization of Typical Clusters

To cross-validate the correctness of the clustering results and preserve the features of each sequence as completely as possible, we used a 61-dimensional feature vector to represent a sequence. We used BRICH (Zhang et al., 1996) to cluster the sequence feature vectors (**Figure 2**). The BRICH method clusters strains in terms of vector distance only, making the number of clusters higher than the number of original typical clusters. When all strains in a BRICH cluster can be found in a typical cluster, we consider that the BRICH cluster corresponds to that typical

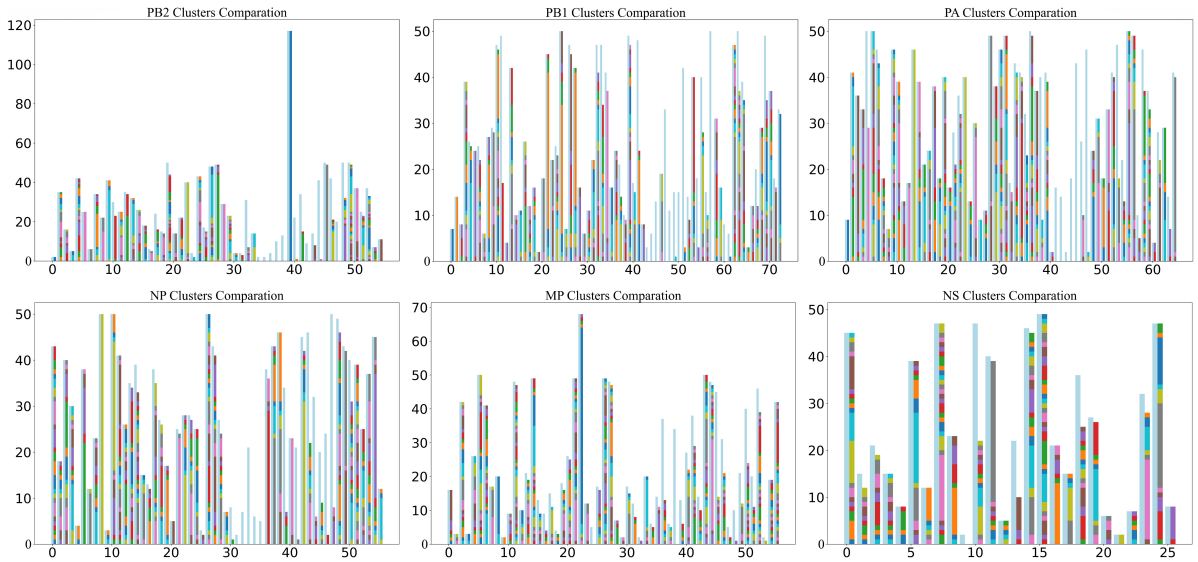


**FIGURE 2 |** Comparison of BRICH cluster results and typical clusters. The horizontal coordinate is the typical cluster number, and the vertical coordinate is the number of strains included. The light blue bars show the strains included in typical clusters, and the different colored bars on the right are the clusters calculated by the BRICH method. When all strains in a BRICH cluster can be found in a typical cluster, the bar representing the BRICH cluster corresponds to the typical cluster, as shown in the figure.

cluster, but the converse is not true. In this analysis, most clusters were observed compared to the phylogenetic clustering method. **Figure 2** shows that some of the resulting BRICH clusters cannot correspond to typical clusters. This phenomenon may occur in part because biological significance is neglected in the mathematical characterization. We analyzed these special typical clusters and found that they were basically composed of H9N2 and H7N9 viruses.

For each internal segment, we calculated the distance matrix among typical clusters based on the center vector of each typical cluster and then normalized the distance matrix. The resulting heatmap, shown in **Figure 3**, indicates that there are obvious differences between each typical cluster. The light-colored areas (marked by a red box) indicate typical clusters that have relatively close distances, which is consistent with the special typical clusters mentioned above.

## Biological Characterization of Typical Clusters

Beyond the mathematical characterization of typical clusters in the core gene pool, we are more interested in the biological characterization of these clusters, which can provide more detailed biological insights. We found that there were obvious differences in geographic distribution among these typical clusters in the core gene pool. As shown in **Figure 4**, the geographical distribution of all typical clusters can be divided into three categories. We named the three categories Asia-Clusters, America-Clusters, and World-Clusters according to the distribution of typical clusters. Of these, Asia-Clusters and America-Clusters account for the majority. The proportions of the three categories in MP and NS segments are different from those in the other four internal segments. In the MP segment, Asia-Clusters account for the majority, while America-Clusters are predominant in the NS segment.

Furthermore, we found relationships between the common mutation sites and geographical distribution of those typical clusters. Taking common mutation sites of the PB2 segment as an example (**Table 3**), we found that over 80% of the strains with PB2 segments including 477I were found in the Americas. Conversely, we found that over 80% of the strains in the Americas have PB2 segments with 477I. As a result, we can infer rationally that strains with 477I in their PB2 segments are likely to be distributed in or originate from the Americas. The complete relationship between mutation sites and geographic distribution is shown in **Supplementary Tables 1–6**.

## Analysis of H7N9 and H9N2 Virus

Among all the reported reassortment events related to the H9N2 virus, the H7N9 virus is highly representative. It is widely distributed and has the ability to infect humans. Notably, it has evolved a lineage with high pathogenicity (Yang et al., 2017). Meanwhile, the H7N9 virus exhibited unique behavior in the above mathematical characterization analysis. As a result, we used the feature vectors of all sequences to construct two-dimensional scatter plots using the TSNE method (Pezzotti et al., 2017). Then, we marked all H9N2 virus sequences and H7N9 virus sequences in the scatter plots (**Figure 5**). Each scatter represents a sequence. For most segments, the H7N9 virus sequences and H9N2 virus sequences are clustered together in the scatter plots. The close distance indicates that these strains have a close relationship. This can also verify the rationality of the feature vectors we extracted and the core gene pool clustering in this analysis.

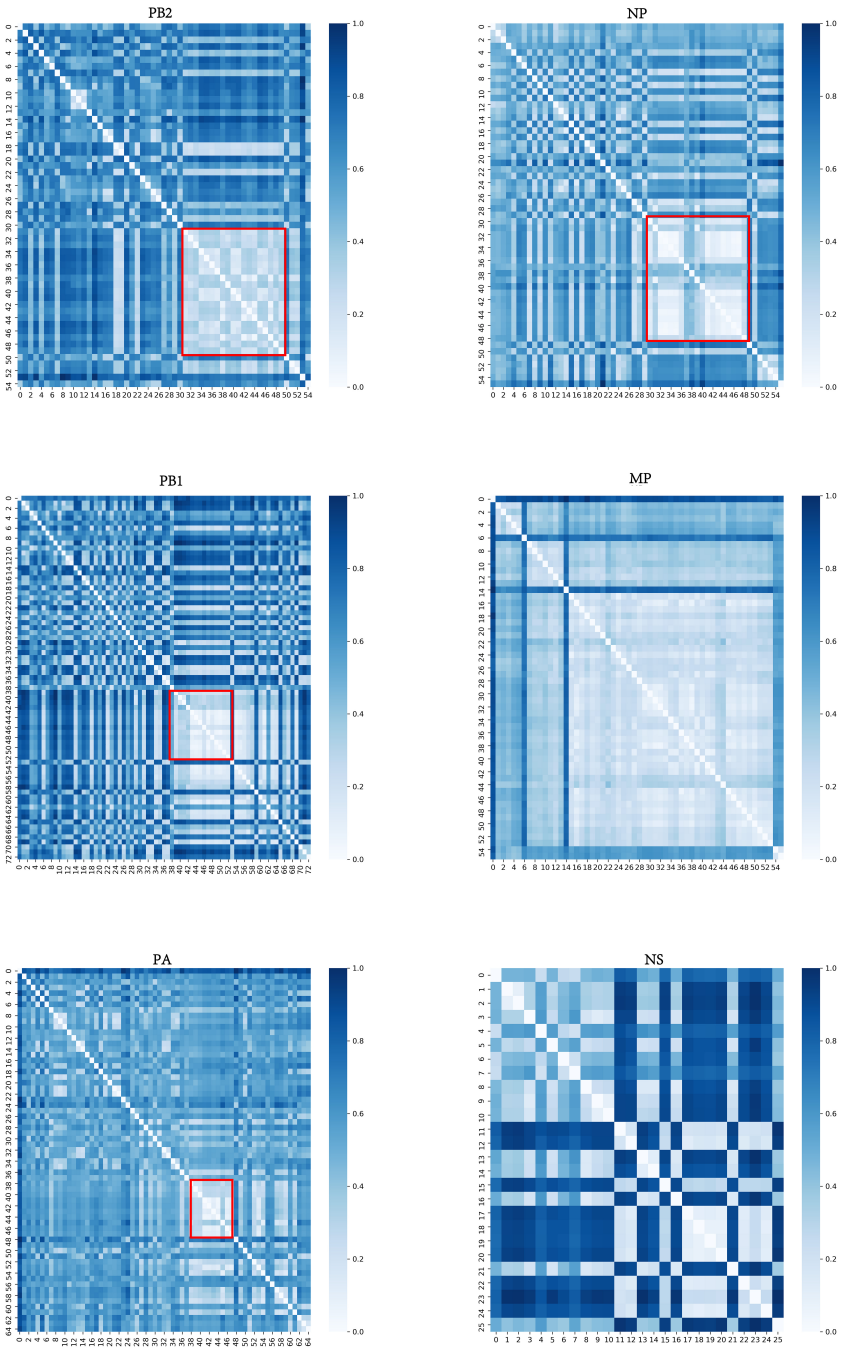


**FIGURE 3 |** Distance matrix of typical clusters of six internal segments. The horizontal and vertical coordinates represent typical clusters. The color shading corresponds to the distance between typical clusters. The darker the color is, the more distant the corresponding two typical clusters are. The light-colored areas (marked by a red box) indicate that those typical clusters have relatively close distances. The distance matrices of MP and NS segments are not marked as they have few significances.

## DISCUSSION

The low pathogenicity and wide distribution of the H9N2 virus make it more likely to be coinfected with other AIV subtypes. As explained above, we consider that the internal segments of the H9N2 virus can be regarded as a gene pool that is in a state of dynamic equilibrium. Avian influenza virus coinfected with the H9N2 virus can be regarded as entering the gene pool of the H9N2 virus, where it may not only provide new internal segments for the gene pool but also receive internal segments from the gene pool and generate novel reassortment AIV subtypes (**Figure 6**). Those internal segments that appear in

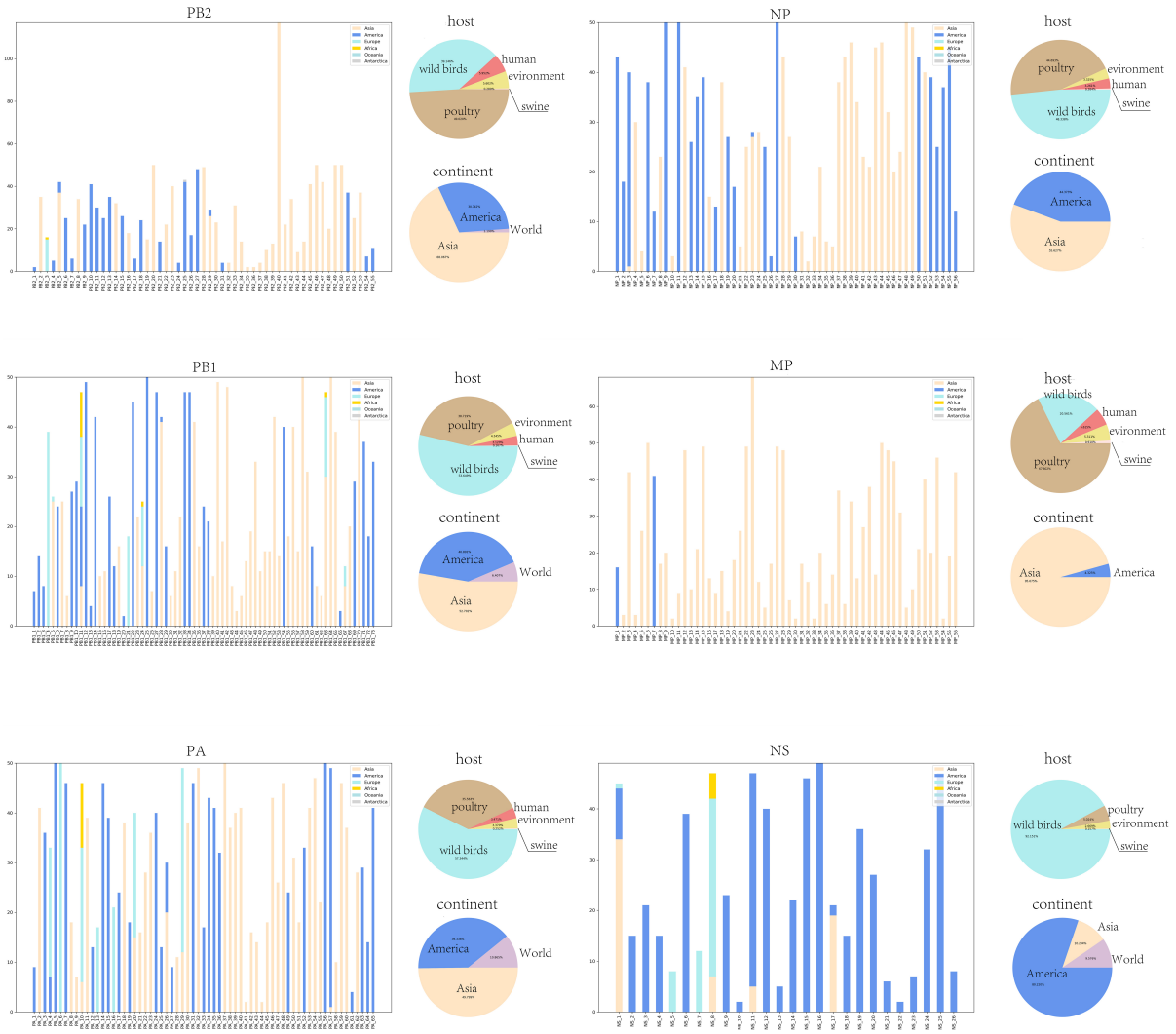


**FIGURE 4 |** Location and host information for typical clusters. The histogram shows the geographical distribution of each typical cluster and the number of strains contained in corresponding regions. The horizontal coordinate of the histogram is the typical cluster number, and the vertical coordinate is the number of strains contained in different regions. The geographical regions counted in the histogram include Asia, America, Europe, Oceania, and Antarctica. The two pie charts show the host species of all strains and their main geographical distributions. The pie chart of host species counts the proportion of five host species including wild birds, human, poultry, swine, and environment. And the pie chart of geographical distributions counts the proportion of three region types including America, Asia, and World.

the gene pool with high frequency constitute the core gene pool of the H9N2 virus.

The establishment of the core gene pool of the H9N2 virus in this article provides new insight into the reassortment characteristics of the H9N2 virus. We conducted systematic phylogenetic analysis and detailed analysis of different characterizations and specific reassortment. The results indicate that the core gene pool of the H9N2 virus affects the evolution direction and geographical distribution of reassortment events related to the H9N2 virus.

The feature vector distance of sequences and the genetic distance of strains show obvious aggregation among strains. Based on the aggregation of different strains, the internal segments of strains can be divided into several typical clusters. The analysis of strain collection locations and collection times indicates that there is geographic isolation among different lineages. The hosts of H9N2 virus and relevant reassortment virus are mainly avian, resulting in rare transmission across continents; this is the main reason for geographic isolation. In

**TABLE 3 |** Relationship between mutation sites and geographic distribution of PB2.

| Location | Mutation site |
|---|---|
| America | 477I, 647M, 452Q, 291M, 450L |
| Asia | 388K, 647V, 273T, 587V, 196N, 597V, 675V, 423S, 105A, 291V |
| Europe | 18V |

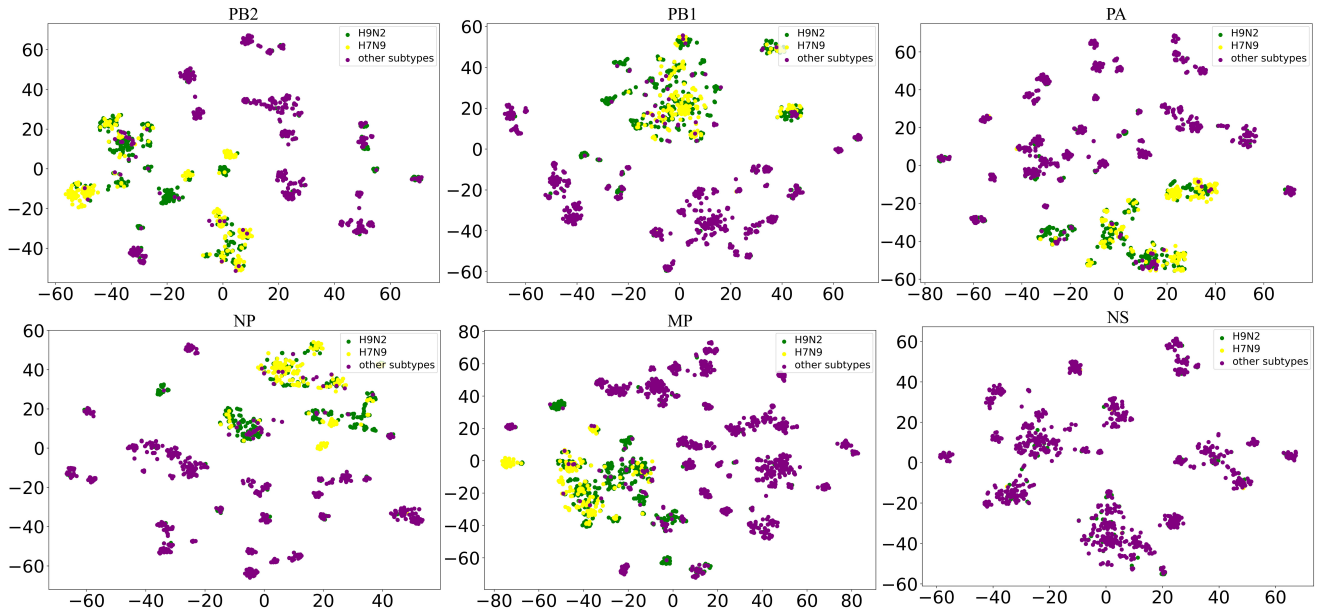


**FIGURE 5 |** Dimensionality reduction scatter plots of H7N9 and H9N2. The horizontal and vertical coordinates are the values of the horizontal and vertical coordinates corresponding to the downscaling of the sequence feature vector to a two-dimensional space, which has no practical significance. A green dot represents a H9N2 virus, while a yellow dot represents a H7N9 virus. The closer the two virus sequence feature vectors are, the more concentrated the two dots are. We only studied the relationship between H9N2 and H7N9, so other AIV subtypes are represented by dark purple dots.

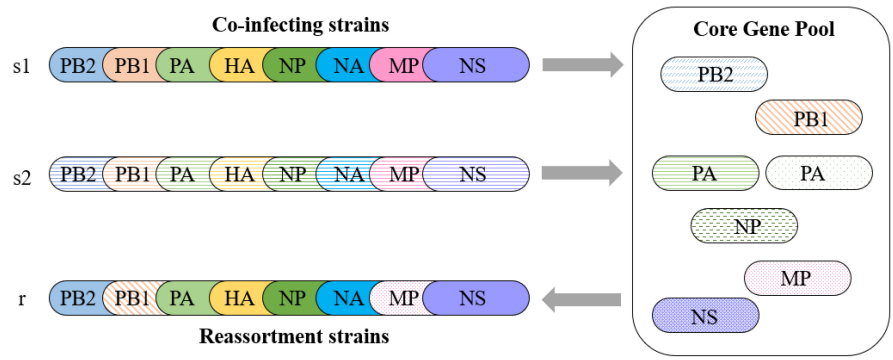


**FIGURE 6 |** Reassortment pattern of the core gene pool. Two strains, s1 and s2, coinfect a host with the H9N2 virus. Strain s1 obtains PB1 and MP internal segments from the core gene pool and produces a reassortment strain r. Strain s2 provides a new PA for the core gene pool.

total, typical clusters located in Asia and the Americas account for the main part of the core gene pool. The distribution differs among different internal segments. Further amino acid mutation site analysis suggests some valuable mutation sites related to geographical distribution. Finally, the analysis of the H7N9 virus visually demonstrated its reassortment relationship with the H9N2 virus, which also verified the rationality of our core gene pool.

It should be noted that the establishment of the core gene pool depends on the existing sequence data. Although we aimed to exclude the impact of sampling bias on the results as much as possible, it is inevitable that our results will differ from the real situation in some ways. Moreover, the analysis of mutation sites in this article is limited to the strains in the core gene pool. We also conducted an analysis of the mutation sites of all available sequences, which produced completely different results. In summary, the core gene pool in this article can help us understand the pattern in which the H9N2 virus donates internal segments during reassortment with other AIV subtypes. In future work, we will further investigated the impact of the core gene pool on the evolution and fitness of the H9N2 virus.

## DATA AVAILABILITY STATEMENT

The original contributions presented in the study are included in the article/**Supplementary Material**, further inquiries can be directed to the corresponding author/s.

## AUTHOR CONTRIBUTIONS

HR, WC, and JY formulated the study. HY and MH performed the research and analyzed the data. BW, YJ, XG, and LL participated in analysis and discussion. HY and HR drafted the manuscript. All authors read and approved the final manuscript.

## FUNDING

This work was supported by the National Natural Science Foundation of China (grant numbers 32070025, 31800136, and 82041019) and Research Project from State Key Laboratory of Pathogen and Biosecurity (grant number SKLPBS1807).

## SUPPLEMENTARY MATERIAL

The Supplementary Material for this article can be found online at: https://www.frontiersin.org/articles/10.3389/fmicb.2021.751142/full#supplementary-material

**Supplementary Figure 1 |** Complete information about typical clusters of PB2.

**Supplementary Figure 2 |** Complete information about typical clusters of PB1.

**Supplementary Figure 3 |** Complete information about typical clusters of PA.

**Supplementary Figure 4 |** Complete information about typical clusters of NP.

**Supplementary Figure 5 |** Complete information about typical clusters of MP.

**Supplementary Figure 6 |** Complete information about typical clusters of NS.

**Supplementary Table 1 |** Complete relationship between mutation sites and geographic distribution of PB2. All mutation information was obtained by comparing the filtered sequence data.

**Supplementary Table 2 |** Complete relationship between mutation sites and geographic distribution of PB1. All mutation information was obtained by comparing the filtered sequence data.

**Supplementary Table 3 |** Complete relationship between mutation sites and geographic distribution of PA. All mutation information was obtained by comparing the filtered sequence data.

**Supplementary Table 4 |** Complete relationship between mutation sites and geographic distribution of NP. All mutation information was obtained by comparing the filtered sequence data.

**Supplementary Table 5 |** Complete relationship between mutation sites and geographic distribution of MP. All mutation information was obtained by comparing the filtered sequence data.

**Supplementary Table 6 |** Complete relationship between mutation sites and geographic distribution of NS. All mutation information was obtained by comparing the filtered sequence data.

## REFERENCES

Bao, Y., Bolotov, P., Dernovoy, D., Kiryutin, B., Zaslavsky, L., Tatusova, T., et al. (2008). The influenza virus resource at the national center for biotechnology information. *J. Virol.* 82, 596–601.

Bi, Y., Li, J., Li, S., Fu, G., and Jin, T. (2020). Dominant subtype switch in avian influenza viruses during 2016–2019 in China. *Nat. Commun.* 11:5909. doi: 10.1038/s41467-020-19671-3

Chen, H. Y., Yuan, H., Gao, R., Zhang, J., Wang, D., Xiong, Y., et al. (2014). Clinical and epidemiological characteristics of a fatal case of avian influenza a H10N8 virus infection: a descriptive study. *Lancet* 383, 714–721. doi: 10.1016/S0140-6736(14)60111-2

Cui, L., Liu, D., Shi, W., Pan, J., Qi, X., Li, X., et al. (2014). Dynamic reassortments and genetic heterogeneity of the human-infecting influenza A (H7N9) virus. *Nat. Commun.* 5:3142. doi: 10.1038/ncomms4142

Gao, R., Cao, B., Hu, Y., Feng, Z., Wang, D., Hu, W., et al. (2013). Human infection with a novel avian-origin influenza A (H7N9) virus. *New England J. Med.* 368, 1888–1897.

Guan, Y., Shortridge, K. F., Krauss, S., and Webster, R. G. (1999). Molecular characterization of H9N2 influenza viruses: were they the donors of the 'internal' genes of H5N1 viruses in Hong Kong? *Proc. Natl. Acad. Sci. U.S.A.* 96, 9363–9367. doi: 10.1073/pnas.96.16.9363

Hoang, D. T., Chernomor, O., von Haeseler, A., Minh, B. Q., and Vinh, L. S. (2018). UFBoot2: improving the ultrafast bootstrap approximation. *Mol. Biol. Evol.* 35, 518–522. doi: 10.1093/molbev/msx281

Hoffmann, E., Stech, J., Leneva, I., Krauss, S., Scholtissek, C., Chin, P. S., et al. (2000). Characterization of the influenza a virus gene pool in avian species in southern china: was H6N1 a derivative or a precursor of H5N1? *J. Virol.* 74, 6309–6315. doi: 10.1128/jvi.74.14.6309-6315.2000

Homme, P. J., and Easterday, B. C. (1970). Avian influenza virus infections. I. characteristics of influenza a/turkey/wisconsin/1966 virus. *Avian. Dis.* 1, 66–74.

Johnson, M., Zaretskaya, I., Raytselis, Y., Merezhuk, Y., McGinnis, S., and Madden, T. L. (2008). NCBI BLAST: a better web interface. *Nucleic Acids Res.* 36, 5–9. doi: 10.1093/nar/gkn201

Kalyaanamoorthy, S., Minh, B. Q., Wong, T. K. F., von Haeseler, A., and Jermiin, L. S. (2017). Model finder: fast model selection for accurate phylogenetic estimates. *Nat. Methods* 14, 587–589. doi: 10.1038/nmeth.4285

Kariin, S., and Burge, C. (1995). Dinucleotide relative abundance extremes: a genomic signature. *Trends Genet.* 11, 283–290. doi: 10.1016/s0168-9525(00)89076-9

Katoh, K., and Standley, D. M. (2013). MAFFT multiple sequence alignment software version 7: improvements in performance and usability. *Mol. Biol. Evolu.* 30, 772–780. doi: 10.1093/molbev/mst010

Kumar, S., Stecher, G., and Tamura, K. (2016). MEGA7: molecular evolutionary genetics analysis version 7.0 for bigger datasets. *Mol. Biol. Evolu.* 33, 1870–1874. doi: 10.1093/molbev/msw054

Li, X., Sun, J., Lv, X., Wang, Y., Li, Y., Li, M., et al. (2020). Novel reassortant avian influenza A(H9N2) virus isolate in migratory waterfowl in hubei province, China. *Front. Microbiol.* 11:220. doi: 10.3389/fmicb.2020.00220

Liu, D., Shi, W., and Gao, G. F. (2014). Poultry carrying H9N2 act as incubators for novel human avian influenza viruses. *Lancet* 383:869. doi: 10.1016/S0140-6736(14)60386-X

Martin, V., Pfeiffer, D. U., Zhou, X., Xiao, X., Prosser, D. J., Guo, F., et al. (2011). Spatial distribution and risk factors of highly pathogenic avian influenza (HPAI) H5N1 in China. *PLoS Pathogens* 7:e1001308. doi: 10.1371/journal.ppat.1001308

Nguyen, L. T., Schmidt, H. A., von Haeseler, A., and Minh, B. Q. (2015). IQ-TREE: a fast and effective stochastic algorithm for estimating maximum likelihood phylogenies. *Mol. Biol. Evol.* 32, 268–274. doi: 10.1093/molbev/msu300

Peacock, T. P., James, J., Sealy, J. E., and Iqbal, M. (2019). A global perspective on H9N2 avian influenza virus. *Viruses* 11:620. doi: 10.3390/v11070620

Peiris, M., Yuen, K. Y., Leung, C. W., Chan, K. H., Ip, P. L. S., Lai, R. W. M., et al. (1999). Human infection with influenza H9N2. *Lancet* 354, 916–917.

Pezzotti, N., Lelieveldt, B. P. F., van der Maaten, L., Höllt, T., and Eisemann, E. (2017). Approximated and user steerable TSNE for progressive visual analytics. *IEEE Trans. Visualiz. Comput. Graphics* 23, 1739–1752. doi: 10.1109/TVCG.2016.2570755

Pu, J., Yin, Y., Liu, J., Wang, X., Zhou, Y., Wang, Z., et al. (2021). Reassortment with dominant chicken H9N2 influenza virus contributed to the fifth H7N9 virus human epidemic. *J. Virol.* 95:e01578-20. doi: 10.1128/JVI.01578-20

Qu, B., Li, X., Cardona, C. J., and Xing, Z. (2020). Reassortment and adaptive mutations of an emerging avian influenza virus H7N4 subtype in China. *PLoS One* 15:e0227597. doi: 10.1371/journal.pone.0227597

Sharp, P. M., Tuohy, T. M., and Mosurski, K. R. (1986). Codon usage in yeast: cluster analysis clearly differentiates highly and lowly expressed genes. *Nucleic Acids Res.* 14, 5125–5143. doi: 10.1093/nar/14.13.5125

Sun, X., Belser, J. A., and Maines, T. R. (2020). Adaptation of H9N2 influenza viruses to mammalian hosts: a review of molecular markers. *Viruses* 12:541. doi: 10.3390/v12050541

Tsirogiannis, C., and Sandel, B. (2014). Computing the skewness of the phylogenetic mean pairwise distance in linear time. *Algor. Mol. Biol.* 9, 15–15. doi: 10.1186/1748-7188-9-15

Yang, L., Zhu, W., Li, X., Chen, M., Wu, J., Yu, P., et al. (2017). Genesis and spread of newly emerged highly pathogenic H7N9 avian viruses in mainland China. *J. Virol.* 91, e01277-17. doi: 10.1128/JVI.01277-17

Yang, Z. F., Mok, C. K. P., Peiris, J. S. M., and Zhong, N.-S. (2015). Human infection with a novel avian influenza A (H5N6) virus. *New England J. Med.* 373, 487–489.

Zhang, T., Ramakrishnan, R., and Livny, M. (1996). BIRCH: an efficient data clustering method for very large databases. *Proc. Int. Conf. Manage. Data* 25, 103–114.

**Conflict of Interest:** The authors declare that the research was conducted in the absence of any commercial or financial relationships that could be construed as a potential conflict of interest.

frontiers in Microbiology

ORIGINAL RESEARCH
published: 16 December 2021
doi: 10.3389/fmicb.2021.793500

# Reassortment Network of Influenza A Virus

*Xingfei Gong[1,2†], Mingda Hu[1†], Wei Chen[2†], Haoyi Yang[1,2], Boqian Wang[1], Junjie Yue[1], Yuan Jin[1*], Long Liang[1*] and Hongguang Ren[1*]*

[1] State Key Laboratory of Pathogen and Biosecurity, Beijing Institute of Biotechnology, Beijing, China, [2] College of Computer, National University of Defense Technology, Changsha, China

Influenza A virus (IAV) genomes are composed of eight single-stranded RNA segments. Genetic exchange through reassortment of the segmented genomes often endows IAVs with new genetic characteristics, which may affect transmissibility and pathogenicity of the viruses. However, a comprehensive understanding of the reassortment history of IAVs remains lacking. To this end, we assembled 40,296 whole-genome sequences of IAVs for analysis. Using a new clustering method based on Mean Pairwise Distances in the phylogenetic trees, we classified each segment of IAVs into clades. Correspondingly, reassortment events among IAVs were detected by checking the segment clade compositions of related genomes under specific environment factors and time period. We systematically identified 1,927 possible reassortment events of IAVs and constructed their reassortment network. Interestingly, minimum spanning tree of the reassortment network reproved that swine act as an intermediate host in the reassortment history of IAVs between avian species and humans. Moreover, reassortment patterns among related subtypes constructed in this study are consistent with previous studies. Taken together, our genome-wide reassortment analysis of all the IAVs offers an overview of the leaping evolution of the virus and a comprehensive network representing the relationships of IAVs.

**Keywords: influenza A virus, evolution, reassortment, network, cross-species**

OPEN ACCESS

***Edited by:***
*Quanjiao Chen,*
*Wuhan Institute of Virology, Chinese Academy of Sciences (CAS), China*

***Reviewed by:***
*Guan-Zhu Han,*
*Nanjing Normal University, China*
*Haizhou Liu,*
*Wuhan Institute of Virology, Chinese Academy of Sciences (CAS), China*

***Correspondence:**
*Hongguang Ren*
*bioren@163.com*
*Long Liang*
*ll@bmi.ac.cn*
*Yuan Jin*
*jin_0220@sina.com*

*† These authors have contributed equally to this work*

***Specialty section:***
*This article was submitted to Virology, a section of the journal Frontiers in Microbiology*

***Received:*** *12 October 2021*
***Accepted:*** *12 November 2021*
***Published:*** *16 December 2021*

***Citation:***
*Gong X, Hu M, Chen W, Yang H, Wang B, Yue J, Jin Y, Liang L and Ren H (2021) Reassortment Network of Influenza A Virus. Front. Microbiol. 12:793500. doi: 10.3389/fmicb.2021.793500*

## INTRODUCTION

Influenza A Virus (IAV) is a highly infectious viral pathogen that causes seasonal epidemics, occasional pandemics, and zoonotic outbreaks, which may lead to substantial human morbidity and mortality and a considerable financial burden worldwide (Liu et al., 2020). It has been more than 100 years since the Spanish flu (H1N1) virus caused the first recorded influenza pandemic, which is considered to be the most lethal natural event in modern history (Smith, 2011; Liu et al., 2018). Since then, there have been three other pandemics caused by A(H2N2), A(H3N2), and A(H1N1)pdm09 viruses—the 1957 Asian flu, the 1968 Hong Kong flu, and the 2009 swine-origin flu, respectively. There are currently 18 HA (hemagglutinin) subtypes and 11 NA (neuraminidase) subtypes in IAVs, most of which spread in wild birds. Comparatively, only three combinations of HA and NA subtypes are known to be widespread in humans: H1N1, H2N2, and H3N2, of which H1N1 and H3N2 subtype viruses cause seasonal epidemics (Petrova and Russell, 2018). The WHO estimated that seasonal influenza viruses infect 5–15% of the human population each year, causing approximately 500,000 deaths worldwide (Stohr, 2002).

As segmented RNA viruses, IAVs can exchange the gene segments through reassortment during co-infection. Specifically, when two or more IAVs infect the same cell, a hybrid virus can be produced by assembling the gene segments of the parental viruses into a nascent virion (McDonald et al., 2016). Reassortment and mutation are both the main driving forces for the evolution of IAVs. However, the effect caused by mutations needs to be accumulated for a long time, while the reassortment is often a leapfrog evolution. Reassortment also plays an important but unclear role in the emergence of the novel viruses and cross-species transmission (Dhanasekaran et al., 2015). The virus that caused the 2009 H1N1 pandemic was generated from a triple-reassortment of H1N1 avian virus, H1N1 classical swine virus, and H3N2 human seasonal virus (Smith et al., 2009). Furthermore, swine has been considered as the "mixing vessels" for IAVs since there are both α-2,3 and α-2,6 sialic acids (SAs) in their respiratory tracts, which provides conditions for the occurrence of reassortment (Ma et al., 2009).

In recent years, a lot of studies for IAVs are based on mutations, especially in the receptor binding region on HA segment, while the study on reassortment detection method and the reassortment history of IAVs is relatively few. Rabadan et al. (2008) proposed a method to detect reassortment by comparing the sequence differences between two viruses. This method considered that the number of differences in each segment sequence of two viruses should be proportional if there is no reassortment. Another algorithm was proposed by de Silva et al. (2012) based on the neighborhood of strains, which determined the reassortant virus by the size of the common neighborhood of two segments. Muller et al. (2020) used a coalescent-based model to study the reassortment pattern of different human influenza datasets and found that the reassortment rates of different human influenza viruses are very different. These rare researches on IAVs reassortment tend to focus on viruses causing a single epidemic or with a single subtype, resulting in a lack of overall understanding of the reassortment history of IAVs. Ding et al. (2020) collected the reassortment events of influenza A virus from published literature and constructed the FlueReassort database. In our work, we proposed a novel genotype nomenclature for IAVs and used it to detect the reassortment in IAV genomes. The reassortment history and gene flow network were constructed, by which we found the characteristics and patterns in frequent reassortment events of IAVs.

# MATERIALS AND METHODS

## Data Preparation and Processing

We assembled all the whole-genomes sequences of IAVs as of October 13, 2020, from the National Centre for Biotechnology Information (NCBI) website resources.[1] After quality control, we obtained 40,296 genomes of IAVs with complete sequence length and essential epidemiological information. Multiple sequence alignment for each segment was performed using MAFFT v7.037 (Katoh and Standley, 2013). To remove redundancy of sampling, we further filtered the genome sequences. Genome sequences with the same host, location, subtype, sampling year, and sharing similarities over 99% were resampled. The relationships among represent strains and other strains were shown in **Supplementary Table 1**.

The phylogenetic tree was reconstructed for each segment by IQ-TREE (Nguyen et al., 2015) using PhyloSuite platform (Zhang et al., 2020) with the GTR + I + G4 + F substitution model. Bat IAVs are used as outgroups to root the trees. We divided the hosts of these IAVs into human, swine, and avian. The avian hosts were further divided into shorebirds, waterfowl, land birds, and domestic birds. The avian host classifications are shown in **Supplementary Table 2**. The locations of the strains were mapped onto 22 areas according to the administrative division, including North America, Western Europe, and East Asia (**Supplementary Table 3**).

## Segment Detailed Type Determination

In order to quantitatively divide the clade of each segment of the virus, we clustered the leaf nodes in the evolutionary tree based on the Mean Pairwise Distance (MPD). Therefore, sequences of each segment of IAVs were divided into different detailed types. MPD is the mean phylogenetic distance between the leaf nodes of an internal node on the phylogenetic tree. For example, the MPD of an internal node with $n$ leaf nodes on PB1 segment phylogenetic tree is calculated as:

$$MPD = \frac{\sum_i^n \sum_j^n \delta_{i,j}}{\binom{n}{2}}$$

$\delta_{i,j}$ is the phylogenetic distance between leaf node $i$ and leaf node $j$. $\binom{n}{2}$ represents the combination number formula. The mean MPD of all internal nodes was used as a threshold to define the leaf nodes of an internal node as a specific cluster, namely a detailed type. We then assigned an index to each detailed type. For example, PB1_1 represents a detailed type of PB1 segment, consisting of a cluster of PB1 sequences.

## Genotype Nomenclature

In the work of Lu et al. (2007), the genotype was defined as the combination of the lineages for each segment in an IAV genome. In this manuscript, the genotype of an IAV genome was defined as the sequential combination of the detailed type for each segment. For example, PB2_292, PB1_415, PA_333, HA_422, NP_463, NA_405, MP_369, and NS_406 is the genotype of a H7N9 virus.

## Reassortment Definition and Identification

A direct way to detect the reassortment of IAVs is to compare the positions on phylogenetic trees of different segments of the genome (Nelson et al., 2008). Based on our genotype nomenclature, a reassortment was defined as a mixation or overlapping of the different genotype combinations. The mixation of different genotype combinations can be understood

[1] https://ftp.ncbi.nih.gov/genomes/INFLUENZA/

as the exchange of segments among different genotypes. If the genotype of a virus can be produced by the combination of the genotypes for two or more parental viruses and their epidemiological information is related, then we consider that this virus might be reassorted from these parental viruses. There may be more than one possible combination of parental viruses to generate the reassortant child. For each strain of each genotype, we screened all the genomes sampled within 5 years before the strain to find the most possible reassortment event with the least evolutionary cost, which was calculated as follows:

$$cost = locNum \cdot parNum + hostNum \cdot parNum + (maxYear - minYear)$$

where *locNum*, *hostNum*, *parNum* is the number of locations, hosts, and parental viruses involved in the reassortment event. *maxYear* and *minYear* is the latest and the earliest year of the parental viruses. In this manuscript, only double-reassortment and triple-reassortment events are examined, as reassortment among more than three strain viruses is considered highly unlikely.

## Gene Flow Network Construction

A connecting network can be constructed using the genotypes as nodes and the relationships among genotypes as edges. We calculated two distance values, *dist* and *diff*, between each pair of genotypes, where *dist* is the number of different segment detailed types between two genotypes, *diff* is the minimum difference of hosts, locations, and sampling years combined among the viruses contained in the genotypes. A minimum spanning tree (MST), representing the gene flow network of IAVs, was established by traversing the network in pursuing the minimal reassortment cost. The MST was visualized using cystoscope v3.6.0 (Shannon et al., 2003).

# RESULTS

## Genotype Definition for Influenza A Virus

We obtained 8,932 high-quality and nonredundant representative IAV genomes from 40,296 whole-genome database, where each segment of IAVs was divided into a detailed type. The segments of IAVs showed high diversity in **Table 1**, in which each segment was divided into hundreds of detailed types. As an example, we showed the detailed type determination result for PB1 segment in **Figure 1**. We listed the year range, hosts, locations, and subtypes where the detailed type emerged. The detailed type determination results for other segments are shown in **Supplementary Figures 1–7**. After determining the detailed types for all segments of IAVs, we got the genotypes of all the IAV genomes, which consists of 6,888 unique genotypes. In fact, these 6,888 genotypes represent the genotypes of the previous 40,296 viruses since each filtered virus can use the genotype of its representative virus as its genotype. The genotype of each virus is shown in **Supplementary Table 4**.

**TABLE 1 |** The number of detailed types for each segment.

| Segment | No. of detailed types |
|---|---|
| PB2 | 534 |
| PB1 | 563 |
| PA | 561 |
| HA | 633 |
| NP | 609 |
| NA | 600 |
| MP | 493 |
| NS | 663 |

## Reassortment Detection

Combining the genotype and the epidemiological information of the virus, we immediately knew a segment detailed type had occurred in which year, which host, which location, and which subtype. Meanwhile, for each segment of the IAV to be analyzed, we also knew which virus had the same segment detailed type. These viruses with identical segment detailed types may provide the reassortment source for the virus in analysis. We showed the result of reassortment analysis for the virus (A/WuXi/0409/2014) in **Figure 2**, where the viruses with identical segment detailed types were listed. The genotype of this H7N9 virus is PB2_292, PB1_415, PA_333, HA_422, NP_463, NA_405, MP_369, and NS_406. Each segment detailed type had spread widely before the virus emerged, indicating that the virus had a high possibility to be a reassortant virus. Later we attempted to identify the reassortment source and found that the virus might be generated from a triple-reassortment of H7N9 virus (A/chicken/Huzhou/3791/2013), H9N2 virus (A/chicken/Suzhou/4954/2013), and H9N2 virus (A/chicken/Jiangsu/SIC11/2013) (**Figure 3**). The triple reassortant virus acquired its HA and NA segments from H7N9 virus (A/chicken/Huzhou/3791/2013). The PB2, PA, NP, and MP segments were derived from the H9N2 virus (A/chicken/Suzhou/4954/2013). Another H9N2 virus (A/chicken/Jiangsu/SIC11/2013) provided PB1 and NS segments for the triple reassortant virus. In a word, the H7N9 virus (A/WuXi/0409/2014) obtained HA and NA segments from its parental H7N9 virus, and internal segments from its parental H9N2 viruses. Obviously, with our segment detailed type determination and genotype nomenclature, it will be an easy task to detect reassortment for IAVs.

## The Reassortment History of Influenza A Virus

In order to construct the reassortment history of IAVs, we detected the reassortment events for all viruses in our dataset, using the method we proposed above. The result of reassortment history was shown in **Figure 4**, in which we displayed each reassortment event as the connections from the parental viruses to the reassortant strain. We also showed another form of the result in **Supplementary Figure 8**. It should be noted that the reassortment event we detected first emerged in North America, but this does not mean that the origin of IAVs was in North

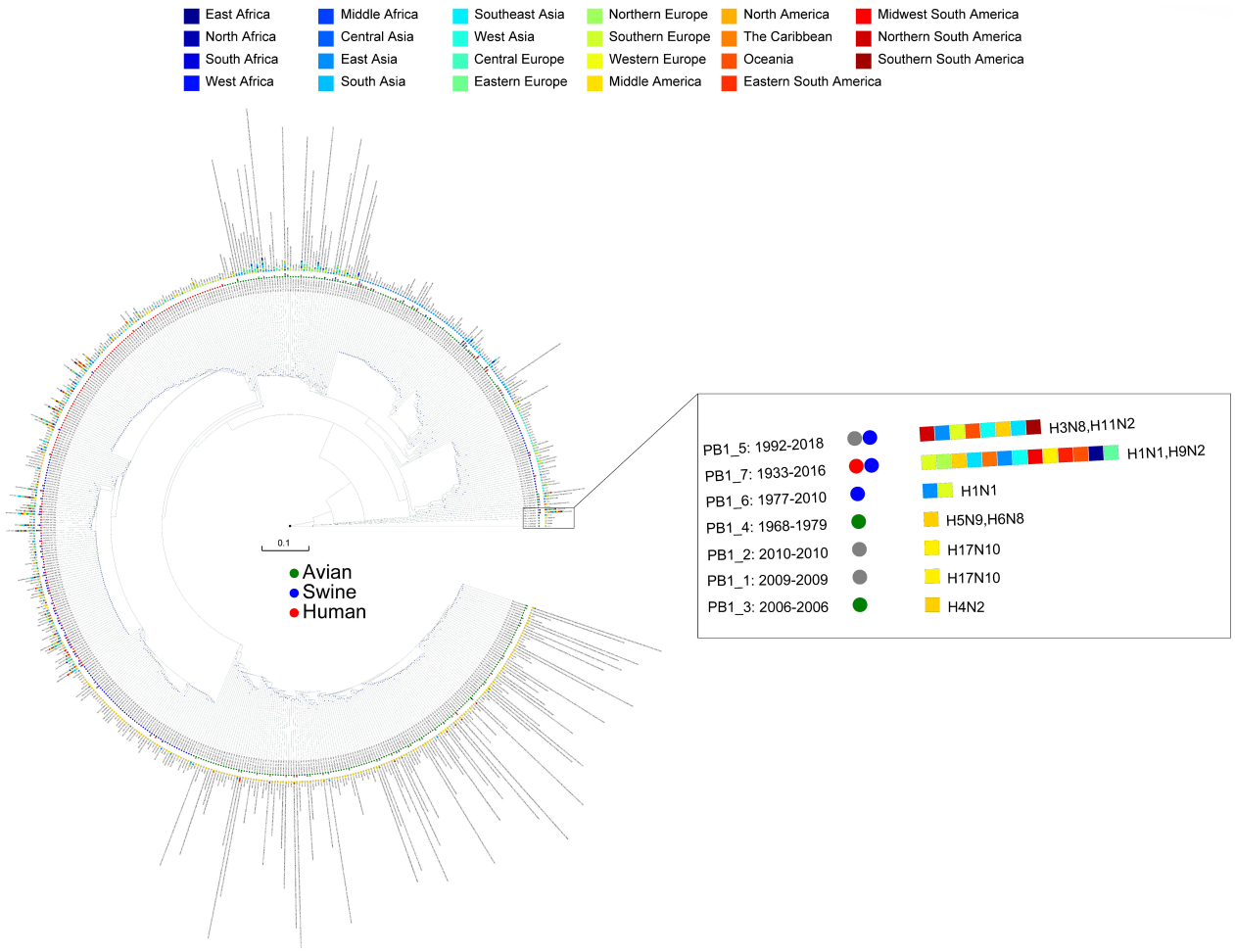


**FIGURE 1 |** The detailed type result for PB1 segment. The year range, hosts, locations, and subtypes are shown after each PB1 type, where the circles represent hosts and the rectangles represent locations. The hosts and locations are distinguished by different colors.

America, since the early sequencing technology around the world was not as advanced as it is now. The reassortment history of IAVs generally reflects the reassortant trend, in which we can know which locations and which hosts are more likely to generate reassortment. In our work, we found that the frequency of inter-locations reassortment is high in various locations of Asia and Europe, which can be illustrated from the large number of red lines in these locations in **Figure 4**. Although the number of reassortment events in North America is large, most of them are intra-locations reassortment. This finding was also reflected in **Figure 5**, in which we counted the number of reassortment events in different locations each year.

## Swine Act as an Intermediate Host in the Reassortment History of Influenza A Virus

In reassortment history of IAVs above, we limited the number of reassortment sources due to the limitation of calculation. The reassortment of IAVs is complicated, since the genome of an IAV can come from 8 different viruses at most. In order to analyze how the genes of IAVs are transmitted during the reassortment, we constructed the gene flow network as shown in **Figure 6**. The network was composed of nodes and edges, where each node was a genotype of IAVs, and the edge represented gene segment flow by reassortment between two genotypes. It should be noted that we found some conclusions which is consistent with previous studies after we added the host information to the network. Swine as an intermediate host played an important role in the gene flow between avian and human IAVs, which can be seen from the swine host nodes in the figure as the hub connecting the avian host nodes and the human host nodes. Actually, it is universally acknowledged that swine are the "mixed vessels" for IAVs since they can be infected by both avian and human IAVs and facilitate the reassortment events of the IAVs (Chastagner et al., 2018). Meanwhile, due to the global live swine trade, swine also play a crucial role in the global spread of IAVs, which provides the possibility of cross-locations reassortment for IAVs (Nelson et al., 2015). Therefore, our result on swine as an intermediate host is consistent with previous studies on the role of swine.

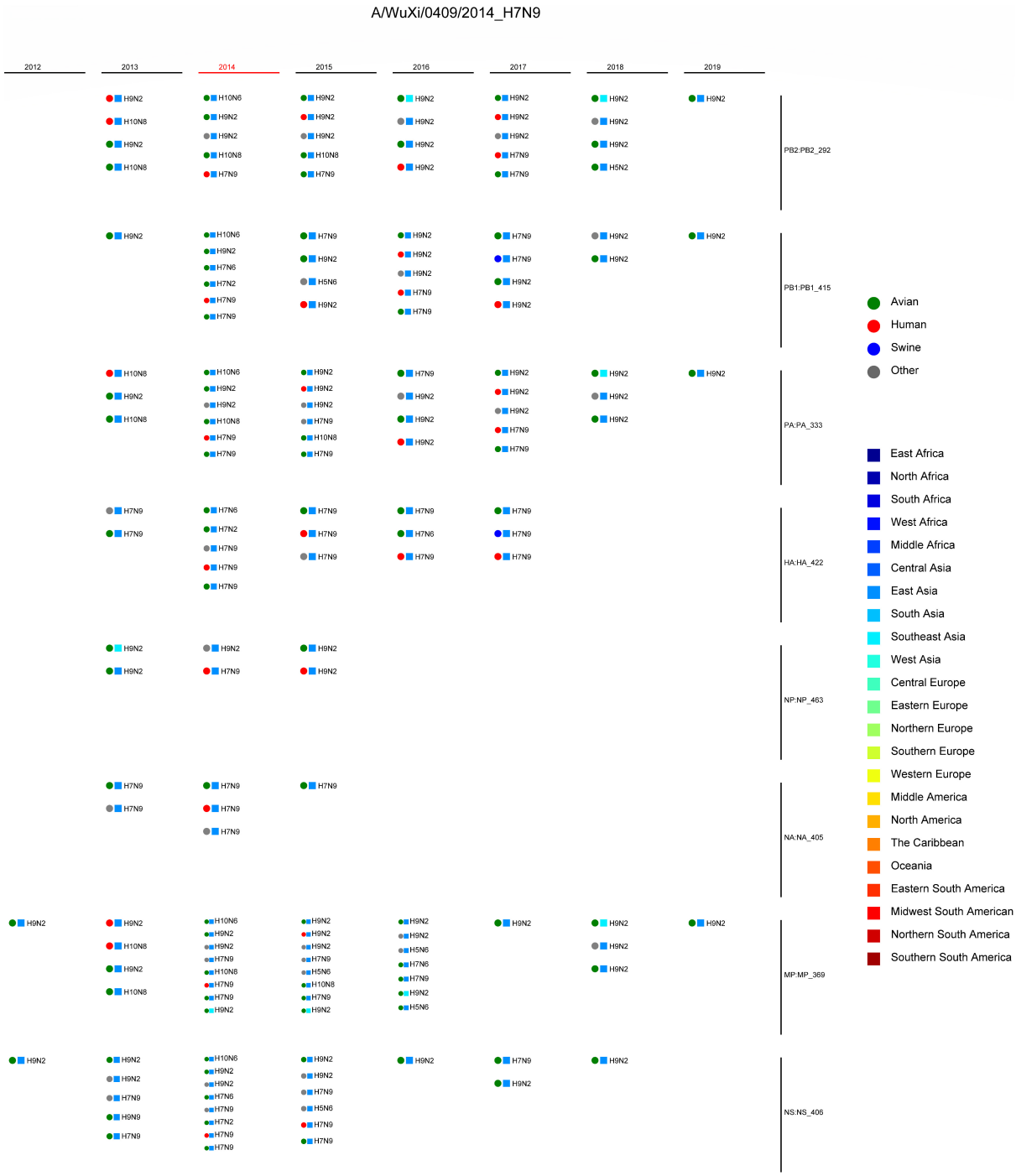


**FIGURE 2 |** Reassortment analysis for the virus (A/WuXi/0409/2014). The genotype of the virus is PB2_292, PB1_415, PA_333, HA_422, NP_463, NA_405, MP_369, and NS_406. The information of the viruses with the same segment detailed types is shown, including host, location, subtype, and year. The circles represent hosts, and the rectangles represent locations, both of which are distinguished by different colors.

## Frequent Reassortment Between H9N2 and H7N9 Viruses

Analyzing the subtypes of IAVs reassortment can also help us understand the patterns of the reassortment. The avian influenza viruses with H9N2 subtype are widely distributed in different regions of China, and provide internal segments for IAVs for other subtypes, which poses a serious threat to public health (Liu et al., 2014). In our study, we also found a similar result after we added the subtype information to the gene flow network. It has been shown in **Supplementary Figure 9** that there are many

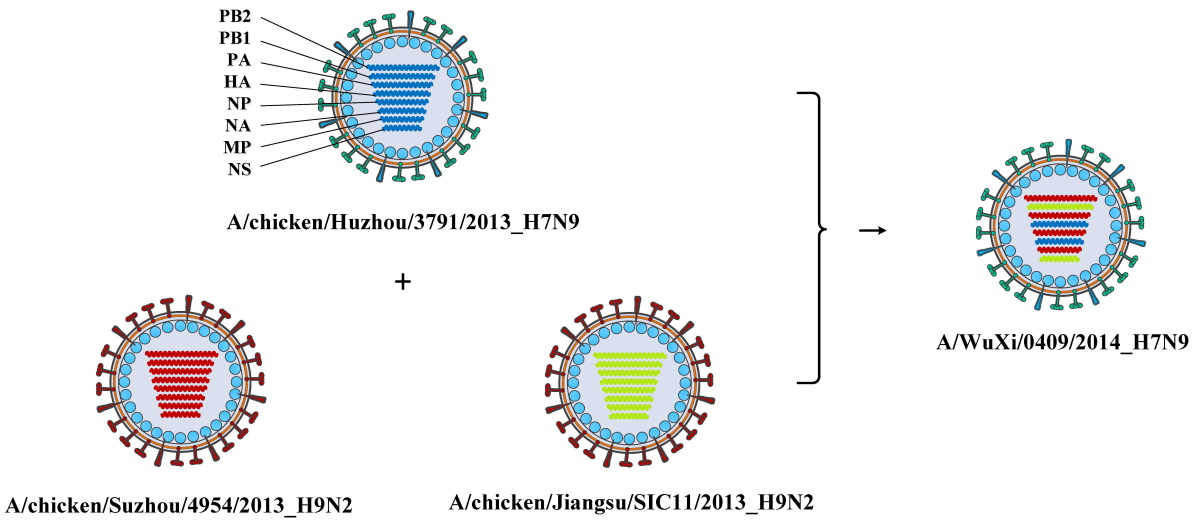


**FIGURE 3 |** The reassortment source of the virus (A/WuXi/0409/2014). The virus was produced by a triple-reassortment of the virus (A/chicken/Suzhou/4954/2013), the virus (A/chicken/Huzhou/3791/2013), and the virus (A/chicken/Jiangsu/SIC11/2013). The genotype of the virus (A/chicken/Huzhou/3791/2013) is PB2_309, PB1_396, PA_284, HA_422, NP_561, NA_405, MP_467, and NS_406, which is indicated by blue. The genotype of the virus (A/chicken/Suzhou/4954/2013) is PB2_292, PB1_252, PA_333, HA_523, NP_463, NA_285, MP_369, and NS_387, which is indicated by red. The genotype of the virus (A/chicken/Jiangsu/SIC11/2013) is PB2_310, PB1_415, PA_307, HA_536, NP_545, NA_385, MP_467, and NS_406, which is indicated by green. The reassortant virus obtained HA and NA segments from an H7N9 virus, and internal segments from two H9N2 viruses.

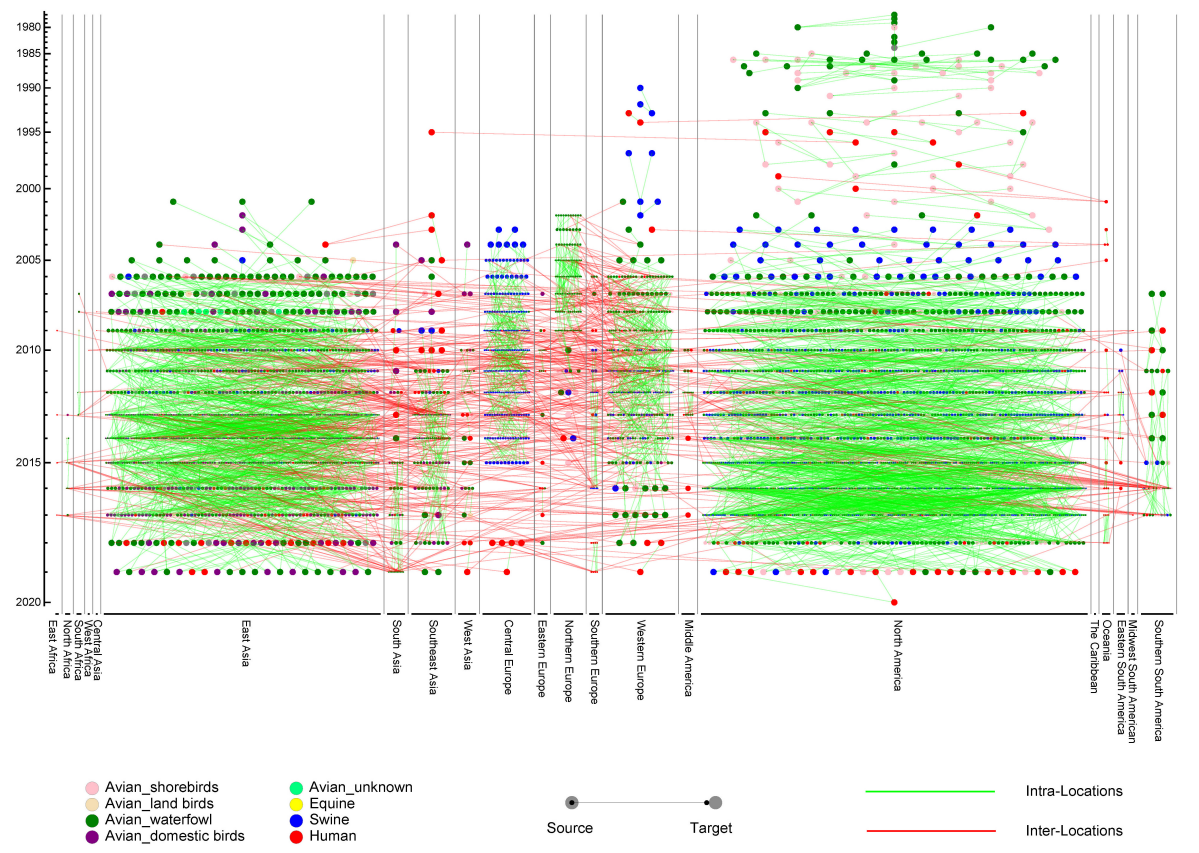


**FIGURE 4 |** The reassortment history of influenza A virus (IAVs). The horizontal axis represents the locations, while the vertical axis represents the years. Each circle represents a virus, with different colors to indicate the hosts. The line from source to target represents the parental virus which produces the reassortant virus. Intra-locations and inter-locations reassortment are indicated by green and red lines, respectively.

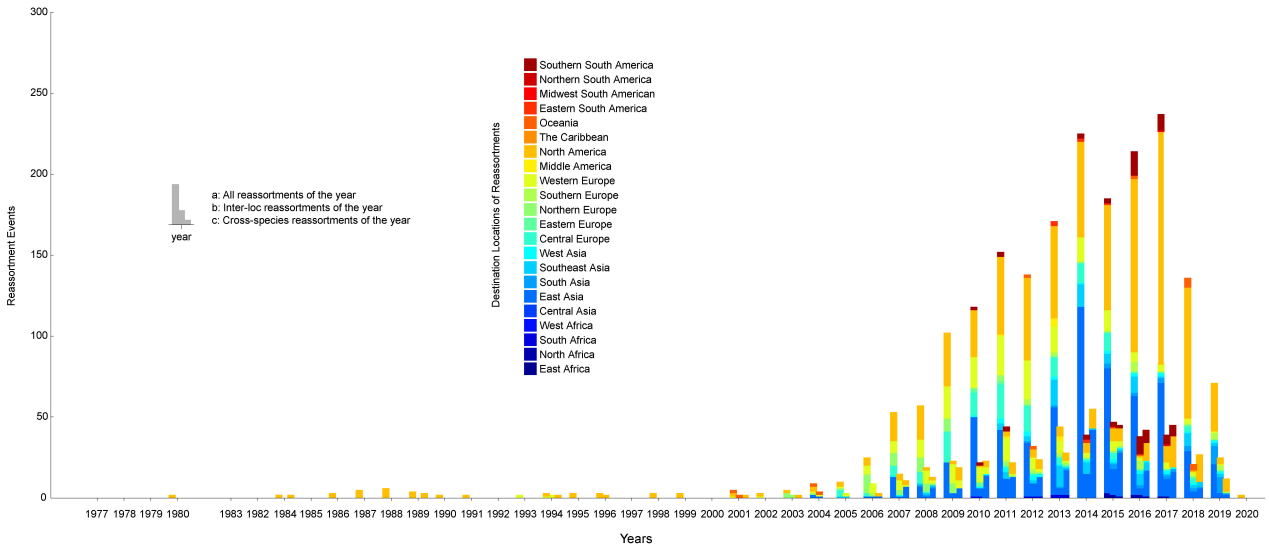


**FIGURE 5 |** The number of reassortment events per year in different locations. The horizontal axis represents the years, and the vertical axis represents the number of reassortment events. The locations of the reassortant viruses are distinguished by different colors. The number of reassortment events per year was divided into three types for statistics: all reassortments, inter-location reassortments, and cross-species reassortments.

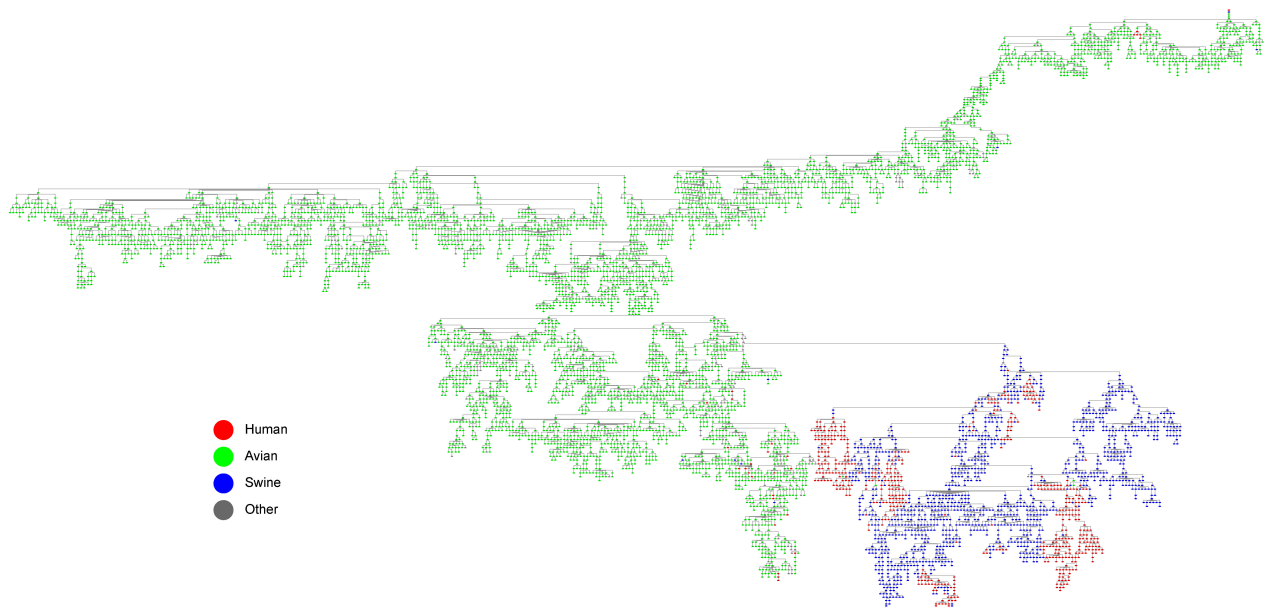


**FIGURE 6 |** The gene flow network of IAVs (with host information annotated). Each node is a genotype of IAVs, and the edge represents gene segment flow by reassortment between two genotypes. The hosts are distinguished by different colors, where red represents human, green represents avian, blue represents swine, and gray represent other hosts.

intersections between H9N2 and H7N9 viruses, which means that frequent reassortments occurred in IAVs with such subtypes. Later we found that almost all these viruses originated from domestic birds in East Asia (**Supplementary Figure 10**). It has been demonstrated that H9N2 has replaced H5N6 and H7N9 as the dominant AIV subtype in both chickens and ducks of China, and the novel viruses generated from reassortment continued to appear and spread among the avian hosts (Bi et al., 2020). The internal segments of some H9N2 viruses have acquired fitness in humans, while viruses with other subtypes such as H7N9 can acquire this fitness through reassortment with them (Liu et al., 2013; Zhang et al., 2013; Lu et al., 2014). The reassortment analysis for the H7N9 virus (A/WuXi/0409/2014) (**Figure 3**) revealed that the virus obtained HA and NA segments from its parental H7N9 virus and internal segments from its parental H9N2 viruses. It is noteworthy that this reassortant virus was

sampled from a human and its parental viruses originated from domestic birds. In other words, the parental viruses completed cross-species transmission through this reassortment patter.

## DISCUSSION

In order to verify the correctness of our clustering method, we used the unified nomenclature system for the highly pathogenic H5N1 avian influenza viruses (WHO, 2011) to cluster HA segments of H5N1 viruses in the database and compared with our result. The unified nomenclature system used three specific clade definition criteria: sharing of a common (clade-defining) node in the phylogenetic tree; monophyletic grouping with a bootstrap value of $\geq$60 at the clade-defining node; and average percentage pairwise nucleotide distances between and within clades of $>$1.5% and $<$1.5%. We marked the clustering results of the two methods on the phylogenetic tree, which was shown in **Supplementary Figure 11**. The inner circle was the clustering result of the unified nomenclature system, and the outer circle was our clustering result. The clustering result of the unified nomenclature system was more detailed than ours, but the clustering boundaries of the two methods were mostly synchronized.

Influenza A Virus are rapidly evolving through reassortment, posing a huge challenge to vaccine development and a serious threat to public health. Traditional studies in IAVs reassortment often focus on the specific virus that causes a certain epidemic, lacking a systematic understanding of IAVs reassortment history. In the present study, we divided each segment of IAVs into detailed types according to the Mean Pairwise Distance (MPD) on the phylogenetic trees. A new method was proposed to define the genotype of IAVs, and the genotype nomenclature was then exploited to analyze whole genomes of IAVs and detect the reassortment. Generally, all the segments of the virus should be compared comprehensively when detecting the reassortment source of IAVs, rather than considering only a single segment. If some segments of a virus have high homology with a parental virus and low homology with another parental virus, and the circumstance in other segments is opposite, the virus is likely to be generated from a reassortment of the two parental viruses (Tian et al., 2011). The reassortment detection method in our work not only compared the source of each segment but also considered the epidemiological information of the IAVs, which is more reasonable. Different from previous reassortment detection method (Suzuki, 2010; Niranjan and Carl, 2011; Yurovsky and Moret, 2011; Svinti et al., 2013), we quantitatively represent the inconsistency of the phylogenetic trees as different segment detailed types. Meanwhile, the results produced by our method are consistent with previous studies, which confirms the effectiveness of our method. Therefore, the method we proposed can indeed effectively define the genotype of IAV and detect the reassortment, especially for large-scale data sets.

Our result only listed the reassortment events we found. Some IAVs were generated from reassortment but we did not detect them because their parental viruses could not be found due to insufficient sampling or incomplete information. Our research was based on the sequence data and the epidemiological information, which benefits from the continuous monitoring and sequencing of IAVs by researchers around the world.

Taken together, we proposed a novel reassortment detection method based on our genotype nomenclature and systematically studied the history and patterns of reassortment in IAVs, which will be beneficial for the prevention and control of IAVs worldwide.

## DATA AVAILABILITY STATEMENT

The original contributions presented in the study are included in the article/**Supplementary Material**, further inquiries can be directed to the corresponding authors.

## AUTHOR CONTRIBUTIONS

HR and LL formulated the study. XG, MH, and WC performed the research and analyzed the data. HY, BW, JY, and YJ participated in analysis and discussion. XG and HR drafted the manuscript. All authors read and approved the final manuscript.

## FUNDING

This work was supported by the National Natural Science Foundation of China (Grant Numbers 32070025, 31800136, and 82041019), and the Research Project from State Key Laboratory of Pathogen and Biosecurity (Grant Number SKLPBS1807).

## SUPPLEMENTARY MATERIAL

The Supplementary Material for this article can be found online at: https://www.frontiersin.org/articles/10.3389/fmicb.2021.793500/full#supplementary-material

## REFERENCES

Bi, Y., Li, J., Li, S., Fu, G., Jin, T., Zhang, C., et al. (2020). Dominant subtype switch in avian influenza viruses during 2016–2019 in China. *Nat. Commun.* 11:5909. doi: 10.1038/s41467-020-19671-3

Chastagner, A., Herve, S., Bonin, E., Queguiner, S., Hirchaud, E., Henritzi, D., et al. (2018). Spatio-temporal distribution and evolution of the A/H1N1 2009 pandemic virus in pigs in France from 2009 to 2017: identification of a potential swine-specific lineage. *J. Virol.* 92, e00988-18. doi: 10.1128/JVI.00988-18

de Silva, U. C., Tanaka, H., Nakamura, S., Goto, N., and Yasunaga, T. (2012). A comprehensive analysis of reassortment in influenza A virus. *Biol. Open* 1, 385–390.

Dhanasekaran, V., Mukerji, R., and Smith, G. (2015). RNA virus reassortment: an evolutionary mechanism for host jumps and immune evasion. *PLoS Pathog.* 11:e1004902. doi: 10.1371/journal.ppat.1004902

Ding, X., Yuan, X., Mao, L., Wu, A., and Jiang, T. (2020). FluReassort: a database for the study of genomic reassortments among influenza vi-ruses. *Brief Bioinform.* 21, 2126–2132. doi: 10.1093/bib/bbz128

Katoh, K., and Standley, D. (2013). MAFFT multiple sequence alignment software version 7: improve-ments in performance and usability. *Mol. Biol. Evol.* 30, 772–780. doi: 10.1093/molbev/mst010

Liu, D., Shi, W., and Gao, G. F. (2014). Poultry carrying H9N2 act as incubators for novel human avian influ-enza viruses. *Lancet* 383, 869–869. doi: 10.1016/S0140-6736(14)60386-X

Liu, D., Shi, W., Shi, Y., Wang, D., Xiao, H., Li, W., et al. (2013). Origin and diversity of novel avian influenza A H7N9 viruses causing human infection: phylogenetic, structural, and coalescent analyses. *Lancet* 381, 1926–1932. doi: 10.1016/S0140-6736(13)60938-1

Liu, W., Bi, Y., Wang, D., and Gao, G. F. (2018). On the centenary of the Spanish flu: being prepared for the next pandemic. *Virol. Sin.* 33, 463–466. doi: 10.1007/s12250-018-0079-1

Liu, W. J., Wu, Y., Bi, Y., Shi, W., Wang, D., Shi, Y., et al. (2020). Emerging HxNy influenza A viruses. *Cold Spring Harb. Perspect. Med.* a038406. doi: 10.1101/cshperspect.a038406

Lu, G., Rowley, T., Garten, R., and Donis, R. O. (2007). FluGenome: a web tool for genotyping influenza A virus. *Nucleic Acids Res.* 35, W275–W279. doi: 10.1093/nar/gkm365

Lu, J., Wu, J., Zeng, X., Guan, D., Zou, L., Yi, L., et al. (2014). Continuing reassortment leads to the genetic diversity of Influenza virus H7N9 in Guangdong, China. *J. Virol.* 88, 8297–8306. doi: 10.1128/jvi.00630-14

Ma, W., Kahn, R. E., and Richt, J. A. (2009). The pig as a mixing vessel for influenza viruses: human and vet-erinary implications. *J. Mol. Genet. Med. Int. J. Biomed. Res.* 3, 158–166.

McDonald, S. M., Nelson, M. I., Turner, P. E., and Patton, J. T. (2016). Reassortment in segmented RNA viruses: mechanisms and outcomes. *Nat. Rev. Microbiol.* 14, 448–460. doi: 10.1038/nrmicro.2016.46

Muller, N. F., Stolz, U., Dudas, G., Stadler, T., and Vaughan, T. G. (2020). Bayesian inference of reassortment networks reveals fitness benefits of reassort-ment in human influenza viruses. *Proc. Natl. Acad. Sci. U. S. A.* 117, 17104–17111. doi: 10.1073/pnas.1918304117

Nelson, M. I., Viboud, C., Simonsen, L., Bennett, R. T., and Griesemer, S. B. (2008). Multiple reassortment events in the evolutionary history of H1N1 influenza A virus since 1918. *PLoS Pathog.* 4:e1000012. doi: 10.1371/journal.ppat.1000012

Nelson, M. I., Viboud, C., Vincent, A. L., Culhane, M. R., Detmer, S. E., Wentworth, D. E., et al. (2015). Global migration of influenza A viruses in swine. *Nat. Commun.* 6:6696.

Nguyen, L.-T., Schmidt, H. A., von Haeseler, A., and Minh, B. Q. (2015). IQ-TREE: a fast and effective stochastic algorithm for estimating maximum-likelihood phylogenies. *Mol. Biol. Evol.* 32, 268–274. doi: 10.1093/molbev/msu300

Niranjan, N., and Carl, K. (2011). GiRaF: robust, computational identification of influenza reassortments via graph mining. *Nucleic Acids Res.* 39:e34. doi: 10.1093/nar/gkq1232

Petrova, V. N., and Russell, C. A. (2018). The evolution of seasonal influenza viruses. *Nat. Rev. Micro Biol.* 16, 47–60. doi: 10.1038/nrmicro.2017.118

Rabadan, R., Levine, A. J., and Krasnitz, M. (2008). Non-random reassortment in human influenza A viruses. *Influenza Other Respir. Viruses* 2, 9–22. doi: 10.1111/j.1750-2659.2007.00030.x

Shannon, P., Markiel, A., Ozier, O., Baliga, N. S., Wang, J. T., Ramage, D., et al. (2003). Cytoscape: a software environment for integrated models of biomolecular interac-tion networks. *Genome Res.* 13, 2498–2504. doi: 10.1101/gr.1239303

Smith, G. J., Vijaykrishna, D., Bahl, J., Lycett, S. J., Worobey, M., Pybus, O. G., et al. (2009). Origins and evolutionary genomics of the 2009 swine-origin H1N1 influenza A epidemic. *Nature* 459, 1122–1125. doi: 10.1038/nature08182

Smith, G. J. D. (2011). The emergence of pandemic influenza viruses. *Int. J. Infect. Dis.* 15, S7–S8.

Stohr, K. (2002). Influenza-WHO cares. *Lancet Infect. Dis.* 2:517. doi: 10.1016/s1473-3099(02)00366-3

Suzuki, Y. (2010). A phylogenetic approach to detecting reassortments in viruses with segmented genomes. *Gene* 464, 11–16. doi: 10.1016/j.gene.2010.05.002

Svinti, V., Cotton, J. A., and McInerney, J. O. (2013). New approaches for unravelling reassortment pathways. *BMC Evol. Biol.* 13:1. doi: 10.1186/1471-2148-13-1

Tian, D., Wang, Y., and Tao, Z. (2011). A novel strategy for exploring the reassortment origins of newly emerging influenza virus. *Bioinformation* 7, 64–68. doi: 10.6026/97320630007064

WHO (2011). *Updated Unified Nomenclature System for the Highly Pathogenic H5N1 Avian Influenza Viruses*. Geneva: WHO.

Yurovsky, A., and Moret, B. (2011). FluReF, an automated flu virus reassortment finder based on phyloge-netic trees. *BMC Genomics* 12(Suppl. 2):S3. doi: 10.1186/1471-2164-12-S2-S3

Zhang, D., Gao, F., Jakovlić, I., Zou, H., Zhang, J., Li, W. X., et al. (2020). PhyloSuite: an integrated and scalable desktop platform for streamlined molecular sequence data management and evolutionary phylogenetics studies. *Mol. Ecol. Resour.* 20, 348–355. doi: 10.1111/1755-0998.13096

Zhang, L., Zhang, Z., and Weng, Z. (2013). Rapid reassortment of internal genes in avian influenza A(H7N9) virus. *Clin. Infect. Dis.* 57, 1059–1061. doi: 10.1093/cid/cit414

**Conflict of Interest:** The authors declare that the research was conducted in the absence of any commercial or financial relationships that could be construed as a potential conflict of interest.

frontiers in Microbiology

ORIGINAL RESEARCH
published: 24 December 2021
doi: 10.3389/fmicb.2021.807458

# Swine Influenza Virus Infection Decreases the Protective Immune Responses of Subunit Vaccine Against Porcine Circovirus Type 2

*Yuhang Sun[1], Jinlong Zhang[1], Zixuan Liu[2], Ying Zhang[1]* and Kehe Huang[2]**

[1] Key Laboratory of Zoonosis of Liaoning Province, College of Animal Science and Veterinary Medicine, Shenyang Agricultural University, Shenyang, China, [2] Department of Animal Nutrition and Immunology, College of Veterinary Medicine, Nanjing Agricultural University, Nanjing, China

OPEN ACCESS

**Edited by:**
*Quanjiao Chen, Wuhan Institute of Virology, Chinese Academy of Sciences (CAS), China*

**Reviewed by:**
*Xusheng Qiu, Shanghai Veterinary Research Institute, Chinese Academy of Agricultural Sciences (CAAS), China*
*Qigai He, Huazhong Agricultural University, China*

***Correspondence:**
*Ying Zhang*
*yingzhang18@syau.edu.cn*
*Kehe Huang*
*khhuang@njau.edu.cn*

**Specialty section:**
*This article was submitted to Virology, a section of the journal Frontiers in Microbiology*

**Received:** *02 November 2021*
**Accepted:** *06 December 2021*
**Published:** *24 December 2021*

**Citation:**
*Sun Y, Zhang J, Liu Z, Zhang Y and Huang K (2021) Swine Influenza Virus Infection Decreases the Protective Immune Responses of Subunit Vaccine Against Porcine Circovirus Type 2. Front. Microbiol. 12:807458. doi: 10.3389/fmicb.2021.807458*

Porcine circovirus type 2 (PCV2) is the primary pathogen of porcine circovirus diseases and porcine circovirus associated diseases. Immunization with a vaccine is considered an effective measure to control these diseases. However, it is still unknown whether PCV2 vaccines have protective immune responses on the animals infected with swine influenza virus (SIV), a pandemic virus in swine herds. In this study, we first compared the effects of 2 different PCV2 vaccines on normal mice and SIV-infected mice, respectively. The results showed that these two vaccines had protective immune responses in normal mice, and the subunit vaccine (vaccine S) had better effects. However, the inactivated vaccine (vaccine I) instead of vaccine S exhibited more immune responses in the SIV-infected mice. SIV infection significantly decreased the immune responses of vaccine S in varying aspects including decreased PCV2 antibody levels and increased PCV2 replication. Mechanistically, further studies showed that SIV infection increased IL-10 expression and M2 macrophage percentage, but decreased TNF-α expression and M1 macrophage percentage in the mice immunized with vaccine S; on the contrary, macrophage depleting by using clodronate-containing liposomes significantly alleviated the SIV infection-induced decrease in the protective immune responses of vaccine S against PCV2. This study indicates that SIV infection decreases the protective immune responses of vaccine S against PCV2. The macrophage polarization induced by SIV infection might facilitate decreased immune responses to vaccine S, which provides new insight into vaccine evaluation and a reference for the analysis of immunization failure.

**Keywords: swine influence virus, subunit vaccine, inactivated vaccine, protectively immune responses, macrophage polarization, porcine circovirus type 2**

## INTRODUCTION

Porcine circovirus type 2 (PCV2) belongs to the *Circoviridae* family and is a single-standard circular DNA virus. As a subtype with pathogenicity, PCV2 has been proved to be the primary etiological agent that cause porcine circovirus associated diseases and post weaning multisystemic wasting syndrome (Hamel et al., 1998; Opriessnig and Meng, 2007), resulting in serious economic losses

(Chae, 2005; Baekbo et al., 2012). In addition, PCV2 has also been proven to be immunosuppressive, which increases the risk of the host infecting other pathogens (Segalés, 2012). Therefore, it is valuable to utilize effective measures to control the PCV2 infection in pigs.

Up to now, vaccination has been always considered one of the most efficient methods of preventing PCV2 infection in pigs. However, the majority of PCV2 vaccine trials were conducted in healthy animals (Wang et al., 2013; Zhang et al., 2017), which is inconsistent with field conditions. The potential infection of other pathogens has always existed in swine herds and is likely to weaken immune responses to PCV2 vaccines. Swine influenza virus (SIV), an especially common virus, is a primary pathogen causing swine flu, an acute respiratory infection with clinical symptoms including coughing, sneezing, nasal discharge, fever, lethargy, and decreased appetite. Its morbidity in pigs can reach 100%, and mortality is generally low (Thacker and Janke, 2008; Pearce et al., 2012). However, its impact on pigs is not negligible because the latent and universality of this virus makes it difficult to be discovered in a timely fashion, thereby greatly influencing the programmed vaccination in pigs. Moreover, SIV is also an immunosuppressive virus. A previous study reported that it could promote alveolar macrophage polarization into immunosuppressive phenotype (Zhao et al., 2014). Therefore, SIV infection may increase PCV2 infection via inducing immunosuppression, but this has not been reported to date.

As the first line of defense, alveolar macrophages have been proven to play an indispensable role in resisting the invasion of SIV (Christoph et al., 2014; Cardani et al., 2017). Alveolar macrophages, a kind of macrophages existing in the lungs, play key roles in innate immunity (Wynn et al., 2013; Byrne et al., 2016). In general, they are classified as two phenotypes: M1 macrophages, which promote inflammatory responses and tissue injury; and M2 macrophages, which inhibit inflammation and promote tissue repair (Byrne et al., 2016; Wynn and Vannella, 2016). Macrophage polarization refers to an estimate of macrophage activation at a given point in space and time, which is a dynamic process and usually associated with inflammatory conditions (Murray, 2017). Multiple growth factors and cytokines including TNF-α and IL-10 can be markers for distinguishing the M1/M2 polarization state (Patel et al., 2016). Toll-like receptors (TLRs) as important components of the pattern recognition receptors, have been found in 13 members (TLR1-TLR13) in mammals, and play an indispensable role in innate immune responses (Fabris et al., 2017). TLR4 is a receptor on the cell membrane that presents a variety of cells, including alveolar macrophages. LPS or viruses can be recognized by TLR4 and then activate innate immune responses and promote inflammation, which is a protection mechanism defense against pathogens (Lu et al., 2008). However, the overexpression of TLR4 often leads to chronic inflammatory disorders and tissue damage *in vivo* (Loretta et al., 2012; Xu et al., 2017), which may weaken immune responses to vaccination. Therefore, in the present study, we examined whether SIV infection could induce excessive inflammation to result in immunosuppression, thereby attenuating the protective immune responses of PCV2 vaccines, providing new insights into vaccine evaluation and a reference for the analysis of immunization failure.

# MATERIALS AND METHODS

## Ethics Statement

The research protocol for this study was approved by the Ethics Committee for Animal Experimentation of Nanjing Agricultural University (approval number: SYXK-SU-2011-0036). All animal care and use procedures were conducted in strict accordance with the Animal Research Committee guidelines of the College of Veterinary Medicine at Nanjing Agricultural University, and all efforts were made to minimize animal suffering and to reduce the number of animals used.

## Viruses and Vaccines

Swine influenza virus (SIV) strain A/swine/Guangxi/18/2011 (H1N1) was kindly provided by Harbin Veterinary Research Institute, Chinese Academy of Agricultural Sciences (Harbin, China). The virus was cultivated in MDCK cells, with serum free medium supplemented with 1 μg/mL TPCK-treated trypsin, in 5% $CO_2$, 37°C condition. The 50% tissue culture infectious doses ($TCID_{50}$) were determined by observing the cytopathic effects at 48 h post-infection. Porcine circovirus type 2 (PCV2NJ2002, PCV2b) was stored in our laboratory (Liu et al., 2017). The virus was cultivated in PK-15 cells, with the Dulbecco's modified eagle medium (DMEM) containing 2% newborn bovine serum free-medium, in 5% $CO_2$, 37°C condition (Zhai et al., 2019). $TCID_{50}$ was determined by indirect immunofluorescence.

PCV2 vaccine I is a commercial inactivated vaccine (SH strain, No. zycp-ym003, O/W adjuvant) purchased from Jiangsu Nannong Hi-Tech Co., Ltd. (Nanjing, China), and the vaccine S was a commercial subunit vaccine (ZJ/c strain, Ingelvac CircoFLEX®, O/W adjuvant) imported from Boehringer-Ingelheim Animal Health Co., Ltd.

## Animal Experiments

The female BALB/c mice (6–8 weeks old) were obtained from the Yangzhou University Experimental Animal Center. All of the animals were monitored at a controlled temperature under a 12 h light/dark cycle with enough standard rodent chow and water for 1-week adaptation. BALB/c mice were challenged with H1N1 SIV as the SIV-infected model, which has been reported as an effective tool for viral replication and pathogenesis *in vivo* (Xin et al., 2015; Qian et al., 2017; Park et al., 2018), and 2 different PCV2 vaccines were immunized on normal mice and the SIV-infected mice for comparison, respectively.

Experiment 1: 80 mice were divided into 8 groups randomly as followed: (a) Blank group; (b) PCV2 control group; (c) SIV control group; (d) SIV and PCV2 control group; (e) Vaccine I and PCV2 group; (f) Vaccine S and PCV2 group; (g) SIV, vaccine I and PCV2 group; (h) SIV, vaccine S and PCV2 group. Mice from c, d, g and h groups were challenged via nasal infection with 1000 $TCID_{50}$ ($TCID_{50} = 10^{-4.5}$) SIV at 1st day, and the negative controls were challenged with equivalent doses of PBS. PCV2 vaccines were immunized via intraperitoneal injection with

0.2 mL for each mouse on the fourth day, and the immunization period lasted 21 days. Then, PCV2 was given via intraperitoneal injection with 1000 $TCID_{50}$ ($TCID_{50} = 10^{-6}$) for each mouse in b, d, e, f, g, and h groups, and the negative control mice were injected with equivalent doses of PBS. The mice challenged with viruses were kept in isolation. At 14 d post-PCV2 infection, all of the animals were euthanized, bronchoalveolar lavage (BAL) fluid, whole blood, lung, thymus, and spleen tissues were collected.

Experiment 2: 20 mice were randomly divided into two groups as follows: (a) SIV + vaccine S + PCV2 + clodronate liposomes group (Clo-lip group); (b) SIV + vaccine S + PCV2 + PBS liposomes group (PBS-lip group). Alveolar macrophages were specifically depleted by intranasally injecting clodronate-containing liposomes according to the instructions of the Clodronate Liposome kit (LIPOSPMA, Shanghai, China). In brief, the mice in the Clo-lip group were challenged via intranasal infection with 50 μL clodronate-containing liposomes every 4 days, and the control mice (PBS-lip group) were administrated with equivalent doses of PBS liposomes at the same time. The administration procedures for SIV, PCV2, and PCV2 vaccines were the same with "Experiment 1." At the end of this experiment, BAL fluid, thymus, and spleen tissues were collected.

## Measurements of Antibody Levels

The serum was collected at 14 and 21 days post-immunization, respectively. The levels of anti-PCV2 specific antibodies were measured by using a sandwich enzyme-linked immunosorbent assay. In brief, the purified recombinant cap protein was coated on 96-well plates for the enzyme-labeled reaction. After antibody incubation and TMB coloration, the OD value was obtained at a wavelength of 450 nm, and the P/N > 2.1 was considered to be positive.

## Quantitative Real-Time PCR

The DNA was extracted from spleens, using the TaKaRa DNA Mini kit (TaKaRa, Dalian, China). The purified DNA was used as a template for qPCR amplification, and a 117-bp fragment from the PCV2 ORF2 gene was amplified with specific primers (forward primer 5′-TAGTATTCAAAGGGCACAG-3′, reverse primer 5′-AAGGCTACCACAGTCAG-3′). A recombinant pMD19 plasmid vector (TaKaRa) containing a PCV2 genome insert was used as a positive control.

Total RNA was extracted from lungs to determine the relative mRNA level of SIV M protein, and from spleens and lungs to detect the relative TLR4, TNF-α mRNA and IL-10 mRNA levels. Target and reference gene primers were designed and synthesized according to the known sequences. Quantitative real-time PCR was conducted using a TaKaRa SYBR Green real-time PCR kit (SYBR Premix Ex Taq) and the ABI Prism Step One Plus detection system (Applied Biosystems, Foster City, United States). Finally, the relative mRNA levels of target genes were calculated by the $2^{-\Delta\Delta CT}$ method with GAPDH as a reference gene.

## Western Blotting Analysis

Lungs were collected to detect the relative expression of SIV NP protein. In brief, total proteins were extracted, and then the protein concentration was measured using a BCA kit (Beyotime, China). Subsequently, the proteins were denatured, subjected to SDS-PAGE, and then transferred to the PVDF membranes. Next, the membranes were blocked with 5% BSA, followed by overnight incubation at 4°C in anti-NP antibody (Abcam, United Kingdom) and 2 h of incubation with an anti-mouse secondary antibody (Cell Signaling Technology, United States) at RT. Finally, the bound antibodies were visualized using an enhanced chemiluminescence kit (Beyotime, China).

## Histopathological Analysis

Spleens and lungs were collected from mice and fixed in 4% neutral-buffered formalin solution. The samples were then embedded in paraffin to be further cut in 4 μm sections for hematoxylin and eosin (HE) staining. The tissue sections were observed and photographed under an optical microscope. The degree of spleen damage was assessed based on the amount of white pulp atrophy, structure disorder, and hemorrhage, and the degree of lung damage was evaluated according to the amount of edema, septal thickening, and cellular infiltration.

## Immunohistochemical Analysis

The fresh spleens were collected and fixed in 4% neutral buffered formalin for IHC staining. In brief, tissue sections were incubated with the specific primary antibodies (anti-cap or anti-TLR4 antibodies) at 37°C for 1 h. After washing in PBS, the sections were incubated with a horseradish peroxidase labeled anti-mouse antibody at 37°C for 1 h. Next, freshly prepared DAB was added into the sections at RT for 5 min. Finally, after hematoxylin staining for 1 min, the sections were dehydrated and mounted by neutral gum, and then examined by an optical microscope. Images were captured with a Pannoramic viewer (Pannoramic MIDI, 3D HISTECH), and data were analyzed using DensitoQuant software (QuantCenter, 3DHISTECH). A histochemistry score (H-score) was calculated as previously described (Sun et al., 2019).

## Bronchoalveolar Lavage Fluid Collection and Macrophage Classification

BAL was conducted to obtain alveolar macrophages from fresh mouse lungs. In brief, each lung was repeatedly flushed with PBS, and cells were harvested from the BAL fluid by centrifugation. Cells from the BAL fluid were incubated with an Fc receptor blocker (BD Biosciences) to reduce non-specific binding and then incubated with specific F4/80-APC, CD11b-PerCP-Cy5.5, CD80-PE, and CD206-FITC antibodies (eBioscience; BD Biosciences) for 30 min at 4°C (Sun et al., 2018). Subsequently, flow cytometry (BD Biosciences) was used to collect and classify the alveolar macrophages, and then data were analyzed using FlowJo for Mac 10.7 (Tree Star, Inc.).

## Statistical Analysis

All statistical analyses were conducted using GraphPad Prism 6. Student's two-tailed *t*-test in two groups and one-way or two-way ANOVA in multiple groups were used, and the results were

expressed as the mean ± standard error (S.E.). $P < 0.05$ was considered statistically significant.

# RESULTS

## The Protective Immune Responses of 2 Porcine Circovirus Type 2 Vaccines on Normal Mice

To explore the immune responses of different PCV2 vaccines on normal animals, mice were treated with subunit vaccine (vaccine S) and inactivated vaccine (vaccine I), respectively, and then challenged by PCV2 at 21 days post-immunization (**Figure 1A**). As expected, no obvious clinical symptoms and abnormal phenomena were observed among all mice. Weight was measured every 2 days, and the results showed that no significance was observed among all mice (**Figure 1B**). Subsequently, spleen index (spleen/body weight percentage) and thymus index (thymus/body weight percentage) were calculated to evaluate the immune organ damage. As demonstrated in **Figures 1C,D**, PCV2 infection significantly decreased the spleen and thymus index, while vaccine S markedly alleviated the decrease in thymus index induced by PCV2 infection, and no significance was observed between the PCV2 group and PCV2 + vaccine I groups. Similar results were demonstrated by HE staining for spleens. As shown in **Figure 1E**, white pulp atrophy, structure disorder, and hemorrhage were observed in the spleens of mice from the PCV2 group, while these pathological damages were relieved by vaccine S.

The PCV2-specific antibody levels in serum were detected at 14 and 21 days post-immunization, respectively, to assess the immune responses of 2 PCV2 vaccines. As shown in **Figure 1F**, higher levels of the PCV2-specific antibodies were produced in vaccine I and vaccine S groups than that in the blank group at 21 days post-immunization, while no significance was observed between vaccine I and S groups. To more accurately assess the immune responses of the 2 vaccines, PCV2 replication was also measured. As indicators to assess PCV2 replication, the PCV2 DNA copies were detected using qRT-PCR, and cap protein was stained for IHC examination. The results showed that PCV2 infection significantly increased PCV2 DNA copies, but the increase was markedly down-regulated by vaccine S, not vaccine I, and PCV2 DNA copies were lower in the PCV2 + vaccine S group than those in the PCV2 + vaccine I group (**Figure 1G**). Similarly, the cap-positive staining (H-score) significantly reduced in 2 vaccine groups compared with the PCV2 control group, and the inhibitory effect was more obvious in PCV2 + vaccine S than that in the PCV2 + vaccine I group (**Supplementary Figure 1**).

Taken together, the vaccine S induced higher levels of PCV2-specific antibodies, significantly reduced PCV2 replication, mitigated the organ damage caused by PCV2 infection, suggesting that it produced protective immune responses on normal PCV2-infected mice. In terms of reducing PCV2 DNA copies, it also had better immune responses compared to vaccine I.

## The Protective Immune Responses of 2 Porcine Circovirus Type 2 Vaccines on the Swine Influenza Virus-Infected Mice

To explore the role SIV infection played in the protective immune responses of PCV2 vaccines, SIV was injected to mice as described in Experiment 1 (**Figure 2A**), and then the immune responses of 2 PCV2 vaccines on the SIV-infected mice were compared. At first, relative SIV M mRNA (**Supplementary Figure 2A**) and NP expression (**Supplementary Figure 2B**) levels, as well as lung damage (**Supplementary Figure 2C**) in the SIV control group were measured to confirm SIV infection. The results showed that the SIV infection model had been successfully established. Next, body weight gain, spleen index, and thymus index were measured. The results demonstrated that the body weight gain significantly increased in 2 vaccine groups relative to the SIV + PCV2 control group (**Figure 2B**). As shown in **Figures 2C,D**, there was significance in both thymus index and spleen index between vaccine I, not vaccine S and SIV + PCV2 control groups; moreover, thymus index was higher in vaccine I group than that in vaccine S group. After SIV and PCV2 infection, white pulp atrophy, structure disorder, and hemorrhage were observed in the spleens of mice, while these pathological damages were relieved by 2 vaccines, and vaccine I had a better effect (**Figure 2E**).

The PCV2-specific antibody titers were detected after SIV infection and vaccine immunization. The results showed that the antibody titers markedly increased in SIV + vaccine S and SIV + vaccine I groups relative to the SIV control group, but there was no significance between SIV + vaccine S and SIV + vaccine I groups (**Figure 2F**). As above mentioned, PCV2 replication was also evaluated. As shown in **Figure 2G**, vaccine I instead of vaccine S significantly decreased the PCV2 DNA copies in the SIV + PCV2 control group, and the PCV2 DNA copies in SIV + PCV2 + vaccine I group were lower than those in SIV + PCV2 + vaccine S. The same tendency was observed in the cap-positive staining (H-score) (**Supplementary Figure 3**).

In summary, these data suggest that vaccine I instead of vaccine S produced adequate immune responses on the SIV-infected mice.

## Swine Influenza Virus Infection Decreased the Protective Responses of Vaccine S, Increased Toll-Like Receptors 4 Expression, and Promoted Alveolar Macrophage Polarization From M1 to M2

To further evaluate the effect of SIV infection on the immune responses of 2 vaccines, the PCV2-specific antibody titers and cap DNA copies were compared between before and after SIV infection. As shown in **Figure 3A**, after SIV infection, the antibody levels of the vaccine S group other than the vaccine I group at 21 days post-immunization were significantly reduced. Meanwhile, the PCV2 DNA copies in the SIV-infected mice immunized by vaccine S instead of vaccine I were significantly increased (**Figure 3B**). These results together

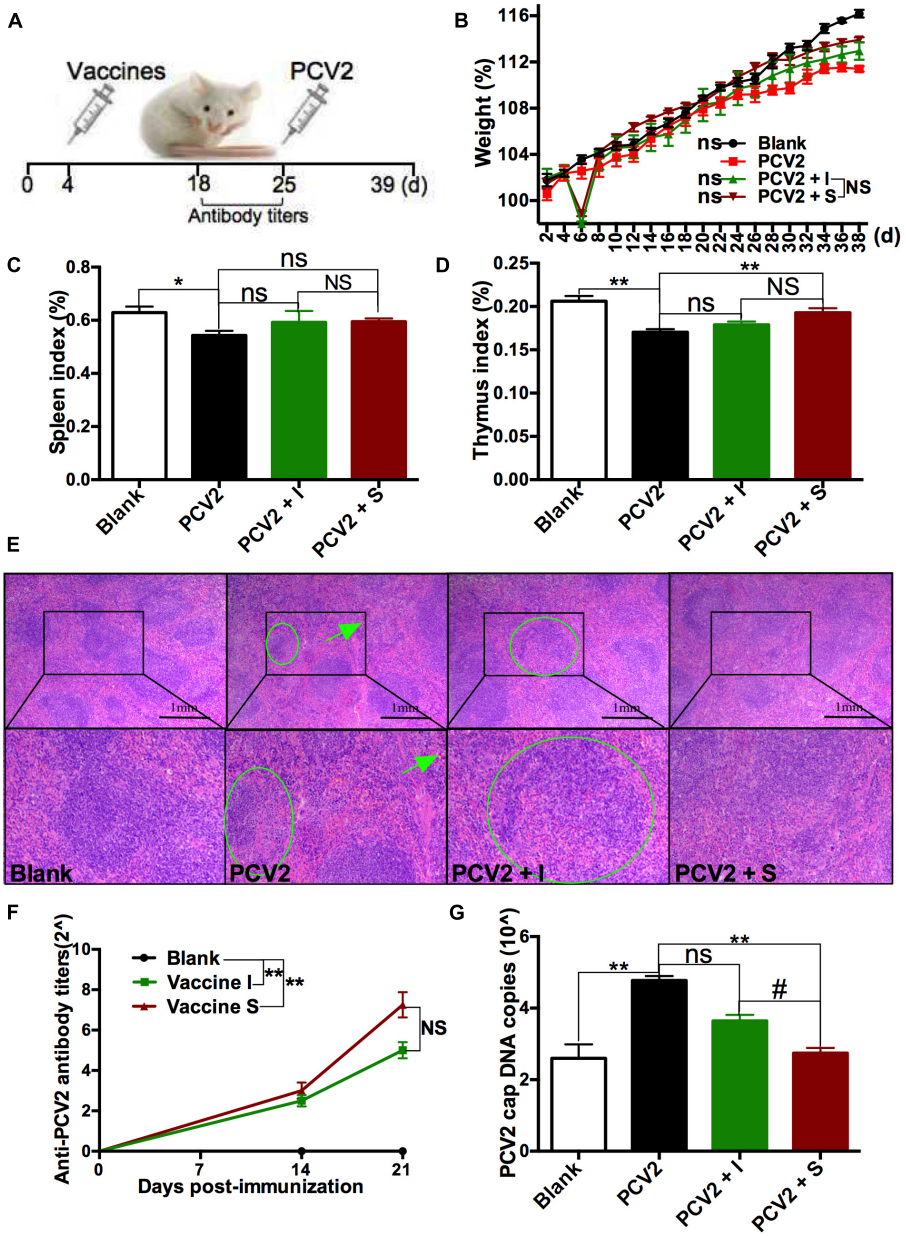


**FIGURE 1 |** Effects of 2 different PCV2 vaccines on normal mice. **(A)** Mice were immunized with subunit vaccine (vaccine S) and inactivated vaccine (vaccine I) at day 4, and then were injected with PCV2 at day 25. **(B)** Weight gain expressed as the percentage of initial weight. **(C)** Spleen index and **(D)** thymus index were calculated by the ratio of spleen or thymus to body weight. **(E)** HE staining for spleens. The green circle and arrow indicated white pulp structure disorder and hemorrhage, respectively. **(F)** PCV2-specific antibody levels in serum were assessed at days 14 and 21 post-immunization. **(G)** The PCV2 DNA copies in spleen. Data were presented as means ± SEM of mice ($n \geq 3$) in each group. Compared with PCV2 group, $^{*}P < 0.05$, $^{**}P < 0.01$, and ns, not significant; Compared with PCV2 + vaccine I group, $^{\#}P < 0.05$ and NS, not significant.

suggest that SIV infection significantly weakened the immune responses of vaccine S.

To explore the reasons why vaccine S was weakened by SIV infection, TLR4, inflammation-related cytokines, and macrophage phenotype were further detected. As expected, TLR4-positive staining (**Figure 3C**) and its mRNA level (**Figure 3D**) significantly enhanced in the PCV2 + vaccine S + SIV group relative to the PCV2 + vaccine S group. Moreover, SIV infection significantly decreased TNF-α mRNA level (**Figure 3E**) but enhanced the IL-10 mRNA level in the PCV2 + vaccine S group (**Figure 3F**). As mentioned in the "Introduction" section, TNF-α and IL-10 are the markers for M1 and M2 macrophages, respectively. Therefore, our results indicated that SIV infection might promote macrophage polarization from M1 to M2. To further verify this conclusion, BAL fluid was collected to detect the alveolar macrophage

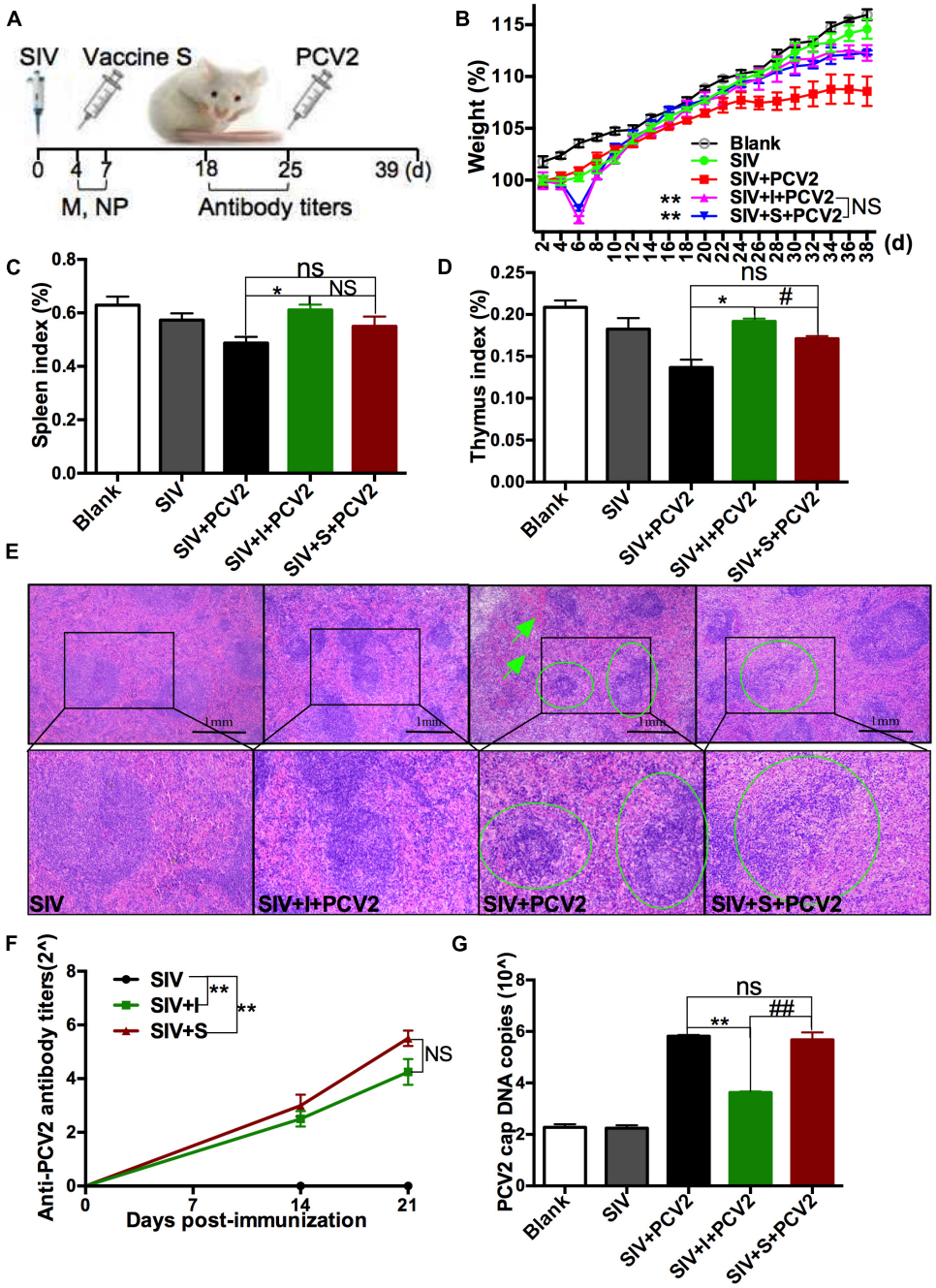


**FIGURE 2 |** Effects of 2 different PCV2 vaccines on the SIV-infected mice. **(A)** Mice were intranasally infected with SIV at day 0, immunized with 2 PCV2 vaccines at day 4, and then injected with PCV2 at day 25. **(B)** Weight gain expressed as the percentage of initial weight. **(C)** Spleen index and **(D)** thymus index were calculated by the ratio of spleen or thymus to body weight. **(E)** HE staining for spleens. The green circle and arrow indicated white pulp structure disorder and hemorrhage, respectively. **(F)** PCV2-specific antibody levels in serum were assessed at days 14 and 21 post-immunization. **(G)** The PCV2 DNA copies in spleen. Data were presented as means ± SEM of mice ($n \geq 3$) in each group. Compared with SIV + PCV2 group, $^{*}P < 0.05$, $^{**}P < 0.01$, and ns, not significant; Compared with SIV + PCV2 + vaccine I group, $^{\#}P < 0.05$, $^{\#\#}P < 0.01$, and NS, not significant.

phenotype considering that the lung was the target organ to infect SIV. The results showed that the mice in the PCV2 + vaccine S group showed a markedly decreased M1 macrophage percentage but significantly increased M2 macrophage percentage after SIV infection (**Figure 4**).

Taken together, these results suggest that SIV infection decreased the protective effects of vaccine S and promoted TLR4 expression and alveolar macrophage polarization from M1 to M2, which could cause the immunization failure of vaccine S on the SIV-infected mice.

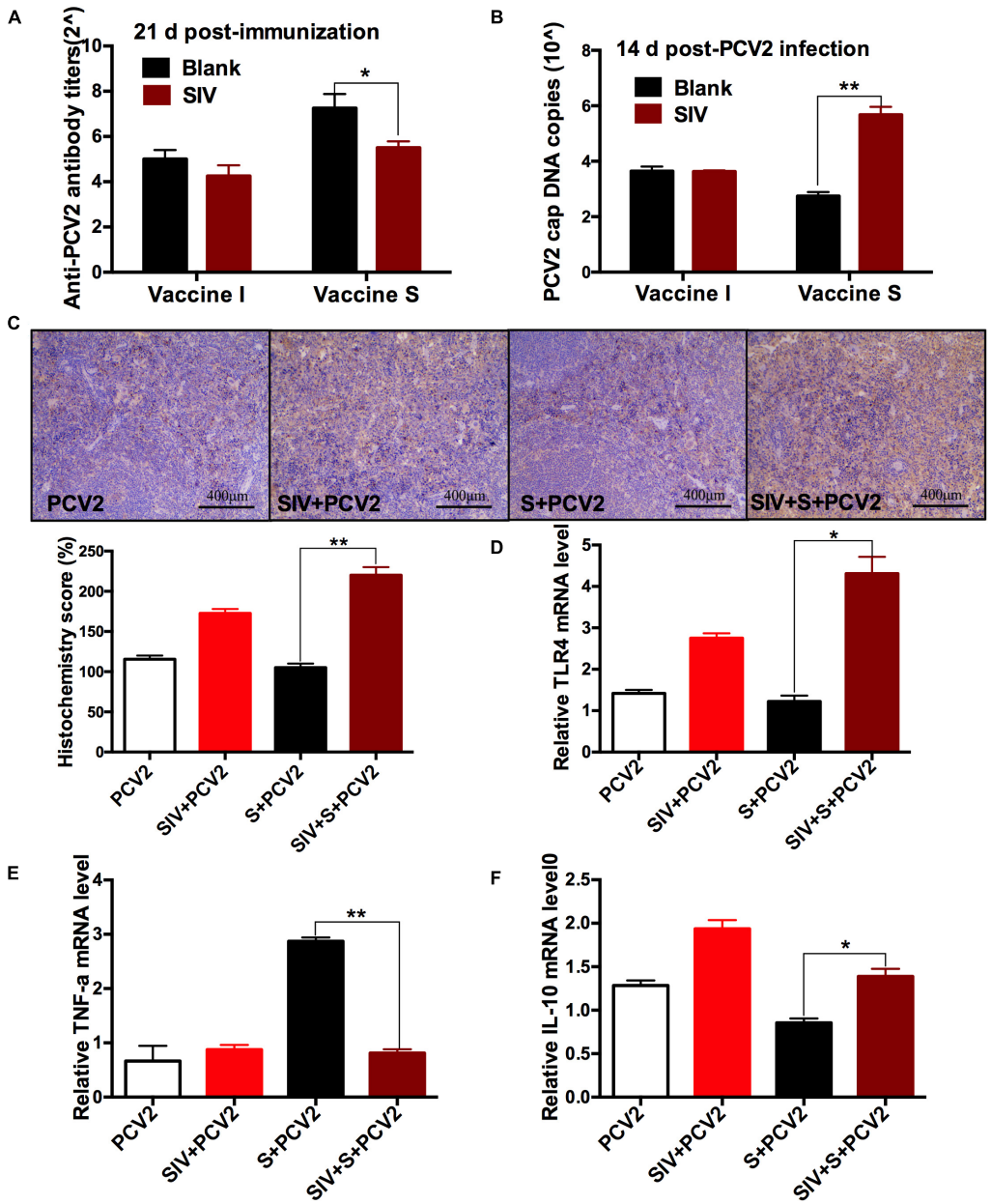


**FIGURE 3 |** The effects of SIV infection on the immune responses of vaccine S. **(A)** PCV2-specific antibody levels in serum were assessed at day 21 post-immunization. **(B)** The PCV2 DNA copies in spleen. **(C)** Immunohistochemical (IHC) analysis for the TLR4 expression in spleens. The TLR4-specific staining intensity was showed by the histochemistry score (H-score). **(D)** The relative TLR4 mRNA level in spleens. **(E)** The relative TNF-α mRNA level in lungs. **(F)** The relative IL-10 mRNA level in lungs. Data were presented as means ± SEM of mice in each group. Data were presented as means ± SEM of mice ($n \geq 3$) in each group. $^{*}P < 0.05$, $^{**}P < 0.01$.

## Macrophage Depletion Alleviated the Swine Influenza Virus Infection-Induced Decrease in the Protective Immune Response of Vaccine S

To further investigate whether SIV infection decreased the protective responses of vaccine S via promoting alveolar macrophage polarization from M1 to M2, clodronate liposome, a macrophage scavenger was used to specifically deplete lung macrophages as described in "Experiment 2" (**Figure 5A**). In order to evaluate the depletion efficiency of Clo-lip, a preliminary test was conducted for a period of 39 days, and the total number of alveolar macrophages in each BAL sample from the Clo-lip group and PBS-lip group was calculated every day as previously described (Garcia-Castillo et al., 2020).

As expected, the number of BAL macrophages decreased by about 80% after one CLP injection, and

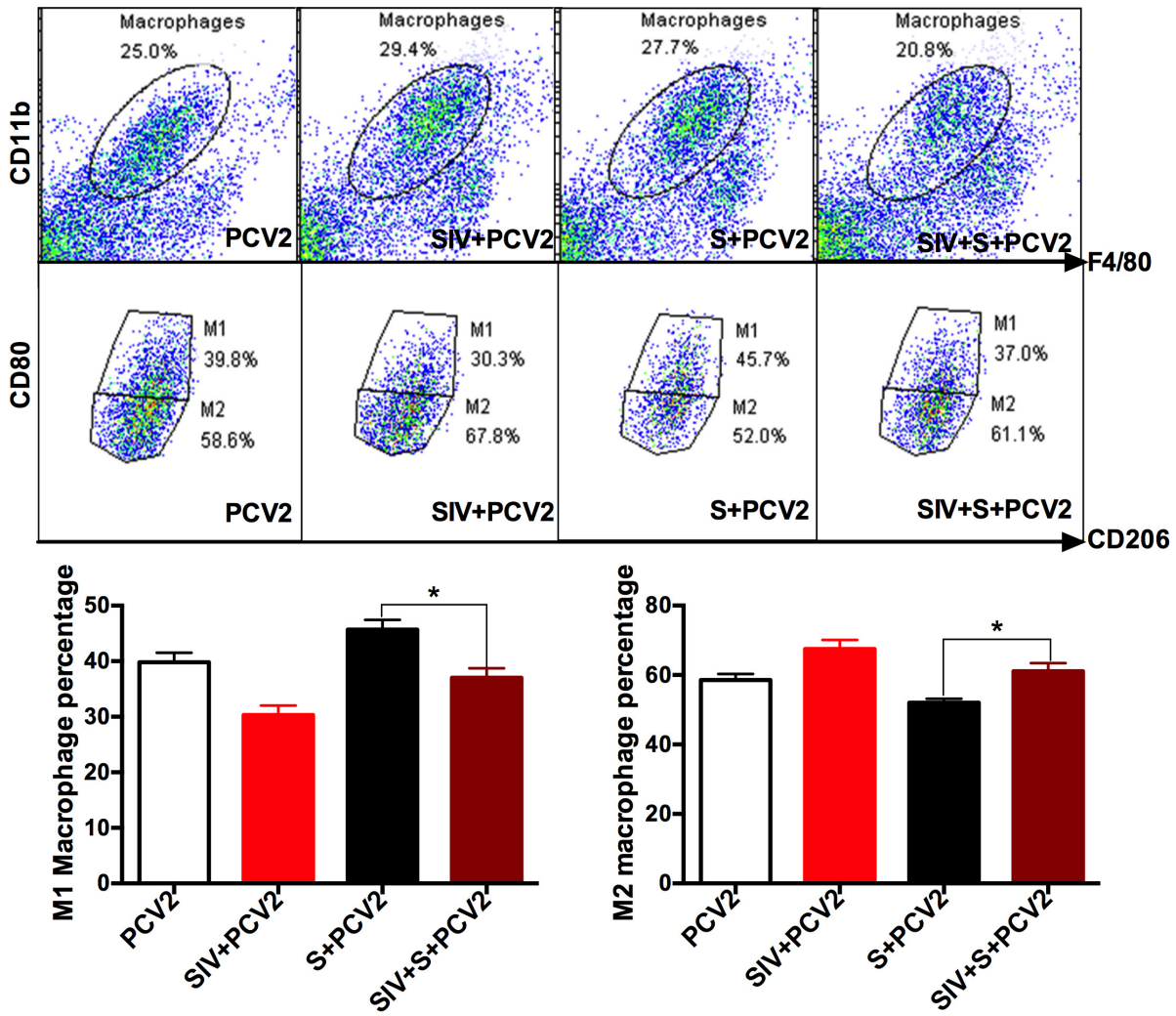


**FIGURE 4 |** SIV promoted macrophage polarization from M1 to M2. Bronchoalveolar lavage (BAL) fluid was detected using a flow cytometer. CD11b and F4/80 were used for marking macrophages; CD80 and CD206 were markers for M1 and M2 macrophages, respectively. The proportion of M1 and M2 macrophages in the total population of macrophages. Data were presented as means ± SEM of mice ($n \geq 3$) in each group. *$P < 0.05$.

then was almost exhausted after multiple CLP injections (**Supplementary Figure 4A**). These results suggested that CLP injection was useful for depleting alveolar macrophages. Next, weight gain (**Figure 5B**), spleen index (**Figure 5C**), thymus index (**Figure 5D**), anti-PCV2 antibody titers (**Figure 5E**), PCV2 DNA copies (**Figure 5F**), and cap-positive staining (**Supplementary Figure 4B**) were measured and compared between Clo-lip and PBS-lip groups. The results showed that weight gain, thymus index, and anti-PCV2 antibody titers significantly increased after macrophage depletion, while PCV2 replication markedly decreased as demonstrated by decreased PCV2 DNA copies and H-score. Taken together, these results demonstrated that macrophage depletion alleviated the SIV infection-induced decrease in the protective immune responses of vaccine S, which suggested that SIV infection might decrease the protective immune responses of vaccine S via promoting alveolar macrophage polarization from M1 to M2.

## DISCUSSION

As an effective measure to prevent pigs from PCV2-related diseases (Opriessnig et al., 2010; Seo et al., 2012), it was important to ensure the effective immune responses of PCV2 vaccines under field conditions. Evidence indicates that most of the available vaccines failed to effectively decrease the mortality of PCV2 infection in herds due to a variety of factors (Beach and Meng, 2012). Of which, the widespread SIV in pigs was considered as a potential reason for immunization failure (Choi et al., 2002). However, the previous PCV2 vaccine evaluation tests were always conducted on healthy animals including piglets (Seo et al., 2014; Huan et al., 2018; Zhang et al., 2018), which made it uncertain whether PCV2 vaccines could effectively work under field conditions. In this present study, the immune responses of two kinds of PCV2 vaccines on SIV-infected mice were tested to imitate a commercial farming condition.

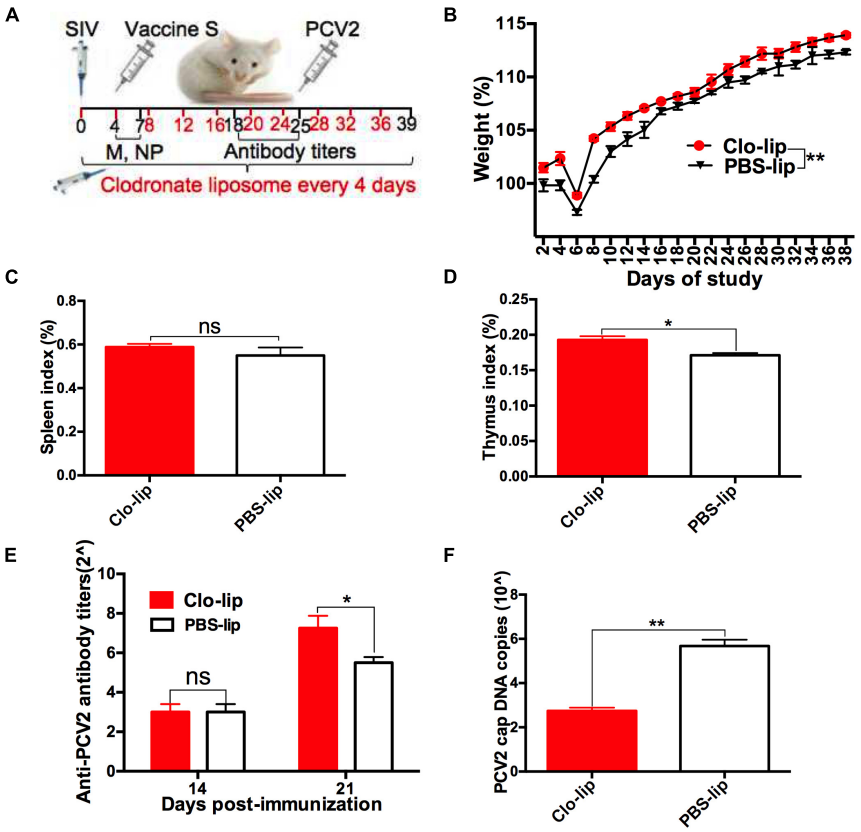


**FIGURE 5 |** Alveolar macrophage depletion attenuated the SIV-induced decrease in the protective immune effect of vaccine S. **(A)** Mice were intranasally infected with SIV at day 0, injected with clodronate-containing liposomes (Clo-lip) or PBS liposomes (PBS-lip) every 4 days, immunized with vaccine S at day 4, and then injected with PCV2 at day 25. **(B)** Weight gain expressed as the percentage of initial weight. **(C)** Spleen index and **(D)** thymus index were calculated by the ratio of spleen or thymus to body weight. **(E)** PCV2-specific antibody levels in serum were assessed at days 14 and 21 post-immunization. **(F)** The PCV2 DNA copies in spleen. Data were presented as means ± SEM of mice ($n \geq 3$) in each group. $^{*}P < 0.05$, $^{**}P < 0.01$, and ns, not significant.

Given that the immune responses of PCV2 vaccines could not be reflected because of invisible clinical symptoms (Deng et al., 2013; Wang et al., 2017), their effects were evaluated based on the growth performance of mice, anti-PCV2 antibody levels, and PCV2 replication *in vivo*. Our results showed that 2 PCV2 vaccines had protective immune responses on normal mice, but the effects of vaccine S were better than those of vaccine I, as demonstrated by the significantly decreased PCV2 DNA copies and organ damage. These results suggested that vaccine S could have more application value than vaccine I on normal mice. In contrast, vaccine I instead of vaccine S produced adequate immune responses on the SIV-infected mice. SIV infection weakened the immune responses of vaccine S, as demonstrated by the significantly decreased anti-PCV2 antibody levels and increased PCV2 replication, which meant that vaccine S only played adequate protective roles in animals without pathogen infection, and there might be a risk of immunization failure due to latent SIV infection. In summary, our results confirmed that the immune responses of vaccine S were inconsistent between the normal and SIV-infected mice.

We try to explain the reason why vaccine S was more easily influenced by SIV than vaccine I. In general, immune responses to vaccination include neutralizing antibodies and cell-mediated immunity (Afghah et al., 2017). The inactivated vaccine often fails to produce sufficient cell-mediated immunity due to the inactivated virus. But the subunit vaccine can increase $CD4^+$ and $CD8^+$ levels thereby producing long-lasting protection (Ferrari et al., 2014), which plays an important role in the immune responses of the subunit vaccine. This difference in action mechanism between inactivated vaccine and subunit vaccine may be one of the reasons for the instability of vaccine S. Moreover, a previous study has reported that the porcine reproductive and respiratory syndrome virus had an adverse effect on naive T cells thereby influencing the immune responses of PCV2 vaccines (Canelli et al., 2016). Given the importance of cell-mediated immunity in the immune responses of subunit vaccines, we concluded that the immunization failure of vaccine S may be related to the immune organ damage or immunosuppression induced by SIV infection.

As our results showed, increased TLR4 expression was detected in the spleens of the mice infected with SIV, and the elevation of TLR4 for at least 5 weeks after SIV infection, which meant that the innate immune responses were continuously activated to resist viral infection. More and more studies have

confirmed that the overexpression or sustained activation of TLR4 could lead to excessive inflammation or tissue damage *in vivo* (Perrone et al., 2008; Tate et al., 2010). Consistently, the SIV-infected mice showed more pronounced thymus damage than the control mice, which further indicates that the adverse effects of SIV infection might be associated with the increased expression of TLR4.

SIV usually invades the body through the respiratory tract and directly acts on alveolar macrophages. Subsequently, macrophages manifest as M1 phenotype to defense against the pathogen at the initial stage of infection and then change into M2 macrophages (Patel et al., 2016). Our data suggested that SIV infection induced the macrophage polarization from M1 to M2, meaning the macrophages exhibited a more stable suppression following excessive inflammatory responses. Due to the compensatory effects and complexity of the body, the immune system of the whole body may be affected, resulting in insufficient responses to antigens and failing to produce effective immune protection. Therefore, the immunization failure of vaccine S in the presence of SIV may be related to the immunosuppression as demonstrated by the alveolar macrophage polarization from M1 to M2 following excessive inflammatory responses. However, studies on the relationship between TLR4 activation and alveolar macrophage polarization from M1 to M2, in this case, remain to be further performed.

## CONCLUSION

In conclusion, PCV2 vaccine S is more effective in defense against PCV2 infection on normal mice, but PCV2 vaccine I instead of vaccine S is better on the SIV-infected mice. SIV infection significantly weakens the protective immune responses of vaccine S, and the risk of immunization failure of the PCV2 vaccine might increase due to the pandemic SIV in herds. These results provided a feasible reference for the clinical analysis of the immunization failure of different vaccines.

## DATA AVAILABILITY STATEMENT

The original contributions presented in the study are included in the article/**Supplementary Material**, further inquiries can be directed to the corresponding author/s.

## ETHICS STATEMENT

The animal study was reviewed and approved by the Ethics Committee for Animal Experimentation of Nanjing Agricultural University.

## AUTHOR CONTRIBUTIONS

YS, YZ, and KH designed this project, wrote, and revised the manuscript. YS, JZ, and ZL conducted the experiments. All authors reviewed the manuscript.

## FUNDING

This work was supported by the China Postdoctoral Science Foundation (2021M692231) and the National Natural Science Foundation of China (NFSC) (32002347) and (31772811).

## SUPPLEMENTARY MATERIAL

The Supplementary Material for this article can be found online at: https://www.frontiersin.org/articles/10.3389/fmicb.2021.807458/full#supplementary-material

**Supplementary Figure 1 |** IHC analysis for the cap expression in spleens of normal mice. The cap-specific staining intensity was showed by H-score. Compared with PCV2 group, $^{**}P < 0.01$; Compared with vaccine I group, NS, not significant.

**Supplementary Figure 2 |** SIV infection measurement. **(A)** SIV M mRNA level, **(B)** NP protein level and **(C)** lung damage were measured to verify SIV infection. The yellow arrow indicated hemorrhage, and the green arrow indicated inflammatory cell infiltration. Data were presented as means ± SEM of mice ($n \geq 3$) in each group. $^{*}P < 0.05$, $^{**}P < 0.01$, and ns, not significant.

**Supplementary Figure 3 |** IHC analysis for the cap expression in spleens of SIV-infected mice. The cap-specific staining intensity was showed by H-score. Compared with PCV2 group, $^{**}P < 0.01$ and ns, not significant; Compared with vaccine I group, $^{\#\#}P < 0.01$.

**Supplementary Figure 4 |** Macrophage numbers and cap expression. **(A)** The number of macrophages from BAL sample was detected and calculated according to the presented time point. **(B)** IHC analysis for the cap expression in spleens. The cap-specific staining intensity was showed by the H-score. Data were presented as means ± SEM of mice ($n \geq 3$) in each group. $^{**}P < 0.01$.

## REFERENCES

Afghah, Z., Webb, B., Meng, X. J., and Ramamoorthy, S. (2017). Ten years of PCV2 vaccines and vaccination: is eradication a possibility? *Vet. Microbiol.* 206, 21–28. doi: 10.1016/j.vetmic.2016.10.002

Baekbo, P., Kristensen, C. S., and Larsen, L. E. (2012). Porcine circovirus diseases: a review of PMWS. *Transboun. Emerg. Dis.* 59, 60–67. doi: 10.1111/j.1865-1682.2011.01288.x

Beach, N. M., and Meng, X. J. (2012). Efficacy and future prospects of commercially available and experimental vaccines against porcine circovirus type 2 (PCV2). *Virus Res.* 164, 33–42. doi: 10.1016/j.virusres

Byrne, A. J., Maher, T. M., and Lloyd, C. M. (2016). Pulmonary macrophages: a new therapeutic pathway in fibrosing lung disease? *Trends Mol. Med.* 22, 303–316. doi: 10.1016/j.molmed.2016.02.004

Canelli, E., Borghetti, P., Ferrari, L., Angelis, E. D., Ferrarini, G., Catella, A., et al. (2016). Immune response to PCV2 vaccination in PRRSV viraemic piglets. *Vet. Rec.* 178:193. doi: 10.1136/vr.103637

Cardani, A., Boulton, A., Kim, T. S., and Braciale, T. J. (2017). alveolar macrophages prevent lethal influenza pneumonia by inhibiting infection of Type-1 alveolar epithelial cells. *PLoS Pathog.* 13:e1006140. doi: 10.1371/journal.ppat.1006140

Chae, C. (2005). A review of porcine circovirus 2-associated syndromes and diseases. *Vet. J.* 169, 326–336. doi: 10.1016/j.tvjl.2004.01.012

Choi, Y. K., Goyal, S. M., and Joo, H. S. (2002). Prevalence of swine influenza virus subtypes on swine farms in the United States. *Arch. Virol.* 147, 1209–1220.

Christoph, S., Nobs, S. P., Heer, A. K., Michael, K., Glynis, K., Nico, V. R., et al. (2014). Alveolar macrophages are essential for protection from respiratory failure and associated morbidity following influenza virus infection. *PLoS Pathog.* 10:e1004053. doi: 10.1371/journal.ppat.1004053

Deng, Z. B., Yuan, A. W., Luo, W., Wang, N. D., Gong, Q. L., Yu, X. L., et al. (2013). Transmission of porcine circovirus type 2b (PCV2b) in Kunming mice. *Acta Vet. Hung.* 61, 234–243. doi: 10.1556/AVet.2013.004

Fabris, T. F., Laporta, J., Corra, F. N., Torres, Y. M., Kirk, D. J., Mclean, D. J., et al. (2017). Effect of nutritional immunomodulation and heat stress during the dry period on subsequent performance of cows. *J. Dairy Sci.* 100, 6733–6742. doi: 10.3168/jds.2016-12313

Ferrari, L., Borghetti, P., Angelis, E. D., and Martelli, P. (2014). Memory T cell proliferative responses and IFN-γ productivity sustain long-lasting efficacy of a Cap-based PCV2 vaccine upon PCV2 natural infection and associated disease. *Vet. Res.* 45:44. doi: 10.1186/1297-9716-45-44

Garcia-Castillo, V., Tomokiyo, M., Raya Tonetti, F., Islam, M. A., Takahashi, H., Kitazawa, H., et al. (2020). Alveolar macrophages are key players in the modulation of the respiratory antiviral immunity induced by orally administered *Lacticaseibacillus rhamnosus* CRL1505. *Front. Immunol.* 11:568636. doi: 10.3389/fimmu.2020.568636

Hamel, A. L., Lin, L. L., and Nayar, G. P. (1998). Nucleotide sequence of porcine circovirus associated with postweaning multisystemic wasting syndrome in pigs. *J. Virol.* 72, 5262–5267. doi: 10.1128/JVI.72.6.5262-5267

Huan, C., Fan, M., Cheng, Q., Wang, X., Gao, Q., Wang, W., et al. (2018). Evaluation of the efficacy and cross-protective immunity of live-attenuated chimeric PCV1-2b vaccine against PCV2b and PCV2d subtype challenge in Pigs. *Front. Microbiol.* 9:455. doi: 10.3389/fmicb.2018.00455

Liu, D., Xu, J., Qian, G., Hamid, M., Gan, F., Chen, X., et al. (2017). Selenizing astragalus polysaccharide attenuates PCV2 replication promotion caused by oxidative stress through autophagy inhibition via PI3K/AKT activation. *Int. J. Biol. Macromol.* 108, 350–359. doi: 10.1016/j.ijbiomac.2017.12.010

Loretta, M., Fumin, D., Maryam, Z., Ashok, K., and Xiaohui, Z. (2012). ABCA1 protein enhances Toll-like receptor 4 (TLR4)-stimulated interleukin-10 (IL-10) secretion through protein kinase A (PKA) activation. *J. Biol. Chem.* 287, 40502–40512. doi: 10.1074/jbc.M112.413245

Lu, Y. C., Yeh, W. C., and Ohashi, P. S. (2008). LPS/TLR4 signal transduction pathway. *Cytokine* 42, 145–151. doi: 10.1016/j.cyto.2008.01.006

Murray, P. J. (2017). Macrophage polarization. *Annu. Rev. Physiol.* 79, 541–566. doi: 10.1146/annurev-physiol-022516-034339

Opriessnig, T., and Meng, X. J. (2007). PG halbur. porcine circovirus Type 2-associated disease: update on current terminology, clinical manifestations, pathogenesis, diagnosis, and intervention strategies. *J. Vet. Diagn. Invest.* 19, 591–615. doi: 10.1177/104063870701900601

Opriessnig, T., Patterson, A. R., Madson, D. M., Pal, N., Ramamoorthy, S., Meng, X. J., et al. (2010). Comparison of the effectiveness of passive (dam) versus active (piglet) immunization against porcine circovirus type 2 (PCV2) and impact of passively-derived PCV2 vaccine-induced immunity on vaccination. *Vet. Microbiol.* 142, 177–183. doi: 10.1016/j.vetmic.2009.09.056

Park, S., Kim, J. I., Bae, J. Y., Yoo, K., Kim, H., Kim, I. H., et al. (2018). Effects of heat-killed *Lactobacillus plantarum* against influenza viruses in mice. *J. Microbiol.* 56, 145–149. doi: 10.1007/s12275-018-7411-1

Patel, U., Rajasingh, S., Samanta, S., Cao, T., Dawn, B., and Rajasingh, J. (2016). Macrophage polarization in response to epigenetic modifiers during infection and inflammation. *Drug Discov. Today* 22, 186–193. doi: 10.1016/j.drudis.2016.08.006

Pearce, M. B., Jayaraman, A., Pappas, C., Belser, J. A., Zeng, H., Gustin, K. M., et al. (2012). Pathogenesis and transmission of swine origin A(H3N2)v influenza viruses in ferrets. *Proc. Natl. Acad. Sci. U.S.A.* 109, 3944–3949. doi: 10.1073/pnas.1119945109

Perrone, L. A., Plowden, J. K., Adolfo, G. S., Katz, J. M., and Tumpey, T. M. (2008). H5N1 and 1918 pandemic influenza virus infection results in early and excessive infiltration of macrophages and neutrophils in the lungs of mice. *PLoS Pathog.* 4:e1000115. doi: 10.1371/journal.ppat.1000115

Qian, G., Liu, D., Hu, J., Gan, F., Hou, L., Chen, X., et al. (2017). Ochratoxin A-induced autophagy in vitro and in vivo promotes porcine circovirus type 2 replication. *Cell Death Dis.* 8:e2909. doi: 10.1038/cddis.2017.303

Segalés, J. (2012). Porcine circovirus type 2 (PCV2) infections: clinical signs, pathology and laboratory diagnosis. *Virus Res.* 164, 10–19. doi: 10.1016/j.virusres.2011.10.007

Seo, H. W., Han, K., Oh, Y., Park, C., and Chae, C. (2012). Efficacy of a reformulated inactivated chimeric PCV1-2 vaccine based on clinical, virological, pathological and immunological examination under field conditions. *Vaccine* 30, 6671–6677. doi: 10.1016/j.vaccine.2012.08.065

Seo, H. W., Park, C., Han, K., and Chae, C. (2014). Effect of porcine circovirus type 2 (pcv2) vaccination on pcv2-viremic piglets after experimental pcv2 challenge. *Vet. Res.* 45:13. doi: 10.1186/1297-9716-45-13

Sun, Y., Liu, Z., Liu, D., Chen, J., Gan, F., and Huang, K. (2018). Low-level Aflatoxin B1 promotes influenza infection and modulates a switch in macrophage polarization from M1 to M2. *Cell Physiol. Biochem.* 49, 1110–1126. doi: 10.1159/000493294

Sun, Y., Su, J., Yang, S., Liu, Z., Liu, D., Gan, F., et al. (2019). Mannan oligosaccharide protects against the Aflatoxin-B(1)-promoted influenza replication and tissue damages in a toll-like-receptor-4-dependent manner. *J. Agric. Food Chem.* 67, 735–745. doi: 10.1021/acs.jafc.8b05829

Tate, M. D., Pickett, D. L., Nico, V. R., Brooks, A. G., and Reading, P. C. (2010). Critical role of airway macrophages in modulating disease severity during influenza virus infection of mice. *J. Virol.* 84, 7569–7580. doi: 10.1128/JVI.00291-10

Thacker, E., and Janke, B. (2008). Swine influenza virus: zoonotic potential and vaccination strategies for the control of avian and swine influenzas. *J. Infect. Dis.* 197(Suppl. 1), S19–S24. doi: 10.1086/524988

Wang, X., Chen, L., Yuan, W., Li, Y., Li, L., Li, T., et al. (2017). Effect of porcine circovirus type 2 (PCV2) on the function of splenic CD11c+ dendritic cells in mice. *Arch. Virol.* 162, 1289–1298. doi: 10.1007/s00705-017-3221-8

Wang, Y. P., Liu, D., Guo, L. J., Tang, Q. H., Wei, Y. W., Wu, H. L., et al. (2013). Enhanced protective immune response to PCV2 subunit vaccine by co-administration of recombinant porcine IFN-γ in mice. *Vaccine* 31, 833–838. doi: 10.1016/j.vaccine.2012.11.062

Wynn, T. A., Ajay, C., and Pollard, J. W. (2013). Macrophage biology in development, homeostasis and disease. *Nature* 496, 445–455. doi: 10.1038/nature12034

Wynn, T. A., and Vannella, K. M. (2016). Macrophages in tissue repair, regeneration, and fibrosis. *Immunity* 44, 450–462. doi: 10.1016/j.immuni.2016.02.015

Xin, Y., Teng, M., Hongsheng, O., Fuwang, C., Zhiyuan, P., Chun, L., et al. (2015). Effect of atovastatin treatment on porcine circovirus 2 infection in BALB/c mice. *Clin. Exp. Pharmacol. Physiol.* 42, 817–821. doi: 10.1111/1440-1681.12434

Xu, H., Hao, S., Gan, F., Wang, H., Xu, J., Liu, D., et al. (2017). In vitro immune toxicity of ochratoxin A in porcine alveolar macrophages: a role for the ROS-relative TLR4/MyD88 signaling pathway. *Chem. Biol. Interact.* 272, 107–116. doi: 10.1016/j.cbi.2017.05.016

Zhai, N., Liu, K., Li, H., Liu, Z., Wang, H., Korolchuk, V. I., et al. (2019). PCV2 replication promoted by oxidative stress is dependent on the regulation of autophagy on apoptosis. *Vet. Res.* 50:19. doi: 10.1186/s13567-019-0637-z

Zhang, D., He, K., Wen, L., and Fan, H. (2018). Protective efficacy of a DNA vaccine encoding capsid protein of porcine circovirus-like virus P1 against porcine circovirus 2 in mice. *Microbiol. Immunol.* 62, 195–199. doi: 10.1111/1348-0421.12571

Zhang, G., Jia, P., Cheng, G., Jiao, S., Ren, L., Ji, S., et al. (2017). Enhanced immune response to inactivated porcine circovirus type 2 (PCV2) vaccine by conjugation of chitosan oligosaccharides. *Carbohyd. Polym.* 166, 64–72. doi: 10.1016/j.carbpol.2017.02.058

Zhao, X., Dai, J., Xiao, X., Wu, L., Zeng, J., Sheng, J., et al. (2014). PI3K/Akt signaling pathway modulates influenza virus induced mouse alveolar macrophage polarization to M1/M2b. *PLoS One* 9:e104506. doi: 10.1371/journal.pone.0104506

**Conflict of Interest:** The authors declare that the research was conducted in the absence of any commercial or financial relationships that could be construed as a potential conflict of interest.

**Publisher's Note:** All claims expressed in this article are solely those of the authors and do not necessarily represent those of their affiliated organizations, or those of the publisher, the editors and the reviewers. Any product that may be evaluated in this article, or claim that may be made by its manufacturer, is not guaranteed or endorsed by the publisher.

frontiers in Microbiology

REVIEW
published: 07 January 2022
doi: 10.3389/fmicb.2021.797789

# Molecular Events Involved in Influenza A Virus-Induced Cell Death

*Rui Gui*[1,2] *and Quanjiao Chen*[1]*

[1] CAS Key Laboratory of Special Pathogens and Biosafety, Center for Biosafety Mega-Science, CAS Center for Influenza Research and Early Warning, Wuhan Institute of Virology, Chinese Academy of Sciences, Wuhan, China, [2] University of Chinese Academy of Sciences, Beijing, China

Viral infection usually leads to cell death. Moderate cell death is a protective innate immune response. By contrast, excessive, uncontrolled cell death causes tissue destruction, cytokine storm, or even host death. Thus, the struggle between the host and virus determines whether the host survives. Influenza A virus (IAV) infection in humans can lead to unbridled hyper-inflammatory reactions and cause serious illnesses and even death. A full understanding of the molecular mechanisms and regulatory networks through which IAVs induce cell death could facilitate the development of more effective antiviral treatments. In this review, we discuss current progress in research on cell death induced by IAV infection and evaluate the role of cell death in IAV replication and disease prognosis.

**Keywords: cell death, influenza A virus, apoptosis, necroptosis, pyroptosis, viral infection**

OPEN ACCESS

***Edited by:***
*Honglin Luo,*
*University of British Columbia, Canada*

***Reviewed by:***
*Yasir Mohamud,*
*University of British Columbia, Canada*
*Shinji Ohno,*
*University of the Ryukyus, Japan*

***Correspondence:**
*Quanjiao Chen*
*chenqj@wh.iov.cn*

***Specialty section:***
*This article was submitted to Virology, a section of the journal Frontiers in Microbiology*

***Received:*** *19 October 2021*
***Accepted:*** *29 November 2021*
***Published:*** *07 January 2022*

***Citation:***
*Gui R and Chen Q (2022) Molecular Events Involved in Influenza A Virus-Induced Cell Death. Front. Microbiol. 12:797789. doi: 10.3389/fmicb.2021.797789*

## INTRODUCTION

Apoptosis, necroptosis, and pyroptosis are the three main patterns of cell death in multicellular organisms, playing vital roles not only in embryonic development; normal tissue homeostasis; and diseases, such as atherosclerosis, cancer, and neurodegeneration, but also in defense reactions against infection (Bellamy et al., 1995; Galluzzi et al., 2008; Fuchs and Steller, 2011; Walsh, 2014; Jorgensen et al., 2017; Gao et al., 2018). The concept of apoptosis was proposed for the first time in 1972 (Kerr et al., 1972). Apoptosis can be activated by two distinct signaling pathways, namely, intrinsic (mitochondrial) and extrinsic (death receptor) pathways (Lowy, 2003). The term "necroptosis" was first used to describe necrotic cell death in 2005 (Degterev et al., 2005). In the next decade, several critical molecules, including receptor interacting protein kinase (RIPK)1/3 and mixed lineage kinase domain like pseudokinase (MLKL) were found to be involved in necroptosis (Holler et al., 2000; Degterev et al., 2005; Cho et al., 2009; He et al., 2009; Zhang et al., 2009; Murphy et al., 2013). Additionally, pyroptotic cell death was first observed in 1986, when a research team found that cultured primary mouse macrophages induced cell death and leakage of cell contents when treated with the lethal toxin anthrax (Friedlander, 1986). In subsequent decades, follow-up research showed that pyroptosis relies on a gasdermin family member to induce cell rupturing and release cellular contents (Kayagaki et al., 2015; Liu et al., 2016; Aglietti and Dueber, 2017; Shi et al., 2017). Although cross-talk exists between apoptosis, necroptosis, and pyroptosis, apoptosis has minimal impact on neighboring cells because it is a non-inflammatory type of cell death; this is the main difference between apoptosis, necroptosis, and pyroptosis. Moreover, in necroptosis and pyroptosis, the release of cellular contents is an intense trigger of innate and adaptive immune responses (Henson et al., 2001; van Delft et al., 2010; Wallach et al., 2016; Shi et al., 2017).

Influenza A virus (IAV) is a negative-sense single-stranded RNA virus that is a member of the Orthomyxoviridae family (Yamauchi, 2020). IAV is among the most notorious respiratory diseases, causing almost 3–5 million cases of critical illness and approximately 250,000–500,000 deaths worldwide each year (Walsh, 2014; Hartmann et al., 2017; Doyon-Plourde et al., 2019). IAV mainly infects the airway epithelial cells, leading to inflammation and cell death, followed by respiratory tract damage, pneumonia, and even respiratory dysfunction or failure (Le Goffic et al., 2007; Cardani et al., 2017; Atkin-Smith et al., 2018). Severe IAV infection is always accompanied by hypercytokinemia, also known as cytokine storm, which is closely related to disease severity and could be a predictor of disease progression and mortality (De Jong et al., 2006; Guo et al., 2015; Zhang Y. et al., 2020). However, cell death and inflammation do not always harm the host; moderate cell death and inflammation can facilitate the elimination of viruses (Kuriakose et al., 2016; Zheng et al., 2020). Therefore, exploring the relative contribution of cell death and inflammation to suppression of viral replication and improvement of prognosis vs. disruption of host homeostasis and physical function, is particularly important for developing novel treatment strategies (Brandes et al., 2013).

In this review, we discuss the mechanisms of the three types of cell death (apoptosis, necroptosis, and pyroptosis) during IAV infection to address how IAV triggers and manipulates cell death and how these processes determine the final fates of viruses, cells, and hosts.

## APOPTOSIS DURING INFLUENZA A VIRUS INFECTION

Characteristic morphological features of intrinsic apoptosis, including flowing nuclear and cytoplasmic condensation, fragmentation of cellular DNA and membrane blebbing with apoptotic body formation during IAV infection were observed in previous studies (Takizawa et al., 1993; Fesq et al., 1994; Hinshaw et al., 1994; Mori et al., 1995). However, the specific mechanisms through which IAV induces apoptosis and the roles of apoptosis in IAV infection remain unclear. In recent years, apoptosis has been documented as a cell defense strategy against invading viruses in most multi-cellular organisms (Robert et al., 2012). Unfortunately, in the battle between viruses and their hosts, viruses have also evolved the ability to subvert apoptosis in the host cells (Danthi, 2016; Orning et al., 2018). Thus, apoptosis has both positive and negative effects on the life cycle of IAV (Galluzzi et al., 2008). In general, early apoptosis reduces viral replication, whereas late apoptosis promotes the release and dissemination of progeny viruses (Zhou et al., 2017).

## INTRINSIC APOPTOSIS

IAV primarily induces intrinsic apoptosis through some viral proteins and the IAV progeny ribonucleoprotein complex (vRNP) (**Table 1**). Research on apoptosis has revealed details of the mechanisms underlying IAV-induced apoptosis (Cardani et al., 2017; Zhou et al., 2017; Atkin-Smith et al., 2018).

These mechanisms may be classified into three types based on how viral proteins of IAV activate apoptosis. First, viral proteins interact with a host protein. Subsequently, mitochondrial membrane permeability is increased, which activates other specific signaling pathways to induce apoptosis (Chen et al., 2001). Second, vRNPs interact directly with DNA-dependent activator of interferon (IFN)-regulatory factor (DAI), which activates caspase-8 and then caspase-3, to induce apoptosis (Thapa et al., 2016). Third, upon IAV infection, endoplasmic reticulum (ER) stress and autophagy are triggered, thereby inducing apoptosis (Frabutt et al., 2018; Yeganeh et al., 2018). Fourth, some viral proteins can regulate apoptosis directly; however, the details of this mechanism are still unclear (Schultz-Cherry et al., 2001).

The viral protein PB1-F2 encoded by *PB1*, which is localized in the mitochondria of MDCK cells infected with IAV, has been shown to induce intrinsic apoptosis (type I) (Gibbs et al., 2003; Zamarin et al., 2005). *In vitro*, microinjection of PB1-F2 into MDCK cells causes its mitochondrial localization, which results in swelling and fragmentation, nuclear shrinkage, and cell death (Zamarin et al., 2005). In a previous study, the release of cytochrome c tagged with green fluorescent protein (Cc-GFP) from mitochondria was observed using flow cytometry when HeLa cells that contained a fusion protein consisting of Cc-GFP overexpressed in the mitochondria were transfected with PB1-F2. The release of Cc-GFP from mitochondria was observed in about 55% of cells in the PB1-F2 treatment group, compared with only 7% in the control group (Chen et al., 2001). In addition, when PB1-F2 was co-transfected with the anti-apoptotic protein Bcl-2 in Cc-GFP HeLa cells, release of Cc-GFP was decreased. Moreover, PB1-F2 can interact with adenine nucleotide translocase 3 (ANT3) and voltage-dependent anion-selective channel 1 (VDAC1), which are critical components of the pore complex on the mitochondrial membrane. When bongkrekic acid, a ANT3 inhibitor, was incubated with PB1-F2, apoptosis was also blocked partially (**Figure 1**; Zamarin et al., 2005).

In addition, the IAV nucleoprotein (NP), which is an essential part of the vRNP, also plays vital roles in promoting apoptosis and viral proliferation (Nailwal et al., 2015). NP induces apoptosis by hijacking host proteins such as clusterin precursor (CLU), RING finger protein 43 (RNF43), and apoptosis inhibitor 5 (API5). CLU was the first host protein identified, and has been shown to interact with NP to regulate apoptosis. CLU binds with Bax to inhibit the mitochondrial translocation of Bax and prevent apoptosis. However, when NP interacts with CLU, the interaction blocks the binding of CLU and Bax, thereby promoting apoptosis (**Figure 1**). Previous studies have evaluated the p53-Bax mitochondrial apoptosis network (McCurrach et al., 1997; Chipuk and Green, 2004; Chipuk et al., 2004; Ohtsuka et al., 2004) and shown that p53 is degraded by the host protein RNF43 through ubiquitination; however, ubiquitination is hampered when NP binds with RNF43, thereby promoting apoptosis (**Figure 1**; Nailwal et al., 2015). API5 is an anti-apoptotic protein whose mRNA and protein levels

**TABLE 1 |** Viral proteins of IAV that are involved in cell death.

| IAV protein | Subtypes | Molecular mechanism | Types of death |
|---|---|---|---|
| HA | H1N1 | - HA promotes apoptosis by enhancing host cell endoplasmic reticulum stress (Frabutt et al., 2018).<br>- Unknown (Hartmann et al., 2017). | Apoptosis<br>Necroptosis |
| NA | H1N1<br>H3N2 | - NA stimulates endoplasmic reticulum stress, enhancing apoptosis (Slaine et al., 2021).<br>-NA interacts with CEACAM6 protein, which increases the tyrosine phosphorylation of FAK, AKT, GSK3β, and Bcl-2, and inhibits cell death (Gaur et al., 2012). | Apoptosis |
| NP | H1N1<br>H1N1<br>H3N2 | - NP directly interacts with the anti-apoptotic protein CLU, which inhibits apoptosis by interacting with Bax, thereby interfering with the function of CLU (Tripathi et al., 2013).<br>- NP promotes apoptosis by down-regulating API5 expression; this interferes with E2F1 recruitment to the *Apaf-1* promoter, leading to down-regulation of *Apaf-1* and impairment of apoptosome formation (Morris et al., 2006; Mayank et al., 2015).<br>- NP interacts with RNF43, which can inhibit apoptosis by interacting with Bax and impairing RNF43 function (Nailwal et al., 2015). | Apoptosis |
| NS1 | H5N1<br>H1N1 | - Unknown (Schultz-Cherry et al., 2001; Lam et al., 2008).<br>- NS1 interacts with MLKL to induce oligomerization and membrane translocation (Gaba et al., 2019). | Apoptosis<br>Necroptosis |
| NS2 | - | - | - |
| M1 | H1N1 | - M1 directly interacts with Hsp70, which then interacts with *Apaf-1* to disrupt apoptosome formation (Halder et al., 2011). | Apoptosis |
| M2 | H1N1 | - M2 interacts with the ATG5/Beclin-1 complex to inhibit autophagosome fusion, promoting apoptosis (Gannage et al., 2009).<br>- M2-mediated perturbation of ion concentrations triggers activation of the NLRP3 inflammasome (Ichinohe et al., 2010). | Apoptosis<br>Pyroptosis |
| PB1-F2 | H3N2<br>H1NI<br>H1N1 | - PB1-F2 activates the NLRP3–ASC inflammasome (McAuley et al., 2013).<br>- PB1-F2 localizes to the mitochondria and alters mitochondrial permeability (Gibbs et al., 2003). | Pyroptosis<br>Apoptosis |
| PA-X | - | - | - |
| PA | H1N1 | - vRNPs are sensed by DAI/ZBP1, which then triggers the downstream cell death signaling pathway (Kuriakose et al., 2016; Thapa et al., 2016). | Apoptosis |
| PB1 | | | Necroptosis |
| PB2 | | | Pyroptosis |

are down-regulated when NP is overexpressed or when the cells were infected with IAV (Mayank et al., 2015). Further studies have demonstrated that NP promotes apoptosis by down-regulating API5, thereby interfering with E2F1. This blocks recruitment of E2F1 to the apoptotic protease-activating factor-1 (*Apaf-1*) promoter, resulting in downregulation of *Apaf-1* and thereby impairing apoptosome formation (**Figure 1**; Mayank et al., 2015). Neuraminidase (NA) protein functions primarily to facilitate the release of progeny virions. However, a recent study showed that NA also interacts with carcinoembryonic antigen-related cell adhesion molecule 6 (CEACAM6) to increase the phosphorylation of Src, AKT, and Bcl-2, resulting in inhibition of apoptosis and promotion of cell survival (**Figure 1**; Gaur et al., 2012).

The microenvironmental perturbations caused by IAV infection include autophagy and ER stress, both of which are implicated in IAV-induced apoptosis (Frabutt et al., 2018; Yeganeh et al., 2018). Both hemagglutinin (HA) which is responsible for viral attachment to cell-surface sialic acid residues and subsequent fusion of the viral and host cell membranes and NA proteins trigger the ER stress response (Frabutt et al., 2018; Slaine et al., 2021). Upon IAV infection, the ER stress markers (transcription factor 6 (ATF6) and endoplasmic reticulum protein 57-kDa (ERp57) are significantly upregulated compared with that in the control group, whereas RNAi knockdown of ATF6 and ERp57 reduces the activity of caspase-3 (Roberson et al., 2012). In addition to the ER stress pathway, autophagy is also implicated in IAV-induced apoptosis. One major characteristic of autophagy is the formation of autophagosomes, which capture cellular components, and fuse with lysosomes, where the cargo is degraded (Gannage et al., 2009; Maiuri et al., 2010). Upon IAV infection, autophagosomes accumulate, and the formation of autophagosome-lysosome complexes can be blocked by M2 ion channels, which function to facilitate fusion between the viral envelope and the endosomal membrane to mediate genome uncoating; these complexes the interact with ATG5/Beclin-1, enabling evasion of autophagy-mediated viral clearance, which significantly enhances apoptosis following IAV infection (Gannage et al., 2009).

The apoptosome consists of *Apaf-1, Apaf-2* (Cyt c), *Apaf-3* (caspase-9 precursor), and dATP. When Apaf-1 interacts with Apaf-3 through its N-terminal CARD domain in the presence

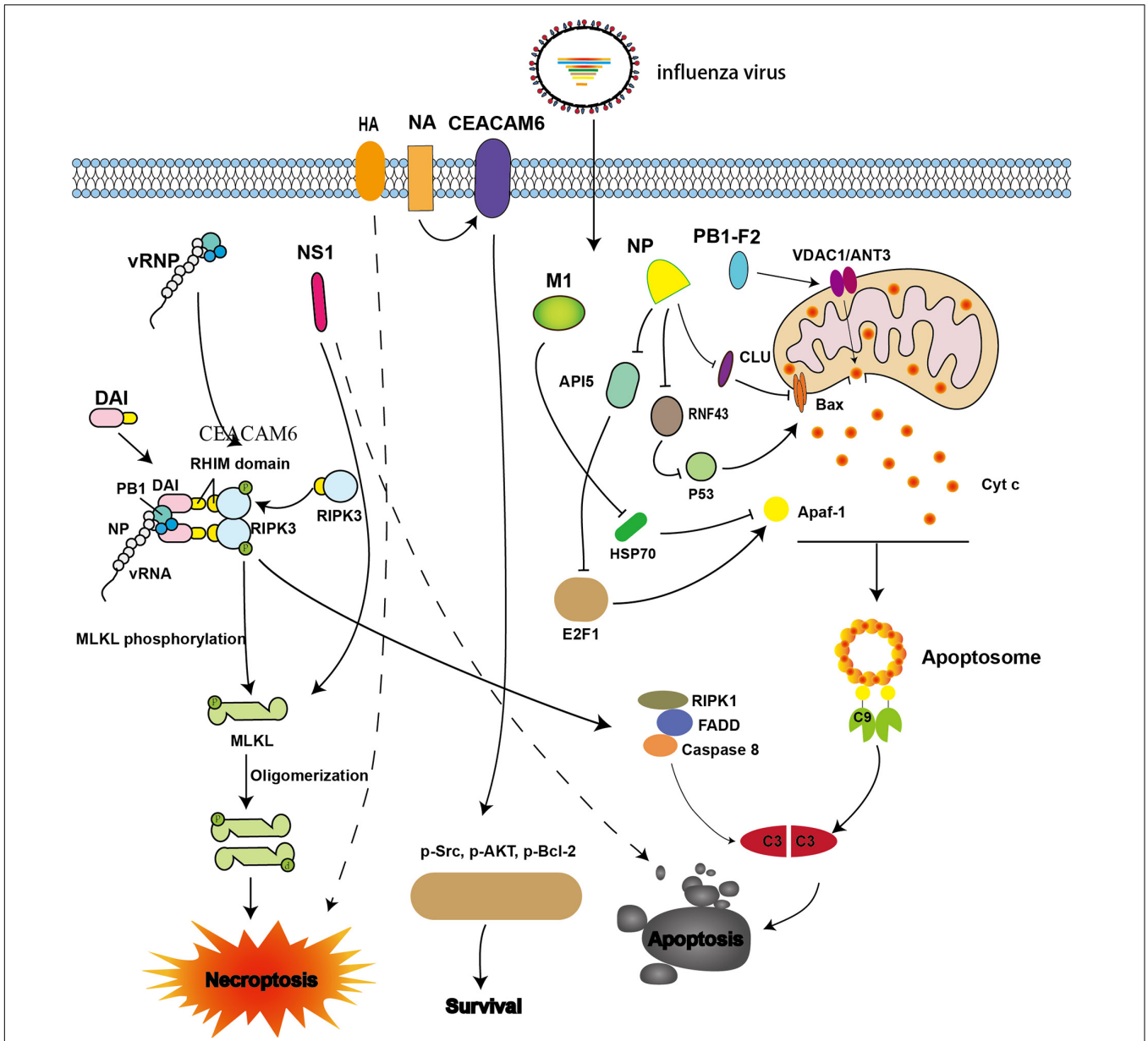


**FIGURE 1 |** Viral proteins involved in intrinsic apoptosis and necroptosis during influenza A virus (IAV) infection. The IAV progeny ribonucleoprotein complex (vRNP) is sensed by DAI via recruitment of RIPK3 to activate MLKL. NS1 directly interacts with MLKL and induces its oligomerization. NS1 also can induce apoptosis; however, the underlying mechanism is not well understood. NA interacts with CEACAM6 and increases the phosphorylation of Src, AKT, and Bcl-2, thereby inhibiting apoptosis. When M1 binds with Hsp70, apoptosome formation is blocked. When NP interacts with CLU and RNF43, its ability to resist apoptosis is weakened by interference with the mitochondrial translocation of Bax. NP also promotes apoptosis by down-regulating API5 expression, thereby inhibiting E2F1 recruitment to the *Apaf-1* promoter. The expression of Apaf-1 is then blocked, and apoptosome formation is impaired. PB1-F2 interacts with ANT3 and VDAC1, resulting in increased permeability of the mitochondrial outer membrane and induction of cytochrome c release.

of Apaf-2 and dATP, pro-caspase-9 is activated and converted to effector caspase-9, which initiates the caspase cascade (Liu et al., 1996; Li et al., 1997). Furthermore, Apaf-1 interacts with the C-terminal of heat shock protein 70 (Hsp70), which inhibits apoptosome formation and reduces apoptosis; however, M1 can bind with the substrate-binding domain of Hsp70 and interferes with the anti-apoptotic function of Hsp70 (**Figure 1**; Halder et al., 2011).

DAI (ZBP1/DLM-1) has been shown to act a cytoplasmic DNA sensor (Wang et al., 2008; Rebsamen et al., 2009; DeFilippis et al., 2010). In addition, upon IAV infection, pattern recognition receptors (PRRs) are also involved in the mechanism of cell death. In particular, DAI, which belongs to the cytosolic DNA sensor family, is one of the most important PRRs and, directly participates in IAV-induced cell death (here, we limit our discussion to its role in apoptosis). Recent studies have

demonstrated that vRNPs with defective viral genomes are directly sensed by the Zα domains of DAI (Thapa et al., 2016; Kesavardhana et al., 2017; Wang et al., 2019; Zhang T. et al., 2020).

During IAV infection, DAI recruits RIPK3 to activate downstream signaling via its RIPK homotypic interaction motif (RHIM) domains (Thapa et al., 2016; Kesavardhana et al., 2017). The activation of caspase-8 and caspase-3 is abrogated in DAI$^{-/-}$and RIPK3$^{-/-}$ cells, thereby inhibiting apoptosis (Kuriakose et al., 2016). Accordingly, IAV may promote apoptosis through the DAI/RIPK3/caspase-8 axis (**Figure 1**).

Non-structural protein 1 (NS1), which is encoded by the IAV *NS* gene, can antagonize innate immunity, e.g., by suppressing IFN-I secretion, and promote viral replication. NS1 has also been shown to be involved in the regulation of apoptosis; however, the mechanism is still unclear (Schultz-Cherry et al., 2001; Zhirnov et al., 2002; Lam et al., 2008). A comparison of apoptosis in cultured cells infected with wild-type (WT) IAVs (A/PR/8/34) and recombinant viruses with a mutant *NS1* gene (Schultz-Cherry et al., 2001) showed that typical apoptotic features, such as DNA fragmentation, were observed in WT IAVs, but not in mutant virus (**Figure 1**; Schultz-Cherry et al., 2001). Further studies are needed to assess the molecular mechanisms.

## EXTRINSIC APOPTOSIS

In addition to intrinsic pathways, IAV can mediate apoptosis via extrinsic signaling. The extrinsic apoptosis pathway is mediated by specific cell surface death receptors belonging to the tumor necrotic factor (TNF) receptor (TNFR) family, namely, TNFR1, Fas, and TRAIL-R1/2 (**Figure 2**; Nagata, 1999; MacFarlane et al., 2005; Vanden Berghe et al., 2015). All of these receptors possess an intracellular death domain (DD), which can recruit downstream adaptor proteins to assemble a set of complexes. The complexes activate caspase-8 and then induce apoptosis through a variety of homotypic interactions (Lee et al., 2012; Nair et al., 2014). These processes are tightly regulated and connected with necroptosis (Guo et al., 2015). TNFR1 plays a major role in mediating extrinsic apoptosis, and this process has been studied thoroughly. Here, we will use the TNRF1 pathway as an example to explain progress in studies of extrinsic apoptosis.

The binding of TNFα and TNFR1 does not always result in cell death. The fate of the cell, i.e., whether it survives or dies, is controlled by multiple key checkpoints (Vanden Berghe et al., 2015). When TNFR1 is activated, it recruits downstream adaptors, such as TRADD, TRAF2, RIPK1, and E3 ubiquitin ligases, and binds to cellular inhibitor of apoptosis 1 (cIAP) 1 and (cIAP2) to assemble complex-I via its DD (Dondelinger et al., 2013; Annibaldi and Meier, 2018). RIPK1 is subsequently ubiquitinated by cIAPs to form linear ubiquitins (Annibaldi and Meier, 2018). Then, these ubiquitin chains act as a signaling scaffold to recruit the kinase complex transforming growth factor (TGF)-β-activated kinase 1 (TAK1)/TGF-β activated kinase 1 binding protein (TAB) 2/TAB3/IκB kinase (IKK) after TNFα stimulation (Jaco et al., 2017; Annibaldi and Meier, 2018). The dissociation of RIPK1 from complex-I to assemble complex-II and its combination with the downstream adaptor protein FADD

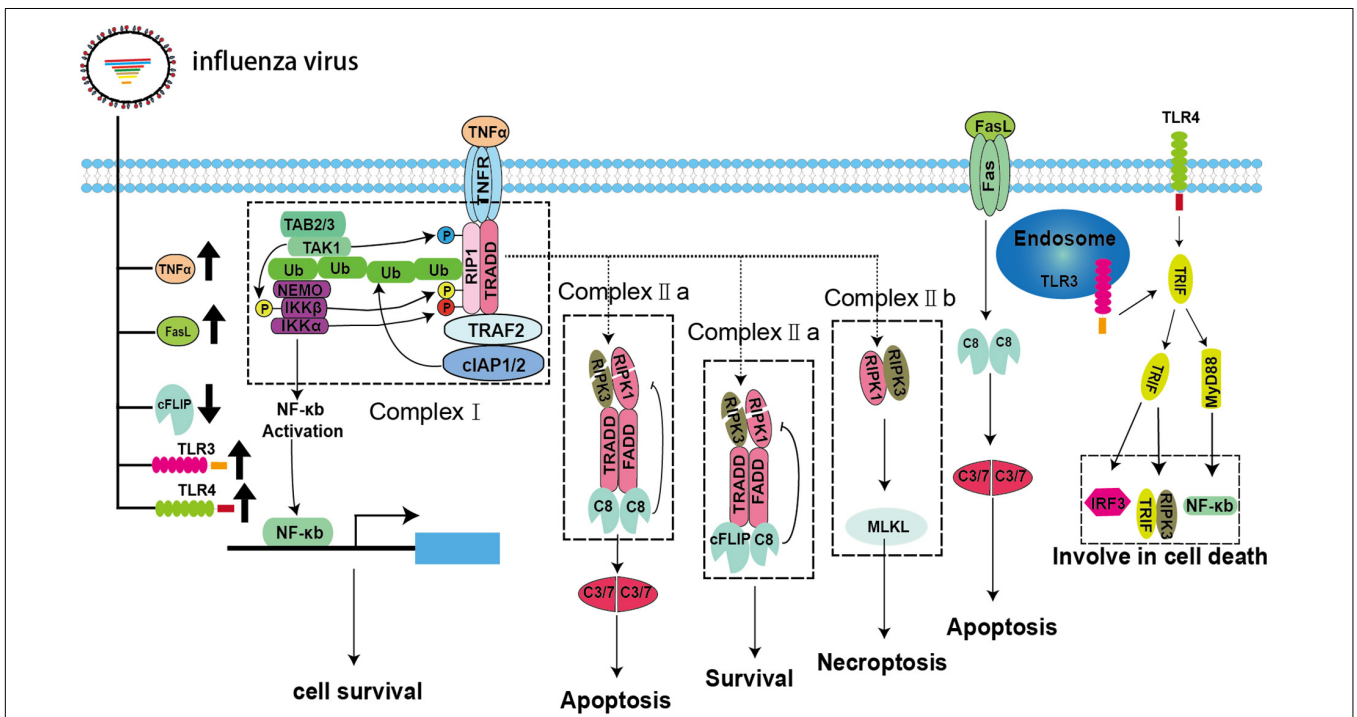


**FIGURE 2 |** Extrinsic apoptosis and necroptosis pathways during IAV infection. IAV infection can lead to upregulation of the death receptor ligands TNFα and FasL and the pattern recognition receptors TLR3/4 as well as downregulation of cFLIP.

and pro-caspase-8 are dependent on some vital checkpoints (Annibaldi and Meier, 2018). In complex-I, RIPK1 is directly phosphorylated by TAK1/IKKα/IKKβ to inhibit complex-II formation and apoptosis (Dondelinger et al., 2015; Annibaldi and Meier, 2018). In addition, MK2 and nuclear factor (NF)-κB can also be activated by TAK1 and IKK, respectively, resulting in the phosphorylation of cytoplasmic RIPK1, thereby, impairing complex-II assembly and the production of pro-survival molecules, such as cellular FADD-like interleukin (IL)-1β-converting enzyme-inhibitory protein (cFLIP), to inhibit the activation of caspase-8 (Dondelinger et al., 2017; Jaco et al., 2017; Annibaldi and Meier, 2018). However, little is known about the strategies developed by IAVs to modulate extrinsic apoptosis. Fortunately, IAV infection may upregulate pro-apoptotic TNFα and FasL and downregulate anti-apoptotic cFLIP *in vivo* and *in vitro*; therefore, we speculate that IAVs can mediate apoptosis via TNFα, FasL, and cFLIP (**Figure 2**; Herold et al., 2008; Monteerarat et al., 2010). Additionally, influenza viruses that use other strategies to manipulate extrinsic apoptosis cannot be excluded.

## NECROPTOSIS DURING INFLUENZA A VIRUS INFECTION

Necroptosis is a newly identified mode of programmed cell death that can be triggered in multiple ways. Based on the molecular events involved, necroptosis can be divided into canonical and non-canonical pathways and is intimately associated with apoptosis through RIPK1 in the canonical pathway (Green and Llambi, 2015). In this pathway, RIPK1, TRADD, and FADD recruit different types of downstream adaptor proteins and assemble into a dynamic complex called complex-IIa after de-ubiquitination, checkpoint escape, and dissociation from complex-I. Complex-IIa determines the ultimate fate of the cell. The homodimer of pro-caspase-8 is recruited to form complex-IIa, which activates pro-caspase-8, thereby inducing apoptosis (Green and Llambi, 2015). Typically, cFLIP, which is a structural analog of pro-caspase-8, recruits complex-IIa to form heterodimers with pro-caspase-8 and prevent its activation (Green and Llambi, 2015). As shown in **Figure 2**, both pro-caspase-8 homodimer and pro-caspase-8/cFLIP heterodimer can cleave essential necrosis modulators, such as RIPK1 and RIPK3. Thus, pro-caspase-8/cFLIP heterodimer can inhibit both apoptosis and necroptosis (Green and Llambi, 2015). However, when the function of either caspase-8 or cFLIP is suppressed, RIPK1 and RIPK3 forms an amyloid-like, intracellular complex-IIb (necrosome) to transmit the necroptosis signal through the downstream protein MLKL. MLKL is a pseudokinase that is phosphorylated and transferred to the cellular membrane after forming oligomers. Then, a pore is formed on the cellular membrane, which can lead to leakage of intracellular contents and induce necroptosis (Green and Llambi, 2015). However, the extent to which IAV is involved in this process is unclear. To date, only NS1 has been shown to interact with MLKL and induce its oligomerization, followed by disruption of the cell membranes (**Figure 1**; Gaba et al., 2019). Toll-like receptor (TLR) 3/4—mediated necroptosis is another non-canonical pathway that involves the downstream adaptor TIR-domain-containing adapter-inducing IFN-β (TRIF), which contains a C-terminal RHIM motif, and recruit RIPK3 to participate in necroptosis (He et al., 2011; Tsai et al., 2014). In fact, TLR3/4 are significantly upregulated *in vivo and in vitro* during IAV infection, and MyD88 and TRIF can be recruited to activate the downstream signaling molecules IFN regulatory factor 3 and NF-κB, which are closely related to inflammation and cell death (**Figure 2**; Le Goffic et al., 2007; He et al., 2011; Matsumoto et al., 2011; Tsai et al., 2014, 2015; Ma et al., 2020; Bertheloot et al., 2021). Current studies have suggested that IAV may trigger necroptosis through the TLR3/4/TRIF pathway, although direct evidence for IAV-induced necroptosis through this axis is lacking (**Figure 2**; Le Goffic et al., 2007; He et al., 2011; Matsumoto et al., 2011; Tsai et al., 2014, 2015).

In addition to its roles in apoptosis, DAI has also been associated with necroptosis. vRNPs are sensed by DAI, which then recruits the downstream protein RIPK3 and activates MLKL to induce necroptosis (Kuriakose et al., 2016; Thapa et al., 2016; Kesavardhana et al., 2017). Necrosomes and the phosphorylated form of MLKL in DAI$^{-/-}$ murine embryo fibroblasts or LET1 cells were undetected after IAV infection (Thapa et al., 2016). However, when MLKL$^{-/-}$ murine bone marrow-derived macrophages (BMDMs) were infected with IAV, the activated forms of caspase-1 and caspase-8 were detected (Kuriakose et al., 2016). Furthermore, cell death in MLKL$^{-/-}$ BMDMs showed no difference compared with that in WT BMDMs (Kuriakose et al., 2016). Intriguingly, a broad spectrum caspase inhibitor, Z-VAD-FMK, prevented cell death in MLKL$^{-/-}$ BMDMs (Kuriakose et al., 2016). These results demonstrated that multiple cell death pathways, including necroptosis, could be activated in IAV-infected cells. Moreover, the HA protein of seasonal IAV seems to be involved in necroptosis (Hartmann et al., 2017). However, the underlying mechanism has not yet been elucidated (**Table 1** and **Figure 1**).

## PYROPTOSIS DURING INFLUENZA A VIRUS INFECTION

For many years, pyroptosis was regarded as a caspase-1 mediated cell death mechanism in monocytes infected with bacteria, and caspase-1 was considered the executioner of pyroptosis (Shi et al., 2017). However, caspase-1 is now considered to a downstream product of inflammasomes, including AIM2/ASC, NLRC4, NLRP3/ASC, Pyrin/ASC, and NLRP1. The real pyroptosis executioner is gasdermin D (GSDMD). GSDMD is cleaved by caspase-1, which leads to exposure of the N domain of GSDMD and pore formation, thereby inducing pyroptosis (Ding et al., 2016). In an addition to caspase-1, caspases-4, −5, −8, and −11 have been shown to cleave GSDMD and trigger pyroptosis directly via a non-canonical pathway (Shi et al., 2014, 2017; Orning et al., 2018).

Pyroptosis has also been observed during IAV infection. Indeed, PB1-F2 from PR8 and H7N9 viruses was shown to induce ASC speck formation, NLRP3 activation, and IL-1β

secretion (Pinar et al., 2017). These results are consistent with previous studies (**Figure 3**; McAuley et al., 2013). The influenza virus M2 protein was found to activate inflammasome and induce pyroptosis by modifying intracellular pH (**Figure 3**; Ichinohe et al., 2010). Several studies have indicated that DAI is also involved in the regulation of pyroptosis during IAV infection (Kuriakose et al., 2016; Thapa et al., 2016). A previous study demonstrated that DAI recognize vRNPs and triggers pyroptosis during IAV infection. Moreover, in DAI$^{-/-}$ or RIPK3$^{-/-}$caspase-8$^{-/-}$ BMDMs, the active form of caspase-1 is completely abolished. Even in RIPK3$^{-/-}$ BMDMs, the activation of caspase-1 is extremely reduced compared with that in WT BMDMs. IL-1β and IL-18 are also significantly downregulated (Kuriakose et al., 2016). These results indicate that RIPK3-caspase-8 is located upstream of GSDMD and downstream of DAI; however, it is not clear how the DAI–RIPK3–caspase-8 signal induces pyroptosis. Nevertheless, GSDMD is cleaved by caspase-8 (Orning et al., 2018; Sarhan et al., 2018) and the

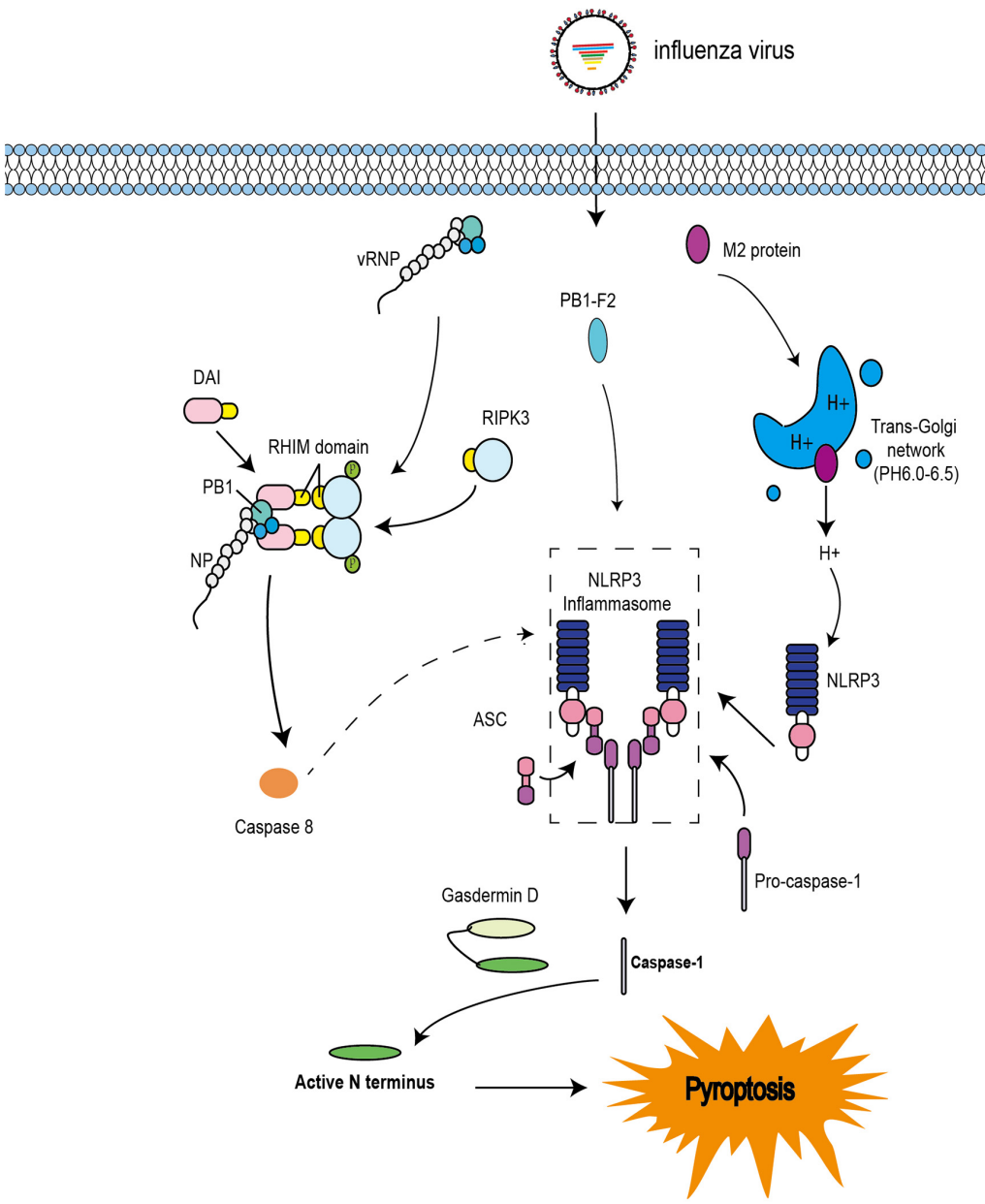


**FIGURE 3 |** Pyroptosis pathways induced by IAV. The IAV progeny ribonucleoprotein complex (vRNP) is sensed by DAI via recruitment of RIPK3 to activate caspase-8. Caspase-8 may cleave GSDMD, and the N-terminal GSDMD fragment then activates NLRP3-dependent caspase-1. PB1-F2 can induce ASC speck formation, NLRP3 activation, and cleavage of caspase-1. M2 is translocated to the Golgi apparatus as a proton ion channel to alter the pH of intracellular compartments and activate inflammasomes.

N-terminal GSDMD fragment, which is the active form of GSDMD, triggers the activation of NLRP3-dependent caspase-1 via non-canonical inflammasome signaling (Kayagaki et al., 2015). Based on these studies, IAV infection may trigger pyroptosis via the RIPK1-RIPK3-caspase-8-GSDMD axis and then induce inflammation, leading to pyroptosis via the NLRP3-dependent caspase-1 activation signal (**Figure 3**).

Cell death is a vital part of the immune response against viral infection, and can suppress virus replication. However, excessive cell death may induce cytokine storms, thereby worsening the disease. This contradictory phenomenon has been observed in previous studies (Kuriakose et al., 2016; Thapa et al., 2016). For example, DAI is a pivotal sensor that can sense the vRNP of IAV and induce cell death (Kesavardhana et al., 2017). In a comparative analysis of WT and DAI$^{-/-}$ mice infected with the PR8 influenza strain, all WT mice recovered from viral infection within 15–18 days post-infection (Thapa et al., 2016). However, 80% of DAI$^{-/-}$ mice succumbed to IAV infection. Higher lung viral titers and longer recovery times were observed in DAI$^{-/-}$ mice compared with those in WT mice (Thapa et al., 2016). Thus, the role of DAI in IAV infection is controversial. Kuriakose et al. (2016) reported a decrease in mortality in IAV-infected DAI$^{-/-}$ mice, although these mice had higher lung viral titers (Kuriakose et al., 2016). Moreover, the inflammatory response and epithelial damage in IAV-infected DAI$^{-/-}$ mice are both reduced (Kuriakose et al., 2016), consistent with the findings of Thapa et al. (2016). However, the differences between these studies remain unexplained. Over all, the results of the animal experiments indicated that IAV-mediated cell death is decreased, whereas viral replication and inflammation responses are attenuated. Further studies are needed to assess whether these features are associated with a good prognosis.

## CROSS-TALK AMONG APOPTOSIS, NECROPTOSIS, AND PYROPTOSIS

Upon infection with IAV, apoptosis, necroptosis, and pyroptosis (PANoptosis) have been observed both *in vitro* and *in vivo* (Lee et al., 2018). DAI has been found to directly recognize vRNPs and recruit an array of molecules, namely, NLRP3, RIPK1, RIPK3, caspase-8, caspase-6, and ASC, to form a multiprotein platform called PANoptosome (Christgen et al., 2020; Zheng et al., 2020). The PANoptosome initiates the cell death signal, i.e., PANoptosis. The interaction between DAI and different adaptors activates distinct forms of cell death (Kuriakose et al., 2016; Thapa et al., 2016). DAI-RIPK1-FADD-CASPASE-8 signaling pathway promotes apoptosis (Thapa et al., 2016). The DAI-RIPK3-MLKL signaling pathway induces necroptosis (Thapa et al., 2016), and the DAI-NLRP3-CASPASE-1 signaling pathway triggers pyroptosis (Kuriakose et al., 2016). Although the critical initiator, DAI, is involved in PANoptosis during IAV infection, the molecular details of the formation and dissociation of the PANoptosome remain poorly understood. Furthermore, although vRNPs are recognized by DAI, it is unclear which cell death signal is activated preferentially, and the precise spatio-temporal order and the mechanisms of different cell death signaling cascades also remain unclear. Thus, further research focusing on elucidating of these mechanisms is necessary to identify novel targets for drug development.

## CELL DEATH AND INFLAMMATION

Eukaryotic cells can die via several distinct biochemical pathways, which exhibit diverse physiological and morphological features (D'Arcy, 2019). Cell death plays a critical role in organism development and host defense (Barber, 2001). IAV infection commits the cell to cell death in the form of apoptosis, necroptosis, and pyroptosis (PANoptosis) (Thapa et al., 2016). Apoptotic cells preserve membrane integrity and are considered an immunologically silent form of cell death, enabling phagocytes to engulf themselves (a process called "efferocytosis") via phosphatidylserine on the apoptotic surface (Elmore, 2007; Poon et al., 2014). By contrast, the persistence of uncleared apoptotic bodies can lead to rupture of the plasma membrane, which releases a series of damage-associated molecular patterns and triggers the inflammatory response (Poon et al., 2014; Venereau et al., 2015). Thus, the efficient clearance of IAV-infected apoptotic bodies by phagocytes is crucial to prevent further exacerbation of the inflammatory response. Phagocytosis of apoptotic bodies and IAV-infected cells by macrophages was discovered in the bronchi alveolar lavage fluid and lung tissue (Atkin-Smith et al., 2018). However, necroptosis and pyroptosis are forms of pro-inflammatory cell death, and the contents of necrotic cells released into the extracellular space elevate inflammation via multiple PRRs (Kang et al., 2014; Venereau et al., 2015). By contrast, pyroptotic cells, through persistent activation and release of the pro-inflammatory cytokines IL-1β and IL-18, ultimately exacerbate inflammation (Kuriakose et al., 2016; Lee et al., 2018). Eventually, excessive cell death within the upper and lower respiratory tracts and lung parenchyma further exacerbates inflammation, compromises the integrity of the epithelial cell barrier, and contributes to respiratory failure (Atkin-Smith et al., 2018).

## CONCLUSION

Although some *in vivo* animal experiments have been performed, most of the research on programmed cell death in IAV infection has been based on *in vitro* experiments, which do not reflect the true course of the IAV infection. Despite the limitations of these experiments, the data can be utilized to elucidate the relationships among cell death, viral replication, and inflammatory responses. For example, CLU and API5 can alleviate the pro-apoptotic effects of NP, and significantly reduce cell death and suppress viral replication (Morris et al., 2006; Mayank et al., 2015). By contrast, one study showed that although the host protein CEACAM6 promotes cell survival, it also enhances viral replication (Gaur et al., 2012). It is unclear why these *in vitro* cell assays have yielded paradoxical results; however, these contradictions may be related to the differences in the influenza viral strains used, infection times, and infection dosages in the testing regime.

More scientifically rigorous methodologies must be developed to address this issue. Moreover, analyses of clinical cases may provide some insights. A recent study of fatal cases of IAV infection revealed diffuse alveolar damage and cell death, providing insights into the relationships between cell death and disease prognosis (De Jong et al., 2006). Importantly, cytokine storm has also been shown to be closely associated with cell death. In addition to cytokine storm in IAV infection, this phenomenon has also been observed in severe acute respiratory syndrome coronavirus (SARS-CoV), Middle East respiratory syndrome coronavirus (MERS-CoV), and SARS-CoV-2 infections and has been shown to be associated with disease severity and mortality (Cao, 2020; Felsenstein et al., 2020; Zhang Y. et al., 2020). Accordingly, these findings suggest that excessive cell death may cause serious severe tissue damage and hypercytokinemia. Further studies are needed to investigate the relationships among cell death, inflammatory reactions, viral replication, and disease prognosis in IAV infection.

## AUTHOR CONTRIBUTIONS

RG wrote the initial draft of the manuscript and prepared the figures. QC carefully revised and corrected the manuscript. Both authors contributed to the article and approved the submitted version.

## FUNDING

This work was supported by the National Science and Technology Major Project (grant no. 2020ZX10001016).

## ACKNOWLEDGMENTS

We would like to thank Editage (www.editage.cn) for English language editing.

## REFERENCES

Aglietti, R. A., and Dueber, E. C. (2017). Recent insights into the molecular mechanisms underlying pyroptosis and gasdermin family functions. *Trends Immunol.* 38, 261–271. doi: 10.1016/j.it.2017.01.003

Annibaldi, A., and Meier, P. (2018). Checkpoints in TNF-induced cell death: implications in inflammation and cancer. *Trends Immunol.* 24, 49–65. doi: 10.1016/j.molmed.2017.11.002

Atkin-Smith, G. K., Duan, M., Chen, W., and Poon, I. K. (2018). The induction and consequences of influenza A virus-induced cell death. *Cell Death Dis.* 9:1002. doi: 10.1038/s41419-018-1035-6

Barber, G. N. (2001). Host defense, viruses and apoptosis. *Cell Death Dis.* 8, 113–126. doi: 10.1038/sj.cdd.4400823

Bellamy, C. O., Malcomson, R. D., Harrison, D. J., and Wyllie, A. H. (1995). Cell death in health and disease: the biology and regulation of apoptosis. *Semin. Cancer Biol.* 6, 3–16. doi: 10.1006/scbi.1995.0002

Bertheloot, D., Latz, E., and Franklin, B. S. (2021). Necroptosis, pyroptosis and apoptosis: an intricate game of cell death. *Cell Mol. Immunol.* 18, 1106–1121. doi: 10.1038/s41423-020-00630-3

Brandes, M., Klauschen, F., Kuchen, S., and Germain, R. N. (2013). A systems analysis identifies a feedforward inflammatory circuit leading to lethal influenza infection. *Cell* 154, 197–212. doi: 10.1016/j.cell.2013.06.013

Cao, X. (2020). COVID-19: immunopathology and its implications for therapy. *Nat. Rev. Immunol.* 20, 269–270. doi: 10.1038/s41577-020-0308-3

Cardani, A., Boulton, A., Kim, T. S., and Braciale, T. J. (2017). Alveolar macrophages prevent lethal influenza pneumonia by inhibiting infection of type-1 alveolar epithelial cells. *PLoS Pathog.* 13:e1006140. doi: 10.1371/journal.ppat.1006140

Chen, W., Calvo, P. A., Malide, D., Gibbs, J., Schubert, U., Bacik, I., et al. (2001). A novel influenza a virus mitochondrial protein that induces cell death. *Nat. Med.* 7, 1306–1312. doi: 10.1038/nm1201-1306

Chipuk, J. E., and Green, D. R. (2004). Cytoplasmic p53: bax and forward. *Cell Cycle* 3, 427–429.

Chipuk, J. E., Kuwana, T., Bouchier-Hayes, L., Droin, N. M., Newmeyer, D. D., Schuler, M., et al. (2004). Direct activation of Bax by p53 mediates mitochondrial membrane a novel influenza a virus mitochondrial protein that induces cell death. Nature medicine permeabilization and apoptosis. *Science* 303, 1010–1014.

Cho, Y. S., Challa, S., Moquin, D., Genga, R., Ray, T. D., Guildford, M., et al. (2009). Phosphorylation-driven assembly of the RIP1-RIP3 complex regulates programmed necrosis and virus-induced inflammation. *Cell* 137, 1112–1123. doi: 10.1016/j.cell.2009.05.037

Christgen, S., Zheng, M., Kesavardhana, S., Karki, R., Malireddi, R. K. S., Banoth, B., et al. (2020). Identification of the PANoptosome: a molecular platform triggering pyroptosis, apoptosis, and necroptosis (PANoptosis). *Front. Cell Infect. Microbiol.* 10:237. doi: 10.3389/fcimb.2020.00237

D'Arcy, M. S. (2019). Cell death: a review of the major forms of apoptosis, necrosis and autophagy. *Cell Biol. Int.* 43, 582–592. doi: 10.1002/cbin.11137

Danthi, P. (2016). Viruses and the diversity of cell death. *Annu. Rev. Virol.* 3, 533–553. doi: 10.1146/annurev-virology-110615-042435

De Jong, M. D., Simmons, C. P., Thanh, T. T., Hien, V. M., Smith, G. J., Chau, T. N. B., et al. (2006). Fatal outcome of human influenza A (H5N1) is associated with high viral load and hypercytokinemia. *Nat. Med.* 12, 1203–1207. doi: 10.1038/nm1477

DeFilippis, V. R., Alvarado, D., Sali, T., Rothenburg, S., and Früh, K. (2010). Human cytomegalovirus induces the interferon response via the DNA sensor ZBP1. *J. Virol.* 84, 585–598. doi: 10.1128/JVI.01748-09

Degterev, A., Huang, Z., Boyce, M., Li, Y., Jagtap, P., Mizushima, N., et al. (2005). Chemical inhibitor of nonapoptotic cell death with therapeutic potential for ischemic brain injury. *Nat. Chem. Biol.* 1, 112–119. doi: 10.1038/nchembio711

Ding, J., Wang, K., Liu, W., She, Y., Sun, Q., Shi, J., et al. (2016). Pore-forming activity and structural autoinhibition of the gasdermin family. *Nature* 535, 111–116. doi: 10.1038/nature18590

Dondelinger, Y., Aguileta, M., Goossens, V., Dubuisson, C., Grootjans, S., Dejardin, E., et al. (2013). RIPK3 contributes to TNFR1-mediated RIPK1 kinase-dependent apoptosis in conditions of cIAP1/2 depletion or TAK1 kinase inhibition. *Cell Death Differ.* 20, 1381–1392. doi: 10.1038/cdd.2013.94

Dondelinger, Y., Delanghe, T., Rojas-Rivera, D., Priem, D., Delvaeye, T., Bruggeman, I., et al. (2017). MK2 phosphorylation of RIPK1 regulates TNF-mediated cell death. *Nat. Cell Biol.* 19, 1237–1247. doi: 10.1038/ncb3608

Dondelinger, Y., Jouan-Lanhouet, S., Divert, T., Theatre, E., Bertin, J., Gough, P. J., et al. (2015). NF-κB-independent role of IKKα/IKKβ in preventing RIPK1 kinase-dependent apoptotic and necroptotic cell death during TNF signaling. *Mol. Cell* 60, 63–76. doi: 10.1016/j.molcel.2015.07.032

Doyon-Plourde, P., Fakih, I., Tadount, F., Fortin, E., and Quach, C. (2019). Impact of influenza vaccination on healthcare utilization–a systematic review. *Vaccine* 37, 3179–3189. doi: 10.1016/j.vaccine.2019.04.051

Elmore, S. (2007). Apoptosis: a review of programmed cell death. *Toxicol. Pathol.* 35, 495–516. doi: 10.1080/01926230701320337

Felsenstein, S., Herbert, J. A., McNamara, P. S., and Hedrich, C. M. (2020). COVID-19: immunology and treatment options. *Clin. Immunol.* 215:108448. doi: 10.1016/j.clim.2020.108448

Fesq, H., Bacher, M., Nain, M., and Gemsa, D. (1994). Programmed cell death (apoptosis) in human monocytes infected by influenza A virus. *Immunobiology* 190, 175–182. doi: 10.1016/S0171-2985(11)80292-5

Frabutt, D. A., Wang, B., Riaz, S., Schwartz, R. C., and Zheng, Y. H. (2018). Innate sensing of influenza a virus hemagglutinin glycoproteins by the host endoplasmic reticulum (ER) Stress pathway triggers a potent antiviral response

via ER-associated protein degradation. *J. Virol.* 92, e1690–e1617. doi: 10.1128/JVI.01690-17

Friedlander, A. M. (1986). Macrophages are sensitive to anthrax lethal toxin through an acid-dependent process. *J. Biol. Chem.* 261, 7123–7126.

Fuchs, Y., and Steller, H. (2011). Programmed cell death in animal development and disease. *Cell* 147, 742–758. doi: 10.1016/j.cell.2011.10.033

Gaba, A., Xu, F., Lu, Y., Park, H.-S., Liu, G., and Zhou, Y. (2019). The NS1 protein of influenza A virus participates in necroptosis by interacting with MLKL and increasing its oligomerization and membrane translocation. *J. Virol.* 93, e1835–e1818. doi: 10.1128/JVI.01835-18

Galluzzi, L., Brenner, C., Morselli, E., Touat, Z., and Kroemer, G. (2008). Viral control of mitochondrial apoptosis. *PLoS Pathog.* 4:e1000018. doi: 10.1371/journal.ppat.1000018

Gannage, M., Dormann, D., Albrecht, R., Dengjel, J., Torossi, T., Ramer, P. C., et al. (2009). Matrix protein 2 of influenza A virus blocks autophagosome fusion with lysosomes. *Cell Host Microbe* 6, 367–380. doi: 10.1016/j.chom.2009.09.005

Gao, Y. L., Zhai, J. H., and Chai, Y. F. (2018). Recent advances in the molecular mechanisms underlying pyroptosis in sepsis. *Mediators Inflamm.* 2018:5823823. doi: 10.1155/2018/5823823

Gaur, P., Ranjan, P., Sharma, S., Patel, J. R., Bowzard, J. B., Rahman, S. K., et al. (2012). Influenza A virus neuraminidase protein enhances cell survival through interaction with carcinoembryonic antigen-related cell adhesion molecule 6 (CEACAM6) protein. *J. Biol. Chem.* 287, 15109–15117. doi: 10.1074/jbc.M111.328070

Gibbs, J. S., Malide, D., Hornung, F., Bennink, J. R., and Yewdell, J. W. (2003). The influenza A virus PB1-F2 protein targets the inner mitochondrial membrane via a predicted basic amphipathic helix that disrupts mitochondrial function. *J. Virol.* 77, 7214–7224. doi: 10.1128/jvi.77.13.7214-7224.2003

Green, D. R., and Llambi, F. (2015). Cell death signaling. *Cold Spring Harb. Perspect. Biol.* 7:a006080. doi: 10.1101/cshperspect.a006080

Guo, J., Huang, F., Liu, J., Chen, Y., Wang, W., Cao, B., et al. (2015). The serum profile of hypercytokinemia factors identified in H7n9-infected patients can predict fatal outcomes. *Sci. Rep.* 5:10942. doi: 10.1038/srep10942

Halder, U., Bagchi, P., Chattopadhyay, S., Dutta, D., and Chawla-Sarkar, M. (2011). Cell death regulation during influenza A virus infection by matrix (M1) protein: a model of viral control over the cellular survival pathway. *Cell Death Dis.* 2, e197–e197. doi: 10.1038/cddis.2011.75

Hartmann, B. M., Albrecht, R. A., Zaslavsky, E., Nudelman, G., Pincas, H., Marjanovic, N., et al. (2017). Pandemic H1N1 influenza A viruses suppress immunogenic RIPK3-driven dendritic cell death. *Nat. Commun.* 8:1931. doi: 10.1038/s41467-017-02035-9

He, S., Liang, Y., Shao, F., and Wang, X. (2011). Toll-like receptors activate programmed necrosis in macrophages through a receptor-interacting kinase-3–mediated pathway. *Proc. Natl. Acad. Sci. U.S.A.* 108, 20054–20059. doi: 10.1073/pnas.1116302108

He, S., Wang, L., Miao, L., Wang, T., Du, F., Zhao, L., et al. (2009). Receptor interacting protein kinase-3 determines cellular necrotic response to TNF-alpha. *Cell* 137, 1100–1111. doi: 10.1016/j.cell.2009.05.021

Henson, P. M., Bratton, D. L., and Fadok, V. A. (2001). Apoptotic cell removal. *Curr. Biol.* 11, R795–R805. doi: 10.1016/s0960-9822(01)00474-2

Herold, S., Steinmueller, M., von Wulffen, W., Cakarova, L., Pinto, R., Pleschka, S., et al. (2008). Lung epithelial apoptosis in influenza virus pneumonia: the role of macrophage-expressed TNF-related apoptosis-inducing ligand. *J. Exp. Med.* 205, 3065–3077. doi: 10.1084/jem.20080201

Hinshaw, V. S., Olsen, C. W., Dybdahl-Sissoko, N., and Evans, D. (1994). Apoptosis: a mechanism of cell killing by influenza A and B viruses. *J. Virol.* 68, 3667–3673. doi: 10.1128/JVI.68.6.3667-3673.1994

Holler, N., Zaru, R., Micheau, O., Thome, M., Attinger, A., Valitutti, S., et al. (2000). Fas triggers an alternative, caspase-8-independent cell death pathway using the kinase RIP as effector molecule. *Nat. Immunol.* 1, 489–495. doi: 10.1038/82732

Ichinohe, T., Pang, I. K., and Iwasaki, A. (2010). Influenza virus activates inflammasomes via its intracellular M2 ion channel. *Nat. Immunol.* 11:404. doi: 10.1038/ni.1861

Jaco, I., Annibaldi, A., Lalaoui, N., Wilson, R., Tenev, T., Laurien, L., et al. (2017). MK2 phosphorylates RIPK1 to prevent TNF-induced cell death. *Mol. Cell* 66, 698.–710. doi: 10.1016/j.molcel.2017.05.003

Jorgensen, I., Rayamajhi, M., and Miao, E. A. (2017). Programmed cell death as a defence against infection. *Nat. Rev. Immunol.* 17, 151–164. doi: 10.1038/nri.2016.147

Kang, R., Lotze, M. T., Zeh, H. J., Billiar, T. R., and Tang, D. (2014). Cell death and DAMPs in acute pancreatitis. *Mol. Med.* 20, 466–477. doi: 10.2119/molmed.2014.00117

Kayagaki, N., Stowe, I. B., Lee, B. L., O'Rourke, K., Anderson, K., Warming, S., et al. (2015). Caspase-11 cleaves gasdermin D for non-canonical inflammasome signalling. *Nature* 526, 666–671. doi: 10.1038/nature15541

Kerr, J. F. R., Wyllie, A. H., and Currie, A. R. (1972). Apoptosis: a basic biological phenomenon with wideranging implications in tissue kinetics. *Br. J. Cancer* 26, 239–257. doi: 10.1038/bjc.1972.33

Kesavardhana, S., Kuriakose, T., Guy, C. S., Samir, P., Malireddi, R. S., Mishra, A., et al. (2017). ZBP1/DAI ubiquitination and sensing of influenza vRNPs activate programmed cell death. *J. Exp. Med.* 214, 2217–2229. doi: 10.1084/jem.20170550

Yamauchi, Y. (2020). Influenza A virus uncoating. *Adv. Virus Res.* 2020, 1–38. doi: 10.1016/bs.aivir.2020.01.001

Kuriakose, T., Man, S. M., Subbarao Malireddi, R. K., Karki, R., Kesavardhana, S., Place, D. E., et al. (2016). ZBP1/DAI is an innate sensor of influenza virus triggering the NLRP3 inflammasome and programmed cell death pathways. *Sci. Immunol.* 1:aag2045. doi: 10.1126/sciimmunol.aag2045

Lam, W. Y., Tang, J. W., Yeung, A. C. M., Chiu, L. C. M., Sung, J. J. Y., and Chan, P. K. S. (2008). Avian influenza virus A/HK/483/97(H5N1) NS1 protein induces apoptosis in human airway epithelial cells. *J. Virol.* 82, 2741–2751. doi: 10.1128/JVI.01712-07

Le Goffic, R., Pothlichet, J., Vitour, D., Fujita, T., Meurs, E., Chignard, M., et al. (2007). Cutting edge: influenza a virus activates TLR3-dependent inflammatory and RIG-I-dependent antiviral responses in human lung epithelial cells. *J. Immunol.* 178, 3368–3372. doi: 10.4049/jimmunol.178.6.3368

Lee, E.-W., Seo, J.-H., Jeong, M.-H., Lee, S.-S., and Song, J.-W. (2012). The roles of FADD in extrinsic apoptosis and necroptosis. *BMB Rep.* 45, 496–508. doi: 10.5483/bmbrep.2012.45.9.186

Lee, S., Hirohama, M., Noguchi, M., Nagata, K., and Kawaguchi, A. (2018). Influenza A virus infection triggers pyroptosis and apoptosis of respiratory epithelial cells through the type I interferon signaling pathway in a mutually exclusive manner. *J. Virol.* 92:14. doi: 10.1128/JVI.00396-18

Li, P., Nijhawan, D., Budihardjo, I., Srinivasula, S. M., Ahmad, M., Alnemri, E. S., et al. (1997). Cytochrome c and dATP-dependent formation of Apaf-1/caspase-9 complex initiates an apoptotic protease cascade. *Cell* 91, 479–489. doi: 10.1016/s0092-8674(00)80434-1

Liu, X., Kim, C. N., Yang, J., Jemmerson, R., and Wang, X. (1996). Induction of apoptotic program in cell-free extracts: requirement for dATP and cytochrome c. *Cell* 86, 147–157. doi: 10.1016/s0092-8674(00)80085-9

Liu, X., Zhang, Z., Ruan, J., Pan, Y., Magupalli, V. G., Wu, H., et al. (2016). Inflammasome-activated gasdermin D causes pyroptosis by forming membrane pores. *Nature* 535, 153–158. doi: 10.1038/nature18629

Lowy, R. J. (2003). Influenza virus induction of apoptosis by intrinsic and extrinsic mechanisms. *Int. Rev. Immunol.* 22, 425–449. doi: 10.1080/08830180305216

Ma, Q., Huang, W., Zhao, J., and Yang, Z. (2020). Liu Shen Wan inhibits influenza a virus and excessive virus-induced inflammatory response via suppression of TLR4/NF-κB signaling pathway in vitro and in vivo. *J. Ethnopharmacol.* 252:112584. doi: 10.1016/j.jep.2020.112584

MacFarlane, M., Kohlhaas, S. L., Sutcliffe, M. J., Dyer, M. J., and Cohen, G. M. (2005). TRAIL receptor-selective mutants signal to apoptosis via TRAIL-R1 in primary lymphoid malignancies. *Cancer Res.* 65, 11265–11270. doi: 10.1158/0008-5472.CAN-05-2801

Maiuri, M. C., Galluzzi, L., Morselli, E., Kepp, O., Malik, S. A., and Kroemer, G. (2010). Autophagy regulation by p53. *Curr. Opin. Cell Biol.* 22, 181–185. doi: 10.1016/j.ceb.2009.12.001

Matsumoto, M., Oshiumi, H., and Seya, T. (2011). Antiviral responses induced by the TLR3 pathway. *Rev. Med. Virol.* 21, 67–77. doi: 10.1002/rmv.680

Mayank, A., Sharma, S., Nailwal, H., and Lal, S. (2015). Nucleoprotein of influenza A virus negatively impacts antiapoptotic protein API5 to enhance E2F1-dependent apoptosis and virus replication. *Cell Death Dis.* 6:e2018. doi: 10.1038/cddis.2015.360

McAuley, J. L., Tate, M. D., MacKenzie-Kludas, C. J., Pinar, A., Zeng, W., Stutz, A., et al. (2013). Activation of the NLRP3 inflammasome by IAV virulence protein PB1-F2 contributes to severe pathophysiology and disease. *PLoS Pathog.* 9:e1003392. doi: 10.1371/journal.ppat.1003392

McCurrach, M. E., Connor, T. M., Knudson, C. M., Korsmeyer, S. J., and Lowe, S. W. (1997). Bax-deficiency promotes drug resistance and oncogenic transformation by attenuating p53-dependent apoptosis. *Proc. Natl. Acad. Sci. U.S.A.* 94, 2345–2349. doi: 10.1073/pnas.94.6.2345

Monteerarat, Y., Sakabe, S., Ngamurulert, S., Srichatraphimuk, S., Jiamtom, W., Chaichuen, K., et al. (2010). Induction of TNF-α in human macrophages by avian and human influenza viruses. *Arch. Virol.* 155, 1273–1279. doi: 10.1007/s00705-010-0716-y

Mori, I., Komatsu, T., Takeuchi, K., Nakakuki, K., Sudo, M., and Kimura, Y. (1995). In vivo induction of apoptosis by influenza virus. *J. Gen. Virol.* 76, 2869–2873. doi: 10.1099/0022-1317-76-11-2869

Morris, E. J., Michaud, W. A., Ji, J.-Y., Moon, N.-S., Rocco, J. W., and Dyson, N. J. (2006). Functional identification of Api5 as a suppressor of E2F-dependent apoptosis in vivo. *PLoS Genet.* 2:e196. doi: 10.1371/journal.pgen.0020196

Murphy, J. M., Czabotar, P. E., Hildebrand, J. M., Lucet, I. S., Zhang, J. G., Alvarez-Diaz, S., et al. (2013). The pseudokinase MLKL mediates necroptosis via a molecular switch mechanism. *Immunity* 39, 443–453. doi: 10.1016/j.immuni.2013.06.018

Nagata, S. (1999). Fas ligand-induced apoptosis. *Annu. Rev. Genet.* 33, 29–55. doi: 10.1146/annurev.genet.33.1.29

Nailwal, H., Sharma, S., Mayank, A., and Lal, S. (2015). The nucleoprotein of influenza A virus induces p53 signaling and apoptosis via attenuation of host ubiquitin ligase RNF43. *Cell Death Dis.* 6:e1768. doi: 10.1038/cddis.2015.131

Nair, P., Lu, M., Petersen, S., and Ashkenazi, A. (2014). Apoptosis initiation through the cell-extrinsic pathway. *Methods Enzymol.* 544, 99–128. doi: 10.1016/B978-0-12-417158-9.00005-4

Ohtsuka, T., Ryu, H., Minamishima, Y. A., Macip, S., Sagara, J., Nakayama, K. I., et al. (2004). ASC is a Bax adaptor and regulates the p53–Bax mitochondrial apoptosis pathway. *Nat. Cell Biol.* 6, 121–128. doi: 10.1038/ncb1087

Orning, P., Weng, D., Starheim, K., Ratner, D., Best, Z., Lee, B., et al. (2018). Pathogen blockade of TAK1 triggers caspase-8–dependent cleavage of gasdermin D and cell death. *Science* 362, 1064–1069. doi: 10.1126/science.aau2818

Pinar, A., Dowling, J. K., Bitto, N. J., Robertson, A. A., Latz, E., Stewart, C. R., et al. (2017). PB1-F2 peptide derived from avian influenza A virus H7N9 induces inflammation via activation of the NLRP3 inflammasome. *J. Biol. Chem.* 292, 826–836. doi: 10.1074/jbc.M116.756379

Poon, I. K., Lucas, C. D., Rossi, A. G., and Ravichandran, K. S. (2014). Apoptotic cell clearance: basic biology and therapeutic potential. *Nat. Rev. Immunol.* 14, 166–180. doi: 10.1038/nri3607

Rebsamen, M., Heinz, L. X., Meylan, E., Michallet, M. C., Schroder, K., Hofmann, K., et al. (2009). DAI/ZBP1 recruits RIP1 and RIP3 through RIP homotypic interaction motifs to activate NF-κB. *EMBO Rep.* 10, 916–922. doi: 10.1038/embor.2009.109

Roberson, E. C., Tully, J. E., Guala, A. S., Reiss, J. N., Godburn, K. E., Pociask, D. A., et al. (2012). Influenza induces endoplasmic reticulum stress, caspase-12-dependent apoptosis, and c-Jun N-terminal kinase-mediated transforming growth factor-beta release in lung epithelial cells. *Am. J. Respir. Cell Mol. Biol.* 46, 573–581. doi: 10.1165/rcmb.2010-0460OC

Robert, G., Gastaldi, C., Puissant, A., Hamouda, A., Jacquel, A., Dufies, M., et al. (2012). The anti-apoptotic Bcl-B protein inhibits BECN1-dependent autophagic cell death. *Autophagy* 8, 637–649. doi: 10.4161/auto.19084

Sarhan, J., Liu, B. C., Muendlein, H. I., Li, P., Nilson, R., Tang, A. Y., et al. (2018). Caspase-8 induces cleavage of gasdermin D to elicit pyroptosis during Yersinia infection. *Proc. Natl. Acad. Sci. U.S.A.* 115, E10888–E10897. doi: 10.1073/pnas.1809548115

Schultz-Cherry, S., Dybdahl-Sissoko, N., Neumann, G., Kawaoka, Y., and Hinshaw, V. S. (2001). Influenza virus ns1 protein induces apoptosis in cultured cells. *J. Virol.* 75, 7875–7881. doi: 10.1128/jvi.75.17.7875-7881.2001

Shi, J., Gao, W., and Shao, F. (2017). Pyroptosis: gasdermin-mediated programmed necrotic cell death. *Trends Biochem. Sci.* 42, 245–254. doi: 10.1016/j.tibs.2016.10.004

Shi, J., Zhao, Y., Wang, Y., Gao, W., Ding, J., Li, P., et al. (2014). Inflammatory caspases are innate immune receptors for intracellular LPS. *Nature* 514, 187–192. doi: 10.1038/nature13683

Slaine, P. D., Kleer, M., Duguay, B. A., Pringle, E. S., Kadijk, E., Ying, S., et al. (2021). Thiopurines activate an antiviral unfolded protein response that blocks influenza A virus glycoprotein accumulation. *J. Virol.* 95, e453–e421. doi: 10.1128/JVI.00453-21

Takizawa, T., Matsukawa, S., Higuchi, Y., Nakamura, S., Nakanishi, Y., and Fukuda, R. (1993). Induction of programmed cell death (apoptosis) by influenza virus infection in tissue culture cells. *J. Gen. Virol.* 74, 2347–2355. doi: 10.1099/0022-1317-74-11-2347

Thapa, R. J., Ingram, J. P., Ragan, K. B., Nogusa, S., Boyd, D. F., Benitez, A. A., et al. (2016). DAI senses influenza A virus genomic RNA and activates RIPK3-dependent cell death. *Cell Host Microbe* 20, 674–681. doi: 10.1016/j.chom.2016.09.014

Tripathi, S., Batra, J., Cao, W., Sharma, K., Patel, J. R., Ranjan, P., et al. (2013). Influenza A virus nucleoprotein induces apoptosis in human airway epithelial cells: implications of a novel interaction between nucleoprotein and host protein Clusterin. *Cell Death Dis.* 4:e562. doi: 10.1038/cddis.2013.89

Tsai, S.-Y., Segovia, J. A., Chang, T.-H., Morris, I. R., Berton, M. T., Tessier, P. A., et al. (2014). DAMP molecule S100A9 acts as a molecular pattern to enhance inflammation during influenza A virus infection: role of DDX21-TRIF-TLR4-MyD88 pathway. *PLoS Pathog.* 10:e1003848. doi: 10.1371/journal.ppat.1003848

Tsai, S.-Y., Segovia, J. A., Chang, T.-H., Shil, N. K., Pokharel, S. M., Kannan, T., et al. (2015). Regulation of TLR3 activation by S100A9. *J. Immunol.* 195, 4426–4437. doi: 10.4049/jimmunol.1500378

van Delft, M. F., Smith, D. P., Lahoud, M. H., Huang, D. C., and Adams, J. M. (2010). Apoptosis and non-inflammatory phagocytosis can be induced by mitochondrial damage without caspases. *Cell Death Differ.* 17, 821–832. doi: 10.1038/cdd.2009.166

Vanden Berghe, T., Kaiser, W. J., Bertrand, M. J., and Vandenabeele, P. (2015). Molecular crosstalk between apoptosis, necroptosis, and survival signaling. *Mol. Cell. Oncol.* 2:e975093. doi: 10.4161/23723556.2014.975093

Venereau, E., Ceriotti, C., and Bianchi, M. E. (2015). DAMPs from cell death to new life. *Front. Immunol.* 6:422. doi: 10.3389/fimmu.2015.00422

Wallach, D., Kang, T. B., Dillon, C. P., and Green, D. R. (2016). Programmed necrosis in inflammation: toward identification of the effector molecules. *Science* 352:aaf2154. doi: 10.1126/science.aaf2154

Walsh, C. M. (2014). Grand challenges in cell death and survival: apoptosis vs. necroptosis. *Front. Cell Dev. Biol.* 2:3. doi: 10.3389/fcell.2014.00003

Wang, Y., Hao, Q., Florence, J. M., Jung, B.-G., Kurdowska, A. K., Samten, B., et al. (2019). Influenza virus infection induces ZBP1 expression and necroptosis in mouse lungs. *Front. Cell Infect. Microbiol.* 9:286. doi: 10.3389/fcimb.2019.00286

Wang, Z., Choi, M. K., Ban, T., Yanai, H., Negishi, H., Lu, Y., et al. (2008). Regulation of innate immune responses by DAI (DLM-1/ZBP1) and other DNA-sensing molecules. *Proc. Natl. Acad. Sci. U.S.A.* 105, 5477–5482. doi: 10.1073/pnas.0801295105

Yeganeh, B., Ghavami, S., Rahim, M. N., Klonisch, T., Halayko, A. J., and Coombs, K. M. (2018). Autophagy activation is required for influenza A virus-induced apoptosis and replication. *Biochim. Biophys. Acta Mol. Cell Res.* 1865, 364–378. doi: 10.1016/j.bbamcr.2017.10.014

Zamarin, D., García-Sastre, A., Xiao, X., Wang, R., and Palese, P. (2005). Influenza virus PB1-F2 protein induces cell death through mitochondrial ANT3 and VDAC1. *PLoS Pathog.* 1:e4. doi: 10.1371/journal.ppat.0010004

Zhang, D. W., Shao, J., Lin, J., Zhang, N., Lu, B. J., Lin, S. C., et al. (2009). RIP3, an energy metabolism regulator that switches TNF-induced cell death from apoptosis to necrosis. *Science* 325, 332–336. doi: 10.1126/science.1172308

Zhang, T., Yin, C., Boyd, D. F., Quarato, G., Ingram, J. P., Shubina, M., et al. (2020). Influenza virus Z-RNAs Induce ZBP1-mediated necroptosis. *Cell* 180, 1115–1129 e1113. doi: 10.1016/j.cell.2020.02.050

Zhang, Y., Yu, L., Tang, L., Zhu, M., Jin, Y., Wang, Z., et al. (2020). A promising anti-cytokine-storm targeted therapy for COVID-19: the artificial-liver blood-purification system. *Engineering* 7, 11–13. doi: 10.1016/j.eng.2020.03.006

Zheng, M., Karki, R., Vogel, P., and Kanneganti, T. D. (2020). Caspase-6 is a key regulator of innate immunity, inflammasome activation, and host defense. *Cell* 181, 674.e–687.e. doi: 10.1016/j.cell.2020.03.040

Zhirnov, O. P., Konakova, T. E., Wolff, T., and Klenk, H. D. (2002). NS1 protein of influenza a virus down-regulates apoptosis. *J. Virol.* 76, 1617–1625. doi: 10.1128/jvi.76.4.1617-1625.2002

Zhou, X., Jiang, W., Liu, Z., Liu, S., and Liang, X. (2017). Virus infection and death receptor-mediated apoptosis. *Viruses* 9:316. doi: 10.3390/v9110316

**Conflict of Interest:** The authors declare that the research was conducted in the absence of any commercial or financial relationships that could be construed as a potential conflict of interest.

**Publisher's Note:** All claims expressed in this article are solely those of the authors and do not necessarily represent those of their affiliated organizations, or those of the publisher, the editors and the reviewers. Any product that may be evaluated in this article, or claim that may be made by its manufacturer, is not guaranteed or endorsed by the publisher.

frontiers | Frontiers in Microbiology

ORIGINAL RESEARCH
published: 12 April 2022
doi: 10.3389/fmicb.2022.854172

# Identification of Neutrophil-Related Factor LCN2 for Predicting Severity of Patients With Influenza A Virus and SARS-CoV-2 Infection

*Zhisheng Huang[1,2], Hui Li[2], Shuai Liu[3], Ju Jia[1,2], Ying Zheng[2,4] and Bin Cao[1,2,4]**

*[1] Graduate School of Peking Union Medical College, Chinese Academy of Medical Sciences, Peking Union Medical College, Beijing, China, [2] Department of Pulmonary and Critical Care Medicine, Center for Respiratory Diseases, China-Japan Friendship Hospital, Beijing, China, [3] Department of Respiratory and Critical Care Medicine, Shandong Provincial Hospital Affiliated to Shandong First Medical University, Jinan, China, [4] China-Japan Friendship Hospital, National Clinical Research Center for Respiratory Diseases, Clinical Center for Pulmonary Infections, Capital Medical University, Beijing, China*

OPEN ACCESS

**Edited by:**
*Quanjiao Chen, Wuhan Institute of Virology Chinese Academy of Sciences (CAS), China*

**Reviewed by:**
*Peng Zhou, Wuhan Institute of Virology Chinese Academy of Sciences (CAS), China*
*Chaohong Liu, Huazhong University of Science and Technology, China*

***Correspondence:**
*Bin Cao*
*caobin_ben@163.com*

**Specialty section:**
*This article was submitted to Virology, a section of the journal Frontiers in Microbiology*

**Received:** *13 January 2022*
**Accepted:** *14 February 2022*
**Published:** *12 April 2022*

**Citation:**
*Huang Z, Li H, Liu S, Jia J, Zheng Y and Cao B (2022) Identification of Neutrophil-Related Factor LCN2 for Predicting Severity of Patients With Influenza A Virus and SARS-CoV-2 Infection. Front. Microbiol. 13:854172. doi: 10.3389/fmicb.2022.854172*

**Background:** Influenza and COVID-19 are respiratory infectious diseases that are characterized by high contagiousness and high mutation and pose a serious threat to global health. After Influenza A virus (IAV) and SARS-CoV-2 infection, severe cases may develop into acute lung injury. Immune factors act as an important role during infection and inflammation. However, the molecular immune mechanisms still remain unclear. We aimed to explore immune-related host factors and core biomarker for severe infection, to provide a new therapeutic target of host factor in patients.

**Methods:** Gene expression profiles were obtained from Gene Expression Omnibus and the Seurat R package was used for data process of single-cell transcriptome. Differentially expressed gene analysis and cell cluster were used to explore core host genes and source cells of genes. We performed Gene Ontology enrichment, Kyoto Encyclopedia of Genes and Genomes analysis, and gene set enrichment analysis to explore potential biological functions of genes. Gene set variation analysis was used to evaluate the important gene set variation score for different samples. We conduct Enzyme-linked immunosorbent assay (ELISA) to test plasma concentrations of Lipocalin 2 (LCN2).

**Results:** Multiple virus-related, cytokine-related, and chemokine-related pathways involved in process of IAV infection and inflammatory response mainly derive from macrophages and neutrophils. LCN2 mainly in neutrophils was significantly upregulated after either IAV or SARS-CoV-2 infection and positively correlated with disease severity. The plasma LCN2 of influenza patients were elevated significantly compared with healthy controls by ELISA and positively correlated with disease severity of influenza patients. Further bioinformatics analysis revealed that LCN2 involved in functions of neutrophils,

including neutrophil degranulation, neutrophil activation involved in immune response, and neutrophil extracellular trap formation.

**Conclusion:** The neutrophil-related LCN2 could be a promising biomarker for predicting severity of patients with IAV and SARS-CoV-2 infection and may as a new treatment target in severe patients.

**Keywords: severe infection, inflammatory response, Lipocalin 2, IAV, SARS-CoV-2**

## INTRODUCTION

Respiratory virus infection represented by influenza and COVID-19 poses a serious threat to global health. Several influenza pandemics happened since the last century, including Spanish influenza in 1918, Asian influenza in 1957, Hong Kong influenza in 1968, and swine influenza in 2009, which have caused serious damage to the global economy and human health (Ziegler et al., 2018). SARS-Cov-2 (Li et al., 2021), a new coronavirus, first reported in 2020 by China, has been spreading around the world for nearly 2 years. By December 31, 2021, a total of 281,808,270 confirmed cases and 5,411,759 deaths have been reported globally by WHO. As the virus evolves, new strains emerge gradually, such as alpha, beta, delta, and omicron, which make the existing vaccine less effective (Callaway, 2021). Options for the treatment of both influenza and COVID-19 are currently limited. Moreover, the effect of antiviral therapy is affected by the timing of administration and emergence of drug-resistant strains (Lampejo, 2020).

Common respiratory viruses including Influenza A virus (IAV) and SARS-Cov-2 belong to RNA virus, and they have limited protein-coding capacity and rely on host factors for replication to complete the life cycle. Meanwhile, expression of host factors is altered by virus stimulation during the process of virus infection. Interaction between hosts and the virus determines prognosis of the disease (Ito et al., 2011; Mahler et al., 2021). Although an effective immune response is indispensible for eliminating virus, exaggerated response characterized by the so-called "cytokine storm" can trigger severe immune pathological damage (Karki et al., 2021; Rappe et al., 2021). Changes in the expression levels of host factors and abnormal immunity, such as cytokine storm (Liu et al., 2016; Guo and Thomas, 2017), lymphopenia (Cheng et al., 2019; Zhang et al., 2020b), and T cell exhaustion (Valero-Pacheco et al., 2013; Diao et al., 2020), during virus infection have been reported. Because of the conserved feature, host factors targeting therapy offers a new approach for the treatment of respiratory viral infection, and it is expected to limit viral replication, alleviate immune-mediated damage, and decrease mortality in severe infection hosts. In recent decades, series host factors have been found to have potential therapeutic value. However, the accurate key molecules and origin cells of host factors remain unclear.

Single-cell transcriptome sequencing (scRNA-seq) has recently emerged as a powerful method to identify cell types and analyze functional status at single-cell level (Dal Molin and Di Camillo, 2019). scRNA-seq is widely used in various fields including cancer (Suvà and Tirosh, 2019), developmental biology (Griffiths et al., 2018), and microbiology (Imdahl and Saliba, 2020) and has become a promising research tool in the fields of life sciences. scRNA-seq results of COVID-19 find that changes of host factors including EN-RAGE, TNFSF14, oncostatin M, ANXA1, FPR1, and S100A8/9 are correlated with disease severity, revealing the possible pathogenesis of severe COVID-19 and potential host therapeutic targets (Arunachalam et al., 2020; Guo et al., 2021; Ren et al., 2021).

To systematically identify the role of host factors in respiratory virus infection, we analyzed the public transcriptomics data of IAV and SARS-CoV-2 infection to further understand changes in host functions and identify important host factors in mice and human. We found that Lipocalin 2 (LCN2) increased in influenza and COVID-19 and positively correlated with disease severity of infected patients, which was associated with neutrophil degranulation, neutrophil associated inflammation, and neutrophil extracellular trap (NET) formation by bioinformatics functional analysis. The plasma LCN2 of clinical influenza patients was elevated significantly compared with healthy controls by enzyme-linked immunosorbent assay (ELISA) and positively correlated with disease severity of influenza patients. Therefore, neutrophil-related LCN2 might be an early biomarker for predicting severity of disease and provide a new method for therapy targeting of host factor in patients with severe IAV and SARS-CoV-2 infection.

## MATERIALS AND METHODS

### Dataset Acquisition

The scRNA-seq data, microarray data, and RNA-seq data obtained from Gene Expression Omnibus (GEO)[1] were included in this study for analysis. The selection criteria of mice datasets were as follows: (1) inclusion lung tissue or whole-blood samples from IAV infection and control mice within 3 days post infection (dpi), datasets involved with other factors (drug intervention and gene knockout) were excluded; (2) every group of dataset contained at least three reduplicate samples; and (3) with the mature of sequencing technology, datasets were selected in 2019–2021. On the basis of these criteria, GSE80011 and GSE124404 were obtained. However, GSE107947 was the only scRNA-seq data of influenza mice in GEO. Given that administration of aerosolized SARS-CoV-2 to K18-hACE2 mice could simulate the real situation well (Fumagalli et al., 2022), GSE184657 was the only dataset included in subsequent analysis of SARS-CoV-2. The scRNA-seq data (GSE107947) of four lung samples of mice

[1]http://www.ncbi.nlm.nih.gov/geo/

were composed of one control sample, two influenza samples (A/PR/8) at 48 hours post infection (hpi), and one influenza sample at 72 hpi, containing 3,840 CD45-negative (CD45-) cells and 3,840 CD45-positive (CD45 +) cells. The microarray dataset (GSE80011) contained three influenza (A/WSN/33) and three control lung samples of mice at 24 hpi. The RNA-seq profiles (GSE124404) of six blood samples included three control mice and three mice with influenza (A/PR/8) at 48 hpi. The RNA-seq profiles (GSE184657) contained four mice with SARS-Cov-2 infection and two control mice at 6 dpi.

The datasets of patients met the following criteria: (1) lung tissue or whole-blood samples from IAV and SARS-Cov-2 infection; (2) datasets contained at least 30 samples; and (3) patients contained various severity classifications. The clinical whole-blood samples of patients with influenza and COVID-19 were composed of GSE111368 and GSE157103. The severity of patients with influenza was divided into mild, moderate, and severe on the basis of whether supplemental oxygen and invasive mechanical ventilation was required. We acquired 130 healthy control samples, the earliest acute stage samples of 94 patients with pH1N1 infection and 44 paired convalescent samples for analysis from GSE111368. The COVID-19 dataset (GSE157103) contained 100 patients, which were recorded clinical information, such as need for admission into the intensive care unit (ICU) and requiring mechanical ventilation support, sequential organ failure assessment (SOFA) scores, and acute physiology and chronic health evaluation (APACHE II) score.

## Single-Cell RNA-seq Data Processing

The Seurat R package 4.0.0 was used for data filtering, statistical analysis, and exploration of the scRNA-seq data. We used the same rigorous method to process data of CD45- cells and CD45 + cells separately. First, we discarded low-quality cells on the basis of the quality control standards that every cell expressed > 200 genes and genes expressed in > 3 cells. Then, the gene expression of remaining cells was normalized, and 2,000 highly variable genes from each sample were identified by the vst method. All genes were scaled, and the principal component analysis was conducted. The cells were clustered by unsupervised clustering (resolution = 0.5) and visualized by t-distributed stochastic neighbor embedding (tSNE) using the top 10 principal components. Last, we annotated cell types through known marker gene in each cluster of CD45- cells and CD45 + cells. Differentially expressed genes (DEGs) were found using the FindMarkers in Seurat R package.

## Differentially Expressed Genes, Functional Enrichment Analysis, Gene Set Enrichment Analysis, and Gene Set Variation Analysis

To estimate the difference among different groups, DEGs were identified using the limma package in R software (version 4.0.4) and selected with the commonly used thresholds of fold change (FC) > 2 and adj. $p$ value < 0.05. Gene Ontology (GO) and Kyoto Encyclopedia of Genes and Genomes (KEGG) pathway enrichment analysis were performed using clusterprofiler package in R software and $p < 0.05$ was considered statistically significant. We performed gene set enrichment analysis (GSEA) between patients with high LCN2 and low LCN2 with the R package clusterprofiler. To investigate intensity of response to virus and inflammatory response pathways in different cell types, we performed gene set variation analysis (GSVA) with GSVA R package.

## Patients and Clinical Information

The clinical study of patients with IAV infection included 25 healthy controls and 43 influenza patients from the Department of Pulmonary and Critical Care Medicine of China-Japan Friendship Hospital during influenza season of 2017–2021. The study was approved by China-Japan Friendship Hospital Ethics Committee (approval no. 2018-120-K86). The patients must meet the following criteria: (i) reverse transcription PCR testing of an appropriate respiratory tract sample was positive; (ii) the time from onset of influenza-like symptoms was ≤14 days; (iii) acute blood samples within 48 h after hospitalization were able to obtain; and (iv) age was > 18 years old. In accordance with the upper classification criteria of severity, severe influenza was defined with respiratory failure that needed invasive mechanical ventilation. Moderate influenza was defined with damage of respiratory function that required supplemental oxygen therapy, including nasal high-flow oxygen therapy and/or non-invasive mechanical ventilatory support. Mild influenza was defined without supplemental oxygen. Forty-three influenza patients contained eight mild patients, 19 moderate patients, and 16 severe patients. Important clinical information including age, sex, and incidence of acute respiratory distress syndrome (ARDS) were obtained from medical records.

## Enzyme-Linked Immunosorbent Assay

Lipocalin 2 expression levels of plasma were measured using the human LCN2 enzyme immunoassay kit (Elabscience, Wuhan, China) according to the manufacturer's instructions.

## Statistical Analysis

The Student's $t$-test or Mann–Whitney U test ($t$-test or wilcox test in R 4.0.4) was used to compare two group differences, as appropriate. $^{*}P < 0.05$, $^{**}P < 0.01$, $^{***}P < 0.001$, and $^{****}P < 0.0001$ represent significant statistical differences.

# RESULTS

## Inflammatory Response Mainly Derives From Macrophages and Neutrophils After IAV Infection

According to quality control standards, 1,228 cells were excluded, and 6,452 cells were included in the scRNA-seq data GSE107947. These cells consisted of 3,211 CD45- cells and 3,241 CD45 + cells using flow cytometry sorting technology. To examine the host immune response characteristics in a cell type–specific manner, 3,211 CD45- cells and 3,241 CD45 + cells were subjected to tSNE on the basis of highly variable genes using the Seurat

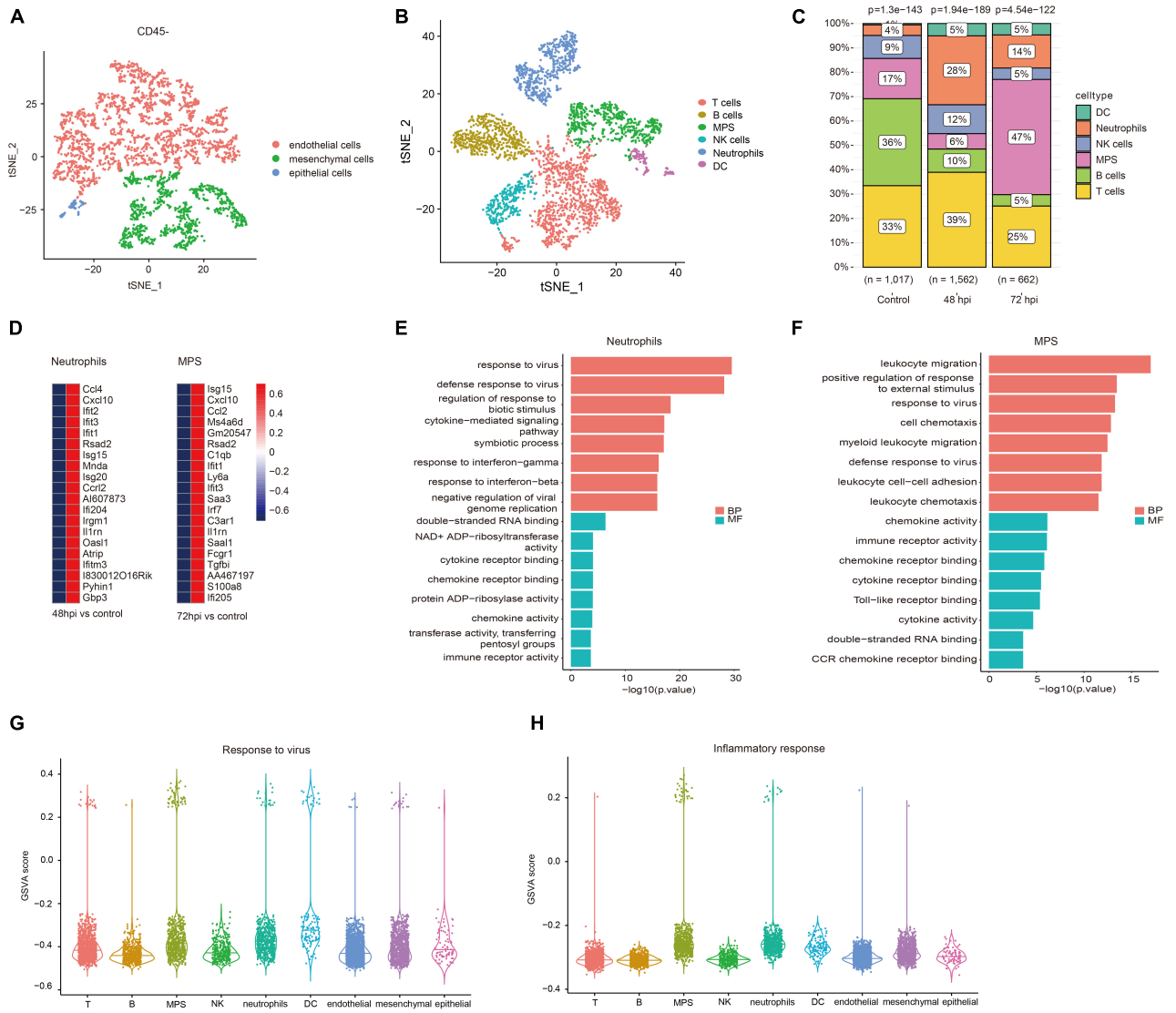


**FIGURE 1 |** Immune landscape associated with IAV infection. Cellular subsets from CD45- **(A)** and CD45 + **(B)** cells in the lung (GSE107947). **(C)** Proportions of immune cells clusters in different studied subjects. **(D)** Top 20 upregulated genes of neutrophils at 48 hpi and MPS at 72 hpi. **(E)** Top eight GO terms of BP and MF in neutrophils. **(F)** Top eight GO terms of BP and MF in MPS. GSVA scores of response to virus **(G)** and inflammatory response **(H)** in different cell types.

package. These cells were successfully classified into 10 different clusters unbiased separately (**Supplementary Figure 1**). These clusters of CD45- cells were assigned to three different cell types (**Figure 1A**), and these clusters of CD45 + cells were annotated to six different cell types (**Figure 1B**) on the basis of well-known marker genes (**Supplementary Figure 2**). The CD45- cells included endothelial cells, mesenchymal cells, and epithelial cells. CD45 + cells contained T cells, B cells, mononuclear phagocyte system (MPS), natural killer (NK) cells, neutrophils, and dendritic cells (DC). To illustrate immunological changes after influenza infection, we analyzed the dynamic change of relative proportions of immune cells in the lung tissue of mice (**Figure 1C**). After influenza infection, the percentage of MPS, neutrophils, and DC significantly increased, whereas that of B cells significantly decreased. In addition, the percentage of NK cells and T cells at 72 hpi decreased slightly compared with that at 48 hpi.

Neutrophils and macrophages were important immune cells that were involved in the important human host mechanism against microorganisms. In this study, neutrophils significantly increased at 48 hpi, and macrophages rose noticeably at 72 hpi. Interferon-stimulated genes (Ifit1, Rsad2, and Isg15), and chemokine (Cxcl10, Ccl2, and Ccl4) were significantly upregulated in neutrophils and macrophages (**Figure 1D**). GO enrichment analysis showed that DEGs were related to antiviral immune-related biological processes and cytokine/chemokine related molecular function in neutrophils (**Figure 1E**). The function analysis of macrophages was also related to leukocyte

migration, antiviral immune, and cytokine/chemokine activity (**Figure 1F**). It is well known that a large number of cytokines (e.g., IL-1β, IL-6, and TNF-α) are produced in the process of inflammatory response and cytokine storm was correlated with disease severity and worse prognosis (Tisoncik et al., 2012). However, what kind of cells is mainly involved in the inflammatory response remains unclear. We evaluated GSVA score of response to virus and inflammatory response among all cell types. The results revealed that MPS and neutrophils showed a higher expression level in both response to virus and inflammatory response pathways (**Figures 1G,H**). It suggests that these cells may mediate hyper-inflammatory features and are an important source of cytokine storm after influenza infection.

## Expression of Lipocalin 2 in Neutrophils Was Upregulated After IAV Infection in Mice

To screen key genes in influenza, difference analysis was performed between control mice and IAV infection mice at 48 and 72 hpi. Top 10 upregulated and downregulated genes at 48 and 72 hpi were selected to take the intersection, and six overlapping upregulated genes were filtered, including Rsad2, Cxcl10, Saa3, Irf7, Il1rn, and LCN2 (**Figure 2A**). Rsad2, Cxcl10 (Yang et al., 2020), Saa3 (Ather et al., 2018), Irf7 (Hatesuer et al., 2017), and Il1rn (Schmitz et al., 2005), which have been reported in influenza, whereas the role of LCN2 in influenza was still unknown. We explored the distribution of LCN2 among all cell types using tSNE and found LCN2 mainly expressed in neutrophils (**Figure 2B**) and partially expressed in CD45- cells (**Supplementary Figure 3**). Moreover, expression of LCN2 in neutrophils was upregulated after influenza infection (**Figure 2C**), and it was also upregulated in little other myeloid cells (**Supplementary Figure 4**).

To verify this finding, the expression levels of LCN2 in mice infected with influenza virus were assessed with another two datasets (GSE80011 and GSE124404). The microarray dataset GSE80011 contained three influenza and three control lung tissues of mice at 24 hpi. As shown in **Figure 2D**, the expression levels of LCN2 was significantly higher in the lung tissues of mice infected with influenza virus, compared with that of the controls ($Log_2FC = 3.06$, adj. $p$ value = 0.0005). Meanwhile, the expression level of LCN2 in peripheral blood samples of mice infected with influenza virus was also upregulated ($Log_2FC = 2.75$, adj. $p$ value = 0.0003) (**Figure 2E**).

## Lipocalin 2 Expression Level in Peripheral Blood Positively Correlated With Disease Severity of Influenza Patients

We further investigated expression characteristics of LCN2 in patients. Ninety-four acute stage samples and 44 paired convalescent samples in GSE111368 dataset were involved in the analysis. The acute stage samples collected from 39 mild patients, 28 moderate patients, and 27 severe patients according to whether need supplemental oxygen and invasive mechanical ventilation. Compared with healthy controls, influenza-infected patients showed significantly higher level of LCN2 in peripheral blood leukocytes (**Figure 3A**). Furthermore, the expression level of LCN2 positively correlated with disease severity (**Figure 3B**). Paired samples revealed that the expression level of LCN2 declined at convalescent stage (**Figure 3C**). Expression of LCN2 was not influenced by age (**Figure 3D**) and gender (**Figure 3E**).

To further clarify the expression level of LCN2 and its correlation with disease severity, we enrolled 43 patients with influenza infection, including eight mild patients, 19 moderate patients, and 16 severe patients. The protein level of LCN2 in plasma samples in acute phase was detected using ELISA. We found that the concentration levels of LCN2 in influenza patients were significantly higher than that in healthy controls (**Figure 4A**). Consistent with the above analysis, patients with severe illness had significantly higher LCN2 levels than those with mild or mild-moderate disease (**Figures 4B,C**). Patients with ARDS exhibited higher levels of LCN2 than those without (**Figure 4D**). Collectively, these findings suggested that plasma levels of LCN2 were positively correlated with severity of IAV infection and may be a clinically relevant biomarker for predicting severity of patients with IAV infection.

## Lipocalin 2 Was Involved in Functions of Neutrophils in Influenza Patients

Because LCN2 was upregulated after influenza infection and correlated with disease severity, we further explored the possible function of LCN2. The influenza patients were equally divided into high-LCN2 group and low-LCN2 group on the basis of the median expression level of LCN2 in GSE111368. A total of 91 DEGs from the influenza patients with high LCN2 were identified by comparing with low LCN2. This total included 62 upregulated genes and 29 downregulated genes, which were indicated in the volcano plot shown in **Figure 5A**. The top 50 upregulated genes of DEGs were represented as a heatmap (**Figure 5B**). GO and KEEG pathway enrichment analysis of DEGs in LCN2-high samples identified an enrichment of genes in pathways related to neutrophils inflammation (neutrophil degranulation and neutrophil activation involved in immune response and antimicrobial humoral response) and NET formation (**Figure 5C**). Using GSEA analysis, we also found that LCN2 was associated with NET formation in influenza (**Figure 5D**).

## Similar Expression Pattern of Lipocalin 2 Was Found in Patients With COVID-19 and Mice

COVID-19 has some similarities in the course of disease development as influenza. The dataset GSE184657 showed the expression level of LCN2 in the lung tissues of mice infected with SARS-CoV-2 was significantly higher ($Log_2FC = 2.93$, $p = 0.0414$) than that of the control at 6dpi (**Supplementary Figure 5**). Compared with patients in general wards, patients with COVID-19 at ICU showed higher level of LCN2

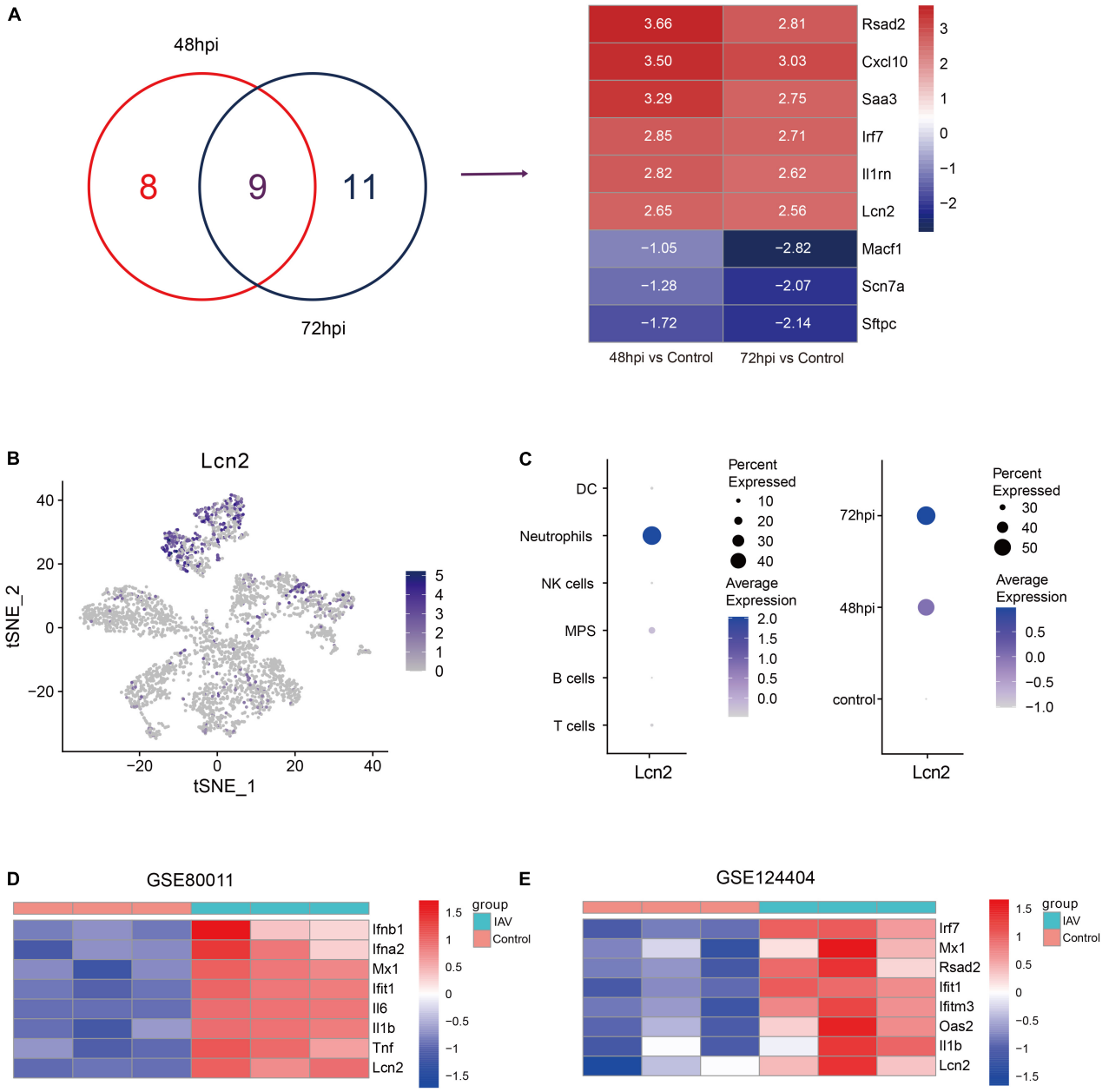


**FIGURE 2 |** Identification and validation of key genes in IAV infection in public dataset. **(A)** Venn diagram to indicate 9 shared genes from DEGs and log2 fold change of shared genes (GSE107947). **(B)** Expression level of LCN2 in immune cells. **(C)** LCN2 expression level of neutrophils in different groups. **(D,E)** Validation of LCN2 in IAV infection.

(**Figure 6A**). Similarly, the expression level of LCN2 was higher in patients who needed mechanical ventilation than those without (**Figure 6B**). APACHE II and SOFA scores, used to stratify the severity of illness, showed a positive correlation with the expression level of LCN2 in in leukocytes from whole blood (**Figures 6C,D**). Similarly, we found that LCN2 was involved in functions of neutrophils in patients with COVID-19, including neutrophil degranulation, neutrophil activation involved in immune response, and NET formation (**Figures 6E–G**).

## DISCUSSION

Increasing evidence indicates that excessive immune response leads to immune-mediated damage and affects disease process and prognosis (Guo et al., 2021; Karki et al., 2021; Rappe et al., 2021). This emphasizes the importance of host factors in predicting clinical progression and prognosis in patients with viral infectious diseases. In this study, we found that a neutrophil-associated host factor LCN2 was significantly elevated and associated with severity in both influenza and

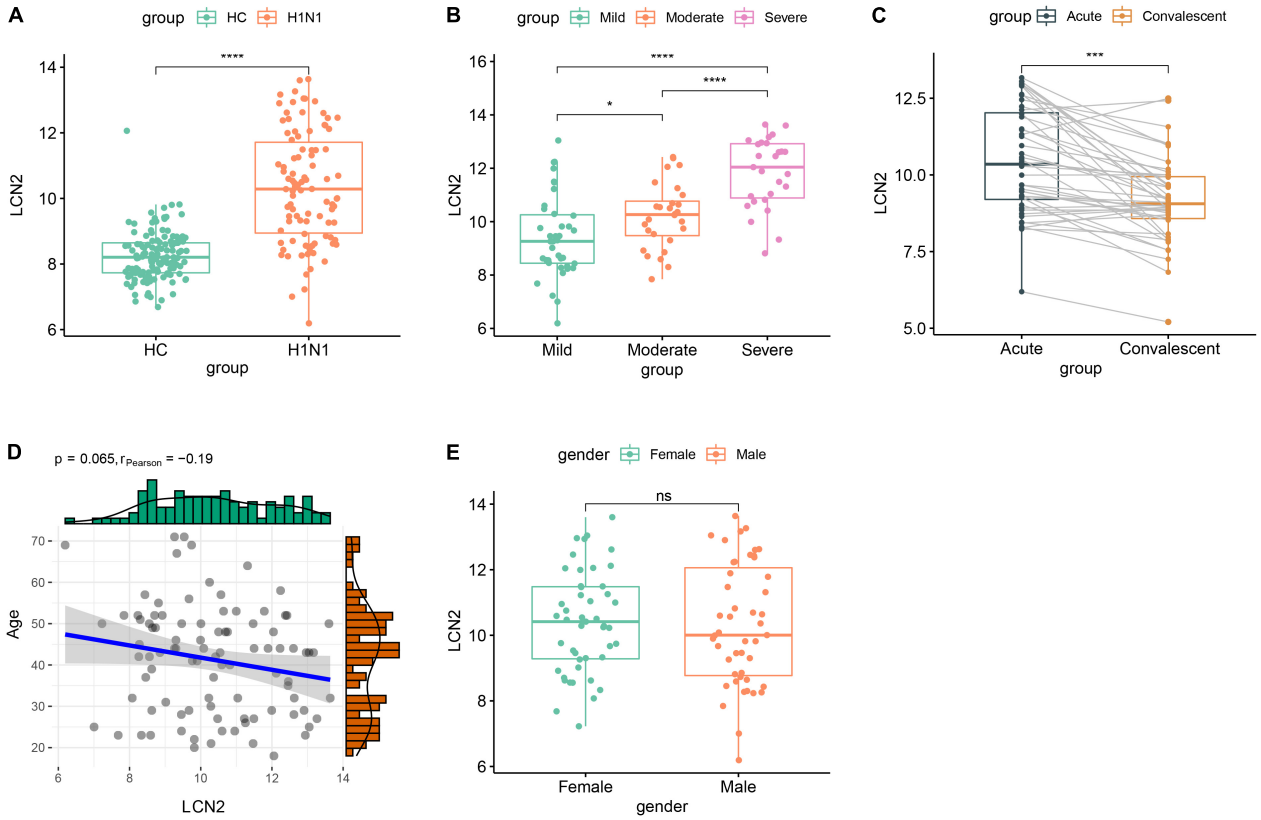


**FIGURE 3 |** Correlation between LCN2 and clinical features of IAV infection in public dataset. **(A)** Expression level of LCN2 in healthy controls and patients with IAV infection (GSE111368). **(B)** Expression level of LCN2 in patients with mild, moderate, and severe influenza. **(C)** Expression level of LCN2 in acute and convalescent patients with IAV infection. **(D)** Association of patients' age with expression level of LCN2. **(E)** Expression level of LCN2 in female and male patients with IAV infection.

patients with COVID-19 by integrated public data analysis. The increase of serum LCN2 level in clinical influenza patients was verified by ELISA and positively correlated with disease severity of influenza patients. Further bioinformatics functional analysis showed LCN2 might influence disease development by affecting neutrophil degranulation, neutrophil activation, and NET formation.

In acute respiratory virus–infected patients, hyper-inflammatory responses involving the release of pro-inflammatory cytokines (e.g., IL-1, IL-6, IL-8, and TNF) impair the function of lung and lead to severe complications (Andreakos et al., 2021). However, it is unclear which types of cells are responsible for the release of large number of cytokines in critical patients. Previous research has shown that inflammation-related factors (IL-1, TNF, CXCL1, CXCL2, S100A8, and S100A9) predominantly express in neutrophils, and neutrophils infiltration largely account for lethal influenza infection (Brandes et al., 2013). In this study, we found that immune response pattern transformed from early antiviral response into inflammatory response gradually with the elimination of influenza virus in the lung tissue. In addition, the inflammatory response was mainly mediated by neutrophils and mononuclear macrophages. These results are consistent with previous report (Zhang et al., 2020a) and suggest that neutrophils may play an important role in the development of severe disease in patients infected with IAV.

Lipocalin 2, also known as neutrophil gelatinase-associated lipocalin, or 24p3, is a secretory glycoprotein involved in various inflammatory processes (Kjeldsen et al., 2000), which is found in various cells, such as neutrophils, macrophages, epithelial cells, and adipocytes. Given that LCN2 is readily detected in plasma, urine, central nervous system, and various body fluids, it has been found to be associated with a variety of diseases (Moschen et al., 2017). In patients with adult-onset Still's disease (AOSD), neutrophil-derived LCN2 is higher than healthy control in plasma and liver tissue, and it could serve as a potent biomarker for identifying liver damage caused by hyper-inflammatory state of AOSD (Jia et al., 2021). LCN2 is also upregulated in serum and liver tissue of patients with non-alcoholic fatty liver (NAFL), and serum LCN2 levels could be a novel biomarker for the diagnosis of non-alcoholic steatohepatitis (NASH), which may be participate in the transition from NAFL to NASH by mediating inflammation. Besides, LCN2 has been demonstrated as a biomarker for inflammatory bowel disease (Thorsvik et al., 2017), vascular dementia (Llorens et al., 2020), neuropsychiatric lupus (Mike et al., 2019), and subarachnoid hemorrhage outcome (Yu

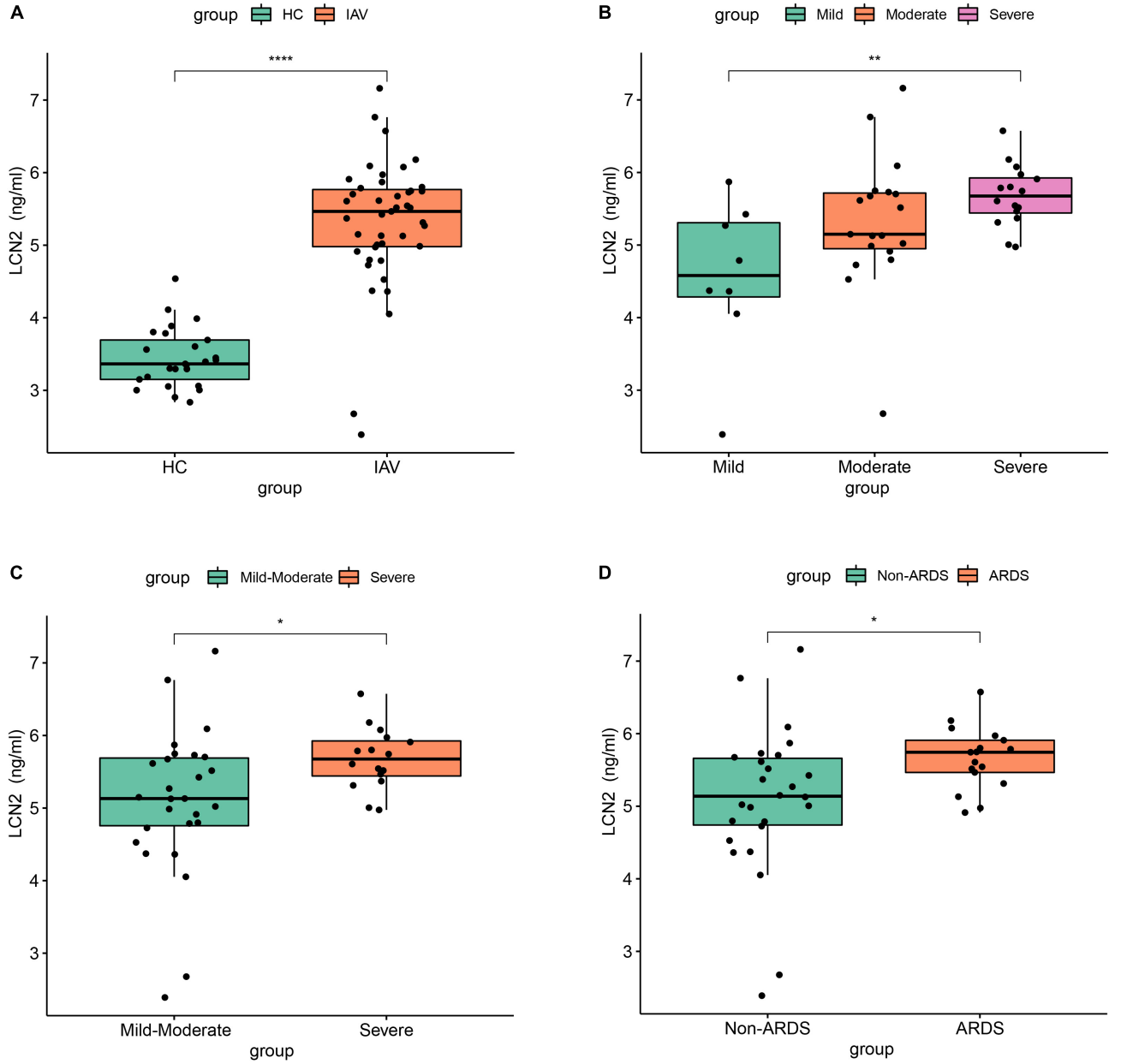


**FIGURE 4 |** The association between LCN2 and disease severity in clinical patients with IAV infection. **(A)** Serum LCN2 levels in healthy controls and patients with IAV infection. **(B,C)** Serum LCN2 levels in patients with mild, moderate, and severe influenza. **(D)** Serum LCN2 levels in ARDS and non-ARDS patients with IAV infection.

et al., 2021). The level of LCN2 could predict disease severity and survival in acute kidney injury (Bennett et al., 2008; Kümpers et al., 2010).

Research studies have revealed that LCN2 is also involved in infectious diseases. LCN2 attenuates bacterial growth by binding and sequestering the iron-scavenging siderophores to prevent bacterial iron acquisition (Goetz et al., 2002). LCN2 from both neutrophils and local epithelium can combat Klebsiella pneumoniae lung infection in mice (Cramer et al., 2017). Genetic deletion of LCN2 gene in neutrophils reduces the bactericidal effect of NETs (Li et al., 2018). However, Warszawska et al. (2013) report that LCN2 deactivates macrophages through an IL-10/STAT3-dependent mechanism and worsens pneumococcal pneumonia outcomes, which may be due to differences cell subset and bacterial strain. Besides, LCN2 can be as a biomarker of systemic inflammation in infants hospitalized with respiratory syncytial virus (RSV) infection (Sawatzky et al., 2019) and as a biomarker of inflammation, monocyte activation, and cardiac stretch during activation of the renin-angiotensin-aldosterone system in human immunodeficiency virus (Bogorodskaya et al., 2019). In this study, we found that neutrophil is one of the main drivers of inflammatory

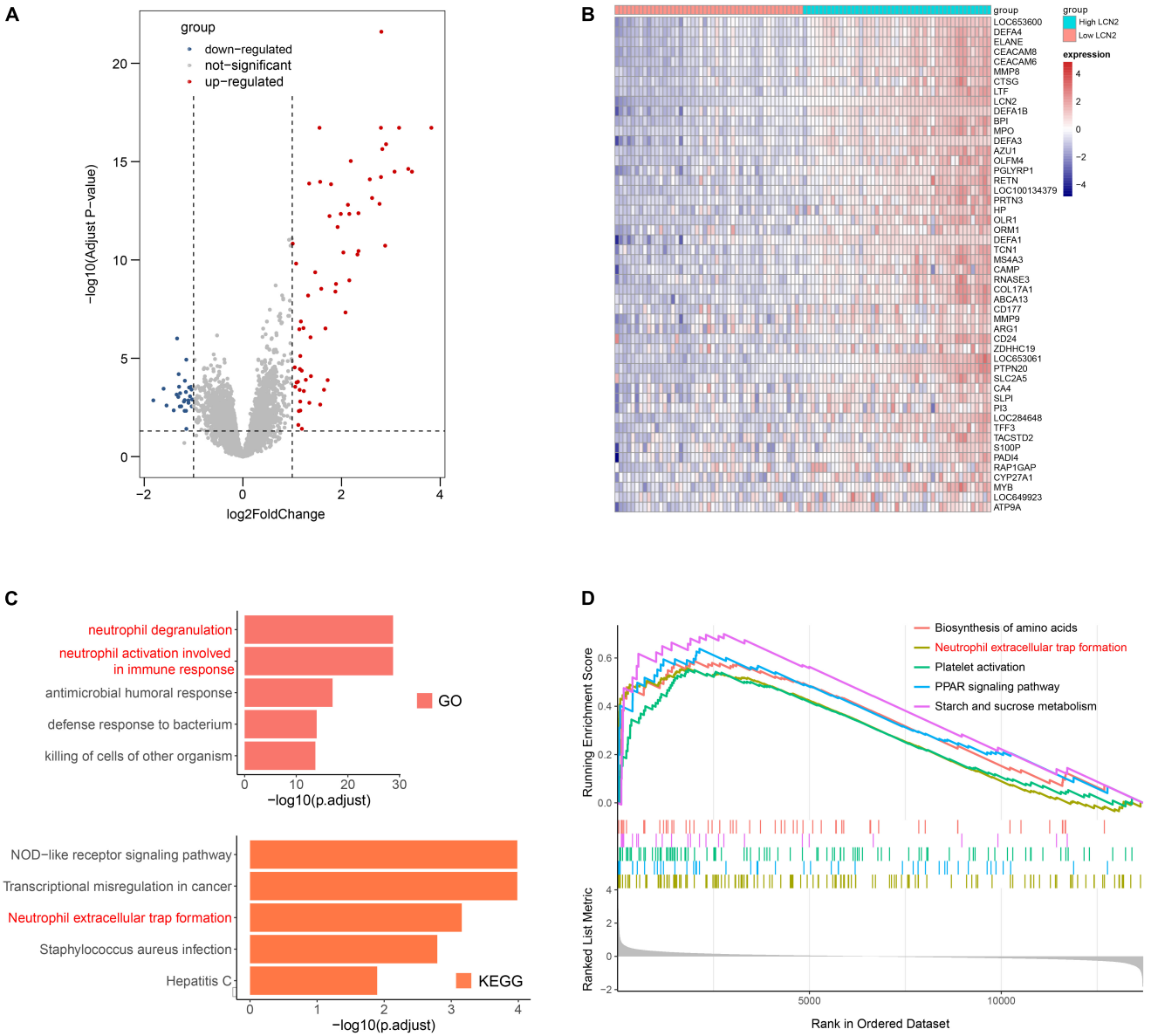


**FIGURE 5 |** Functional analysis of LCN2 in patients with IAV. **(A)** DEGs between patients with low LCN2 and high LCN2 with IAV infection (GSE111368). **(B)** Heatmap of DEGs between patients with low LCN2 and high LCN2 with IAV infection. **(C)** GO terms and KEGG pathway enrichment analysis of DEGs between patients with low LCN2 and high LCN2 with IAV infection. **(D)** GSEA in groups with patients with high LCN2.

response after virus infection. As an important functional gene of neutrophil, LCN2 was upregulated in both plasma and lung tissue after IAV and SARS-CoV-2 infection. Plasma LCN2 level was positively associated with disease severity. Therefore, neutrophil-related LCN2 might serve as a potential biomarker for predicting disease severity in both patients with influenza and COVID-19. Meanwhile, we also found that the difference between mild and severe clinical patients had not multiplied obviously compared with the difference in mice. This difference may be caused by time point of clinical infection patients, and patients come to the hospital only when the apparent symptoms appear, as neutrophils are generated enriched at early infection and LCN2 is mainly expressed in neutrophils.

Lipocalin 2 is involved in various biological processes, including immune inflammatory response and iron homeostasis (Xiao et al., 2017). LCN2 acts as a scavenger of bacterial siderophores and has antibacterial activity against siderophores dependent bacteria (Saiga et al., 2008). In addition, LCN2 can also interact with LCN2 receptor 24p3R of neutrophils to activate ERK pathway and regulate neutrophil migration and adhesion (Schroll et al., 2012). In the study, functional analysis demonstrated that LCN2 was associated with NET formation, which may reveal that LCN2 influences the development of

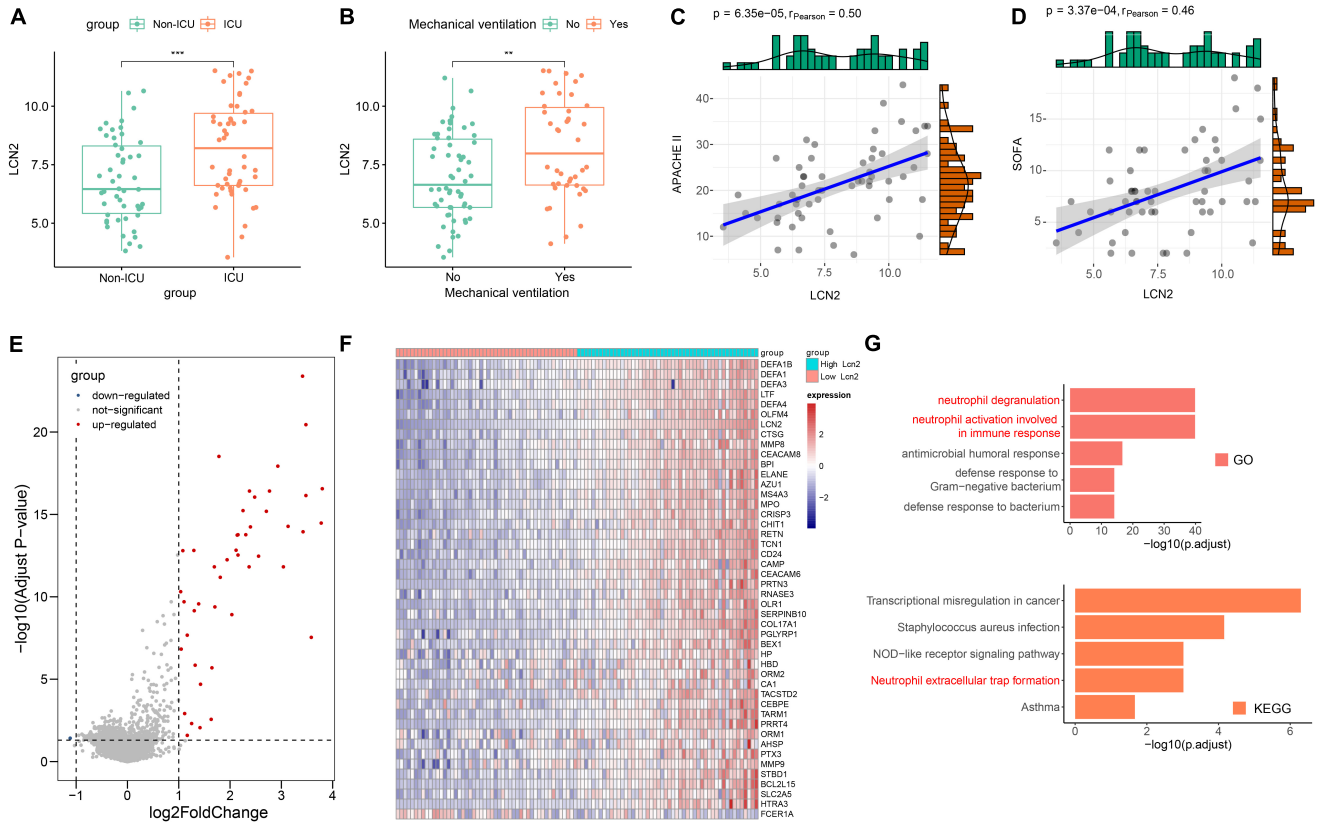


**FIGURE 6 |** The role of LCN2 in patients with COVID-19. **(A)** Expression level of LCN2 in ICU and non-ICU patients with COVID-19 (GSE157103). **(B)** Expression level of LCN2 in patients with COVID-19 with mechanical ventilation and without mechanical ventilation support. **(C,D)** Correlation analysis between LCN2 and SOFA, APACHE II in patients with COVID-19. **(E)** DEGs between patients with low LCN2 and high LCN2 with COVID-19. **(F)** Heatmap of DEGs between patients with low LCN2 and high LCN2 with COVID-19. **(G)** GO terms and KEGG pathway enrichment analysis of DEGs between patients with low LCN2 and high LCN2 with COVID-19.

disease through NETs. NETs, composed of a scaffold of DNA with histones and cytotoxic neutrophil-derived proteins, are released by neutrophils to contain invading microbes during infection and inflammation (Brinkmann et al., 2004). NETs were originally thought to eliminate bacteria but, now, are proved to protect against many viral pathogens, including influenza virus, RSV, and dengue virus (Schönrich and Raftery, 2016). NETs capture viral particles through the NETs structure and eliminate the virus through high concentration MPO and defensin or prevent the spread of the virus (Brinkmann and Zychlinsky, 2007). Therefore, the appropriate level of LCN2 possesses a protective role in mild virus infection (Watzenboeck et al., 2021). Nevertheless, NETs not only can eliminate invading pathogens but can also harm the host as well. The high level of NETs is able to kill epithelial and endothelial cells (Saffarzadeh et al., 2012). The level of NETs is higher in severe than that in mild influenza patients and is significantly associated with APACHE II score, multiple organ dysfunction syndrome (MODS), and patient survival rate of clinical influenza patients (Zhu et al., 2018). The high level of NETs is also closely associated with thrombosis in patients with COVID-19 (Middleton et al., 2020). At present, the role and exact molecular mechanism of LCN2 are still unclear and need to be further explored in severe viral infection.

There are limitations in this study. In the validation of clinical samples, we only detected the expression level of LCN2 in the plasma of patients, whereas the expression level of LCN2 in the alveolar lavage fluid of patients is unclear. In recent years, because there are fewer patients with influenza and COVID-19 in China, the sample size is small. In future studies, we will try to collect bronchoalveolar lavage fluid (BALF) from patients as much as possible and increase the sample size of the study to improve the stability of the results.

## CONCLUSION

In conclusion, we identify that a host factor LCN2 associated with neutrophils through comprehensive analysis of public database and data from clinical influenza patient samples could be used as potential biomarkers of predicting severity of patients with IAV and SARS-CoV-2 infection and provide a new direction for targeted treatment of host factor in respiratory virus infection. However, the specific mechanism of LCN2 is still unclear, which needs to be further verified by molecular biology experiments.

## DATA AVAILABILITY STATEMENT

Publicly available datasets used in the study were downloaded from GEO database: GSE107947, GSE80011, GSE124404, GSE184657, GSE111368, and GSE157103.

## ETHICS STATEMENT

The studies involving human participants were reviewed and approved by China-Japan Friendship Hospital Ethics Committee. The patients/participants provided their written informed consent to participate in this study.

## AUTHOR CONTRIBUTIONS

BC: conception and design. ZH, SL, JJ, and YZ: acquisition of data. ZH and HL: analysis and interpretation of data. ZH: writing the draft. BC, HL, and SL: revising of manuscript. All authors contributed to the article and approved the submitted version.

## FUNDING

This study was provided by the Natural Science Foundation of China (Nos. 81970010/H0104 and 82030002/H0102).

## ACKNOWLEDGMENTS

The authors thank for Shengrui Mu and Xiaoyan Deng for helpful discussions and technical support.

## SUPPLEMENTARY MATERIAL

The Supplementary Material for this article can be found online at: https://www.frontiersin.org/articles/10.3389/fmicb.2022.854172/full#supplementary-material

## REFERENCES

Andreakos, E., Papadaki, M., and Serhan, C. N. (2021). Dexamethasone, pro-resolving lipid mediators and resolution of inflammation in COVID-19. *Allergy* 76, 626–628. doi: 10.1111/all.14595

Arunachalam, P. S., Wimmers, F., Mok, C. K. P., Perera, R. A. P. M., Scott, M., Hagan, T., et al. (2020). Systems biological assessment of immunity to mild versus severe COVID-19 infection in humans. *Science* 369, 1210–1220. doi: 10.1126/science.abc6261

Ather, J. L., Dienz, O., Boyson, J. E., Anathy, V., Amiel, E., and Poynter, M. E. (2018). Serum Amyloid A3 is required for normal lung development and survival following influenza infection. *Sci. Rep.* 8:16571. doi: 10.1038/s41598-018-34901-x

Bennett, M., Dent, C. L., Ma, Q., Dastrala, S., Grenier, F., Workman, R., et al. (2008). Urine NGAL predicts severity of acute kidney injury after cardiac surgery: a prospective study. *Clin. J. Am. Soc. Nephrol.* 3, 665–673. doi: 10.2215/CJN.04010907

Bogorodskaya, M., Fitch, K. V., Burdo, T. H., Maehler, P., Easly, R. M., Murray, G. R., et al. (2019). Serum Lipocalin 2 (Neutrophil Gelatinase-Associated Lipocalin) in Relation to Biomarkers of Inflammation and Cardiac Stretch During Activation of the Renin-Angiotensin-Aldosterone System in Human Immunodeficiency Virus. *J. Infect. Dis.* 220, 1420–1424. doi: 10.1093/infdis/jiz346

Brandes, M., Klauschen, F., Kuchen, S., and Germain, R. N. (2013). A systems analysis identifies a feedforward inflammatory circuit leading to lethal influenza infection. *Cell* 154, 197–212. doi: 10.1016/j.cell.2013.06.013

Brinkmann, V., Reichard, U., Goosmann, C., Fauler, B., Uhlemann, Y., Weiss, D. S., et al. (2004). Neutrophil extracellular traps kill bacteria. *Science* 303, 1532–1535.

Brinkmann, V., and Zychlinsky, A. (2007). Beneficial suicide: why neutrophils die to make NETs. *Nat. Rev. Microbiol.* 5, 577–582. doi: 10.1038/nrmicro1710

Callaway, E. (2021). Omicron likely to weaken COVID vaccine protection. *Nature*.600, 367–368 doi: 10.1038/d41586-021-03672-3

Cheng, Y., Zhao, H., Song, P., Zhang, Z., Chen, J., and Zhou, Y.-H. (2019). Dynamic changes of lymphocyte counts in adult patients with severe pandemic H1N1 influenza A. *J. Infect. Public Health* 12, 878–883. doi: 10.1016/j.jiph.2019.05.017

Cramer, E. P., Dahl, S. L., Rozell, B., Knudsen, K. J., Thomsen, K., Moser, C., et al. (2017). Lipocalin-2 from both myeloid cells and the epithelium combats lung infection in mice. *Blood* 129, 2813–2817. doi: 10.1182/blood-2016-11-753434

Dal Molin, A., and Di Camillo, B. (2019). How to design a single-cell RNA-sequencing experiment: pitfalls, challenges and perspectives. *Brief. Bioinform.* 20, 1384–1394. doi: 10.1093/bib/bby007

Diao, B., Wang, C., Tan, Y., Chen, X., Liu, Y., Ning, L., et al. (2020). Reduction and Functional Exhaustion of T Cells in Patients With Coronavirus Disease 2019 (COVID-19). *Front. Immunol.* 11:827. doi: 10.3389/fimmu.2020.00827

Fumagalli, V., Ravà, M., Marotta, D., Di Lucia, P., Laura, C., Sala, E., et al. (2022). Administration of aerosolized SARS-CoV-2 to K18-hACE2 mice uncouples respiratory infection from fatal neuroinvasion. *Sci. Immunol.* 7:eabl9929. doi: 10.1126/sciimmunol.abl9929

Goetz, D. H., Holmes, M. A., Borregaard, N., Bluhm, M. E., Raymond, K. N., and Strong, R. K. (2002). The neutrophil lipocalin NGAL is a bacteriostatic agent that interferes with siderophore-mediated iron acquisition. *Mol. Cell* 10, 1033–1043. doi: 10.1016/s1097-2765(02)00708-6

Griffiths, J. A., Scialdone, A., and Marioni, J. C. (2018). Using single-cell genomics to understand developmental processes and cell fate decisions. *Mol. Syst. Biol.* 14:e8046. doi: 10.15252/msb.20178046

Guo, Q., Zhao, Y., Li, J., Liu, J., Yang, X., Guo, X., et al. (2021). Induction of alarmin S100A8/A9 mediates activation of aberrant neutrophils in the pathogenesis of COVID-19. *Cell Host Microbe* 29, 222–235.e4. doi: 10.1016/j.chom.2020.12.016

Guo, X.-Z. J., and Thomas, P. G. (2017). New fronts emerge in the influenza cytokine storm. *Semi. Immunopathol.* 39, 541–550. doi: 10.1007/s00281-017-0636-y

Hatesuer, B., Hoang, H. T. T., Riese, P., Trittel, S., Gerhauser, I., Elbahesh, H., et al. (2017). Deletion of Irf3 and Irf7 Genes in Mice Results in Altered Interferon Pathway Activation and Granulocyte-Dominated Inflammatory Responses to Influenza A Infection. *J Innate Immun.* 9, 145–161. doi: 10.1159/000450705

Imdahl, F., and Saliba, A.-E. (2020). Advances and challenges in single-cell RNA-seq of microbial communities. *Curr. Opin. Microbiol.* 57, 102–110. doi: 10.1016/j.mib.2020.10.001

Ito, Y., Torii, Y., Ohta, R., Imai, M., Hara, S., Kawano, Y., et al. (2011). Increased levels of cytokines and high-mobility group box 1 are associated with the development of severe pneumonia, but not acute encephalopathy, in 2009 H1N1 influenza-infected children. *Cytokine* 56, 180–187. doi: 10.1016/j.cyto.2011.07.016

Jia, J., Yang, L., Cao, Z., Wang, M., Ma, Y., Ma, X., et al. (2021). Neutrophil-derived lipocalin-2 in adult-onset Still's disease: a novel biomarker of disease activity and liver damage. *Rheumatology* 60, 304–315. doi: 10.1093/rheumatology/keaa368

Karki, R., Sharma, B. R., Tuladhar, S., Williams, E. P., Zalduondo, L., Samir, P., et al. (2021). Synergism of TNF-α and IFN-γ Triggers Inflammatory Cell Death, Tissue Damage, and Mortality in SARS-CoV-2 Infection and Cytokine Shock Syndromes. *Cell* 184, 149–168.e17

Kjeldsen, L., Cowland, J. B., and Borregaard, N. (2000). Human neutrophil gelatinase-associated lipocalin and homologous proteins in rat and mouse. *Biochimi. Biophys. Acta* 1482, 272–283. doi: 10.1016/s0167-4838(00)00152-7

Kümpers, P., Hafer, C., Lukasz, A., Lichtinghagen, R., Brand, K., Fliser, D., et al. (2010). Serum neutrophil gelatinase-associated lipocalin at inception of renal replacement therapy predicts survival in critically ill patients with acute kidney injury. *Critic. Care* 14:R9. doi: 10.1186/cc8861

Lampejo, T. (2020). Influenza and antiviral resistance: an overview. *Eur. J. Clin. Microbiol. Infect. Dis.* 39, 1201–1208. doi: 10.1007/s10096-020-03840-9

Li, H., Feng, D., Cai, Y., Liu, Y., Xu, M., Xiang, X., et al. (2018). Hepatocytes and neutrophils cooperatively suppress bacterial infection by differentially regulating lipocalin-2 and neutrophil extracellular traps. *Hepatology* 68, 1604–1620. doi: 10.1002/hep.29919

Li, J., Lai, S., Gao, G. F., and Shi, W. (2021). The emergence, genomic diversity and global spread of SARS-CoV-2. *Nature*.600, 408–418 doi: 10.1038/s41586-021-04188-6

Liu, Q., Zhou, Y.-H., and Yang, Z.-Q. (2016). The cytokine storm of severe influenza and development of immunomodulatory therapy. *Cell. Mol. Immunol.* 13, 3–10 doi: 10.1038/cmi.2015.74

Llorens, F., Hermann, P., Villar-Piqué, A., Diaz-Lucena, D., Nägga, K., Hansson, O., et al. (2020). Cerebrospinal fluid lipocalin 2 as a novel biomarker for the differential diagnosis of vascular dementia. *Nat. Commun.* 11:619. doi: 10.1038/s41467-020-14373-2

Mahler, M., Meroni, P.-L., Infantino, M., Buhler, K. A., and Fritzler, M. J. (2021). Circulating Calprotectin as a Biomarker of COVID-19 Severity. *Exp. Rev. Clin. Immunol.* 17, 431–443. doi: 10.1080/1744666X.2021.1905526

Middleton, E. A., He, X.-Y., Denorme, F., Campbell, R. A., Ng, D., Salvatore, S. P., et al. (2020). Neutrophil extracellular traps contribute to immunothrombosis in COVID-19 acute respiratory distress syndrome. *Blood* 136, 1169–1179. doi: 10.1182/blood.2020007008

Mike, E. V., Makinde, H. M., Gulinello, M., Vanarsa, K., Herlitz, L., Gadhvi, G., et al. (2019). Lipocalin-2 is a pathogenic determinant and biomarker of neuropsychiatric lupus. *J. Autoimmun.* 96, 59–73. doi: 10.1016/j.jaut.2018.08.005

Moschen, A. R., Adolph, T. E., Gerner, R. R., Wieser, V., and Tilg, H. (2017). Lipocalin-2: A Master Mediator of Intestinal and Metabolic Inflammation. *Trends Endocrinol. Metabol.* 28, 388–397. doi: 10.1016/j.tem.2017.01.003

Rappe, J. C. F., Finsterbusch, K., Crotta, S., Mack, M., Priestnall, S. L., and Wack, A. (2021). A TLR7 antagonist restricts interferon-dependent and -independent immunopathology in a mouse model of severe influenza. *J. Exp. Med.* 218. doi: 10.1084/jem.20201631

Ren, X., Wen, W., Fan, X., Hou, W., Su, B., Cai, P., et al. (2021). COVID-19 immune features revealed by a large-scale single-cell transcriptome atlas. *Cell* 184, 1895–1913.e19

Saffarzadeh, M., Juenemann, C., Queisser, M. A., Lochnit, G., Barreto, G., Galuska, S. P., et al. (2012). Neutrophil extracellular traps directly induce epithelial and endothelial cell death: a predominant role of histones. *PloS One* 7:e32366. doi: 10.1371/journal.pone.0032366

Saiga, H., Nishimura, J., Kuwata, H., Okuyama, M., Matsumoto, S., Sato, S., et al. (2008). Lipocalin 2-dependent inhibition of mycobacterial growth in alveolar epithelium. *J. Immunol.* 181, 8521–8527. doi: 10.4049/jimmunol.181.12.8521

Sawatzky, J., Soo, J., Conroy, A. L., Bhargava, R., Namasopo, S., Opoka, R. O., et al. (2019). Biomarkers of Systemic Inflammation in Ugandan Infants and Children Hospitalized With Respiratory Syncytial Virus Infection. *Pediatric infect. Dis. J.* 38, 854–859. doi: 10.1097/INF.0000000000002343

Schmitz, N., Kurrer, M., Bachmann, M. F., and Kopf, M. (2005). Interleukin-1 is responsible for acute lung immunopathology but increases survival of respiratory influenza virus infection. *J. Virol.* 79, 6441–6448. doi: 10.1128/JVI.79.10.6441-6448.2005

Schönrich, G., and Raftery, M. J. (2016). Neutrophil Extracellular Traps Go Viral. *Front. Immunol.* 7:366. doi: 10.3389/fimmu.2016.00366

Schroll, A., Eller, K., Feistritzer, C., Nairz, M., Sonnweber, T., Moser, P. A., et al. (2012). Lipocalin-2 ameliorates granulocyte functionality. *Eur. J. Immunol.* 42, 3346–3357. doi: 10.1002/eji.201142351

Suvà, M. L., and Tirosh, I. (2019). Single-Cell RNA Sequencing in Cancer: Lessons Learned and Emerging Challenges. *Mol. Cell* 75, 7–12 doi: 10.1016/j.molcel.2019.05.003

Thorsvik, S., Damås, J. K., Granlund, A. V., Flo, T. H., Bergh, K., Østvik, A. E., et al. (2017). Fecal neutrophil gelatinase-associated lipocalin as a biomarker for inflammatory bowel disease. *J. Gastroenterol. Hepatol.* 32, 128–135. doi: 10.1111/jgh.13598

Tisoncik, J. R., Korth, M. J., Simmons, C. P., Farrar, J., Martin, T. R., and Katze, M. G. (2012). Into the eye of the cytokine storm. *Microbiol. Mol. Biol. Rev.* 76, 16–32.

Valero-Pacheco, N., Arriaga-Pizano, L., Ferat-Osorio, E., Mora-Velandia, L. M., and Pastelin-Palacios, R. (2013). PD-L1 expression induced by the 2009 pandemic influenza A(H1N1) virus impairs the human T cell response. *Clin. Dev. Immunol.* 2013:989673. doi: 10.1155/2013/989673

Warszawska, J. M., Gawish, R., Sharif, O., Sigel, S., Doninger, B., Lakovits, K., et al. (2013). Lipocalin 2 deactivates macrophages and worsens pneumococcal pneumonia outcomes. *J. Clin. Invest.* 123, 3363–3372. doi: 10.1172/JCI67911

Watzenboeck, M. L., Drobits, B., Zahalka, S., Gorki, A.-D., Farhat, A., and Quattrone, F. (2021). Lipocalin 2 modulates dendritic cell activity and shapes immunity to influenza in a microbiome dependent manner. *PLoS Pathogens* 17:e1009487. doi: 10.1371/journal.ppat.1009487

Xiao, X., Yeoh, B. S., and Vijay-Kumar, M. (2017). Lipocalin 2: An Emerging Player in Iron Homeostasis and Inflammation. *Ann. Rev. Nutr.* 37, 103–130. doi: 10.1146/annurev-nutr-071816-064559

Yang, L., Wang, S., Wang, Y., Zhao, P., Cui, C., Tu, L., et al. (2020). Diversity of locally produced IFN-α subtypes in human nasopharyngeal epithelial cells and mouse lung tissues during influenza virus infection. *Appl. Microbiol. Biotechnol.* 104, 6351–6361. doi: 10.1007/s00253-020-10676-y

Yu, F., Saand, A., Xing, C., Lee, J. W., Hsu, L., Palmer, O. P., et al. (2021). CSF lipocalin-2 increases early in subarachnoid hemorrhage are associated with neuroinflammation and unfavorable outcome. *J. Cereb. blood Flow Metab.* 41, 2524–2533. doi: 10.1177/0271678X211012110

Zhang, J., Liu, J., Yuan, Y., Huang, F., Ma, R., Luo, B., et al. (2020a). Two waves of pro-inflammatory factors are released during the influenza A virus (IAV)-driven pulmonary immunopathogenesis. *PLoS Pathog.* 16:e1008334. doi: 10.1371/journal.ppat.1008334

Zhang, X., Tan, Y., Ling, Y., Lu, G., Liu, F., Yi, Z., et al. (2020b). Viral and host factors related to the clinical outcome of COVID-19. *Nature* 583, 437–440. doi: 10.1038/s41586-020-2355-0

Zhu, L., Liu, L., Zhang, Y., Pu, L., Liu, J., Li, X., et al. (2018). High Level of Neutrophil Extracellular Traps Correlates With Poor Prognosis of Severe Influenza A Infection. *J. Infect. Dis.* 217, 428–437. doi: 10.1093/infdis/jix475

Ziegler, T., Mamahit, A., and Cox, N. J. (2018). 65 years of influenza surveillance by a World Health Organization-coordinated global network. *Influenza Other Respir. Viruses* 12, 558–565. doi: 10.1111/irv.12570

**Conflict of Interest:** The authors declare that the research was conducted in the absence of any commercial or financial relationships that could be construed as a potential conflict of interest.

**Publisher's Note:** All claims expressed in this article are solely those of the authors and do not necessarily represent those of their affiliated organizations, or those of the publisher, the editors and the reviewers. Any product that may be evaluated in this article, or claim that may be made by its manufacturer, is not guaranteed or endorsed by the publisher.

frontiers | Frontiers in Microbiology

REVIEW
published: 21 April 2022
doi: 10.3389/fmicb.2022.869406

# A Review and Meta-Analysis of Influenza Interactome Studies

*Sonja Courtney Jun Hui Chua*[1,2,3,4], *Jianzhou Cui*[1,2,3], *David Engelberg*[4,5,6] and *Lina Hsiu Kim Lim*[1,2,3]*

[1]Department of Physiology, Yong Loo Lin School of Medicine, National University of Singapore, Singapore, Singapore, [2]Immunology Translational Research Program, Yong Loo Lin School of Medicine, National University of Singapore, Singapore, Singapore, [3]NUS Immunology Program, Life Sciences Institute, National University of Singapore, Singapore, Singapore, [4]CREATE-NUS-HUJ Cellular & Molecular Mechanisms of Inflammation Programme, National University of Singapore, Singapore, Singapore, [5]Department of Microbiology, Yong Loo Lin School of Medicine, National University of Singapore, Singapore, Singapore, [6]Department of Biological Chemistry, The Institute of Life Science, The Hebrew University of Jerusalem, Jerusalem, Israel

Annually, the influenza virus causes 500,000 deaths worldwide. Influenza-associated mortality and morbidity is especially high among the elderly, children, and patients with chronic diseases. While there are antivirals available against influenza, such as neuraminidase inhibitors and adamantanes, there is growing resistance against these drugs. Thus, there is a need for novel antivirals for resistant influenza strains. Host-directed therapies are a potential strategy for influenza as host processes are conserved and are less prone mutations as compared to virus-directed therapies. A literature search was performed for papers that performed viral–host interaction screens and the Reactome pathway database was used for the bioinformatics analysis. A total of 15 studies were curated and 1717 common interactors were uncovered among all these studies. KEGG analysis, Enrichr analysis, STRING interaction analysis was performed on these interactors. Therefore, we have identified novel host pathways that can be targeted for host-directed therapy against influenza in our review.

**Keywords: influenza, host-pathogen interactions, influenza proteins, interactome analysis, bioinformatics**

OPEN ACCESS

***Edited by:***
*Yizhi Tao,*
*Rice University, United States*

***Reviewed by:***
*Yang Li,*
*Fudan University, China*
*Irene Ramos,*
*Icahn School of Medicine at Mount Sinai, United States*

***Correspondence:**
*Lina Hsiu Kim Lim*
*linalim@nus.edu.sg*

***Specialty section:***
*This article was submitted to Virology, a section of the journal Frontiers in Microbiology*

***Received:*** *04 February 2022*
***Accepted:*** *23 March 2022*
***Published:*** *21 April 2022*

***Citation:***
*Chua SCJH, Cui J, Engelberg D and Lim LHK (2022) A Review and Meta-Analysis of Influenza Interactome Studies. Front. Microbiol. 13:869406. doi: 10.3389/fmicb.2022.869406*

## INTRODUCTION

Influenza viruses are negative-sense single-stranded RNA viruses from the *Orthomyxoviridae* family that cause respiratory diseases (MacLachlan and Dubovi, 2017). Of the 4 influenza virus types, A, B, C, and D, type A is the most prolific as it infects numerous hosts and is the main causative agent of the seasonal and pandemic influenza (Shen et al., 2015). Influenza viruses constantly evolve with antigenic shifts (reassortment of viral segments, resulting in dramatically different viruses) and drifts (small antigenic changes to increase immune evasion). Due to the viral adaptation and reassortment, highly virulent strains may appear and result in local epidemics or global pandemics, such as the 1918 H1N1 Spanish pandemic, 2005 H5N1 Bird flu, and the 2009 H1N1 Swine flu (Shen et al., 2015). Influenza's genome, which is composed of eight segments of symmetrical helixes, encodes ten proteins. Those include the surface glycoproteins haemagglutinin (HA) and neuraminidase (NA), matrix protein (M1), matrix ion channel (M2), Nucleoprotein (NP), PA (polymerase acid subunit),

polymerase basic subunit 1 (PB1), and polymerase basic subunit 2 (PB2), which form the RNA-dependent RNA polymerase complex, NS1 (non-structural protein 1) and NS2, non-structural protein 2 or nuclear export protein (NEP; Noda, 2012). Segments of some influenza A virus strains may encode a second or third polypeptide in alternative reading frames (McCauley et al., 2012). These functional proteins (Jagger et al., 2012), such as PB1-F2 and PA-X, are known to modulate the host response to the virus (Klemm et al., 2018). The influenza A virus can be further classified based on its HA and NA glycoproteins into different subtypes. There are 18 haemagglutinin and 11 neuraminidase subtypes known today (Tong et al., 2013). Only the H1, H2, H3, N1, and N2 subtypes have caused epidemics in humans (Bouvier and Palese, 2008).

## Current Prophylaxis and Treatment of Influenza

Vaccination is available for influenza and is the main form of prevention against influenza. Vaccine efficacy is around 60% if matched to the current circulating strains of the virus, but effectiveness can be as low as 10–20% if there is a mismatch between the vaccine and current strains of the virus (Eisenstein, 2019). The current method of developing influenza vaccines is lengthy, with the Centre for Disease Control (CDC) characterizing around 2,000 influenza viruses. These viruses are monitored for drifts and shifts and compared to viruses included in the current influenza vaccine. This provides an indication of the vaccine's ability to produce an immune response against current circulating strains of influenza (CDC, 2019). There are three main kinds of vaccines: egg-based vaccines, attenuated vaccines, and recombinant vaccines. However, due to the constantly evolving nature of influenza, there are problems associated with vaccine mismatches (Paules et al., 2018) and poor immunogenicity of vaccines in the elderly (DiazGranados et al., 2014). Moreover, there is a lack of a universal influenza vaccine covering all strains and subtypes of influenza (Krammer et al., 2018).

Hence, there is a need for antiviral therapy for breakthrough infections and for infection with influenza strains not covered by vaccines. M2 ion channel inhibitors (e.g., amantadine and rimantadine) and NA inhibitors (e.g., oseltamivir and zanamivir) are the original two drug classes approved for influenza treatment (Krammer et al., 2018). Resistant virus strains have emerged and have rendered M2 inhibitors ineffective for clinical use while there is also increasing NA inhibitor resistance, such as the H274Y mutation, found in the 2009 H1N1 strain which conferred oseltamivir resistance (Arias et al., 2009; Shen et al., 2015). Recently, baloxavir (cap-dependent endonuclease inhibitor) was approved by the FDA in 2018 and worked by interfering influenza's ability to multiply *via* inhibition of viral transcription (Hayden et al., 2018). There are a limited number of compounds under development or in trials (Davidson, 2018). Hence, there is an increasing focus to research and developing host-directed therapies given there is a lower drug resistance potential (Lou et al., 2014). We hypothesized that by combining various influenza interactome studies, there might be novel insights into viral–host interactors and processes that could be targeted for antiviral therapy. In this study, we identified novel host interactors of influenza *via* literature and database search. We further analyzed the data set by bioinformatics. This resulted in the identification of core cellular processes and druggable targets that could be further studied. This provides an overall landscape of conserved host processes targeted by various influenza strains for future drug development and better understanding the influenza life cycle.

# MATERIALS AND METHODS

## Data Collection

In order to identify host interactions that are ubiquitous across the various influenza A strains, data was extracted from the Reactome database (Fabregat et al., 2018; Jassal et al., 2020) and Host Pathogen Interaction Database (HPIDB; Ammari et al., 2016) while a PubMed and Scopus search of primary literature that performed interaction studies. Papers were chosen if they had found specific interactions between a host protein and influenza proteins. Host interactions with viral complexes and novel accessory viral proteins, such as PA-X and PB1-F2, were excluded. This is because not all influenza A strains express these accessory proteins. A total of 15 papers were retrieved, and their methodology, as well as virus strain (s) studied, are listed **Supplementary Table S1**. Reactome is a free, online, curated, open-source pathway database contains the influenza infection pathway (REACT_6167.3), specifically NS1 Mediated Effects on Host Pathways (Homo sapiens). This pathway was last reviewed on 1 May 2007, thus does not contain any information from the studies utilized in this project. Despite its age, it was still included as a point of reference for subsequent analysis. (Fabregat et al., 2018; Jassal et al., 2020).

HPIDB was chosen as it contains a comprehensive set of host–virus interactions (Ammari et al., 2016). This includes experimentally derived HPI, predicted HPI *via* network analysis, and molecular interactions from other databases which include VirHostNet[1] and UniProtKB (Consortium, 2012).[2] Currently, in its third version, it has 69,787 unique protein interactions between 66 host and 668 pathogen species. In this project, all ten characterized influenza protein interactions (HA, NA, PA, PB1, PB2, NP, M1, M2, NS1, and NS2) from various influenza A strains with human proteins were extracted from the various studies and databases, compiled, and matched to reveal which are key interactors of influenza. The compiled data can be found in **Supplementary Table S1**.

## Data Set Analysis

Using the filtered gene data set, we performed the following analysis. Enrichr (Chen et al., 2013; Kuleshov et al., 2016) was used for gene set enrichment analysis. Kyoto Encyclopedia of Genes and Genomes (KEGG)[3] pathwayanalysis was conducted

[1]http://virhostnet.prabi.fr
[2]https://www.uniprot.org/
[3]http://www.genome.jp/kegg/pathway.html

to identify genes at the biologically functional level (Kummer et al., 2014). For all enrichment analysis, a value of p cutoff of 0.05 was used as significant. **Figure 1** shows the analysis workflow for the bioinformatics analysis.

# RESULTS AND DISCUSSION

## Meta-Analysis of Influenza–Host Interactions

In order to better understand the landscape of influenza–host interactions, we performed an analysis of influenza host interactors. We compiled virus–host protein–protein interaction data from HPIDB, Reactome, and published interactome studies. The published studies and their methodology are described in **Supplementary Table S1**. This data set covered various strains of influenza A, such as H3N2, H1N1, and H7N9. This data set contained protein interactions from different experimental methods—Affinity purification-mass spectrometry (AP-MS), Yeast 2 hybrid (Y2H), RNA immunoprecipitation, and bioinformatics prediction of interactions. Given that single interactome studies may result in false positives, a host interactor was considered to be true if it appeared in at least 3 different studies and databases. Altogether, our review uncovered 1,717 host interactions among the ten viral proteins. Both KEGG and Enrichr functional analysis were performed for the interactors of each viral protein. Details of the specific host–viral interactions can be found from **Supplementary Table S2**.

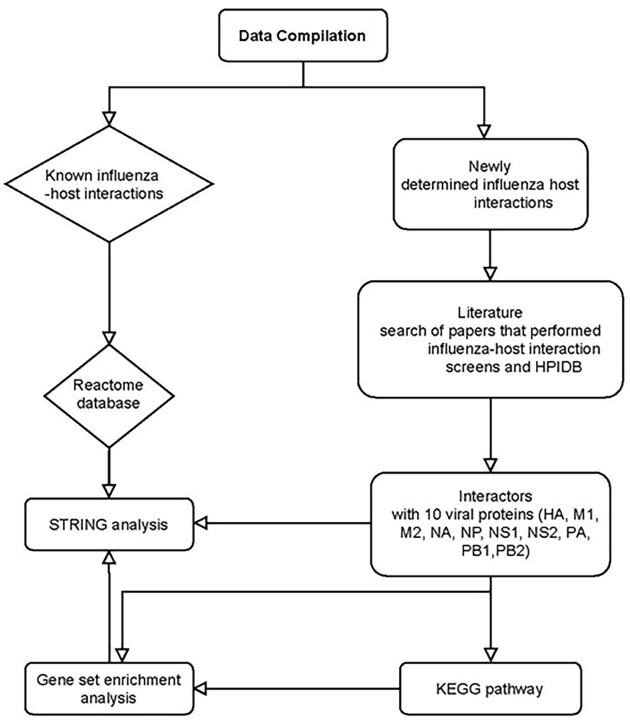


**FIGURE 1 |** Bioinformatics analysis of influenza and host interactors. HPIDB: Human Pathogen Interactions Database. Host interactors of influenza were separated into known and newly determined interactions. PubMed search of Viral–host interactome studies (IP-MS, Y2H, computer homology) was conducted. Papers were filtered if they were in English and full data set was available for analysis. Compiled data set of interactors was analyzed using STRING, Gene set enrichment analysis, and KEGG pathway.

## HA Interactors Are Mainly Involved in Protein Processing

HA is a trimer of identical subunits, each containing two polypeptides that result from proteolytic cleavage of a singular precursor (Skehel and Wiley, 2000). This cleavage is essential to activate membrane fusion potential and hence infectivity (Garten and Klenk, 1999; Steinhauer, 1999). A newly synthesized 70 kDa HA is cleaved into HA1 and HA2, which are linked by disulfide bonds. HA1 contains the sialic acid binding site. After binding, the virus is internalized into endosomes. Endosomal acidification triggers a marked and irreversible change in HA, which results in the dissociation of HA1 from the endosomal membrane and HA1 moving away from HA2. There is a loop-to-helix transition in HA2 which enables the fusion peptide at the N-terminus of HA2 to attach to the endosomal membrane. This promotes the fusion of the viral and endosomal membranes and this results in the vRNP release into the cytoplasm (Das et al., 2010).

HA binding to sialic acid receptor determines the species-specific infectivity of the influenza virus (Rogers and Paulson, 1983). Avian and equine viruses prefer α-2,3-galactose-linked sialic acid, human viruses prefer α-2,6-linked sialic acid and swine viruses appear to bind to both linkages of sialic acid (Rogers and D'Souza, 1989; Gambaryan et al., 1997; Ito et al., 1998).

Based on our meta-analysis, 36 common host interactors were found across the various studies. The top KEGG pathway identified for HA interactors was the proteasomal pathway (i.e., PSMD6 and PSMD7), protein processing in endoplasmic reticulum (i.e., RPN1, CALR, and PDIA6), and adherens junction (i.e., ACTN1 and ACTN4; **Figure 2A; Supplementary Figure S1A**). The functional analysis of the interactors revealed that they were mainly involved in the immune pathway (i.e., PSMD6, PSMD7, ACTN4, ARF1, and ANXA2), protein processing (i.e., PSMD6, PSMD7, CALR), and post-translational modification (i.e., PSMD6, PSMD7, CALU, and PDIA6; **Figure 2B; Supplementary Figure S1B**). Given that HA is being transcribed and translated in the infected cell during the viral life cycle, this would point to the importance of the protein processing being key in influenza replication. Any drug targeting this process would affect the formation of new virions. This is supported by a previous study which showed HA being synthesized by ER-bound biosynthetic machinery and interacting with ER chaperone proteins calnexin and calreticulin (Hebert et al., 1997). Any drug targeting this process would affect the formation of new virions. Moreover, HA requires glycosylation for binding to sialic receptors (de Vries et al., 2010), while palmitoylation of HA is essential for the virus to form infectious virions (Chen et al., 2005). Therefore, this presents a key druggable target for a new therapy to target or prevent influenza infection. DAS181 has already been developed as a sialidase fusion protein

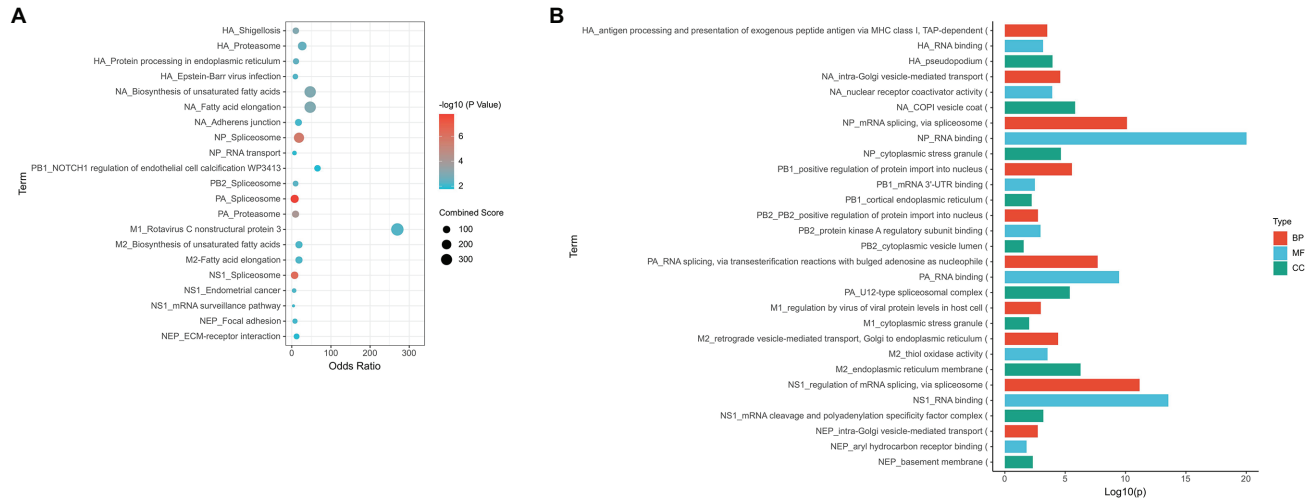


**FIGURE 2 |** Summary of the main processes found to be represented for each viral protein. **(A)** Enriched KEGG pathway for interactors of each viral protein **(B)** GO analysis of interactors of each viral protein. Proteins were analyzed using Enrichr BP, MF, and CC represent Biological Process, Molecular Function, and Cellular Component groups of gene ontology (GO).

to prevent the binding of haemagglutinin to sialic acid receptors. It has reached late-stage clinical trials (Koszalka et al., 2017).

An interesting observation was that immune-related processes were highly enriched from the gene set analysis. A previous study had reported that HA subunit 1 drove the IFN receptor chain IFNAR1 degradation, thus suppressing IFN-triggered JAK/STAT. The reduced JAK/STAT activation would lead to lower type I interferon production, resulting in decreased immune response and thereby increasing viral replication (Xia et al., 2016). This would confirm that HA is involved in regulating the host immune response as part of the influenza life cycle.

## NA Interactors Are Involved in Vesicle Transport

NA is a mushroom-shaped protein and is found as a tetramer of identical subunits, with the mushroom head suspended from the viral membrane on a thin, long stalk. Each subunit that forms the mushroom head is made up of a six-bladed propeller-like structure (Varghese et al., 1983).

During viral replication, NA removes sialic acid from cellular glycoproteins and glycolipids, as well as from both viral glycoproteins. This prevents newly assembled viruses from rebinding to the infected cell surface and with self-aggregate through HA-sialic acid interactions. New virions are then released from the cell to infect new cells and further the infection spread (Gamblin and Skehel, 2010). It is also thought that NA aids viral infectivity by breaking down the mucins in the respiratory tract secretions to allow the penetration of the virus to the respiratory epithelium and may play a role in viral entry into respiratory epithelial cells (Matrosovich et al., 2004).

A total of 36 NA interactors were found across the various studies. These proteins are involved in fatty acid metabolism (i.e., TECR and HACD3); focal adhesion tight and adherens junction (i.e., ACTN1 and ACTN4), and cell cycle (i.e., MCM7 and PRKDC) *via* KEGG analysis (**Figure 2A; Supplementary Figure S2A**). Functional analysis of NA interactors found that the most highly enriched processes were intra-Golgi vesicle transport and vesicle transport (i.e., COPB2, COPA, and COPG1; **Figure 2B; Supplementary Figure S2B**). Given that acetylation of α-tubulin occurs as part of the viral release (Husain and Harrod, 2011), this would suggest that NA is involved in this mechanism.

## NP, PB1, PB2, PA Interactors Are Involved in Spliceosome Activity

NP is a structural protein with no enzymatic activity but is the most abundant viral protein in infected cells (Hu et al., 2017). It is an important part of the vRNP complex and its functions include RNA packing (Eisfeld et al., 2015), nuclear trafficking (Amorim et al., 2013; Chutiwitoonchai and Aida, 2016), and vRNA transcription and replication (Eisfeld et al., 2015). A NP monomer has a molecular weight of 56 kDa that is able to bind to 24 bases of RNA (Hu et al., 2017). It is crescent-shaped with head, body, RNA binding, and tail domains (Cianci et al., 2013). The residues in the basic loop (residues 73–91) were found to be required for RNA binding (Ng et al., 2008). NP oligomerization occurs *via* a flexible tail-loop (residues 402–428) that can insert into the body domain of a neighboring NP monomer (Ye et al., 2006). This tail insertion is facilitated by R419 and E339 which forms a critical salt bridge for stabilization (Cianci et al., 2013). NP also directly interacts with PB1 and PB2 subunits of the viral polymerase (Biswas et al., 1998; Fodor, 2013; Eisfeld et al., 2015; Davis et al., 2017). The C-terminus of NP (aa 340 to 498) contains a PB2 binding site and a sequence that regulates the NP-PB2 interaction.

In addition to its role in the vRNP, NP has been found to induce apoptosis in host cells (Tripathi et al., 2013; Nailwal et al., 2015) and inhibit PKR activation *via* Hsp40 (Sharma et al., 2011).

The vRNP polymerase complex is a heterotrimer formed together by PB1 with PB2 and PA in the viral polymerase (Eisfeld et al., 2015). PB1 itself has the polymerase activity and is enclosed by the PA linker on one side (Ma et al., 2017) and the N-terminal domain of PB2 at the other side (Stevaert and Naesens, 2016). PA contains the endonuclease domain while PB2 has the cap-binding domain (te Velthuis and Fodor, 2016). The LLFL motif in PB1 N-terminus (residue 7–10) interacts with the PA C-terminus hydrophobic core (F411, M595, L666, W706, F710, V636, and L640; Massari et al., 2016). Based on a crystal structure, the C-terminus of PB1 (residues 678–757) was found to complex with the N-terminus of PB2 (residues 1–37; Sugiyama et al., 2009).

Among the three subunits of the vRNP polymerase complex, PB1 had the least interactome studies and the least number of interactors. The most identified interactor for PB1 was PP6R3. Among all the studies, PA had 316 interactors while NP had 51 interactors and PB2 had 45 interactors. The interactors of NP, PB2, and PA are mostly involved in spliceosome based on the KEGG pathway (**Figure 2A; Supplementary Figures S3A–C**). The common process for all the interactors of NP, PB2, and PB1 is the transportation of proteins into the nucleus (i.e., NCBP1, SRSF1, PHAX, U2AF1, SRRM1, BAG3, UBR5, and IPO5; **Figure 2B; Supplementary Figures S3D–G**). This is expected as the vRNP is required to enter the nucleus for viral replication. In addition, spliceosome pathway is a common process for the interactors of all the vRNP components (i.e., SF3B4, DDX5, SF3B2, SF3B3, SF3B6, SRSF1, U2AF1, CHERP, TRA2B, DHX15, SRSF3, SRSF6, SRSF7, SF3B1, RBMX, DDX5, FXR2, NCBP1, PCBP1, and SNRPA). These interactors are also involved in general RNA processing (**Supplementary Figures S3D–G**). This may explain the spliceosome being identified with these host interactors, since the spliceosome is part of the RNA processing pathway (Licatalosi and Darnell, 2010; Wilkinson et al., 2020). This is a unique observation as NS1 has traditionally been the viral protein associated with spliceosome inhibition due to its binding to CPSF4 (Twu et al., 2006; Ramos et al., 2013). It was previously reported that the vRNP complex is required to stabilize the NS1-CPSF30 complex, specifically NP and PA (Kuo and Krug, 2009). However, the role of the viral polymerase complex alone in spliceosome regulation has yet to be studied.

The proteasome pathway was a specific pathway identified for PA interactors (i.e., PSMD6, PSMD7, PSMD4, PSMD2, PSMD3, and PSMD1). This would correlate to other studies which has found that treatment with proteasome inhibitors resulted in an antiviral state in cells (Dudek et al., 2010; Haasbach et al., 2011). It was also reported that treatment with the clinical approved proteasomal inhibitor PS-341 resulted in degradation of IκB and the activation of NF-κB and JNK/AP-1 pathway (Dudek et al., 2010). Hence, this suggests that the proteasomal pathway may be present a novel method of targeting influenza.

An interesting finding was that Annexin A2 (ANXA2) was identified as an interactor of PA across 3 papers (Bradel-Tretheway et al., 2011; Watanabe et al., 2014; Heaton et al., 2016) and HPIDB. Previously, it was reported that ANXA2 binds to highly pathogenic H5N1 influenza NS1 to enhance viral replication. Moreover, ANXA2 is incorporated into IAV particles to enhance viral replication, *via* the conversion of plasminogen to plasmin (LeBouder et al., 2008).

## M2 Interactors Are Involved in Fatty Acid Metabolism

The M gene encodes for both M1 and M2 proteins (Lamb et al., 1981). M1 protein consists of 252 amino acids, with 2 domains (N-terminal domain from amino acid 1 to 164 and the C-terminal domain from amino acid 165 to 252) linked by a protease-sensitive loop (Ito et al., 1991). It forms the matrix layer by oligomerizing directly below the lipid envelope and binds the viral ribonucleoproteins. It has the important function of stabilizing the whole envelope structure of a fully formed virion (Harris et al., 2001; Calder et al., 2010; Schaap et al., 2012; Adachi et al., 2017). M1 contacts with both viral RNA and NP, promoting the vRNP complex formation and cause the RNP dissociation from the nuclear matrix (Wakefield and Brownlee, 1989; Elster et al., 1994, 1997; Nasser et al., 1996; Chaimayo et al., 2017). M1 plays an important role in assembly by recruiting viral components to the assembly and an essential role in budding, such as viral particle formation (Gómez-Puertas et al., 2000; Latham and Galarza, 2001). M1 had the least interactome studies and only three common interactors were found: EZRI, HSP7C, and STAU1. Based on these three interactors, the interactors were found to be positive regulators of virus replication (**Figure 2; Supplementary Figures S4A,B**).

The M2 protein comprises of 97 amino acids with three domains: extracellular (24 amino acids), transmembrane domain (19 amino acids), and cytoplasmic domain (54 amino acids). It is a membrane protein which is inserted into the viral envelope and projects from the surface of the virus as tetramers (Lamb et al., 1985; Holsinger and Alams, 1991). The M2 protein is a proton channel and is required in the acidification of the viral particle upon endocytosis (Lamb et al., 1985) and prior to membrane fusion to enable the release of vRNPs into the cytosol (Helenius, 1992). It is also required to prevent the Golgi lumen pH from becoming too acidic so that the nascent HA do not undergo premature conformational arrangement while being transported to the plasma membrane (Sugrue and Hay, 1991).

Eighty-nine host proteins were found to interact with M2 across the various interactome studies. The most common interactors were 4F2, AFG32, ECHB, SPTC1, and TMX3. KEGG analysis revealed that these proteins were mainly involved in fatty acid metabolism (i.e., TECR and HACD3) and DNA replication (i.e., RFC3 and MCM7; **Figure 2A; Supplementary Figure S4C**). Functional enrichment analysis showed that these proteins were involved in vesicle transport (i.e., COPB2, COPA, ZW10, GBF1, and COPG1; **Figure 2B;**

**Supplementary Figure S4D**). Given that ubiquitination of M2 is required for viral packaging and release (Su et al., 2018), this would confirm the importance of the vesicle pathway for influenza *via* M2.

An interesting observation was the involvement of M2 interactors in fatty acid metabolism. Fatty acid oxidation was found to be reduced in influenza-infected mice (Ohno et al., 2020), while supplying palmitic acid increased influenza replication (Limsuwat et al., 2020). Influenza replication could be reduced by a fatty acid import inhibitor (Limsuwat et al., 2020). Hence, this would suggest that M2 may be involved in the fatty acid metabolism dysregulation caused by influenza infection. In addition, a recent study reported that M2 clustering which enables membrane scission is mediated by cholesterol (Elkins et al., 2017). Given that cholesterol is involved in viral membrane fusion, viral genome release, and viral budding, this may explain the efficacy of cholesterol-lowering drugs, gemfibrozil, and lovastatin in reducing the stability and infectivity of progeny virus (Bajimaya et al., 2017). It was also demonstrated that overexpression of Annexin A6 as well as the addition of U18666A, a hydrophobic polyamine, was able to reduce cholesterol levels in the plasma membrane and inhibit viral replication (Musiol et al., 2013).

## NS1 Interacting Partners Are Involved in Spliceosome and Autophagy

NS1 is not part of the virion structural component, but it is expressed at high levels in infected cells (Hale et al., 2008). It is composed of 231–237 amino acids, depending on the strain, and has a molecular mass of around 26 kDa (Hale et al., 2008). It has two distinct functional domains: an N-terminal RNA binding domain (amino acids 1–73) and a C-terminal effector domain (amino acids 86-231/237), which mediates binding with host cell proteins (Wang et al., 2002; Kochs et al., 2007; Hale et al., 2008; Das et al., 2010). NS1 was reported to have multiple functions that contribute to viral replication and virulence (Kochs et al., 2007; Hale et al., 2008; Fournier et al., 2014). These include: (i) temporarily regulating viral RNA synthesis (Hale et al., 2008; Ayllon and García-Sastre, 2015); (ii) viral mRNA splicing control (Hale et al., 2008, Ayllon and García-Sastre, 2015); (iii) enhancing viral mRNA translation *via* PKR inhibition (Li et al., 2006); (iv) regulating the creation of the virus particle structure (Hale et al., 2008; Pereira et al., 2017); (v) suppressing the host immune or apoptotic responses (Ehrhardt et al., 2007; Kochs et al., 2007; Iwai et al., 2010; Jia et al., 2010; Mata et al., 2011; Gao et al., 2012; Anastasina et al., 2016); (vi) activating phosphoinositide 3-kinase (Ehrhardt et al., 2007; Gaur et al., 2011; Ayllon and García-Sastre, 2015); and (vii) involvement in strain-dependent pathogenesis (Hale et al., 2008). NS1 exists as a homodimer. The RNA binding domain binds to RNA and the binding is dependent on R38 and other charged residues, such as R35 and K41 (Lalime and Pekosz, 2014; Ayllon and García-Sastre, 2015). In addition, the effector domain of NS1 has been found to bind to CPSF30, which results in reduced IFN-β mRNA production. The key amino acid residue for the CPSF30 interaction is W187 (Engel, 2013). Moreover, multiple mutations in NS1 have been found to increase virulence (Ozawa et al., 2011; DeDiego et al., 2016) and viral pathogenicity (Ehrhardt et al., 2007; Engel, 2013; Nogales et al., 2017).

NS1 had the most interactome studies among all the viral proteins. A total of 252 interactors were found among the interactome studies. The most common interactor found was STAU1 found in nine studies, followed by PRKRA. Based on the KEGG pathway, these interactors are involved in spliceosome (i.e., SF3B2, SNW1, FUS, NCBP2, PCBP1, TRA2B, TRA2A, DHX15, SRSF3, SRSF6, SRSF7, and RBMX) and autophagy (i.e., IRS1, BAD, IRS4, RAF1, and TANK; **Figure 2A**; **Supplementary Figure S5A**). Enrichr analysis also revealed that these interacting partners are involved in mRNA splicing (i.e., DDX17, PRDX6, QKI, FXR1, PTBP1, FXR2, SNW1, SON, TRA2B, TRA2A, SRSF3, SRSF6, SRSF7, and RBMX) and RNA processing (i.e., CPSF4, SF3B2, CHTOP, RBM14, CPSF1, FUS, NCBP2, CPSF2, PTBP1, SNW1, SON, PCBP1, TRA2B, TRA2A, DHX15, SRSF3, RALY, SRSF6, SRSF7, and RBMX; **Figure 2B; Supplementary Figure S5B**). NS1 is a well-known interactor of the spliceosome pathway, given its interactions with CPSF4 and NS1-BP (Wolff et al., 1998; Thompson et al., 2018; Zhang et al., 2018). It has been previously reported that NS1 interacts with hnRNP-F to modulate host mRNA processing (Lee et al., 2010). In addition, NS1 is required for unspliced M1 nuclear export (Pereira et al., 2017). NS1 is also a well-known inducer of autophagy (Zhirnov and Klenk, 2013; Zhang et al., 2019). It was previously reported that NS1 induced autophagy *via* its interaction with JNK (Zhang et al., 2019).

## NS2 Interactors Are Mainly Involved in Focal Adhesion and ECM–Receptor Interaction

NEP or non-structural protein 2 (NS2) is a structural protein and is associated with M1 (Yasuda et al., 1993). NEP mediates vRNP nuclear export into the cytoplasm *via* an export signal (O'Neill et al., 1998) through XPO1 interaction (Neumann et al., 2000). NEP has also been found to interact with nucleoporins and is suggested to act as an adaptor between vRNPs and the nuclear pore complex (O'Neill et al., 1998). It has been proposed that NEP is involved in the transcription and replication of the influenza virus (Robb et al., 2009).

Forty host proteins were found to be NS2 interactors across the different studies. These proteins are involved in focal adhesion and ECM–receptor interaction (i.e., LAMC3, ZYX, and LAMB1), and ubiquitin-mediated proteolysis (i.e., PIAS3 and SKP1) *via* KEGG analysis (**Figure 2A; Supplementary Figure S6A**). Functional enrichment analysis showed that these proteins are involved in microtubule reorganization (i.e., DCTN2, CENPH, and ZWINT) and ER-Golgi transport (i.e., COG8 and COG6; **Figure 2; Supplementary Figure S6B**).

## Influenza Interacting Partners Are Involved in the Spliceosome, Focal Adhesions, and Protein Processing in the ER

A global analysis of the protein interactors revealed that most of these interactors are involved in the spliceosome, followed

by focal adhesion and protein processing in the ER *via* KEGG analysis. Given the large proportion of NS1 interactome studies, this may have resulted in spliceosome being the top process. However, it was interesting to note that focal adhesion and protein processing in the ER was one of the top processes revealed for influenza interactors.

A previous study revealed that actin reorganization is required for influenza assembly and budding *via* cofilin-1 phosphorylation (Liu et al., 2014). Focal adhesion kinase (FAK) is a non-receptor tyrosine kinase (non-PTK) and part of focal adhesions that tether actin cytoskeleton to the extracellular matrix. It was previously shown that FAK is involved in phosphatidylinositol-3-kinase (PI3K) activation and reorganization of cytoskeleton for endosomal trafficking during IAV entry (Elbahesh et al., 2014). In addition, FAK was found to positively regulate IAV replication and polymerase activity of different IAV strains (Elbahesh et al., 2016). FAK-dependent regulation of innate immune responses was observed during severe IAV infection in mice (Bergmann and Elbahesh, 2019). Given that HA, NA, and NS2 have interactors involved in focal adhesions or ECM, this may be a potential target for novel influenza therapy.

In addition, a novel finding was the involvement of these interactors in protein processing in the ER. **Figure 3** describes the interaction of the influenza proteins and host proteins involved in ER protein processing. It was previously reported that influenza modulates vesicle trafficking *via* disruption of the Golgi complex (Yadav et al., 2016). In addition, brefeldin A, an ER to Golgi transport inhibitor, was found to affect the intracellular distribution of HA (Russ et al., 1991; Ciampor et al., 1997) and induce apoptosis in influenza-infected cells (Saito et al., 1996). Monensin, a Golgi complex disruptor, was found to reduce viral budding and HA localization to the cell membrane (Edwardson, 1984).

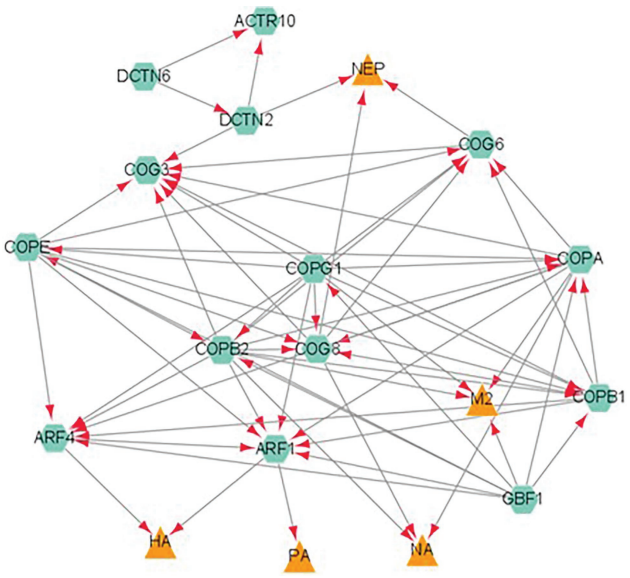


**FIGURE 3 |** A network analysis of influenza proteins and host proteins involved in ER protein processing. Proteins classified as belonging to the ER protein processing pathway were analyzed by STRING database. The viral proteins are represented by orange triangles and host interactors are represented by green hexagons. Each interaction is represented by edges connecting the two nodes with the arrow reflecting a positive association between two proteins.

Given the role of influenza proteins, NS1, NP, PA, and PB1 in spliceosome activity, targeting this pathway may be a potential target for influenza. Cdc2-like kinase 1 (CLK1) is a kinase that regulates alternative splicing of pre-mRNA (Bullock et al., 2009). CLK1 inhibition by TG003 or CLK1 knockdown was shown to decrease M2 mRNA generation and downstream M2 protein expression, thus reducing IAV propagation (Karlas et al., 2010).

A total of 190 host proteins had more than 1 viral protein interaction. 4F2 was the most promiscuous host protein with 6 viral protein interactions. ADT3, ANXA2, PSD11, PSD12, PSD13, and TCPE had 5 viral protein interactions each. Given that these proteins have interactions with multiple viral proteins, this may indicate that these proteins are key for multiple aspects of viral replication and life cycle and, hence, should be further studied for novel host-directed therapy.

## CONCLUSIONS AND FUTURE WORK

Identifying novel host interactors in influenza is key in understanding the viral life cycle as well as for the development of novel therapies against the virus. Our review of influenza interactors has comprehensively compiled influenza interactome studies together with host–virus interaction databases. While other studies have done interactome studies on influenza proteins, no study has done a comprehensive review on influenza interactors. Using interactome studies to derive our data set also enables a more direct virus–host interaction compared to RNAi studies and would include essential genes which may lead to cell death in RNAi studies, thus reducing false negatives (Watanabe et al., 2010). While Watanabe et al. (2010) and Tripathi et al. (2015) both did meta-analysis of RNAi studies, no other study has done a meta-analysis of interactome studies for influenza. Our study has revealed novel influenza interactors which can be potentially targeted for novel therapies against influenza. It also filters out possible false positives that may be derived from a single interactome study. Given that we used a benchmark of at least three separate studies to filter out true positive, this would reflect the sensitivity of our study to detect conserved host interactors of influenza. Moreover, given that our study included various strains of influenza A, this would increase the likelihood that these pathways are globally used by all influenza A strains for their life cycle. Hence, these pathways can be further studied as potential universal therapy against influenza.

Based on our bioinformatics analysis of influenza proteins, we observed that protein transport to the ER is one of the top biological processes exploited by influenza (**Figure 2**). This supports the previous study by Heaton et al. (2016), where they identified Sec61 knockdown was found to reduce influenza replication. This suggests that the protein transport to the ER is one of the key processes that influenza exploits for its life

cycle. In addition, ER transport is a key process in the innate immunity. A member of the COPII complex, Sec13, was previously identified in a CRIPSR knockout screen to reduce influenza replication (Li et al., 2020). This would support the important role of ER processing for influenza. Hence, more studies into how it can be targeted for influenza treatment should be undertaken. Several pro-inflammatory cytokines, such as IL6 and IFN-β, are secreted (Murray and Stow, 2014) *via* the ER-Golgi pathway. Influenza's control over this pathway would enable it to replicate without detection from immune cells and this would reflect the importance of the protein transport system. Moreover, influenza's ability to overstimulate the immune response *via* cytokine storm has been shown to be correlated to virus virulence (Kido, 2015; Li et al., 2018; Short et al., 2018). This correlates with other RNAi studies performed in influenza which reflect the importance of the ER to Golgi transport pathway in viral replication (Tripathi et al., 2015). Given the importance of post-translational modification of influenza proteins in viral replication and host response, as discussed by Hu et al. (2020), this would be a potential target for influenza treatment, especially in the context of severe influenza. This finding can be extrapolated to other viruses as discussed in the review (Ravindran et al., 2016). Both enveloped and non-enveloped viruses were described to hijack the ER for replication. HIV utilizes the ER to synthesize its envelope glycoprotein (Checkley et al., 2011). Antiviral therapeutics that impair ER-resident glycan trimming enzymes α-glucosidases I and II have been shown inhibit viral infection by DNA and RNA viruses (Chang et al., 2013). Moreover, an inhibitor against HSP70, a cytosolic chaperone that controls ER-associated degradation, has been shown to inhibit flavivirus infection (Taguwa et al., 2015).

Future work would be to validate the targets identified in this review *via in vitro* and *in vivo* models. However, this review has reflected the key processes that can be potentially targeted for host-directed therapy against influenza. Given the key role these processes play in influenza as well as normal host cell maintenance, it would be important to find key differences between normal cellular maintenance and viral infection. This would enable specific targeting of influenza-driven pathways without killing the host. Another aspect that would need to be studied is how these processes contribute to severe influenza, which is still currently unknown. Therefore, a more detailed analysis of IAV–host interactions would provide clues for therapeutic targeting and molecular mechanisms of viral replication.

## AUTHOR CONTRIBUTIONS

SC, JC, DE, and LL designed the experiments. SC performed the experiments. SC, JC, and LL analyzed the data. SC wrote the manuscript. DE and LL did the final editing of the manuscript. All authors contributed to the article and approved the submitted version.

## FUNDING

LL and DE are supported by the Singapore National Research Foundation under its HUJ-NUS partnership program at the Campus for Research Excellence and Technology Enterprise (CREATE). SC is funded by a PHD scholarship from NUS and the Hebrew University. This study was funded by a grant from the National Research Foundation of Singapore (SHARE MMID-2).

## ACKNOWLEDGMENTS

DE holds a Wolfson family chair in Biochemistry.

## SUPPLEMENTARY MATERIAL

The Supplementary Material for this article can be found online at: https://www.frontiersin.org/articles/10.3389/fmicb.2022.869406/full#supplementary-material

## REFERENCES

Adachi, A., Koizumi, M., and Ohsumi, Y. (2017). Autophagy induction under carbon starvation conditions is negatively regulated by carbon catabolite repression. *J. Biol. Chem.* 292, 19905–19918. doi: 10.1074/jbc.M117.817510

Ammari, M. G., Gresham, C. R., Mccarthy, F. M., and Nanduri, B. (2016). HPIDB 2.0: a curated database for host–pathogen interactions. *Database* 2016:baw103. doi: 10.1093/database/baw103

Amorim, M. J., Kao, R. Y., and Digard, P. (2013). Nucleozin targets cytoplasmic trafficking of viral ribonucleoprotein-Rab11 complexes in influenza A virus infection. *J. Virol.* 87, 4694–4703. doi: 10.1128/JVI.03123-12

Anastasina, M., Le May, N., Bugai, A., Fu, Y., Söderholm, S., Gaelings, L., et al. (2016). Influenza virus NS1 protein binds cellular DNA to block transcription of antiviral genes. *Biochim. Biophys. Acta* 1859, 1440–1448. doi: 10.1016/j.bbagrm.2016.09.005

Arias, C. F., Escalera-Zamudio, M., Soto-Del Rio Mde, L., Cobian-Guemes, A. G., Isa, P., and Lopez, S. (2009). Molecular anatomy of 2009 influenza virus A (H1N1). *Arch. Med. Res.* 40, 643–654. doi: 10.1016/j.arcmed.2009.10.007

Ayllon, J., and García-Sastre, A. (2015). "The NS1 protein: a multitasking virulence factor," in *Influenza Pathogenesis and Control – Volume II*. eds. M. B. A. Oldstone and R. W. Compans (Cham: Springer International Publishing).

Bajimaya, S., Frankl, T., Hayashi, T., and Takimoto, T. (2017). Cholesterol is required for stability and infectivity of influenza A and respiratory syncytial viruses. *Virology* 510, 234–241. doi: 10.1016/j.virol.2017.07.024

Bergmann, S., and Elbahesh, H. (2019). Targeting the proviral host kinase, FAK, limits influenza a virus pathogenesis and NFkB-regulated pro-inflammatory responses. *Virology* 534, 54–63. doi: 10.1016/j.virol.2019.05.020

Biswas, S. K., Boutz, P. L., and Nayak, D. P. (1998). Influenza virus nucleoprotein interacts with influenza virus polymerase proteins. *J. Virol.* 72, 5493–5501. doi: 10.1128/JVI.72.7.5493-5501.1998

Bouvier, N. M., and Palese, P. (2008). The biology of influenza viruses. *Vaccine* 26(Suppl 4), D49–D53. doi: 10.1016/j.vaccine.2008.07.039

Bradel-Tretheway, B. G., Mattiacio, J. L., Krasnoselsky, A., Stevenson, C., Purdy, D., Dewhurst, S., et al. (2011). Comprehensive proteomic analysis of influenza virus polymerase complex reveals a novel association with mitochondrial proteins and RNA polymerase accessory factors. *J. Virol.* 85, 8569–8581. doi: 10.1128/JVI.00496-11

Bullock, A. N., Das, S., Debreczeni, J. É., Rellos, P., Fedorov, O., Niesen, F. H., et al. (2009). Kinase domain insertions define distinct roles of CLK kinases

in SR protein phosphorylation. *Structure* 17, 352–362. doi: 10.1016/j.str.2008.12.023

Calder, L. J., Wasilewski, S., Berriman, J. A., and Rosenthal, P. B. (2010). Structural organization of a filamentous influenza A virus. *Proc. Natl. Acad. Sci. U. S. Am.* 107, 10685–10690. doi: 10.1073/pnas.1002123107

CDC (2019). Seasonal Influenza (Flu): Antigenic Characterization [Online]. Available at: https://www.cdc.gov/flu/about/professionals/antigenic.htm (Accessed 30 August, 2021).

Chaimayo, C., Hayashi, T., Underwood, A., Hodges, E., and Takimoto, T. (2017). Selective incorporation of vRNP into influenza A virions determined by its specific interaction with M1 protein. *Virology* 505, 23–32. doi: 10.1016/j.virol.2017.02.008

Chang, J., Block, T. M., and Guo, J. T. (2013). Antiviral therapies targeting host ER alpha-glucosidases: current status and future directions. *Antiviral Res* 99, 251–260. doi: 10.1016/j.antiviral.2013.06.011

Checkley, M. A., Luttge, B. G., and Freed, E. O. (2011). HIV-1 envelope glycoprotein biosynthesis, trafficking, and incorporation. *J. Mol. Biol.* 410, 582–608. doi: 10.1016/j.jmb.2011.04.042

Chen, B. J., Takeda, M., and Lamb, R. A. (2005). Influenza virus hemagglutinin (H3 subtype) requires palmitoylation of its cytoplasmic tail for assembly: M1 proteins of two subtypes differ in their ability to support assembly. *J. Virol.* 79, 13673–13684. doi: 10.1128/JVI.79.21.13673-13684.2005

Chen, E. Y., Tan, C. M., Kou, Y., Duan, Q., Wang, Z., Meirelles, G. V., et al. (2013). Enrichr: interactive and collaborative HTML5 gene list enrichment analysis tool. *BMC Bioinf.* 14:128. doi: 10.1186/1471-2105-14-128

Chutiwitoonchai, N., and Aida, Y. (2016). NXT1, a novel influenza A NP binding protein, promotes the nuclear export of NP via a CRM1-dependent pathway. *Viruses* 8:209. doi: 10.3390/v8080209

Ciampor, F., Závodská, E., Cmarko, D., Cmarková, J., and Varecková, E. (1997). Effects of brefeldin A on the expression and transport of influenza A virus haemagglutinin, M1 and M2 proteins within the cell. *Acta Virol* 41, 83–91.

Cianci, C., Gerritz, S. W., Deminie, C., and Krystal, M. (2013). Influenza nucleoprotein: promising target for antiviral chemotherapy. *Antiviral Chem. Chemother.* 23, 77–91. doi: 10.3851/IMP2235

Consortium, U. (2012). Update on activities at the universal protein resource (UniProt) in 2013. *Nucleic Acids Res.* 41, D43–D47. doi: 10.1093/nar/gks1068

Das, K., Aramini, J. M., Ma, L. C., Krug, R. M., and Arnold, E. (2010). Structures of influenza A proteins and insights into antiviral drug targets. *Nat Struct Mol Biol* 17, 530–538. doi: 10.1038/nsmb.1779

Davidson, S. (2018). Treating influenza infection, from now and into the future. *Front. Immunol.* 9:1946. doi: 10.3389/fimmu.2018.01946

Davis, A. M., Ramirez, J., and Newcomb, L. L. (2017). Identification of influenza A nucleoprotein body domain residues essential for viral RNA expression expose antiviral target. *Virol. J.* 14, 22. doi: 10.1186/s12985-017-0694-8

De Vries, R. P., De Vries, E., Bosch, B. J., De Groot, R. J., Rottier, P. J., and De Haan, C. A. (2010). The influenza A virus hemagglutinin glycosylation state affects receptor-binding specificity. *Virology* 403, 17–25. doi: 10.1016/j.virol.2010.03.047

Dediego, M. L., Nogales, A., Lambert-Emo, K., Martinez-Sobrido, L., and Topham, D. J. (2016). NS1 protein mutation I64T affects interferon responses and virulence of circulating H3N2 human influenza A viruses. *J. Virol.* 90, 9693–9711. doi: 10.1128/JVI.01039-16

Diazgranados, C. A., Dunning, A. J., Kimmel, M., Kirby, D., Treanor, J., Collins, A., et al. (2014). Efficacy of high-dose versus standard-dose influenza vaccine in older adults. *New Eng. J. Med.* 371, 635–645. doi: 10.1056/NEJMoa1315727

Dudek, S. E., Luig, C., Pauli, E.-K., Schubert, U., and Ludwig, S. (2010). The clinically approved proteasome inhibitor PS-341 efficiently blocks influenza A virus and vesicular stomatitis virus propagation by establishing an antiviral state. *J. Virol.* 84, 9439–9451. doi: 10.1128/JVI.00533-10

Edwardson, J. M. (1984). Effects of monensin on the processing and intracellular transport of influenza virus haemagglutinin in infected MDCK cells. *J. Cell Sci.* 65, 209–221. doi: 10.1242/jcs.65.1.209

Ehrhardt, C., Wolff, T., Pleschka, S., Planz, O., Beermann, W., Bode, J. G., et al. (2007). Influenza A virus NS1 protein activates the PI3K/Akt pathway to mediate antiapoptotic signaling responses. *J. Virol.* 81, 3058–3067. doi: 10.1128/JVI.02082-06

Eisenstein, M. (2019). Towards a universal flu vaccine. *Nature* 573, S50–S52. doi: 10.1038/d41586-019-02751-w

Eisfeld, A. J., Neumann, G., and Kawaoka, Y. (2015). At the centre: influenza A virus ribonucleoproteins. *Nat. Rev. Microbiol.* 13, 28–41. doi: 10.1038/nrmicro3367

Elbahesh, H., Bergmann, S., and Russell, C. J. (2016). Focal adhesion kinase (FAK) regulates polymerase activity of multiple influenza A virus subtypes. *Virology* 499, 369–374. doi: 10.1016/j.virol.2016.10.002

Elbahesh, H., Cline, T., Baranovich, T., Govorkova, E. A., Schultz-Cherry, S., and Russell, C. J. (2014). Novel roles of focal adhesion kinase in cytoplasmic entry and replication of influenza A viruses. *J. Virol.* 88, 6714–6728. doi: 10.1128/JVI.00530-14

Elkins, M. R., Williams, J. K., Gelenter, M. D., Dai, P., Kwon, B., Sergeyev, I. V., et al. (2017). Cholesterol-binding site of the influenza M2 protein in lipid bilayers from solid-state NMR. *Proc. Nat. Acad. Sci.* 114, 12946–12951. doi: 10.1073/pnas.1715127114

Elster, C., Fourest, E., Baudin, F., Larsen, K., Cusack, S., and Ruigrok, R. W. H. (1994). A small percentage of influenza virus M1 protein contains zinc but zinc does not influence in vitro M1-RNA interaction. *J. Gen. Virol.* 75, 37–42. doi: 10.1099/0022-1317-75-1-37

Elster, C., Larsen, K., Gagnon, J., Ruigrok, R. W., and Baudin, F. (1997). Influenza virus M1 protein binds to RNA through its nuclear localization signal. *J. Gen. Virol.* 78, 1589–1596. doi: 10.1099/0022-1317-78-7-1589

Engel, D. A. (2013). The influenza virus NS1 protein as a therapeutic target. *Antiviral Res.* 99, 409–416. doi: 10.1016/j.antiviral.2013.06.005

Fabregat, A., Sidiropoulos, K., Viteri, G., Marin-Garcia, P., Ping, P., Stein, L., et al. (2018). Reactome diagram viewer: data structures and strategies to boost performance. *Bioinformatics* 34, 1208–1214. doi: 10.1093/bioinformatics/btx752

Fodor, E. (2013). The RNA polymerase of influenza a virus: mechanisms of viral transcription and replication. *Acta Virol.* 57, 113–122. doi: 10.4149/av_2013_02_113

Fournier, G., Chiang, C., Munier, S., Tomoiu, A., Demeret, C., Vidalain, P. O., et al. (2014). Recruitment of RED-SMU1 complex by influenza A virus RNA polymerase to control viral mRNA splicing. *PLoS Pathog.* 10:e1004164. doi: 10.1371/journal.ppat.1004164

Gambaryan, A. S., Tuzikov, A. B., Piskarev, V. E., Yamnikova, S. S., Lvov, D. K., Robertson, J. S., et al. (1997). Specification of receptor-binding phenotypes of influenza virus isolates from different hosts using synthetic sialylglycopolymers: non-egg-adapted human H1 and H3 influenza A and influenza B viruses share a common high binding affinity for 6′-sialyl(N-acetyllactosamine). *Virology* 232, 345–350. doi: 10.1006/viro.1997.8572

Gamblin, S. J., and Skehel, J. J. (2010). Influenza hemagglutinin and neuraminidase membrane glycoproteins. *J. Biol. Chem.* 285, 28403–28409. doi: 10.1074/jbc.R110.129809

Gao, S., Song, L., Li, J., Zhang, Z., Peng, H., Jiang, W., et al. (2012). Influenza A virus-encoded NS1 virulence factor protein inhibits innate immune response by targeting IKK. *Cell. Microbiol.* 14, 1849–1866. doi: 10.1111/cmi.12005

Garten, W., and Klenk, H. D. (1999). Understanding influenza virus pathogenicity. *Trends Microbiol.* 7, 99–100. doi: 10.1016/S0966-842X(99)01460-2

Gaur, P., Munjal, A., and Lal, S. K. (2011). Influenza virus and cell signaling pathways. *Med. Sci. Monit.* 17, RA148–RA154. doi: 10.12659/MSM.881801

Gómez-Puertas, P., Albo, C., Pérez-Pastrana, E., Vivo, A., and Portela, A. N. (2000). Influenza virus matrix protein is the major driving force in virus budding. *J. Virol.* 74, 11538–11547. doi: 10.1128/JVI.74.24.11538-11547.2000

Haasbach, E., Pauli, E. K., Spranger, R., Mitzner, D., Schubert, U., Kircheis, R., et al. (2011). Antiviral activity of the proteasome inhibitor VL-01 against influenza A viruses. *Antiviral Res.* 91, 304–313. doi: 10.1016/j.antiviral.2011.07.006

Hale, B. G., Randall, R. E., Ortin, J., and Jackson, D. (2008). The multifunctional NS1 protein of influenza A viruses. *J. Gen. Virol.* 89, 2359–2376. doi: 10.1099/vir.0.2008/004606-0

Harris, A., Forouhar, F., Qiu, S., Sha, B., and Luo, M. (2001). The crystal structure of the influenza matrix protein M1 at neutral pH: M1-M1 protein interfaces can rotate in the oligomeric structures of M1. *Virology* 289, 34–44. doi: 10.1006/viro.2001.1119

Hayden, F. G., Sugaya, N., Hirotsu, N., Lee, N., De Jong, M. D., Hurt, A. C., et al. (2018). Baloxavir marboxil for uncomplicated influenza in adults and adolescents. *N. Engl. J. Med.* 379, 913–923. doi: 10.1056/NEJMoa1716197

Heaton, N. S., Moshkina, N., Fenouil, R., Gardner, T. J., Aguirre, S., Shah, P. S., et al. (2016). Targeting viral proteostasis limits influenza virus, HIV, and dengue virus infection. *Immunity* 44, 46–58. doi: 10.1016/j.immuni.2015.12.017

Hebert, D. N., Zhang, J. X., Chen, W., Foellmer, B., and Helenius, A. (1997). The number and location of glycans on influenza hemagglutinin determine folding and association with calnexin and calreticulin. *J. Cell Biol.* 139, 613–623. doi: 10.1083/jcb.139.3.613

Helenius, A. (1992). Unpacking the incoming influenza virus. *Cell* 69, 577–578. doi: 10.1016/0092-8674(92)90219-3

Holsinger, L. J., and Alams, R. (1991). Influenza virus M2 integral membrane protein is a homotetramer stabilized by formation of disulfide bonds. *Virology* 183, 32–43. doi: 10.1016/0042-6822(91)90115-R

Hu, Y., Sneyd, H., Dekant, R., and Wang, J. (2017). Influenza A virus nucleoprotein: a highly conserved multi-functional viral protein as a hot antiviral drug target. *Curr. Top. Med. Chem.* 17, 2271–2285. doi: 10.2174/1568026617666170224122508

Hu, J., Zhang, L., and Liu, X. (2020). Role of post-translational modifications in influenza A virus life cycle and host innate immune response. *Front. Microbiol.* 11:517461. doi: 10.3389/fmicb.2020.517461

Husain, M., and Harrod, K. S. (2011). Enhanced acetylation of alpha-tubulin in influenza A virus infected epithelial cells. *FEBS Lett.* 585, 128–132. doi: 10.1016/j.febslet.2010.11.023

Ito, T., Couceiro, J. N., Kelm, S., Baum, L. G., Krauss, S., Castrucci, M. R., et al. (1998). Molecular basis for the generation in pigs of influenza A viruses with pandemic potential. *J. Virol.* 72, 7367–7373. doi: 10.1128/JVI.72.9.7367-7373.1998

Ito, T., Gorman, O. T., Kawaoka, Y., Bean, W. J., and Webster, R. G. (1991). Evolutionary analysis of the influenza A virus M gene with comparison of the M1 and M2 proteins. *J. Virol.* 65, 5491–5498. doi: 10.1128/jvi.65.10.5491-5498.1991

Iwai, A., Shiozaki, T., Kawai, T., Akira, S., Kawaoka, Y., Takada, A., et al. (2010). Influenza A virus polymerase inhibits type I interferon induction by binding to interferon beta promoter stimulator 1. *J. Biol. Chem.* 285, 32064–32074. doi: 10.1074/jbc.M110.112458

Jagger, B. W., Wise, H. M., Kash, J. C., Walters, K.-A., Wills, N. M., Xiao, Y.-L., et al. (2012). An overlapping protein-coding region in influenza A virus segment 3 modulates the host response. *Science* 337, 199–204. doi: 10.1126/science.1222213

Jassal, B., Matthews, L., Viteri, G., Gong, C., Lorente, P., Fabregat, A., et al. (2020). The reactome pathway knowledgebase. *Nucleic Acids Res.* 48, D498–D503. doi: 10.1093/nar/gkz1031

Jia, D., Rahbar, R., Chan, R. W., Lee, S. M., Chan, M. C., Wang, B. X., et al. (2010). Influenza virus non-structural protein 1 (NS1) disrupts interferon signaling. *PLoS One* 5:e13927. doi: 10.1371/journal.pone.0013927

Karlas, A., Machuy, N., Shin, Y., Pleissner, K.-P., Artarini, A., Heuer, D., et al. (2010). Genome-wide RNAi screen identifies human host factors crucial for influenza virus replication. *Nature* 463, 818–822. doi: 10.1038/nature08760

Kido, H. (2015). Influenza virus pathogenicity regulated by host cellular proteases, cytokines and metabolites, and its therapeutic options. *Proc. Jpn. Acad. Ser. B Phys. Biol. Sci.* 91, 351–368. doi: 10.2183/pjab.91.351

Klemm, C., Boergeling, Y., Ludwig, S., and Ehrhardt, C. (2018). Immunomodulatory nonstructural proteins of influenza A viruses. *Trends Microbiol.* 26, 624–636. doi: 10.1016/j.tim.2017.12.006

Kochs, G., García-Sastre, A., and Martínez-Sobrido, L. (2007). Multiple anti-interferon actions of the influenza A virus NS1 protein. *J. Virol.* 81, 7011–7021. doi: 10.1128/JVI.02581-06

Koszalka, P., Tilmanis, D., and Hurt, A. C. (2017). Influenza antivirals currently in late-phase clinical trial. *Influenza Other Respir. Viruses* 11, 240–246. doi: 10.1111/irv.12446

Krammer, F., Smith, G. J. D., Fouchier, R. A. M., Peiris, M., Kedzierska, K., Doherty, P. C., et al. (2018). Influenza. *Nat. Rev. Dis. Primers* 4:3. doi: 10.1038/s41572-018-0002-y

Kuleshov, M. V., Jones, M. R., Rouillard, A. D., Fernandez, N. F., Duan, Q., Wang, Z., et al. (2016). Enrichr: a comprehensive gene set enrichment analysis web server 2016 update. *Nucleic Acids Res.* 44, W90–W97. doi: 10.1093/nar/gkw377

Kummer, S., Flottmann, M., Schwanhausser, B., Sieben, C., Veit, M., Selbach, M., et al. (2014). Alteration of protein levels during influenza virus H1N1 infection in host cells: a proteomic survey of host and virus reveals differential dynamics. *PLoS One* 9:e94257. doi: 10.1371/journal.pone.0094257

Kuo, R. L., and Krug, R. M. (2009). Influenza a virus polymerase is an integral component of the CPSF30-NS1A protein complex in infected cells. *J. Virol.* 83, 1611–1616. doi: 10.1128/JVI.01491-08

Lalime, E. N., and Pekosz, A. (2014). The R35 residue of the influenza A virus NS1 protein has minimal effects on nuclear localization but alters virus replication through disrupting protein dimerization. *Virology* 458-459, 33–42. doi: 10.1016/j.virol.2014.04.012

Lamb, R. A., Lai, C. J., and Choppin, P. W. (1981). Sequences of mRNAs derived from genome RNA segment 7 of influenza virus: colinear and interrupted mRNAs code for overlapping proteins. *Proc. Natl. Acad. Sci. U S A* 78, 4170–4174. doi: 10.1073/pnas.78.7.4170

Lamb, R. A., Zebedee, S. L., and Richardson, C. D. (1985). Influenza virus M2 protein is an integral membrane protein expressed on the infected-cell surface. *Cell* 40, 627–633. doi: 10.1016/0092-8674(85)90211-9

Latham, T., and Galarza, J. M. (2001). Formation of wild-type and chimeric influenza virus-like particles following simultaneous expression of only four structural proteins. *J. Virol.* 75, 6154–6165. doi: 10.1128/JVI.75.13.6154-6165.2001

Lebouder, F., Morello, E., Rimmelzwaan, G. F., Bosse, F., Péchoux, C., Delmas, B., et al. (2008). Annexin II incorporated into influenza virus particles supports virus replication by converting plasminogen into plasmin. *J. Virol.* 82, 6820–6828. doi: 10.1128/JVI.00246-08

Lee, J. H., Kim, S. H., Pascua, P. N., Song, M. S., Baek, Y. H., Jin, X., et al. (2010). Direct interaction of cellular hnRNP-F and NS1 of influenza A virus accelerates viral replication by modulation of viral transcriptional activity and host gene expression. *Virology* 397, 89–99. doi: 10.1016/j.virol.2009.10.041

Li, H., Bradley, K. C., Long, J. S., Frise, R., Ashcroft, J. W., Hartgroves, L. C., et al. (2018). Internal genes of a highly pathogenic H5N1 influenza virus determine high viral replication in myeloid cells and severe outcome of infection in mice. *PLOS Pathogens* 14:e1006821. doi: 10.1371/journal.ppat.1006821

Li, B., Clohisey, S. M., Chia, B. S., Wang, B., Cui, A., Eisenhaure, T., et al. (2020). Genome-wide CRISPR screen identifies host dependency factors for influenza A virus infection. *Nat. Commun.* 11:164. doi: 10.1038/s41467-020-19935-y

Li, S., Min, J.-Y., Krug, R. M., and Sen, G. C. (2006). Binding of the influenza A virus NS1 protein to PKR mediates the inhibition of its activation by either PACT or double-stranded RNA. *Virology* 349, 13–21. doi: 10.1016/j.virol.2006.01.005

Licatalosi, D. D., and Darnell, R. B. (2010). RNA processing and its regulation: global insights into biological networks. *Nat. Rev. Genet.* 11, 75–87. doi: 10.1038/nrg2673

Limsuwat, N., Boonarkart, C., Phakaratsakul, S., Suptawiwat, O., and Auewarakul, P. (2020). Influence of cellular lipid content on influenza A virus replication. *Archives of Virology* 165, 1151–1161. doi: 10.1007/s00705-020-04596-5

Liu, G., Xiang, Y., Guo, C., Pei, Y., Wang, Y., and Kitazato, K. (2014). Cofilin-1 is involved in regulation of actin reorganization during influenza A virus assembly and budding. *Biochem. Biophys. Res. Commun.* 453, 821–825. doi: 10.1016/j.bbrc.2014.10.036

Lou, Z., Sun, Y., and Rao, Z. (2014). Current progress in antiviral strategies. *Trends in Pharmacological Sciences* 35, 86–102. doi: 10.1016/j.tips.2013.11.006

Ma, Y., Sun, J., Gu, L., Bao, H., Zhao, Y., Shi, L., et al. (2017). Annexin A2 (ANXA2) interacts with nonstructural protein 1 and promotes the replication of highly pathogenic H5N1 avian influenza virus. *BMC Microbiol.* 17:191. doi: 10.1186/s12866-017-1097-0

Massari, S., Goracci, L., Desantis, J., and Tabarrini, O. (2016). Polymerase acidic protein–basic protein 1 (PA–PB1) protein–protein interaction as a target for next-generation anti-influenza therapeutics. *J. Med. Chem.* 59, 7699–7718. doi: 10.1021/acs.jmedchem.5b01474

Mata, M. A., Satterly, N., Versteeg, G. A., Frantz, D., Wei, S., Williams, N., et al. (2011). Chemical inhibition of RNA viruses reveals REDD1 as a host defense factor. *Nat. Chem. Biol.* 7, 712–719. doi: 10.1038/nchembio.645

Matrosovich, M. N., Matrosovich, T. Y., Gray, T., Roberts, N. A., and Klenk, H.-D. (2004). Neuraminidase is important for the initiation of influenza virus infection in human airway epithelium. *J. Virol.* 78, 12665–12667. doi: 10.1128/JVI.78.22.12665-12667.2004

Mccauley, J., Hongo, S., Kaverin, N., Kochs, G., Lamb, R., Matrosovich, M., et al. (2012). "Family – orthomyxoviridae," in *Virus Taxonomy*. eds. A. M. Q. King, M. J. Adams, E. B. Carstens and E. J. Lefkowitz (San Diego: Elsevier).

MacLachlan, N. J., and Dubovi, E. J. (2017). "Chapter 21 – Orthomyxoviridae," in *Fenner's Veterinary Virology. 5th Edn.* eds. N. J. Maclachlan and E. J. Dubovi (Boston, MA: Academic Press).

Murray, R. Z., and Stow, J. L. (2014). Cytokine secretion in macrophages: SNAREs, Rabs, and membrane trafficking. *Front. Immunol.* 5:538. doi: 10.3389/fimmu.2014.00538

Musiol, A., Gran, S., Ehrhardt, C., Ludwig, S., Grewal, T., Gerke, V., et al. (2013). Annexin A6-balanced late endosomal cholesterol controls influenza A replication and propagation. *mBio* 4:e00608-13. doi: 10.1128/mBio.00608-13

Nailwal, H., Sharma, S., Mayank, A. K., and Lal, S. K. (2015). The nucleoprotein of influenza A virus induces p53 signaling and apoptosis via attenuation of host ubiquitin ligase RNF43. *Cell Death Dis.* 6:e1768. doi: 10.1038/cddis.2015.131

Nasser, E. H., Judd, A. K., Sanchez, A., Anastasiou, D., and Bucher, D. J. (1996). Antiviral activity of influenza virus M1 zinc finger peptides. *J. Virol.* 70, 8639–8644. doi: 10.1128/jvi.70.12.8639-8644.1996

Neumann, G., Hughes, M. T., and Kawaoka, Y. (2000). Influenza A virus NS2 protein mediates vRNP nuclear export through NES-independent interaction with hCRM1. *EMBO J.* 19, 6751–6758. doi: 10.1093/emboj/19.24.6751

Ng, A. K.-L., Zhang, H., Tan, K., Li, Z., Liu, J.-H., Chan, P. K.-S., et al. (2008). Structure of the influenza virus A H5N1 nucleoprotein: implications for RNA binding, oligomerization, and vaccine design. *FASEB J.* 22, 3638–3647. doi: 10.1096/fj.08-112110

Noda, T. (2012). Native morphology of influenza virions. *Front. Microbiol.* 2:269. doi: 10.3389/fmicb.2011.00269

Nogales, A., Martinez-Sobrido, L., Topham, D. J., and Dediego, M. L. (2017). NS1 protein amino acid changes D189N and V194I affect interferon responses, thermosensitivity, and virulence of circulating H3N2 human influenza A viruses. *J. Virol.* 91:e01930-16. doi: 10.1128/JVI.01930-16

O'neill, R. E., Talon, J., and Palese, P. (1998). The influenza virus NEP (NS2 protein) mediates the nuclear export of viral ribonucleoproteins. *EMBO J.* 17, 288–296. doi: 10.1093/emboj/17.1.288

Ohno, M., Sekiya, T., Nomura, N., Daito, T. J., Shingai, M., and Kida, H. (2020). Influenza virus infection affects insulin signaling, fatty acid-metabolizing enzyme expressions, and the tricarboxylic acid cycle in mice. *Sci. Rep.* 10:10879. doi: 10.1038/s41598-020-67879-6

Ozawa, M., Basnet, S., Burley, L. M., Neumann, G., Hatta, M., and KAWAOKA, Y., (2011). Impact of amino acid mutations in PB2, PB1-F2, and NS1 on the replication and pathogenicity of pandemic (H1N1) 2009 influenza viruses. *J. Virol.* 85, 4596–4601. doi: 10.1128/JVI.00029-11

Paules, C. I., Sullivan, S. G., Subbarao, K., and Fauci, A. S. (2018). Chasing seasonal influenza—the need for a universal influenza vaccine. *N. Engl. J. Med.* 378, 7–9. doi: 10.1056/NEJMp1714916

Pereira, C. F., Read, E. K. C., Wise, H. M., Amorim, M. J., and Digard, P. (2017). Influenza A virus NS1 protein promotes efficient nuclear export of unspliced viral M1 mRNA. *J. Virol.* 91:e00528-17. doi: 10.1128/JVI.00528-17

Ramos, I., Carnero, E., Bernal-Rubio, D., Seibert, C. W., Westera, L., García-Sastre, A., et al. (2013). Contribution of double-stranded RNA and CPSF30 binding domains of influenza virus NS1 to the inhibition of type I interferon production and activation of human dendritic cells. *J. Virol.* 87, 2430–2440. doi: 10.1128/JVI.02247-12

Ravindran, M. S., Bagchi, P., Cunningham, C. N., and Tsai, B. (2016). Opportunistic intruders: how viruses orchestrate ER functions to infect cells. *Nat. Rev. Microbiol.* 14, 407–420. doi: 10.1038/nrmicro.2016.60

Robb, N. C., Smith, M., Vreede, F. T., and Fodor, E. (2009). NS2/NEP protein regulates transcription and replication of the influenza virus RNA genome. *J. General Virol.* 90, 1398–1407. doi: 10.1099/vir.0.009639-0

Rogers, G. N., and D'Souza, B. L. (1989). Receptor binding properties of human and animal H1 influenza virus isolates. *Virology* 173, 317–322. doi: 10.1016/0042-6822(89)90249-3

Rogers, G. N., and Paulson, J. C. (1983). Receptor determinants of human and animal influenza virus isolates: differences in receptor specificity of the H3 hemagglutinin based on species of origin. *Virology* 127, 361–373. doi: 10.1016/0042-6822(83)90150-2

Russ, G., Bennink, J. R., Bächi, T., and Yewdell, J. W. (1991). Influenza virus hemagglutinin trimers and monomers maintain distinct biochemical modifications and intracellular distribution in brefeldin A-treated cells. *Cell Regulation* 2, 549–563. doi: 10.1091/mbc.2.7.549

Saito, T., Tanaka, M., and Yamaguchi, I. (1996). Effect of brefeldin A on influenza A virus-induced apoptosis in vitro. *J. Vet. Med. Sci.* 58, 1137–1139. doi: 10.1292/jvms.58.11_1137

Schaap, I. A. T., Eghiaian, F., Des Georges, A., and Veigel, C. (2012). Effect of envelope proteins on the mechanical properties of influenza virus. *The Journal of Biological Chemistry* 287, 41078–41088. doi: 10.1074/jbc.M112.412726

Sharma, K., Tripathi, S., Ranjan, P., Kumar, P., Garten, R., Deyde, V., et al. (2011). Influenza A virus nucleoprotein exploits Hsp40 to inhibit PKR activation. *PLoS One* 6:e20215. doi: 10.1371/journal.pone.0020215

Shen, Z., Lou, K., and Wang, W. (2015). New small-molecule drug design strategies for fighting resistant influenza A. *Acta Pharm. Sin. B* 5, 419–430. doi: 10.1016/j.apsb.2015.07.006

Short, K. R., Kedzierska, K., and Van De Sandt, C. E. (2018). Back to the future: lessons learned from the 1918 influenza pandemic. *Front. Cell. Infect. Microbiol.* 8:343. doi: 10.3389/fcimb.2018.00343

Skehel, J. J., and Wiley, D. C. (2000). Receptor binding and membrane fusion in virus entry: the influenza hemagglutinin. *Annu. Rev. Biochem.* 69, 531–569. doi: 10.1146/annurev.biochem.69.1.531

Steinhauer, D. A. (1999). Role of hemagglutinin cleavage for the pathogenicity of influenza virus. *Virology* 258, 1–20. doi: 10.1006/viro.1999.9716

Stevaert, A., and Naesens, L. (2016). The influenza virus polymerase complex: an update on its structure, functions, and significance for antiviral drug design. *Med. Res. Rev.* 36, 1127–1173. doi: 10.1002/med.21401

Su, W. C., Yu, W. Y., Huang, S. H., and Lai, M. M. C. (2018). Ubiquitination of the cytoplasmic domain of influenza A virus M2 protein is crucial for production of infectious virus particles. *J. Virol.* 92:e01972-1. doi: 10.1128/JVI.01972-17

Sugiyama, K., Obayashi, E., Kawaguchi, A., Suzuki, Y., Tame, J. R. H., Nagata, K., et al. (2009). Structural insight into the essential PB1-PB2 subunit contact of the influenza virus RNA polymerase. *EMBO J.* 28, 1803–1811. doi: 10.1038/emboj.2009.138

Sugrue, R. J., and Hay, A. J. (1991). Structural characteristics of the M2 protein of influenza A viruses: evidence that it forms a tetrameric channel. *Virology* 180, 617–624. doi: 10.1016/0042-6822(91)90075-M

Taguwa, S., Maringer, K., Li, X., Bernal-Rubio, D., Rauch, J. N., Gestwicki, J. E., et al. (2015). Defining Hsp70 subnetworks in dengue virus replication reveals key vulnerability in Flavivirus infection. *Cell* 163, 1108–1123. doi: 10.1016/j.cell.2015.10.046

Te Velthuis, A. J. W., and Fodor, E. (2016). Influenza virus RNA polymerase: insights into the mechanisms of viral RNA synthesis. *Nat. Rev. Micro* 14, 479–493. doi: 10.1038/nrmicro.2016.87

Thompson, M. G., Muñoz-Moreno, R., Bhat, P., Roytenberg, R., Lindberg, J., Gazzara, M. R., et al. (2018). Co-regulatory activity of hnRNP K and NS1-BP in influenza and human mRNA splicing. *Nat. Commun.* 9:2407. doi: 10.1038/s41467-018-04779-4

Tong, S., Zhu, X., Li, Y., Shi, M., Zhang, J., Bourgeois, M., et al. (2013). New world bats harbor diverse influenza A viruses. *PLOS Pathog.* 9:e1003657. doi: 10.1371/journal.ppat.1003657

Tripathi, S., Batra, J., Cao, W., Sharma, K., Patel, J. R., Ranjan, P., et al. (2013). Influenza A virus nucleoprotein induces apoptosis in human airway epithelial cells: implications of a novel interaction between nucleoprotein and host protein Clusterin. *Cell Death Dis.* 4:e562. doi: 10.1038/cddis.2013.89

Tripathi, S., Pohl, M. O., Zhou, Y., Rodriguez-Frandsen, A., Wang, G., Stein, D. A., et al. (2015). Meta- and orthogonal integration of influenza "OMICs" data defines a role for UBR4 in virus budding. *Cell Host Microbe* 18, 723–735. doi: 10.1016/j.chom.2015.11.002

Twu, K. Y., Noah, D. L., Rao, P., Kuo, R.-L., and Krug, R. M. (2006). The CPSF30 binding site on the NS1A protein of influenza A virus is a potential antiviral target. *J. Virol.* 80, 3957–3965. doi: 10.1128/JVI.80.8.3957-3965.2006

Varghese, J. N., Laver, W. G., and Colman, P. M. (1983). Structure of the influenza virus glycoprotein antigen neuraminidase at 2.9 A resolution. *Nature* 303, 35–40. doi: 10.1038/303035a0

Wakefield, L., and Brownlee, G. G. (1989). RNA-binding properties of influenza A virus matrix protein M1. *Nucleic Acids Res.* 17, 8569–8580. doi: 10.1093/nar/17.21.8569

Wang, X., Basler, C. F., Williams, B. R., Silverman, R. H., Palese, P., and Garcia-Sastre, A. (2002). Functional replacement of the carboxy-terminal two-thirds of the influenza A virus NS1 protein with short heterologous dimerization domains. *J. Virol.* 76, 12951–12962. doi: 10.1128/JVI.76.24.12951-12962.2002

Watanabe, T., Kawakami, E., Shoemaker, J. E., Lopes, T. J., Matsuoka, Y., Tomita, Y., et al. (2014). Influenza virus-host interactome screen as a platform for antiviral drug development. *Cell Host Microbe* 16, 795–805. doi: 10.1016/j.chom.2014.11.002

Watanabe, T., Watanabe, S., and Kawaoka, Y. (2010). Cellular networks involved in the influenza virus life cycle. *Cell Host Microbe* 7, 427–439. doi: 10.1016/j.chom.2010.05.008

Wilkinson, M. E., Charenton, C., and Nagai, K. (2020). RNA splicing by the spliceosome. *Ann. Rev. Biochem.* 89, 359–388. doi: 10.1146/annurev-biochem-091719-064225

Wolff, T., O'neill, R. E., and Palese, P. (1998). NS1-binding protein (NS1-BP): a novel human protein that interacts with the influenza A virus nonstructural NS1 protein is relocalized in the nuclei of infected cells. *J. Virol.* 72, 7170–7180. doi: 10.1128/JVI.72.9.7170-7180.1998

Xia, C., Vijayan, M., Pritzl, C. J., Fuchs, S. Y., Mcdermott, A. B., Hahm, B., et al. (2016). Hemagglutinin of influenza A virus antagonizes type I interferon (IFN) responses by inducing degradation of type I IFN receptor 1. *J. Virol.* 90, 2403–2417. doi: 10.1128/JVI.02749-15

Yadav, V., Panganiban, A. T., Honer Zu Bentrup, K., and Voss, T. G. (2016). Influenza infection modulates vesicular trafficking and induces Golgi complex disruption. *Virusdisease* 27, 357–368. doi: 10.1007/s13337-016-0347-3

Yasuda, J., Nakada, S., Kato, A., Toyoda, T., and Ishihama, A. (1993). Molecular assembly of influenza virus: association of the NS2 protein with virion matrix. *Virology* 196, 249–255. doi: 10.1006/viro.1993.1473

Ye, Q., Krug, R. M., and Tao, Y. J. (2006). The mechanism by which influenza A virus nucleoprotein forms oligomers and binds RNA. *Nature* 444, 1078–1082. doi: 10.1038/nature05379

Zhang, J., Ruan, T., Sheng, T., Wang, J., Sun, J., Wang, J., et al. (2019). Role of c-Jun terminal kinase (JNK) activation in influenza A virus-induced autophagy and replication. *Virology* 526, 1–12. doi: 10.1016/j.virol.2018.09.020

Zhang, K., Shang, G., Padavannil, A., Wang, J., Sakthivel, R., Chen, X., et al. (2018). Structural–functional interactions of NS1-BP protein with the splicing and mRNA export machineries for viral and host gene expression. *Proc. Nat. Acad. Sci.* 115, E12218–E12227. doi: 10.1073/pnas.1818012115

Zhirnov, O. P., and Klenk, H. D. (2013). Influenza A virus proteins NS1 and hemagglutinin along with M2 are involved in stimulation of autophagy in infected cells. *J. Virol.* 87, 13107–13114. doi: 10.1128/JVI.02148-13

**Conflict of Interest:** The authors declare that the research was conducted in the absence of any commercial or financial relationships that could be construed as a potential conflict of interest.

**Publisher's Note:** All claims expressed in this article are solely those of the authors and do not necessarily represent those of their affiliated organizations, or those of the publisher, the editors and the reviewers. Any product that may be evaluated in this article, or claim that may be made by its manufacturer, is not guaranteed or endorsed by the publisher.

frontiers | Frontiers in Microbiology

ORIGINAL RESEARCH
published: 26 April 2022
doi: 10.3389/fmicb.2022.859420

# The Interaction of Influenza A NS1 and Cellular TRBP Protein Modulates the Function of RNA Interference Machinery

*Qi Wang[1,2], Jiaxin Wang[1,2], Yan Xu[1,2], Zhe Li[1], Binbin Wang[1,2] and Yang Li[2]**

[1]State Key Laboratory of Genetic Engineering, School of Life Sciences, Fudan University, Shanghai, China, [2]CAS Key Laboratory of Animal Ecology and Conservation Biology, Institute of Zoology, Chinese Academy of Sciences, Beijing, China

Influenza A virus (IAV), one of the most prevalent respiratory diseases, causes pandemics around the world. The multifunctional non-structural protein 1 (NS1) of IAV is a viral antagonist that suppresses host antiviral response. However, the mechanism by which NS1 modulates the RNA interference (RNAi) pathway remains unclear. Here, we identified interactions between NS1 proteins of Influenza A/PR8/34 (H1N1; IAV-PR8) and Influenza A/WSN/1/33 (H1N1; IAV-WSN) and Dicer's cofactor TAR-RNA binding protein (TRBP). We found that the N-terminal RNA binding domain (RBD) of NS1 and the first two domains of TRBP protein mediated this interaction. Furthermore, two amino acid residues (Arg at position 38 and Lys at position 41) in NS1 were essential for the interaction. We generated TRBP knockout cells and found that NS1 instead of NS1 mutants (two-point mutations within NS1, R38A/K41A) inhibited the process of microRNA (miRNA) maturation by binding with TRBP. PR8-infected cells showed masking of short hairpin RNA (shRNA)-mediated RNAi, which was not observed after mutant virus-containing NS1 mutation (R38A/K41A, termed PR8/3841) infection. Moreover, abundant viral small interfering RNAs (vsiRNAs) were detected *in vitro* and *in vivo* upon PR8/3841 infection. We identify, for the first time, the interaction between NS1 and TRBP that affects host RNAi machinery.

**Keywords: influenza A virus, non-structural protein 1 of IAV, TRBP, antiviral RNAi response, RNA interference machinery**

OPEN ACCESS

***Edited by:***
*Quanjiao Chen,*
*Wuhan Institute of Virology (CAS), China*

***Reviewed by:***
*Xiulong Xu,*
*Rush University, United States*
*Ke Zhang,*
*Institut Pasteur of Shanghai (CAS), China*

****Correspondence:***
*Yang Li*
*yangli15@fudan.edu.cn*

***Specialty section:***
*This article was submitted to Virology, a section of the journal Frontiers in Microbiology*

***Received:*** *21 January 2022*
***Accepted:*** *29 March 2022*
***Published:*** *26 April 2022*

***Citation:***
*Wang Q, Wang J, Xu Y, Li Z, Wang B and Li Y (2022) The Interaction of Influenza A NS1 and Cellular TRBP Protein Modulates the Function of RNA Interference Machinery. Front. Microbiol. 13:859420. doi: 10.3389/fmicb.2022.859420*

## INTRODUCTION

Influenza A viruses (IAVs) are widespread pathogens causing severe respiratory disease around the world (Neumann et al., 2010; Su et al., 2015; Coughlan and Palese, 2018). Seasonal epidemics of influenza affect 5%–15% of the global population, and cause about 250,000 to 500,000 respiratory deaths annually, with influenza A causing considerable morbidity and mortality (Li et al., 2018; Yassine et al., 2018). IAVs are negative-stranded RNA viruses belonging to the *Orthomyxoviridae* family, which contain 8 segments encoding approximately 14 proteins (Krammer et al., 2018; Ampomah and Lim, 2020). Different subtypes of IAVs are classified according to two glycoproteins, haemagglutinin (HA) and neuraminidase (NA). The three polymerase proteins

(PA, PB1, and PB2) form a viral ribonucleoprotein (vRNP) with the nucleoprotein (NP)-encapsidated RNA segment in the replication of IAVs.

Non-structural protein 1 (NS1) consists of 215 to 237 amino acids (aa) and consists of an N-terminal RNA binding domain (RBD; 1 to 73 aa) and a C-terminal effector domain (ED; 85 aa to end) and joined by a linker domain (LD; 74 to 84 aa; Hale et al., 2008; Krug, 2015). The RBD non-specifically binds double-stranded RNA (dsRNA) of different lengths and mediates several interactions (Chien et al., 2004; Hale et al., 2008). Highly expressed NS1 performs a range of activities to inhibit the host antiviral response by interacting with interferon (IFN)-induced proteins and antagonizing IFN production during infection (Krug et al., 2003; Krug, 2015). Two residues of NS1, arginine 38 (R38) and lysine 41 (K41), are the key functional sites for binding dsRNA and retinoic acid-inducible gene I (RIG-I) to inhibit signal transduction (Qian et al., 1994; Wang et al., 1999; Talon et al., 2000; Wang et al., 2000; Mibayashi et al., 2007). NS1 competes with 2′-5′-oligoadenylate synthetase (2′-5'-OAS) for interaction with dsRNA, thereby blocking cleavage by RNase L of viral and cellular mRNA (Ji-Young Min, 2006). The ED also mediates functional interactions with host proteins. The interaction between NS1 and ubiquitin ligase TRIM25 suppresses RIG-I signal transduction, which requires E96/E97 residues in the ED of NS1 (Gack et al., 2009). NS1 binds to protein kinase R (PKR) at residues 123–127, which in turn inhibits PKR-mediated eukaryotic translation initiation factor eIF2α phosphorylation (Li et al., 2006; Min et al., 2007; Schierhorn et al., 2017). Furthermore, the cellular cleavage and polyadenylation specific factor 30 (CPSF30) binds to the ED, in turn blocking the maturation of pre-mRNA (Nemeroff et al., 1998).

RNA interference (RNAi) has been recognized as an important gene silencing mechanism in mammals (Ding, 2010; Guo et al., 2019). In the processing of RNAi, the stem-loop structure of precursor microRNAs (pre-miRNAs) or viral double-stranded RNA replicative intermediates (dsRNA-vRIs) are cleaved into ~22 nucleotide (nt) miRNAs or viral small interfering RNAs (vsiRNAs) by Dicer, an enzyme belonging to the RNase III family (Bernstein et al., 2001; Hutvágner et al., 2001). Then, these small RNAs (sRNAs) are loaded into Argonaute-2 (AGO2) protein, an important component of RNA-induced silencing complex (RISC), leading to silencing or degradation of target sequences (Jinek and Doudna, 2009; Ding et al., 2018). As another essential member of RISC, TRBP serves as a cofactor of Dicer in the processing of miRNAs (Chendrimada et al., 2005; Haase et al., 2005; Takahashi et al., 2018). However, whether TRBP affects miRNA abundance or isoforms remains controversial (Chendrimada et al., 2005; Haase et al., 2005; Melo et al., 2009; Lee and Doudna, 2012; Kim et al., 2014). Numerous proteins, including adenosine deaminases acting on RNA-1 (ADAR1) and the protein activator of PKR (PACT), have also been reported to enhance the cleavage activity of Dicer (Lee et al., 2006; Ota et al., 2013; Heyam et al., 2015).

Many studies indicate that host miRNA expression levels are regulated to resist viral infections. In hepatocytes, hepatitis C virus (HCV)-induced IFN-β regulates the expression of cellular miRNAs including miR-196, miR-351, and miR-431, which target the RNA genome of HCV to inhibit viral replication (Pedersen et al., 2007). Increased expression of miR-296-5p directly targets VP1 and VP3 coding sequences of the genome to inhibit the Enterovirus 71 (EV71) replication in rhabdomyosarcoma (RD) and human neuroblastoma (SKN-SH) cells (Zheng et al., 2013). In addition, miR-32 targets viral nucleic acids, which restricts the expression of primate foamy virus type 1 (PFV-1) mRNA in 293 T cells (Lecellier et al., 2005). Many viruses in turn inhibit host miRNA maturation for viral replication. Flaviviruses, including dengue viruses (DENV), Kunjin virus (KUNV), and Japanese encephalitis virus (JEV), suppress miRNA production through non-coding subgenomic flavivirus RNAs (sfRNAs) that associate with Dicer and AGO2 in infected cells (Moon et al., 2015). Human cytomegalovirus (HCMV) encodes intergenic sequences that are complementary to miR-17, resulting in its degradation (Lee et al., 2013). In addition, Zika virus (ZIKV) capsid protein binds to Dicer to dampen miRNA production in neural stem cells (NSCs; Zeng et al., 2020).

On the other hand, there is growing evidence that siRNA-based antiviral immunity plays an important role in mammals (Li et al., 2013; Maillard et al., 2013; Li et al., 2016; Qiu et al., 2017; Han et al., 2020; Zeng et al., 2020). Recent studies including ours have shown several viruses, such as Nodamura virus (NoV), IAV, Sindbis virus (SINV), and ZIKV induce vsiRNA production *in vitro* or *in vivo* (Li et al., 2013; Li et al., 2016; Zhang et al., 2020; Zhang et al., 2021). To counter the defense mechanism, many viruses encode viral suppressors of RNAi (VSRs), including NoV B2, IAV NS1, Ebolavirus (EBOV) VP35, and human enterovirus 71 (HEV71) 3A (Fabozzi et al., 2011; Li et al., 2013; Li et al., 2016; Qiu et al., 2017). For instance, VP35 directly interacts with TRBP and PACT to suppress the effects of siRNAs (Fabozzi et al., 2011). 3A inhibits siRNAs production by sequestrating viral dsRNA (Qiu et al., 2017).

Similar to several viruses, IAV has also been recognized to functionally regulate cellular miRNA expression (Terrier et al., 2013; Tan et al., 2014; Jiao et al., 2019). Moreover, our previous study has shown that vsiRNAs are detected in mammalian cells only when infected with IAV lacking NS1, suggesting that NS1 blocks vsiRNA production (Li et al., 2016). Our emerging study also determines that NS1 encoded by influenza A/WSN/1/33 (WSN) interacts with AGO2, which induces nuclear import of AGO2 (Wang et al., 2020). In addition, multiple studies have observed that NS1 interacts with many host proteins including ADAR1 and PACT that participate in the RNAi process (de Chassey et al., 2013; Tawaratsumida et al., 2014).

Although IAV NS1 has been shown to inhibit the production of sRNAs, few studies have clarified the mechanism underlying suppression by NS1. Here, we show the interaction between PR8 NS1 and TRBP, which inhibits some miRNAs production. Further analysis reveals that R38 and K41 of NS1 are vital sites for this binding. Moreover, our findings provide the first evidence for the *in vivo* production canonical duplex vsiRNAs by mutant IAV virus. Our work explains the mechanism of

NS1 in modulating RNA interference machinery from a new perspective.

## MATERIALS AND METHODS

### Cell Culture and Viruses

Human embryonic kidney cells (293 T) were cultured in Dulbecco's modified Eagle's medium (DMEM; Sigma) containing 10% fetal bovine serum (FBS; Gibco) at 37°C with 5% $CO_2$. Influenza A/Puerto Rico/8/34 (H1N1), designated PR8-wild type (WT), Influenza A/WSN/1/33 (H1N1), designated WSN-WT, and the mutant virus, designated PR8/3841, were gifts from Dr. A. García-Sastre.

### Plasmids and Molecular Cloning

The sequences encoding NS1, N-NS1, C-NS1, and NS1 38/41 of PR8-WT and the sequences encoding NS1, NS1 38/41 of WSN-WT were generated by reverse transcription–polymerase chain reaction (RT-PCR) and cloned into pcDNA3.1 vector digested by EcoRI and HindIII (NEB) to generate pcDNA-NS1, pcDNA-N-NS1, pcDNA-C-NS1 and pcDNA-NS1 38/41. The open reading frame (ORF) of EGFP was cloned into the EcoRI and HindIII sites of the pcDNA3.1 vector to generate pcDNA-EGFP. The plasmids expressing EGFP, TRBP, T7, and different mutants of TRBP (TA, TB, and TC) were constructed into pCMV vectors with an N-terminal 3xFLAG epitope digested by HindIII and EcoRI to generate pCMV-3Flag-EGFP, pCMV-3Flag-TRBP, pCMV-3Flag-T7, pCMV-3Flag-TA, pCMV-3Flag-TB, and pCMV-3Flag-TC. The ORFs of EGFP and TRBP were cloned with C-terminal His tag into the SalI and XhoI sites of pDEST-myc-DICER (Addgene, Cat. #19873) to generate pDEST-His-EGFP and pDEST-His-TRBP. The sequence encoding TRBP was cloned into pGEX-4 T-1 digested by BamHI and SalI to generate GST-TRBP. The expression plasmid for human Dicer was purchased from Addgene (Cat. #41584). Human miRNA expression plasmid MIR-21 (pCMV-MIR-21) was purchased from OriGene (Cat. #SC400271). The designed short hairpin RNAs (shRNAs) targeting EGFP or luciferase were cloned into pLKO.5 vector (gift from Dr. Feng Qian) digested by AgeI and EcoRI to produce pLKO-sh-EGFP (shEGFP) and pLKO-sh-LUC (shLUC). The CRISPR/Cas9 plasmids were gifts from Dr. Yongming Wang (Xie et al., 2017). Two designed guide RNAs (gRNAs), gRNA1 and gRNA2, were ligated with tracrRNA-U6 sequence from gRNAU6 plasmid. Then, the fragment was constructed into an epiCRISPR vector that was digested by BspQI to generate epiCRISPR-TRBP. The primer sequences and gRNA sequences are shown in **Supplementary Tables 1 and 2**.

### Cell Culture Infection and Transfection

293 T cells were seeded in a 6-cm plate at a density of $2 \times 10^6$/plate 1 day before infection. Approximately 24 h after inoculation with serum-free DMEM (mock), PR8-WT, or PR8/3841 at a multiplicity of infection (MOI) of 1 as previously described (Li et al., 2016), the infected cells were lysed in TRIzol (Invitrogen) for RNA and protein extraction using the manufacturer's protocol.

To identify the interaction between NS1 and TRBP, 293 T cells ($6 \times 10^5$ cells/well) were seeded into a 6-well plate 1 day before transfection. Plasmids expressing NS1 (2 μg) and FLAG-TRBP (2 μg) were co-transfected into 293 T cells using Lipofectamine 2000 (Life Technologies) for 48 h. 293 T cells were transfected with plasmids expressing FLAG-TRBP (2 μg) or FLAG-EGFP (2 μg) for 24 h and then inoculated with PR8-WT (MOI = 1) or WSN-WT (MOI = 1) or PR8/3841 (MOI = 1) in different wells for 24 h.

To determine the effect of the interaction on miRNA production, 293 T cells ($6 \times 10^5$ cells/well) were seeded into a 6-well plate 1 day before transfection. Plasmids expressing FLAG-TRBP (2 μg) were transfected into TRBP-KO cells using Lipofectamine 2000 for 48 h or TRBP-KO cells were transfected with pCMV-MIR-21 (2 μg) and FLAG-TRBP (2 μg) or FLAG-EGFP (2 μg) for 24 h and then inoculated with DMEM (mock) or PR8-WT (MOI = 1) or PR8/3841 (MOI = 1) in different wells for 24 h.

For the EGFP RNAi assay, 293 T cells ($4 \times 10^5$ cells/well) were seeded into a 12-well plate one day before transfection. pCMV-3Flag-EGFP (0.1 μg) and shEGFP (0.3 μg) or shLUC (0.3 μg) were co-transfected into cells using Lipofectamine 2000. Six hours post-transfection, the cells were infected with PR8-WT (MOI = 1) or PR8/3841 (MOI = 1). After 48 h post-transfection, cells were washed with PBS and lysed in TRIzol for RNA and protein extraction using the manufacturer's protocol.

### Co-immunoprecipitation and AGO-Immunoprecipitation

293 T cells transfected with Flag-tagged plasmids or infection with viruses were co-immunoprecipitated (co-IP) by anti-FLAG affinity resin (GenScript). Briefly, 293 T cells lysates in lysis buffer (20 mM Tris–HCl [pH 7.5], 150 mM NaCl, 0.5% NP-40, 5 mM $MgCl_2$, 10% glycerol) mixed with a protease inhibitor (Roche) were incubated with 30 μl anti-FLAG affinity resin for 4 h at 4°C in the presence or absence of 10 μg/ml RNase A (Thermo Fisher Scientific) and 5 U/ml RNase III (NEB). After five times washes with 1 × wash buffer (IBA BioTAGnology), the precipitated complexes were used to detect specific proteins by Western blotting.

For AGO-IP, cells lysates in 1 ml RIPA (Cell Signaling Technology) were precleared by incubation with 20 μl of protein A/G PLUS-Agarose (Santa Cruz Biotechnology) and 2 μg of mouse IgG (Santa Cruz Biotechnology) for 1 h at 4°C for pre-clearing. 2 μg of Anti-pan Ago antibody (Millipore) or 2 μg of mouse IgG antibodies (Santa Cruz Biotechnology) and 20 μl of protein A/G PLUS-Agarose were added into the lysates and incubated together for 4 h at 4°C followed by washing five times with 1 × wash buffer. Total RNAs were extracted from the precipitated complexes using TRIzol to construct small RNA libraries.

### Protein Purification and GST Pulldown

Plasmids expressing GST and GST-TRBP were expressed in Escherichia coli BL21 (DE3) strain cells. The cells were harvested

and sonicated in lysis buffer (50 mM Tris–HCl [pH 8.0], 50 mM NaCl, 5 mM $\beta$-mercaptoethanol, 5% glycerol). Then, lysates were cleared by centrifugation at 20,000 *g* for 30 min at 4°C. The supernatants were purified with Glutathione Resin (GenScript) and dialyzed overnight at 4°C. GST and GST-TRBP proteins were detected by SDS-PAGE and used for GST pulldown.

For GST pulldown, the GST and GST-TRBP proteins were bound to glutathione beads and incubated with lysates expressing NS1 or NS1 38/41 protein for 5 h at 4°C in the presence or absence of 10 μg /ml RNase A and 5 U/ml RNase III. After five times washes with 1 × wash buffer, the bound proteins were detected by SDS-PAGE and Western blotting analysis.

## Western and Northern Blotting Assays

Two assays were performed as previously described (Li et al., 2016; Wang et al., 2020). The following primary antibodies were used for detection: $\beta$-actin (Cell Signaling Technology), TRBP, PACT, Dicer, and EGFP (Santa Cruz Biotechnology), Flag and His (GenScript). The antibody of IAV-NS1 was gift of Dr. Yan Zhou. For Northern blotting, 10 μg of total RNA was used to detect miRNA. The probes used in this study are listed in **Supplementary Table 3**.

## Generation of KO Cell Lines

293 T cells ($1 \times 10^6$ cells/well) were seeded into a 6-well plate 1 day before transfection. The CRISPR/Cas9 plasmid (2 μg) were transfected into 293 T cells (80%–90% confluent) with Lipofectamine 2000. 24 h after transfection, cells were selected by puromycin (2.5 μg/ml). 72 h after selection, cells were identified by PCR and Western blotting. For analysis of single cell-derived clones, separated cells were plated at a density of 100–300 cells per 100 cm dish and were incubated for 2 weeks until colony formation. The KO cell lines were confirmed by DNA sequencing and Western blotting.

## RT-qPCR

One microgram of RNA was reverse transcribed to cDNA using HiScript III First Strand cDNA Synthesis kit (+gDNA wiper; Vazyme). qPCR was performed using ChamQ Universal SYBR qPCR Master Mix (Vazyme). All samples were performed in triplicate. The results were normalized to $\beta$-actin mRNA. The expression levels of specific miRNAs were analyzed by quantitative PCR with specific stem-loop RT primer. The results were normalized to U6 small nuclear RNA. The primer sequences used in RT-qPCR are listed in **Supplementary Table 4**.

## Animals

BALB/c and C57BL/6 mice were purchased from Charles River Laboratory (Shanghai, China). All animal experiments were carried out under the guidelines of the Institutional Animal Care and Use Committee, Fudan University of China.

## Intranasal Infections

Six- to eight-week-old female BALB/c and C57BL/6 mice were kept under specific pathogen-free conditions in individual ventilated cages. Briefly, mice were anesthetized by intraperitoneal injection of a mixture of atropine, diazepam, and pentobarbital and infected intranasally with $10^4$ PFU PR8/3841 in 50 μl of PBS or $10^4$ PFU PR8-WT in 50 μl of PBS. Total RNAs were extracted from the lung tissues of mice 4 days post-infection (dpi).

## Construction of Small RNA Libraries

RNA extractions were used for the construction of small RNA libraries by the method that depends on the 5′ monophosphate of small RNAs as previously described with the TruSeq Small RNA Sample Preparation Kit of Illumina (San Diego, CA; Li et al., 2016).

## Deep Sequencing and Bioinformatic Analysis of Small RNAs

Libraries of small RNAs were cloned from the RNA samples and sequenced by Illumina HiSeq 2000/2500. Small RNA reads were mapped to the virus genome references or compared to mature miRNAs with a perfect match by Bowtie 1.1.2 before removed from adapter sequences. Bioinformatics analysis of virus-derived small RNAs was conducted using in-house Perl scripts as previously described (Li et al., 2016). Pairs of complementary 22-nt vsiRNAs in each library with different base-pairing lengths were computed using a previously described algorithm (Li et al., 2013). Content and properties of the small RNA libraries sequenced are shown in **Supplementary Table 5**. The following reference sequences were used in this study:

PR8-WT: The sequences were downloaded from NCBI: AF389115.1, AF389116.1, AF389117.1, AF389118.1, AF389119.1, AF389120.1, AF389121.1, and AF389122.1.

PR8/3841: Obtained from PR8-WT by mutating amino acids R38A and K41A in the NS1 segment.

Mature miRNAs: miRbase 21 (http://www.mirbase.org/).

# RESULTS

## IAV NS1 Interacts With Host TRBP Protein

To explore RNAi suppression by the NS1 protein of IAV, we conducted co-immunoprecipitation (co-IP) experiments to identify interactions between IAV NS1 and cellular proteins that are involved in RNAi. We detected NS1 in TRBP immunoprecipitants when plasmids encoding FLAG-tagged TRBP or FLAG-tagged EGFP (negative control) and plasmid encoding PR8 NS1 or WSN NS1 were co-transfected into 293 T cells (**Figure 1A**, lanes 1–6 and **Figure 1B**, lanes 1–6). To confirm whether NS1 is associated with TRBP upon IAV infection, 293 T cells were infected with PR8-wildtype (WT) or WSN-WT after ectopically expressing TRBP protein. NS1 was specifically co-immunoprecipitated with TRBP with viral infection, whereas NS1 was undetected in the control of EGFP (**Figure 1A**, lanes 7–12, **Figure 1B**, lanes 7–12, and **Supplementary Figure 1**). Because NS1 and TRBP are both dsRNA binding proteins (dsRBPs), we then examined whether the interaction is dependent on

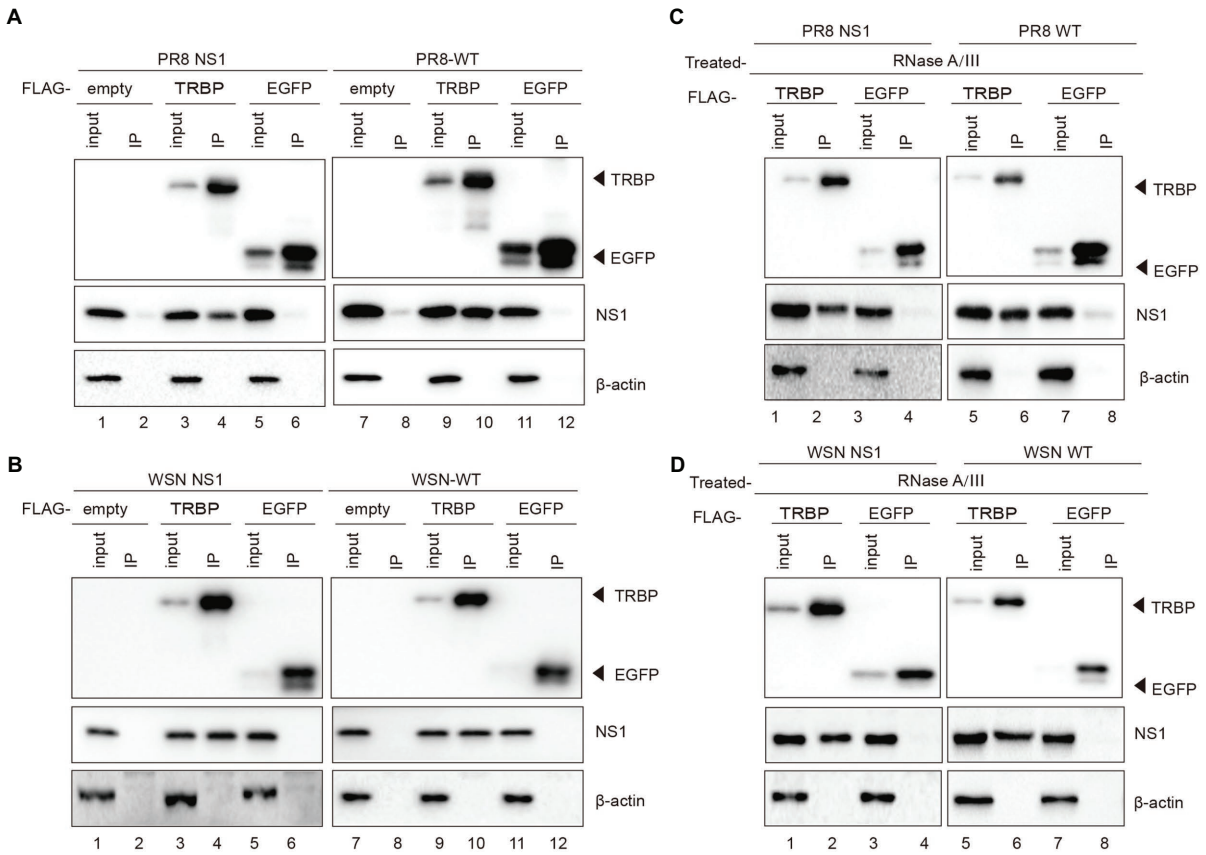


**FIGURE 1 |** IAV NS1 interacts with TRBP. **(A)** Plasmids encoding PR8 NS1 and FLAG-TRBP or FLAG-EGFP or empty vector were co-transfected into 293 T cells for 48 h (lanes 1–6). 293 T cells were transfected with FLAG-TRBP or FLAG-EGFP or empty vector for 24 h before infected with PR8-WT (MOI = 1) for 24 h (lanes 7–12). Immunoprecipitations were performed with anti-FLAG antibody. FLAG-tagged proteins, NS1, and $\beta$-actin were detected with specific antibodies. **(B)** Plasmids encoding WSN NS1 and FLAG-TRBP or FLAG-EGFP or empty vector were co-transfected into 293 T cells for 48 h (lanes 1–6). 293 T cells were transfected with FLAG-TRBP or FLAG-EGFP or empty vector for 24 h before infected with WSN-WT (MOI = 1) for 24 h (lanes 7–12). Immunoprecipitations were performed and processed as in **(A)**. **(C,D)** The NS1-specific interaction with TRBP persists in the presence of RNase. RNase A (10 mg/ml) and RNase III (5 U/ml) were treated with cell lysates. Immunoprecipitations were performed with anti-FLAG antibody. Samples were analyzed by SDS–PAGE with the indicated antibodies.

RNA. RNase A and RNase III were added into the cell lysate to exclude potential interactions mediated by single-stranded RNA (ssRNA) and dsRNA (**Supplementary Figure 2**). The NS1-TRBP interaction was maintained with RNase A and RNase III treatment (**Figures 1C,D**). These results suggest that the NS1-TRBP interaction is likely mediated by protein–protein binding instead of RNA.

To further characterize complex formation, we aimed to validate the interaction using purified NS1 and TRBP. Unfortunately, full-length NS1 protein was observed to aggregate at various concentrations, consistent with those previously reported (Bornholdt and Prasad, 2008; Koliopoulos et al., 2018; Chen et al., 2020b). We finally purified the recombinant glutathione-S-transferase (GST)-fusion TRBP protein and performed GST pull-down experiments. PR8 NS1 or WSN NS1 from ectopic expression or viral infection in 293 T cells was incubated with GST-TRBP or GST purified from E. coli (**Figure 2A**). We found that NS1 bound with high affinity to GST-TRBP but not to GST with RNase treatment (**Figure 2B**). Together, these results demonstrate that IAV NS1 physically binds to the host TRBP protein.

## R38A and K41A Mutations in NS1 Abolish the NS1-TRBP Interaction

It has been demonstrated that a variety of important sites mediate interactions between NS1 and cellular proteins (Ji-Young Min, 2006; Mibayashi et al., 2007; Hale et al., 2008; Krug, 2015; Moriyama et al., 2016; Schierhorn et al., 2017). To further identify the binding sites in NS1, we constructed the C-terminal deletion mutant of NS1 (N-NS1) and the N-terminal deletion mutant of NS1 (C-NS1; **Figure 3A**). N-NS1 was specifically co-immunoprecipitated with TRBP (**Figure 3B**). However, we did not detect the interaction between C-NS1 and TRBP protein (**Figure 3C**). It was inferred that the N-terminal domain of IAV NS1 harbored critical sites that mediated the interaction with TRBP protein. We thus

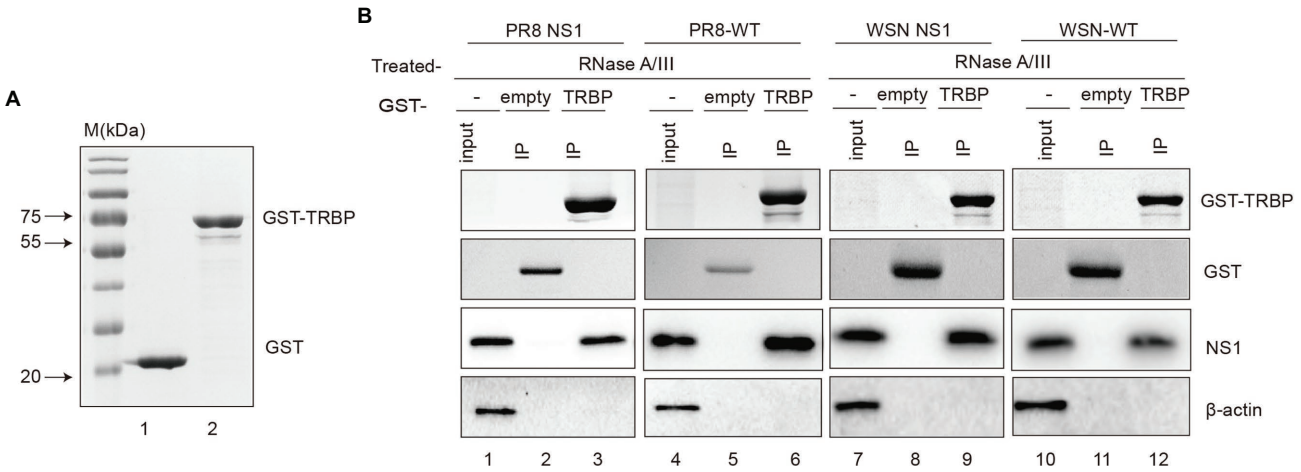


**FIGURE 2 |** GST pull-down assays of NS1 and TRBP. **(A)** Purification of GST and GST-TRBP proteins. **(B)** GST pull-down assay showing the interaction between NS1 and TRBP. Lysates of 293 T cells transfected with PR8 NS1 or WSN NS1 or infected with PR8-WT (MOI = 1) or WSN-WT (MOI = 1) were incubated with an equal amount of GST or GST-TRBP bound to glutathione-sepharose 4B beads with RNase A (10 mg/ml) and RNase III (5 U/ml) treatment. Samples were analyzed by SDS–PAGE with the indicated antibodies.

generated NS1 mutants and found that two-point mutations within NS1 (R38A/K41A) completely abolished NS1-TRBP interaction (**Figures 3D,E**). Furthermore, a recombinant virus carrying the R38A-K41A substitutions in NS1 (PR8/3841) was rescued to identify the interaction. The results of the virus-infected group were consistent with the plasmid-transfected group (**Figure 3F**). These results demonstrate that the region comprised of R38 and K41 is essential to bind TRBP protein.

## The First Two Domains of the TRBP Protein Mediate the Interaction With NS1

TRBP contains three dsRNA binding domains (dsRBDs), including dsRBD-A, dsRBD-B, and dsRBD-C (Chendrimada et al., 2005; Haase et al., 2005; Kok et al., 2007). The first two domains bind dsRNA, while the third domain mediates protein–protein interactions including the Dicer protein (Daniels et al., 2009). To determine which domain NS1 binds to, we constructed FLAG-tagged plasmids expressing different domains of TRBP (**Figure 4A**). NS1 and each plasmid encoding TRBP including full-length plasmid (TRBP-WT) and truncated plasmids (TA, TB, and TC) were co-transfected into 293 T cells. Co-IP assays and Western blotting were conducted to identify the interaction region. It showed that the dsRBD-A and dsRBD-B of TRBP were responsible for NS1-TRBP interaction (**Figure 4B**).

TRBP forms a complex with Dicer and promotes the activity of Dicer in the processing of sRNAs (Chendrimada et al., 2005; Takahashi et al., 2014; Kurzynska-Kokorniak et al., 2015). To confirm the relationship between NS1 and Dicer in viral infection, we expressed FLAG-tagged Dicer or FLAG-tagged T7 (negative control) in 293 T cells and infected with PR8-WT. The results showed a weak interaction between NS1 and Dicer (**Figure 4C**). We subsequently tested whether the interaction between TRBP and Dicer was influenced by NS1. FLAG-Dicer and His-tagged TRBP or His-tagged EGFP (negative control) were co-transfected into 293 T cells and then infected with mock or PR8-WT or PR8/3841. Co-IP analysis were performed to examine the interaction between Dicer-TRBP and Dicer-NS1. The TRBP-Dicer interaction was not influenced with or without viral infection. However, the NS1-Dicer interaction was enhanced during PR8-WT infection (**Figure 4D**). We previously found that TRBP interacted with NS1 *via* its RBD instead of the ED that interacted with Dicer. Therefore, we inferred that the NS1 protein might be in the complex with TRBP and Dicer during sRNAs production.

## NS1-TRBP Interaction Reduces the Expression of Endogenous miRNAs

The effect of TRBP on the expression level of miRNA has remained elusive (Chendrimada et al., 2005; Melo et al., 2009; Ota et al., 2013; Kim et al., 2014). To verify the effect of TRBP on miRNAs, TRBP knockout (KO) 293 T cells were generated with the CRISPR/Cas9 system. Western blot analysis was performed to confirm the depletion of full-length TRBP protein in TRBP-KO cells. The expression of key protein components of the RISC, including Dicer, AGO, and PACT proteins, were similar between parental and TRBP-KO cells (**Figure 5A**). Northern blot analysis was performed to confirm miRNA production. We identified that the expression levels of let-7a-5p and the abundance of 22-nt miR-126-3p decreased in the absence of TRBP (**Figure 5B** and **Supplementary Figure 3A**), which were concordant to the results of a previous study (Chendrimada et al., 2005; Kim et al., 2014).

To validate the function of TRBP, TRBP-KO cells were transfected with FLAG-TRBP plasmid. It showed that TRBP

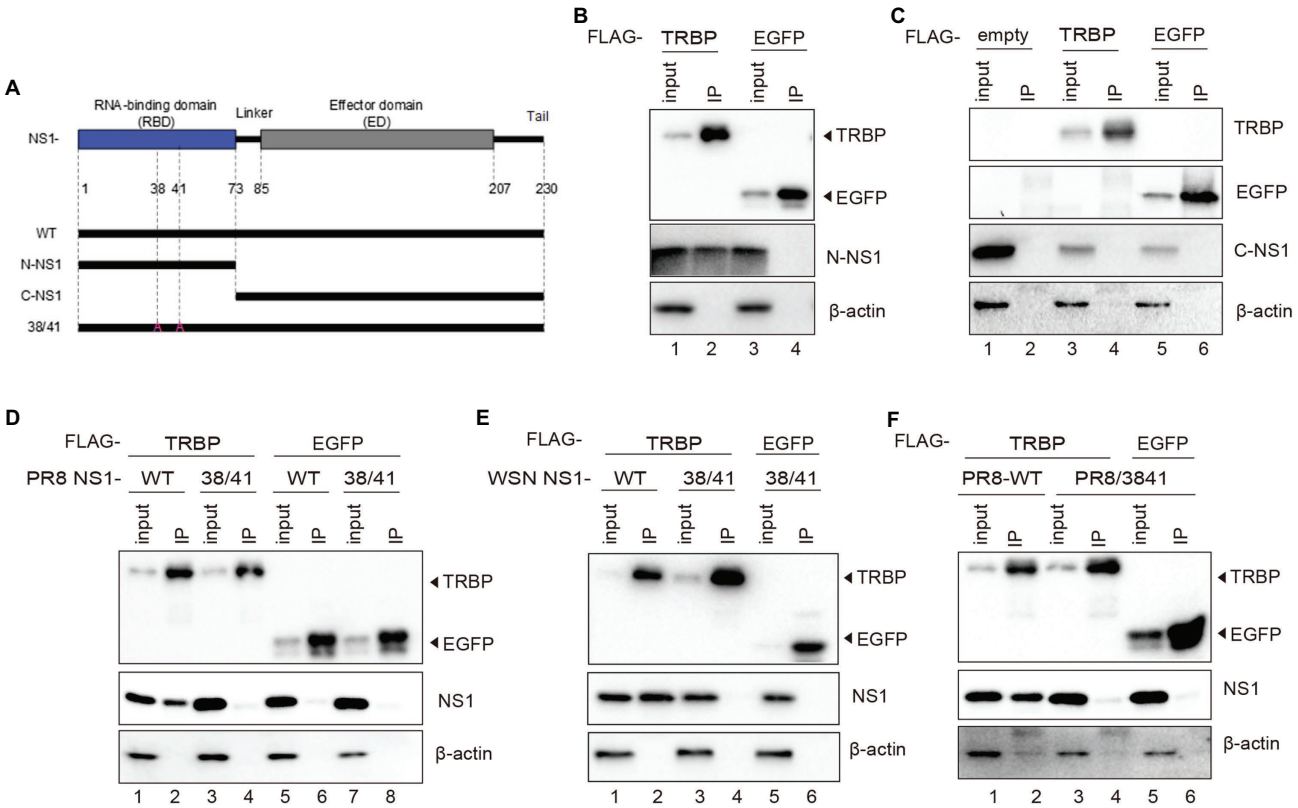


**FIGURE 3 |** R38A and K41A mutations in NS1 abolish the NS1-TRBP interaction. **(A)** Domain architecture of PR8 NS1 protein (NS1-WT) and the generated mutant constructs (N-NS1, C-NS1, NS1 38/41). **(B)** Immunoprecipitation of N-NS1 protein with the TRBP protein. Plasmids encoding FLAG-TRBP or FLAG-EGFP and N-NS1 were co-transfected into 293T cells for 48 h. Immunoprecipitations were performed with anti-FLAG antibody. FLAG-tagged proteins, N-NS1, and $\beta$-actin were detected with specific antibodies. **(C)** Immunoprecipitation of C-NS1 protein with the TRBP protein. Plasmids encoding FLAG-TRBP or FLAG-EGFP and C-NS1 were co-transfected into 293T cells for 48 h and processed as in **(B)**. **(D)** Plasmids encoding FLAG-TRBP or FLAG-EGFP and PR8 NS1-WT or PR8 NS1 38/41 were co-transfected into 293T cells for 48 h and processed as in **(B)**. **(E)** Plasmids encoding FLAG-TRBP or FLAG-EGFP and WSN NS1-WT or WSN NS1 38/41 were co-transfected into 293T cells for 48 h and processed as in **(B)**. **(F)** 293T cells were transfected with FLAG-TRBP or FLAG-EGFP for 24 h before infected with PR8-WT (MOI = 1) or PR8/3841 (MOI = 1) for 24 h and processed as in **(B)**.

overexpression indeed upregulated let-7a-5p (**Figure 5C** and **Supplementary Figure 3B**). We also evaluated the expression level of exogenous miR-21 as previously described (Wang et al., 2020). The human miR-21 expressing plasmid and FLAG-TRBP or FLAG-EGFP (negative control) were co-transfected into TRBP-KO cells. It revealed that TRBP also affected exogenous miR-21 expression (**Figure 5D** and **Supplementary Figure 3C**). These results demonstrate that TRBP affects the maturation of miRNAs in 293T cells.

To further elucidate the role of NS1 in miRNA expression mediated by TRBP, we first compared the expression level of the specific miRNA after viral infection of WT and TRBP-KO cells. We found that the abundance of let-7a-5p was significantly reduced in PR8-infected WT cells (**Figure 6A**, lanes 1–3 and **Supplementary Figure 3D**). In contrast, infection with or without virus did not alter the expression of let-7a-5p in TRBP-KO cells (**Figure 6A**, lanes 4–6 and **Supplementary Figure 3E**). We then transfected FLAG-TRBP in TRBP-KO cells and then infected with mock or PR8-WT or PR8/3841. The same results were observed that PR8-WT instead of PR8/3841 inhibited the production of let-7a-5p (**Figure 6B** and **Supplementary Figure 3F**), which suggested that NS1-TRBP interaction affected the production of the endogenous miRNA. NS1 has been shown to be involved in the regulation of miRNAs processing (Terrier et al., 2013; Tan et al., 2014; Bamunuarachchi et al., 2021). To exclude the potential effect of the endogenous miRNA, we also examined the expression of exogenous miR-21. A reduction in miR-21 expression was observed after infection with PR8-WT, while NS1 mutants did not affect miR-21 expression (**Figures 6C,D**, and **Supplementary Figures 3G,H**). Taken together, IAV NS1 influences the function of Dicer by binding to the TRBP protein.

## R38A-K41A Substitutions Abolish the Inhibition of shRNA-Mediated RNAi by NS1

Dicer can cleave short hairpin RNA (shRNA) into siRNAs (Haasnoot et al., 2007; Jinek and Doudna, 2009; Qian et al., 2020). As a VSR, NS1 modulates functions of

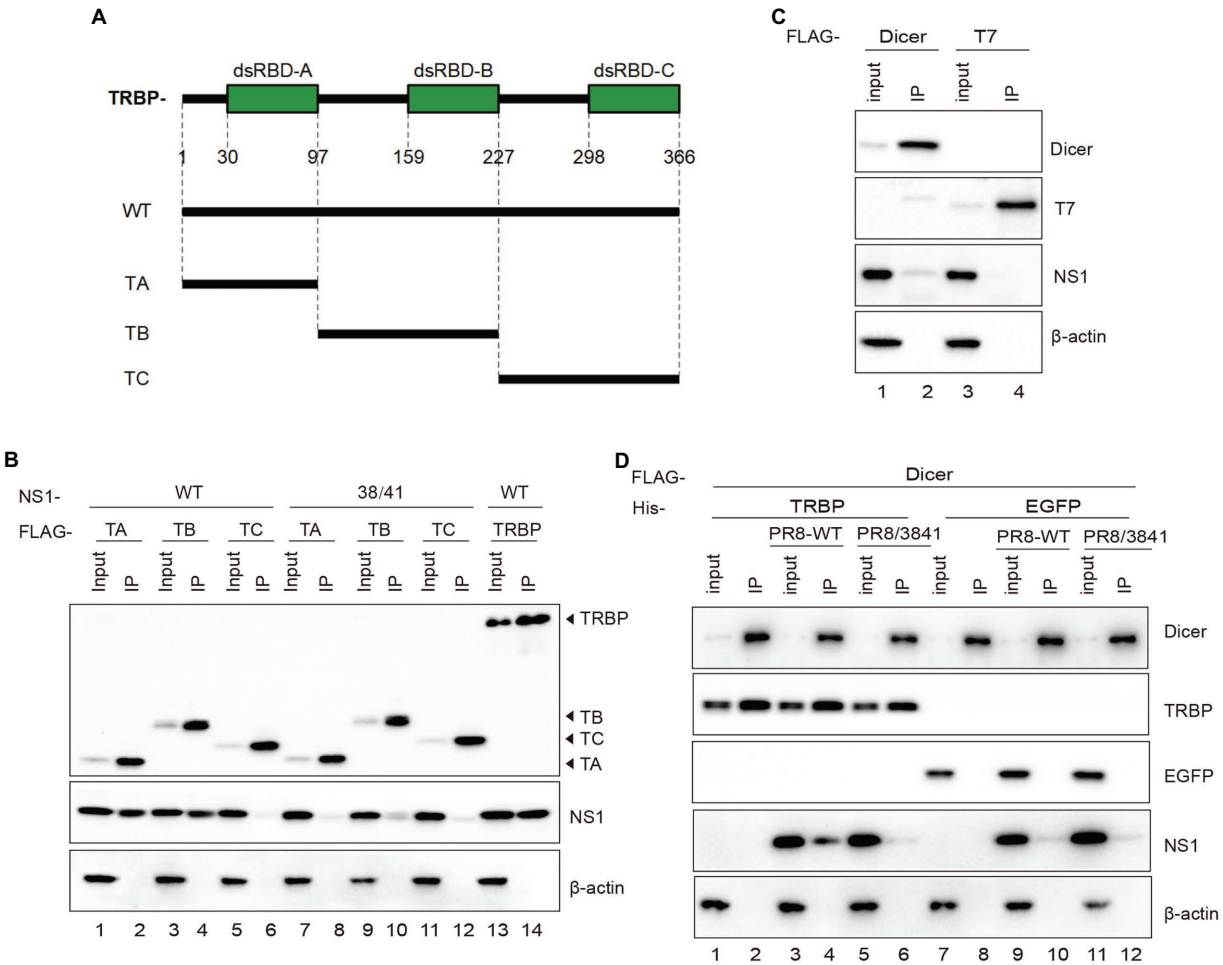


**FIGURE 4 |** The dsRBD-A and dsRBD-B of TRBP are critical for interacting with NS1. **(A)** Domain architecture of TRBP protein (TRBP-WT) and the generated mutant constructs (TA, TB, and TC). **(B)** Immunoprecipitation of PR8 NS1 protein with different mutants of TRBP proteins. PR8 NS1 and the indicated FLAG-tagged constructs were co-transfected into 293 T cells, followed by FLAG immunoprecipitation. FLAG-tagged proteins, NS1, and $\beta$-actin were detected with specific antibodies. **(C)** The weak interaction between Dicer and NS1. 293 T cells were transfected with FLAG-Dicer or FLAG-T7 for 24 h before infected with PR8-WT (MOI = 1) for 24 h and processed as in **(B)**. **(D)** NS1 participates in the complex with TRBP and Dicer. 293 T cells were co-transfected with FLAG-Dicer and His-EGFP or His-TRBP for 24 h before infected with mock or PR8-WT (MOI = 1) or PR8/3841 (MOI = 1) and then processed as in **(B)**.

Dicer to facilitate viral replication and pathogenesis (Bucher et al., 2004; Li et al., 2004; de Vries et al., 2009). To further determine whether mutant NS1 was capable of affecting Dicer's activities, shRNAs were assessed. The EGFP-specific short hairpin RNA (shEGFP) can induce shRNA-mediated silencing to destroy the EGFP transcript. Luciferase-specific shRNA (shLUC) was used as a negative control. We observed that, compared to co-transfection of EGFP with shLuc in 293 T cells, transfection with EGFP and shEGFP statistically significantly reduced EGFP mRNA level (**Figure 7A**). We then infected 293 T cells with PR8-WT or PR8/3841 after transfection with EGFP and shEGFP. Quantitative real-time PCR (qRT-PCR) and Western blotting analysis showed that the mRNA expression level of EGFP was recovered in PR8-WT-infected cells instead of PR8/3841-infected cells (**Figures 7A,B**). These results show that infection of PR8-WT effectively suppresses shRNA-induced silencing in 293 T cells. However, PR8/3841 is deficient in the ability to suppress the process.

## Abundant vsiRNAs are Produced *in vitro* and *in vivo* With PR8/3841 Infection

We previously reported that IAV-WT suppressed vsiRNAs production in mammalian cells. We next investigated whether the 38/41 amino acid sites of NS1 were associated with vsiRNAs induction. Total RNAs from PR8/3841 infected 293 T cells without or with AGO-IP were sequenced. We detected abundant vsiRNAs that were predominantly 22-nt in size from viral positive and negative strands

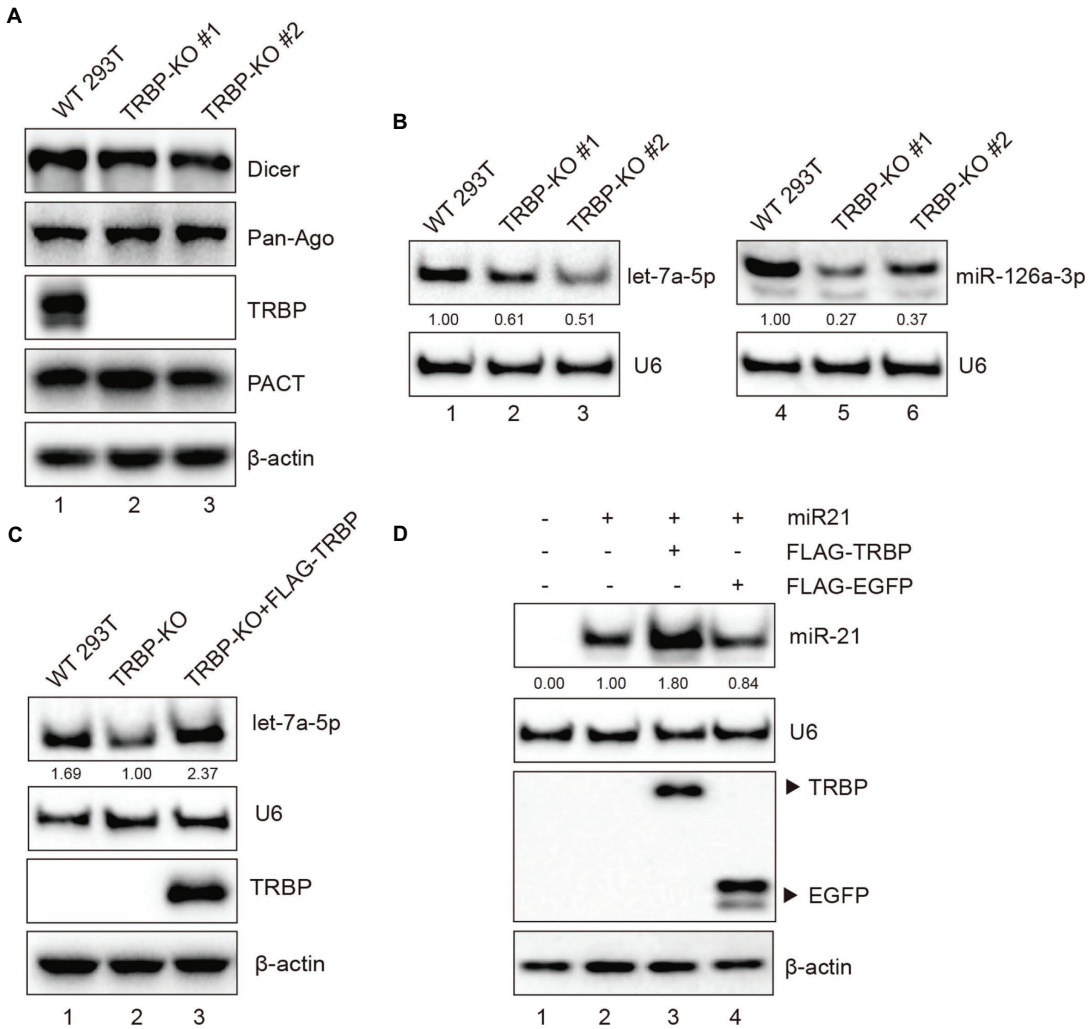


**FIGURE 5 |** TRBP affects miRNAs production. **(A)** RISC-associated proteins of 293T and TRBP-KO cells were detected by Western blotting. **(B)** Northern blotting analysis of miR-126a-3p and let-7a-5p expression levels in the indicated cells. The relative expression levels of miRNAs are normalized to that of U6 small nuclear RNA and to the miRNA level from the WT 293T cells. **(C)** TRBP promotes endogenous let-7a-5p expression. FLAG-TRBP was transfected into TRBP-KO cells for 48 h. Northern blotting and Western blotting were performed to detect let-7a-5p, U6, TRBP, and $\beta$-actin expressions in the indicated cells. The relative expression level of let-7a-5p is normalized to that of U6 small nuclear RNA and to the miRNA level from the TRBP-KO cells. **(D)** TRBP promotes exogenous miR-21 expression. TRBP-KO cells were transfected with a miR-21 expressing plasmid and FLAG-TRBP or FLAG-EGFP for 48 h. Northern blotting and Western blotting were performed to detect expression levels of miR-21, U6, FLAG-tagged proteins and $\beta$-actin. The relative expression level of miR-21 is normalized to that of U6 small nuclear RNA and to the miRNA level from the miR-21-transfected TRBP-KO cells.

(**Figure 8A**). The vsiRNA reads were mainly derived from the first three segments (PB2, PB1, and PA), and exhibited a discrete distribution pattern (**Figure 8C**). In conclusion, amino acids 38/41 of NS1 are key sites to induce and suppress vsiRNA production in mammalian somatic cells.

To date, no study on IAV-derived siRNAs *in vivo* has been reported. We sequenced sRNAs from lung tissues of PR8-WT or PR8/3841 infected C57BL/6 and BALB/c mice by intranasal inoculation. PR8-WT did not generate the visible properties vsiRNAs in C57BL/6 mice (**Figure 8B**). In contrast, it showed a 22-nt predominant size distribution of IAV-specific siRNAs for both viral positive and negative strands in the PR8/3841-infected C57BL/6 and BALB/C mice (**Figure 8B**). To further identify the distribution of vsiRNAs on the genome, 21–23-nt vsiRNAs were mapped onto the viral genome and exhibited a discrete distribution pattern with high abundance in the segment PB2, PB1, and NP, especially NP (**Figure 8C**). 46% of the viral reads were derived from the NP segment in PR8/3841-infected BALB/c mice, while the length of NP segment accounted for 11.5% of the length of the viral genome. In contrast, we previously found that most of the vsiRNA reads were mapped to the segment NS in PR8/delNS1-infected 293T cells (Li et al., 2016), suggesting the distribution of vsiRNAs varied from

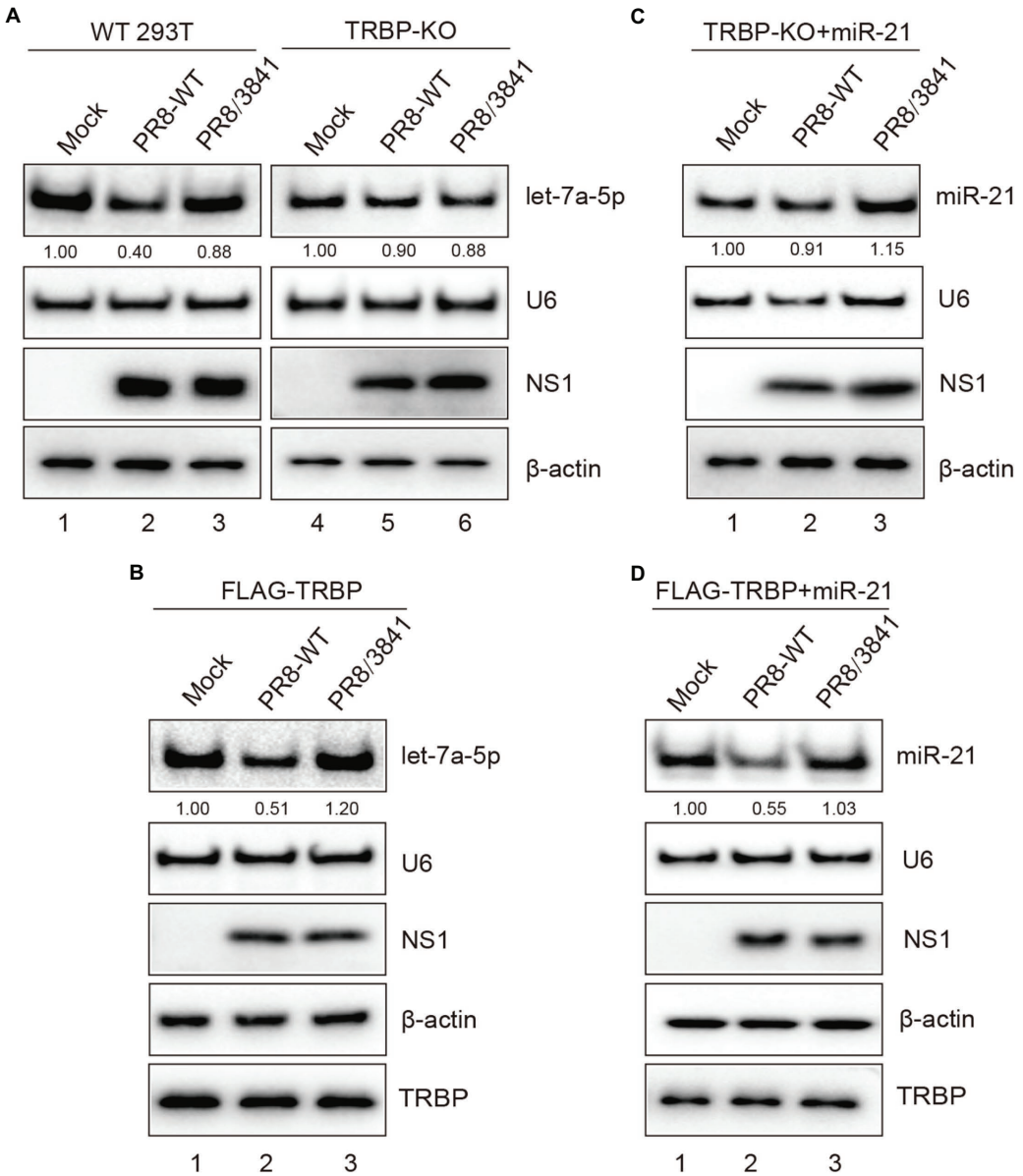


**FIGURE 6 |** NS1-TRBP interaction reduces miRNAs production. **(A)** The expression level of let-7a-5p is downregulated in PR8-infected WT cells. WT 293T cells and TRBP-KO cells were infected with mock or PR8-WT (MOI = 1) or PR8/3841 (MOI = 1) for 48 h. Northern blotting and Western blotting were performed to detect expression levels of let-7a-5p, U6, NS1, and *β*-actin. The relative expression level of let-7a-5p is normalized to that of U6 small nuclear RNA and to the miRNA level from the uninfected WT 293T cells or the uninfected TRBP-KO cells. **(B)** NS1-TRBP interaction reduces the expression of endogenous let-7a-5p. TRBP-KO cells were transfected with FLAG-TRBP for 24 h before infected with PR8-WT or PR8/3841 for 24 h. Northern blotting detection of let-7a-5p and U6 expressions. The relative expression level of let-7a-5p is normalized to that of U6 small nuclear RNA and to the miRNA level from the uninfected cells. Western blotting detection of TRBP, NS1, and *β*-actin proteins. **(C, D)** NS1-TRBP interaction reduces the expression of exogenous miR-21. **(C)** TRBP-KO cells were transfected with a miR-21 expressing plasmid for 24 h before infected with mock or PR8-WT or PR8/3841 for 24 h. **(D)** TRBP-KO cells were co-transfected with FLAG-TRBP and miR-21 expressing plasmid for 24 h before infected with mock or PR8-WT or PR8/3841 for 24 h. Northern blotting detection expressions of miR-21 and U6. The relative expression level of miR-21 is normalized to that of U6 small nuclear RNA and to the miRNA level from the uninfected cells. Western blotting detection of TRBP, NS1, and *β*-actin proteins.

recombinant virus-expressing NS1 protein with different mutations. Together, our findings show that vsiRNAs are readily detectable *in vitro* and *in vivo* after infection with PR8/3841.

## DISCUSSION

Many studies have demonstrated the suppressor role of influenza virus NS1 protein in RNAi. NS1 from different

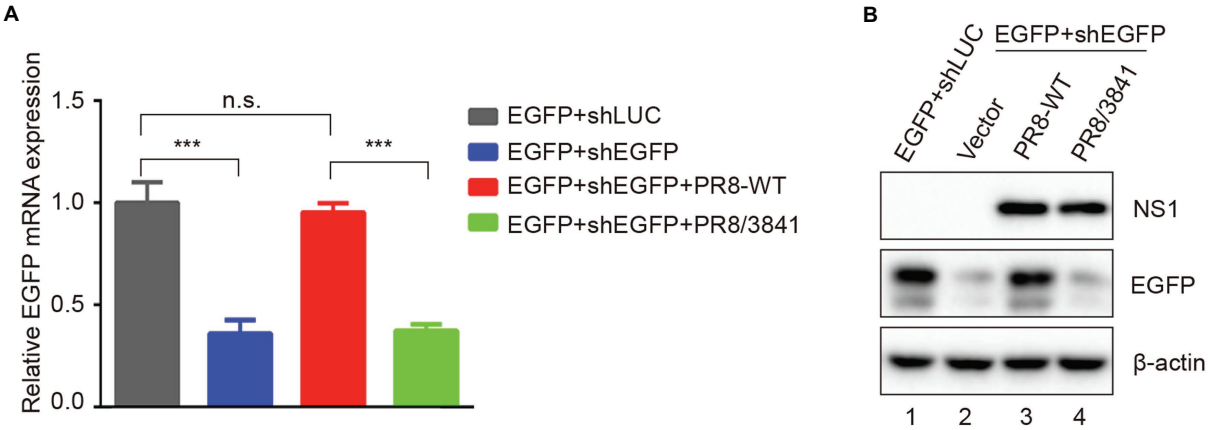


**FIGURE 7 |** R38A-K41A substitutions in NS1 abolish the inhibition of shRNA-mediated RNAi. **(A)** Relative mRNA levels of EGFP as quantified by qRT-PCR. 293 T cells were co-transfected with a plasmid encoding EGFP and EGFP-specific shRNA (shEGFP) or luciferase-specific shRNA (shLUC) as a negative control and then infected with PR8-WT (MOI = 1) or PR8/3841 (MOI = 1). After 48 h post-transfection, total RNAs were extracted, and the level of EGFP mRNA was examined by qRT-PCR. The experiments were repeated three times independently. The mRNA level of EGFP+shLUC group was set as 1. ***$p < 0.001$ (Student's t-test). ns indicates no significance. **(B)** Western blotting detection of EGFP, NS1, and $\beta$-actin proteins.

subtypes of influenza viruses suppress RNA silencing *via* dsRBD in Drosophila (Li et al., 2004). NS1 of IAV binds to siRNA and serves as a suppressor of RNA silencing in plants (Bucher et al., 2004). Moreover, we previously reported that NS1 inhibits the generation of vsiRNAs in IAV-infected mammalian cells (Li et al., 2016). An important function of NS1 RBD is binding dsRNA to mediate protein–protein interactions (Chen et al., 2020a). However, not all interactions that occur in RBD are associated with dsRNA. For instance, NS1 directly interacts with importin-α isoforms *via* its amino acids R35, R38, and K41 (Melen et al., 2007). In this study, RNase A and RNase III were used to remove ssRNA and dsRNA. Our results showed that NS1 likely formed an RNA-independent complex with TRBP *in vitro* and TRBP may not compete with dsRNA for binding to NS1. Therefore, as a VSR, NS1 uses various mechanisms for not only dsRNA binding but also interacting with TRBP to interfere with Dicer-mediated sRNA induction (**Figure 9**). In addition to the role in small RNA processing, TRBP also functions as a PKR inhibitor to suppress the phosphorylation of PKR and eIF2α in interferon response (Park et al., 1994). Besides, NS1 interacts with PKR *via* its 123–127 aa and inhibits translation (Min et al., 2007). The interaction of NS1 and TRBP is likely to affect the activity of PKR indirectly. Future studies should examine whether virus replication is affected by the PKR pathway.

MiRNA expression is influenced by multiple factors. Two factors that we are mainly concerned with include the TRBP protein and viral infection. In this study, we generated 293 T TRBP-KO cells and found that the isoform of miR126-3p and the abundance let-7a-5p were significantly downregulated, which are consistent with the findings of previous studies (Chendrimada et al., 2005; Ota et al., 2013; Kim et al., 2014). There are several reports about the inhibition of IAV in miRNA maturation. Terrier et al. reveal that five miRNAs (miR-21, miR-29a, miR-29b, miR-146a, and miR-452) are downregulated in human lung epithelial cells (A549) infected with H1N1 and H3N2 IAV (Terrier et al., 2013). MiRNA microarray has been used to demonstrate that four miRNAs (miR-221-3p, miR-22-3p, miR-20a-5p, and miR-3,613-3p) are upregulated and two miRNAs (miR-3,178 and miR-4,505) are downregulated in HEK293 cells stably expressing the NS1 protein of H5N1 IAV (Jiao et al., 2019). Another microarray study indicates that 22 and 114 miRNAs in lungs are downregulated at 7 and 15 days post-infection when BALB/c mice are infected with PR8-WT (Tan et al., 2014). However, the mechanism by which the IAV NS1 protein regulates miRNAs is unclear. Here, we compared the effects of miRNA production between NS1 and NS1 38/41 and found that let-7a-5p and miR-21 were downregulated by NS1-TRBP interaction. Based on these results, there are still some issues needed to be resolved in future studies. First, we only tested a few miRNAs, which may not reflect the overall miRNA expression. Second, more types of cells need to be analyzed, preferably the results of *in vivo* IAV infection.

Previous studies have demonstrated that the recombinant viruses containing R38A and K41A mutations in NS1 increase the expression of IFN-$\alpha/\beta$ and are attenuated in cells and mice (Talon et al., 2000; Donelan et al., 2003; Ramos et al., 2013). In our study, PR8/3841 induces vsiRNAs following infection, activating the antiviral RNAi *in vivo* and *in vitro*. Dicer-mediated cleavage of viral dsRNAs into vsiRNAs leads to suppression of viral replication by knocking down viral genes. Our recent study indicates that NoV-derived siRNAs have antiviral function *in vivo* by constructing a recombinant SINV containing part of NoV genomic RNA 1 sequences (Zhang et al., 2021). In addition, Zhou and colleagues designed peptides targeting the 3A protein of enterovirus A71 (EV-A71), which abrogate VSR function and promote

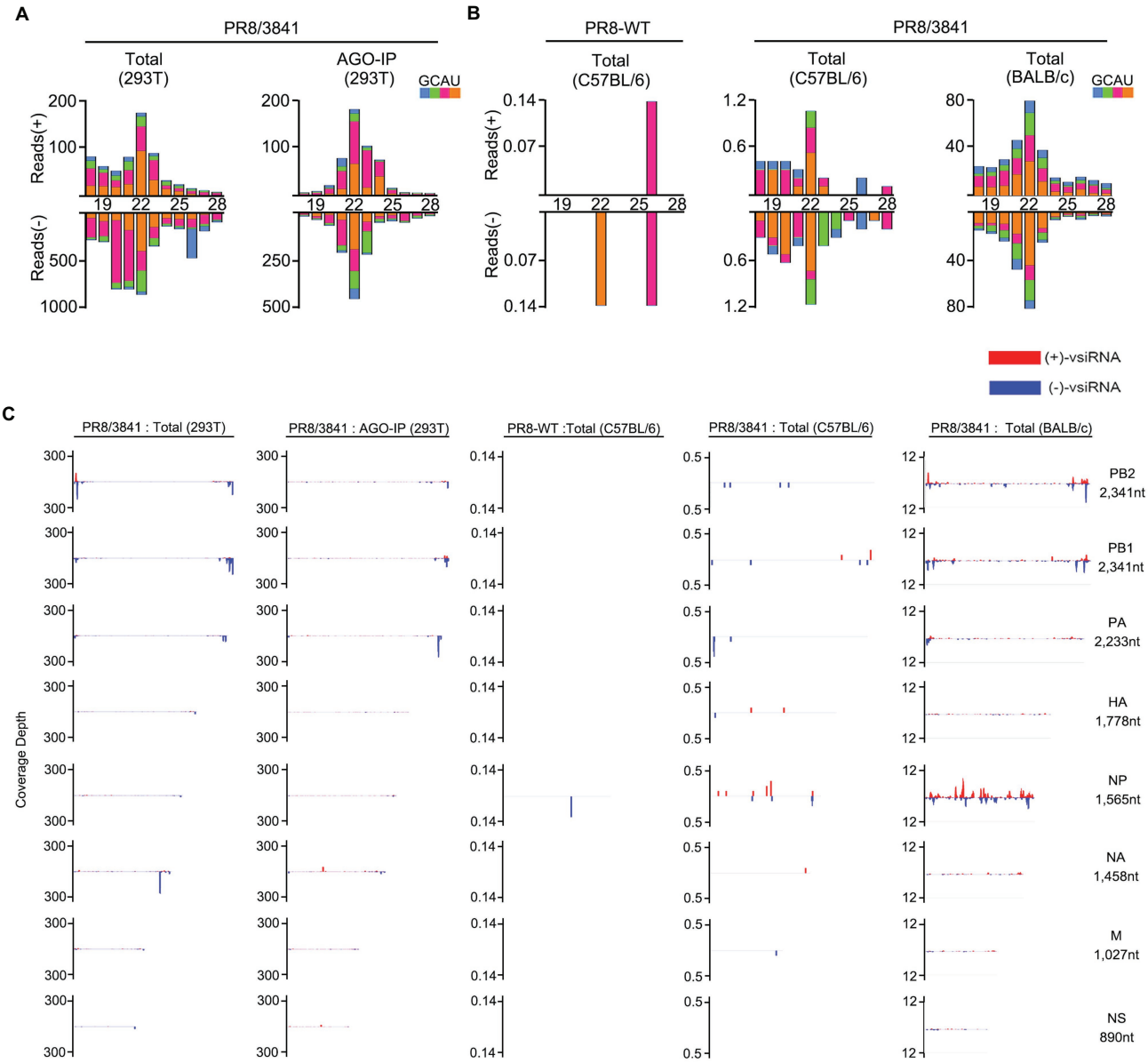


**FIGURE 8 |** The abundant vsiRNAs produced in mammalian cells and mice with PR8/3841 infection. **(A)** Properties of vsiRNAs (per million total mature miRNAs) sequenced from 293T cells without or with AGO-IP (at 1 dpi). Size distribution, abundance, the 5′-nucleotide preference of vsiRNAs (per million total 18–28 nt reads) with PR8/3841 infection. **(B)** Properties of vsiRNAs (per million total mature miRNAs) sequenced from adult C57BL/6 or BALB/c mice (at 4 dpi) infected with PR8-WT or PR8/3841. Size distribution, abundance, the 5′-nucleotide preference of vsiRNAs (per million total 18–28 nt reads) with PR8-WT or PR8/3841 infection. **(C)** Relative abundance of 21–23 nt vsiRNA hotspots mapped to PR8-WT or PR8/3841 genomic RNAs, presented from the 3′ end to the 5′ end.

vsiRNAs production (Fang et al., 2021). These vsiRNAs are able to load into AGO proteins and silence cognate viral RNA *in vivo*. In present work, we show for the first time the production of IAV-derived siRNAs *in vivo*. These IAV vsiRNAs have the characteristics of canonical viral siRNAs and are likely to have antiviral functions. Because both NoV and SINV can infect the muscle tissue of mice, we generated the SINV reporting system to detect the function of vsiRNAs from the NoV virus (Zhang et al., 2021). Unfortunately, because IAV mainly replicates in lung tissues, the SINV reporting system is not suitable for testing the function of IAV vsiRNAs. Future work needs to establish an optimized reporter system to confirm the antiviral function of these IAV siRNAs *in vivo*.

## DATA AVAILABILITY STATEMENT

The datasets presented in this study can be found in online repositories. The names of the repository/repositories and

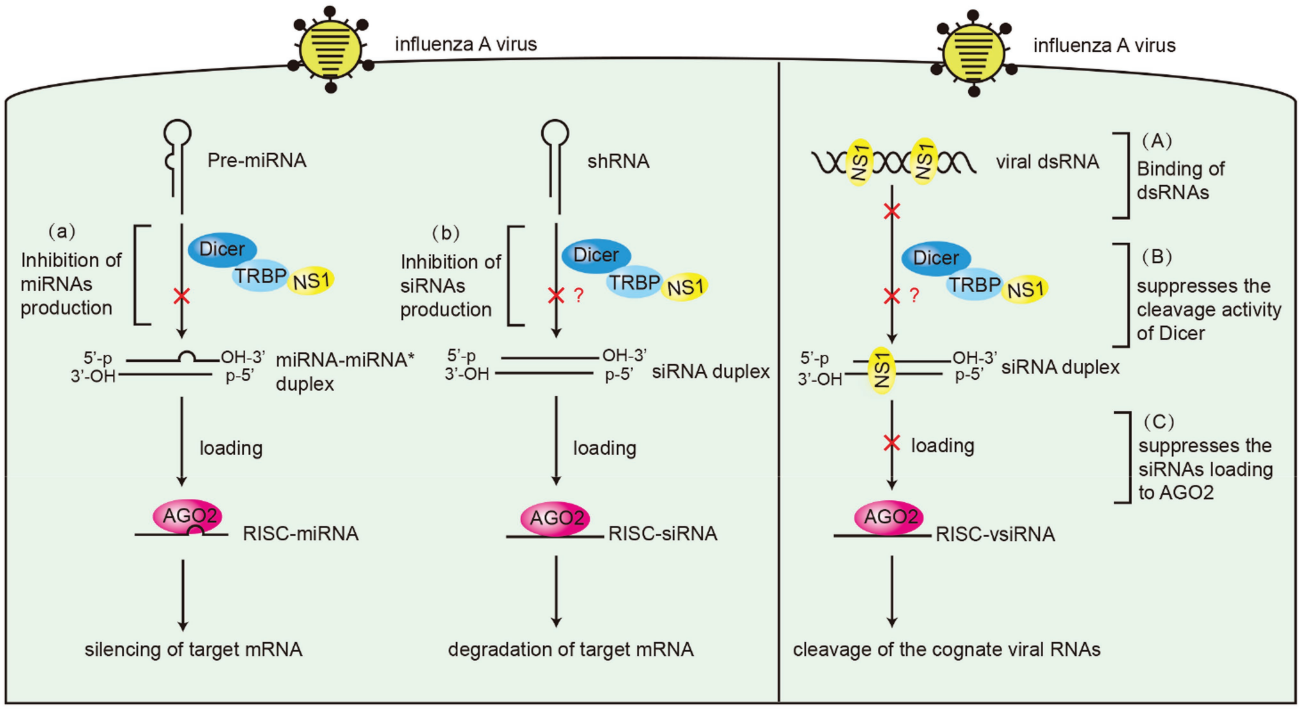


**FIGURE 9 |** Schematic model of the suppressor roles of NS1 in RNAi. Left panel: **(A)** NS1 inhibits miRNAs production by interacting with TRBP. **(B)** NS1 inhibits shRNA-mediated RNAi by interacting with TRBP. Right panel: **(A)** NS1 inhibits siRNA production by directly binding to dsRNAs. **(B)** NS1 suppresses the cleavage activity of Dicer by interacting with TRBP. **(C)** NS1 suppresses siRNA loading onto AGO2 by directly binding to siRNAs.

accession number(s) can be found at: https://www.ncbi.nlm.nih.gov/geo/, GSE189776.

## ETHICS STATEMENT

The animal study was reviewed and approved by all animal experiments were carried out under the guidelines of the Institutional Animal Care and Use Committee, Fudan University of China.

## AUTHOR CONTRIBUTIONS

QW and YL performed all infection experiments and wrote the final manuscript. YX performed bioinformatics analyses. JW, ZL, and BW assisted with some experiments. YL conceived the study and designed experiments. All authors contributed to the article and approved the submitted version.

## FUNDING

This study was supported by grants from the National Natural Science Foundation of China (31770179 and 91640111) and Innovation Program of Shanghai Municipal Education Commission (2017-01-07-00-07-E00015).

## ACKNOWLEDGMENTS

The authors thank A. García-Sastre and Y. Zhou for providing materials.

## SUPPLEMENTARY MATERIAL

The Supplementary Material for this article can be found online at: https://www.frontiersin.org/articles/10.3389/fmicb.2022.859420/full#supplementary-material

## REFERENCES

Ampomah, P. B., and Lim, L. H. K. (2020). Influenza A virus-induced apoptosis and virus propagation. *Apoptosis* 25, 1–11. doi: 10.1007/s10495-019-01575-3

Bamunuarachchi, G., Pushparaj, S., and Liu, L. (2021). Interplay between host non-coding RNAs and influenza viruses. *RNA Biol.* 18, 767–784. doi: 10.1080/15476286.2021.1872170

Bernstein, E., Caudy, A. A., Hammond, S. M., and Hannon, G. J. (2001). Role for a bidentate ribonuclease in the initiation step of RNA interference. *Nature* 409, 363–366. doi: 10.1038/35053110

Bornholdt, Z. A., and Prasad, B. V. (2008). X-ray structure of NS1 from a highly pathogenic H5N1 influenza virus. *Nature* 456, 985–988. doi: 10.1038/nature07444

Bucher, E., Hemmes, H., de Haan, P., Goldbach, R., and Prins, M. (2004). The influenza A virus NS1 protein binds small interfering RNAs and

suppresses RNA silencing in plants. *J. Gen. Virol.* 85, 983–991. doi: 10.1099/vir.0.19734-0

Chen, Z., Li, Z., Hu, X., Xie, F., Kuang, S., Zhan, B., et al. (2020b). Structural basis of human helicase DDX21 in RNA binding, unwinding, and antiviral signal activation. *Adv Sci (Weinh)* 7:2000532. doi: 10.1002/advs.202000532

Chen, G., Ma, L. C., Wang, S., Woltz, R. L., Grasso, E. M., Montelione, G. T., et al. (2020a). A double-stranded RNA platform is required for the interaction between a host restriction factor and the NS1 protein of influenza A virus. *Nucleic Acids Res.* 48, 304–315. doi: 10.1093/nar/gkz1094

Chendrimada, T. P., Gregory, R. I., Kumaraswamy, E., Norman, J., Cooch, N., Nishikura, K., et al. (2005). TRBP recruits the dicer complex to ago 2 for micro RNA processing and gene silencing. *Nature* 436, 740–744. doi: 10.1038/nature03868

Chien, C., Xu, Y., Xiao, R., Aramini, J. M., Sahasrabudhe, P. V., Krug, R. M., et al. (2004). Biophysical characterization of the complex between double-stranded RNA and the N-terminal domain of the NS1 protein from influenza A virus: evidence for a novel RNA-binding mode. *Biochemistry* 43, 1950–1962. doi: 10.1021/bi030176o

Coughlan, L., and Palese, P. (2018). Overcoming barriers in the path to a universal influenza virus vaccine. *Cell Host Microbe* 24, 18–24. doi: 10.1016/j.chom.2018.06.016

Daniels, S. M., Melendez-Pena, C. E., Scarborough, R. J., Daher, A., Christensen, H. S., El Far, M., et al. (2009). Characterization of the TRBP domain required for dicer interaction and function in RNA interference. *BMC Mol. Biol.* 10:38. doi: 10.1186/1471-2199-10-38

de Chassey, B., Aublin-Gex, A., Ruggieri, A., Meyniel-Schicklin, L., Pradezynski, F., Davoust, N., et al. (2013). The interactomes of influenza virus NS1 and NS2 proteins identify new host factors and provide insights for ADAR1 playing a supportive role in virus replication. *PLoS Pathog.* 9:e1003440. doi: 10.1371/journal.ppat.1003440

de Vries, W., Haasnoot, J., Fouchier, R., de Haan, P., and Berkhout, B. (2009). Differential RNA silencing suppression activity of NS1 proteins from different influenza A virus strains. *J. Gen. Virol.* 90, 1916–1922. doi: 10.1099/vir.0.008284-0

Ding, S. W. (2010). RNA-based antiviral immunity. *Nat. Rev. Immunol.* 10, 632–644. doi: 10.1038/nri2824

Ding, S. W., Han, Q., Wang, J., and Li, W. X. (2018). Antiviral RNA interference in mammals. *Curr. Opin. Immunol.* 54, 109–114. doi: 10.1016/j.coi.2018.06.010

Donelan, N. R., Basler, C. F., and Garcia-Sastre, A. (2003). A recombinant influenza A virus expressing an RNA-binding-defective NS1 protein induces high levels of beta interferon and is attenuated in mice. *J. Virol.* 77, 13257–13266. doi: 10.1128/jvi.77.24.13257-13266.2003

Fabozzi, G., Nabel, C. S., Dolan, M. A., and Sullivan, N. J. (2011). Ebolavirus proteins suppress the effects of small interfering RNA by direct interaction with the mammalian RNA interference pathway. *J. Virol.* 85, 2512–2523. doi: 10.1128/JVI.01160-10

Fang, Y., Liu, Z., Qiu, Y., Kong, J., Fu, Y., Liu, Y., et al. (2021). Inhibition of viral suppressor of RNAi proteins by designer peptides protects from enteroviral infection in vivo. *Immunity* 54, 2231–2244.e6. doi: 10.1016/j.immuni.2021.08.027

Gack, M. U., Albrecht, R. A., Urano, T., Inn, K. S., Huang, I. C., Carnero, E., et al. (2009). Influenza A virus NS1 targets the ubiquitin ligase TRIM25 to evade recognition by the host viral RNA sensor RIG-I. *Cell Host Microbe* 5, 439–449. doi: 10.1016/j.chom.2009.04.006

Guo, Z., Li, Y., and Ding, S. W. (2019). Small RNA-based antimicrobial immunity. *Nat. Rev. Immunol.* 19, 31–44. doi: 10.1038/s41577-018-0071-x

Haase, A. D., Jaskiewicz, L., Zhang, H., Laine, S., Sack, R., Gatignol, A., et al. (2005). TRBP, a regulator of cellular PKR and HIV-1 virus expression, interacts with dicer and functions in RNA silencing. *EMBO Rep.* 6, 961–967. doi: 10.1038/sj.embor.7400509

Haasnoot, J., de Vries, W., Geutjes, E. J., Prins, M., de Haan, P., and Berkhout, B. (2007). The Ebola virus VP35 protein is a suppressor of RNA silencing. *PLoS Pathog.* 3:e86. doi: 10.1371/journal.ppat.0030086

Hale, B. G., Randall, R. E., Ortin, J., and Jackson, D. (2008). The multifunctional NS1 protein of influenza A viruses. *J. Gen. Virol.* 89, 2359–2376. doi: 10.1099/vir.0.2008/004606-0

Han, Q., Chen, G., Wang, J., Jee, D., Li, W. X., Lai, E. C., et al. (2020). Mechanism and function of antiviral RNA interference in mice. *mBio* 11, e03278–03219. doi: 10.1128/mBio.03278-19

Heyam, A., Lagos, D., and Plevin, M. (2015). Dissecting the roles of TRBP and PACT in double-stranded RNA recognition and processing of noncoding RNAs. *Wiley Interdiscip Rev RNA* 6, 271–289. doi: 10.1002/wrna.1272

Hutvágner, G., McLachlan, J., Pasquinelli Amy, E., Bálint, É., Tuschl, T., and Zamore Phillip, D. (2001). A cellular function for the RNA-interference enzyme dicer in the maturation of the let-7 small temporal RNA. *Science* 293, 834–838. doi: 10.1126/science.1062961

Jiao, H., Zheng, Z., Shuai, X., Wu, L., Chen, J., Luo, Y., et al. (2019). Micro RNA expression profiles from HEK293 cells expressing H5N1 avian influenza virus non-structural protein 1. *Innate Immun.* 25, 110–117. doi: 10.1177/1753425919826342

Jinek, M., and Doudna, J. A. (2009). A three-dimensional view of the molecular machinery of RNA interference. *Nature* 457, 405–412. doi: 10.1038/nature07755

Ji-Young Min, R. M. K. (2006). The primary function of RNA binding by the influenza A virus NS1 protein in infected cells: inhibiting the 2`-5` oligo (A) synthetase/RNase L pathway. *PNAS* 103, 7100–7105. doi: 10.1073/pnas.0602184103

Kim, Y., Yeo, J., Lee, J. H., Cho, J., Seo, D., Kim, J. S., et al. (2014). Deletion of human tarbp 2 reveals cellular micro RNA targets and cell-cycle function of TRBP. *Cell Rep.* 9, 1061–1074. doi: 10.1016/j.celrep.2014.09.039

Kok, K. H., Ng, M. H., Ching, Y. P., and Jin, D. Y. (2007). Human TRBP and PACT directly interact with each other and associate with dicer to facilitate the production of small interfering RNA. *J. Biol. Chem.* 282, 17649–17657. doi: 10.1074/jbc.M611768200

Koliopoulos, M. G., Lethier, M., van der Veen, A. G., Haubrich, K., Hennig, J., Kowalinski, E., et al. (2018). Molecular mechanism of influenza A NS1-mediated TRIM25 recognition and inhibition. *Nat. Commun.* 9:1820. doi: 10.1038/s41467-018-04214-8

Krammer, F., Smith, G. J. D., Fouchier, R. A. M., Peiris, M., Kedzierska, K., Doherty, P. C., et al. (2018). Influenza. *Nat. Rev. Dis. Primers* 4:3. doi: 10.1038/s41572-018-0002-y

Krug, R. M. (2015). Functions of the influenza A virus NS1 protein in antiviral defense. *Curr. Opin. Virol.* 12, 1–6. doi: 10.1016/j.coviro.2015.01.007

Krug, R. M., Yuan, W., Noah, D. L., and Latham, A. G. (2003). Intracellular warfare between human influenza viruses and human cells: the roles of the viral NS1 protein. *Virology* 309, 181–189. doi: 10.1016/s0042-6822(03)00119-3

Kurzynska-Kokorniak, A., Koralewska, N., Pokornowska, M., Urbanowicz, A., Tworak, A., Mickiewicz, A., et al. (2015). The many faces of dicer: the complexity of the mechanisms regulating dicer gene expression and enzyme activities. *Nucleic Acids Res.* 43, 4365–4380. doi: 10.1093/nar/gkv328

Lecellier, C.-H., Dunoyer, P., Arar, K., Lehmann-Che, J., Eyquem, S., Himber, C., et al. (2005). A cellular MicroRNA mediates antiviral defense in human cells. *Science* 308, 557–560. doi: 10.1126/science.1108784

Lee, H. Y., and Doudna, J. A. (2012). TRBP alters human precursor microRNA processing in vitro. *RNA* 18, 2012–2019. doi: 10.1261/rna.035501.112

Lee, Y., Hur, I., Park, S. Y., Kim, Y. K., Suh, M. R., and Kim, V. N. (2006). The role of PACT in the RNA silencing pathway. *EMBO J.* 25, 522–532. doi: 10.1038/sj.emboj.7600942

Lee, S., Song, J., Kim, S., Kim, J., Hong, Y., Kim, Y., et al. (2013). Selective degradation of host MicroRNAs by an intergenic HCMV noncoding RNA accelerates virus production. *Cell Host Microbe* 13, 678–690. doi: 10.1016/j.chom.2013.05.007

Li, Y., Basavappa, M., Lu, J., Dong, S., Cronkite, D. A., Prior, J. T., et al. (2016). Induction and suppression of antiviral RNA interference by influenza A virus in mammalian cells. *Nat. Microbiol.* 2:16250. doi: 10.1038/nmicrobiol.2016.250

Li, W.-X., Li, H., Lu, R., Li, F., Dus, M., Atkinson, P., et al. (2004). Interferon antagonist proteins of influenza and vaccinia viruses are suppressors of RNA silencing. *Proc. Natl. Acad. Sci. U. S. A.* 101, 1350–1355. doi: 10.1073/pnas.0308308100

Li, Y., Lu, J., Han, Y., Fan, X., and Ding, S. W. (2013). RNA interference functions as an antiviral immunity mechanism in mammals. *Science* 342, 231–234. doi: 10.1126/science.1241911

Li, S., Min, J. Y., Krug, R. M., and Sen, G. C. (2006). Binding of the influenza A virus NS1 protein to PKR mediates the inhibition of its activation by either PACT or double-stranded RNA. *Virology* 349, 13–21. doi: 10.1016/j.virol.2006.01.005

Li, L., Wong, J. Y., Wu, P., Bond, H. S., Lau, E. H. Y., Sullivan, S. G., et al. (2018). Heterogeneity in estimates of the impact of influenza on population

mortality: a systematic review. *Am. J. Epidemiol.* 187, 378–388. doi: 10.1093/aje/kwx270

Maillard, P. V., Ciaudo, C., Marchais, A., Li, Y., Jay, F., Ding, S. W., et al. (2013). Antiviral RNA interference in mammalian cells. *Science* 342, 235–238. doi: 10.1126/science.1241930

Melen, K., Kinnunen, L., Fagerlund, R., Ikonen, N., Twu, K. Y., Krug, R. M., et al. (2007). Nuclear and nucleolar targeting of influenza A virus NS1 protein: striking differences between different virus subtypes. *J. Virol.* 81, 5995–6006. doi: 10.1128/JVI.01714-06

Melo, S. A., Ropero, S., Moutinho, C., Aaltonen, L. A., Yamamoto, H., Calin, G. A., et al. (2009). A TARBP2 mutation in human cancer impairs microRNA processing and DICER1 function. *Nat. Genet.* 41, 365–370. doi: 10.1038/ng.317

Mibayashi, M., Martinez-Sobrido, L., Loo, Y. M., Cardenas, W. B., Gale, M., and Garcia-Sastre, A. (2007). Inhibition of retinoic acid-inducible gene I-mediated induction of beta interferon by the NS1 protein of influenza A virus. *J. Virol.* 81, 514–524. doi: 10.1128/JVI.01265-06

Min, J. Y., Li, S., Sen, G. C., and Krug, R. M. (2007). A site on the influenza A virus NS1 protein mediates both inhibition of PKR activation and temporal regulation of viral RNA synthesis. *Virology* 363, 236–243. doi: 10.1016/j.virol.2007.01.038

Moon, S. L., Dodd, B. J., Brackney, D. E., Wilusz, C. J., Ebel, G. D., and Wilusz, J. (2015). Flavivirus sf RNA suppresses antiviral RNA interference in cultured cells and mosquitoes and directly interacts with the RNAi machinery. *Virology* 485, 322–329. doi: 10.1016/j.virol.2015.08.009

Moriyama, M., Chen, I. Y., Kawaguchi, A., Koshiba, T., Nagata, K., Takeyama, H., et al. (2016). The RNA- and TRIM25-binding domains of influenza virus NS1 protein are essential for suppression of NLRP3 Inflammasome-mediated interleukin-1beta secretion. *J. Virol.* 90, 4105–4114. doi: 10.1128/JVI.00120-16

Nemeroff, M. E., Barabino, S. M. L., Li, Y., Keller, W., and Krug, R. M. (1998). Influenza virus NS1 protein interacts with the cellular 30 kDa subunit of CPSF and inhibits 3′ end formation of cellular pre-mRNAs. *Mol. Cell* 1, 991–1000. doi: 10.1016/S1097-2765(00)80099-4

Neumann, G., Chen, H., Gao, G. F., Shu, Y., and Kawaoka, Y. (2010). H5N1 influenza viruses: outbreaks and biological properties. *Cell Res.* 20, 51–61. doi: 10.1038/cr.2009.124

Ota, H., Sakurai, M., Gupta, R., Valente, L., Wulff, B. E., Ariyoshi, K., et al. (2013). ADAR1 forms a complex with dicer to promote microRNA processing and RNA-induced gene silencing. *Cell* 153, 575–589. doi: 10.1016/j.cell.2013.03.024

Park, H., Davies, M. V., Langland, J. O., Chang, H. W., Nam, Y. S., Tartaglia, J., et al. (1994). TAR RNA-binding protein is an inhibitor of the interferon-induced protein kinase PKR. *Proc. Natl. Acad. Sci.* 91, 4713–4717. doi: 10.1073/pnas.91.11.4713

Pedersen, I. M., Cheng, G., Wieland, S., Volinia, S., Croce, C. M., Chisari, F. V., et al. (2007). Interferon modulation of cellular microRNAs as an antiviral mechanism. *Nature* 449, 919–922. doi: 10.1038/nature06205

Qian, X. Y., Alonso-Caplen, F., and Krug, R. M. (1994). Two functional domains of the influenza virus NS1 protein are required for regulation of nuclear export of mRNA. *J. Virol.* 68, 2433–2441. doi: 10.1128/jvi.68.4.2433-2441.1994

Qian, Q., Zhou, H., Shu, T., Mu, J., Fang, Y., Xu, J., et al. (2020). The capsid protein of Semliki Forest virus antagonizes RNA interference in mammalian cells. *J. Virol.* 94, e01233–e01219. doi: 10.1128/JVI.01233-19

Qiu, Y., Xu, Y., Zhang, Y., Zhou, H., Deng, Y. Q., Li, X. F., et al. (2017). Human virus-derived small RNAs can confer antiviral immunity in mammals. *Immunity* 46, 992–1004.e5. doi: 10.1016/j.immuni.2017.05.006

Ramos, I., Carnero, E., Bernal-Rubio, D., Seibert, C. W., Westera, L., Garcia-Sastre, A., et al. (2013). Contribution of double-stranded RNA and CPSF30 binding domains of influenza virus NS1 to the inhibition of type I interferon production and activation of human dendritic cells. *J. Virol.* 87, 2430–2440. doi: 10.1128/JVI.02247-12

Schierhorn, K. L., Jolmes, F., Bespalowa, J., Saenger, S., Peteranderl, C., Dzieciolowski, J., et al. (2017). Influenza A virus virulence depends on two amino acids in the N-terminal domain of its NS1 protein to facilitate inhibition of the RNA-dependent protein kinase PKR. *J. Virol.* 91, e00198–e0019817. doi: 10.1128/JVI.00198-17

Su, S., Bi, Y., Wong, G., Gray, G. C., Gao, G. F., and Li, S. (2015). Epidemiology, evolution, and recent outbreaks of avian influenza virus in China. *J. Virol.* 89, 8671–8676. doi: 10.1128/JVI.01034-15

Takahashi, T., Nakano, Y., Onomoto, K., Murakami, F., Komori, C., Suzuki, Y., et al. (2018). LGP2 virus sensor regulates gene expression network mediated by TRBP-bound microRNAs. *Nucleic Acids Res.* 46, 9134–9147. doi: 10.1093/nar/gky575

Takahashi, T., Zenno, S., Ishibashi, O., Takizawa, T., Saigo, K., and Ui-Tei, K. (2014). Interactions between the non-seed region of si RNA and RNA-binding RLC/RISC proteins, ago and TRBP, in mammalian cells. *Nucleic Acids Res.* 42, 5256–5269. doi: 10.1093/nar/gku153

Talon, J., Horvath Curt, M., Polley, R., Basler Christopher, F., Muster, T., Palese, P., et al. (2000). Activation of interferon regulatory factor 3 is inhibited by the influenza A virus NS1 protein. *J. Virol.* 74, 7989–7996. doi: 10.1128/JVI.74.17.7989-7996.2000

Tan, K. S., Choi, H., Jiang, X., Yin, L., Seet, J. E., Patzel, V., et al. (2014). Micro-RNAs in regenerating lungs: an integrative systems biology analysis of murine influenza pneumonia. *BMC Genomics* 15:587. doi: 10.1186/1471-2164-15-587

Tawaratsumida, K., Phan, V., Hrincius, E. R., High, A. A., Webby, R., Redecke, V., et al. (2014). Quantitative proteomic analysis of the influenza A virus nonstructural proteins NS1 and NS2 during natural cell infection identifies PACT as an NS1 target protein and antiviral host factor. *J. Virol.* 88, 9038–9048. doi: 10.1128/JVI.00830-14

Terrier, O., Textoris, J., Carron, C., Marcel, V., Bourdon, J. C., and Rosa-Calatrava, M. (2013). Host microRNA molecular signatures associated with human H1N1 and H3N2 influenza A viruses reveal an unanticipated antiviral activity for mi R-146a. *J. Gen. Virol.* 94, 985–995. doi: 10.1099/vir.0.049528-0

Wang, X., Li, M., Zheng, H., Muster, T., Palese, P., Beg Amer, A., et al. (2000). Influenza A virus NS1 protein prevents activation of NF-κB and induction of alpha/Beta interferon. *J. Virol.* 74, 11566–11573. doi: 10.1128/JVI.74.24.11566-11573.2000

Wang, W. R. K., Lynch, P., Chien, C. Y., Montelione, G. T., and Krug, R. M. (1999). RNA binding by the novel helical domain of the influenza virus NS1 protein requires its dimer structure and a small number of specific basic amino acids. *RNA* 5, 195–205. doi: 10.1017/S1355838299981621

Wang, H., Tian, Z., Xu, Y., Wang, Q., Ding, S.-W., and Li, Y. (2020). Altering intracellular localization of the RNA interference factors by influenza A virus non-structural protein 1. *Front. Microbiol.* 11:590904. doi: 10.3389/fmicb.2020.590904

Xie, Y., Wang, D., Lan, F., Wei, G., Ni, T., Chai, R., et al. (2017). An episomal vector-based CRISPR/Cas 9 system for highly efficient gene knockout in human pluripotent stem cells. *Sci. Rep.* 7:2320. doi: 10.1038/s41598-017-02456-y

Yassine, H. M., McTamney, P. M., Boyington, J. C., Ruckwardt, T. J., Crank, M. C., Smatti, M. K., et al. (2018). Use of Hemagglutinin stem probes demonstrate prevalence of broadly reactive group 1 influenza antibodies in human sera. *Sci. Rep.* 8:8628. doi: 10.1038/s41598-018-26538-7

Zeng, J., Dong, S., Luo, Z., Xie, X., Fu, B., Li, P., et al. (2020). The Zika virus capsid disrupts Corticogenesis by suppressing dicer activity and mi RNA biogenesis. *Cell Stem Cell* 27, 618–632.e9. doi: 10.1016/j.stem.2020.07.012

Zhang, Y., Li, Z., Ye, Z., Xu, Y., Wang, B., Wang, C., et al. (2020). The activation of antiviral RNA interference not only exists in neural progenitor cells but also in somatic cells in mammals. *Emerg Microbes Infect* 9, 1580–1589. doi: 10.1080/22221751.2020.1787798

Zhang, Y., Xu, Y., Dai, Y., Li, Z., Wang, J., Ye, Z., et al. (2021). Efficient dicer processing of virus-derived double-stranded RNAs and its modulation by RIG-I-like receptor LGP2. *PLoS Pathog.* 17:e1009790. doi: 10.1371/journal.ppat.1009790

Zheng, Z., Ke, X., Wang, M., He, S., Li, Q., Zheng, C., et al. (2013). Human microRNA hsa-miR-296-5p suppresses enterovirus 71 replication by targeting the viral genome. *J. Virol.* 87, 5645–5656. doi: 10.1128/JVI.02655-12

**Conflict of Interest:** The authors declare that the research was conducted in the absence of any commercial or financial relationships that could be construed as a potential conflict of interest.

**Publisher's Note:** All claims expressed in this article are solely those of the authors and do not necessarily represent those of their affiliated organizations, or those of the publisher, the editors and the reviewers. Any product that may

be evaluated in this article, or claim that may be made by its manufacturer, is not guaranteed or endorsed by the publisher.

frontiers | Frontiers in Microbiology

TYPE Original Research
PUBLISHED 01 August 2022
DOI 10.3389/fmicb.2022.963218



OPEN ACCESS

EDITED BY
Quanjiao Chen,
Wuhan Institute of Virology (CAS), China

REVIEWED BY
Juan Li,
Shandong First Medical University, China
Guan-Zhu Han,
Nanjing Normal University, China

*CORRESPONDENCE
Min Liao
liaomin4545@zju.edu.cn
Jiyong Zhou
jyzhou@zju.edu.cn

SPECIALTY SECTION
This article was submitted to Virology, a section of the journal Frontiers in Microbiology

RECEIVED 07 June 2022
ACCEPTED 04 July 2022
PUBLISHED 01 August 2022

CITATION
Cui M, Huang Y, Wang X, Bian X, Du L, Yan Y, Gu J, Dong W, Zhou J and Liao M (2022) Genetic characterization and evolution of H6N6 subtype avian influenza viruses. *Front. Microbiol.* 13:963218. doi: 10.3389/fmicb.2022.963218



# Genetic characterization and evolution of H6N6 subtype avian influenza viruses

Mingxian Cui[1], Yanming Huang[1], Xingbo Wang[1], Xiyi Bian[1], Liuyang Du[1], Yan Yan[1], Jinyan Gu[1], Weiren Dong[1], Jiyong Zhou[1,2]* and Min Liao[1]*

[1]MOA Key Laboratory of Animal Virology, Department of Veterinary Medicine and Center of Veterinary Medical Sciences, Zhejiang University, Hangzhou, China, [2]Collaborative Innovation Center and State Key Laboratory for Diagnosis and Treatment of Infectious Diseases, The First Affiliated Hospital, Zhejiang University, Hangzhou, China

H6-subtype avian influenza virus (AIV) was prevalent in the world and could sporadically infect humans. Here, a new chicken-derived H6N6-subtype AIV strain A/chicken/Zhejiang/49/2021 (ZJ49) was isolated in Zhejiang Province, China in 2021. Phylogenetic analysis by Maximum likelihood methods showed that H6-subtype AIVs were classed into 13 groups according to HA gene. The ZJ49 strain belonged to the G12 group, which mainly consisted of strains from Asian and dominated in recent years. Based on NA gene, H6-subtype AIVs were divided into N6.1 and N6.2 clades according to the NA gene. The ZJ49 isolate was located in the N6.2e clade, which mainly consisted of the H5N6-subtype AIVs. Phylogenetic analysis by Bayesian methods showed that the effective quantity size of H6-subtype AIVs increased around 1990, reached a peak around 2015, declined after 2015, then kept in a stable level after 2018. The reassortment analysis predicted that the PB2, PA, and NA genes of ZJ49 may recombine with H5-subtype AIVs. The amino acid at 222 position of HA gene of ZJ49 strain mutated from A to V, suggesting that ZJ49 has a potential ability to cross species barriers. The four glycosylation sites were highly conserved, implying less impact on the fold and conception of HA stem structure. Our results revealed the complicated evolution, reassortment, and mutations of receptor binding sites of H6-subtype AIVs, which emphasize the importance to continuously monitor the epidemiology and evolution of H6-subtype AIVs.

KEYWORDS

**H6N6-subtype AIVs, genetic evolutionary, reassortment, SA receptors, glycosylation sites**

## Introduction

Avian influenza is a kind of avian infectious disease caused by the avian influenza viruses (Avian Influenza viruses, AIVs) characterized by respiratory system lesions or systemic sepsis. AIVs can be divided into low pathogenic AIVs (LPAIVs) and high pathogenic AIVs (HPAIVs; Germeraad et al., 2019). Compared with HPAIVs, LPAIVs

caused continuous effects to chickens in reducing egg production and even became a potential threat to human public health (Wang et al., 2014). H6-subtype AIVs belong to LPAIVs (Lin et al., 2020; Li et al., 2021). The H6 subtype AIV was first isolated from a turkey in 1965 (Munster et al., 2007; Rimondi et al., 2011), and subsequently from shorebirds and wild ducks (Downie et al., 1973; Sharp et al., 1993). Currently, the H6 viruses became one of the most predominant virus subtypes circulating in wild birds and domestic poultry throughout different continents (Hoque et al., 2015; Lee et al., 2017; Rimondi et al., 2018) and they were undergoing constant reassortment with different subtypes of viruses (Yuan et al., 2016; Kumar et al., 2018; Li et al., 2019). H6-subtype AIVs highly occurred in China as compared to other countries. Five subtypes of H6 influenza virus (H6N1, H6N2, H6N5, H6N6 and H6N8) co-circulated in Eastern China (Zhao et al., 2011), which formed a significant part of the natural influenza virus reservoir in domestic ducks. In China, the most representative strain, A/teal/Hong Kong/W312/97 (W312), was isolated during the "bird flu" incident in Hong Kong in 1997 (Cheung et al., 2007). The duck-derived H6N2 viruses were most frequently detected in China from 2002 to 2008, then the H6N6 viruses became the most epidemic subtype since 2009 (Zhao et al., 2011). H6N6 viruses had become the main circulating H6 subtype AIVs from 2014 to 2018 (Li et al., 2019; Cui et al., 2021).

Remarkably, H6 subtype AIVs can not only infect birds but also infect mammals. A strain of H6N6 was isolated from swine in Yangzhou, Eastern China in 2009 (Zhao et al., 2013). The first human infection with the A/Taiwan/2/2013 (H6N1) was reported on June 21, 2013 (Shi et al., 2013; Wei et al., 2013). Due to the lack of a commercial available vaccine, H6-subtype AIVs had continuously evolved and diversified into many distinct lineages in China and other Asian countries (Huang et al., 2010, 2012). These findings suggest that H6 subtype AIVs could cross the species barrier and infect mammals, including humans. Antigenic variation in the influenza virus had the potential to cause rapid adaptation and led to an unexpected evolutionary road (Liu et al., 2013; Morens et al., 2013). Therefore, extensive monitoring of influenza virus variation is necessary for understanding of the epidemiology of influenza virus. Here, a new H6N6-subtype AIV strain from chickens named A/chicken/Zhejiang/49/2021 (ZJ49) was isolated in Zhejiang, China in 2021. The genetic evolutionary, reassortment, and mutations of receptor binding sites of H6-subtype AIVs were analyzed to investigate the genetic evolution regulations and molecular characteristics. Our findings revealed that H6N6-subtype AIVs were likely to spread across species and recombine with highly pathogenic viruses.

# Materials and methods

## Sample collection and virus isolation

To investigate the prevalence of AIVs in Zhejiang Province, fixed location surveillance in poultry farms were conducted in four cities of Zhejiang Province in 2021. A total of 923 oropharyngeal and cloacal swabs including 810 from chickens and 113 from ducks were collected from apparently healthy poultry from four cities in Zhejiang, including Jiaxing ($n = 389$), Huzhou ($n = 294$), Zhoushan ($n = 100$), and Taizhou ($n = 140$). The samples in Zhoushan were free-range samples from farmers. The total RNA extracted from the samples was detected by RT-PCR using universal primers targeting the M gene (M-F: CGTAGACG CTTTGTCCAAAATGCC; M-R: AAGACGATCAAGAATCC ACAATA). All RT-PCR positive samples were isolated with 10-day-73 old SPF chicken embryos for 96 h at 37 °C for virus isolation. Hemagglutinin-positive samples were further confirmed by RT-PCR with above primers M-F and M-R. The isolate was serially passaged on chicken embryos and subjected to extract RNA for Next-generation sequencing (NGS).

## Whole-genome sequencing of AIV isolates and sequencing data assembly

The ultra-concentrated virus was sent to Genergy Bio-Technology (SHANGHAI) CO., LTD for Next-generation sequencing. The main methods were as follows: NGS (van Dijk et al., 2014) was used to determine the whole-genome sequences of AIV isolates. For NGS, the viral RNAs were quantified using the 2,100 Bio-analyzer System (Agilent Technologies). RT-PCR and cDNA synthesis were conducted using the Prime Script One-Step RT-PCR kit (Takara), with influenza A random primer. The sequencing libraries with an insert size of 200–400 bp were prepared by end-repairing, dA-tailing, adaptor ligation, and PCR amplification, all according to the instructions provided by the manufacturer (Illumina). The libraries were sequenced on an Illumina NovaSeq 6,000 Sequencer (Dillies et al., 2013) by 150 bp paired-end sequencing, and sequencing depth for AIVs isolates was 2G per sample.

NGS sequencing reads were processed and assembled as described previously (Yu et al., 2014). The filtered reads were mapped to the Influenza database to choose the best-matching reference sequences and determine genotypes. Burrows-Wheeler Aligner (BWA version 0.7.17; Li and Durbin, 2009) and SAMtools (version 1.10; Li et al., 2009) were then used to perform the reference-based assembly.

## Sequence retrieval and phylogenetic reconstruction

In order to describe the spatiotemporal evolution of H6-subtype AIVs, the H6NX and HXN6 influenza viruses were focused in this study. The data of the global distribution of H6NX are listed in Supplementary Table S1. The gene sequences of isolates with the full-length gene sequences of all H6NX HA gene sequences, HXN6 NA gene sequences, and all H6N6 internal fragments in the GISAID and Genbank Influenza Research Databases were combined. Identical sequences were removed

through RAxML-ng. Sequences derived from laboratory strains and containing ambiguous characters were also removed from the dataset. The Visual Studio code was used to remove the noncoding region and to keep the full length of the ORFs encoding each fragment genes. Only the longest ORFs were retained for each sequence. Nucleotide sequences were aligned using MAFFT (Katoh et al., 2002). Identical sequences were removed again by RAxML-ng. The total number of sequences for HA, NA, MP, NP, NS, PA, PB1, and PB2 were 2063, 3,338, 386, 386, 376, 308, 259, and 266, respectively. The accession number and the sequence source were listed in Supplementary Table S2.

All HA sequences from GISAID and Genbank were used to determine the distribution ratios of various subtypes across continents. Coding region sequences (CDS) were used for phylogenetic reconstruction using RAxML v8.2.4 (Stamatakis, 2014) based on the general time-reversible model and gamma distribution (GTR + G) model. The auto MRE bootstrapping convergence criterion (Pattengale et al., 2010) was applied to determine the most suitable number of replicates instead of the default 1,000 replicates. The selection of most suitable replicates of bootstrap was done as follow: after 50 replicates, all of the generated bootstrapped trees were repeatedly (1,000 permutations) split into two equal subsets and the Weighted Robinson–Foulds (WRF) distance was calculated between the majority-rule consensus trees of both subsets (for each permutation). Bootstrapping convergence was considered to be reached if over 99% of permutations have low WRF distances (<3%). In this case, convergence was reached after 400, 650, 900, 1,000, 750, 550, 420, and 550 replicates.

The phylogenetic tree was visualized using iTOL v4 (Letunic and Bork, 2016). For further analysis, the big HA tree was split into several different groups. The criteria for group selection were as follows: Collapse all clades whose average branch length distance to their leaves is below 0.15. The naming of branches and sub-branches in the NA evolutionary tree follows the topological rules of the evolutionary tree: The naming of primary branches follows "name of subtype/gene + '.' + number," Subclades are named with alternating letters and numbers, such as H5.2a. Try to follow the order of host (avian > human > swine > horse > dog) > space (Western hemisphere > Eastern hemisphere) > time (early period > later period).

## Evolutionary and reassortment analysis

The TempEst was used to assessed temporal signal in our data sets (Rambaut et al., 2016) and Path-sampling and Stepping-stone estimation approaches were used to assess the best fitting model through marginal likelihood estimation (Baele et al., 2013, 2016). The BEAST package (v2.6.6) was used to construct the maximum clade credibility (MCC) tree (Suchard et al., 2018). The best-fit nucleotide substitution model was selected using IQ-tree (Nguyen et al., 2015). We selected GTR + G distributed rate variation among sites in nucleotide substitution model, uncorrelated relaxed lognormal clock set in the molecular clock, Coalescent: Bayesian Skyline set in prior, total chain length was $4 \times 10^8$ and sampling every 1,000 steps. Four dependently runs were combined using Logcombiner. In addition, we used a coalescent-based nonparametric skyline prior to the tree topologies to model the effective avian size over time.

The reassortment events among the H6N6-subtype and other subtype viruses were carried out with the sequences which information were listed in Supplementary Table S3. ML phylogenetic trees inferred for HXN6-subtype AIVs HA and NA using RAxML under the general time-reversible substitution model with gamma-distributed rates across sites. In total, 1,000 bootstraps were evaluated to assess support values. Full genomes sequences were analyzed separately to detect reassortment events using RDP5 (He et al., 2020) and Similarity plot (Soli et al., 2019). A total of eight methods including RDP, GENECONV, 3Seq, Chimaera, SiScan, MaxChi, BootScan, and LARD implemented in RDP5 were applied. Reassortment detected by at least three of the eight methods with a value of $p$ cut off of 0.05 was considered as true reassortment (Sabir et al., 2016).

## The haemagglutinin binding site and N-glycosylation site

Amino acid glycosylation sites of ZJ49 isolate were predicted by NetNGlyc-1.0 prediction server[1] (Wang et al., 2006). The tertiary structure model (The template was 4wss.1.A) of ZJ49 HA protein was constructed through the SWISS-MODEL online server[2] (Waterhouse et al., 2018), and PyMOL (Version 2.0.7) was used for visual analysis to map the spatial location of receptor binding sites and glycosylation sites (Lu, 2020).

# Results

## Spatial distribution of the H6-subtype influenza virus

In 2021, a total of 923 pharyngeal and anal swabs were collected from Zhejiang Province, China. A total of 71 positive samples were detected, with a positive rate of 7.69% for AIV detection. Among them, the AIV positive rates of samples from Jiaxing, Huzhou, Zhoushan and Taizhou were 4.88% (19/389), 8.16% (24/294), 28% (28/100) and 0 (0/140), respectively. A strain of chicken-derived H6N6 virus (A/chicken/Zhejiang/49/2021, ZJ49) was isolated from the samples of Huzhou. The nucleotide sequence lengths of PB2, PB1, PA, HA, NA, NP, M, and NS fragments of ZJ49 were 2,280, 2,274, 2,151, 1701, 1,380, 1,497, 982, and 838 (Supplementary Table S4). Total of 2064 H6NX genome sequences including ZJ49 were collected from GISAID and Genbank (Supplementary Table S1), which strain informations were subjected to analysis of spatial distribution of H6NX subtype AIVs. There

1 https://services.healthtech.dtu.dk/service.php?NetNGlyc-1.0
2 https://swissmodel.expasy.org/interactive/

were differences in the proportion of isolates of each H6NX subtype in each continent, with the highest proportion of H6N6 isolates in Asia (about 43.25%; Figure 1A). H6N6-subtype AIVs were found in the three continents including Asia, Europe, and North America, with the highest distribution in Asia (about 96.73%; Figure 1A).

According to the phylogenetic tree (Figure 1B), 13 genetically distinct groups based on HA genes were identified. Most of the strains in the H6NX ML tree were isolated from ducks, indicating that ducks are the main host for H6-subtype AIVs. The number of strains originating from chickens was relatively small, and they were mainly distributed in China. The strains isolated in the early 1970s were mainly concentrated in North America to form G1 and G2 groups. H6N2 and H6N6-subtype AIVs co-evolved and were mainly distributed in the Asia continent especially China. The ZJ49 isolate was located in the G12 group and was most genetically related to A/duck/Hunan/2.06_YYGK86J3-OC/2018 (H6N6), which was consistent with the analysis by BLAST (Figure 1B; Supplementary Table S4). The genome nucleotide homology between these two strains was 98.53% (Supplementary Table S4). The NA subtypes of the G13 strains were more abundant and mainly composed of Eurasian strains and American strains. The strain of H6N1 isolated from human was located in this group.

The NA genes of the N6-subtype AIVs can be divided into two primary branches, N6.1 and N6.2, corresponding to the branches dominated by North America and Eurasia, respectively (Figure 1C). The North American clade was mainly composed of the H4N6-subtype AIVs, and the European clade was jointly composed of H4N6, H5N6 and H6N6-subtype AIVs. Five secondary clades were named N6.1a ~ e, within the N6.1 clade. The N6.1a ~ d branches correspond to the HXN6-subtype AIVs isolated earlier. Five secondary clades were named N6.2a ~ e within the N6.2 branch. The N6.2a ~ c branch was mainly composed of H4N6. N6.2d and N6.2e were dominated by H6N6 and H5N6, respectively. Among them, H4N6 and H5N6 were cross-distributed in N6.2a, and H5N6 and H6N6 were cross-distributed in N6.2d and N6.2e, suggesting that H5N6 may recombine with H4N6 and H6N6. The ZJ49 isolate was located in the N6.2e branch, which was mainly consisted of the H5N6-subtype AIVs.

According to the ML trees constructed based on the internal fragments of H6N6 (Figure 2), the distribution of H6N6 can be divided into the seven countries, including China, Viet Nam, United States, Canada, Korea, Russian Federation, and Japan. The results were consistent with the results of phylogenetic analysis based on the HA gene, in which the H6N6-subtype AIVs was mainly prevalent in China.

## Temporal distribution of the H6-subtype influenza virus

We explored temporal signal in sequence alignments using TempEst, as assessed by visual inspection and the correlation coefficient, $R^2$. The result indicated a positive correlation between genetic divergence and sampling time ($R^2 = 0.4008$) and appeared to be suitable for phylogenetic molecular clock analysis in BEAST (Figure 3A). The Stepping-stone and Path-sampling estimation approaches showed that the log marginal likelihood of Bayesian Skyline was −63461.546 (Figure 3B) and − 63407.094 (Figure 3C), respectively, indicating that the Bayesian skyline was the best fitting model. Due to the increasing number of samples, the effective quantity size increased around 1990, reached a peak around 2015, while declined after 2015, then kept in a stable level after 2018. (Figure 3D). The structure of the MCC tree based on HA was similar to the ML tree. The H6 subtype AIVs were clearly divided into G1–G13 (Figure 3E). Base on the MCC tree, the H6-subtype AIVs spread from North America to Eurasia around 1976. In recent years, H6-subtype AIVs were mainly distributed in G12 and G13 groups. In the NA gene genetic tree, N6.2d mainly consisted of H6N6 strains prevalent in Asia after 2005, and N6.2e mainly consisted of H5N6 strains prevalent in Asia after 2015 (Figure 1C). According to the phylogenetic tree (Figure 2), the ML tree constructed by the internal fragments of H6N6 can be also divided into the early branch and modern branch according to time.

## Reassortment analysis of the H6N6-subtype AIVs

A total of 37 HXN6 genome sequences were collected from GenBank (Supplementary Table S3). The results of reassortment analysis showed that the H6N6-subtype AIVs and H5N6-subtype AIVs recombined frequently (Figure 4A). To explore the reassortment events in ZJ49 isolates, we integrated the sequences that were genetically close to ZJ49 for reassortment prediction. The Simplot results showed that the full genomes sequences of ZJ49 had the highest similarity to the H6N6-subtype AIVs, but the PB2 and PA genes were closer to A/chicken/Zhejiang/194/2016 (H5N2) and the NA gene was closer to A/duck/Guangdong/GD01/2014(H5N6; Figure 4B). Among the RDP detection methods, there were 7 methods (RDP, GENECONV, 3Seq, Chimaera, SiScan, MaxChi, and BootScan) that also can detect the reassortment of ZJ49 (Figure 4C). The results showed that the ZJ49 isolate underwent genetic reassortment with the Major Parent A/duck/Guangdong/GD01/2014(H5N6) and the Minor Parent A/chicken/Zhejiang/194/2016 (H5N2). This result was consistent with the above result showed in Figure 4B. In conclusion, there was a high possibility that the ZJ49 gene recombined with the H5-subtype AIVs.

## Molecular characterization of the H6N6-subtype AIVs

The length of the ZJ49 HA coding region was 1701 bp, encoding a total of 566 amino acids. The HA trimer projects of ZJ49 can be divided into two domains: the membrane-distal

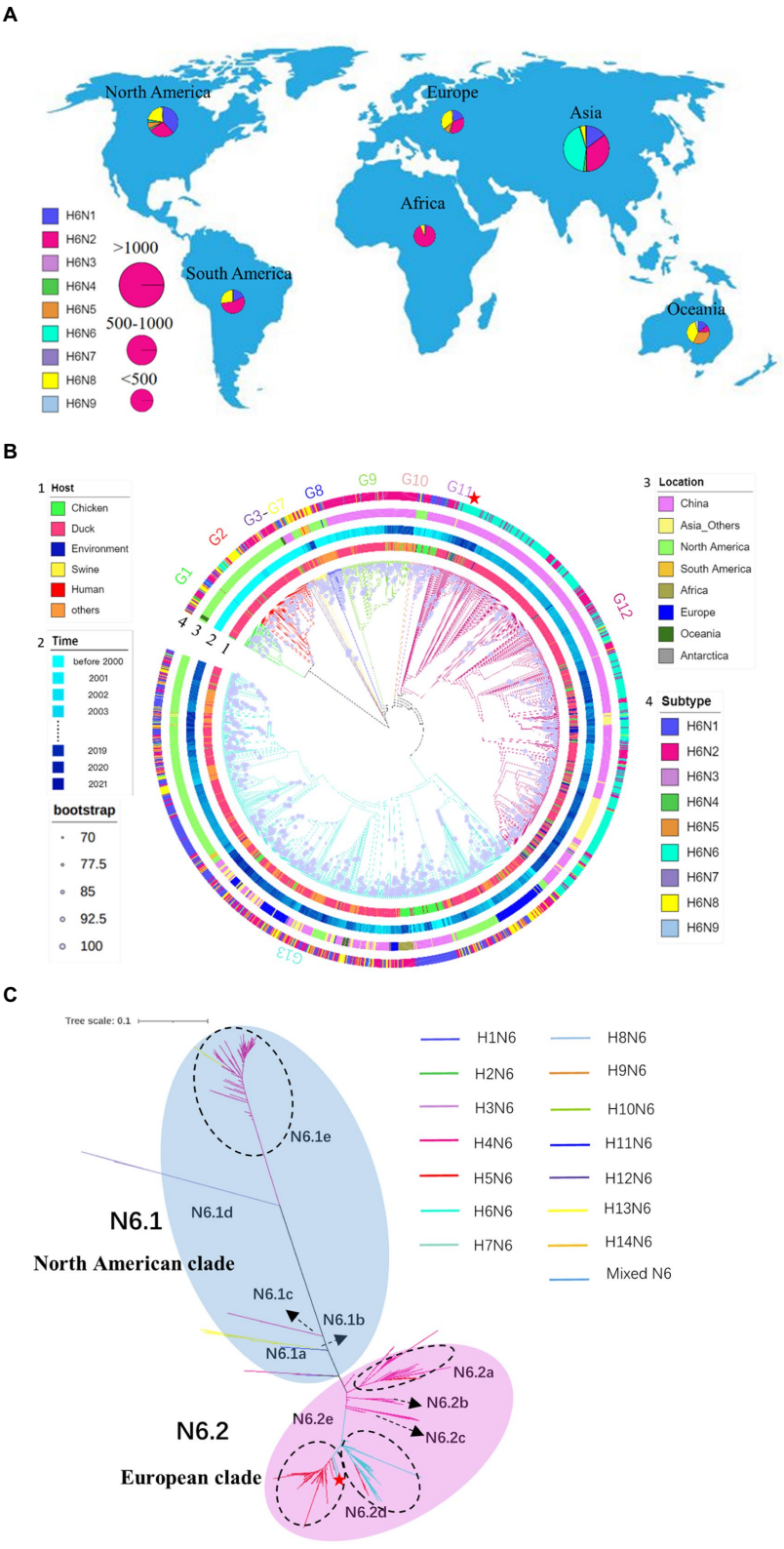


FIGURE 1
Spatial distribution of the H6-subtype influenza virus. **(A)** Global distribution of H6NX isolates. The proportion of isolates for each subtype category is visualized in a pie chart. The size of the pie chart is proportional to the number of isolates in each continent. **(B)** Phylogeny and groups of H6NX HA. Only bootstrap values≥70% are visualized as a purple circle in the middle of the branch. The size of the circle is proportional to the bootstrap value. Categories of virus (such as subtype, host, location, time) are identified by different colors of circles in the outer part of the tree. Phylogenetic independent groups are indicated with different colors of branches. **(C)** Phylogeny and groups of HXN6 NA. Tree scale is 0.1. Different subtypes are represented by different colored branches. ZJ49 is indicated by a red five-pointed star.

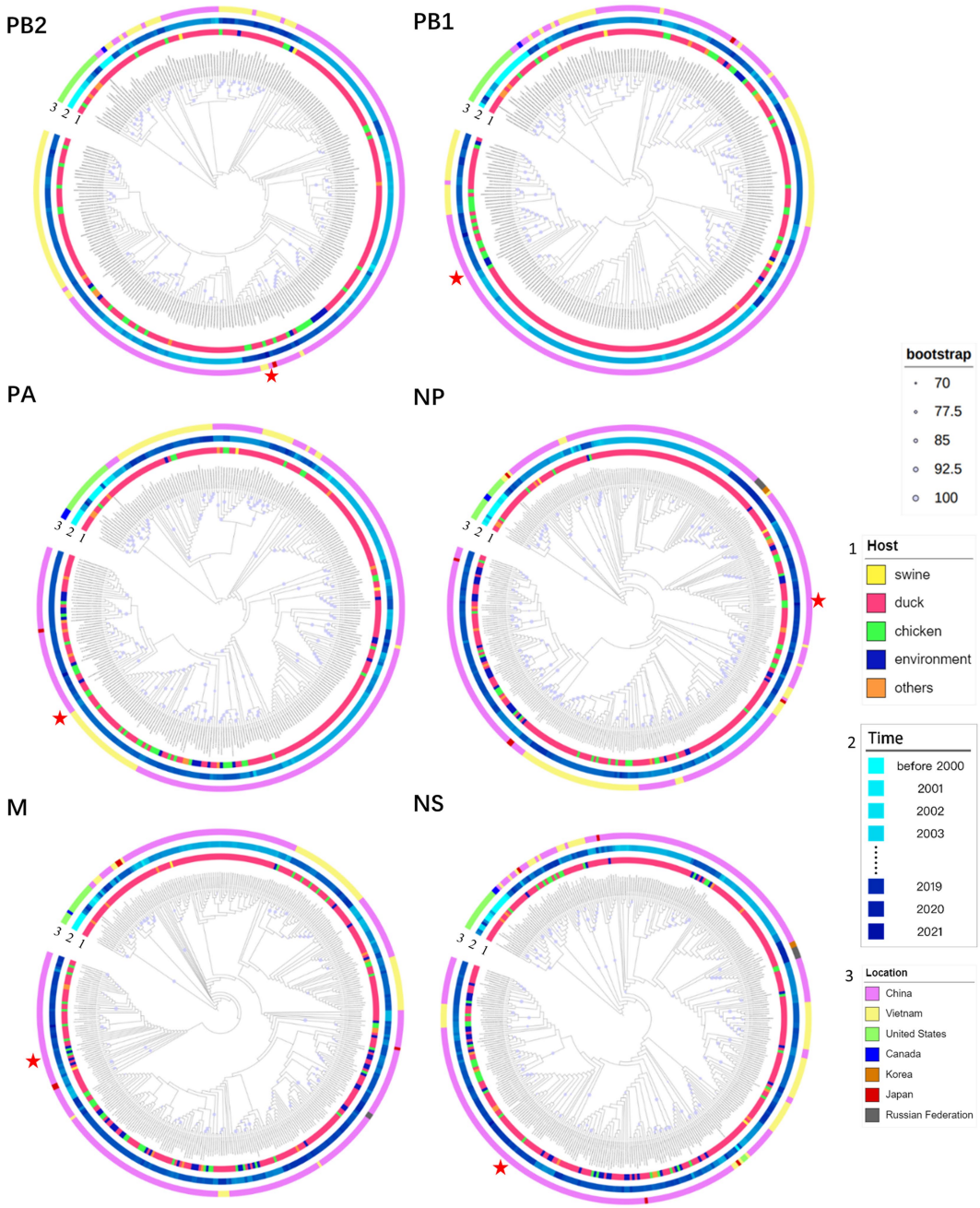


FIGURE 2
Phylogeny and groups of PB2, PB1, PA, NP, M, and NS of H6N6. Only bootstrap values≥70% are indicated as a purple circle in the middle of the branch. The size of the circle is proportional to the bootstrap value. Categories of viruses (such as host, and location) are identified by different colors. ZJ49 is indicated by a red five-pointed star.

globular domain and the membrane-proximal stem domain (Figure 5A). The results of amino acid variation sites of the HA gene of all H6N6-subtype AIVs were shown in Supplementary Table S5. The result showed that the mutation rate of the G228 site of H6N6-subtype AIVs was 0.95%. Moreover, strains isolated from pigeon, swine, and duck have G228S mutant sites. H6N6-subtype AIVs had a high mutation rate (28.44%) at the A222 site, of which the mutation rate from A to V was 8.40%. The mutation rate of A222V was 15.91% before 2010, 31.82% from 2011 to 2015, and 52.27% after 2015. Moreover, strains isolated from pigeons and swine, and some strains from chickens and ducks have A222V mutant sites. Sequencing by NGS showed that the nucleotide of 222 site of HA gene of ZJ49 mutated from GCT t-o GTT, namely A222V mutation exsists (data not shown). The G228S and A222V played an important role in the cross-species transmission of the H6N6-subtype AIVs. However, there

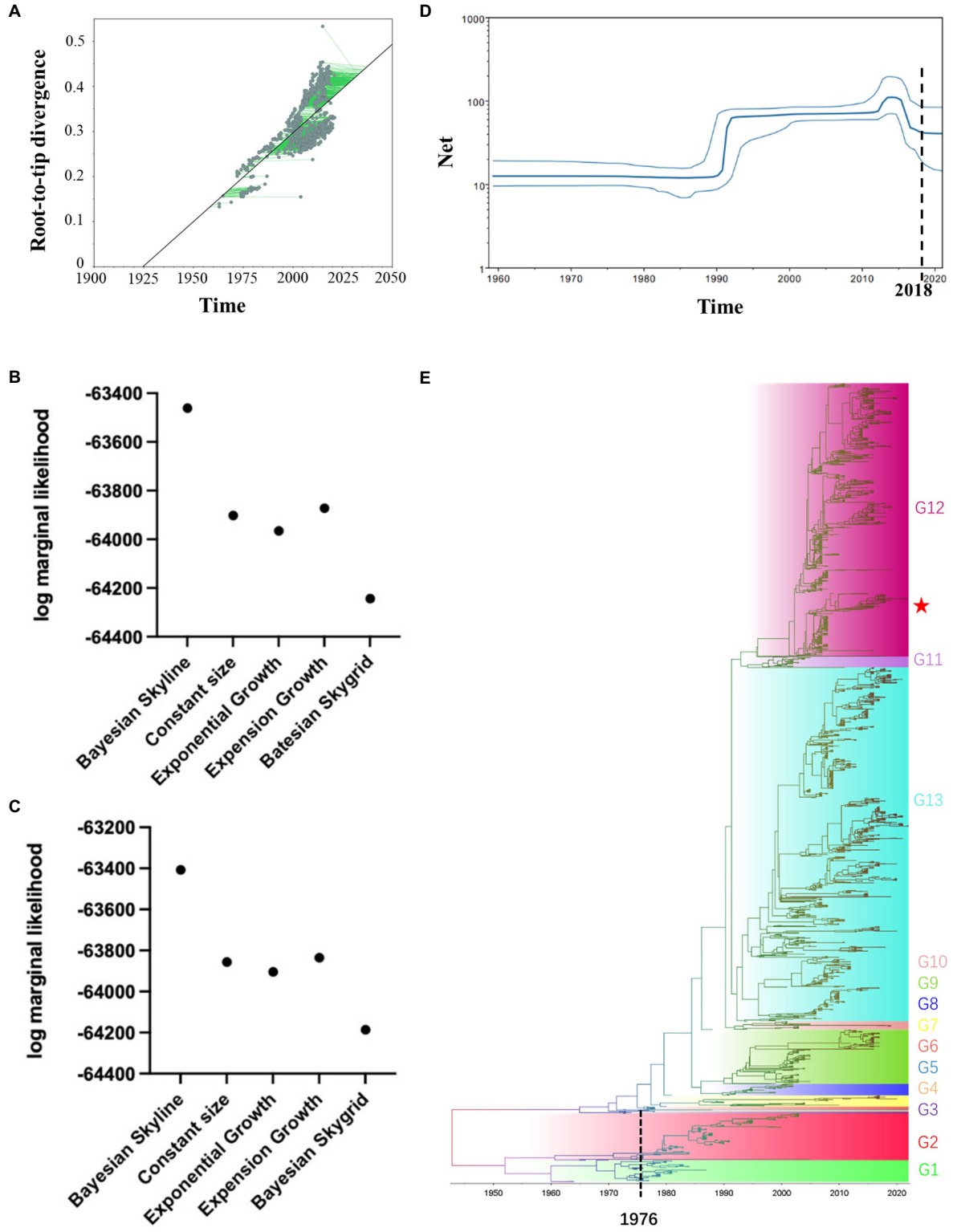


FIGURE 3
Temporal distribution of the H6-subtype influenza virus. **(A)** Root-to-tip regression analyses. Plots of the root-to-tip genetic distance against sampling time were shown for phylogenies estimated from 2063 HA gene sequences. **(B)** Stepping-stone estimation approaches were used to assess the best fitting model through marginal likelihood estimation. **(C)** Path-sampling estimation approaches were used to assess the best fitting model through marginal likelihood estimation. **(D)** The Bayesian skyline plot was based on the individuals infected by H6NX-subtype AIVs. **(E)** Maximum clade credibility tree of HA gene. The MCC tree was constructed by BEAST (v2.6.6) with GTR+G distribution nucleotide substitution model, relaxed molecular clock, the tree prior was Coalescent: Bayesian Skyline and $4\times10^8$ total chain length, sample every 1,000 steps.

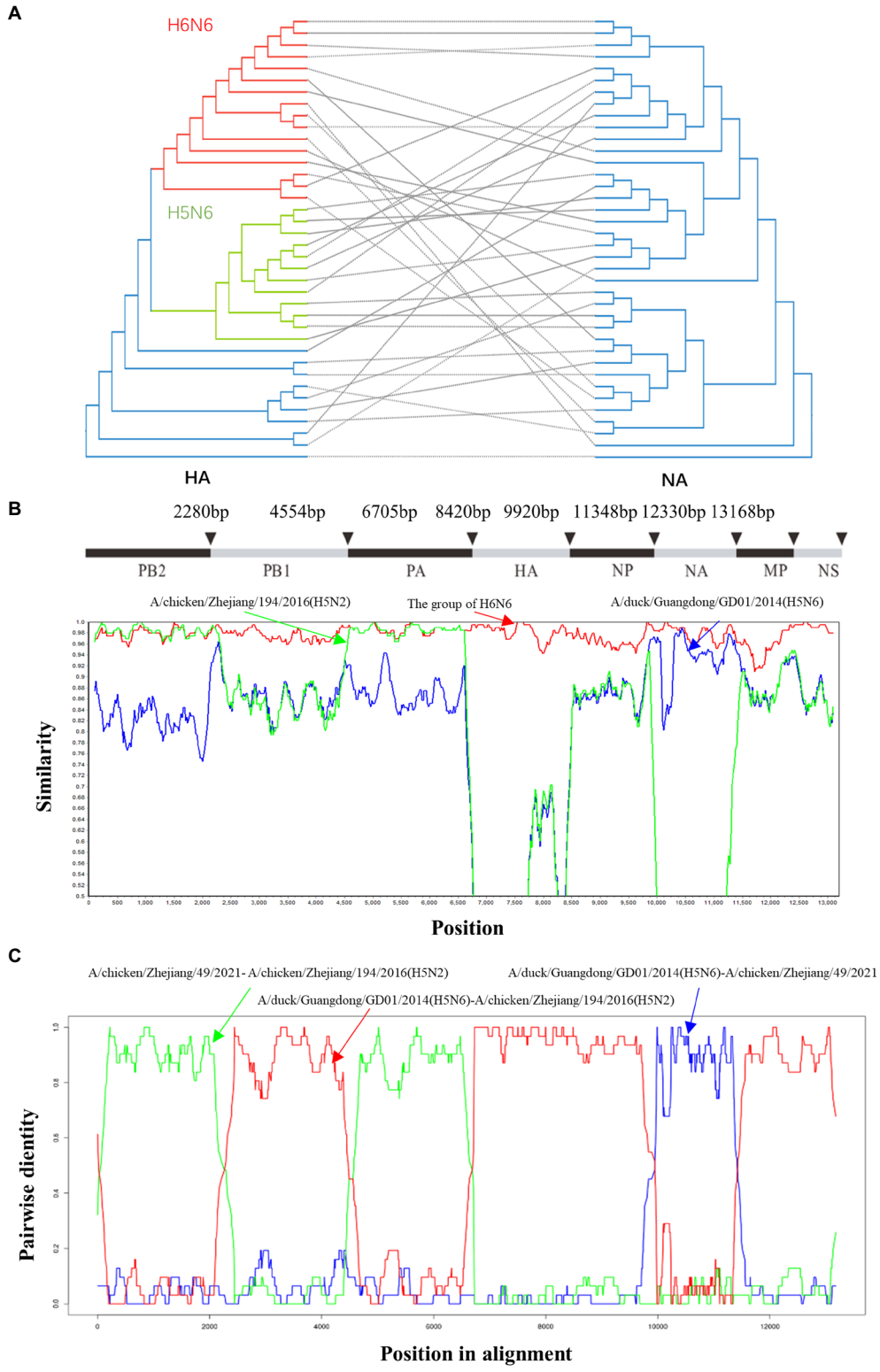


FIGURE 4
Reassortment analysis on concatenated H6N6 virus genomes. **(A)** ML phylogenetic trees inferred for HXN6-subtype AIVs HA and NA using RAxML under the general time-reversible substitution model with gamma-distributed rates across sites. In total, 1,000 bootstraps were evaluated to assess support values. **(B)** Reassortment analysis was performed using Simplot (v.3.5.1). The H6N6 group mainly included the following strains: A/duck/Jiangxi/10.30_NCNP67B3-OC/2017 (H6N6), A/duck/Ganzhou/GZ151/2016 (H6N6), A/chicken/Hunan/1.12_YYGK22H3-OC/2018 (H6N6), A/environment/Jiangxi/2.06_SRXZJG016-E/2017 (H6N6), A/duck/Hunan/2.06_YYGK86J3-OC/2018 (H6N6), and A/duck/Hunan/2.06_YYGK73J3-OC/2018 (H6N6). **(C)** Reassortment analysis was performed using RDP (v.5.5).

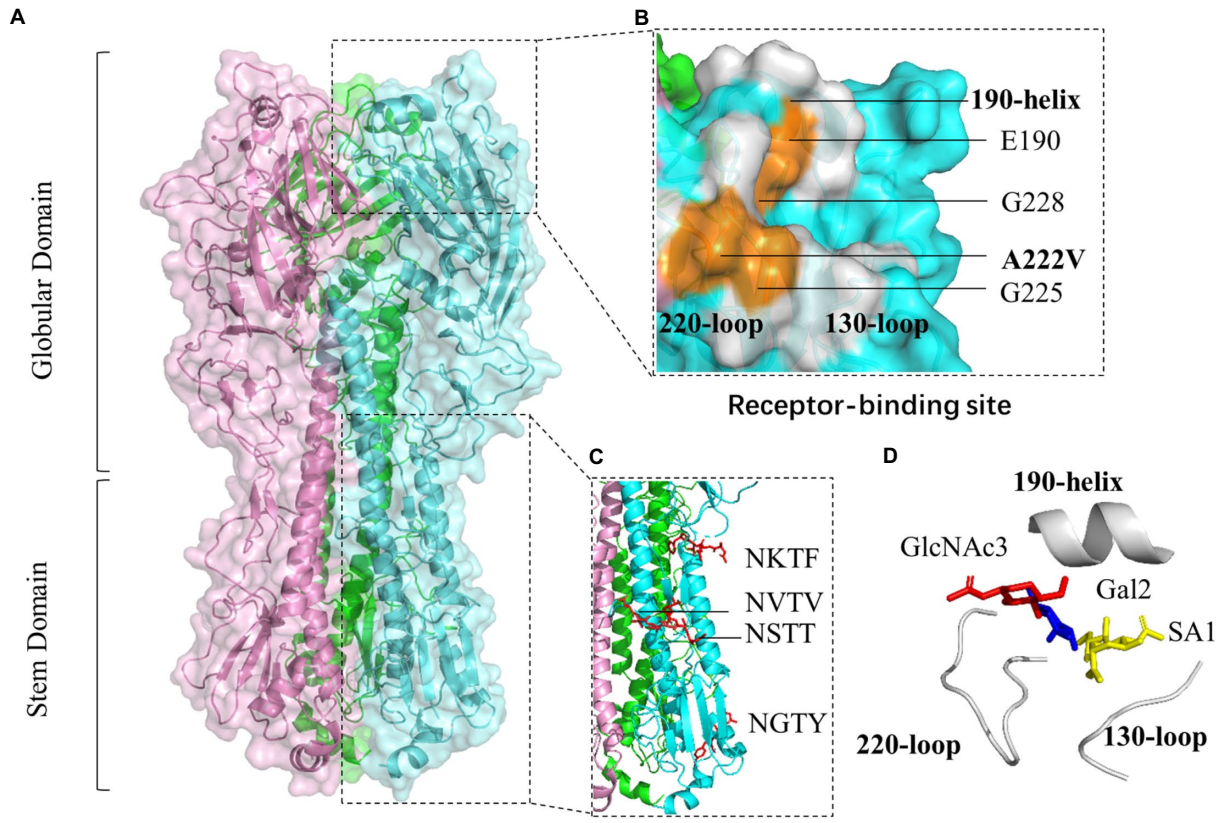


FIGURE 5
Molecular characterization of the H6N6-subtype AIVs. **(A)** The crystal structure of the ectodomain of haemagglutinin (HA) reveals two distinct domains: the globular domain and the stem domain. Each monomer is represented by pink, green, and blue, respectively. **(B)** Three secondary structural elements (in white color) and the sites associated with H6 receptor-binding properties (in orange color). **(C)** N-glycosylation sites (in red color). **(D)** The H6N6 HA receptor analogue (α2, 3-linked sialylated glycan receptor). Sialylated glycans of the host receptors that influenza viruses bind to contain the three-terminal saccharides: the terminal sialic acid SA1, the galactose ring Gal2 (at position two relative to SA), and N-acetylglucosamine GlcNAc3 (at position three relative to SA).

were no corresponding mutations at 190 and 225 sites, which were cross-species related to H6-subtype AIVs. In the newly isolated ZJ49 strain, the E190 site was located on 190-helix, and the V222, G225, G228 sites were all located on 220-loop, except for the mutation from A to V at site 222, the other sites associated with H6 receptor-binding properties were not mutated (Figure 5B). The avian α2, 3-linked SA receptor of ZJ49 adopted a trans conformation, and the glycan rings interacted with the 220-loop of HA (Figure 5D). HAs had a total of five potential glycosylation sites on each monomer (NSTT, NVTV, NKTF, NGTY, NGSM), at HA1 11 (NSTT), 23 (NVTV), 290 (NKTF), HA2 154 (NGTY), and 213 (NGSM). In the structures, four glycans on the stem domain were found, which were 11, 23, 290 sites on HA1 and 154 sites on HA2 (Figure 5C).

## Discussion

The H6-subtype AIVs are widespread in poultry, with a host range extending to mammals such as swine and even human. In recent years, 11 duck samples were infected with H6N6-subtype AIVs in 2017 in Vietnam (Tran et al., 2020). Cui et al. reported that 83 H6 AIVs were isolated from poultry farms between 2014 and 2018 in China, including 38 strains from ducks, 13 from farm environment, and two from geese. These H6 viruses have undergone frequent reassortment, resulting in the formation of 19 different genotypes (Cui et al., 2021). In September 2019, an H6N6-AIV (KNU2019-48) was isolated in South Korea, which was the first reported AIV in Korea. In fact, the H6-subtype viruses had co-circulated in China, Vietnam, and Korea for half a decade (Durairaj et al., 2022). Therefore, the monitoring and prevention of the H6-subtype AIVs, especially H6N6 subtype, should not be taken lightly.

According to the phylogenetic analysis of the HA gene, all H6-subtype AIVs were classified into the gene pools of the Americas and Eurasia. The Eurasian lineage was further divided into three major groups (I, II, and III), ST339-like, ST2853-like, HN573-like (Huang et al., 2010). Our results show that the H6-subtype AIVs were mainly prevalent in the Eurasian continent, and mainly concentrated in China. The

ducks were the main host of the H6-subtype AIVs. The evolutionary tree of the 8 segments can be divided into two major branches, namely the Eurasian branch and the North American branch. ST339-like, W312-like, ST2853-like, HN573-like branches are located in G9, G11, G12, and G13 groups. The W312-like branch was closer to the ST2853-like branch, the HN573-like and Taiwan branch was in the same group, and they all evolved from the ST339-like branch and the above results were consistent with previous reports (Zou et al., 2016). In this paper, a new H6N6 strain (ZJ49) was isolated from chickens in Zhejiang Province, China in November 2021. This ZJ49 isolate was located in the G12 group where the ST2853-like branch was also clustered in this group. In recent years, the G12 group became dominant wordwide.

The H6-subtype AIVs spread from North America to Eurasia around 1976. The effective quantity size increased around 1990, reached a peak around 2015, declined after 2015, then kept in a stable level after 2018. However, newly isolated virus strains had been found in China, Vietnam, South Korea and other places. Whether H6-subtype AIV will cause a large-scale re-epidemic in poultry in above mention countries beside North America and Eurasia is unclear. Therefore, it's important to continuously monitor the genetic characterization and evolution of H6-subtype AIVs to get better control of their epidemic.

The high mutation rate of amino acids enabled AIVs to evolve rapidly, thereby helping them overcome host barriers. Antigenic shift and antigenic drift were two major kinds of antigenic variation occurring in AIVs. Antigenic shift was a result of the reassortment of viral genome segments. To overcome selective pressures and get a better adaptation to the new environments or hosts, the homologous RNA reassortments within segments produced a diverse subtype in most viruses (He et al., 2009; Lam et al., 2013; Ge et al., 2017; Wei and Li, 2018). The H6-subtype AIVs were characterized as LPAIVs, but the reassortment with other influenza virus subtypes may result in the emergence of HPAIVs (Bi et al., 2016; Li et al., 2019). According to the report, A/duck/Guangdong/GD01/2014 was a strain of HPAIV and its NA gene was clustered with some H6N6 viruses circulating in China (Shen et al., 2015). Our results showed that the H6N6-subtype AIVs and H5N6-subtype AIVs recombined frequently. The reassortment analysis predicted that the PB2, PA, and NA genes of ZJ49 were more similar to H5-subtype AIVs. It provided the possibility for H6-subtype AIV recombining with highly pathogenic viruses.

HA protein was a homotrimer, with each monomer containing two polypeptide chains, HA1 and HA2. The receptor-binding site formed a shallow pocket at the tip of the globular domain and comprised three secondary structural elements and one base element (Gamblin and Skehel, 2010). The three secondary elements, namely the 130-loop, the 190-helix, and the 220-loop, formed the edges of the receptor-binding site, and four highly conserved residues (Y98, W153, H183, Y195) formed the base (the numbers correspond to the amino acids in the H3 subtype; Shi et al., 2014). HA proteins exhibited specific binding affinities for the different SA-linked glycoproteins. AIVs preferentially bond to SA-linked terminal oligosaccharides by an α2, 3-linked SA receptor (which is referred to as the avian receptor), whereas human strains favored the α2, 6-linked SA receptor (which is referred to as the human receptor; Shi et al., 2014). Specific amino acid mutations in HA led to a change in receptor-binding preference and thus altered host specificity and tropism of AIVs. The E190V, A222V, G225D, and G228S substitutions of H6-subtype were important to acquire the human receptor-binding capacity (Wang et al., 2015; de Vries et al., 2017; Sun et al., 2017). Our results showed that H6N6-subtype AIVs had a high mutation rate at the A222V site. The ZJ49 strain had no mutations at the E190, G225, and G228 sites, but the A222 site was mutated from A to V leading to a potential risk of its spreading across species. The addition of glycans to the HA was thought to be an important mechanism contributing to antigenic drift (Schulze, 1997; Abe et al., 2004). Oligosaccharides attached to the stem/stalk region of the viral HA tend to be conserved across different viruses strains, whereas those ones attached to the globular head displayed considerable variation in both number and location (Wagner et al., 2000). Glycans in the stalk region were critical for fold and conformation of the HA molecule, while the trimerization, folding, transport of HA to the cell surface, and the sensitivity of HA to changes in pH were impaired by removing these sites from the stalk (Daniels et al., 2003; Tate et al., 2014). According to the three-dimensional structure of this isolate, four conserved glycosylation sites were found in the stem of HA performing less impact on the fold and conception of HA structure.

## Conclusion

This is a study that broadens the knowledge of H6-subtype AIVs from genetic evolutionary, reassortment, and mutations of receptor binding sites. Continuous monitoring and molecular characterization of the H6-subtype AIVs, especially H6N6 subtype, will be required for a better understanding of the evolutionary dynamics of the virus, which can further assist in improving control measures for the diseases.

## Data availability statement

The data presented in the study are deposited in the https://www.ncbi.nlm.nih.gov/nuccore/?term=ON692794:ON692801[accn] repository, accession number ON692794-ON692801.

## Author contributions

MC, YH, and JZ conceived and designed the experiments. MC, YH, and XB performed the experiments. MC and YH analyzed the data. MC and ML wrote the paper. All authors contributed to the article and approved the submitted version.

## Funding

This work was supported by the National Science Foundation of China (grant no. 32192454) and the China Agriculture Research System (grant no. CARS-40-K13).

## Conflict of interest

The authors declare that the research was conducted in the absence of any commercial or financial relationships that could be construed as a potential conflict of interest.

## Publisher's note

All claims expressed in this article are solely those of the authors and do not necessarily represent those of their affiliated organizations, or those of the publisher, the editors and the reviewers. Any product that may be evaluated in this article, or claim that may be made by its manufacturer, is not guaranteed or endorsed by the publisher.

## Supplementary material

The Supplementary material for this article can be found online at: https://www.frontiersin.org/articles/10.3389/fmicb.2022.963218/full#supplementary-material

**SUPPLEMENTARY TABLE S1**
The information of the global distribution of H6NX.

**SUPPLEMENTARY TABLE S2**
The information of the 8 fragment sequences for construction of the ML tree.

**SUPPLEMENTARY TABLE S3**
The information of sequences for reassortment analysis of HXN6.

**SUPPLEMENTARY TABLE S4**
The information of the 8 gene fragments of the maximum similarity reference strain to ZJ49.

**SUPPLEMENTARY TABLE S5**
The amino acid variation sites of the HA gene of H6N6-subtype AIVs.

## References

Abe, Y., Takashita, E., Sugawara, K., Matsuzaki, Y., Muraki, Y., and Hongo, S. (2004). Effect of the addition of oligosaccharides on the biological activities and antigenicity of influenza A/H3N2 virus hemagglutinin. *J. Virol.* 78, 9605–9611. doi: 10.1128/JVI.78.18.9605-9611.2004

Baele, G., Lemey, P., and Suchard, M. A. (2016). Genealogical working distributions for Bayesian model testing with phylogenetic uncertainty. *Syst. Biol.* 65, 250–264. doi: 10.1093/sysbio/syv083

Baele, G., Li, W. L., Drummond, A. J., Suchard, M. A., and Lemey, P. (2013). Accurate model selection of relaxed molecular clocks in bayesian phylogenetics. *Mol. Biol. Evol.* 30, 239–243. doi: 10.1093/molbev/mss243

Bi, Y., Chen, Q., Wang, Q., Chen, J., Jin, T., Wong, G., et al. (2016). Genesis, evolution and prevalence of H5N6 avian influenza viruses in China. *Cell Host Microbe* 20, 810–821. doi: 10.1016/j.chom.2016.10.022

Cheung, C. L., Vijaykrishna, D., Smith, G. J., Fan, X. H., Zhang, J. X., Bahl, J., et al. (2007). Establishment of influenza A virus (H6N1) in minor poultry species in southern China. *J. Virol.* 81, 10402–10412. doi: 10.1128/JVI.01157-07

Cui, J., Cui, P., Shi, J., Fan, W., Xing, X., Gu, W., et al. (2021). Continued evolution of H6 avian influenza viruses isolated from farms in China between 2014 and 2018. *Transbound. Emerg. Dis.* [Epub ahead of print]. doi: 10.1111/tbed.14212

Daniels, R., Kurowski, B., Johnson, A. E., and Hebert, D. N. (2003). N-linked glycans direct the cotranslational folding pathway of influenza hemagglutinin. *Mol. Cell* 11, 79–90. doi: 10.1016/s1097-2765(02)00821-3

de Vries, R. P., Tzarum, N., Peng, W., Thompson, A. J., Ambepitiya Wickramasinghe, I. N., de la Pena, A. T. T., et al. (2017). A single mutation in Taiwanese H6N1 influenza hemagglutinin switches binding to human-type receptors. *EMBO Mol. Med.* 9, 1314–1325. doi: 10.15252/emmm.201707726

Dillies, M. A., Rau, A., Aubert, J., Hennequet-Antier, C., Jeanmougin, M., Servant, N., et al. (2013). A comprehensive evaluation of normalization methods for Illumina high-throughput RNA sequencing data analysis. *Brief. Bioinform.* 14, 671–683. doi: 10.1093/bib/bbs046

Downie, J. C., Webster, R. G., Schild, G. C., Dowdle, W. R., and Laver, W. G. (1973). Characterization and ecology of a type A influenzavirus isolated from a sheawater. *Bull. World Health Organ.* 49, 559–566.

Durairaj, K., Trinh, T. T., Yun, S. Y., Yeo, S. J., Sung, H. W., and Park, H. (2022). Molecular characterization and pathogenesis of H6N6 low pathogenic avian influenza viruses isolated from mallard ducks (*Anas platyrhynchos*) in South Korea. *Viruses* 14:1001. doi: 10.3390/v14051001

Gamblin, S. J., and Skehel, J. J. (2010). Influenza hemagglutinin and neuraminidase membrane glycoproteins. *J. Biol. Chem.* 285, 28403–28409. doi: 10.1074/jbc.R110.129809

Ge, Y., Chai, H., Fan, Z., Wang, X., Yao, Q., Ma, J., et al. (2017). New H6 influenza virus reassortment strains isolated from *Anser fabalis* in Anhui Province China. *Virol. J.* 14:36. doi: 10.1186/s12985-017-0680-1

Germeraad, E. A., Sanders, P., Hagenaars, T. J., Jong, M. C. M., Beerens, N., and Gonzales, J. L. (2019). Virus shedding of avian influenza in poultry: A systematic review and Meta-analysis. *Viruses* 11:412. doi: 10.3390/v11090812

He, W.-T., Ji, X., He, W., Dellicour, S., Wang, S., Li, G., et al. (2020). Genomic epidemiology, evolution, and transmission dynamics of porcine Deltacoronavirus. *Mol. Biol. Evol.* 37, 2641–2654. doi: 10.1093/molbev/msaa117

He, C. Q., Xie, Z. X., Han, G. Z., Dong, J. B., Wang, D., Liu, J. B., et al. (2009). Homologous recombination as an evolutionary force in the avian influenza A virus. *Mol. Biol. Evol.* 26, 177–187. doi: 10.1093/molbev/msn238

Hoque, M. A., Burgess, G. W., Cheam, A. L., and Skerratt, L. F. (2015). Epidemiology of avian influenza in wild aquatic birds in a biosecurity hotspot, North Queensland, Australia. *Prev. Vet. Med.* 118, 169–181. doi: 10.1016/j.prevetmed.2014.11.009

Huang, K., Bahl, J., Fan, X. H., Vijaykrishna, D., Cheung, C. L., Webby, R. J., et al. (2010). Establishment of an H6N2 influenza virus lineage in domestic ducks in southern China. *J. Virol.* 84, 6978–6986. doi: 10.1128/JVI.00256-10

Huang, K., Zhu, H., Fan, X., Wang, J., Cheung, C.-L., Duan, L., et al. (2012). Establishment and lineage replacement of H6 influenza viruses in domestic ducks in southern China. *J. Virol.* 86, 6075–6083. doi: 10.1128/JVI.06389-11

Katoh, K., Misawa, K., Kuma, K.-I., and Miyata, T. (2002). MAFFT: a novel method for rapid multiple sequence alignment based on fast Fourier transform. *Nucleic Acids Res.* 30, 3059–3066. doi: 10.1093/nar/gkf436

Kumar, M., Nagarajan, S., Murugkar, H. V., Saikia, B., Singh, B., Mishra, A., et al. (2018). Emergence of novel reassortant H6N2 avian influenza viruses in ducks in India. *Infect. Genet. Evol.* 61, 20–23. doi: 10.1016/j.meegid.2018.03.005

Lam, T. T., Chong, Y. L., Shi, M., Hon, C. C., Li, J., Martin, D. P., et al. (2013). Systematic phylogenetic analysis of influenza A virus reveals many novel mosaic genome segments. *Infect. Genet. Evol.* 18, 367–378. doi: 10.1016/j.meegid.2013.03.015

Lee, E. K., Kang, H. M., Song, B. M., Lee, Y. N., Heo, G. B., Lee, H. S., et al. (2017). Surveillance of avian influenza viruses in South Korea between 2012 and 2014. *Virol. J.* 14:54. doi: 10.1186/s12985-017-0711-y

Letunic, I., and Bork, P. (2016). Interactive tree of life (iTOL) v3: an online tool for the display and annotation of phylogenetic and other trees. *Nucleic Acids Res.* 44, W242–W245. doi: 10.1093/nar/gkw290

Li, H., and Durbin, R. (2009). Fast and accurate short read alignment with burrows-wheeler transform. *Bioinformatics* 25, 1754–1760. doi: 10.1093/bioinformatics/btp698

Li, H., Handsaker, B., Wysoker, A., Fennell, T., Ruan, J., Homer, N., et al. (2009). The sequence alignment/map format and SAMtools. *Bioinformatics* 25, 2078–2079. doi: 10.1093/bioinformatics/btp352

Li, Y., Li, M., Tian, J., Bai, X., and Li, Y. (2021). Genetic characteristics and pathogenicity of novel reassortant H6 viruses isolated from wild birds in China. *Vet. Microbiol.* 254:108978. doi: 10.1016/j.vetmic.2021.108978

Li, J., Quan, C., Xie, Y., Ke, C., Nie, Y., Chen, Q., et al. (2019). Continued reassortment of avian H6 influenza viruses from southern China, 2014-2016. *Transbound. Emerg. Dis.* 66, 592–598. doi: 10.1111/tbed.13037

Lin, W., Cui, H., Teng, Q., Li, L., Shi, Y., Li, X., et al. (2020). Evolution and pathogenicity of H6 avian influenza viruses isolated from southern China during 2011 to 2017 in mice and chickens. *Sci. Rep.* 10:20583. doi: 10.1038/s41598-020-76541-0

Liu, D., Shi, W., Shi, Y., Wang, D., Xiao, H., Li, W., et al. (2013). Origin and diversity of novel avian influenza A H7N9 viruses causing human infection: phylogenetic, structural, and coalescent analyses. *Lancet* 381, 1926–1932. doi: 10.1016/S0140-6736(13)60938-1

Lu, X.-J. (2020). DSSR-enabled innovative schematics of 3D nucleic acid structures with PyMOL. *Nucleic Acids Res.* 48:e74. doi: 10.1093/nar/gkaa426

Morens, D. M., Taubenberger, J. K., and Fauci, A. S. (2013). Pandemic influenza viruses--hoping for the road not taken. *N. Engl. J. Med.* 368, 2345–2348. doi: 10.1056/NEJMp1307009

Munster, V. J., Baas, C., Lexmond, P., Waldenstrom, J., Wallensten, A., Fransson, T., et al. (2007). Spatial, temporal, and species variation in prevalence of influenza A viruses in wild migratory birds. *PLoS Pathog.* 3:e61. doi: 10.1371/journal.ppat.0030061

Nguyen, L.-T., Schmidt, H. A., von Haeseler, A., and Minh, B. Q. (2015). IQ-TREE: a fast and effective stochastic algorithm for estimating maximum-likelihood phylogenies. *Mol. Biol. Evol.* 32, 268–274. doi: 10.1093/molbev/msu300

Pattengale, N. D., Alipour, M., Bininda-Emonds, O. R. P., Moret, B. M. E., and Stamatakis, A. (2010). How many bootstrap replicates are necessary? *J. Comput. Biol.* 17, 337–354. doi: 10.1089/cmb.2009.0179

Rambaut, A., Lam, T. T., Max Carvalho, L., and Pybus, O. G. (2016). Exploring the temporal structure of heterochronous sequences using TempEst (formerly path-O-gen). *Virus. Evol.* 2:vew007. doi: 10.1093/ve/vew007

Rimondi, A., Gonzalez-Reiche, A. S., Olivera, V. S., Decarre, J., Castresana, G. J., Romano, M., et al. (2018). Evidence of a fixed internal gene constellation in influenza A viruses isolated from wild birds in Argentina (2006-2016). *Emerg. Microbes. Infect.* 7:194. doi: 10.1038/s41426-018-0190-2

Rimondi, A., Xu, K., Craig, M. I., Shao, H., Ferreyra, H., Rago, M. V., et al. (2011). Phylogenetic analysis of H6 influenza viruses isolated from rosy-billed pochards (*Netta peposaca*) in Argentina reveals the presence of different HA gene clusters. *J. Virol.* 85, 13354–13362. doi: 10.1128/JVI.05946-11

Sabir, J. S. M., Lam, T. T. Y., Ahmed, M. M. M., Li, L., Shen, Y., Abo-Aba, S. E. M., et al. (2016). Co-circulation of three camel coronavirus species and recombination of MERS-CoVs in Saudi Arabia. *Science* 351, 81–84. doi: 10.1126/science.aac8608

Schulze, I. T. (1997). Effects of glycosylation on the properties and functions of influenza virus hemagglutinin. *J. Infect. Dis.* 176, S24–S28. doi: 10.1086/514170

Sharp, G. B., Kawaoka, Y., Wright, S. M., Turner, B., Hinshaw, V., and Webster, R. G. (1993). Wild ducks are the reservoir for only a limited number of influenza A subtypes. *Epidemiol. Infect.* 110, 161–176. doi: 10.1017/s0950268800050780

Shen, H., Wu, B., Chen, Y., Bi, Y., and Xie, Q. (2015). Influenza A(H5N6) virus Reassortant, southern China, 2014. *Emerg. Infect. Dis.* 21, 1261–1262. doi: 10.1016/j.chom.2016.10.022

Shi, W., Shi, Y., Wu, Y., Liu, D., and Gao, G. F. (2013). Origin and molecular characterization of the human-infecting H6N1 influenza virus in Taiwan. *Protein Cell* 4, 846–853. doi: 10.1007/s13238-013-3083-0

Shi, Y., Wu, Y., Zhang, W., Qi, J., and Gao, G. F. (2014). Enabling the 'host jump': structural determinants of receptor-binding specificity in influenza A viruses. *Nat. Rev. Microbiol.* 12, 822–831. doi: 10.1038/nrmicro3362

Soli, R., Kaabi, B., Barhoumi, M., Maktouf, C., and Ahmed, S. B. (2019). Bayesian phylogenetic analysis of the influenza-A virus genomes isolated in Tunisia, and determination of potential recombination events. *Mol. Phylogenet. Evol.* 134, 253–268. doi: 10.1016/j.ympev.2019.01.019

Stamatakis, A. (2014). RAxML version 8: a tool for phylogenetic analysis and post-analysis of large phylogenies. *Bioinformatics* 30, 1312–1313. doi: 10.1093/bioinformatics/btu033

Suchard, M. A., Lemey, P., Baele, G., Ayres, D. L., Drummond, A. J., and Rambaut, A. (2018). Bayesian phylogenetic and phylodynamic data integration using BEAST 1.10. *Virus. Evol.* 4:vey016. doi: 10.1093/ve/vey016

Sun, H., Kaplan, B. S., Guan, M., Zhang, G., Ye, J., Long, L. P., et al. (2017). Pathogenicity and transmission of a swine influenza A(H6N6) virus. *Emerg. Microbes. Infect.* 6:e17, 1–13. doi: 10.1038/emi.2017.3

Tate, M. D., Job, E. R., Deng, Y. M., Gunalan, V., Maurer-Stroh, S., and Reading, P. C. (2014). Playing hide and seek: how glycosylation of the influenza virus hemagglutinin can modulate the immune response to infection. *Viruses* 6, 1294–1316. doi: 10.3390/v6031294

Tran, Q. A., Le Thi, H., Thi Thanh Le, X., and To Long, T. (2020). The presence of poultry influenza strains in two live bird markets near the east-west boundary of Vietnam. *Biomed. Res. Int.* 2020, 1487651–1487655. doi: 10.1155/2020/1487651

van Dijk, E. L., Auger, H., Jaszczyszyn, Y., and Thermes, C. (2014). Ten years of next-generation sequencing technology. *Trends Genet.* 30, 418–426. doi: 10.1016/j.tig.2014.07.001

Wagner, R., Wolff, T., Herwig, A., Pleschka, S., and Klenk, H. D. (2000). Interdependence of hemagglutinin glycosylation and neuraminidase as regulators of influenza virus growth: a study by reverse genetics. *J. Virol.* 74, 6316–6323. doi: 10.1128/jvi.74.14.6316-6323.2000

Wang, G., Deng, G., Shi, J., Luo, W., Zhang, G., Zhang, Q., et al. (2014). H6 influenza viruses pose a potential threat to human health. *J. Virol.* 88, 3953–3964. doi: 10.1128/JVI.03292-13

Wang, L., Li, F., Sun, W., Wu, S., Wang, X., Zhang, L., et al. (2006). Concanavalin A-captured glycoproteins in healthy human urine. *Mol. Cell. Proteomics* 5, 560–562. doi: 10.1074/mcp.D500013-MCP200

Wang, F., Qi, J., Bi, Y., Zhang, W., Wang, M., Zhang, B., et al. (2015). Adaptation of avian influenza A (H6N1) virus from avian to human receptor-binding preference. *EMBO J.* 34, 1661–1673. doi: 10.15252/embj.201590960

Waterhouse, A., Bertoni, M., Bienert, S., Studer, G., Tauriello, G., Gumienny, R., et al. (2018). SWISS-MODEL: homology modelling of protein structures and complexes. *Nucleic Acids Res.* 46, W296–W303. doi: 10.1093/nar/gky427

Wei, K., and Li, Y. (2018). Global genetic variation and transmission dynamics of H9N2 avian influenza virus. *Transbound. Emerg. Dis.* 65, 504–517. doi: 10.1111/tbed.12733

Wei, S.-H., Yang, J.-R., Wu, H.-S., Chang, M.-C., Lin, J.-S., Lin, C.-Y., et al. (2013). Human infection with avian influenza A H6N1 virus: an epidemiological analysis. *Lancet Respir. Med.* 1, 771–778. doi: 10.1016/S2213-2600(13)70221-2

Yu, X., Jin, T., Cui, Y., Pu, X., Li, J., Xu, J., et al. (2014). Influenza H7N9 and H9N2 viruses: coexistence in poultry linked to human H7N9 infection and genome characteristics. *J. Virol.* 88, 3423–3431. doi: 10.1128/JVI.02059-13

Yuan, R., Zou, L., Kang, Y., Wu, J., Zeng, X., Lu, J., et al. (2016). Reassortment of avian influenza A/H6N6 viruses from live poultry markets in Guangdong China. *Front. Microbiol.* 7:65. doi: 10.3389/fmicb.2016.00065

Zhao, G., Chen, C., Huang, J., Wang, Y., Peng, D., and Liu, X. (2013). Characterisation of one H6N6 influenza virus isolated from swine in China. *Res. Vet. Sci.* 95, 434–436. doi: 10.1016/j.rvsc.2013.06.013

Zhao, G., Lu, X., Gu, X., Zhao, K., Song, Q., Pan, J., et al. (2011). Molecular evolution of the H6 subtype influenza A viruses from poultry in eastern China from 2002 to 2010. *Virol. J.* 8:470. doi: 10.1186/1743-422X-8-470

Zou, S., Gao, R., Zhang, Y., Li, X., Chen, W., Bai, T., et al. (2016). Molecular characterization of H6 subtype influenza viruses in southern China from 2009 to 2011. *Emerg. Microbes. Infect.* 5:e73, 1–8. doi: 10.1038/emi.2016.71

frontiers | Frontiers in Microbiology

TYPE Original Research
PUBLISHED 16 August 2022
DOI 10.3389/fmicb.2022.895779



OPEN ACCESS

EDITED BY
Yizhi Tao,
Rice University,
United States

REVIEWED BY
Yang Li,
Institute of Zoology (CAS), China
Ya-Fang Chiu,
Chang Gung University, Taiwan

*CORRESPONDENCE
Yan Li
yanli3@zju.edu.cn

SPECIALTY SECTION
This article was submitted to Virology, a section of the journal Frontiers in Microbiology

RECEIVED 14 March 2022
ACCEPTED 29 July 2022
PUBLISHED 16 August 2022

CITATION
Ling Y-H, Wang H, Han M-Q, Wang D, Hu Y-X, Zhou K and Li Y (2022) Nucleoporin 85 interacts with influenza A virus PB1 and PB2 to promote its replication by facilitating nuclear import of ribonucleoprotein. *Front. Microbiol.* 13:895779. doi: 10.3389/fmicb.2022.895779



# Nucleoporin 85 interacts with influenza A virus PB1 and PB2 to promote its replication by facilitating nuclear import of ribonucleoprotein

Yue-Huan Ling[1], Hao Wang[1], Mei-Qing Han[1], Di Wang[1], Yi-Xiang Hu[1,2], Kun Zhou[1] and Yan Li[1,2,3]*

[1]Department of Veterinary Medicine and Institute of Preventive Veterinary Sciences, Zhejiang University College of Animal Sciences, Hangzhou, Zhejiang, China, [2]Hainan Institute, Zhejiang University, Sanya, Hainan, China, [3]Zhejiang Provincial Key Laboratory of Preventive Veterinary Medicine, Hangzhou, Zhejiang, China

Transcription and replication of the influenza A virus (IAV) genome take place in the nucleus of infected cells, which rely on host factors to aid viral ribonucleoprotein (vRNP) to cross the nuclear pore complex (NPC) and complete the bidirectional nucleocytoplasmic trafficking. Here, we showed that nucleoporin 85 (NUP85), a component of NPC, interacted with RNP subunits polymerase basic 1 (PB1) and polymerase basic 2 (PB2) in an RNA-dependent manner during IAV infection. Knockdown of NUP85 delayed the nuclear import of vRNP, PB1 and PB2, inhibiting polymerase activity and ultimately suppressing viral replication. Further analysis revealed that NUP85 assisted the binding of PB1 to nuclear transport factor Ran-binding protein 5 (RanBP5) and the binding of PB2 to nuclear transport factor importin α1 and importin α7. We also found that NUP85 expression was downregulated upon IAV infection. Together, our study demonstrated that NUP85 positively regulated IAV infection by interacting with viral PB1 and PB2, which may provide new insight into the process of vRNP nuclear import and a novel target for effective antivirals.

KEYWORDS

**influenza A virus, NUP85, RNP, PB1, PB2, nuclear import**

## Introduction

Influenza A virus (IAV) belongs to the family *Orthomyxoviridae* and represents important pathogens of humans and animals. IAV has caused the yearly epidemics and multiple pandemics over the past century. Thus, it poses a massive threat to public health and results in significant economic losses (Taubenberger and Morens, 2008; Neumann et al., 2009; Taubenberger et al., 2019). Influenza A virus is a single- and negative-stranded RNA virus with eight RNA segments (PB2, PB1, PA, NP, HA, NA, M, and NS). Each viral

RNA (vRNA) segment is encapsidated by multiple nucleoprotein (NP) molecules and is also associated with a single, trimeric polymerase complex that comprises polymerase basic protein 1 (PB1), polymerase basic protein 2 (PB2), polymerase acidic protein (PA). Each subunit of vRNA–NP–polymerase is referred to as a viral ribonucleoprotein (vRNP) complex (Eisfeld et al., 2015; Te Velthuis and Fodor, 2016).

The transcription and replication of the IAV genome are performed by the viral RNA-dependent RNA polymerase that is compacted into the vRNP complex. The vRNP complex plays a crucial role in the viral life cycle, viral genome replication, and expression (Noda and Kawaoka, 2010; Resa-Infante et al., 2010; Moeller et al., 2012; Eisfeld et al., 2015). Unlike many other single-stranded RNA viruses, for which the replication cycle is confined to the cytoplasm, influenza viral RNA synthesis takes place in the host cellular nucleus. After viral entry and release of eight vRNPs into the cytoplasm, the vRNPs are transported into the nucleus for the primary transcription and replication that results in the production of both viral messenger RNAs (mRNAs) and complementary RNAs (cRNAs) that serve as templates for vRNAs production. Then the mRNAs are exported into the cytoplasm for protein translation in ribosomes. The newly formed viral proteins, such as PB2, NP monomers, and PA-PB1 heterodimers, traffic back into the nucleus for genome replication and progeny RNPs production. With the assistance of M1 and NEP proteins, progeny vRNPs are exported to cytoplasm and subsequently transported into the cell membrane for the progeny virions assembly and budding. Finally, the released progeny virions infect adjacent cells for a new life cycle (Eisfeld et al., 2015; Peacock et al., 2019).

Due to the limited genome capacity, vRNPs rely on host factors to traffic in and out of the nucleus for efficient viral genome transcription and replication. Following viral entry, internalization, and release of vRNP in the cytoplasm, vRNPs were transported into the nucleus through the nuclear pore complex (NPC) by importin-α:β heterodimer (O'Neill et al., 1995). Importin-α recognizes the nuclear localization sequences (NLSs) on NP and associates with importin-β (Gorlich et al., 1995; Wu et al., 2007; Wu and Pante, 2009). After primary transcription and translation, newly formed polymerase subunits need to form a catalytically active hetero-trimer in the nucleus. It has been shown that newly synthesized PB2 enters into the nucleus by its NLS binding of importin-α isotypes, such as importin-α1 (IMP-α1), importin-α3 (IMP-α3), importin-α5 (IMP-α5), and importin-α7 (IMP-α7) (Resa-Infante et al., 2008), and PA and PB1 translocate to nucleus by the binding of β-importin Ran-binding protein 5 (RanBP5; also known as importin-5 and karyopherin-β3) (Deng et al., 2006). Factors that affect the nuclear import of ribonucleoprotein (RNP) tend to have effects on viral replication, such as Heat Shock Protein 90 (HSP90) (Naito et al., 2007b), Phospholipid scramblase 1 (PLSCR1) (Luo et al., 2018), translation elongation factor 1 delta (eEF1D) (Gao et al., 2020), and LYAR (Yang et al., 2018).

Besides, the transportation of vRNP relies on the host nuclear machineries. NPC is a part of nuclear machinery, and its function coordinates the bidirectional transport of macromolecules between the cytoplasm and nucleus (Terry and Wente, 2007; Lim et al., 2008; Hampoelz et al., 2019; Lin and Hoelz, 2019). It is composed of multiple copies of ~30 different proteins termed nucleoporins (NUPs) to form a basket-like structure (Beck and Hurt, 2017). Nucleoporins have also been reported to play roles in influenza virus replication, such as NUP98, NUP93, NUP214, and NUP153 (Satterly et al., 2007; Muhlbauer et al., 2015; Furusawa et al., 2018; Li et al., 2020; Senbas Akyazi et al., 2020). As a part of the Nup107-160 complex, NUP85 (also known as FROUNT) is required for NPC assembly and maintenance (Harel et al., 2003). It has been found to interact with HIV Tat protein in the cellular nucleus (Brass et al., 2008; Gautier et al., 2009), be involved in inflammation (Terashima et al., 2020), be associated with the chemokine receptor CCR2 and CCR5 to regulate chemokine signaling (Zannettino et al., 2008; Toda et al., 2009, 2014) and tumor progression (Terashima et al., 2020). However, the association of NUP85 with influenza virus infection and its role in influenza virus replication and its mechanisms have not been investigated.

In this study, we found that NUP85 interacted with IAV PB1 and PB2 proteins. Meanwhile, the knockdown of NUP85 delayed the nuclear transportation of vRNP, hindered IAV polymerase activity, and significantly hampered the replication of various subtypes of influenza viruses. Further investigation indicated that NUP85 facilitated the nuclear import of vRNP by assisting the interactions of PB1 with nuclear transporter factor RanBP5, and PB2 with nuclear transporter factor IMP-α1 and IMP-α7. We also found that NUP85 mRNA and protein levels were reduced in A549 cells upon IAV infection. Our results strongly demonstrate that NUP85 is a host factor essential for influenza A virus infection.

# Materials and methods

## Cells and viruses

Human alveolar adenocarcinoma epithelial (A549) cells, human embryonic kidney (HEK 293 T) cells, and Madin–Darby canine kidney (MDCK) cells were used in this study. A549 cells, MDCK cells and HEK 293 T cells were cultured in Ham's F-12 medium, Dulbecco's modified Eagle's medium (DMEM), and minimum essential medium (MEM), respectively. The media were purchased from Thermo Fisher (Waltham, MA, United States), and were supplemented with 10% fetal bovine serum (FBS; ExCell Biology, shanghai, China), 100 U/ml penicillin, and 0.1 mg/ml streptomycin. All cells were cultured at 37°C in a 5% $CO_2$ humidified incubator.

The IAVs used in experiments were Influenza A/Puerto Rico/8/1934 (H1N1), A/Zhejiang /163/2020 (H3N2), and A/swine/Jiangsu/C1/2008 (H9N2). All the viruses were propagated in 10-day-old specific-pathogen-free (SPF) chicken embryos, and viral titers were determined by calculating $TCID_{50}$ per milliliter using the Reed–Muench method in MDCK cells.

TABLE 1 List of primers used for PCR in this study.

| Target gene | Sequence(5′ to 3′) |
|---|---|
| HA-NUP85 | F-ATGGAGGAGCTCGATGGCGA |
| | R-TCAGGAACCTTCCAGTGAGCC |
| Importin | F-ATGTCCACCAACGAGAATGCTAATACACCAGCTGCC |
| α1 | R-GGTACCTAAAAGTTAAAGGTCCCAGGAGCCCCATCC |
| Importin | F-ATGGCGGACAACGAGAAACTGGACAACCAACG |
| α3 | R-CGGTACCTAAAACTGGAACCCTTCTGTTGGTACATTGGC |
| Importin | F-ATGACCACCCCAGGAAAAGAGAACTTTCGCCT |
| α5 | R-CTTAAAGCTGGAAACCTTCCATAGGAGCCTCACA |
| Importin | F-ATGGAGACCATGGCGAGCCCAGGGAAAGACAATTA |
| α7 | R-TTATAGCTGGAAGCCCTCCATGGGGGCCTCA |
| RanBP5 | F-ATGGCGGCGGCCGCGGCGGAGCAGCAACAGTTC |
| | R-TCACGCAGAGTTCAGGAGCTCCTGAATGGCGGCCTGC |

TABLE 2 List of sequences for siRNAs used in this study.

| siRNAs | Sequence(5′ to 3′) |
|---|---|
| siRNA1 | F-GGGUCGAUUACUUUGAUUATT |
| | R-UAAUCAAAGUAAUCGACCCTT |
| siRNA2 | F-GAGCAUGUAUGGAGGAAAUTT |
| | R-GGAGGAGTGGGTGTCGCTG |

## Antibodies and reagents

Antibodies used for Western blot, immunoprecipitation, and indirect immunofluorescence were anti-NUP85 rabbit polyclonal antibody (catalogue No. 19370-1-AP, Proteintech, Rosemont, United States), anti-Flag mouse monoclonal antibody (catalogue No. 66008-3-Ig, Proteintech, Rosemont, United States), anti-IAV NS1 rabbit polyclonal antibody (catalogue No. GTX125990, GeneTex, CA, United States); anti-HA rabbit polyclonal antibody (catalogue No. 51064-2-AP, Proteintech, Rosemont, United States), anti-GAPDH mouse monoclonal antibody, goat anti-rabbit HRP and goat anti-mouse HRP (catalogue No. FD0063, FDR007, and FDM007, FD bio, Hangzhou, China), Tritc Conjugated goat mouse polyclonal antibody (catalogue No. HA1017, HuaBio, Hangzhou, China), anti-Histone H3 mouse monoclonal antibody (catalogue No. EM30605, HuaBio, Hangzhou, China) and Alexa Fluor 488 conjugated goat rabbit polyclonal antibody (catalogue No. HA1121, HuaBio, Hangzhou, China), Anti-Flag M2 beads (Sigma, MO, United States) and DAPI (Beyotime, Shanghai, China).

## Plasmids, small interfering RNAs and transfection

The nucleic acid for wild-type NUP85 (Nucleoporin 85, GenBank accession No. NM024844.5), RanBP5 (IPO5 importin 5, GenBank accession No. NM002271.6), and the full-length open reading frames (ORFs) of human importin α1 (GenBank accession No. BC005978.1), importin α3 (GenBank accession No. AK291041), importin α5 (GenBank accession No. CR456743.1), and importin α7 (GenBank accession No. AF060543) were obtained from the A549 cells by RT-PCR and subsequently subcloned into eukaryotic expression vector pCMV-HA at EcoRI and KpnI sites, respectively. The PA (GenBank accession No. CY147539), PB1 (GenBank accession No. CY147540), PB2 (GenBank accession No. CY147541), and NP (GenBank accession No. CY147537) of the PR8 H1N1 virus were amplified from viral supernatant and cloned into the vector pCMV-Flag at HindIII and KpnI sites, respectively. All plasmid constructs were confirmed by sequencing.

Small interfering RNAs targeting NUP85 (siRNA1 and siRNA2) and a validated negative control siRNA (NC siRNA) were purchased from GenePharma (Shanghai, China). The knockdown efficiency was examined by qRT-PCR. The primer sequences of PCR for plasmids construction are listed in Table 1, and the sequences for siRNAs are listed in Table 2.

Transfection of Plasmids and siRNAs to HEK293 cells was performed using GeneTwin (Biomed, Beijing, China), DMEM medium without serum and antibiotics. Briefly, plasmids, siRNAs, and GeneTwin were diluted to equal volumes with DMEM and incubated for 5 min at room temperature. The diluted GeneTwin and the diluted DNA (or RNA) were mixed and incubated for 10 min at room temperature, and then the mixture was added to the cells. Transfection of siRNA in A549 cells was mediated by jetPRIME (Polyplus, California, United States) according to the manufacture's instruction. Four hours post-transfection, transfection reagents were replaced with medium containing 10% FBS.

## Virus infection and titration

When the A549 cells in 12-well plates grew to ~95% confluent monolayer, the cell culture medium was withdrawn, and the cells were washed twice with phosphate-buffered saline (PBS). Then viruses in the viral growth medium, which is the medium supplemented with 2% BSA (Sigma, MO, United States) and 2 μg/ml of tosylsulfonyl phenylalanyl chloromethyl ketone (TPCK)-trypsin (Sigma, MO, United States), were inoculated in the cells at indicated MOIs. After adsorption at 37°C for 1 h, the inoculum was removed and replaced with a viral growth medium. And viral supernatants were harvested at the indicated time points post-infection.

To measure the viral titers in the supernatant, we plated MDCK cells in 96-well plates and let them grow to 90%–95% confluence overnight. The supernatant was diluted serially in MEM supplemented with 2% BSA and 2 μg/ml of TPCK-trypsin and inoculated into the cells with PBS washed twice. The IAV-induced cytopathic effect (CPE) was monitored for 24–96 h. $TCID_{50}$ was then calculated by the Reed-Muench formula.

## RNA isolation and qRT-PCR

A two-step real-time quantitative RT-PCR was used to examine specific mRNA levels. Cells were lysed for quantitative reverse transcription-PCR (qRT-PCR), and total RNA was extracted according to the manufacturer's instructions (Easy-do Bio, Zhejiang, China). Reverse transcription was carried out with HiScript Q Select RT SuperMix for qPCR (+gDNA wiper; Vazyme, Nanjing, China). To detect the viral NP mRNA, we used oligo(dT) primer for the reverse transcription. And to detect the viral NP cRNA and vRNA, we used primer specifically targeting IAV H9N2 JSC1 cRNA and vRNA for reverse transcription. Quantitative PCR was performed using ChamQ Universal SYBR qPCR Master Mix (Vazyme, Nanjing, China), and run on an Mx3005P quantitative PCR system(Agilent, California, US). The primers of RT-PCR were designed using PrimerQuest Tool. The sequences of primers for qRT-PCR are listed in Table 3. Each gene was amplified in triplicate, and the mean threshold (Ct) values were calculated. GAPDH was used for normalization in gene expression analysis. Relative fold changes in gene expression among groups were determined using the $2^{-\Delta\Delta Ct}$ method.

## Western blot assay

Cells were collected and washed with PBS and then lysed with RIPA lysis buffer (Beyotime, Shanghai, China) containing Phenylmethanesulfonylfluoride (PMSF, Beyotime, Shanghai, China). The cell lysates were centrifuged at 12,000 g for 10 min at 4°C, and the supernatant was collected, then added with SDS-PAGE sample loading buffer (Beyotime, Shanghai, China) and boiled for 10 min. Equal amounts of protein samples were subjected to SDS-polyacrylamide gel (FD Bio, Hangzhou, China) electrophoresis and transferred to PVDF membrane (Millipore, Darmstadt, Germany). The membrane was probed with various primary antibodies as indicated and detected using the ECL system (Beyotime, Shanghai, China and Thermo Fisher, Massachusetts, United States) with alkaline phosphatase-conjugated secondary antibodies according to the manufacturer's protocol.

TABLE 3 List of primers for qRT-PCR assay in this study.

| Target genes | Sequence(5′ to 3′) |
|---|---|
| GAPDH | F-GCTAAGGCTGTGGGCAAGG |
| | R-GGAGGAGTGGGTGTCGCTG |
| NUP85 | F-GCCAACAGTCACTTTGATTCC |
| | R-CACATACCAGCATCTCCCCTG |
| NS1 | F-TCGAAACAGCTACTCGTGCG |
| | R-ACTGTGAAGCAGGCACAGAA |
| 18 s RNA | F-AGTTGGTGGAGCGATTTGT |
| | R-TGAGCCAGTCAGTGTAGCG |
| NP | F-CAAAGAGGAGATCAGGAGGA |
| | R-TTCCAGTACGCACGAGAGCT |

## Cell viability assay

To detect the effect of NUP85 silencing on cell proliferation, we measured the cell viability of A549 cells transfected with NUP85 siRNA1 or NC siRNA by Cell Counting Kit-8 (CCK-8) activity according to the manufacturer's instructions (APE Bio, Texas, United States). In brief, different amounts of cells in 96-well plates were transfected with NUP85 siRNA1 or NC siRNA, and cell viability was measured at 36 h post-transfection. The CCK-8 reagent was added to each well of the 96-well plates, and cells were incubated at 37°C for 2 h; the absorbance at 450 nm was measured by a microplate reader (Bio-Tek, Vermont, United States).

## Minigenome assay

The minigenome assay was performed as described previously (Zhou et al., 2011). We firstly knocked down NUP85 expression by small interfering RNAs treatment for 24 h, and then we transfected HEK293T cells with 0.2 ug of pPoll-NS-luc plasmid that contains the firefly luciferase gene flanked by the non-coding regions of influenza nonstructural (NS) gene segment and 0.5 ug of each of the reverse genetic plasmids encoding PR8 PB2, PB1, PA, and NP by using 30 ul transfection reagent (GeneTwin). Simultaneously, 50 ng of the Renilla luciferase plasmid pRL-TK (Promega) was co-transfected as a transfection efficiency control. At 24 and 48 h post-transfection, the relative polymerase activity (firefly normalized to Renilla) was measured using the dual-luciferase assay kit (Vazyme, Nanjing, China) according to the manufacturer's instructions. The polymerase activity in the cells co-transfected with NC siRNA was set as 100%, and the activity in the cells co-transfected with NUP85 siRNA was determined relative to that in cells with NC siRNA. The results shown are from three independent experiments performed in triplicate.

## Indirect immunofluorescence assay and confocal microscopy

A549 cells were grown on coverslips to 50% confluence and were transfected with 2 μg of small interfering RNAs. After 24 h, cells were infected with an indicated influenza A virus for 3, 6, and 9 h. Then, cells were fixed with 4% paraformaldehyde (PFA) at 4°C overnight. The next day, cells were washed with PBS three times and permeabilized using 0.2% (vol/vol) Triton X-100 for 15 min, then blocked with 2% (wt/vol) bovine serum albumin (BSA) in PBS for 2 h. Coverslips were incubated with specific antibodies for NUP85 and NP at 4°C for 2 h. After washing with PBS, cells were incubated with indicated Alexa Fluor conjugated secondary antibodies for 2 h at room temperature. After washing the secondary antibodies, nuclei were stained with DAPI for 15 min at room temperature. These samples were observed by confocal microscope (IX81-FV1000; Nikon, Tokyo, Japan) after washing with PBS three times.

## Immunoprecipitation and RNase treatment

HEK293T cells were transfected with the 4 μg of small interfering RNAs for 24 h, and then the cells were transfected with 4 μg plasmids encoding the RNP subunits using GeneTwin (Biomed, Beijing, China) according to the manufacturer's instructions. After 24 h transfection, the cells were lysed with RIPA lysis buffer (Beyotime, Shanghai, China) with Phenylmethanesulfonylfluoride (PMSF, Beyotime, Shanghai, China) supplement. Then the supernatant was collected and used to set up immunoprecipitation assay. For RNase treatment, 100 μg/ml RNase was added to the cell lysate, and the mix was incubated at 37°C for 45 min. Cell extracts were mixed with anti-Flag M2 Magnetic Beads (Sigma, MO, United States) and incubated at 4°C for overnight. The next day, the beads were washed thrice with PBS, and protein-antibody complexes were eluted in buffer (20 mM Tris; 150 mM NaCl; 0.15% HCl; 0.05% Tween). The immunoprecipitated proteins and remaining cell lysates were separated on SDS-PAGE followed by transferring to nitrocellulose for Western blot.

## Nuclear and cytoplasmic protein fractionation

HEK293T cells treated with small interfering RNAs for 24 h were transfected with Flag-PB2 or co-transfected with Flag-PB1 and PA plasmids using GeneTwin (Biomed, Beijing, China) according to the manufacturer's instructions. After 24 h post-transfection, cells were harvested with PBS and collected by centrifugation at 1,000 rpm for 5 min. Nuclear and Cytoplasmic Protein Extraction Kit (Beyotime, Shanghai, China) was used to prepare nuclear and cytoplasmic lysates. For protein isolation, the whole lysates and the cytoplasmic and nuclear fractions were added with SDS-PAGE sample loading buffer (Beyotime, Shanghai, China) and boiled for 10 min, followed by Western blot analysis.

## Cytoplasmic and nuclear RNA fractionation

HEK293T cells treated with small interfering RNAs for 24 h were infected with influenza A viruses. At 6 and 12 h post-infection, cells were collected and washed with PBS three times and then lysed with 0.5% Nonidet P-40 (Sangon Biotech, Shanghai, China) containing RNase Inhibitor and DL-Dithiothreitol (Beyotime, Shanghai, China). The cell lysates were centrifuged at 12,000 g for 5 min at 4°C. The supernatant was collected for cytoplasmic RNA extraction and the precipitate was collected for nuclear RNA extraction.

## Statistical analysis

All data were expressed as mean ± standard deviation (SD) from at least three independent experiments. The statistical analyses were performed with a two-tailed Student's *t*-test and a two-way ANOVA test. Differences between groups were considered significant if $p < 0.05$ (indicated with *), highly significant if $p < 0.01$ (indicated with **) and extremely significant if $p < 0.001$ (indicated with ***).

# Results

## Knockdown of NUP85 suppresses IAV replication

Previous analysis has shown that NUP85 potentially plays a role in influenza virus replication (Li et al., 2020). To determine the role of NUP85 during IAV infection, we applied small interfering RNAs (siRNA) to knockdown NUP85 in A549 cells. Firstly, we confirmed the knockdown efficiency by measuring the NUP85 mRNA level by qRT-PCR. As shown in Figure 1A, expression of NUP85 in the A549 cells that were transfected with two different siRNAs targeted to NUP85 (NUP85 siRNA1 and NUP85 siRNA2) was reduced by 70% ~ 80% as compared to the cells that were transfected with negative control RNAi (NC siRNA) at 6 h post-transfection (h.p.t.). The silencing efficiency went down over time as the degradation of siRNA happened in the cells, but still, the NUP85 expression level was reduced by 40 ~ 70% of control cells at 12 and 24 h.p.t. (Figure 1A). We selected the NUP85 siRNA1, whose silencing efficiency was a little higher than NUP85 siRNA2 for the following experiments. Also, the cell viability was measured by Cell Counting Kit-8 (CCK-8) assay, and the results showed that knockdown of NUP85 by NUP85 siRNA transfection does not have a cytotoxic effect on A549 cells (Figure 1B).

To examine the function of NUP85 during virus replication, we infected A549 cells with influenza virus A/Puerto Rico/8/1934 (H1N1) (PR8), A/swine/Jiangsu/C1/2008 (H9N2) (JSC1), A/Zhejiang/163/2020 (H3N2) (HZ163) after NUP85 siRNA or NC siRNA transfection. Samples were collected at 0, 3, 6, 12, 24, and 36 h post-infection (h.p.i.), and Western blot was performed to detect viral NS1 protein in the infected cells. The result showed much less viral NS1 protein was detected in the cells with NUP85 siRNA treatment compared with NC siRNA treatment at different time points post-infection by three different strains of viruses (Figures 1C,E,G). To further confirm the impact of NUP85 knockdown on IAV replication, we determined the growth kinetics of H1N1 PR8, H3N2 HZ163, and H9N2 JSC1 in NUP85 siRNA- or NC siRNA-treated A549 cells. Supernatant samples were collected at 3, 6, 12, 24, and 36 h.p.i., and the viral titers were examined by 50% tissue culture infective dose ($TCID_{50}$) assay in MDCK cells. The results showed that the viral loads of H1N1 PR8, H3N2 HZ163, and H9N2 JSC1 were significantly decreased in NUP85 siRNA-treated cells compared to NC siRNA-treated cells (Figures 1D,F,H). Taken together, these results showed that the knockdown of NUP85 suppressed IAV replication.

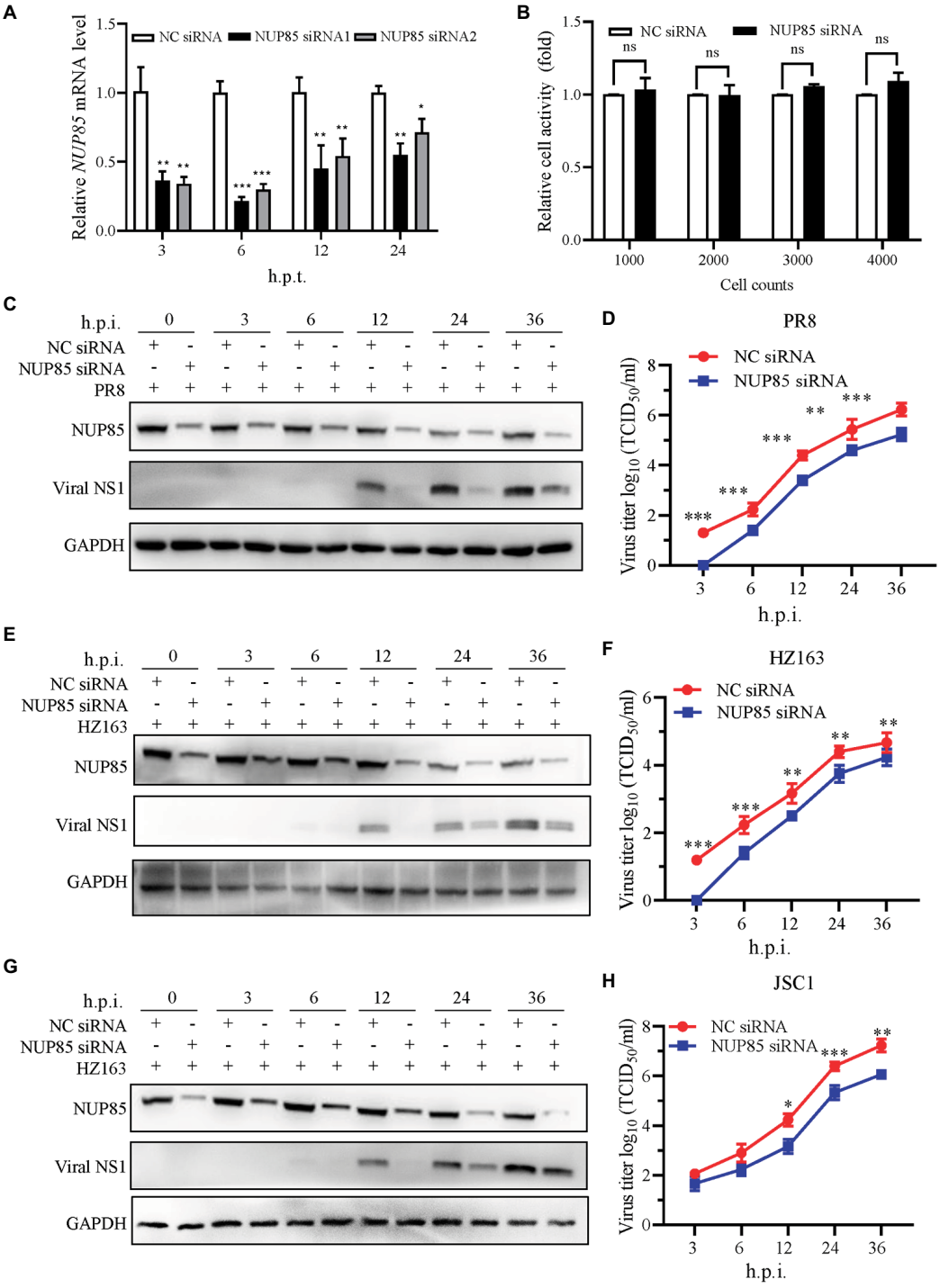


FIGURE 1
NUP85 knockdown suppresses IAV replication. **(A)** The silencing efficiency of *NUP85*-specific siRNAs. A549 cells were transfected with two individual siRNAs targeted to *NUP85* (NUP85 siRNA1 and NUP85 siRNA2) or non-target siRNA as negative control (NC siRNA), and the cells were harvested for RNA isolation at 3, 6, 12, and 24h.p.t., followed by qRT-PCR to detect the relative expression level of *NUP85*. **(B)** The effect of NUP85 siRNA1 on A549 cell viability. Indicated numbers of A549 cells were transfected with NUP85 siRNA1 and NC siRNA for 36h.p.i. Cell viability was measured by Cell Counting Kit-8 (CCK-8) assay. **(C,E,G)** The effect of siRNA on the expression of IAV NS1 protein. A549 cells were transfected with NUP85 siRNA and NC siRNA and then infected with H1N1 PR8, H3N2 HZ163, and H9N2 JSC1 (MOI=0.1). Whole cell lysates were collected at the indicated time points and subjected to Western blot to detect the NUP85 and viral NS1 protein levels. GAPDH was used as an internal control. Images are from one of three independent experiments. **(D,F,H)** A549 cells were transfected with NUP85 siRNA and NC siRNA and then infected with influenza A virus JSC1, PR8 and HZ163 (MOI=0.01). Cell supernatants were harvested at 3, 6, 12, 24, and 36h.p.i. Virus titers were determined by $TCID_{50}$ assay on MDCK cells. Data are mean±SD of three independent experiments. Significance is calculated by unpaired *T*-test; *indicates $p$ <0.05; **indicates $p$ <0.01; *** indicates $p$ <0.001.

## Knockdown of NUP85 inhibits polymerase activity and suppresses RNA synthesis during IAV infection

IAV uses an RNA-dependent RNA polymerase (RdRp) compacted into RNP to transcribe and replicate its RNA genome. To investigate whether deduction of viral replication in NUP85 knockdown cells would result from the decreased polymerase activity, we performed a well-established mini-replicon assay to examine the effect of NUP85 on the polymerase activity of the H1N1 PR8 virus (Lutz et al., 2005). In the assay, HEK293T cells treated with NUP85 siRNA or NC siRNA were transfected with plasmids encoding RNP subunits PB1, PB2, PA, and NP, as well as a Poll-driven RNA expression plasmid encoding the firefly luciferase gene which was franked by viral NS non-coding sequences. The experiment showed that knockdown of NUP85 resulted in an approximately 55% reduction in the polymerase activity at 24 h.p.t. and ~40% reduction in the polymerase activity at 48 h.p.t. compared with control. The lowered deduction of polymerase activity at 48 h.p.t. may result from the decreased silencing efficiency along with the degradation of the interfering RNA (Figure 2A). The result indicates that NUP85 silencing reduces viral polymerase activity, thereby inhibiting IAV replication.

To further determine whether NUP85 knockdown affected viral genome replication, A549 cells were transfected with the NC siRNA and NUP85 siRNA, followed by infection of H9N2 JSC1 at an MOI of 2. Cells were collected, and viral RNAs were examined at 3, 6, and 9 h post-infection. The levels of viral RNAs (vRNA, cRNA, and mRNA) were considerably lower in the NUP85 siRNA-treated cells than those in NC siRNA-treated cells (Figures 2B–D). The results indicated that NUP85 is essential in viral RNA synthesis.

## Knockdown of NUP85 hinders the vRNP import into nucleus

Transcription and replication of influenza A viral gene happen in the nucleus, so the nuclear import of vRNP is pivotal to the transcription and replication of influenza A viral gene. We hypothesized that NUP85 knockdown might affect the nuclear import of vRNPs in A549 cells. Viral NP is a major component of the vRNP complex, and it mediates the nuclear import of the vRNP complex *via* its nuclear localization signals (NLSs) (Naito et al., 2007a; Kawaguchi et al., 2011; Luo et al., 2018). We examined the cellular distribution of vRNP by imaging viral NP in A549 cells. A549 cells treated with NUP85 siRNA or NC siRNA were infected with H9N2 JSC1, and then viral NP and nucleus were stained to display the vRNP subcellular localization by immunofluorescence microscopy. In NC siRNA-treated cells, NP had clearly accumulated exclusively in the nucleus of approximately 45% of cells, and it accumulated both in the nucleus and cytoplasm of roughly 40% of cells at 3 h.p.i., and then it was predominantly located in the nucleus (81% of the cells) at 6 h.p.i. (Figures 3A,B). While none of the cells treated with NUP85 siRNA had NP exclusively localized in the nucleus at 3 h.p.i., and most NP was still distributed in the cytoplasm at the time point. At 6 h.p.i., the percentage of exclusive nuclear localization of viral NP in the NUP85 knockdown cells decreased over 20% compared with control cell (Figures 3A,B). After the primary transcription of the viral genes, the newly synthesized RNP subunit mRNA was exported from the nucleus to the cytoplasm for protein translation to form more RNPs (Matsuoka et al., 2013). At a later stage (9 h.p.i.), NP started to re-localization into the cytoplasm in NC siRNA-treated cells, but it still predominantly localized in the nuclear in the NUP85 siRNA-treated cells. These results suggest that knockdown of NUP85 hinders the nuclear import of vRNP, which leads to decreased polymerase activity and reduced viral replication.

To further confirm the defective nuclear import of vRNP when NUP85 was knocked down, we fractionated the cytoplasm and nucleus of infected cells and examined vRNP distribution indicated by NP expression at 3, 6, and 9 h post-infection by Western blot. As shown in Figure 3C, the nuclear distribution of vRNP decreased by 37% at 3 h.p.i. in the NUP85-knockdown cells compared with the control cells. The number changed to 21% as more vRNPs entered into the nucleus at 6 h.p.i., but the total amount of vRNP in the nuclear and cytoplasm is less in the NUP85-knockdown cells than in the control cells. At a later stage (9 h.p.i.), there is only one-third of vRNPs distributed in the nucleus in control cells, and there are still nearly a half vRNP in the nucleus in the NUP85 knockdown cells. The results are consistent with what we have seen in the immunofluorescent microscopy assay (Figures 3A,B). Furthermore, we examined vRNA levels in the cytoplasmic and nuclear fractions at 6 and 12 h post-infection by qRT-PCR. The NP vRNA in the nucleus in the NUP85 knockdown cells was only around a half when compared with the control cell at 6 and 12 h post-infection. The NP vRNA in the cytoplasm in the NUP85 knockdown cells was only 23% compared to that in the control cell at 6 h post-infection (Figure 3D). And the total vRNA in the nucleus and cytoplasm decreased by 45% in the NUP85 knockdown cells compared to that in the control cells at 6 h post-infection, and it decreased by 60% in the NUP85 knockdown cells at 12 h post-infection (Figure 3D). The results indicated that the knockdown of NUP85 impaired nuclear import of vRNP and further resulted in the decreased polymerase activity and reduced viral replication.

## NUP85 binds to IAV RNP subunits PB1 and PB2

NUP85 is a component of the Nup107-160 subunit of the nuclear pore complex, which is embedded in the nuclear envelope and mediates bidirectional transport of macromolecules between the cytoplasm and nucleus (Beck and Hurt, 2017). IAV vRNP transports into the nucleus by interacting with host factors. To

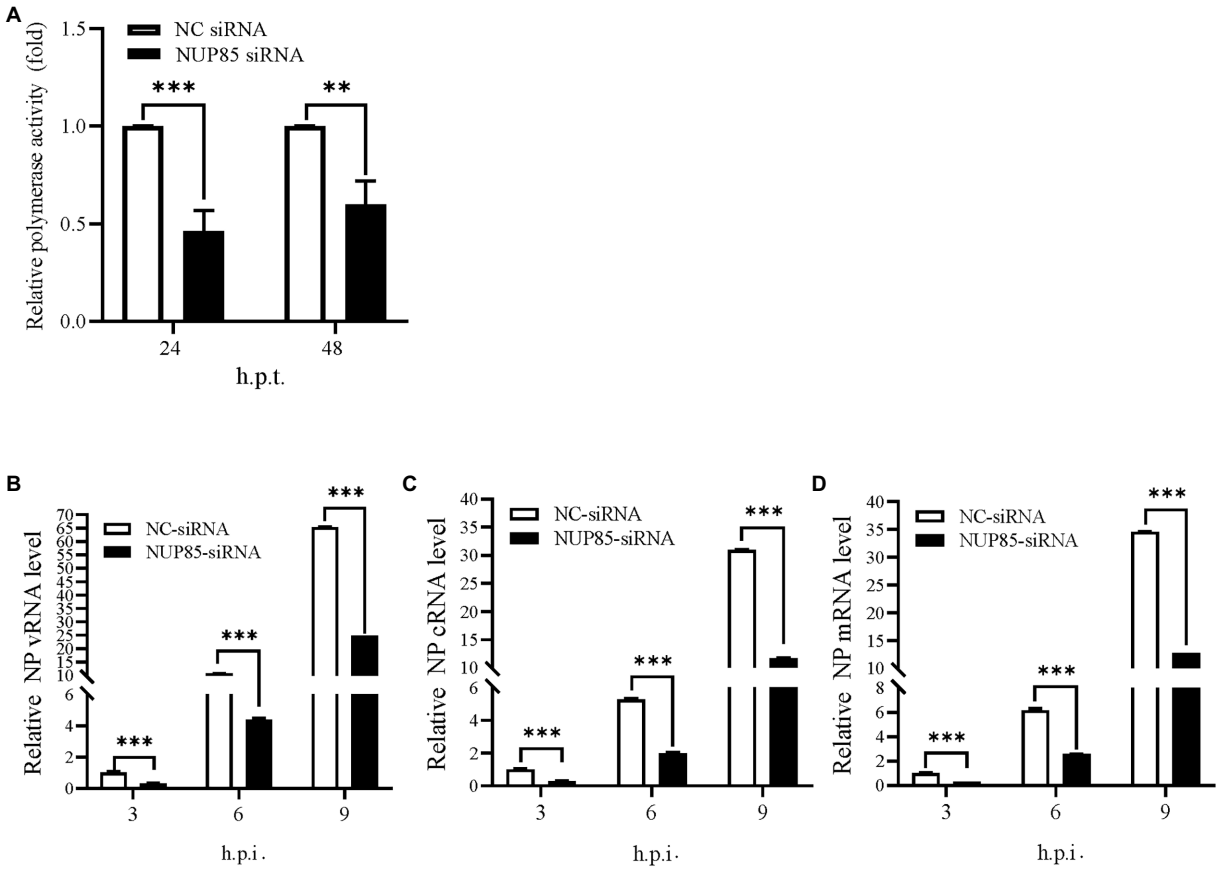


FIGURE 2
Knockdown of NUP85 inhibits polymerase activity and suppresses RNA synthesis during IAV infection. **(A)** HEK293T cells treated with NUP85 siRNA or NC siRNA were transfected with vRNP reconstitution plasmids together with Renilla plasmids. Luciferase activities were measured at 24 and 48h.p.t., and Renilla luciferase was used as an internal control. **(B–D)** A549 cells were transfected with NUP85 siRNA and NC siRNA for 24h and then infected with influenza A virus JSC1 (MOI=2). Cells were harvested for RNA isolation at 3, 6, and 9h.p.t., followed by qRT-PCR to detect vRNA, cRNA and mRNA relative expression level of NP. The viral RNA levels were normalized to the 18S rRNA level. Data are mean±SD of three independent experiments. Significance is measured by unpaired *T*-test; ** indicates $p<0.01$. *** indicates $p<0.001$.

determine the associations between NUP85 and each RNP subunit, Flag-PA, Flag-PB1, Flag-PB2, or Flag-NP and hemagglutinin (HA)-NUP85 were co-transfected into HEK293T cells, respectively. Then, co-immunoprecipitation (co-IP) was performed at 24h post-transfection. Results showed that NUP85 could co-precipitate with Flag-PB1 and Flag-PB2, but not with Flag-NP and Flag-PA (Figure 4A). Since IAV RNP subunits were the RNA-binding proteins, we also performed the same co-IP assays under RNase A treatment. Results showed that NUP85 was not co-precipitated with Flag-PB1 and Flag-PB2 under the RNase A treatment (Figures 4B,C), suggesting that NUP85 binds to PB1 and PB2 in an RNA-dependent manner.

## Knockdown of NUP85 impedes nuclear import of IAV RNP subunits PB1 and PB2

Since NUP85 knockdown hindered the nuclear import of vRNP and the interaction of NUP85 with RNP subunits PB1 and PB2, we further examined the effect of NUP85 on the nuclear import of PB1 and PB2. Since PB1 enters the nucleus with PA as a dimer, A549 cells were treated with NUP85 siRNA or NC siRNA, then transfected with plasmids expressing Flag-PB1 and Flag-PA for 24h. The results of nuclear and cytoplasmic fractionation showed that the relative protein level of Flag-PB1 in the cytoplasmic was raised by about 44%, and that in the nucleus was decreased by about 29% in the NUP85 siRNA-treated cells compared with the NC siRNA-treated cells (Figure 5A). To examine the nucleocytoplasmic distribution of viral PB2, we transfected Flag-PB2 into the NUP85 siRNA- or NC siRNA-treated cells and determined the PB2 protein levels in cellular nuclear and cytoplasmic parts. Similar to PB1, the relative Flag-PB2 protein level in the cytoplasmic was raised about 23%, and that in the nucleus was decreased by about 23% in the NUP85 siRNA-treated cells compared with the NC siRNA-treated cells (Figure 5B). To further confirm the effect of NUP85 on the nuclear import of IAV RNP subunits PB1 and PB2 is specific, we also examined the nuclear import of IAV RNP subunit PA. PA contains NLS and does not bind with NUP85. As shown in Figure 5C, the knockdown of

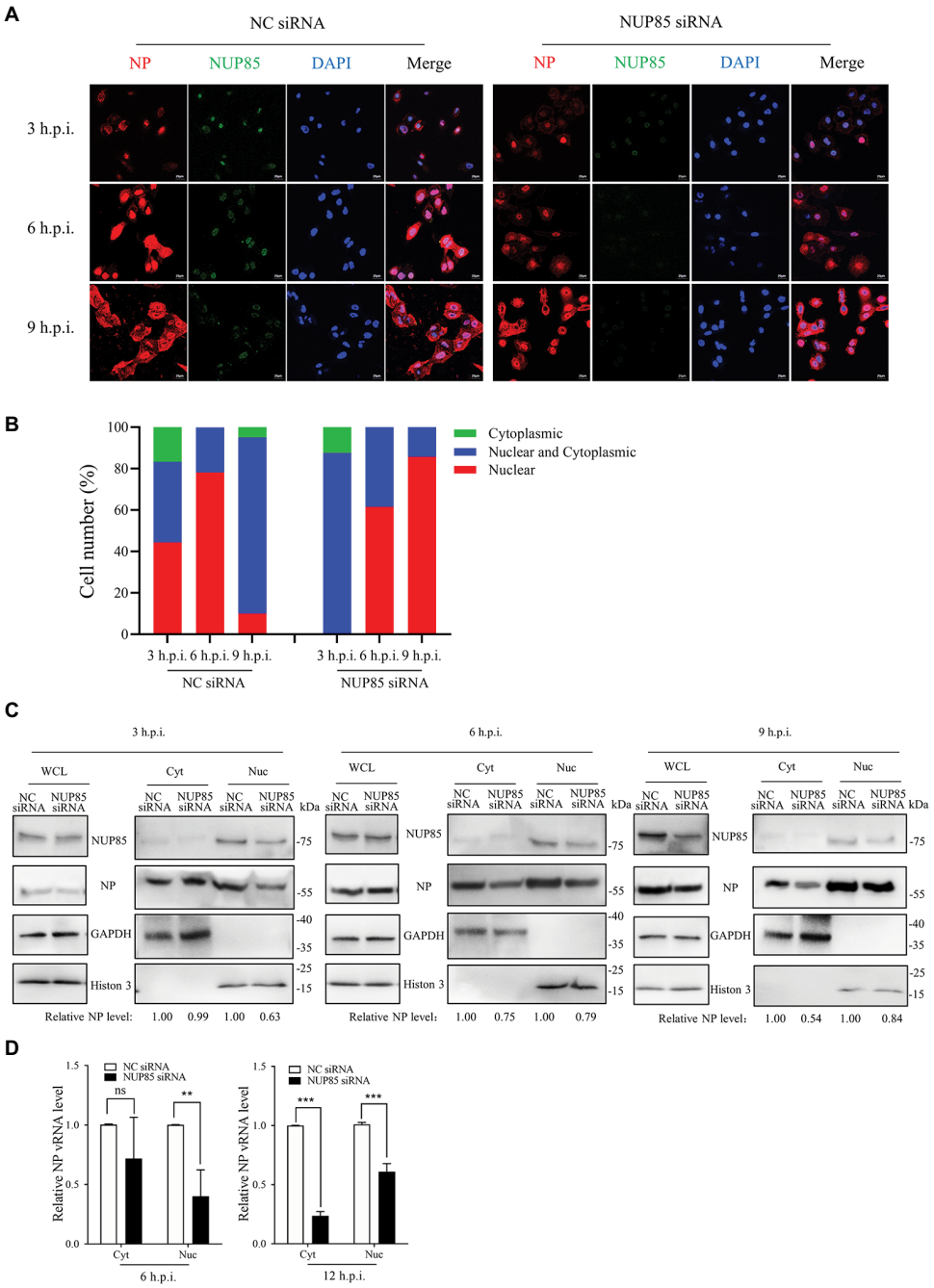


FIGURE 3
Knockdown of NUP85 inhibits the nuclear import of vRNP. **(A)** Confocal microscopy analysis of the nucleocytoplasmic distribution of vRNP in virus-infected NUP85 knockdown cells. A549 cells were treated with NUP85 siRNA or NC siRNA and then were infected with the H9N2 JSC1 virus (MOI=3). At 3, 6, and 9h post-infection, cells were fixed, permeabilized, and stained with mouse anti-NP (red), rabbit anti-NUP85 (green) and DAPI (blue). The scale bar represents 20μm. Images are representative of three independent experiments. **(B)** Quantitative analysis of vRNP localization in the infected cells was performed by calculating cell numbers with related fluorescence. At least 100 cells in each group were scored. **(C)** Western blot analysis of the distribution of NP in the cytoplasmic and nuclear fractions in virus-infected NC siRNA and NUP85 siRNA-treated cells. A549 cells were treated with NUP85 siRNA or NC siRNA and then were infected with the H9N2 JSC1 virus (MOI=3). Cells were harvested at 3, 6, and 9h.p.i. Then, the nucleocytoplasmic distribution of NP was examined by Western blot and grayscale analysis. The relative protein level of NP in nucleus is indicated with its gray intensity divided by that of Histone 3, and the relative protein level of NP in cytoplasmic is indicated with its gray intensity divided by GAPDH. Then they are normalized by that of control group, the results of which are shown at the bottom panel. Images are representative of three independent experiments. **(D)** qRT-PCR analysis of the distribution of viral vRNA in the cytoplasmic and nuclear fractions in virus-infected NC siRNA and NUP85 siRNA-treated cells. A549 cells were treated with NUP85 siRNA or NC siRNA and then were infected with the H9N2 JSC1 virus (MOI=3). Cells were harvested and the cytoplasmic and nuclear parts were fractionated at 6, and 12h.p.i., followed by qRT-PCR to detect the relative level of NP vRNA. Data are mean±SD of three independent experiments. Significance is measured by unpaired *T*-test; ns, no significance. ** indicates $p$ <0.01. *** indicates $p$ <0.001.

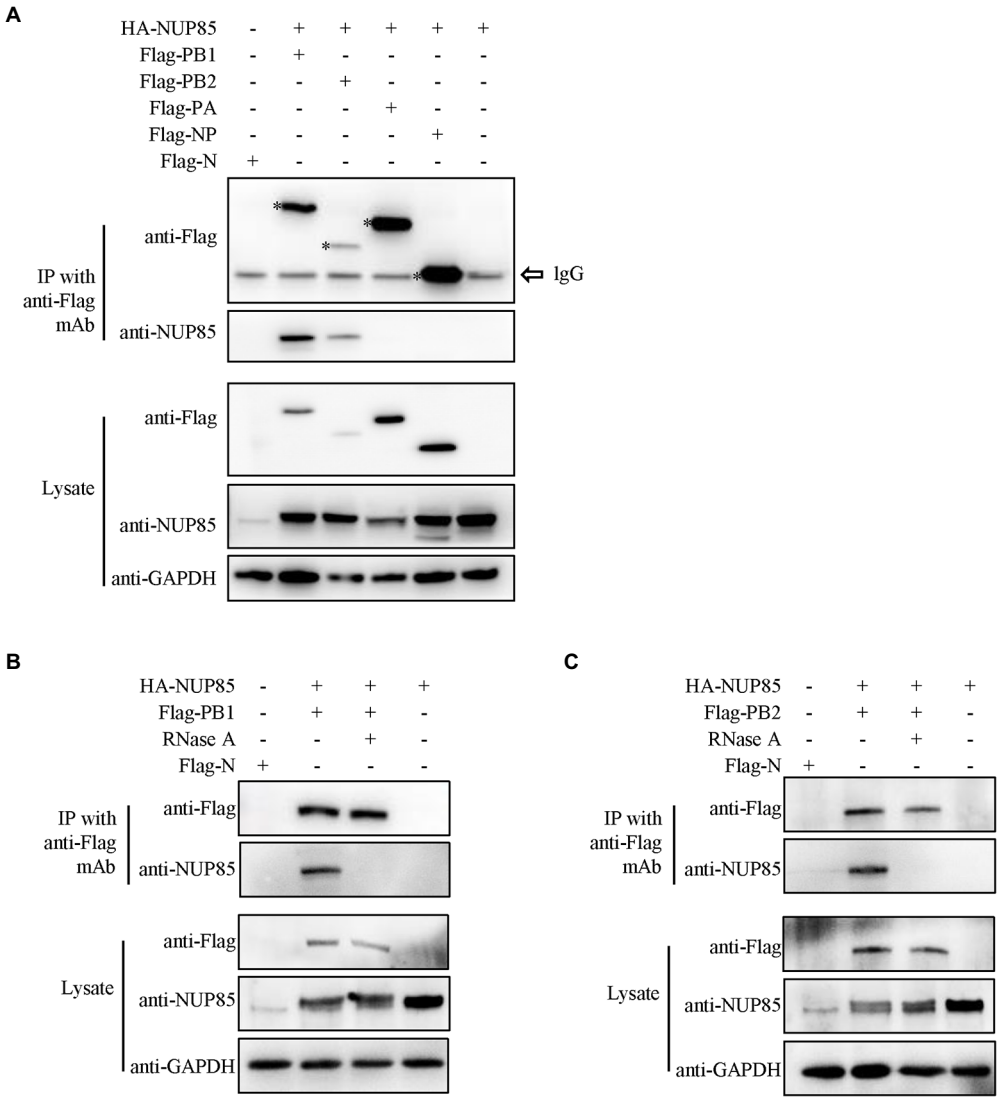


FIGURE 4
Interactions between NUP85 and RNP subunits. **(A)** HEK293T cells were co-transfected with HA-NUP85 and Flag-PA, Flag-PB1, Flag-PB2, Flag-NP, or Flag-N, respectively. Cells were then lysed at 24h post-transfection, and immunoprecipitation was performed using anti-Flag antibodies followed by Western blot. **(B)** HEK293T cells were co-transfected with HA-NUP85 with Flag-PB1 and Flag-N or HA-NUP85, respectively. Cells were lysed and treated the RNase at 24h post-transfection, and immunoprecipitation was performed using anti-Flag antibodies followed by Western blot. **(C)** HEK293T cells were co-transfected with HA-NUP85 with Flag-PB2 and Flag-N or HA-NUP85, respectively. Cells were lysed and treated the RNase at 24h post-transfection, and immunoprecipitation was performed using anti-Flag antibodies followed by Western blot.

NUP85 did affect the nuclear import of NP. These results indicate that NUP85 affects the nuclear import of RNP subunits PB1 and PB2, and the process relies on the interaction of NUP85 with PB1 and PB2.

## NUP85 assists the binding of PB1 to RanBP5 and the binding of PB2 to importin α1 and importin α7

Previous studies have already reported that IAV PB1 enters the nucleus *via* a non-classical transport pathway mediated by RanBP5 (Deng et al., 2006; Huet et al., 2010; Hutchinson et al., 2011), and viral PB2 enters the nucleus by binding multiple isoforms of importin α in the classic importin α - importinβ1 pathway (Resa-Infante et al., 2008; Gabriel et al., 2011; Beck and Hurt, 2017). However, unlike PB2, which can accumulate efficiently in the nucleus in the absence of other viral proteins, PB1 and PA can be efficiently imported into the nucleus only after they form a dimer in the cytoplasm (Jones et al., 1986; Smith et al., 1987; Hutchinson and Fodor, 2012). To test the hypothesis that NUP85 might play a role in the interaction between PB1 and RanBP5, we co-transfected the HEK293T cells with plasmids expressing Flag-PB1, HA-RanBP5 and PA

in the NUP85 siRNA or NUP85 expressing plasmids treated 293 T cells and detected the effect of NUP85 knockdown or overexpression on the PB1 and RanBP5 interaction by co-immunoprecipitation. The results showed that PB1 bound to RanBP5 as reported previously, but the relative amount of PB1 binding to RanBP5 was obviously decreased when NUP85 was knocked down and significantly increased when NUP85 was overexpressed (Figure 6A). The results suggest that NUP85 is involved in the interaction between PB1 and RanBP5. Since knockdown of NUP85 impedes nuclear import of PB2, and PB2 relies on the interaction with importin α1, α3, α5, and α7 to mediate its nuclear import (Mukaigawa and Nayak, 1991; Tarendeau et al., 2007; Gabriel et al., 2011), we hypothesized that NUP85 knockdown might affect the interaction between PB2 and importin α. To test the hypothesis, we treated HEK293T cells with NUP85 siRNA or NUP85 expressing plasmids for 24 h, then transfected with plasmids expressing Flag-PB2 and HA-importin α. The results of immunoprecipitation showed that PB2 bound to all four isoforms of importin α, and NUP85 knockdown obviously reduced the amounts of importin α1 and importin α7 immunoprecipitated with PB2 (Figures 6B,E), but not the amounts of immunoprecipitated importin α3 and importin α5 (Figures 6C,D), indicating that NUP85 knockdown interfered with the interaction between PB2 with both importin α1 and importin α7. Accordingly, NUP85 overexpression obviously increased the relative amounts of importin α1 and importin α7 immunoprecipitated with PB2 (Figures 6B,E), but not the relative amounts of immunoprecipitated importin α3 and importin α5 (Figures 6C,D). These results suggest that NUP85 facilitates the nuclear import of PB1 by enhancing the interaction of PB1 with RanBP5, and it facilitates the nuclear import of PB2 by enhancing the interaction of PB2 with importin α1 and importin α7.

## IAV infection decreases NUP85 expression

To investigate NUP85 expression during IAV infection, we detected the mRNA and protein levels of NUP85 in A549 cells after infection with three strains of IAV (influenza A H1N1 PR8, H3N2 HZ163, H9N2 JSC1), respectively. The mRNA level of NUP85 was detected by qRT-PCR at different time points post-infection. We observed a gradual decrease in NUP85 mRNA level in the process of each virus infection, and the level decreased by half at 12 h.p.i. (Figures 7A–C). And about a two-fold decrease in NUP85 protein level was observed in the infected A549 cells at 24 h.p.i. (Figure 7D). Meanwhile, treatment with a synthetic analog of viral double-stranded RNA polyinosinic-polycytidylic acid (Poly(I: C)) does not decrease NUP85 expression (Figures 7E,F). These data demonstrated that NUP85 expression was downregulated upon IAV infection.

# Discussion

Influenza A viruses are responsible for seasonal flu and even some pandemics. Several antivirals were developed for binding the viruses. Due to the rapid mutation of the viral genes, the evolution of resistance to the antiviral vaccine and therapy is rapid (Peacock et al., 2019). Understanding the interaction of virus and host factors would be of great importance in developing novel, effective antivirals. After influenza A virus invades the host cell, vRNPs are released into the cytoplasm, then they enter the nucleus through the nuclear pore for viral gene transcription and replication (Banerjee et al., 2014; Miyake et al., 2019; Sempere Borau and Stertz, 2021). IAV gene transcription and genome replication are mediated by the RNA-dependent RNA polymerase, which comprises PB1, PB2, and PA. PB1 is a critical factor of polymerase complex, and its N-terminal region binds to the C-terminal region of PA. The C-terminal region of PB1 interacts with the N-terminal region of PB2 (Te Velthuis and Fodor, 2016). In addition, NP interacts with PB1 and PB2 but not with PA (Biswas et al., 1998). For successful viral transcription and replication, vRNPs must pass through the NPC to the nucleus for primary gene transcription. Following the primary protein synthesis in the cytoplasm, newly formed viral proteins, including PB2, NP, PB1, and PA, are translocated back into the nucleus for vRNP assembly. Then the assembled progeny vRNP would be exported from the nuclear to the cytoplasm, and it finally reaches the cell membrane for progeny virus budding and release (Eisfeld et al., 2015; Peacock et al., 2019). In this study, we demonstrated that NUP85 interacted with the PB1 and PB2 in an RNA-dependent manner. Knockdown of NUP85 delayed the nuclear localization of vRNP in the early life cycle, weakened the binding of PB1 to RanBP5 and the binding of PB2 to importin α1 and importin α7, therefore leading to a smaller amount of nuclear PB1 and PB2, and further resulting in the reduced polymerase activity and suppressed virus replication. A proposed model of the mechanism NUP85 utilizes in the IAV infection is illustrated in Figure 8.

It has been well studied that vRNP utilizes the nuclear localization signals (NLSs) of NP for its nuclear translocation *via* the classic nuclear import pathway (Naito et al., 2007a; Hutchinson and Fodor, 2012). But whether NLSs of the polymerase subunits also contribute to the import of RNPs remains to be determined (Wu and Pante, 2009; Hutchinson and Fodor, 2012). In this study, we showed that NUP85 interacted with PB1 and PB2 in an RNA-dependent manner rather than with NP and PA. As RNA polymerase and nucleoprotein, all IAV RNP subunits are capable of binding viral RNA. NP can bind small RNA as well (Labaronne et al., 2016). What kind of RNA mediating interaction of NUP85 with PB1 and PB2 is not clear and worthy of further study. Knockdown of NUP85 significantly delayed vRNP entry into the nucleus at 3 h post-infection, inhibiting polymerase activity and suppressing viral replication.

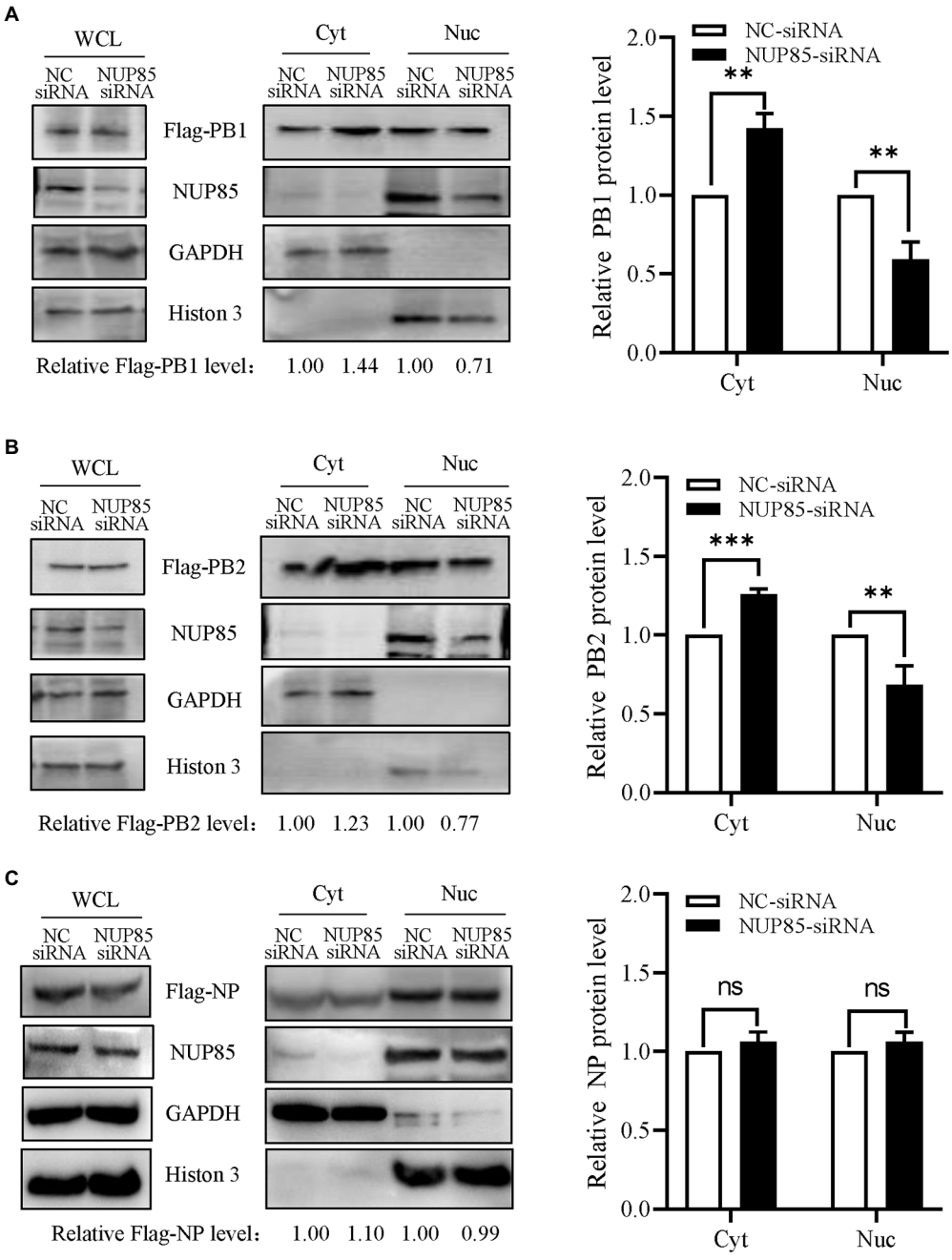


FIGURE 5
Knockdown of NUP85 affects the nucleocytoplasmic distribution of viral PB1 and PB2, but not NP. **(A)** Plasmids expressing Flag-PB1 and PA were transfected into HEK293T cells treated with NUP85 siRNA or NC siRNA, and the nucleocytoplasmic distribution of Flag-PB1 was examined by Western blot and densitometry analysis. Statistical analysis of PB1 distribution in the NC siRNA-treated or NUP85 siRNA-treated cells was shown on the right. **(B,C)** Plasmids expressing Flag-PB2 **(B)** or Flag-NP **(C)** were transfected into HEK293T cells treated with NUP85 siRNA or NC siRNA, and the nucleocytoplasmic distribution of Flag-PB2 was examined by Western blot and grayscale analysis. The statistical analysis of relative band intensity of PB2 **(B)** or NP **(C)** was shown on the right. Western blot densitometry analysis was performed using software ImageJ. Histone 3 and GAPDH were used as loading controls for nuclear and cytoplasmic fractions, respectively. The relative protein level of PB1, PB2, and NP in nucleus is indicated with its gray intensity divided by that of Histone 3, and the relative protein level of PB1, PB2, and NP in cytoplasmic is indicated with its gray intensity divided by GAPDH. Then they are normalized by that of control group, the results of which are shown at the bottom panels **(A–C)**. Data are mean ± SD of three independent experiments. Significance is measured by unpaired *T*-test; ** indicates $p<0.01$. *** indicates $p<0.001$. ns, no significance.

The study may provide a new possibility that NLSs of PB1 and PB2 also play a specific role in the nuclear import of RNPs. The classic IMP α-IMP β1 pathway used by viral protein includes cargo, importin-α, and importin-β1 (Tarendeau et al., 2007; Gabriel et al., 2008; Lange et al., 2010). The NLS-containing cargo protein binds to importin-α, and importin-α binds to importin-β1

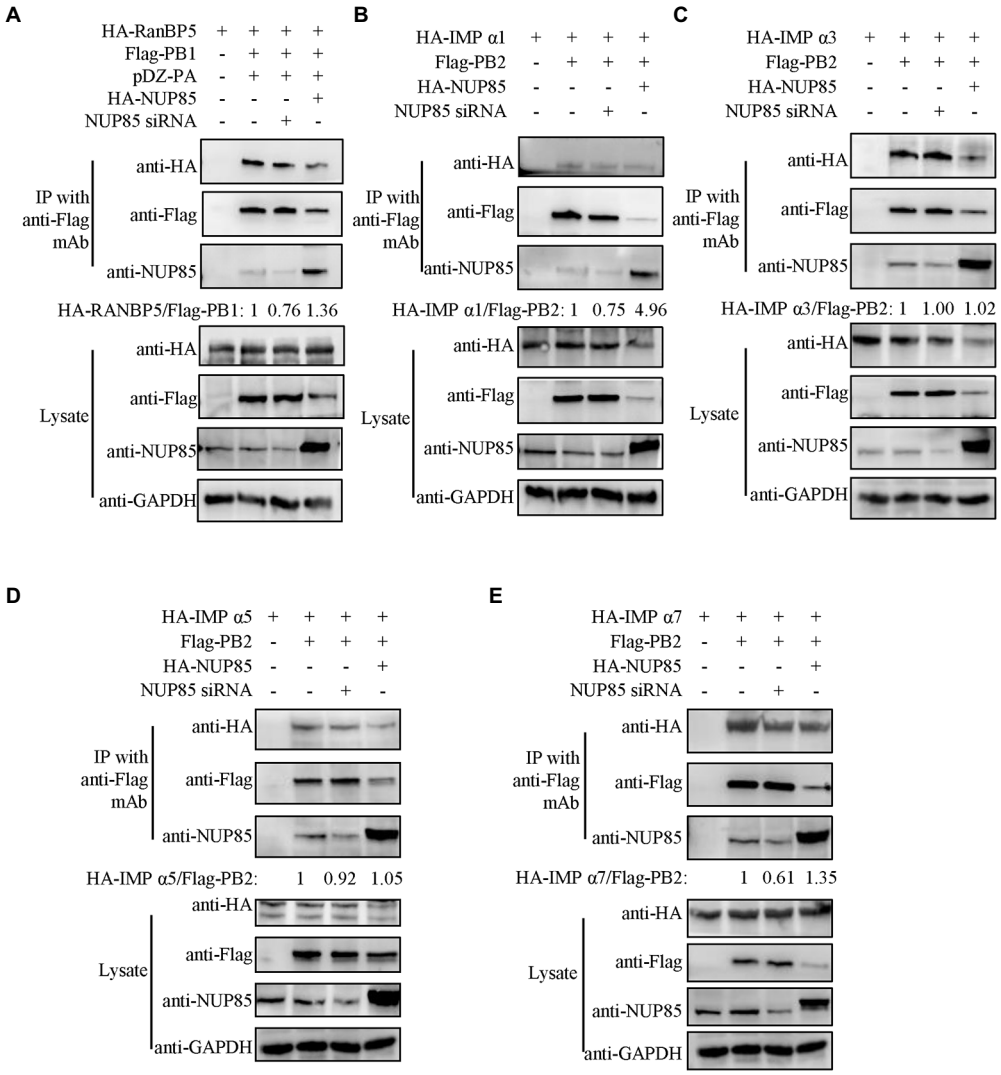


FIGURE 6
NUP85 facilitates IAV PB1-RanBP5, PB2-importin α1, and PB2-importin α7 interactions. **(A)** Effect of NUP85 on the interaction between RanBP5 in PB1. HEK293T cells were treated with NUP85 siRNA or NUP85 expressing plasmids and then transfected with the indicated plasmids for 24h. Cell lysates were immunoprecipitated with an anti-Flag antibody. RanBP5 and Flag-PB1 levels were detected *via* Western blot. The band intensities were quantified by ImageJ, and relative precipitated HA-RanBP5 /Flag-PB1 ratios are shown at the bottom. **(B–E)** Interaction of PB2 with importin α family members, importin α1 **(B)**, importin α3 **(C)**, importin α5 **(D)**, and importin α7 **(E)** in the NUP85 siRNA or NUP85 expressing plasmid treated cells. Cell lysates were immunoprecipitated with a mouse anti-Flag antibody. The bound proteins were detected by Western blot with a rabbit anti-HA antibody, a mouse anti-Flag antibody, or a rabbit anti-NUP85 antibody to detect importin α family members, NP, NUP85, and GAPDH, respectively. Images are representative of three independent experiments. The band intensities were quantified by ImageJ. The binding ratio of importin and PB1 or PB2 was calculated with the gray value of the importin divided by that of Flag, and then normalized by the that of control group, the results of which are present at the bottom of the panels. Images are representative of three independent experiments.

through its N-terminal IBB domain, which constructs the complex of cargo-importin-α-importin-β1 (Cingolani et al., 1999; Lott et al., 2010). It has been shown that the ternary complex (cargo-importin-α-importin-β1) or binary complex (cargo-RanBP5) is transported through NPC by the interaction of importin-β with phenylalanine and glycine (FG)-riched nuclear pore proteins (Beck and Hurt, 2017; Hampoelz et al., 2019). Interestingly, NUP85 does not contain FG-repeat, which implies that nuclear transporter factors RanBP5 or importin-β1 may not bind to NUP85. Our study reveals that NUP85 silencing inhibits the nuclear entry of PB1 and PB2, suggesting that NUP85 is indeed associated with cargo-importin-α -Importin-β1 and cargo-RanBP5 complex. But the mechanism remains elusive, and it could be one of the future directions.

NUP85 is a part of subcomplex Nup107-160, which forms the out ring of NPC and is critical for NPC assembly (Walther et al., 2003). NUP85 is also a cytoplasmic protein (known as FROUNT), and its overexpression amplified the chemokine-elicited PI(3)K–Rac–lamellipodium protrusion cascade (Terashima et al., 2005). We tried to overexpress NUP85 to test

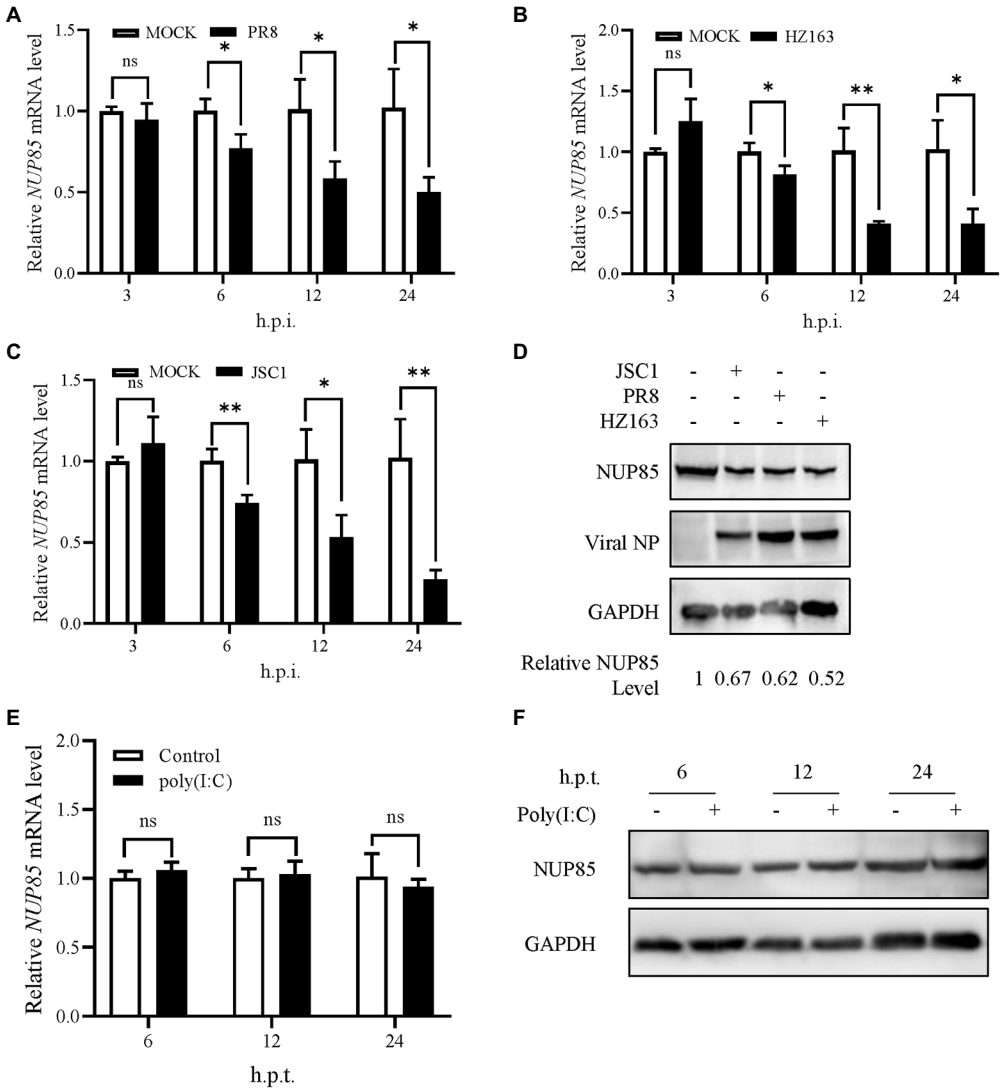


FIGURE 7
Influenza A virus infection decreased NUP85 expression. **(A–C)** A549 cells were infected with H1N1 PR8, H3N2 HZ163, and H9N2 JSC1, respectively (MOI=0.1). Cells were harvested for RNA isolation at 3, 6, 12, and 24h.p.i. The relative expression level of NUP85 was determined by qRT-PCR. Data are mean±SD of three independent experiments. Significance is measured by two-way ANOVA test; * indicates $p$ <0.05, ** indicates $p$ <0.01. **(D)** A549 cells were infected with H9N2 JSC1, H1N1 PR8, and H3N2 HZ163 at indicated MOIs and harvested at 24h.p.i. for Western blot analysis of NUP85, viral NP, and GAPDH protein levels. GAPDH was used as a loading control. **(E,F)** A549 cells were treated with 1μg/ml poly(I:C) with (+) or without (–) transfection reagent for 6, 12, and 24h, then collected for Western blot and qRT-PCR analysis of NUP85. Data are mean±SD of three independent experiments. Significance is measured by unpaired $T$-test; * indicates $p$ <0.05. ** indicates $p$ <0.01.

its effect on vRNP import and viral replication. Still, we failed it as the cells became too unwell to do viral infection after NUP85 introduction either by transient transfection or by lentivirus transduction. It seems excessive NUP85 is not friendly to the A549 cells cell, and whether excessive NUP85 affected normal cellular metabolism due to NUP85 accumulating in the cytoplasm is elusive and worthy of further investigation. NUP85 interacts with HIV Tat protein in the cellular nucleus. Here, we showed that NUP85 interacted with IAV PB1 and PB2 protein, which was required for vRNP, PB1, and PB2 import into the nucleus. Other NUPs have also been shown to be essential for IAV infection. NUP62 is required for the nuclear export of IAV mRNA and vRNA (Morita et al., 2013). NUP93 is involved in the nuclear export of IAV RNA (Furusawa et al., 2018). NUP98 interacts with IAV NS2/nuclear export protein through its FG repeat, and overexpression of the domain inhibits virus propagation (Chen et al., 2010). In addition, the influenza A virus down-regulates Nup98 to facilitate its infection (Satterly et al., 2007). Moreover, Panda et al. showed that Nup98 directly binds to the promoters of virus-induced genes and promotes antiviral gene expression (Panda et al., 2014). But we did not see any difference in the mRNA levels of multiple immune-related factors in the NUP85 siRNA and NC siRNA-treated A549 cells after influenza A virus JSC1 H9N2

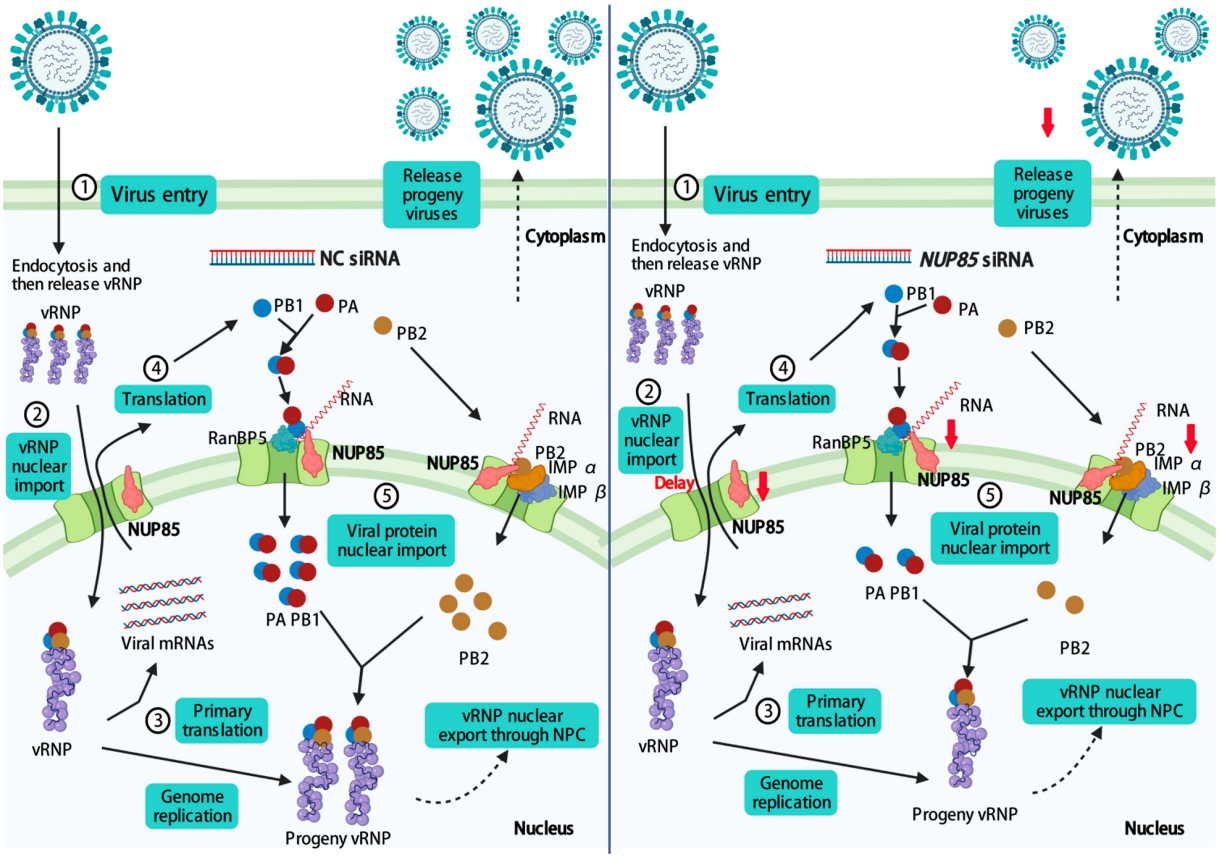


FIGURE 8
Proposed model for NUP85 facilitating nuclear import of vRNP and therefore promoting viral replication. Knockdown of NUP85 delays the nuclear import of vRNP, PB1, and PB2, which finally hinders viral replication. The figure was drawn at biorender.com under the agreement number of MT23YJ15J1.

infection. It indicated knockdown of NUP85 did not affect the antiviral status of the infected cells. Therefore, the significantly decreased viral replication is mainly due to the decreased RNP import into the nucleus in the NUP85 knockdown cells. Furthermore, NUP85 protein expression significantly decreased during IAV infection (Figure 7). It is possible that the host cells used some strategies that merit further investigation to alter the NPC against IAV infection. NPC components would be the potential targets for influenza treatments.

## Conclusion

In conclusion, our data showed that NUP85 is a novel PB1 and PB2 binding protein and is pivotal for IAV replication. NUP85 knockdown impedes the nuclear import of vRNP, PB1 and PB2, thus inhibiting IAV replication. Importantly, we uncovered the underlying mechanisms that NUP85 assists the formation of a complex of viral PB2 and importin α1 and importin α7, PB1 and RanBP5 also. These results will advance our understanding that host proteins regulate the RNP nuclear import of IAV.

## Data availability statement

The original contributions presented in the study are included in the article/supplementary material, further inquiries can be directed to the corresponding author.

## Author contributions

YHL and YL designed the experiments, drafted the manuscript, and revised the manuscript. YHL, HW, MQH, and DW performed the experiments. YHL, YXH, KZ, and YL analyzed and interpreted the data. All authors contributed to the article and approved the submitted version.

## Funding

This work was supported by the National Natural Science Foundation of China (31872837), the National Program on Key

Research Project of China (2019YFE0103900) as well as the European Union's Horizon 2020 Research and Innovation Program under grant agreement no. 861917—SAFFI, the National Science Foundation for Distinguished Young Scholars (32102620), and the Natural Science Foundation of Zhejiang Province (LZ22C180004).

## Acknowledgments

We thank the staff (Dr. Ying Shan) in the Shared Experimental Platform for Core Instruments, Zhejiang University College of Animal Sciences, for assistance with the laser confocal microscopy imaging analysis.

## Conflict of interest

The authors declare that the research was conducted in the absence of any commercial or financial relationships that could be construed as a potential conflict of interest.

## Publisher's note

All claims expressed in this article are solely those of the authors and do not necessarily represent those of their affiliated organizations, or those of the publisher, the editors and the reviewers. Any product that may be evaluated in this article, or claim that may be made by its manufacturer, is not guaranteed or endorsed by the publisher.

## References

Banerjee, I., Miyake, Y., Nobs, S. P., Schneider, C., Horvath, P., Kopf, M., et al. (2014). Influenza A virus uses the aggresome processing machinery for host cell entry. *Science* 346, 473–477. doi: 10.1126/science.1257037

Beck, M., and Hurt, E. (2017). The nuclear pore complex: understanding its function through structural insight. *Nat. Rev. Mol. Cell Biol.* 18, 73–89. doi: 10.1038/nrm.2016.147

Biswas, S. K., Boutz, P. L., and Nayak, D. P. (1998). Influenza virus nucleoprotein interacts with influenza virus polymerase proteins. *J. Virol.* 72, 5493–5501. doi: 10.1128/JVI.72.7.5493-5501.1998

Brass, A. L., Dykxhoorn, D. M., Benita, Y., Yan, N., Engelman, A., Xavier, R. J., et al. (2008). Identification of host proteins required for HIV infection through a functional genomic screen. *Science* 319, 921–926. doi: 10.1126/science.1152725

Chen, J., Huang, S., and Chen, Z. (2010). Human cellular protein nucleoporin hNup98 interacts with influenza A virus NS2/nuclear export protein and overexpression of its GLFG repeat domain can inhibit virus propagation. *J. Gen. Virol.* 91, 2474–2484. doi: 10.1099/vir.0.022681-0

Cingolani, G., Petosa, C., Weis, K., and Muller, C. W. (1999). Structure of importin-beta bound to the IBB domain of importin-alpha. *Nature* 399, 221–229. doi: 10.1038/20367

Deng, T., Engelhardt, O. G., Thomas, B., Akoulitchev, A. V., Brownlee, G. G., and Fodor, E. (2006). Role of ran binding protein 5 in nuclear import and assembly of the influenza virus RNA polymerase complex. *J. Virol.* 80, 11911–11919. doi: 10.1128/JVI.01565-06

Eisfeld, A. J., Neumann, G., and Kawaoka, Y. (2015). At the Centre: influenza A virus ribonucleoproteins. *Nat. Rev. Microbiol.* 13, 28–41. doi: 10.1038/nrmicro3367

Furusawa, Y., Yamada, S., and Kawaoka, Y. (2018). Host factor Nucleoporin 93 is involved in the nuclear export of influenza virus RNA. *Front. Microbiol.* 9:1675. doi: 10.3389/fmicb.2018.01675

Gabriel, G., Herwig, A., and Klenk, H. D. (2008). Interaction of polymerase subunit PB2 and NP with importin alpha1 is a determinant of host range of influenza A virus. *PLoS Pathog.* 4:e11. doi: 10.1371/journal.ppat.0040011

Gabriel, G., Klingel, K., Otte, A., Thiele, S., Hudjetz, B., Arman-Kalcek, G., et al. (2011). Differential use of importin-alpha isoforms governs cell tropism and host adaptation of influenza virus. *Nat. Commun.* 2:156. doi: 10.1038/ncomms1158

Gao, Q., Yang, C., Ren, C., Zhang, S., Gao, X., Jin, M., et al. (2020). Eukaryotic translation elongation factor 1 Delta inhibits the nuclear import of the nucleoprotein and PA-PB1 heterodimer of influenza A virus. *J. Virol.* 95:01391-20. doi: 10.1128/JVI.01391-20

Gautier, V. W., Gu, L., O'Donoghue, N., Pennington, S., Sheehy, N., and Hall, W. W. (2009). In vitro nuclear interactome of the HIV-1 tat protein. *Retrovirology* 6:47. doi: 10.1186/1742-4690-6-47

Gorlich, D., Vogel, F., Mills, A. D., Hartmann, E., and Laskey, R. A. (1995). Distinct functions for the two importin subunits in nuclear protein import. *Nature* 377, 246–248. doi: 10.1038/377246a0

Hampoelz, B., Andres-Pons, A., Kastritis, P., and Beck, M. (2019). Structure and assembly of the nuclear pore complex. *Annu. Rev. Biophys.* 48, 515–536. doi: 10.1146/annurev-biophys-052118-115308

Harel, A., Orjalo, A. V., Vincent, T., Lachish-Zalait, A., Vasu, S., Shah, S., et al. (2003). Removal of a single pore subcomplex results in vertebrate nuclei devoid of nuclear pores. *Mol. Cell* 11, 853–864. doi: 10.1016/s1097-2765(03)00116-3

Huet, S., Avilov, S. V., Ferbitz, L., Daigle, N., Cusack, S., and Ellenberg, J. (2010). Nuclear import and assembly of influenza A virus RNA polymerase studied in live cells by fluorescence cross-correlation spectroscopy. *J. Virol.* 84, 1254–1264. doi: 10.1128/JVI.01533-09

Hutchinson, E. C., and Fodor, E. (2012). Nuclear import of the influenza A virus transcriptional machinery. *Vaccine* 30, 7353–7358. doi: 10.1016/j.vaccine.2012.04.085

Hutchinson, E. C., Orr, O. E., Man Liu, S., Engelhardt, O. G., and Fodor, E. (2011). Characterization of the interaction between the influenza A virus polymerase subunit PB1 and the host nuclear import factor ran-binding protein 5. *J. Gen. Virol.* 92, 1859–1869. doi: 10.1099/vir.0.032813-0

Jones, I. M., Reay, P. A., and Philpott, K. L. (1986). Nuclear location of all three influenza polymerase proteins and a nuclear signal in polymerase PB2. *EMBO J.* 5, 2371–2376. doi: 10.1002/j.1460-2075.1986.tb04506.x

Kawaguchi, A., Momose, F., and Nagata, K. (2011). Replication-coupled and host factor-mediated encapsidation of the influenza virus genome by viral nucleoprotein. *J. Virol.* 85, 6197–6204. doi: 10.1128/JVI.00277-11

Labaronne, A., Swale, C., Monod, A., Schoehn, G., Crepin, T., and Ruigrok, R. W. (2016). Binding of RNA by the nucleoproteins of influenza viruses A and B. *Viruses* 8:247. doi: 10.3390/v8090247

Lange, A., McLane, L. M., Mills, R. E., Devine, S. E., and Corbett, A. H. (2010). Expanding the definition of the classical bipartite nuclear localization signal. *Traffic* 11, 311–323. doi: 10.1111/j.1600-0854.2009.01028.x

Li, B., Clohisey, S. M., Chia, B. S., Wang, B., Cui, A., Eisenhaure, T., et al. (2020). Genome-wide CRISPR screen identifies host dependency factors for influenza A virus infection. *Nat. Commun.* 11:164. doi: 10.1038/s41467-019-13965-x

Lim, R. Y., Ullman, K. S., and Fahrenkrog, B. (2008). Biology and biophysics of the nuclear pore complex and its components. *Int. Rev. Cell Mol. Biol.* 267, 299–342. doi: 10.1016/S1937-6448(08)00632-1

Lin, D. H., and Hoelz, A. (2019). The structure of the nuclear pore complex (an update). *Annu. Rev. Biochem.* 88, 725–783. doi: 10.1146/annurev-biochem-062917-011901

Lott, K., Bhardwaj, A., Mitrousis, G., Pante, N., and Cingolani, G. (2010). The importin beta binding domain modulates the avidity of importin beta for the nuclear pore complex. *J. Biol. Chem.* 285, 13769–13780. doi: 10.1074/jbc.M109.095760

Luo, W., Zhang, J., Liang, L., Wang, G., Li, Q., Zhu, P., et al. (2018). Phospholipid scramblase 1 interacts with influenza A virus NP, impairing its nuclear import and thereby suppressing virus replication. *PLoS Pathog.* 14:e1006851. doi: 10.1371/journal.ppat.1006851

Lutz, A., Dyall, J., Olivo, P. D., and Pekosz, A. (2005). Virus-inducible reporter genes as a tool for detecting and quantifying influenza A virus replication. *J. Virol. Methods* 126, 13–20. doi: 10.1016/j.jviromet.2005.01.016

Matsuoka, Y., Matsumae, H., Katoh, M., Eisfeld, A. J., Neumann, G., Hase, T., et al. (2013). A comprehensive map of the influenza A virus replication cycle. *BMC Syst. Biol.* 7:97. doi: 10.1186/1752-0509-7-97

Miyake, Y., Keusch, J. J., Decamps, L., Ho-Xuan, H., Iketani, S., Gut, H., et al. (2019). Influenza virus uses transportin 1 for vRNP debundling during cell entry. *Nat. Microbiol.* 4, 578–586. doi: 10.1038/s41564-018-0332-2

Moeller, A., Kirchdoerfer, R. N., Potter, C. S., Carragher, B., and Wilson, I. A. (2012). Organization of the influenza virus replication machinery. *Science* 338, 1631–1634. doi: 10.1126/science.1227270

Morita, M., Kuba, K., Ichikawa, A., Nakayama, M., Katahira, J., Iwamoto, R., et al. (2013). The lipid mediator protectin D1 inhibits influenza virus replication and improves severe influenza. *Cell* 153, 112–125. doi: 10.1016/j.cell.2013.02.027

Muhlbauer, D., Dzieciolowski, J., Hardt, M., Hocke, A., Schierhorn, K. L., Mostafa, A., et al. (2015). Influenza virus-induced caspase-dependent enlargement of nuclear pores promotes nuclear export of viral ribonucleoprotein complexes. *J. Virol.* 89, 6009–6021. doi: 10.1128/JVI.03531-14

Mukaigawa, J., and Nayak, D. P. (1991). Two signals mediate nuclear localization of influenza virus (A/WSN/33) polymerase basic protein 2. *J. Virol.* 65, 245–253. doi: 10.1128/JVI.65.1.245-253.1991

Naito, T., Kiyasu, Y., Sugiyama, K., Kimura, A., Nakano, R., Matsukage, A., et al. (2007a). An influenza virus replicon system in yeast identified tat-SF1 as a stimulatory host factor for viral RNA synthesis. *Proc. Natl. Acad. Sci. U. S. A.* 104, 18235–18240. doi: 10.1073/pnas.0705856104

Naito, T., Momose, F., Kawaguchi, A., and Nagata, K. (2007b). Involvement of Hsp90 in assembly and nuclear import of influenza virus RNA polymerase subunits. *J. Virol.* 81, 1339–1349. doi: 10.1128/JVI.01917-06

Neumann, G., Noda, T., and Kawaoka, Y. (2009). Emergence and pandemic potential of swine-origin H1N1 influenza virus. *Nature* 459, 931–939. doi: 10.1038/nature08157

Noda, T., and Kawaoka, Y. (2010). Structure of influenza virus ribonucleoprotein complexes and their packaging into virions. *Rev. Med. Virol.* 20, 380–391. doi: 10.1002/rmv.666

O'Neill, R. E., Jaskunas, R., Blobel, G., Palese, P., and Moroianu, J. (1995). Nuclear import of influenza virus RNA can be mediated by viral nucleoprotein and transport factors required for protein import. *J. Biol. Chem.* 270, 22701–22704. doi: 10.1074/jbc.270.39.22701

Panda, D., Pascual-Garcia, P., Dunagin, M., Tudor, M., Hopkins, K. C., Xu, J., et al. (2014). Nup98 promotes antiviral gene expression to restrict RNA viral infection in drosophila. *Proc. Natl. Acad. Sci. U. S. A.* 111, E3890–E3899. doi: 10.1073/pnas.1410087111

Peacock, T. P., Sheppard, C. M., Staller, E., and Barclay, W. S. (2019). Host determinants of influenza RNA synthesis. *Annu. Rev. Virol.* 6, 215–233. doi: 10.1146/annurev-virology-092917-043339

Resa-Infante, P., Jorba, N., Zamarreno, N., Fernandez, Y., Juarez, S., and Ortin, J. (2008). The host-dependent interaction of alpha-importins with influenza PB2 polymerase subunit is required for virus RNA replication. *PLoS One* 3:e3904. doi: 10.1371/journal.pone.0003904

Resa-Infante, P., Recuero-Checa, M. A., Zamarreno, N., Llorca, O., and Ortin, J. (2010). Structural and functional characterization of an influenza virus RNA polymerase-genomic RNA complex. *J. Virol.* 84, 10477–10487. doi: 10.1128/JVI.01115-10

Satterly, N., Tsai, P. L., van Deursen, J., Nussenzveig, D. R., Wang, Y., Faria, P. A., et al. (2007). Influenza virus targets the mRNA export machinery and the nuclear pore complex. *Proc. Natl. Acad. Sci. U. S. A.* 104, 1853–1858. doi: 10.1073/pnas.0610977104

Sempere Borau, M., and Stertz, S. (2021). Entry of influenza A virus into host cells - recent progress and remaining challenges. *Curr. Opin. Virol.* 48, 23–29. doi: 10.1016/j.coviro.2021.03.001

Senbas Akyazi, B., Pirincal, A., Kawaguchi, A., Nagata, K., and Turan, K. (2020). Interaction of influenza A virus NS2/NEP protein with the amino-terminal part of Nup214. *Turk. J. Biol.* 44, 82–92. doi: 10.3906/biy-1909-49

Smith, G. L., Levin, J. Z., Palese, P., and Moss, B. (1987). Synthesis and cellular location of the ten influenza polypeptides individually expressed by recombinant vaccinia viruses. *Virology* 160, 336–345. doi: 10.1016/0042-6822(87)90004-3

Tarendeau, F., Boudet, J., Guilligay, D., Mas, P. J., Bougault, C. M., Boulo, S., et al. (2007). Structure and nuclear import function of the C-terminal domain of influenza virus polymerase PB2 subunit. *Nat. Struct. Mol. Biol.* 14, 229–233. doi: 10.1038/nsmb1212

Taubenberger, J. K., Kash, J. C., and Morens, D. M. (2019). The 1918 influenza pandemic: 100 years of questions answered and unanswered. *Sci. Transl. Med.* 11:eaau5485. doi: 10.1126/scitranslmed.aau5485

Taubenberger, J. K., and Morens, D. M. (2008). The pathology of influenza virus infections. *Annu. Rev. Pathol.* 3, 499–522. doi: 10.1146/annurev.pathmechdis.3.121806.154316

Te Velthuis, A. J., and Fodor, E. (2016). Influenza virus RNA polymerase: insights into the mechanisms of viral RNA synthesis. *Nat. Rev. Microbiol.* 14, 479–493. doi: 10.1038/nrmicro.2016.87

Terashima, Y., Onai, N., Murai, M., Enomoto, M., Poonpiriya, V., Hamada, T., et al. (2005). Pivotal function for cytoplasmic protein FROUNT in CCR2-mediated monocyte chemotaxis. *Nat. Immunol.* 6, 827–835. doi: 10.1038/ni1222

Terashima, Y., Toda, E., Itakura, M., Otsuji, M., Yoshinaga, S., Okumura, K., et al. (2020). Targeting FROUNT with disulfiram suppresses macrophage accumulation and its tumor-promoting properties. *Nat. Commun.* 11:609. doi: 10.1038/s41467-020-14338-5

Terry, L. J., and Wente, S. R. (2007). Nuclear mRNA export requires specific FG nucleoporins for translocation through the nuclear pore complex. *J. Cell Biol.* 178, 1121–1132. doi: 10.1083/jcb.200704174

Toda, E., Terashima, Y., Esaki, K., Yoshinaga, S., Sugihara, M., Kofuku, Y., et al. (2014). Identification of a binding element for the cytoplasmic regulator FROUNT in the membrane-proximal C-terminal region of chemokine receptors CCR2 and CCR5. *Biochem. J.* 457, 313–322. doi: 10.1042/BJ20130827

Toda, E., Terashima, Y., Sato, T., Hirose, K., Kanegasaki, S., and Matsushima, K. (2009). FROUNT is a common regulator of CCR2 and CCR5 signaling to control directional migration. *J. Immunol.* 183, 6387–6394. doi: 10.4049/jimmunol.0803469

Walther, T. C., Alves, A., Pickersgill, H., Loiodice, I., Hetzer, M., Galy, V., et al. (2003). The conserved Nup107-160 complex is critical for nuclear pore complex assembly. *Cell* 113, 195–206. doi: 10.1016/s0092-8674(03)00235-6

Wu, W. W., and Pante, N. (2009). The directionality of the nuclear transport of the influenza A genome is driven by selective exposure of nuclear localization sequences on nucleoprotein. *Virol. J.* 6:68. doi: 10.1186/1743-422X-6-68

Wu, W. W., Sun, Y. H., and Pante, N. (2007). Nuclear import of influenza A viral ribonucleoprotein complexes is mediated by two nuclear localization sequences on viral nucleoprotein. *Virol. J.* 4:49. doi: 10.1186/1743-422X-4-49

Yang, C., Liu, X., Gao, Q., Cheng, T., Xiao, R., Ming, F., et al. (2018). The Nucleolar protein LYAR facilitates Ribonucleoprotein assembly of influenza A virus. *J. Virol.* 92:01042-18. doi: 10.1128/JVI.01042-18

Zannettino, A. C., Psaltis, P. J., and Gronthos, S. (2008). Home is where the heart is: via the FROUNT. *Cell Stem Cell* 2, 513–514. doi: 10.1016/j.stem.2008.05.012

Zhou, B., Li, Y., Halpin, R., Hine, E., Spiro, D. J., and Wentworth, D. E. (2011). PB2 residue 158 is a pathogenic determinant of pandemic H1N1 and H5 influenza a viruses in mice. *J. Virol.* 85, 357–365. doi: 10.1128/JVI.01694-10

frontiers | Frontiers in Microbiology

TYPE Original Research
PUBLISHED 11 January 2023
DOI 10.3389/fmicb.2022.957830



OPEN ACCESS

EDITED BY
Nejat Duzgunes,
University of the Pacific, United States

REVIEWED BY
Liu Sidang,
Shandong Agricultural University, China
Mira C. Patel,
Centers for Disease Control and Prevention, United States

*CORRESPONDENCE
Heiko Adler
✉ h.adler@helmholtz-muenchen.de
Claudia A. Staab-Weijnitz
✉ staab-weijnitz@helmholtz-muenchen.de

SPECIALTY SECTION
This article was submitted to Virology, a section of the journal Frontiers in Microbiology

RECEIVED 31 May 2022
ACCEPTED 19 December 2022
PUBLISHED 11 January 2023

CITATION
Nakayama M, Marchi H, Dmitrieva AM, Chakraborty A, Merl-Pham J, Hennen E, Le Gleut R, Ruppert C, Guenther A, Kahnert K, Behr J, Hilgendorff A, Hauck SM, Adler H and Staab-Weijnitz CA (2023) Quantitative proteomics of differentiated primary bronchial epithelial cells from chronic obstructive pulmonary disease and control identifies potential novel host factors post-influenza A virus infection.
*Front. Microbiol.* 13:957830.
doi: 10.3389/fmicb.2022.957830



# Quantitative proteomics of differentiated primary bronchial epithelial cells from chronic obstructive pulmonary disease and control identifies potential novel host factors post-influenza A virus infection

Misako Nakayama[1,2], Hannah Marchi[3,4], Anna M. Dmitrieva[5], Ashesh Chakraborty[1], Juliane Merl-Pham[6], Elisabeth Hennen[1], Ronan Le Gleut[3], Clemens Ruppert[7], Andreas Guenther[7], Kathrin Kahnert[8], Jürgen Behr[8], Anne Hilgendorff[1], Stefanie M. Hauck[6], Heiko Adler[5,9]* and Claudia A. Staab-Weijnitz[1]*

[1]Institute of Lung Health and Immunity and Comprehensive Pneumology Center with the CPC-M BioArchive, Helmholtz Zentrum München, Member of the German Center of Lung Research (DZL), Munich, Germany, [2]Division of Pathogenesis and Disease Regulation, Department of Pathology, Shiga University of Medical Science, Otsu, Japan, [3]Core Facility Statistical Consulting, Helmholtz Zentrum München, Munich, Germany, [4]Faculty of Business Administration and Economics, Bielefeld University, Bielefeld, Germany, [5]Research Unit Lung Repair and Regeneration, Helmholtz Zentrum München, Member of the German Center of Lung Research (DZL), Munich, Germany, [6]Metabolomics and Proteomics Core, Helmholtz Zentrum München, Neuherberg, Germany, [7]Department of Internal Medicine, Medizinische Klinik II, Member of the German Center of Lung Research (DZL), Giessen, Germany, [8]Department of Medicine V, Ludwig Maximilian University (LMU) Munich, Member of the German Center of Lung Research, University Hospital, Munich, Germany, [9]Institute of Asthma and Allergy Prevention, Helmholtz Zentrum München, Member of the German Center of Lung Research (DZL), Munich, Germany

**Background:** Chronic obstructive pulmonary disease (COPD) collectively refers to chronic and progressive lung diseases that cause irreversible limitations in airflow. Patients with COPD are at high risk for severe respiratory symptoms upon influenza virus infection. Airway epithelial cells provide the first-line antiviral defense, but whether or not their susceptibility and response to influenza virus infection changes in COPD have not been elucidated. Therefore, this study aimed to compare the susceptibility of COPD- and control-derived airway epithelium to the influenza virus and assess protein changes during influenza virus infection by quantitative proteomics.

**Materials and methods:** The presence of human- and avian-type influenza A virus receptor was assessed in control and COPD lung sections as well as in fully differentiated primary human bronchial epithelial cells (phBECs) by lectin- or antibody-based histochemical staining. PhBECs were from COPD lungs, including cells from moderate- and severe-stage diseases, and from age-,

sex-, smoking, and history-matched control lung specimens. Protein profiles pre- and post-influenza virus infection *in vitro* were directly compared using quantitative proteomics, and selected findings were validated by qRT-PCR and immunoblotting.

**Results:** The human-type influenza receptor was more abundant in human airways than the avian-type influenza receptor, a property that was retained *in vitro* when differentiating phBECs at the air–liquid interface. Proteomics of phBECs pre- and post-influenza A virus infection with A/Puerto Rico/8/34 (PR8) revealed no significant differences between COPD and control phBECs in terms of flu receptor expression, cell type composition, virus replication, or protein profile pre- and post-infection. Independent of health state, a robust antiviral response to influenza virus infection was observed, as well as upregulation of several novel influenza virus-regulated proteins, including PLSCR1, HLA-F, CMTR1, DTX3L, and SHFL.

**Conclusion:** COPD- and control-derived phBECs did not differ in cell type composition, susceptibility to influenza virus infection, and proteomes pre- and post-infection. Finally, we identified novel influenza A virus-regulated proteins in bronchial epithelial cells that might serve as potential targets to modulate the pathogenicity of infection and acute exacerbations.

KEYWORDS

**organotypic, proteomics, flu receptor, primary human bronchial epithelial cells, COPD**

## 1. Introduction

Chronic obstructive pulmonary disease (COPD) is an umbrella term used to describe chronic and progressive lung diseases that cause limitations in lung airflow, which are not fully reversible. Currently, at least sixty-five million people suffer from moderate-to-severe COPD, with the prevalence being increasing and thus COPD has become the third leading cause of death worldwide (World Health Organization [WHO], 2021). The primary cause of COPD is tobacco smoke in high- and middle-income countries and biomass smoke and other fuels in low-income countries (Decramer et al., 2012). Exacerbation, defined as a sudden worsening of clinical manifestations and decrease in lung function, is related to a significantly worse survival outcome (Viniol and Vogelmeier, 2018), and the influenza virus is one of the respiratory viruses triggering COPD exacerbations (Bouquet et al., 2020). However, the underlying mechanisms of acute COPD exacerbations by influenza viruses have not been fully elucidated (Decramer et al., 2012; Viniol and Vogelmeier, 2018; Ji et al., 2022; Wu et al., 2022).

Respiratory viruses are associated with 40–64% of acute COPD exacerbations, and influenza virus infections cause substantial declines in lung function parameters (Smith et al., 1980). Seasonal influenza virus causes annual epidemics, with an estimation of 10% of the global population catching the disease, and the detection rates of influenza virus among hospitalized patients with acute exacerbation of COPD were reported as 8–36% (Mallia and Johnston, 2007; Viniol and Vogelmeier, 2018). Therefore, it is important to elucidate the mechanisms underlying the susceptibility and pathogenicity of influenza viruses in patients with COPD.

Given that the airway epithelium provides the first-line antiviral defense, it is a highly relevant question whether or not susceptibility to virus infection and virus replication is altered in COPD airway cells. Different responses of airway epithelium upon infection have been reported in patients with COPD compared with healthy controls (Hsu et al., 2015, 2016), suggesting that targeted treatment of exacerbations might serve to improve the prognosis of COPD.

Primary human bronchial epithelial cells (phBECs) differentiated at the air–liquid interface (ALI) represent a powerful tool to assess the airway-specific first-line defense against external stimuli. The resulting organotypic bronchoepithelium closely resembles the *in vivo* airway and is frequently used in studies of toxicology, infection, and drug delivery (Pezzulo et al., 2011; Lenz et al., 2014; Singanayagam et al., 2019; Berthold et al., 2022; Mastalerz et al., 2022). The fully differentiated epithelium, obtained 4 weeks after the airlift, contains all major bronchial epithelial cell types and displays physiologically important functional properties like mucus

secretion and ciliary beating (Lodes et al., 2020). The model also allows for differentiating phBECs from different disease origins and assessing viral replication and antiviral epithelial responses after infection (Zarcone et al., 2017; Singanayagam et al., 2019).

Sialic acids on the surface of airway epithelial cells serve as receptors for influenza A viruses. Human influenza A viruses preferentially bind to sialic acids bound to galactose by the α2,6 linkage (SAα2,6Gal), the human-type flu receptor, whereas avian influenza A viruses preferentially bind to SAα2,3Gal, the avian-type flu receptor (Ito et al., 1997). Although the human airway epithelium predominantly displays the human-type flu receptor, the avian-type flu receptor has also been reported to be displayed by a minor proportion of cells (Shinya et al., 2006; Davis et al., 2015; Hsu et al., 2016). Considering that a major natural reservoir of influenza A virus is wild aquatic birds and that several subtypes of avian influenza A viruses have crossed the species barrier resulting in higher mortality rates than those caused by human influenza A viruses (Krammer et al., 2018), not only the human-type but also the avian-type flu receptor was assessed in this study.

The aims of this study were 2-fold. (1) To assess the susceptibility of airway epithelium of patients with COPD and controls to influenza virus. For this aim, we evaluated the expression of flu receptors in COPD and control lung sections as well as in a human organotypic model of the bronchial epithelium derived from COPD and control lung airway cells. (2) To identify novel molecular targets for the treatment of acute exacerbations caused by the influenza virus. Here, we performed quantitative proteomics in organotypic bronchoepithelia with phBECs derived from patients with COPD and controls.

# 2. Materials and methods

## 2.1. Subjects

Lectin-based and immunofluorescent staining of lung tissue was carried out in samples obtained from the UGMLC/DZL biobank, where biospecimen collection was approved by votes from the Ethics Committee of the Justus-Liebig-University School of Medicine (no. 111/08 and 58/15). Here, lung sections were from lung explants of patients with COPD, i.e., lungs with end-stage disease (GOLD stage IV; mean age 55 ± 6 years; three females, two males), or from donor's lungs (mean age 52 ± 13 years, three females, two males).

All phBECs used in this study were obtained from the CPC-M BioArchive. PhBECs were derived from patients with COPD and controls, and were selected based on the following criteria: (1) male, (2) age over 60 years, (3) ex-smoker (more than 5 years), (4) a smoking history of more than 11 pack-years, and (5) the definition and classification provided by the Global Initiative for Chronic Obstructive Lung Disease (GOLD). The majority of phBECs, including all controls and COPD-derived phBECS from GOLD stage II/III, were derived from patients undergoing lung tumor resections and isolated from histologically normal regions adjacent to the resected lung tumors as assessed by an experienced pathologist. For the patients with COPD ($n$ = 4), one patient was from GOLD stage IV, another from GOLD stage III, and two patients from GOLD stage II. The patient with COPD stage IV was a recipient of a lung transplant who had his lung resected at the University Hospital of the Ludwig Maximilians University Munich. Other patients underwent lobectomy at Asklepios clinic, Munich-Gauting, with a lung tumor as the primary diagnosis. All control subjects ($n$ = 3) had normal lung functions and also underwent lobectomy at Asklepios clinic with a lung tumor as the primary diagnosis (**Table 1**). These patients received different multiple medications (outlined in **Supplementary Table 1**). The study was approved by the Ethics Committee of the Ludwig Maximilians University Munich, Germany (Ethic vote #333-10, #382-10). Written informed consent was obtained from all study participants.

## 2.2. Culture of primary human bronchial epithelial cells

The primary human bronchial epithelial cells were expanded and cultured as described previously (Berthold et al., 2022; Mastalerz et al., 2022). For more details, refer to the online **Supplementary material**.

## 2.3. Lectin-based and immunohistochemical fluorescent staining

### 2.3.1. Sample preparation

Formalin-fixed, paraffin-embedded lung sections were deparaffinized with xylene, rehydrated in 100–50% ethanol, and rinsed in tap water. Antigen retrieval was performed in 10 mM citrate buffer, pH 6, with heat (125°C for 30 s, followed by 90°C for 10 s). Slides were washed 3 times in 1 × Tris-buffered saline. Paraformaldehyde-fixed phBECs on membranes were washed once with PBS and cut into 1/6 of the whole membrane with a scalpel.

### 2.3.2. Lectin-based histochemical staining for detection of human-type flu receptor

To prepare a negative control, slides/phBECs on membranes were incubated with neuraminidase from *Arthrobacter ureafaciens* (Merck KGaA, #10269611001) with a 1:100 dilution in acetic acid buffer, pH 5.5, for 20 h at 37°C. Slides/phBECs on membranes incubated with and without neuraminidase were then blocked with 5% BSA in PBS for 30 min at room

TABLE 1 Patient information and bronchial diameter of specimens used for cell isolation.

| | GOLD stage | Smoking status | Smoking-free period (years) | Pack-years | Sex | Age | Primary diagnosis | Bronchial diameter |
|---|---|---|---|---|---|---|---|---|
| COPD | IV | Ex | 5 | 45 | m | 67 | COPD | ≈15 mm |
| COPD | III | Ex | 5 to 10 | 40 to 60 | m | 60 | Squamous cell carcinoma | ≈8.5 mm |
| COPD | II | Ex | > 20 | 21 to 40 | m | 67 | Squamous cell carcinoma | ≈11 mm |
| COPD | II | Ex | 6 to 10 | > 60 | m | 70 | Carcinoma | ≈15 mm |
| Control | NA | Ex | > 20 | 20 to 40 | m | 72 | Primary histiocytic sarcoma | ≈15 mm |
| Control | NA | Ex | 5 to 10 | 40 to 60 | m | 71 | Pleomorphic carcinoma | ≈8 mm |
| Control | NA | Ex | 11 to 20 | 11 to 20 | m | 69 | Adenocarcinoma | ≈5 mm |

temperature and incubated overnight at 4°C with fluorescein isothiocyanate-conjugated *Sambucus nigra* lectin (FITC-SNA) (SNAI, US Bio, S0071-20A.2) (1:50 in 5% BSA in PBS, final concentration 40 μg/ml).

### 2.3.3. Immunohistochemistry

Slides/phBECs on membranes were incubated overnight at 4°C with antibodies against the avian-type flu receptor, acetylated tubulin (acTub), mucin 5AC (MUC5AC), club cell-specific protein 10 (CC10), or cytokeratin 5 (CK5) diluted in 5% BSA in PBS. After washing three times with PBS, slides/phBECs on membranes were incubated with secondary antibodies and 4′,6-diamidino-2-phenylidole (DAPI) (1:2,000 in 5% BSA in PBS) for 1 h at room temperature. For phBECs on membranes, cells were permeabilized in 0.2% Triton X-100 in PBS for 10 min at room temperature prior to applying primary antibodies for differentiation markers. Permeabilization was not performed to detect flu receptors, since the cell-surface display is important for the virus to attach. Primary and secondary antibodies are listed in **Supplementary Tables 2, 3**, respectively. After washing 3 times with PBS, lung sections on glass slides were covered with mounting medium (DAKO). Membranes with phBECs were put on glass slides, covered in mounting medium, and coverslips were placed on top. Fluorescent microscopy was performed using the Axiovert II (Carl Zeiss AG, Oberkochen, Germany). For phBECs, immunofluorescence quantification was performed using the Imaris 7.4.0 software (Bitplane). Briefly, z-stack images of stained transwell membranes were generated by fluorescent microscopy, and individual cells were analyzed for the positivity of specific markers, largely as described previously (Schamberger et al., 2015; Mastalerz et al., 2022). For patient lung sections, quantification was performed using NIS Elements version 5.41.00 (Nikon Solutions Co., Ltd.) as follows: the apical area of the bronchus was selected above the bronchial epithelial nuclear layer and along the apical surface to yield the bronchial region of interest (ROI). Pneumocytes were selected in three randomly selected alveolar walls to yield the alveolar/pneumocyte ROI. Areas positive for the human-type flu receptor (SNA, green) or avian-type flu receptor (HYB4, red) were detected by the same threshold in all samples and recorded as binary areas. Data are given as binary area/ROI area × 100%.

## 2.4. Transepithelial electrical resistance measurements

The transepithelial electrical resistance (TEER) measurements were largely performed as described previously (Mastalerz et al., 2022). For more details, refer to the online **Supplementary material**.

## 2.5. Infection of fully differentiated phBECs

Transwell plates were placed in the 37°C incubator for 30 min with 500 μl of pre-warmed HBSS on the apical side. Mucus was carefully removed by pipetting up and down in each insert 5 times, followed by aspiration of HBSS and the addition of another 500 μl of HBSS on the apical side. This cycle was repeated for a total of 5 times to completely remove mucus. To each well, $1.25 \times 10^5$ $TCID_{50}$ PR8 viruses in 100 μl of HBSS, or 100 μl of HBSS for mock infection, was added to the apical side of inserts (Zhang et al., 2005; Newby et al., 2006). The infectious dose was adapted from the procedure described by Wu et al. (2022). If all the cells in the insert were exposed to and susceptible to influenza A virus infection, this would correspond to a multiplicity of infection (MOI) of approximately 0.1. However, this MOI has to be seen in the context of three-dimensional cultures composed of different cell types (Newby et al., 2006): compared with two-dimensional cultures in which MOI indicates the number of infectious viral particles that can infect each cell, the organotypic bronchoepithelium includes multiple cell types, with basal cells not facing the apical surface. In addition, not all cell types express influenza A virus receptors. Following infection, plates were gently rocked several times and incubated at 37°C for 2 h. The apical side was gently washed with 500 μl of pre-warmed HBSS two times to remove unbound viral particles, and another 500 μl of HBSS was added and collected

for viral titration for day 0. The basolateral side was washed two times with 1 ml of pre-warmed HBSS, and 1 ml of pre-warmed PneumaCult-ALI medium was added. For sample collection on days 1 and 3 post-infection, 500 μl of HBSS was added to the apical side of inserts, and plates were incubated for 30 min at 37°C in a humidified cell incubator at 37°C with 95% air and 5% $CO_2$. After gently pipetting up and down 5 times, apical washes and phBECs on membranes were collected and stored at −80°C until RNA and protein extraction.

## 2.6. Quantitative mass spectrometry in data-independent acquisition mode

Equal total protein amounts (10 μg) of the cell lysate were digested with a modified filter-aided sample preparation procedure (Wisniewski et al., 2009) using Lys-C and trypsin as proteases and Microcon® centrifugal filters (Sartorius Vivacon 500, 30 kDa) for buffer exchange and on-filter digest. Approximately 0.5 μg of peptides per sample were measured in a randomized manner on a Q-Exactive™ HF mass spectrometer online coupled to an Ultimate 3000 nano-RSLC (Thermo Scientific) in data-independent acquisition (DIA) mode as described previously (Lepper et al., 2018; Mattugini et al., 2018). Briefly, peptides were automatically loaded on a trap column [300 μm inner diameter (ID) × 5 mm, Acclaim PepMap100 C18, 5 μm, 100 Å, LC Packings] prior to C18 reversed phase chromatography on the analytical column (nanoEase MZ HSS T3 Column, 100 Å, 1.8 μm, 75 μm × 250 mm, Waters) at 250 nl/min flow rate in a 105 min non-linear acetonitrile gradient from 3 to 40% in 0.1% formic acid. Profile precursor spectra from 300 to 1,650 m/z were recorded at 120,000 resolution with an automatic gain control (AGC) target of 3e6 and a maximum injection time of 120 ms. Subsequently, fragment spectra were recorded in 37 overlapping DIA isolation windows of variable size covering a total of 300–1,650 m/z, each at 30,000 resolution with an AGC target of 3e6 and a normalized collision energy of 28. The recorded raw files were analyzed using the Spectronaut Pulsar software (Biognosys) (Bruderer et al., 2015) with a peptide and protein identification false discovery rate setting of < 1%, using an in-house human spectral library that was generated using Proteome Discoverer 2.1 (Thermo Scientific), the Byonic search engine (Protein Metrics), and the Swissprot Human database (release 2017_02). Quantification was based on MS2 area levels of all unique peptides per protein fulfilling the percentile 0.25 setting. Normalized protein quantifications were exported and used for calculations of fold changes and significance values. The mass spectrometry proteomics data have been deposited to the ProteomeXchange Consortium *via* the PRIDE (Perez-Riverol et al., 2022) partner repository with the data set identifier PXD031461.

## 2.7. Statistical analysis of quantitative mass spectrometry data

For the whole protein expression analysis, we used R (version 4.0.4). The data was pre-processed by variance stabilization and normalization (vsn package) (Huber et al., 2002). A reduction in the dimension of the data using tSNE (Krijthe, 2015) allowed us to identify the different patients as a batch effect. The data were corrected from the patient effect using ComBat (Leek et al., 2012, 2020), and the interaction between time and condition as covariates. Due to the induced correlation structure in the corrected data, ComBat might lead to the exaggerated significance and, therefore, to higher FDR (Li et al., 2021). This might artificially increase the effect of condition and time when correcting the data from the batch effect. For protein expression analysis, we used the R package limma (Ritchie et al., 2015). We specified a generalized linear mixed model with a random intercept for patients and the interaction between condition and time as a fixed effect. For sensitivity analysis, we additionally built the model with adjustment for health state, which revealed very similar results.

## 2.8. Gene expression analysis by qRT-PCR and Western blot

Real-time quantitative reverse transcription polymerase chain reaction (qRT-PCR) and Western blot analysis were performed as described previously (Mastalerz et al., 2022). For more details including antibodies used for Western Blot analysis (**Supplementary Tables 2, 3**) and primers used for qRT-PCR (**Supplementary Table 4**), please refer to the online **Supplementary material**.

# 3. Results

## 3.1. The human-type flu receptor is detected more frequently than the avian-type in human lung sections and organotypic bronchoepithelia

First, to assess the display of human- and avian-type flu receptors in the peripheral airway epithelium of patients with COPD and controls, formalin-fixed, paraffin-embedded lung sections (COPD $n = 5$, control $n = 5$) were stained with (1) FITC-SNA, which specifically binds to sialic acids bound to galactose by the α2,6 linkage (SAα2,6Gal), the human-type flu receptor (Ito et al., 1997) and (2) a monoclonal antibody (clone HYB4) that specifically binds to SAα2,3Gal, the avian-type flu receptor (Hidari et al., 2013). Pretreatment of a serial section with neuraminidase, an enzyme that cleaves sialic acids, resulted

in a drastic reduction of the SNA signal, validating the specificity of the lectin-based histochemical staining (**Supplementary Figure 1A**). In the bronchial region, the human-type flu receptor was much more frequently detected than the avian-type flu receptor in patients with COPD and controls, while in alveolar regions, human- and avian-type flu receptors were displayed at similar levels (**Supplementary Figures 1B, 2A, B**). Despite considerable heterogeneity of flu receptor display across the samples, our results indicate that the levels of both humans- and avian-type flu receptors are decreased in patients with COPD compared with controls (**Supplementary Figure 2**). Staining with SNA targeting the human-type flu receptor in combination with antibodies against acetylated tubulin (acTub), mucin 5AC (MUC5AC), club cell-specific protein 10 (CC10), and cytokeratin 5 (CK5) demonstrated that the human-type flu receptor was not displayed by ciliated or basal cells, but rather by goblet and club cells (**Figure 1A**, **Supplementary Figure 1B**). The very infrequently detected avian-type flu receptor was not or little displayed by ciliated cells, never by the club or basal cells, but maybe by goblet cells (**Supplementary Figure 1B**). The latter was not directly assessed because both anti-MUC5AC and anti-SAα2,3Gal antibodies were of mouse origin (**Supplementary Figure 1B**).

Having confirmed the expression of flu receptors in small airways of patients with COPD and controls in lung sections, we made use of the organotypic model of phBECs differentiated at ALI. PhBECs from patients with COPD ($n$ = 4) and controls ($n$ = 3), matched for age and sex (**Table 1**), were differentiated for 28 days at ALI. Males were chosen considering the gender-specific prevalence of COPD (Ntritsos et al., 2018) as well as in efforts to reduce sample heterogeneity. Again, the specificity of lectin histochemistry in phBECs was confirmed by pretreating cells with neuraminidase (**Supplementary Figure 1C**). On ALI day 0, where the culture consists exclusively of basal cells, almost no expression of the human-type receptor was observed. The avian-type flu receptor, in contrast, was observed in all controls and patients with COPD at this time point, even if in relatively few cells only (up to 11%) (**Figures 1B, C**). On ALI days 14 and 28, in parallel to the emergence of all major differentiated cell types, the number of human-type flu receptor-positive cells increased in phBECs from controls and patients with COPD (**Figures 1B, C**). The avian-type receptor was still detectable in all cultures at similar levels at an intermediate time point of differentiation (day 14) but mostly lost at day 28 (**Figure 1C**).

As opposed to the tissue section staining, flu receptor display was similar for COPD- and control-derived cells *in vitro*. The much higher prevalence of human-type to avian-type flu receptors, however, agreed well with our observations in human lung sections, supporting the usefulness of our *in vitro* model for studies with influenza A virus infection where flu receptors serve as a major determinant of host susceptibility.

## 3.2. Patients with COPD- and control-derived cells show similar differentiation potential

The expression of differentiation markers assessed by immunofluorescence and qRT-PCR showed similar differentiation potential in cells from patients with COPD and controls. TEER value increased and reached a similar value on day 28 (**Supplementary Figure 3**). Ciliated cells continued to increase until day 28, goblet cells increased on day 14 and decreased on day 28, and club cells continued to increase until day 28 (**Supplementary Figures 4A, B**). *FOXJ1*, encoding a transcription factor specifically required for motile cilia, *MUC5AC,* and *SCGB1A1* (*CC10*) were expressed at similar levels on days 14 and 28 (unpaired, two-sided Mann–Whitney $U$ test, $p > 0.05$) (**Supplementary Figure 4C**). PhBECs from patients with COPD tends to show a more heterogeneous expression of differentiation markers compared with those from controls.

## 3.3. COPD- and control-derived fully differentiated phBECs display largely similar protein profiles pre-infection

To compare the protein expression in fully differentiated phBECs from patients with COPD and controls, cells were collected on ALI day 28 (**Figure 2A**) and subjected to proteomic analysis. The heatmap displaying overall protein changes in all subjects demonstrated that COPD- and control-derived phBECs did not cluster separately. Interestingly, however, the COPD GOLD stage IV-derived phBECs without a tumor background stood out with a unique protein profile (**Figure 2B**).

## 3.4. PhBECs derived from a COPD GOLD stage IV patient show distinct COPD-like features

Having observed that the COPD GOLD stage IV-derived phBECs displayed a unique protein profile compared to control and COPD GOLD stage II/III phBECs, we assessed to which extent this may reflect a more advanced COPD airway phenotype. Indeed, in particular, at day 28, the phBECs derived from the GOLD stage IV patient ($n$ = 1) displayed a striking COPD-like phenotype in comparison to the control and less severe stage-derived cells: cells from that patient showed a lower TEER value, reduced levels of human-type flu receptor, and fewer ciliated and more goblet cells (**Supplementary Figure 5A–C**). Finally, from a panel of 20 genes known to be upregulated in COPD airway epithelial cells (Steiling et al., 2013; Wei et al., 2015), 14 showed

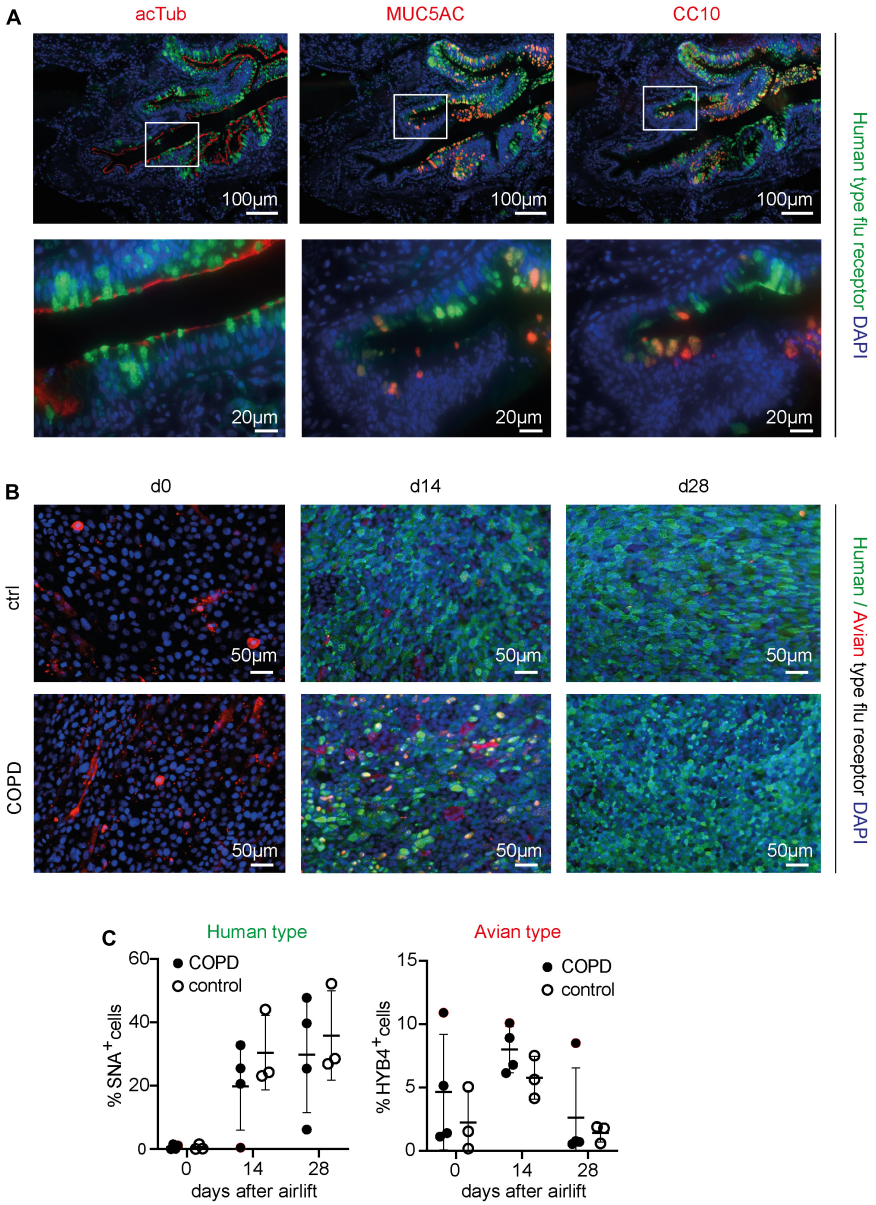


FIGURE 1
Detection of the human- and avian-type flu receptors in lung sections and organotypic bronchoepithelium from patients with chronic obstructive pulmonary disease (COPD) and controls. Human lung sections (COPD $n$ = 5, control $n$ = 5) and primary human bronchial epithelial cells (phBECs) from patients with COPD ($n$ = 4) and controls ($n$ = 3) were stained with Sambucus Nigra lectin (SNA) that specifically binds to sialic acids bound to galactose by the α2,6 linkage, SAα2,6Gal, the human-type flu receptor, and a monoclonal antibody (clone HYB4) that specifically binds to SAα2,3Gal, the avian-type flu receptor. **(A)** Detection of human-type flu receptor (green) in co-staining with antibodies directed toward acetylated tubulin (acTub), mucin 5AC (MUC5AC), or club cell-specific protein CC10 (red), for the identification of ciliated, goblet, or club cells, respectively, in formalin-fixed, paraffin-embedded human lung sections. The example shown is from a COPD lung explant. **(B)** Detection of human-type flu receptor (green) and avian-type flu receptor (red) in phBECs from COPD and control on days 0, 14, and 28 after airlift. **(C)** Quantification of the human- and avian-type flu receptors in phBECs on days 0, 14, and 28 after airlift. Panel **(A)** shows representative images for $n$ = 5 (COPD) and $n$ = 5 (control lung sections). Panel **(B)** shows representative images for $n$ = 3 (control phBECs; here second control, see **Table 1**) and $n$ = 4 (COPD phBECs; here GOLD stage III-derived phBECs); quantification of those data is given in panel **(C)**. For panel **(C)**, statistical analysis was performed using an unpaired, two-sided Mann–Whitney $U$ test, but with a cutoff value of $p < 0.05$, no statistically significant differences were observed.

increased levels in the GOLD stage IV phBECs as compared to the GOLD stage II/III and control phBECs (**Supplementary Figure 5D**). However, following infection, the PR8 virus still replicated similarly in these cells (**Supplementary Figure 5E**), indicating little biological influence of these features on infection.

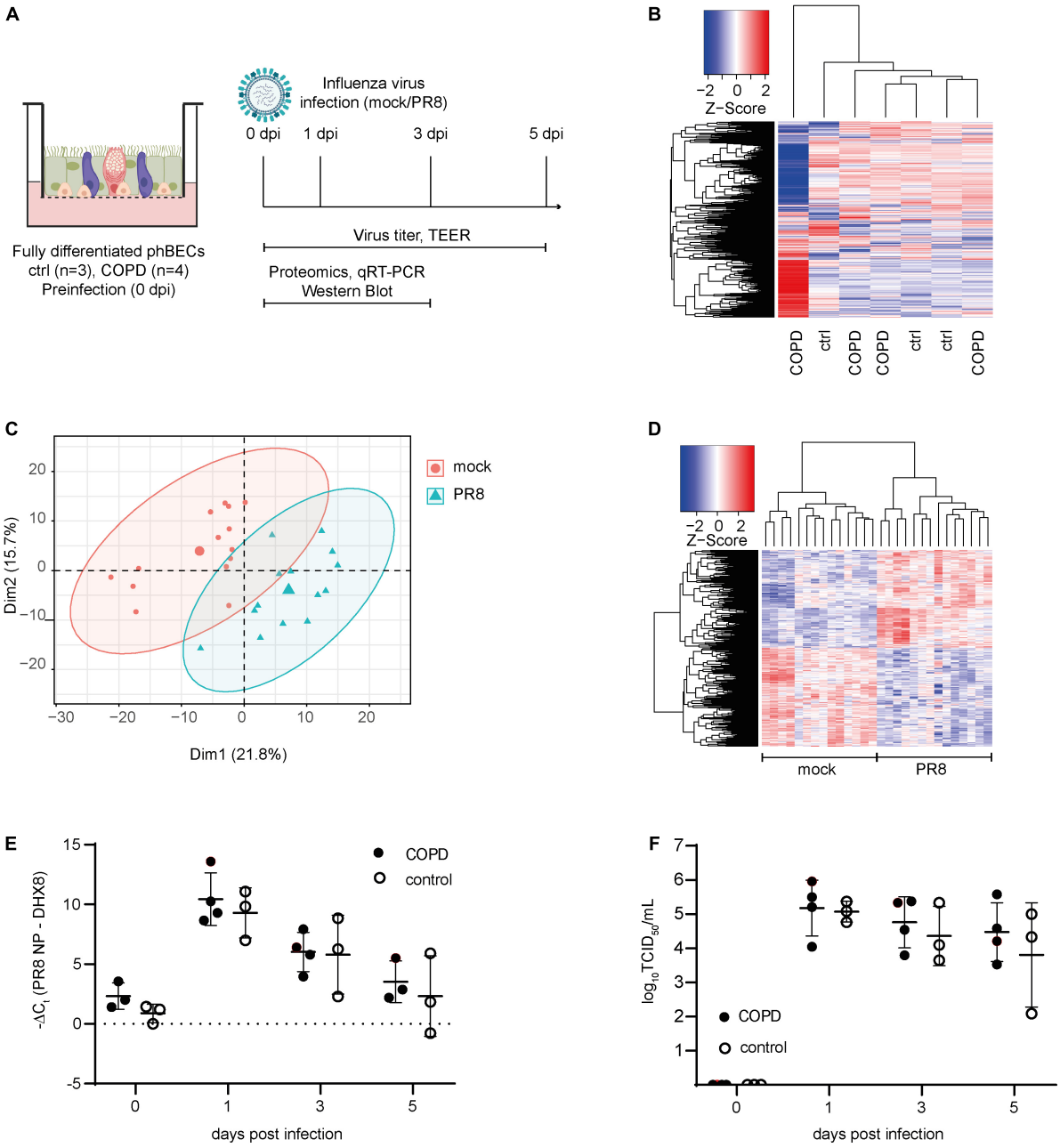


FIGURE 2
Proteomics pre- and post-influenza virus infection in fully differentiated primary human bronchial epithelial cells (phBECs). PhBECs from patients with chronic obstructive pulmonary disease (COPD) ($n$ = 4) and controls ($n$ = 3) were differentiated for 28 days at the air–liquid interface and either mock-infected or infected with influenza A virus PR8. Cells were harvested for proteomics on day 28 after airlift (pre-infection), and on days 1 and 3 post-infection. To examine viral replication, cells and apical washes were harvested on day 0 (after incubating the cells with the virus to allow attachment, and after removing the unattached virus by washing) and on days 1, 3, and 5 post-infection. **(A)** Scheme of culture, infection, and sample analysis. An illustration was created with biorender.com. TEER, transepithelial electrical resistance. **(B)** Heatmap of proteomics pre-infection. The protein profile of the COPD GOLD stage IV-derived phBECs is shown in the outermost left lane. **(C)** Principal component analysis of proteomics post-infection. **(D)** Heatmap of significantly altered proteins post-infection with all patients/controls and all time points (PR8 vs. mock, $n$ = 7). A protein was considered to be differentially expressed if the comparison resulted in a false discovery rate (FDR) of less than 5% with the Benjamini–Hochberg (BH) correction to correct multiple testing. **(E)** Total RNA was extracted from cells and mRNA levels of PR8 nucleoprotein transcripts were examined by RT-qPCR. DHX8 was used as a housekeeping gene. **(F)** Infectious viral particles in apical washes were quantified by an end point dilution assay. $TCID_{50}$: 50% tissue culture infectious dose. For panels **(E,F)**, statistical analysis was performed using an unpaired, two-sided Mann–Whitney $U$ test, but with a cutoff point of $p < 0.05$, no statistically significant differences were observed.

### 3.5. Viral replication after influenza A virus infection does not differ in COPD- and control-derived fully differentiated phBECs

To evaluate the susceptibility and response of fully differentiated phBECs derived from patients with COPD and controls to influenza A virus infection, cells were infected with PR8, a widely used strain in *in vitro* studies (Kroeker et al., 2012, 2013; Short et al., 2016; Han et al., 2018). On ALI day 28, phBECs were infected with PR8 (**Figure 2A**) and proteomes were analyzed at days 1 and 3 post-infection (**Figures 2C, D**). Viral RNA of nucleoprotein within the cells and infectious viral particles in apical washes peaked at day 1 in phBECs from patients with COPD and controls and from then gradually decreased, with no statistical differences at any time point (unpaired, two-sided Mann–Whitney *U* test, **Figures 2E, F**).

### 3.6. COPD- and control-derived fully differentiated phBECs display similar protein profiles post-influenza A virus infection

Cellular protein was collected from phBECs on days 1 and 3 post-infection and subjected to proteomic analysis (**Figure 2A**). Principal component analysis (PCA) and a heatmap displaying the significantly altered proteins showed a clear separation between PR8- and mock-infected cells (**Figures 2C, D**), but not between disease origin (health state: COPD vs. control). An alternative dimensionality reduction method, t-Distributed Stochastic Neighbor Embedding (t-SNE), also indicated that only the condition effect (PR8-infected vs. mock-infected) separated the two groups, but not disease origin (COPD vs. control), time (day 1 vs. day 3 post-infection), or patients' origin (**Supplementary Figure 6**). Moreover, the heatmap of significantly altered proteins on days 1 and 3 post-infection also did not indicate any separation between disease origin, and we found no significant changes in influenza virus-induced gene expression between control- and COPD-derived cells (**Supplementary Figures 7, 8**).

### 3.7. PhBECs display a robust antiviral response post-influenza A virus infection and upregulate several novel influenza virus-induced proteins

Given the absence of disease-specific effects, we focused on differences between PR8- and mock-infected cells, independent of the disease origin ($n = 7$). In this analysis, 31 and 234 proteins were differentially expressed (adj. $p < 0.05$) on day 1 and day 3 post-infection (PR8/mock), respectively, with a robust upregulation of interferon (IFN)-regulated genes (**Figure 3**, **Supplementary Figures 7, 8**, and **Supplementary data** file "Protein List," data sheets "ConditionsDay1" and "ConditionsDay3"). Taking into account both time points, 290 proteins were differentially expressed post-infection (adj. $p < 0.05$) among the total 4,341 variables (PR8/mock; Supplementary data file "Protein List," data sheet "ConditionsOverallTime"). Pathway enrichment analysis of those 290 proteins demonstrated that variants of the (innate) immune system and cytokine signaling, in particular IFN signaling, were the dominating top enriched pathways (**Figure 4A**). For instance, a strong upregulation of established IFN-regulated genes like interferon-regulatory factor 9 (IRF9), interferon-induced GTP-binding protein Mx1 (MX1), 2′–5′-oligoadenylate synthase 1 (OAS1), signal transducer and activator of transcription 1-α/β (STAT1), ubiquitin-like protein ISG15 (ISG15), and interferon-induced protein with tetratricopeptide repeats 1 (IFIT1) was observed (**Figures 4B–G**). In addition to these drastically upregulated proteins demonstrating a robust antiviral response, several novel proteins appeared as significantly upregulated (adj. $p < 0.05$). Those proteins were phospholipid scramblase 1 (PLSCR1), human leukocyte antigen class I histocompatibility antigen, α chain F (HLA-F), cap-specific mRNA (nucleoside-2′-*O*-)-methyltransferase 1 (CMTR1), E3 ubiquitin–protein ligase DTX3L (DTX3L), and shiftless antiviral inhibitor of ribosomal frameshifting protein SHFL, previously called RyDEN (c19orf66) (**Figure 5A**). Upregulation of all these genes was assessed by RT-qPCR (**Figure 5B**) and, for PLSCR1, HLA-F, and DTX3L, by Western blot analysis (**Figure 5C**, **Supplementary Figure 9**). Upregulation on protein level was validated for all three proteins assessed, while upregulation on transcript level was only observed for PLSCR1 and HLA-F, demonstrating significant post-transcriptional regulation mechanisms.

## 4. Discussion

Studies comparing proteomes between COPD- and control-derived phBECs in fully differentiated organotypic bronchoepithelia pre- and post-influenza virus infection are lacking. Performing such a comparison, we have not found disease-dependent changes. Independent of disease status, we have, however, observed a robust IFN-mediated antiviral response and identified several upregulated proteins following PR8 infection, which have not or only recently been linked to the host response to the influenza virus. Notably, those proteins have not been reported in studies where undifferentiated primary normal human bronchotracheal epithelial cells were infected with influenza virus PR8 (Kroeker et al., 2012, 2013). Our study has thus identified novel influenza-regulated proteins

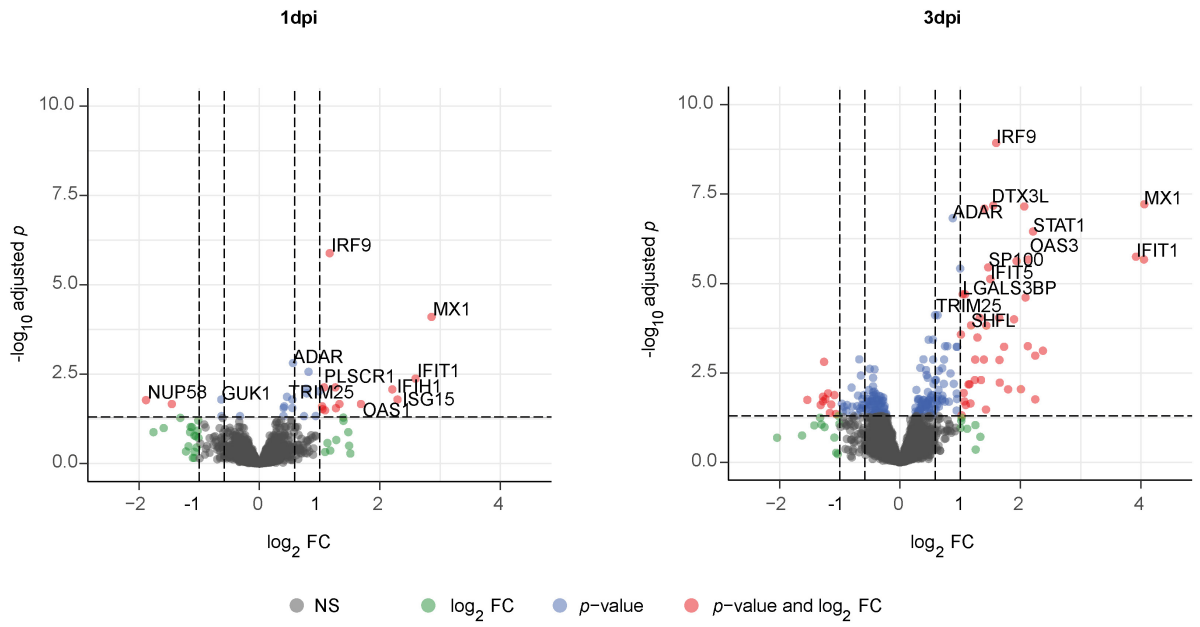


FIGURE 3
Volcano plot of significantly altered proteins in fully differentiated primary human bronchial epithelial cells (phBECs) on days 1 and 3 post-influenza virus infection. Fully differentiated phBECs from patients with chronic obstructive pulmonary disease (COPD) ($n$ = 4) and controls ($n$ = 3) were either mock-infected or infected with influenza A virus PR8. Cells were harvested for proteomics on days 1 and 3 post-infection (dpi). Volcano plot of significantly altered proteins (PR8/mock) on days 1 **(left)** and 3 **(right)** post-infection, independent of the disease state. A protein was considered to be differentially expressed if the comparison resulted in a false discovery rate (FDR) of less than 5% with the Benjamini–Hochberg (BH) correction to correct multiple testing.

in the fully differentiated bronchial epithelium that may qualify as targets to modulate the pathogenicity of infection and acute exacerbation caused by the influenza virus.

In agreement with previously published reports, we observed that the human-type flu receptor is much more frequent in human airways and fully differentiated phBECs than the avian-type (Shinya et al., 2006; Davis et al., 2015; Hsu et al., 2016) and predominantly localized on bronchial secretory cells (Matrosovich et al., 2004). The specific bronchial epithelial cell types presenting the avian-type flu receptor, however, remain poorly identified. While the display of the avian-type flu receptor on ciliated cells has been reported by others (Matrosovich et al., 2004), our results do not provide evidence for this (**Supplementary Figure 1B**). However, it must be acknowledged that the overall low presentation of the avian-type flu receptor in the human airway (Matrosovich et al., 2004; Nicholls et al., 2007; Davis et al., 2015) represents a challenge for a systematic assessment of the cell types displaying it. In addition, discrepancies between studies may also stem from different detection systems and protocols. For instance, it has been reported that *Maackia amurensis* agglutinin (MAA) lectins, frequently used to detect the avian-type flu receptor, differ in their binding affinity to SAα2,3 depending on supplier and MAA isoform used (Matrosovich et al., 2004; Nicholls et al., 2007). Here, we took advantage of a more recently developed specific monoclonal mouse antibody (HYB4) (Hidari et al., 2013; **Supplementary Figure 1B**), which allowed for circumventing the known variability in lectin binding but restricted our choice of specific antibodies to co-stain with. Therefore, even if our results, by way of exclusion, suggest display of the avian-type receptor by goblet cells in human bronchial epithelium, we have not been able to directly demonstrate this. The cell types displaying the avian-type flu receptor thus remain elusive and need further investigation.

Interestingly, despite considerable patient heterogeneity, fluorescent staining-based quantification suggested that flu receptors overall may be downregulated in patients with COPD. Also, the thickened mucus layer and increased expression of mucins in patients with COPD may protect them from influenza virus infection both because cell membranes are less accessible and because heavily sialylated mucins act as decoy receptors (Ehre et al., 2012; Wallace et al., 2021). Here, before *in vitro* infection of phBECs, we removed the mucus layer in effort to focus on cell-associated differences in virus susceptibility. Furthermore, as opposed to flu receptors in patients' epithelium, we did not see any significant changes in flu receptor display in COPD-derived vs. control-derived phBECs *in vitro*. These two aspects may explain why viral replication was similar for control- and COPD-derived phBECs *in vitro*. Flu receptor display not being conserved in COPD-derived cells *in vitro* could, on the one hand, be due to optimized growth and differentiation conditions that certainly do not reflect the

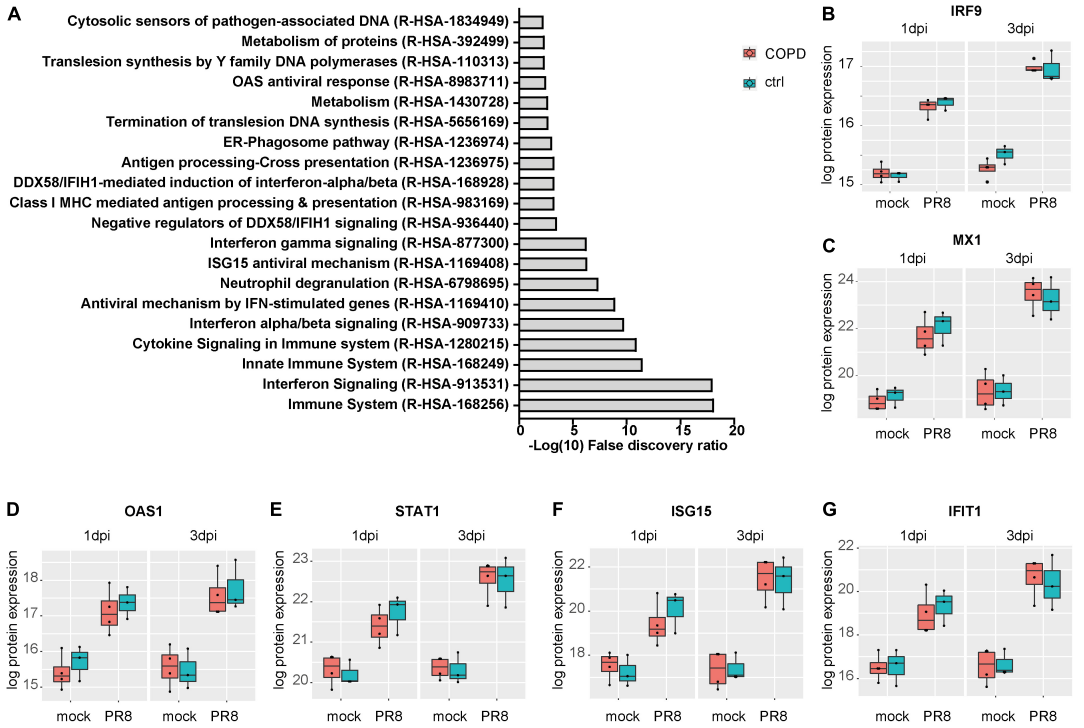


FIGURE 4
Upregulation of interferon-regulated pathways and proteins in fully differentiated primary human bronchial epithelial cells (phBECs) independent of disease state post-influenza virus infection. **(A)** Pathway analysis performed using the tool PANTHER and all 290 differentially expressed proteins post-infection, independent of disease state and taking account of both time points. **(B–G)** Box plots of interferon-regulated proteins depicting the median (middle horizontal line), the 25 and 75% percentile (lower and upper edge of the box), and the range between largest and smallest value up to a maximum of 1.5 × interquartile range (vertical lines). Data points beyond that range are regarded as outliers and are shown as individual points. IRF9, interferon-regulatory factor 9; MX1, Interferon-induced GTP-binding protein Mx1; OAS1, 2′–5′-oligoadenylate synthase 1; STAT1, signal transducer and activator of transcription 1-α/β; ISG15, ubiquitin-like protein ISG15; IFIT1, interferon-induced protein with tetratricopeptide repeats 1.

microenvironment in COPD airways. On the other hand, a decrease in flu receptor display may also only manifest in later stages of COPD: while we mainly used COPD GOLD stage II/III-derived cells for differentiation, lung specimens used for staining and quantification of flu receptors *in vivo* were derived from end-stage patients with COPD. In support of this, human-type flu receptor display is drastically reduced in phBECs derived from a COPD GOLD stage IV patient ($n$ = 1, **Supplementary Figure 5B**). Overall, these observations rather support a lower susceptibility of patients with COPD to influenza virus infection. However, interestingly, during the differentiation of phBECs, we regularly observed more avian-type receptors at early time points, where basal cells are overrepresented and where the culture thus reflects properties of a regenerating bronchial epithelium (Schamberger et al., 2015; Mastalerz et al., 2022). This suggests that, under conditions of acute airway injury and ongoing regeneration or in smoking-induced airway basal cell hyperplasia (Crystal, 2014), bronchial epithelial cells may be more susceptible to infection by the avian influenza viruses. These observations warrant further studies in models of airway regeneration and hyperplasia.

Comparisons between COPD- and control-derived phBECs have been done by direct transcriptomic analysis of bronchial brushings, identifying several differentially expressed genes that characterized COPD-derived phBECs (Steiling et al., 2013). It has also been shown that phBECs derived from GOLD stage IV patients differentiate differently relative to control cells, resulting in altered cell type compositions (Gohy et al., 2019). Here, we selected phBECs from age-, sex-, and smoking history-matched control and COPD lungs (GOLD stage II/III), all isolated from non-tumorous airways in the context of a lung tumor resection, except for one GOLD stage IV specimen from an end-stage explant. However, in our differentiated organotypic bronchoepithelia, we did not find any statistically significant differences between COPD- and control-derived phBECs in terms of proteomes and differentiation potential. Identification of such differences may have been hampered by the following limitations in our study design: first, we included phBECs from different COPD GOLD stages, including mild-to-moderate COPD. Several large COPD cohort studies showed that the COPD GOLD stage is not necessarily a stable or progressive criterion (due to diagnosis by spirometry and work-related

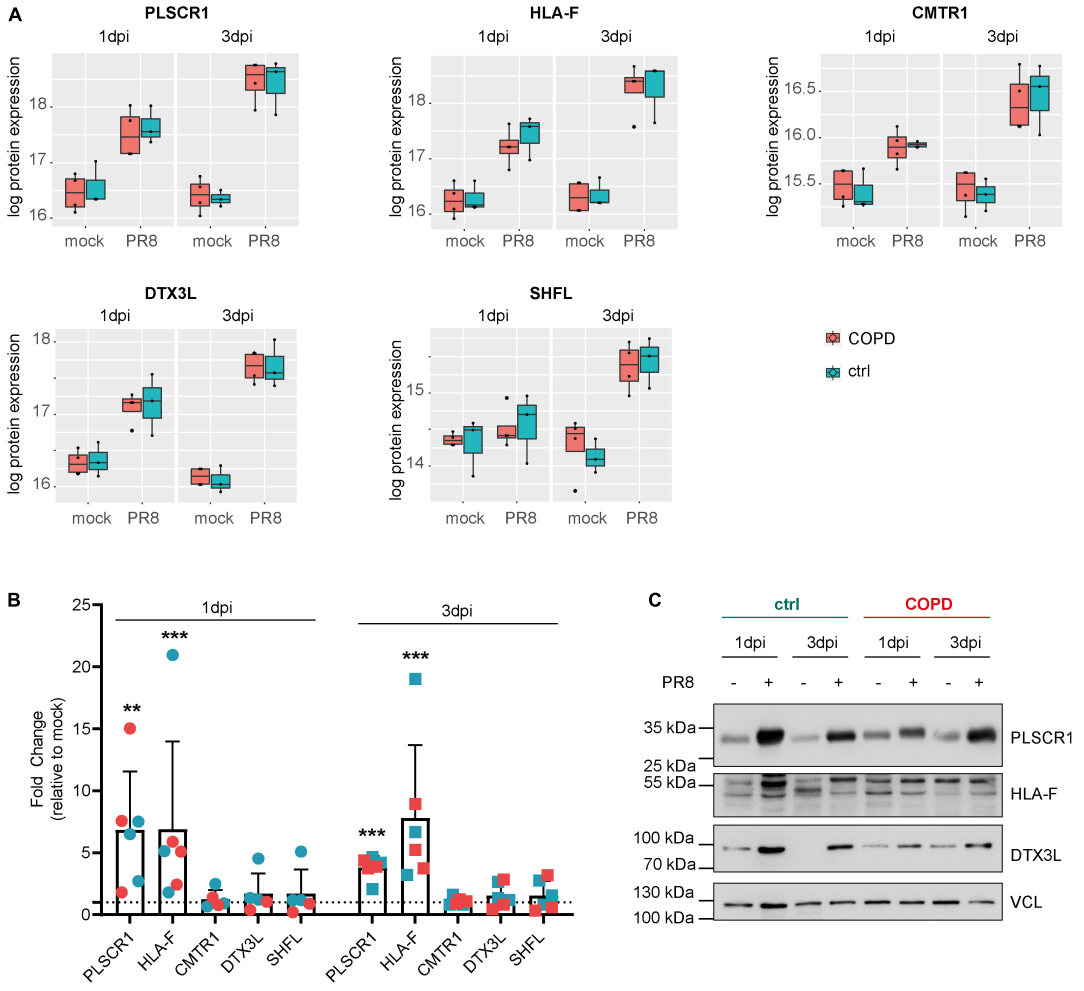


FIGURE 5
Novel proteins upregulated in fully differentiated primary human bronchial epithelial cells (phBECs) independent of disease state post-influenza virus infection. **(A)** Box plots of significantly upregulated novel proteins in fully differentiated phBECs on days 1 and 3 post-influenza virus infection (dpi). PLSCR1, phospholipid scramblase 1; HLA-F, human leukocyte antigen class I histocompatibility antigen, α chain F; CMTR1, cap-specific mRNA (nucleoside-2′-*O*-)-methyltransferase 1; DTX3L, E3 ubiquitin–protein ligase DTX3L; SHFL, shiftless antiviral inhibitor of ribosomal frameshifting protein. Box plots depict the median (middle horizontal line), the 25 and 75% percentile (lower and upper edge of the box), and the range between the largest and smallest value up to a maximum of 1.5 × interquartile range (vertical lines). Data points beyond that range are regarded as outliers and are shown as individual points. **(B)** mRNA expression of novel genes 1 and 3 dpi (PR8/mock). For some COPD phBECs samples, the obtained amount of RNA was insufficient to cover all qPCR reactions, restricting the COPD-derived samples to $n = 3$ and $n = 2$ on 1 dpi. Symbol legend (in analogy to panels A and C): Cyan squares, ctrl samples; red squares, COPD samples. **(C)** Western blots of PLSCR1, HLA-F, and DTX3L. VCL (vinculin) was used as a loading control. Irrelevant parts of the Western blot images were cropped to only present the areas of interest. Uncropped Western blot images are given in **Supplementary Figure 9**.

lung function diagnostics). Especially patients who initially meet the criteria for mild-to-moderate COPD are sometimes later diagnosed with lower COPD GOLD stages or even with normal lung function, or vice versa, over a series of annual visits (Aaron et al., 2017). This suggests reversibility of disease stage unless cells are from severe or very severe patients with COPD, which may in part be reflected by the capacity of airway epithelial cells to differentiate normally *in vitro* when given the appropriate growth factors. Second, given the known individual variations in patient-derived cells including a highly diverse medication history (**Supplementary Table 1**), the low number of control- and COPD-derived phBECs used in our study may have been insufficient to detect significant differences (Mindaye et al., 2017). Third, it cannot be completely excluded that tumor environment-derived factors may have ultimately masked COPD-specific effects for all but phBECs from the stage IV patient without a tumor background.

Although influenza A virus infection has been studied using proteomics in basal-like phBECs under submerged conditions (Kroeker et al., 2012, 2013), an advantage of our study is that we used fully differentiated phBECs, which reflect the cell type complexity of the bronchial epithelium *in vivo* and

thus recapitulate the orchestration of numerous host factors better than undifferentiated cells or cell lines. Nevertheless, our *in vitro* model does not recapitulate all features of the bronchial epithelium *in vivo* including epithelial–immune cells or epithelial–mesenchymal crosstalk. Such interactions, however, may be key in the context of acute exacerbation and COPD progression (Barnes, 2019; Guo-Parke et al., 2020). Therefore, future studies on influenza virus infection should make use of phBECs derived from very severe or severe COPD GOLD stage lungs, which typically retain a disease phenotype *in vitro*, ideally in combination with non-tumorous and, in terms of age and sex, well-matched control samples. Furthermore, the influence of deregulated immune or mesenchymal cells should be studied in more advanced organoid co-culture models.

Next to a strong and mostly IFN signaling-related antiviral response, we discovered several influenza virus-induced proteins that have not or only recently been linked to influenza virus infection and may thus represent novel host factors in that context. PLSCR1, for instance, is an IFN-regulated gene with multiple functions including the regulation of viral uptake and replication by interacting with viral proteins at the plasma membrane as well as within the cytoplasm (Dal Col et al., 2022). The few studies that addressed its role in influenza virus infection have demonstrated binding to nucleoprotein NP and prevention of its nuclear translocation (Luo et al., 2018; Liu et al., 2022). Interestingly, PLSCR1 has also been described to be secreted and interact with extracellular matrix protein 1 (ECM1) in the dermal–epidermal junction of human skin (Merregaert et al., 2010). This raises the intriguing hypothesis that PLSCR1 could also play a role in epithelial–mesenchymal crosstalk and, for instance, promote small airway fibrosis upon influenza virus infection. Notably, small airway fibrosis is increasingly recognized as the major driver of COPD progression, but the underlying causative mechanisms remain poorly understood (Hogg et al., 2017; Barnes, 2019). Hence, further investigation is warranted to assess the role of this protein in the context of airway fibrosis.

Cap-specific mRNA (nucleoside-2'-O-)-methyltransferase 1 (CMTR1) and SHFL have been described as host factors that facilitate the expression of viral proteins. Upon influenza A virus infection, CMTR1 is required for efficient cap snatching and regulation of a cell's autonomous immune response (Li et al., 2020). A function of SHFL has not yet been described in the context of influenza virus infection, but it is known to promote programmed-1 ribosomal frameshift (−1 PRF) in SARS-CoV-2 viral gene expression (Baggen et al., 2021; Sun et al., 2021). Importantly, an inhibitor of −1 PRF, merafloxacin, restricted SARS-CoV-2 replication in VERO E6 cells (Sun et al., 2021). Taken together, these observations warrant further studies into CMTR1 and SHFL as potential influenza virus host factors and targets to modulate influenza pathogenicity.

E3 ubiquitin-protein ligase DTX3L (DTX3L), an E3 ubiquitin–protein ligase, has been little investigated in the context of virus infection, except for a study that reports protein mono-ADP-ribosyltransferase PARP9 (PARP9)-DTX3L ubiquitin ligase to target host histone and viral protease to enhance IFN signaling (Zhang et al., 2015). It is known that the ubiquitin–proteasome system is important for the replication of influenza A viruses and that ubiquitination also plays an essential role in innate immunity to the influenza A virus (Rudnicka and Yamauchi, 2016). DTX3L may thus be a hitherto unidentified factor in this context.

Finally, recent studies have been revealing the significance of natural killer (NK) cells in maintaining immune system homeostasis and their involvement in COPD pathogenesis (Rao et al., 2021). NK cells, as innate immune cells, provide the first line of defense at the border of airway epithelium and the microenvironment. HLA-F, upregulated in our model upon influenza virus infection, has been the least investigated among the HLA class I family; it has only recently been demonstrated to exert an important role in immune regulation by presenting peptides and regulating immunity through interactions with NK cells (Dulberger et al., 2017; Lin and Yan, 2019). Interestingly, increased protein levels of HLA-F and interaction with NK cells have been indicated after infection with BK polyomavirus, HIV, and HCV (Lunemann et al., 2018; Kiani et al., 2019; Koyro et al., 2021). Our study indicates a role for HLA-F after influenza virus infection in the human airway, presumably by interaction with NK cells. Since the functions of NK cells in COPD have remained unclear (Rao et al., 2021), the differentiated organotypic bronchoepithelia might serve as a simplified model to unravel the interaction of NK cells with HLA-F upon viral infection.

## Conclusion

Our study demonstrated the dominant presentation of human-type vs. avian-type flu receptors in human lung sections and in fully differentiated phBECs. COPD- and control-derived cells showed similar differentiation potential, similar susceptibility to influenza A virus infection, and similar proteomes pre- and post-infection. Pooling all post-infection proteome data enabled us to identify novel influenza A virus-regulated proteins. Our results warrant further studies of these proteins' functions in the context of the pathogenicity of infection and acute exacerbation caused by the influenza virus.

## Data availability statement

The datasets presented in this study can be found in online repositories. The names of the repository/repositories

and accession number(s) can be found below: http://www.proteomexchange.org/, PXD031461.

## Ethics statement

The studies involving human participants were reviewed and approved by Ethics Committee of the Justus-Liebig-University School of Medicine, Gießen, Germany, Ethics Committee of the Ludwig-Maximilians University of Munich, Germany. The patients/participants provided their written informed consent to participate in this study.

## Author contributions

MN, HA, and CS-W conceived and designed the research and wrote the manuscript. HA and CS-W supervised the project. MN, CS-W, HA, AD, AC, and EH planned and performed the experiments and analyzed the data. JM-P and SH performed the proteomics and data analysis. HM and RL performed the statistical analysis on proteomics data. CR, AG, KK, JB, and AH provided the clinical samples, patient parameters, and resources. All authors read and approved the manuscript.

## Funding

This work was supported by the German Federal Institute for Risk Assessment (BfR, 1328-570, to CS-W), the German Center for Lung Research (DZL), the German Research Foundation (DFG) in the context of GRK2338 (CS-W and AH), and the Helmholtz Association. MN was supported by an overseas grant from the Shiga University of Medical Science and the Uehara Memorial Foundation.

## Acknowledgments

We gratefully acknowledge the provision of human biomaterial and clinical data from the CPC-M BioArchive and its partners at the Asklepios Biobank Gauting, the LMU Hospital, and the Ludwig Maximilians Universität München as well as from the UGMLC/DZL biobank, Gießen. We thank the patients and their families for their support. We also thank Prof. Dr. med. Susanne Herold (University of Giessen and Marburg Lung Center), Prof. Dr. Silke Meiners, Dr. Ilona Kammerl for providing PR8, and Drs.Takahisa Nakayama and Takaaki Kinoshita for meaningful discussions. We are grateful to Dr. Andrea Schamberger for providing the protocols related to cell culture, Ms. Beatrix Steer, Ms. Heike Hofmann, Dr. Gerald Burgstaller, Ms. Daniela Dietel, and Ms. Marisa Neumann for their technical help.

## Conflict of interest

The authors declare that the research was conducted in the absence of any commercial or financial relationships that could be construed as a potential conflict of interest.

## Publisher's note

All claims expressed in this article are solely those of the authors and do not necessarily represent those of their affiliated organizations, or those of the publisher, the editors and the reviewers. Any product that may be evaluated in this article, or claim that may be made by its manufacturer, is not guaranteed or endorsed by the publisher.

## Supplementary material

The Supplementary Material for this article can be found online at: https://www.frontiersin.org/articles/10.3389/fmicb.2022.957830/full#supplementary-material

## References

Aaron, S. D., Tan, W. C., Bourbeau, J., Sin, D. D., Loves, R. H., Macneil, J., et al. (2017). Diagnostic instability and reversals of chronic obstructive pulmonary disease diagnosis in individuals with mild to moderate airflow obstruction. *Am. J. Respir. Crit. Care Med.* 196, 306–314. doi: 10.1164/rccm.201612-2531OC

Baggen, J., Vanstreels, E., Jansen, S., and Daelemans, D. (2021). Cellular host factors for SARS-CoV-2 infection. *Nat. Microbiol.* 6, 1219–1232. doi: 10.1038/s41564-021-00958-0

Barnes, P. J. (2019). Small airway fibrosis in COPD. *Int. J. Biochem. Cell Biol.* 116:105598. doi: 10.1016/j.biocel.2019.105598

Berthold, E. J., Ma-Lauer, Y., Chakraborty, A., Von Brunn, B., Hilgendorff, A., Hatz, R., et al. (2022). Effects of immunophilin inhibitors and non-immunosuppressive analogs on coronavirus replication in human infection models. *Front. Cell. Infect. Microbiol.* 12:958634. doi: 10.3389/fcimb.2022.958634

Bouquet, J., Tabor, D. E., Silver, J. S., Nair, V., Tovchigrechko, A., Griffin, M. P., et al. (2020). Microbial burden and viral exacerbations in a longitudinal multicenter COPD cohort. *Respir. Res.* 21:77. doi: 10.1186/s12931-020-01340-0

Bruderer, R., Bernhardt, O. M., Gandhi, T., Miladinovic, S. M., Cheng, L. Y., Messner, S., et al. (2015). Extending the limits of quantitative proteome profiling with data-independent acquisition and application to acetaminophen-treated

three-dimensional liver microtissues. *Mol. Cell. Proteom.* 14, 1400–1410. doi: 10.1074/mcp.M114.044305

Crystal, R. G. (2014). Airway basal cells. The "smoking gun" of chronic obstructive pulmonary disease. *Am. J. Respir. Crit. Care Med.* 190, 1355–1362. doi: 10.1164/rccm.201408-1492PP

Dal Col, J., Lamberti, M. J., Nigro, A., Casolaro, V., Fratta, E., Steffan, A., et al. (2022). Phospholipid scramblase 1: A protein with multiple functions via multiple molecular interactors. *Cell Commun. Signal.* 20:78. doi: 10.1186/s12964-022-00895-3

Davis, A. S., Chertow, D. S., Moyer, J. E., Suzich, J., Sandouk, A., Dorward, D. W., et al. (2015). Validation of normal human bronchial epithelial cells as a model for influenza A infections in human distal trachea. *J. Histochem. Cytochem.* 63, 312–328. doi: 10.1369/0022155415570968

Decramer, M., Janssens, W., and Miravitlles, M. (2012). Chronic obstructive pulmonary disease. *Lancet* 379, 1341–1351. doi: 10.1016/S0140-6736(11)60968-9

Dulberger, C. L., Mcmurtrey, C. P., Hölzemer, A., Neu, K. E., Liu, V., Steinbach, A. M., et al. (2017). Human leukocyte antigen F presents peptides and regulates immunity through interactions with NK-cell receptors. *Immunity* 46, 1018–1029.e1017. doi: 10.1016/j.immuni.2017.06.002

Ehre, C., Worthington, E. N., Liesman, R. M., Grubb, B. R., Barbier, D., O'neal, W. K., et al. (2012). Overexpressing mouse model demonstrates the protective role of Muc5ac in the lungs. *Proc. Natl. Acad. Sci. U. S. A.* 109, 16528–16533. doi: 10.1073/pnas.1206552109

Gohy, S., Carlier, F. M., Fregimilicka, C., Detry, B., Lecocq, M., Ladjemi, M. Z., et al. (2019). Altered generation of ciliated cells in chronic obstructive pulmonary disease. *Sci. Rep.* 9:17963. doi: 10.1038/s41598-019-54292-x

Guo-Parke, H., Linden, D., Weldon, S., Kidney, J. C., and Taggart, C. C. (2020). Mechanisms of virus-induced airway immunity dysfunction in the pathogenesis of COPD disease, progression, and exacerbation. *Front. Immunol.* 11:1205. doi: 10.3389/fimmu.2020.01205

Han, J., Perez, J. T., Chen, C., Li, Y., Benitez, A., Kandasamy, M., et al. (2018). Genome-wide CRISPR/Cas9 screen identifies host factors essential for influenza virus replication. *Cell Rep.* 23, 596–607. doi: 10.1016/j.celrep.2018.03.045

Hidari, K. I., Yamaguchi, M., Ueno, F., Abe, T., Yoshida, K., and Suzuki, T. (2013). Influenza virus utilizes N-linked sialoglycans as receptors in A549 cells. *Biochem. Biophys. Res. Commun.* 436, 394–399. doi: 10.1016/j.bbrc.2013.05.112

Hogg, J. C., Paré, P. D., and Hackett, T. L. (2017). The contribution of small airway obstruction to the pathogenesis of chronic obstructive pulmonary disease. *Physiol. Rev.* 97, 529–552. doi: 10.1152/physrev.00025.2015

Hsu, A. C., Parsons, K., Moheimani, F., Knight, D. A., Hansbro, P. M., Fujita, T., et al. (2016). Impaired antiviral stress granule and IFN-beta enhanceosome formation enhances susceptibility to influenza infection in chronic obstructive pulmonary disease epithelium. *Am. J. Respir. Cell Mol. Biol.* 55, 117–127. doi: 10.1165/rcmb.2015-0306OC

Hsu, A. C., Starkey, M. R., Hanish, I., Parsons, K., Haw, T. J., Howland, L. J., et al. (2015). Targeting PI3K-p110 alpha suppresses influenza virus infection in chronic obstructive pulmonary disease. *Am. J. Respir. Crit. Care Med.* 191, 1012–1023. doi: 10.1164/rccm.201501-0188OC

Huber, W., Von Heydebreck, A., Sultmann, H., Poustka, A., and Vingron, M. (2002). Variance stabilization applied to microarray data calibration and to the quantification of differential expression. *Bioinformatics* 18, S96–S104. doi: 10.1093/bioinformatics/18.suppl_1.S96

Ito, T., Suzuki, Y., Takada, A., Kawamoto, A., Otsuki, K., Masuda, H., et al. (1997). Differences in sialic acid-galactose linkages in the chicken egg amnion and allantois influence human influenza virus receptor specificity and variant selection. *J. Virol.* 71, 3357–3362. doi: 10.1128/jvi.71.4.3357-3362.1997

Ji, S., Dai, M. Y., Huang, Y., Ren, X. C., Jiang, M. L., Qiao, J. P., et al. (2022). Influenza a virus triggers acute exacerbation of chronic obstructive pulmonary disease by increasing proinflammatory cytokines secretion via NLRP3 inflammasome activation. *J. Inflammat.* 19:8. doi: 10.1186/s12950-022-00305-y

Kiani, Z., Bruneau, J., Geraghty, D. E., and Bernard, N. F. (2019). HLA-F on autologous HIV-infected cells activates primary NK cells expressing the activating killer immunoglobulin-like receptor KIR3DS1. *J. Virol.* 93, e00933–e919. doi: 10.1128/JVI.00933-19

Koyro, T. F., Kraus, E., Lunemann, S., Hölzemer, A., Wulf, S., Jung, J., et al. (2021). Upregulation of HLA-F expression by BK polyomavirus infection induces immune recognition by KIR3DS1-positive natural killer cells. *Kidney Int.* 99, 1140–1148. doi: 10.1016/j.kint.2020.12.014

Krammer, F., Smith, G. J. D., Fouchier, R. A. M., Peiris, M., Kedzierska, K., Doherty, P. C., et al. (2018). Influenza. *Nat. Rev. Dis. Primers* 4:3. doi: 10.1038/s41572-018-0002-y

Krijthe, J. H. (2015). *Rtsne: T-distributed stochastic neighbor embedding using barnes-hut implementation. R package version 0.16 ed.*

Kroeker, A. L., Ezzati, P., Coombs, K. M., and Halayko, A. J. (2013). Influenza A infection of primary human airway epithelial cells up-regulates proteins related to purine metabolism and ubiquitin-related signaling. *J. Proteome Res.* 12, 3139–3151. doi: 10.1021/pr400464p

Kroeker, A. L., Ezzati, P., Halayko, A. J., and Coombs, K. M. (2012). Response of primary human airway epithelial cells to influenza infection: A quantitative proteomic study. *J. Proteome Res.* 11, 4132–4146. doi: 10.1021/pr300239r

Leek, J. T., Johnson, W. E., Parker, H. S., Fertig, E. J., Jaffe, A. E., Zhang, Y., et al. (2020). *Sva: Surrogate variable analysis. R package version 3.36.0 ed.*

Leek, J. T., Johnson, W. E., Parker, H. S., Jaffe, A. E., and Storey, J. D. (2012). The sva package for removing batch effects and other unwanted variation in high-throughput experiments. *Bioinformatics* 28, 882–883. doi: 10.1093/bioinformatics/bts034

Lenz, A. G., Stoeger, T., Cei, D., Schmidmeir, M., Semren, N., Burgstaller, G., et al. (2014). Efficient bioactive delivery of aerosolized drugs to human pulmonary epithelial cells cultured in air-liquid interface conditions. *Am. J. Respir. Cell Mol. Biol.* 51, 526–535. doi: 10.1165/rcmb.2013-0479OC

Lepper, M. F., Ohmayer, U., Von Toerne, C., Maison, N., Ziegler, A. G., and Hauck, S. M. (2018). Proteomic landscape of patient-derived CD4+ T cells in recent-onset type 1 diabetes. *J. Proteome Res.* 17, 618–634. doi: 10.1021/acs.jproteome.7b00712

Li, B., Clohisey, S. M., Chia, B. S., Wang, B., Cui, A., Eisenhaure, T., et al. (2020). Genome-wide CRISPR screen identifies host dependency factors for influenza A virus infection. *Nat. Commun.* 11:164. doi: 10.1038/s41467-019-13965-x

Li, T., Zhang, Y., Patil, P., and Johnson, W. E. (2021). Overcoming the impacts of two-step batch effect correction on gene expression estimation and inference. *Biostatistics* [Preprint]. doi: 10.1101/2021.01.24.428009

Lin, A., and Yan, W. H. (2019). The emerging roles of human leukocyte antigen-F in immune modulation and viral infection. *Front. Immunol.* 10:964. doi: 10.3389/fimmu.2019.00964

Liu, Y., Lin, S., Xie, Y., Zhao, L., Du, H., Yang, S., et al. (2022). ILDR1 promotes influenza A virus replication through binding to PLSCR1. *Sci. Rep.* 12:8515. doi: 10.1038/s41598-022-12598-3

Lodes, N., Seidensticker, K., Perniss, A., Nietzer, S., Oberwinkler, H., May, T., et al. (2020). Investigation on ciliary functionality of different airway epithelial cell lines in three-dimensional cell culture. *Tissue Eng.* 26, 432–440. doi: 10.1089/ten.tea.2019.0188

Lunemann, S., Schöbel, A., Kah, J., Fittje, P., Hölzemer, A., Langeneckert, A. E., et al. (2018). Interactions between KIR3DS1 and HLA-F activate natural killer cells to control HCV replication in cell culture. *Gastroenterology* 155, 1366–1371.e1363. doi: 10.1053/j.gastro.2018.07.019

Luo, W., Zhang, J., Liang, L., Wang, G., Li, Q., Zhu, P., et al. (2018). Phospholipid scramblase 1 interacts with influenza A virus NP, impairing its nuclear import and thereby suppressing virus replication. *PLoS Pathog.* 14:e1006851. doi: 10.1371/journal.ppat.1006851

Mallia, P., and Johnston, S. L. (2007). Influenza infection and COPD. *Int. J. Chron. Obstruct. Pulmon. Dis.* 2, 55–64. doi: 10.2147/copd.2007.2.1.55

Mastalerz, M., Dick, E., Chakraborty, A., Hennen, E., Schamberger, A. C., Schroppel, A., et al. (2022). Validation of in vitro models for smoke exposure of primary human bronchial epithelial cells. *Am. J. Physiol.* 322, L129–L148. doi: 10.1152/ajplung.00091.2021

Matrosovich, M. N., Matrosovich, T. Y., Gray, T., Roberts, N. A., and Klenk, H. D. (2004). Human and avian influenza viruses target different cell types in cultures of human airway epithelium. *Proc. Natl. Acad. Sci. U. S. A.* 101, 4620–4624. doi: 10.1073/pnas.0308001101

Mattugini, N., Merl-Pham, J., Petrozziello, E., Schindler, L., Bernhagen, J., Hauck, S. M., et al. (2018). Influence of white matter injury on gray matter reactive gliosis upon stab wound in the adult murine cerebral cortex. *Glia* 66, 1644–1662. doi: 10.1002/glia.23329

Merregaert, J., Van Langen, J., Hansen, U., Ponsaerts, P., El Ghalbzouri, A., Steenackers, E., et al. (2010). Phospholipid scramblase 1 is secreted by a lipid raft-dependent pathway and interacts with the extracellular matrix protein 1 in the dermal epidermal junction zone of human skin. *J. Biol. Chem.* 285, 37823–37837. doi: 10.1074/jbc.M110.136408

Mindaye, S. T., Ilyushina, N. A., Fantoni, G., Alterman, M. A., Donnelly, R. P., and Eichelberger, M. C. (2017). Impact of influenza A virus infection on the proteomes of human bronchoepithelial cells from different donors. *J. Proteome Res.* 16, 3287–3297. doi: 10.1021/acs.jproteome.7b00286

Newby, C. M., Rowe, R. K., and Pekosz, A. (2006). Influenza A virus infection of primary differentiated airway epithelial cell cultures derived from Syrian golden hamsters. *Virology* 354, 80–90. doi: 10.1016/j.virol.2006.06.024

Nicholls, J. M., Bourne, A. J., Chen, H., Guan, Y., and Peiris, J. S. (2007). Sialic acid receptor detection in the human respiratory tract: Evidence for widespread distribution of potential binding sites for human and avian influenza viruses. *Respir. Res.* 8:73. doi: 10.1186/1465-9921-8-73

Ntritsos, G., Franek, J., Belbasis, L., Christou, M. A., Markozannes, G., Altman, P., et al. (2018). Gender-specific estimates of COPD prevalence: A systematic review and meta-analysis. *Int. J. Chron. Obstruct. Pulmon. Dis.* 13, 1507–1514. doi: 10.2147/COPD.S146390

Perez-Riverol, Y., Bai, J., Bandla, C., Garcia-Seisdedos, D., Hewapathirana, S., Kamatchinathan, S., et al. (2022). The PRIDE database resources in 2022: A hub for mass spectrometry-based proteomics evidences. *Nucleic Acids Res.* 50, D543–D552. doi: 10.1093/nar/gkab1038

Pezzulo, A. A., Starner, T. D., Scheetz, T. E., Traver, G. L., Tilley, A. E., Harvey, B. G., et al. (2011). The air-liquid interface and use of primary cell cultures are important to recapitulate the transcriptional profile of in vivo airway epithelia. *Am. J. Physiol.* 300, L25–L31. doi: 10.1152/ajplung.00256.2010

Rao, Y., Le, Y., Xiong, J., Pei, Y., and Sun, Y. (2021). NK cells in the pathogenesis of chronic obstructive pulmonary disease. *Front. Immunol.* 12:666045. doi: 10.3389/fimmu.2021.666045

Ritchie, M. E., Phipson, B., Wu, D., Hu, Y., Law, C. W., Shi, W., et al. (2015). Limma powers differential expression analyses for RNA-sequencing and microarray studies. *Nucleic Acids Res.* 43:e47. doi: 10.1093/nar/gkv007

Rudnicka, A., and Yamauchi, Y. (2016). Ubiquitin in influenza virus entry and innate immunity. *Viruses* 8:293. doi: 10.3390/v8100293

Schamberger, A. C., Staab-Weijnitz, C. A., Mise-Racek, N., and Eickelberg, O. (2015). Cigarette smoke alters primary human bronchial epithelial cell differentiation at the air-liquid interface. *Sci. Rep.* 5:8163. doi: 10.1038/srep08163

Shinya, K., Ebina, M., Yamada, S., Ono, M., Kasai, N., and Kawaoka, Y. (2006). Avian flu: Influenza virus receptors in the human airway. *Nature* 440, 435–436. doi: 10.1038/440435a

Short, K. R., Kasper, J., Van Der Aa, S., Andeweg, A. C., Zaaraoui-Boutahar, F., Goeijenbier, M., et al. (2016). Influenza virus damages the alveolar barrier by disrupting epithelial cell tight junctions. *Eur. Respir. J.* 47, 954–966. doi: 10.1183/13993003.01282-2015

Singanayagam, A., Loo, S. L., Calderazzo, M., Finney, L. J., Trujillo Torralbo, M. B., Bakhsoliani, E., et al. (2019). Antiviral immunity is impaired in COPD patients with frequent exacerbations. *Am. J. Physiol.* 317, L893–L903. doi: 10.1152/ajplung.00253.2019

Smith, C. B., Kanner, R. E., Golden, C. A., Klauber, M. R., and Renzetti, A. D. Jr. (1980). Effect of viral infections on pulmonary function in patients with chronic obstructive pulmonary diseases. *J. Infect. Dis.* 141, 271–280. doi: 10.1093/infdis/141.3.271

Steiling, K., Van Den Berge, M., Hijazi, K., Florido, R., Campbell, J., Liu, G., et al. (2013). A dynamic bronchial airway gene expression signature of chronic obstructive pulmonary disease and lung function impairment. *Am. J. Respir. Crit. Care Med.* 187, 933–942. doi: 10.1164/rccm.201208-1449OC

Sun, Y., Abriola, L., Niederer, R. O., Pedersen, S. F., Alfajaro, M. M., Silva Monteiro, V., et al. (2021). Restriction of SARS-CoV-2 replication by targeting programmed -1 ribosomal frameshifting. *Proc. Natl. Acad. Sci. U. S. A.* 118:e2023051118. doi: 10.1073/pnas.2023051118

Viniol, C., and Vogelmeier, C. F. (2018). Exacerbations of COPD. *Eur. Respir. Rev.* 27:170103. doi: 10.1183/16000617.0103-2017

Wallace, L. E., Liu, M., Van Kuppeveld, F. J. M., De Vries, E., and De Haan, C. A. M. (2021). Respiratory mucus as a virus-host range determinant. *Trends Microbiol.* 29, 983–992. doi: 10.1016/j.tim.2021.03.014

Wei, L., Xu, D., Qian, Y., Huang, G., Ma, W., Liu, F., et al. (2015). Comprehensive analysis of gene-expression profile in chronic obstructive pulmonary disease. *Int. J. Chron. Obstruct. Pulmon. Dis.* 10, 1103–1109. doi: 10.2147/COPD.S68570

Wisniewski, J. R., Zougman, A., Nagaraj, N., and Mann, M. (2009). Universal sample preparation method for proteome analysis. *Nat. Methods* 6, 359–362. doi: 10.1038/nmeth.1322

World Health Organization [WHO] (2021). *Chronic obstructive pulmonary disease (COPD)*. Available online at: https://www.who.int/news-room/fact-sheets/detail/chronic-obstructive-pulmonary-disease-(copd) (accessed Nov 26, 2021).

Wu, W., Alexander, J. S., and Metcalf, J. P. (2022). In vivo and in vitro studies of cigarette smoke effects on innate responses to influenza virus: A matter of models? *Viruses* 14:1824. doi: 10.3390/v14081824

Zarcone, M. C., Van Schadewijk, A., Duistermaat, E., Hiemstra, P. S., and Kooter, I. M. (2017). Diesel exhaust alters the response of cultured primary bronchial epithelial cells from patients with chronic obstructive pulmonary disease (COPD) to non-typeable *Haemophilus influenzae*. *Respir. Res.* 18:27. doi: 10.1186/s12931-017-0510-4

Zhang, L., Bukreyev, A., Thompson, C. I., Watson, B., Peeples, M. E., Collins, P. L., et al. (2005). Infection of ciliated cells by human parainfluenza virus type 3 in an in vitro model of human airway epithelium. *J. Virol.* 79, 1113–1124. doi: 10.1128/JVI.79.2.1113-1124.2005

Zhang, Y., Mao, D., Roswit, W. T., Jin, X., Patel, A. C., Patel, D. A., et al. (2015). PARP9-DTX3L ubiquitin ligase targets host histone H2BJ and viral 3C protease to enhance interferon signaling and control viral infection. *Nat. Immunol.* 16, 1215–1227. doi: 10.1038/ni.3279

# Frontiers in Microbiology

**Explores the habitable world and the potential of microbial life**

The largest and most cited microbiology journal which advances our understanding of the role microbes play in addressing global challenges such as healthcare, food security, and climate change.

---

## Discover the latest Research Topics

See more →


**Frontiers**

Avenue du Tribunal-Fédéral 34
1005 Lausanne, Switzerland
frontiersin.org

**Contact us**

+41 (0)21 510 17 00
frontiersin.org/about/contact